A New Class of Terpene Antibiotics from Actinobacteria: Discovery, Characterization, and Biosynthesis

Dissertation
zur Erlangung des Grades
des Doktors der Naturwissenschaften
der Naturwissenschaftlich-Technischen Fakultät
der Universität des Saarlandes

von
Dmytro Bratiichuk

Saarbrücken
2025

Tag des Kolloquiums:	09.04.2026
Dekan:	Prof. Dr.-Ing. Dirk Bähre
Berichterstatter:	Prof. Dr. Andriy Luzhetskyy Prof. Dr. Christoph Wittmann Prof. Dr. Andreas Bechthold
Vorsitz:	Prof. Dr. Alexandra K. Kiemer
Akad. Mitarbeiter:	Dr. Stefan Boettcher

Diese Arbeit entstand unter der Anleitung von Prof. Dr. Andriy Luzhetskyy in der Fachrichtung 8.2, Pharmazeutische Biotechnologie der Naturwissenschaftlich-Technischen Fakultät der Universität des Saarlandes, von April 2021 bis August 2025.

Acknowledgements

First and foremost, I would like to express my deepest gratitude to my doctoral father, Prof. Dr. Andriy Luzhetskyy, for giving me the opportunity to pursue my PhD in his group. I am deeply thankful for his constant optimism, invaluable guidance, encouragement, for interesting and challenging projects, which helped me to grow personally and gain new skills and knowledge. Thank you for believing in me throughout all these years.

I want to thank my second supervisor, Prof. Dr. Christoph Wittmann, for his helpful suggestions and constructive feedback during my thesis committee meetings and for reviewing my thesis.

Furthermore, I would like to thank Dr. Maksym Myronovskyi, for leading me during my PhD and generously sharing his expertise and skills. I am grateful for his patience and dedication in answering my questions, reviewing my presentations and manuscripts, and his help in my personal life. Moreover, I want to thank Birgit Rosenkränzer for helping me in the lab during the first months of my PhD. I am grateful to Anja Palusczak for sharing her knowledge of HPLC/MS systems, measuring all the never-ending samples, and for our small talks. Many thanks to Dr. Marc Stierhof and Dr. Josef Zapp for performing the NMR experiments. Thank you, Marc, for never refusing to measure the countless new derivatives, for your help, and for our cheerful conversations. I also want to thank Prof. Dr. Rolf Müller and Franziska Fries for all the functional studies and manuscript reviews. Thank you, Franzi, for always accepting the endless derivatives, despite the protest of zebra fish. Special thanks go to Dr. Olena Kurylenko for her teaching, guidance, and encouragement to pursue a PhD, and to Dr. Yuriy Rebets for introducing me to the world of actinobacteria, for his generous help, support, and instruction in many new methods.

I would like to express my heartfelt gratitude to all my AMEG colleagues, past and present. Your support, laughter, conversations, coffee breaks, inspiration, and all the moments we shared both inside and outside the lab have made these years truly unforgettable.

Lastly, I would like to thank my family. Я вдячний моїм батькам за те, що подарували мені життя, за віру у мене, розуміння та підтримку у всіх моїх починаннях. Дякую, що завжди були поруч. Особливу подяку висловлюю своїй коханій дружині Анастасії. Завдяки тобі моє життя не припиняє наповнюватись радістю, щастям та любов'ю. Без твоєї безмежної підтримки, терпіння, безсонних ночей і непохитної віри в мене значна частина цієї роботи не була б можливою. Дякую тобі, кохана, за нашого сина та за те, що ви завжди поруч і даруєте мені силу й натхнення!

Abstract

Actinomycetes are a prolific source of structurally diverse and bioactive natural products with high pharmaceutical potential. This work describes the discovery and characterization of novel terpene antibiotics, gromomycins and darumycins. Identified through the screening of an actinomycete library and heterologously produced in *Streptomyces* chassis strains, gromomycins represent a new class of pentacyclic triterpenes featuring a cyclic guanidino group and exhibiting potent antimicrobial activity. The corresponding biosynthetic gene cluster was identified by transposon mutagenesis after bioinformatic analyses failed to detect it, revealing a biosynthetic pathway independent of the canonical squalene route. Gromomycins represent a new type of biosynthetic logic in secondary metabolism, utilizing a unique cyclization path based on a hexaprenylguanidine precursor. Identification, cloning and expression of related clusters uncovered new gromomycin derivatives, expanding their phylogenetic distribution. Mechanistic studies demonstrated that gromomycins disrupt bacterial membrane integrity, leading to cell lysis. Further genome mining led to the discovery of guanidine-bearing sesterterpenoids, darumycins. Targeted gene deletions combined with in vitro analyses provided important insights into their biosynthesis. Overall, these findings expand the understanding of terpene diversity and reveal new potential for antimicrobial discovery.

Zusammenfassung

Actinomyceten sind eine bedeutende Quelle strukturell vielfältiger und bioaktiver Naturstoffe mit hohem pharmazeutischem Potenzial. Diese Arbeit beschreibt die Entdeckung und Charakterisierung neuartiger Terpen-Antibiotika, Gromomycins und Darumycins. Gromomycins, identifiziert durch das Screening einer Actinomyceten-Bibliothek und heterolog exprimiert in *Streptomyces*-Chassis-Stämmen, stellen eine neue Klasse pentazyklischer Triterpene mit zyklischer Guanidinogruppe dar und zeigen ausgeprägte antimikrobielle Aktivität. Das zugehörige Biosynthesegencluster wurde mittels Transposonmutagenese identifiziert, nachdem bioinformatische Analysen erfolglos blieben, was auf einen vom Squalenweg unabhängigen Biosyntheseweg hinweist. Gromomycins repräsentieren eine neuartige Biosyntheselogik mit einzigartiger Cyclisierungsweg über einen Hexaprenylguanidin-Präkursor. Die Identifizierung, Klonierung und Expression verwandter Cluster deckte neue Gromomycin-Derivate auf und erweiterte deren phylogenetische Verbreitung. Wirkmechanistische Untersuchungen zeigten, dass Gromomycins die bakterielle Membranintegrität stören und Zelllyse auslösen. Genomanalysen führten zudem zur Entdeckung guanidinhaltiger Sesterterpenoide, Darumycins. Zielgerichtete Gen-Deletionen und in-vitro-Analysen ermöglichten wesentliche Einblicke in deren Biosynthese. Insgesamt erweitern diese Ergebnisse das Verständnis der Terpenvielfalt und eröffnen neue Perspektiven für die Entdeckung antimikrobieller Wirkstoffe.

Publications

Publications created in the course of this work:

I. Tistechok S‡., **Bratiichuk D‡.**, Sucipto H., Gummerlich N., Stierhof M., Gromyko O., Fries F., Fedorenko V., Müller R., Zapp J., Myronovskyi M., Luzhetskyy A. Gromomycins: An Unprecedented Class of Triterpene Antibiotics Produced by a Novel Biosynthetic Pathway. *Angew. Chem. Int. Ed.* **2025**, 64, e202422270.

‡ authors contributed equally.

II. **Bratiichuk D‡.**, Fries F‡., Stierhof M., Morguet L., Zapp J., Rebets Y., Müsken M., Myronovskyi M., Müller R., Herrmann J., Luzhetskyy A. Genome Mining – Driven Isolation of New Gromomycins and Insights into Their Mode of Action. *Submitted to ACS Chem. Biol.* **2025**.

‡ authors contributed equally.

III. **Bratiichuk D.**, Redzic I., Kolling D., Stierhof M., Fries F., Zapp Y., Müller R., Köhnke J., Myronovskyi M., Luzhetskyy A. Expanding the Chemical Space of Sesterterpene Antibiotics: Discovery and Characterization of Darumycins. *To be submitted*.

Publications that are not a part of the dissertation:

Melnyk, S., Stierhof, M., **Bratiichuk, D.**, Fries, F., Müller, R., Rebets, Y., Luzhetskyy, A., Ostash, B. Uncovering the Genetic Basis of Antiviral Polyketide Limocrocin Biosynthesis Through Heterologous Expression. *Microbial Cell Factories*. **2025**. 24(1):17. https://doi.org/10.1186/s12934-024-02621-9.

Melnyk, S., Rebets, Y., **Bratiichuk, D**., Luzhetskyy, A., Ostash, B. Gene *amir_2071* of *Actinosynnema mirum* DSM 43827 Encodes a Dimethylallyltryptophan Synthase Superfamily Protein Responsible for the Production of Prenylated Tyrosine. *Folia Microbiol* **2025**. https://doi.org/10.1007/s12223-025-01305-0.

Conference Contributions

Bratiichuk D., Tistechok S., Sucipto H., Gummerlich N., Stierhof M., Gromyko O., Zapp J., Fries F., Müller R., Myronovskyi M., Luzhetskyy A. Gromomycins – A Novel Class of Antibiotics Active Against Various Gram-Negative and Gram-Positive Pathogens. *International VAAM Symposium: Biology of Bacterial Natural Producers, Saarbrücken, Germany*, **2023** (talk).

Bratiichuk D., Tistechok S., Sucipto H., Gummerlich N., Stierhof M., Gromyko O., Zapp J., Fries F., Müller R., Myronovskyi M., Luzhetskyy A. Gromomycins: An Unprecedented Class of Triterpene Antibiotic Exhibiting Biosynthetic Uniqueness. *International VAAM Symposium: Biology of Bacterial Natural Producers, Würzburg, Germany*, **2024** (talk).

Bratiichuk D., Tistechok S., Sucipto H., Gummerlich N., Stierhof M., Gromyko O., Fedorenko V., Zapp J., Fries F., Müller R., Myronovskyi M., Luzhetskyy A. Gromomycins: An Unprecedented Class of Triterpene Antibiotics Produced by a Novel Biosynthetic Pathway. *20th International Symposium on the Biology of Actinomycetes (ISBA2025), Egmond aan Zee, Netherlands,* **2025** (poster).

Redzic I., **Bratiichuk D.,** Stierhof M., Zapp J., Fries F., Müller R., Kolling D., Köhnke J., Myronovskyi M., Luzhetskyy A. Biosynthetic Engineering of Darumycin, a Novel Sesterterpene Compound. *20th International Symposium on the Biology of Actinomycetes (ISBA2025), Egmond aan Zee, Netherlands,* **2025** (poster).

Matthias Klees, **Dmytro Bratiichuk**, Marc Stierhof, Maksym Myronovskyi, Andriy Luzhetskyy. Discovery of a Novel Tricyclic-Acetal-Lactone: Structural Echoes of Echinosporin and Unfolding Clues to a Shikimate Biosynthesis. *20th International Symposium on the Biology of Actinomycetes (ISBA2025), Egmond aan Zee, Netherlands,* **2025** (poster).

Table of Contents

1. Introduction

1.1. Terpene Natural Products

Natural products (NPs) are compounds derived from natural sources, such as plants, animals, and microorganisms.[1-4] NPs are broadly categorized into primary and secondary metabolites.[5-6] Primary metabolites, such as nucleic acids, amino acids, sugars, and fatty acids, are essential for survival as they form the building blocks of macromolecules.[7-8] Secondary metabolites, on the other hand, are not essential for survival, but they do provide ecological advantages by influencing interactions with other organisms and enhancing the producer's competitiveness.[9-11] They encompass various structural classes, such as alkaloids, polyketides, shikimates (phenylpropanoids), and terpenes.[12-15]

Terpenes form the most diverse class of NPs, numbering over 100,000 known compounds[16] with diverse structures, chemical and biological properties. Terpenes are hydrocarbons consisting solely of carbon and hydrogen atoms.[17-18] In contrast, modified terpenes with various functional groups, oxidized methyl groups at different locations or other structural modifications are referred to as terpenoids[19]. Terpenes and terpenoids are found in all domains of life, but are particularly abundant in plants, fungi, marine invertebrates, and less common in bacteria.[20-22] Being important components of both primary and secondary metabolism, these compounds are among the most studied and well-known natural products.[23-25] They present by diverse classes of biological molecules fulfilling different functions, including vitamins (vitamins A and D); steroids (cholesterol, testosterone); plant hormones (cytokinins, gibberellins) photosynthetic pigments (chlorophyll, having terpenoid phytol tail, carotenoids, phycobilins), flavours and fragrances (limonene, pinene, geraniol, menthol), and a variety of successful drugs (etoposide, taxol, vincristine, artemisinin).[20, 26-29]

Terpenoids of bacterial origin are relatively rare, pepresenting less than 2% of all known terpenes of bacterial origin.[20, 30] However, they have a broad spectra of activities, from geosmin and sodorifen with ecological, signalling functions, to platensimycin, azamerone, madeirone, and neomarinone, glaciapyrroles, bacterial terpenoids with therapeutic potential.[31-36] Analysis of the large amount of genomic data accumulated over the past decades has revealed the presence of countless putative terpene biosynthetic genes within bacterial genomes.[37] Terpenes and terpenoids, especially those of bacterial origin, represent a vast but underexplored source of structurally diverse bioactive compounds.[20, 38-40] The identification and development of these compounds comprises significant potential for their utilization as pharmaceuticals and in a variety of industrial and commercial applications.[37, 40]

1.2. Classification of Terpenes

Terpenes are essentially oligomers or polymers of 2-methyl-1,3-butadiene (isoprene), a 5-carbon "building block".[41] The general formula of terpenes can be written as $(C_5H_8)_n$, where n means the number of isoprene units.[42] Terpenes are classified according to the number and structural arrangement of isoprene units, which are first joined into a linear chain and then undergo cyclization and rearrangements of the carbon skeleton.[23] This principle, known as the **isoprene rule**, was proposed by Otto Wallach and refined by Leopold Ružička, provides a framework for understanding the biosynthesis of terpenes and terpenoids.[43-44] The isoprene (2-methyl-1,3-butadiene) molecule can be conceptualized as a figure with a "head" at the branched end of the molecule, and the "tail" on the opposite end.[45] However, the free isoprene unit is not a direct substrate used in polymerization step in isoprenoids biosynthesis. Instead, precursor molecules dimethylallyl diphosphate (DMAPP) and isopentenyl diphosphate (IPP) are the substrates utilized by enzymes terpene synthases to form longer isoprene skeletons. The general concept views the DMAPP and IPP molecules as a "fish" with the "head" at the phosphorylated end, and the "tail" at the branched end.[46] Hence, in principle, two isoprene units could be joined as regular, or head-to-tail fusions (the most common), or irregular (head-to-head, tail-to-tail or head-to-middle) fusions.[45, 47]

According to the number of isoprene units (n) in the molecule, terpenes can be divided into hemiterpenes (C_5), monoterpenes (C_{10}), sesquiterpenes, (C_{15}), diterpenes (C_{20}), sesterterpenes (C_{25}), triterpenes (C_{30}) tetraterpenes (C_{40}) and polyterpenes ($C_{>40}$) (**Table1**).[17]

Table 1. Classification of terpenes.

Number of carbon atoms	Value of n	Terpene class
5	1	hemiterpenes (C_5H_8)
10	2	monoterpenes
15	3	sesquiterpenes
20	4	diterpenes
25	5	sesterterpenes
30	6	triterpenes
40	8	tetraterpenes
>40	>8	polyterpenes

Hemiterpenes (n=1, C_5H_8, **Figure 1**, compounds 1-4) are in terms of structure, the simplest terpenes, which are mainly found in plants (e. g. eucalyptus). The best-known representatives include isoprene, prenol, isoprenol (also isolated from bacteria), as well as tiglic and isovaleric acid.[20]

Monoterpenes (n=2, $C_{10}H_{16}$, **Figure 1**, compounds 5-8) are derived from geranyl diphosphate (GPP) and can be in acyclic, monocyclic, or bicyclic form, with more than 30 known carbon skeletons.[48] Structurally, they may either be simple unsaturated hydrocarbons or may contain functional groups and be classified as alcohols, ketones or aldehydes.[19] Their representatives include pinene, limonene, menthol, camphene, which are active ingredients in various industrial applications.[49] Bacteria are also known to produce monoterpenoids, such as methyl geranate, borneol, and many others.[20]

Sesquiterpenes (n=3, $C_{15}H_{24}$, **Figure 1**, compounds 9-11) are composed of three isoprene units (farnesyldiphosphate) and found in both linear and cyclic (bicyclic and tricyclic) forms.[50] These compounds are naturally found in plants, fungi, insects and bacteria (geosmin, known as the earthy odor), in the form of hydrocarbons or oxygenated derivatives, such as alcohols, acids, ketones, aldehydes, and lactones.[51] Sesquiterpenoids are also widely used in medicine (artemisinin, in the treatment of malaria), agriculture and other industries.[52]

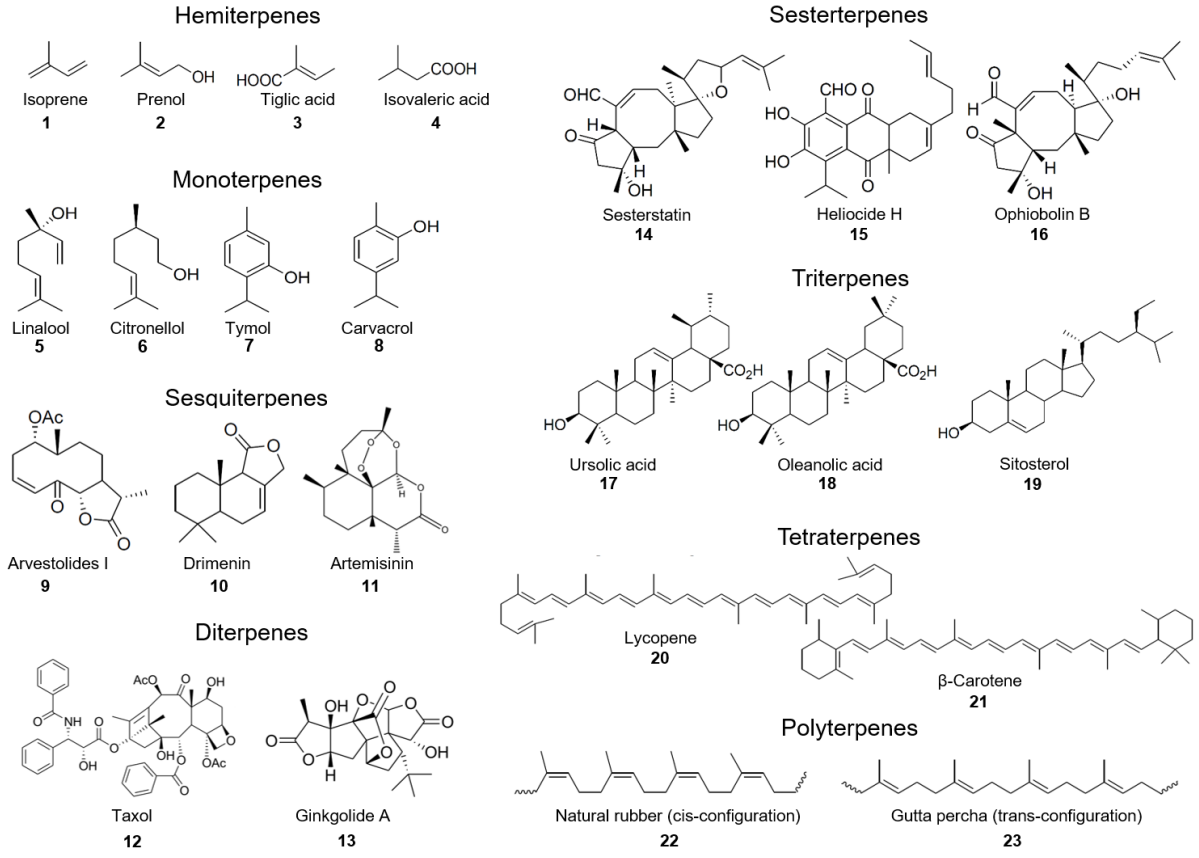

Figure 1. Examples of common terpenes and terpenoids. Structures adapted from PubChem.

Diterpenes (n=4, $C_{20}H_{32}$, **Figure 1**, compounds 12-13) are derived from geranylgeranyl diphosphate (GGPP), containing four isoprene units. Depending on their skeletal core, they can be classified as linear, bi-, tri-, tetra-, penta-, or macrocyclic diterpenes.[53] Found mostly in plants (phytol, taxol, and other derivatives), fungi, and less common in bacteria, diterpenes possess various biological activities, including antibacterial, anti-cancer, antioxidant, and anti-inflammatory.[54] Sesterterpenes (n=5, $C_{25}H_{40}$ **Figure 1**, compounds 14-16) consist of 25 carbon atoms and five isoprene units and are rare compared to other classes.[55] Over 1,600 structurally and functionally diverse compounds belong to this class, most of which come from plants and sponges, some found in bacteria.[56]

Triterpenes (n=6, $C_{30}H_{48}$, **Figure 1**, compounds 17-19) are a large and diverse group of NPs with a carbon skeleton containing six isoprene units.[57] Found in a wide variety of plants, animals, fungi, and bacteria, they fulfil a different functions: from hormone signaling, membrane rigidity, stabilization, and organization, to antibacterial, anti-cancer, anti-inflammatory, and antioxidant properties.[58]

Tetraterpenes (n=8, $C_{40}H_{64}$, **Figure 1**, compounds 20-21) are often called carotenoids, and contain two C_{20} units fused in the head-to-head manner.[59] They play crucial roles in plants as pigments in photosynthesis and photoprotection, as well as in human health, as antioxidants, sources of provitamin A, and precursors to essential vitamins.[60] Polyterpenes (n > 8, $(C_5H_8)n$, **Figure 1**, compounds 22-23) consist of more than eight isoprene units and are essentially polymeric isoprenoid hydrocarbons. Typical representatives are found in plants, with structures like natural rubber and gutta-percha.[61] Another example is bactoprenol, a polyterpenoid (C55 isoprenoid alcohol) found in bacteria, which is essential for transporting cell wall building blocks, like Lipid II.[62]

In addition to the previously mentioned classical terpenoids, there are also irregular or noncanonical terpenoids.[63] They deviate from the standard carbon skeleton patterns of five carbon isoprene units, possessing irregular carbon skeletons (C7, C11, C12, C16, C24, C27 etc.) as a result of enzymatic modifications such as the methylation of substrate units.[64]

Notably, there are other hybrid NPs with only a partial terpenoid structure, called meroterpenoids.[65] Meroterpenoids ("mero" - part, partial) are a class of NPs with a hybrid structure formed from a combination of terpenoid and polyketide, as well as other non-terpenoid parts (phenols, alkaloids).[66]

1.3. Discovery and Diversity of Terpenes

1.3.1. Terpenes from Natural and Synthetic Sources

The history of terpenes begins with their widespread use by many ancient cultures, who, before understanding their chemical nature, recognized the aromatic and medicinal properties of plants containing terpenes.[67] Later, the discovery of distillation of plant resins and essential oils resulted in the isolation of turpentine oil, as the earliest known terpene source.[68] In 1818, J.J. Houtou de La Billardière re analyzed turpentine and established the 5:8 carbon-to-hydrogen ratio that would later define all so-called “true” terpenes.[69] Afterwards, during the 19th century, compounds like camphor, menthol, thymol, and many others were described, though their structures remained unknown until systematic chemical studies in the late 1800s.[67] The “isoprene rule”, mentioned in the previous chapter, finally provided the framework to unify these early discoveries. The term "terpene" was suggested by August Kekulé in 1866, as an abbreviation of the German “Terpentin” or English “Turpentine”.[68] Turpentine, also known as the "resin of pine trees" contains the "resin acids" and certain hydrocarbons, which were at first called terpenes, with the suffix "ene" indicating the presence of olefinic (alkene) bonds.[57] Originally describing $C_{10}H_{16}$ hydrocarbons in volatile essential oils, this term was later broadened to include oxygenated derivatives (such as thymol, menthol, camphor) and, eventually, all compounds built from isoprene units.[57, 67]

Terpenes are now known to be the universal biomolecules, displaying various chemical and structural features along with important biological activities.[24] They are produced across all domains of life, in Bacteria (synthesize isoprenoids for quinones, carotenoids, and membrane stability), Archaea (use ether-linked isoprenoid chains as their unique membrane components), and Eukaryotes (in plants monoterpenes, sesquiterpenes, diterpenes, triterpenes, carotenoids, sterols; in fungi ergosterol, meroterpenes; and cholesterol, steroid hormones, dolichols in animals).[57, 70] Although first recognized from natural sources, terpenes were also among the earliest natural products to be synthesized in the laboratory. Semmler and Tiemann achieved early terpene syntheses in the late 19th century, followed by development of total synthesis of camphor, citral, and other terpenoids in the early 20th century.[45, 71] Synthetic terpenes and terpenoids today are indispensable in production of perfumes, flavors, vitamins, and pharmaceuticals (menthol, nootkatone).[23, 72-73] Natural terpenes play an important ecological function in plant protection, attracting pollinators, or communicating with other organisms.[74-75] In human life, terpenes are of great importance in medicine (taxol and its derivatives, utilized as one of the most effective antitumor drugs; artemisinin, an antimalarial antibiotic), industry (rubber, resins), and culture (fragrances, flavors).[23-24, 76]

However, while most terpenes were isolated from Eukaryotes such as plants, the field of bacterial-derived terpenes remains underexplored.[77] Only with the development of genome analysis instruments it become obvious that microorganisms are also capable of producing many secondary metabolites of this group.[30, 78]

1.3.2. Guanidine-Bearing Terpenes

The emergence of antibiotic resistance highlights a growing need for antimicrobial NPs with novel and unconventional scaffolds, as they are more likely to overcome existing resistance mechanisms.[79-80] In this context, terpenes carrying a guanidine moiety are considered as promising candidates, due to their unique structural features and often potent biological activity.[81-83] The guanidine functionale group is particularly important in biological interractions, as guanidine-rich molecules are cationic at physiological pH, and this charge often enhances their interaction with biological membranes or negatively charged biomolecules (such as phosphates and carboxylates).[84-85] This chapter will discuss current knowledge about guanidine-bearing terpenoids, including their properties, prevalence and biological activities.

Despite the vast diversity of terpenes, only a limited number of compounds of this class with a guanidine group in their structure have been identified to date. The first example is the cyclic sesterpenoid cytoscalarol.[86] The compound was isolated from the cultured terrestrial cyanobacterium *Scytonema* sp. UTEX 1163, as its crude extract exhibited antibacterial activity against *Bacillus anthracis*. According to Mo et al. (2009), scytoscalarol was the first sesterterpene documented in cyanobacteria, as well as the first sesterterpene with a guanidine moiety to be isolated from a natural source.[86] It possesses a tetracyclic scalarane skeleton with a hydroxy group and a guanidine moiety (**Figure 2**). Scytoscalarol displays a broad antimicrobial profile, it is inhibiting *Staphylococcus aureus* and *B. anthracis* at low micromolar concentrations (MIC 2–6 μM), exhibit moderate activity against *Candida albicans* (MIC 4 μM), weak antimycobacterial effect (MIC of 110 μM against *Mycobacterium tuberculosis*). It also has a relatively low cytotoxicity (IC_{50} of approx. 135 μM in Vero cells).[87-88] Scytoscalarol represents natural product chemistry rarely seen in terpenes: a cyanobacterium-derived terpenoid of scalarane type that is functionally decorated with a guanidine group.[86]

Cybastacins are another known representatives of guanidine-bearing terpenes (**Figure 2, cybastacines A and B**). They are produced by the cyanobacteria strain *Nostoc* sp. BEA-0956, collected in the Canary Islands.[89]

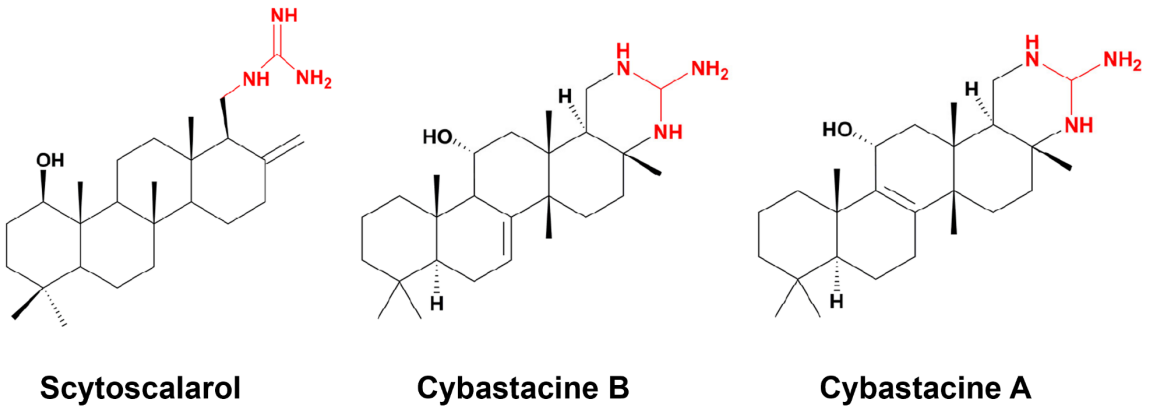

Figure 2. Structure of the terpenoids Scytoscalarol, and Cybastacines A-B. In red, the guanidine group is shown. Structures adapted from[90]

Cybastacines are distinguished by their unusual architecture, which features a pentacyclic carbon skeleton with an incorporated guanidine group forming one of the rings.[89] This distinguishes from the free guanidine moiety found in scytoscalarol (**Figure 2**). Cybastacines are biologically active, with cybastacine A displaying modest activity with MIC values in a range of 16–32 μg/mL (with an exception MIC of 8 μg/mL for *Tsukamurella pulmonis*).[89] By contrast, cybastacine B demonstrated a stronger antibacterial profile, inhibiting multiple relevant pathogens including the clinical isolates of *Nocardia* spp., *M. abscessus*, *Enterococcus* spp., and *Staphylococcus* spp. with MICs below 4 μg/mL (in case of *T. pulmonis* the observed MIC was ≤ 2 μg/mL).[89, 91]

Zillamycin, another isoprenyl guanidine alkaloid, was discovered from *Streptomyces griseofuscus* extracts, through a method called Deuterium Adduct Bioactivity Screening (DABS).[92] Structurally, zillamycin is a linear isoprenyl chain, decorated with guanidine moiety. This compound showed both anti-cancer and antimicrobial activities.[82]

A review of the relevant literature reveals other examples of guanidine-bearing terpenes, including diacylguanidines dotofide and actinofide isolated from the marine slug *Doto pinnatifida* and mollusk *Actinocyclus papillatus*, respectively.[93] Dotofide was discovered through a targeted chemical investigation of the nudibranch *D. pinnatifida*.[94] Nudibranchs have evolved a cryptic appearance as a part of a defence mechanism. At the same time, it is hypothesized that as compensation for the absence of protective structures like spicules or cnidarian nematocysts in *Dotidae*, they can also protect themselves by predator-deterrent chemicals such as dotofide.[94] Structurally, the compound is distinguished by its unusual terpenoid skeleton, which is interrupted by a guanidine moiety, resulting in a hybrid structure combining sesquiterpenoid and hemiterpenoid units (**Figure 3**). The sesquiterpenoid unit contains a substituted cyclohexane ring similar to the one found in carotenoids (β- and α-ionone

ring),[95] while the hemiterpene unit is linked through the guanidine moiety. It is noteworthy that *D. pinnatifida* feeds exclusively on the hydrozoans, such as *Nemertesia antennina*, which does not contain dotofide. This strongly suggests that the slug itself synthesizes the metabolite de novo, rather than absorbing it from its prey.[94]

Actinofide (**Figure 3**) was purified from the skin extract of the dorid nudibranch *A. papillatus*, collected in the South China Sea.[93] It is a diacylguanidine which contains a guanidine unit acylated by farnesoyl and senecioyl (3,3-dimethylacryloyl) residues. Actinofide shares a structural similarity with the previously described dotofide. However, its distinguishing feature is the presence of a linear C_{15} isoprenoid moiety, in contrast to the monocyclic farnesoic unit found in dotofide (**Figure 3**). Furthermore, the chemical synthesis of actinofide and its synthetic analogues was performed, based on the two-step coupling of guanidine with two terpenoid acid units, according to the previously reported synthetic procedure for dotofide.[81, 96] While their antimicrobial activity was not reported, both actinofide (with its analogues) and dotofide were evaluated for the growth inhibitory activity against several cancer cell lines. Consequently, dotofide exhibited moderate antiproliferative activity, actinofide, and notably its synthetic derivative *N*, *N′*-difarnesoyl-guanidine, showed higher potency than dotofide in certain cases.[93]

Agelasidines are another NTs featuring guanidine functional groups. They were isolated from marine sponges *Agelas* sp.[97] In addition to the unique hypotaurocyamine

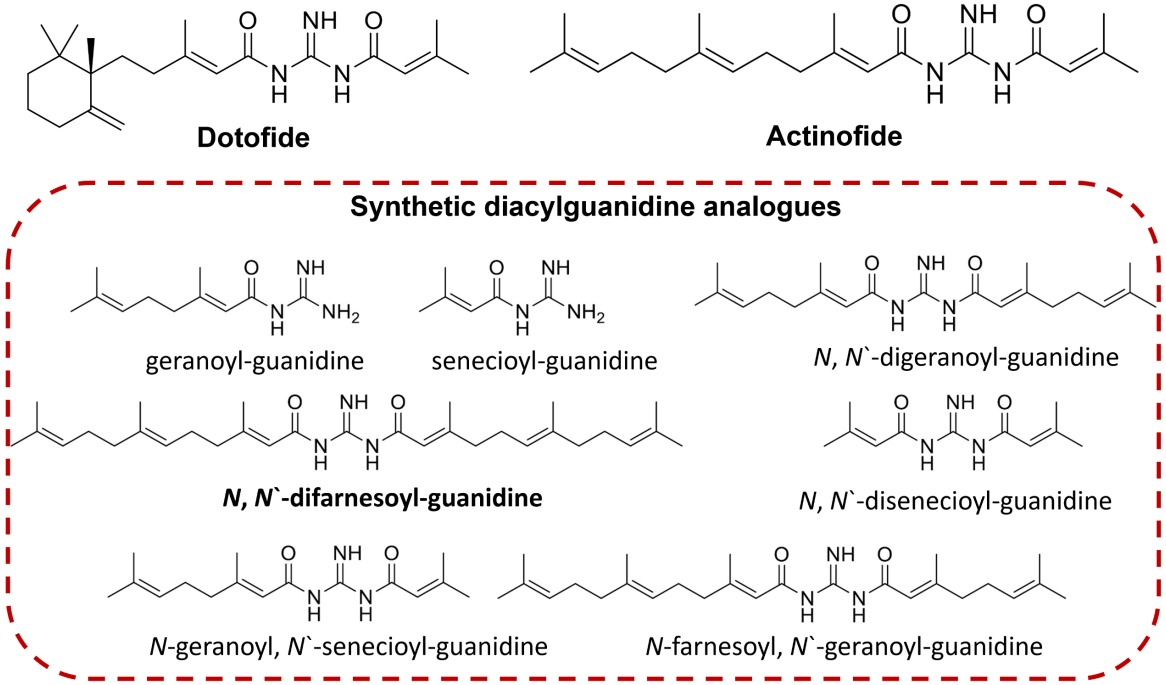

Figure 3. Structures of dotofide, actinofide, and synthetic diacylguanidine analogues. Structures adapted from[81, 83]

diterpene skeleton, these compounds displayed inhibitory effects against pathogenic *Candida* species.[97-98]

Guanidine-bearing terpenoids are not exclusive to bacteria or animals; they have also been found in plants. For example, four prenylated guanidines, galegine, nitensidine A, pterogynidine, and pterogynine, were isolated from the higher plant *Pterogyne nitens*.[82] These compounds have different numbers of isoprenyl moieties at their amino nitrogens (**Figure 4**). Notably, galegine (amino nitrogen has one isoprenyl moiety) and pterogynidine (amino nitrogen has two isoprenyl moieties) exhibited potent yet mild antibacterial activity against *S. aureus* strains, ranging between 20 and 31 μM.[99] Another study examined the biological effects of nitensidine A (two amino nitrogens have one geranyl moiety) and pterogynine (two amino nitrogens have one isoprenyl moiety) on osteoclasts, displaying anti-osteoclastic effects at 10 μM by decreasing the number of osteoclasts on the culture plate.[100]

The widespread occurrence and broad spectra of biological activity of natural guanidine-containing terpenes have prompted synthetic efforts to obtain new compounds of this group. For example, Zarraga et al. (2008) reported synthesis of 11-guanidinodrimene, a new sesquiterpenoid derived from drimenol.[101] According to the findings of the study, the addition of the guanidine group to the drimenol C-11 carbon led to an increase in antifungal activity against *Candida albicans* (MIC 32 mg/mL), which is among the most prevalent human pathogens.[101] G. Duca et al. (2018) have obtained dihomodrimane and 14,15-bis-norlabdane guanidine-bearing terpenoids, synthesized from commercially available sesquiterpene lactone sclareolide and diterpenoid sclareol.[83] The compounds demonstrated potent antiproliferative

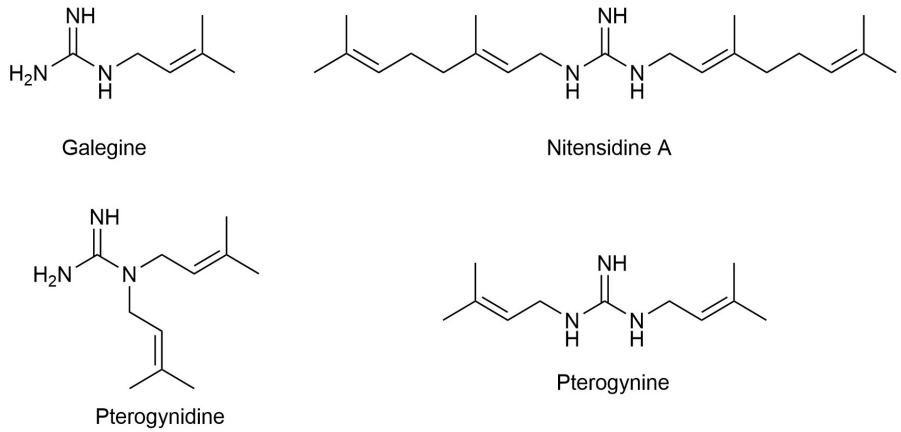

Figure 4. Structures of plant-derived guanidine terpenoids: galegine, nitensidine A, pterogynidine and pterogynine.[99]

and cytotoxic properties against the Colo 205 and Colo 320 cell lines, suggesting the potential for their application in cancer chemotherapy.[83]

Furthermore, a recent study has reported the synthesis of novel guanidine-functionalized labdane type diterpenoids.[102] Two compounds, namely labdan-8,13(*R*)-epoxy-15-oyl guanidine and 8,13(*S*)-epoxy-15-oyl guanidine (**Figure 5**) were shown to exhibit a substantial antimicrobial activity against Gram-positive and Gram-negative bacteria (MIC of up to 4 μg/ml), while with moderate toxicity on zebrafish embryos.[102]

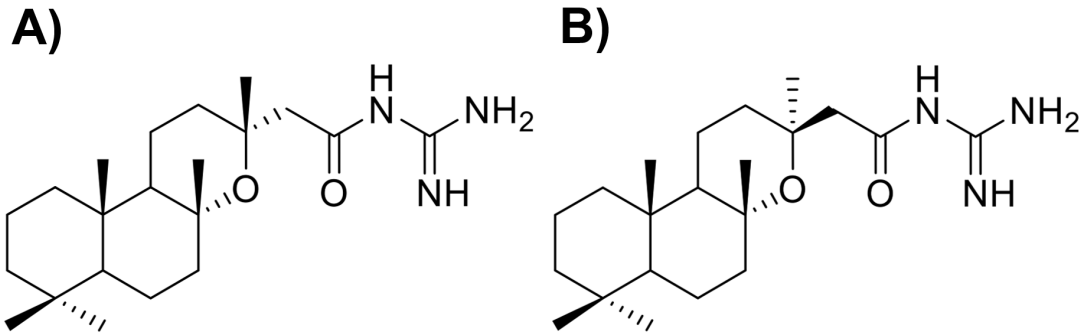

Figure 5. Synthetic guanidine-functionalized labdane type diterpenoids: **A)** labdan-8,13(R)-epoxy-15-oyl guanidine, and **B)** 8,13(S)-epoxy-15-oyl guanidine. Structures modified from[102].

1.4. Biosynthesis of Terpenes

Biosynthesis of terpenes can generally be described as follows: **(1)** synthesis of five-carbon isoprenoid precursors isopentenyl pyrophosphate (IPP) and dimethylallyl pyrophosphate (DMAPP); **(2)** condensation of isoprene precursors into isoprenoid diphosphates of a certain length (elongation to form a linear precursor); **(3)** conversion of the linear precursors by terpene synthases into linear and cyclic (or polycyclic) terpenes; and **(4)** subsequent modification (functionalization) by various enzymes to generate final structure (**Figure 6**).[68]

The **(1)** step in the biosynthesis of terpenes is the generation of C_5 building blocks, the IPP and DMAPP. This step is part of primary metabolism and is present in all living species. Both compounds are produced either via the mevalonate pathway (MVA) or methylerythritol phosphate (MEP) pathway (is also called non-mevalonate, DOXP (1-deoxy-D-xylulose 5-phosphate), or the Rohmer pathway).[103] There is a clear separation of both pathways distribution: animals, fungi, and archaea use the MVA pathway, while algae and the majority of bacteria utilize the MEP pathway.[104] Interestingly, some bacteria, such as *Staphylococcus*, *Streptococcus*, and *Borrelia*, rely on the MVA pathway.[105] In contrast, others, such as *Streptomyces*, may have both.[106] Plants use both pathways simultaneously (MVA in the cytosol and MEP in the chloroplasts).[107]

In the next **(2)** step, a condensation reaction between a DMAPP molecule and one or more IPP molecules produces a methyl-substituted polyene chain of a specific length (geranyl diphosphate (C_{10}), farnesyl diphosphate(C_{15}), geranylgeranyl diphosphate (C_{20}), or geranyl farnesyl diphosphate (C_{25}) typically in head-to-tail orientation). The size of such chains is determined by the respective prenyltransferase (PT), controlling the number of the incorporated

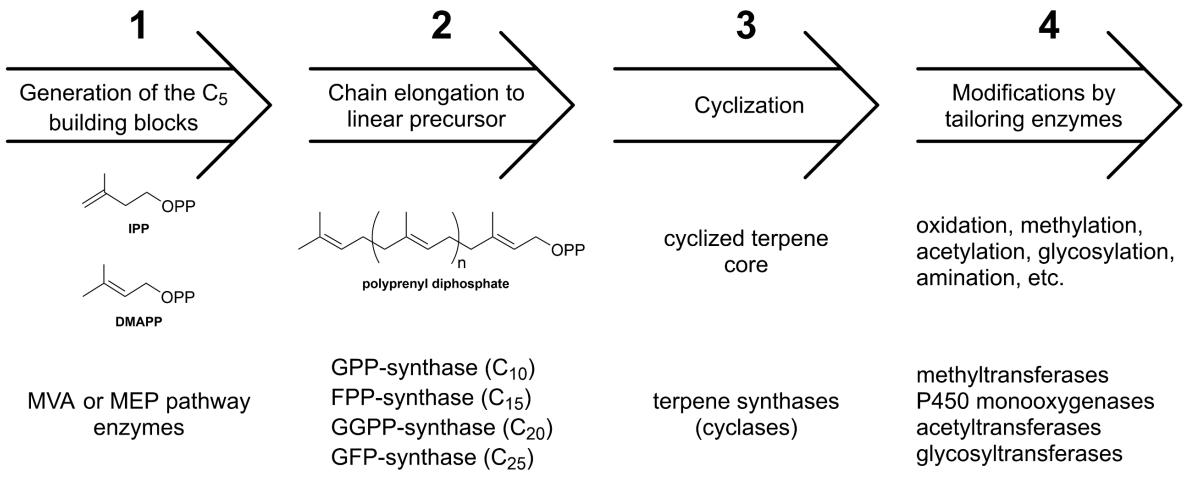

Figure 6. Schematic representation of terpene biosynthesis.

isoprene monomer units.[108] In this way, various C_{10}–C_{40} (or longer) precursors are processed by terpene synthases and tailoring enzymes allowing the generation of the final terpenes and terpenoids.[109] Subsequently **(3)**, terpene cyclase (TC) folds such a chain into a specific conformation, which results in a sequence of intramolecular cyclization and rearrangements that form the cyclic core of the compound.[47] This core can undergo further modifications by tailoring enzymes **(4)**, including oxidation, methylation, acetylation, glycosylation, amination, and other modifications, which ultimately result it the final compound. In most cases, these modifications are important for the biologically active form of the compound (functionalization).[110-111]

Each of the above-mentioned steps in the biosynthesis of terpenes will be discussed in more details in the following sections.

1.4.1. Overview of IPP and DMAPP Biosynthesis

1.4.1.1. Mevalonate (MVA) Pathway

The mevalonate pathway is a complex and important metabolic pathway that provides cells with building blocks for sterol and non-sterol isoprenoids.[112] It was discovered in the 1950s, when Konrad Bloch and Feodor Lynen traced the origin of cholesterol by feeding animals with isotopically labelled acetate, an experiment that resulted in the Nobel Prize.[113-114] The pathway itself contains six main enzymes and seventh called isopentenyl diphosphate isomerase (IDI) (**Figure 7**). It begins with the acetyl-CoA synthase (thiolase) catalyzing condensation of two acetyl-CoA molecules into acetoacetyl-CoA. Which is then followed by an aldole condensation with a third acetyl-CoA molecule by 3-hydroxy-3-methylglutaryl-CoA synthase (HMGS), yielding 3-hydroxy- 3-methylglutaryl-CoA (HMG-CoA).[110] This six-carbon intermediate is then transferred to 3-hydroxy-3-methylglutaryl-CoA reductase (HMGR), which reduces it to mevalonate, using NADPH as a reducing agent. From mevalonate onward, two ATP-dependent enzymes: mevalonate kinase and phosphomevalonate kinase phosphorylate the substrate, producing first mevalonate-5-phosphate, followed by mevalonate-5-diphosphate.[108]

Afterwards, mevalonate diphosphate decarboxylase cleaves off a carboxyl group, releasing both CO_2 and IPP. Finally, an isopentenyl diphosphate isomerase (IDI) converts IPP into DMAPP, ensuring both isoprene units are available.[105] Once IPP and DMAPP are synthetized, terpene prenyltransferases can condense them into longer chains of 10, 15, 20 or

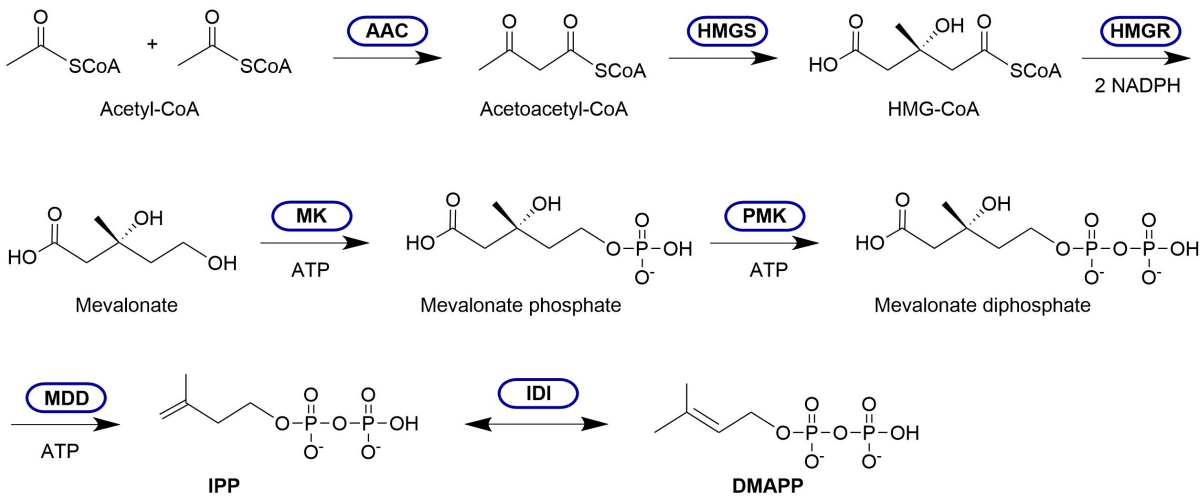

Figure 7. Scheme of the mevalonate pathway. AAC: acetyl-CoA synthase; HMGS: hydroxymethylglutaryl-CoA synthase; HMGR: hydroxymethylglutaryl-CoA reductase; MK: mevalonatekinase; PMK: phosphomevalonate kinase, MDD: diphosphomevalonate decarboxylase; IDI: isopentenyl diphosphate isomerase; NADPH: nicotinamide adenine dinucleotide phosphate; ATP: adenosine triphosphate; HMG-CoA: 3-hydroxy-3-methylglutaryl-CoA.

more carbons,which in turn generates the vast terpene family: geranyl pyrophosphate (C_{10}) for monoterpenes, farnesyl pyrophosphate (C_{15}) for sesquiterpenes (and triterpenes), and geranylgeranyl pyrophosphate (C_{20}) for diterpenes (and tetraterpenes).[110]

1.4.1.2. Methylerythritol Phosphate (MEP/DOXP) Pathway

The methylerythritol phosphate (MEP) pathway, also called the DOXP (1-deoxy-D-xylulose 5-phosphate) pathway, is the other major route for isoprenoids synthesis (**Figure 8**).[110] Unlike the mevalonate pathway, the MEP route occurs mainly in bacteria, algae, and plant plastids.[105] It was also discovered much later, in the 1990s, when Michel Rohmer and Duilio Arigoni noticed that certain organisms were still producing terpenes, even though they lacked the classic mevalonate machinery.[115] That discovery changed the way scientists thought about the previous single-pathway view of isoprenoid biosynthesis.[116]

The MEP pathway also directs carbon into the same five-carbon building blocks IPP and DMAPP.[110] But in this case, the starting material is different: pyruvate and glyceraldehyde-3-phosphate, two intermediates from of glycolysis. The first enzyme, 1-deoxy-D-xylulose-5-phosphate synthase (DXS), combines them together in a thyamine pyrophosphate mediated reaction into 1-deoxy-D-xylulose 5-phosphate (DOXP). DOXP is then quickly rearranged and reduced to 2-C-methylerythritol 4-phosphate (MEP) by 1-deoxy-D-xylulose-5-phosphate reductoisomerase (DXR or IspC). From MEP, the pathway unfolds through a series of transformations: the phosphate group of MEP is substituted with a cytidine diphosphate by a 2-C-methyl-D-erythritol-4-phosphate cytidylyltransferase (IspD), generating 4-diphosphocytidyl-2-C-methyl-D-erythritol (CDP-ME).[116]

Next, the 4-diphosphocytidyl-2-C-methyl-D-erythritol kinase (IspE) phosphorylates the previous substrate, producing the 4-diphosphocytidyl-2-C-methyl-D-erythritol-2-phosphate (CDP-ME2P). This intermediate is further rearranged by 2-C-methyl-D-erythritol-2,4-cyclodiphosphate synthase (IspF) into the cyclic diphosphate named 2-C-methyl-D-erythritol-2,4-cyclodiphosphate (MEcDP). Afterwards, the (E)-4-hydroxy-3-methylbut-2-enyl-diphosphate synthase (IspG) is involved for the (E)-4-hydroxy-3-methylbut-2-enyl diphosphate (HMBPP) formation.[115] Following, the (E)-4-hydroxy-3-methylbut-2-enyl-diphosphate synthase (IspG) is involved in the (E)-4-hydroxy-3-methylbut-2-enyl diphosphate (HMBPP) formation. In the final step, this molecule is reduced to the IPP and DMAPP (in the approx. ratio 5:1) by the (E)-4-hydroxy-3-methylbut-2-enyl-diphosphate reductase.[117] Additionally, an isopentenyl diphosphate isomerase (IDI) balances the IPP and DMAPP ratio if needed.

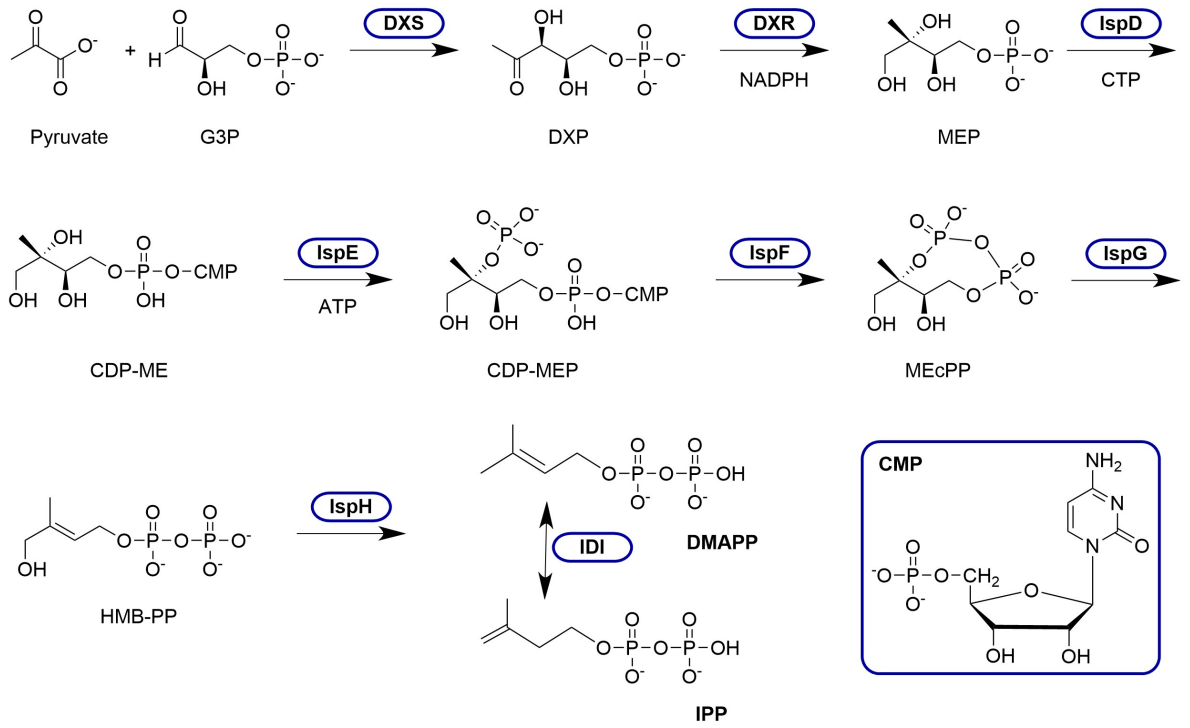

Figure 8. Scheme of the deoxyxylulose phosphate pathway. DXS: 1-deoxy-D-xylulose-5-phosphate synthase; DXR: 1-deoxy-D-xylulose 5-phosphate reductoisomerase; IspD: 4-diphosphocytidyl-2-C-methyl-D-erythritol synthase; IspE: 4-diphosphocytidyl-2-C-methyl-D-erythritol kinase; IspF: 2-C-methyl-D-erythritol-2,4-cyclodiphosphate synthase; IspG: 4-hydroxy-3-methylbut-2-enyl diphosphate synthase; IspH: 4-hydroxy-3-methylbut-2-enyl diphosphate reductase; IDI: isopentenyl diphosphate isomerase; G3P: glyceraldehyde 3-phosphate; DXP: 1-Deoxy-D-xylulose 5-phosphate; MEP: 2-C-methylerythritol 4-phosphate; CDP-ME: 4-diphosphocytidyl-2-C-methylerythritol; CDP-MEP: 4-diphosphocytidyl-2-C-methyl-D-erythritol 2-phosphate; MEcPP: 2-C-methyl-D-erythritol 2,4-cyclodiphosphate; HMB-PP: (E)-4-Hydroxy-3-methyl-but-2-enyl pyrophosphate; NADPH: nicotinamide adenine dinucleotide phosphate; ATP: adenosine triphosphate; CTP: cytidine triphosphate; CMP: cytidine monophosphate.

In plants, the MEP pathway supplies carotenoids for photosynthesis, plastoquinones for electron transport, and phytohormones like gibberellins and abscisic acid.[104] In bacteria, it provides the isoprenoids needed for the synthesis of quinones and cell wall precursors.[118]

1.4.2. Biosynthesis of Isoprenoid Chains

Once IPP and DMAPP precursors are synthesized, terpene synthases, also called prenyltransferases (or isoprenyl diphosphate synthases), can fuse them into longer chains of specific length, determining which terpene class will be produced.[110] These enzymes generate prenyl diphosphates, which are the universal precursors of all terpenoids.[108] Prenyltransferases are a large and diverse family of enzymes that can be classified into two main groups based on their function: **isoprenoid-coupled** enzymes (catalyse regular **head-to-tail**, or irregular: **head-**

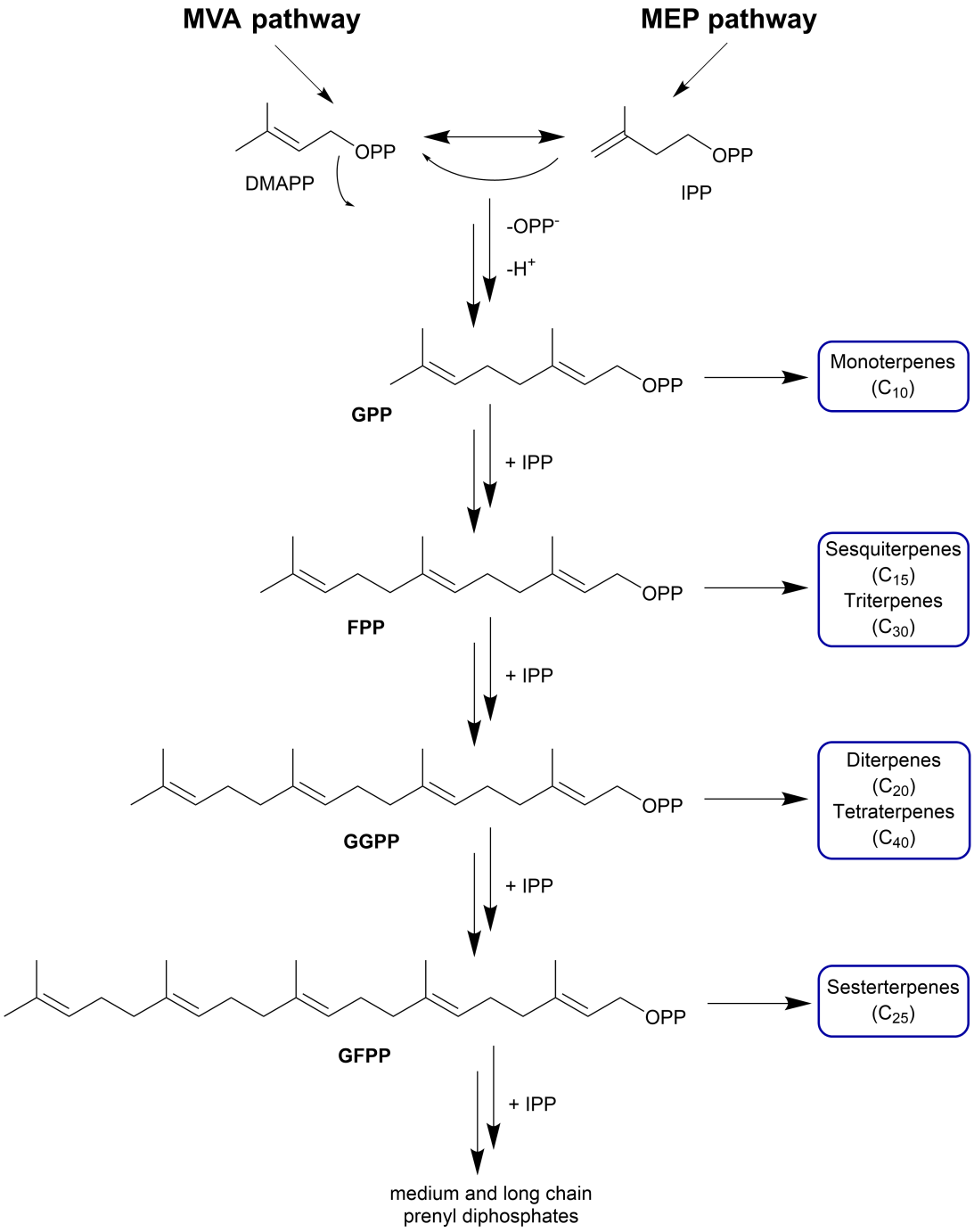

Figure 9. Overview of terpene biosynthesis from IPP and DMAPP: chain elongation.

to-head, head-to-middle, or **tail-to-tail** condensations), and **aromatic prenyltransferases**.[119-120] Additionally, based on the stereochemistry of the double bonds formed during isoprenoid condensation, there are *trans* (*E*) and *cis* (*Z*) prenyltransferases. Most terpene natural products are known to be synthesized from *E*-linear precursors; nonetheless, *Z*-linear precursors also exist in nature.

PTs feature domain architecture with various combinations of six basic domains: α, β, γ (the most common), and δ, ε, ζ.[121] They have conserved aspartate-rich motifs (typically DDXXD) in the active site, which enable the binding of divalent metal ions (such as Mg^{2+}), necessary for substrate recognition and the subsequent elimination of diphosphate groups. Notably, both chain length and structure of the enzyme product depend on the nature of the catalyzing prenyltransferase. The structure of the enzyme`s active site acts as a molecular ruler, controlling the termination of each prenyltransferase reaction at a specific length.

The typical reaction starts with the condensation of IPP with DMAPP in a nucleophilic substitution reaction, producing geranyl diphosphate (GPP, C_{10}), a precursor to monoterpenes.[110] Such **head-to-tail** condensations (**Figure 10**) are the most common and follow the same mechanistic principle: ionization of the allylic diphosphate generates a carbocation, which is then attacked by the double bond of IPP, with subsequent release of pyrophosphate and proton elimination to form the elongated isoprenoid chain (**Figure 10**).[47] In the next step, farnesyl diphosphate synthase (FPPS) catalyzes the condensation of GPP with another IPP unit to produce farnesyl diphosphate (FPP, C_{15}), the precursor of sesquiterpenes (and triterpenes).[122] Afterwards, the geranylgeranyl diphosphate synthase (GGPPS) can generate geranylgeranyl diphosphate (GGPP, C_{20}), a precursor to diterpenes (and tetraterpenes), including carotenoids.[123] Geranylfarnesyl diphosphate synthases (GFPPS) extend the chain of GGPP to geranylfarnesyl diphosphate (GFPP, C_{25}), the precursor of sesterterpenes.[47] A large group of enzymes called *cis*-prenyltransferases can generate longer chains ($C_{30} - C_{100}$, or more), which are precursors to dolichols or side chains of ubiquinones.[124-125] Notably, DMAPP and IPP themselves can also serve as a precursor of hemiterpenes.[126]

Head-to-head condensation (**Figure 10**) couples two allylic diphosphates (FPPs). The most studied representatives of this group of PTs include squalene synthase, which utilizes 2 molecules of FPP to form squalene (C_{30}), the precursor of triterpenoids and steroids; and phytoene synthase (two GGPP to produce phytoene, C_{40}), which initiates carotenoids biosynthesis.[47,127]

Head-to-middle condensation reaction, occurs between the internal carbon (**middle**) of the first substrate and the **head** of a second isoprenyl diphosphate molecule.[119] A good example is the biosynthesis of isosesquivandulyl diphosphate (**Figure 10**). This coupling is rare in Bacteria and Archaea, and is mainly found in Eukaryotes.[128] Another unconventional condensation mode is **tail-to-tail**. An example of such enzymes is Archaeal tetraether synthase (TES). Unlike previous types, this radical SAM enzyme catalyzes the condensation of the terminal methyl groups of prenyl chains (**tails**) during the biosynthesis of membrane components glycerol dibiphytanyl glycerol tetraethers.[129]

Aromatic prenyltransferases are enzymes that catalyze the attachment of isoprenoid chains to molecules originating from other metabolic pathways, such as indoles, polyketides, or other aromatic compounds (ubiquinone, menaquinone, vitamin E, amino acids, or prenylation of proteins).[130-131] This essentially links terpenoid metabolism to other biosynthetic pathways).[132-133]

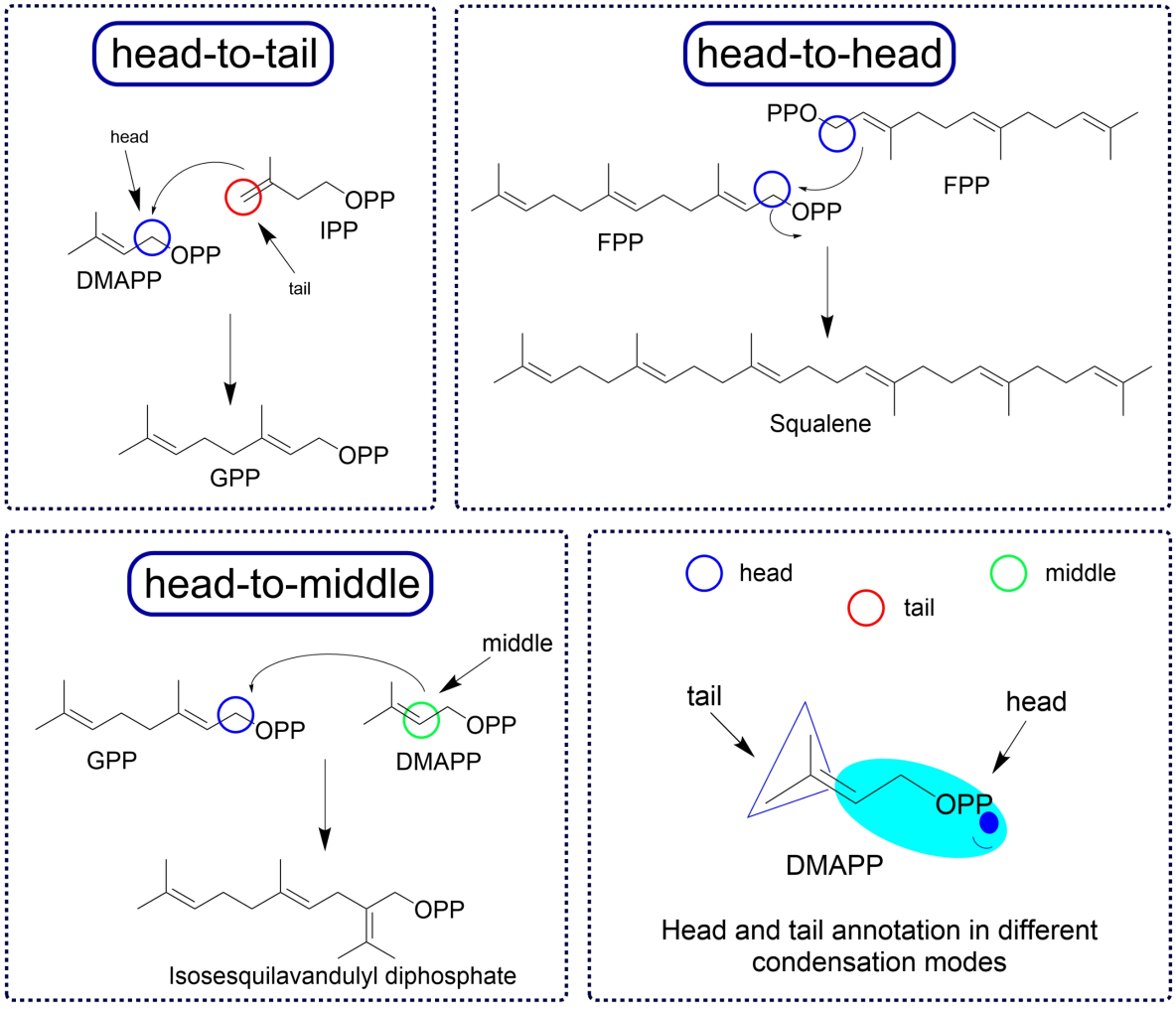

Figure 10. Illustration of different condensation modes during isoprenoid chain biosynthesis.

1.4.3. Terpene Cyclization

The third step in terpene biosynthesis is the cyclization of linear isoprenyl diphosphates into diverse cyclic backbones.[77] This transformation is catalyzed by terpene synthases (TSs) or cyclases (TCs), as mentioned in previous chapters. These enzymes utilize various prenyl diphosphate substrates produced by prenyltransferases, such as geranyl diphosphate (GPP, C_{10}), farnesyl diphosphate (FPP, C_{15}), geranylgeranyl diphosphate (GGPP, C_{20}), geranylfarnesyl diphosphate (GFPP, C_{25}), or other.[47] Noteworthy, both TCs and PTs can be structured in two main ways: as distinct proteins, represented by physically colocalized gene pairs (most often seen in plants and bacteria), or as chimeric (single, bifunctional proteins, as found in fungi), with C-terminal prenyltransferase and N-terminal cyclase domains.[134] The prenyltransferase domain synthesizes isoprenoid pyrophosphate precursors assembly, which the cyclase domain then uses as a substrate in subsequent cyclisation.[135-136]

Terpene cyclisation is among the most complex reactions known in nature.[110, 137-138] In multi-step cascades, over half of the substrate carbon atoms undergo changes in bonding, hybridization, and stereochemistry during a single enzyme-catalyzed reaction.[47, 139] The mechanism of cyclization depends on the enzyme class. There are two main classes of TCs: **class I** cyclase, which initiate the reaction by ionization of the diphosphate group, assisted by divalent metal ions (such as Mg^{2+}), generating a highly reactive carbocation intermediate; and **class II** enzymes, which employ protonation of a double bond or epoxide by a conserved acidic residue to activate the substrate, and produce the carbocation.[47, 136, 140] Once the carbocation is formed, it undergoes a cascade of intramolecular cyclizations, alkyl shifts, ring contractions, and expansions. In some cases, proton transfer is also proposed to occur.[141-142]

In **class I** enzymes, activation occurs through cleavage of the diphosphate leaving group. This step is mediated by a cluster of divalent metal ions (such as Mg^{2+}, less frequently Mn^{2+}, Co^{2+}), which are coordinated by conserved amino-acid motifs (typically DDXXD and NSE/DTE sequences, as shown in **Figure 11**). The active site of an enzyme binds both the metal ion cluster and the isoprenyl pyrophosphate substrate while precisely orienting the linear isoprenyl chain in a specific folding pattern. This stabilizes and polarizes the substrate diphosphate, promoting its departure and the formation of an allylic carbocation. The highly reactive carbocation initiates a series of rearrangements that ultimately result in various cyclic skeletons.

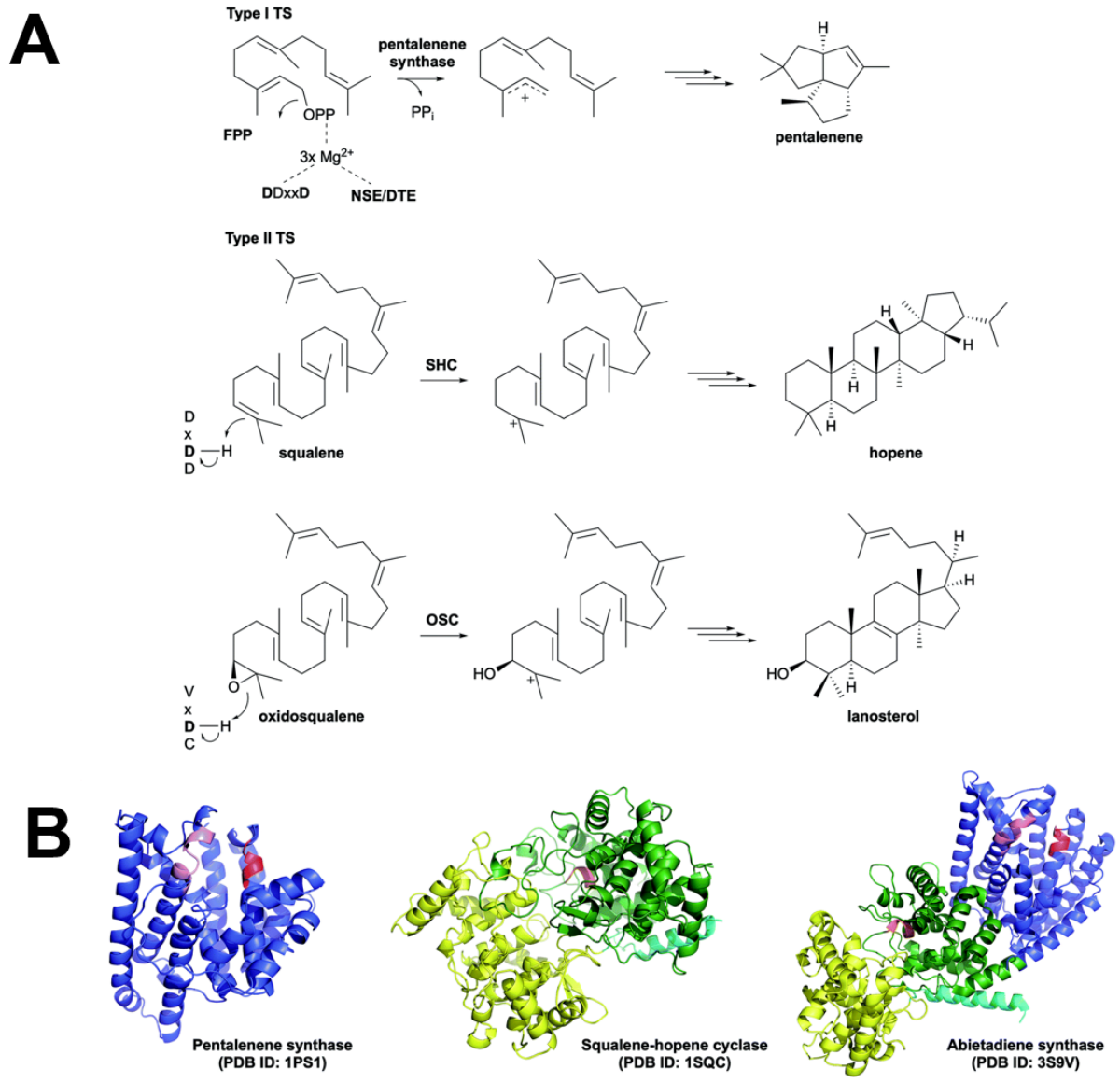

Figure 11. Canonical terpene synthases (cyclases). (**A**) Cyclization mechanisms of **type I** (pentalenene synthase) and **type II** synthases (squalene-hopene cyclase (SHC) and oxidosqualene cyclase (OHC)), catalyzing pentalenene, hopene and lanosterol cyclizations, respectively. (**B**) Structures of **pentalenene** synthase (left, consists of an α domain (**blue**), Mg^{2+}-binding Asp rich motifs and are colored in **red** (DDxxD) and **pink** (NSE/DTE)); **squalene-hopene** cyclase (middle, with two domains, shown in **green** (β) and **yellow** (γ), with Asp rich motif DxDD colored in **orange**, and N-terminal helix of the β domain in **cyan**); and the **abietadiene** synthase, as a representative of bifunctional TSs, with all αβγ domains. Adapted from Rudolf J.D. and Chang C.-Y.[141]

Pentalenene synthase is a classic representative of the cyclization mechanism by class I terpene synthases. This enzyme initiates the cyclization of FPP substrate, which ultimately leads to the production of pentalenene sesquiterpene (**Figure 11**).[141] Many other TCs belong to class I, including monoterpene cyclases (limonene synthase, bornyl diphosphate synthase, terpinene synthase, cineole synthase); sesquiterpene cyclases (aristolochene synthase, trichodiene synthase, selinadiene synthase, bisabolol and bisabolene synthases, previously mentioned pentalenene synthase and many others); diterpene cyslases (taxadiene synthase, labdane-related

diterpene cyclase, cyclooctatenol synthase, *ent*-kaurene synthase); sesterterpene cyclases (ophiobolin synthase, sesterfisherol synthase, as well as AtTPS06, AtTPS22, AtTPS29 reported from *Arabidopsis thaliana*).[47, 143-144]

In contrast, **class II synthases** use a protonation-initiated mechanism that does not depend on metal-assisted diphosphate cleavage.[110] In this case, a conserved DxDD motif gives a proton to a double bond or an epoxide, which generates a carbocation that initiates polycyclization.[141] Squalene-hopene cyclase (SHC) and oxidosqualene cyclase (OSC) are model class II enzymes. They convert squalene/oxidosqualene substrates into complex polycyclic structures such as hopene or lanosterol, which serve as scaffolds of triterpenoids and sterols (**Figure 11**).[145-147] Structurally, the active site of class II synthases resides at the interface between the β and γ domains of a protein that possesses a βγ or αβγ domain architecture.[47] For instance, in the OSC, the active site forms a long, hydrophobic tunnel that accepts the substrate and promotes a precise folding pattern with the sequence of ring closures.[148] Other examples of class II synthases include: sesquiterpene cyclases (such as drimenyl diphosphate synthase, found in *Streptomyces showdoensis*),[149] diterpene cyclases (*ent*-copalyl diphosphate synthase from *A. Thaliana*, or its homologue from *Streptomyces platensis*); triterpene cyclases (the above mentioned SHC and OSC superfamilies); or sesquarterpene cyclases (involved in C_{35} terpenes production, e.g. heptaprenyl diphosphate synthase,[150] or tetraprenyl- β-curcumene cyclase identified in *Bacillus*).[47, 151-152] Notably, since class II synthases do not require a diphosphate moiety to initiate cyclization activation, their substrates also do not need to be diphosphates. Therefore, these enzymes can process prenyl diphosphates while leaving the diphosphate group intact for a subsequent reaction with a class I synthase. In this case, the $Mg^{2+}$is proposed to facilitate substrate binding through Coulomb interaction with the negatively charged phosphate group, and not to the Asp-rich motif as in **class I**.[141, 153]

There are also bifunctional terpene synthases, containing both class II and class I catalytic domains within a single polypeptide. In short, they are represented with geosmin synthase (a sesquiterpene cyclase, produced by various soil-dwelling *Streptomyces* species), abietadiene synthase (a diterpene cyclase, involved in resin acid biosynthesis), and fusicoccadiene synthase (a diterpene synthase, which produces the precursor for fusicoccins, a class of diterpene glucosides with antitumor activity). [47]

The incredible structural variety of terpenoid skeletons produced by terpene cyclases should be especially noted. Depending on the specific enzyme, a single substrate such as FPP can be transformed into numerous distinct skeletons.[154-157] For example, amorpha-4,11-diene synthase forms the sesquiterpene backbone which is further used in the production of the

antimalarial drug artemisinin.[158] While other enzyme, aristolochene synthase produces the precursor of a number of fungal toxins.[159] Similarly, monoterpene synthases convert GPP into compounds as limonene, myrcene, pinene, linalool and many others, which are key components of essential oils.[160]

1.4.4. Tailoring Enzymes

Terpene prenyltransferases and cyclases are responsible for terpene hydrocarbon scaffolds (backbone) formation.[47] However, this is often not the final form of a compound. Terpenes also differ in final structures by functional groups, which are important for their diverse chemical and biological properties.[161] The diversity of terpene structures is largely determined by tailoring modifications catlysed by specific enzymes. They can be categorized into **oxidoreductases** and **transferases**, which modify the hydrocarbon scaffold (oxidation/reduction, methylation, acetylation, glycosylation, amination, etc.), resulting in highly functionalized molecules.[162] The **oxidoreductases** are mainly represented by cytochrome P450 monooxygenases (P450s, or CYPs), flavin-dependent monooxygenases (FMOs), non-heme iron α-ketoglutarate-dependent oxygenases, or NAD-dependent dehydrogenases/reductases.[162] Arguably, CYPs heme monooxygenases are the main and most abundant superfamily of terpene tailoring enzymes, reported to modify more than 97% of all terpenoids.[163] Typically, they function by introducing oxygen atoms through a hydroxylation reaction, but other types, such as epoxidation, dealkylation, formation of aldehydes and ketones, reduction, and dehalogenation, can also be catalyzed by these enzymes.[163-164]

Among **transferases** the most common are methyltransferases (MTs), acetyltransferases (ATs), and glycosyltransferases (GTs). For instance, MTs usually catalyze *C*- or *O*-methylations, with *N*-methylation also reported.[162, 165] On the other hand, ATs function by transferring the acetyl group from acetyl-CoA to the hydroxyl group(s) of the terpenoids.[111, 166-168] Glycosylation is another modification reaction, catalyzed by glycosyltransferases (GTs) to form terpenoid glycosides.[169] It was reported that this enzymatic modification can enhance terpenoids solubility and thus affect their bioactivity.[170] Noteworthy, in reactions where terpene scaffolds are combined with alkaloids or polyketides (meroterpenes), the transfer of the isoprenoid moiety is catalyzed by prenyltransferases, as mentioned in the previous chapter.[171-172]

Altogether, these enzymes contribute to chemical diversity of the terpene structure, by modifying its stability, reactivity, as well as interaction with different biological targets.[162]

Terpene tailoring enzymes are distributed across all domains of life. In plants, they are crucial for the chemical diversity of terpenes involved in defense, or pollinator attraction.[173] For example, cytochrome P450 monooxygenases found in the plant *Artemisia annua* oxidise amorpha-4,11-diene in order to produce artemisinic acid, which serves as a precursor to the antimalarial compound artemisinin.[174] Another example is P450s from *Solanum lycopersicum*, which modify certain sesquiterpenes into oxygenated derivatives, such as santalene and bergamotene, which are toxic to whiteflies and different microorganisms.[175] In addition, plant MTs are reported to be involved in floral scent production, as shown in the *Clarkia breweri* S-adenosyl-L-methionine dependent *O*-methyltransferase, which methylates eugenol or isoeugenol to make methyleugenol or isomethyleugenol.[176]

In animals, tailoring modifications of terpenes occurs during the biosynthesis of cholesterol or steroid hormones.[177] For instance, CYP51 enzymes catalyze oxidative demethylation of lanosterol, which is an important step in cholesterol biosynthesis in mammals.[178] Moreover, other enzymes such as sulfotransferases are involved in mechanisms of cellular detoxification, as well as bioavailability and signaling activity of steroid hormones.[179]

As for fungi and bacteria, the genes for tailoring enzymes are usually organized together with genes eocoding terpene synthases into biosynthetic gene clusters, responsible for production of various metabolites with antibacterial and antifungal properties.[180-181] Well-known examples include the fungus *Aspergillus fumigatus* with fumagillin gene cluster, which includes genes coding for P450 dioxygenase and flavin monooxygenase. These enzymes make various modifications of the meroterpenoid core structure produced by terpene cyclase and polyketide synthase that lead to the formation of fumagillin, the anti-angiogenic compound used in cancer research.[182] In bacteria the terpene oxidoreductases, in particular cytochrome P450s, were shown to be important for the antibiotic activity of pentalenolactone and albaflavenone.[78, 183]

1.5. Biological Roles and Importance of Terpenes

The roles that terpenes play in living organisms can generally be categorized into three distinct classes: functional, communication, and defense.[17, 23, 45, 57] An example of the functional role of terpenes is vitamin A, a diterpenoid and the precursor to rhodopsin, which detects light, and is therefore critical for vision.[184-185] Other notable examples include vitamin D_2, a derivative of ergosterol, which plays a crucial role in regulating calcium and phosphorus metabolism in the body, a process essential for healthy bones and teeth;[186] and vitamin E, an effective antioxidant that prevents free radicals formation.[187] In addition, cholesterol, a derivative of triterpenes, serves as a critical component of membranes and a precursor to steroid hormones.[46, 188] In a similar manner, fungi are dependent on ergosterol, a triterpene, for membrane stability and signaling, mirroring the role of cholesterol in animals.[189-190] In plants, tetraterpene carotenoids serve as natural dyes and play a crucial role in photosynthesis by capturing light and protecting photosystems from photooxidative damage.[191-193] In Archaea, isoprenoid-based lipids offer distinctive survival strategies.[194] For instance, many Archaea have hydrocarbon chains with branched methyl groups as components of their cell membranes, which gives them exceptional resistance to environmental factors such as high temperatures, pressure, salinity, and acidity.[195] In Bacteria, bactoprenol is a C_{55} terpenoid alcohol which plays a vital role as a lipid carrierin cell wall biosynthesis.[62, 196] In addition, certain bacterial species can synthesize hopanoids, which are pentacyclic triterpenes that strengthen their membranes.[197-198]

In addition to their role in sustaining life, terpenes are also used as messengers for communication within (hormones) and between organisms (pheromones).[45] In plants, volatile monoterpenes, including limonene, linalool, cineole, myrcene, are released by flowers to attract pollinators or by fruits to direct various seed dispersers.[73, 199] In addition, the diterpenoid gibberellins function as growth regulators, affecting a range of processes from seed germination to flowering.[200] In animals, terpenoid signaling affects behavior and reproduction.[201-203] For instance, a monocyclic diterpene neocembrene, is a major component of the trail-following pheromone in the *Prorhinotermes* termites.[204] Another example is the sesquiterpenoid juvenile hormone, which regulates development and caste structure in social insects such as bees and ants.[205-206] Terpenoid derivatives have also been identified as contributing factors to scent marking (territorial boundaries), and mate attraction in mammals.[201, 207] Furthermore, different fungi species are known to use volatile terpenoids to mediate ecological interactions.[208] The characteristic aromas of fungi often come from sesquiterpenes, which attract spore-dispersing insects.[209] Whereas bacterial volatile terpenoids can influence microbial behaviors, such as stress resistance and microbe-microbe communication.[210-211]

Besides their functional and communicative roles, terpenes are also known to have a protective functions, for instance against herbivores,[212] pathogens, and fungi.[59, 73] Many plant monoterpenes and sesquiterpenes, found in resins and essential oils, have pesticidal activities, acting as a deterrents to herbivores and limiting the proliferation of pathogens.[213-214] Certain marine sponges can accumulate terpenoid compounds and use them to deter pathogens and predators.[215] A considerable number of fungi species have been described to produce terpenoids that exhibit potent antibacterial or antifungal properties.[61] For instance, *C. albicans* was reported to produce farnesol, a sesquiterpene alcohol that disrupts bacterial quorum sensing and thereby inhibits the growth of competing microbes.[216] *Fusarium*, a genus of pathogenic fungi, produces trichothecenes, sesquiterpenoids that were shown to inhibit protein synthesis in eukaryotic cells by binding to ribosomes.[217]

Furthermore, bacteria synthesize a variety of antimicrobial terpenes.[38, 78] For example, *Streptomyces* species produce a sesquiterpene antibiotic albaflavenone, active against Gram-positive bacteria,[218] or the indolosesquiterpenoids xiamycins with an antiviral activity.[219] Others can produce diterpenoids, such as the previously mentioned platensimycin,[220] which inhibits fatty acid biosynthesis in competing microbes; phenalinolactones and tiancilactones with antibacterial activity, and immunosuppressants brasilicardins; or cyclooctatins with relatively weaker antimicrobial activities.[20] Moreover, genome mining in Actinobacteria has shown that many of these bacteria have terpene-synthase gene clusters encrypted in their genomes which are encoding known and uncharacterized sesquiterpenes and diterpenes.[221] Sesterterpenoid antimicrobials include the previously mentioned scytiscalarol[86] and cybastacines,[89] as well as atolypenes and sestermobaraenes.[222-223] Bacterial triterpenoids include hopanoids (diploptene, homohopanoid)[224-225] as well as sterols,[226] involved in stress tolerance, lipid raft formation or nitrogen fixation.[20] Tetraterpenoids, represented primarily by carotenoids, play important roles as pigments, antioxidants, photoprotection against UV (especially in cyanobacteria), and contribute to cell membrane integrity.[192] Altogether, these compounds give bacteria a competitive advantage in complex ecosystems, where survival depends on chemical interactions.[30, 32, 192, 227]

1.6. Outline of the Work.

The present dissertation comprises a single, coherent narrative, divided into three chapters. The **first chapter (2.1)** describes the discovery of a new class of guanidine-containing triterpene antibiotics, entitled gromomycins. Identified through screening of an actinomycetes library, and subsequently produced in *S. albus* chassis strain, these pentacyclic triterpenes harbor a cyclic guanidino group, and were found to possess significant antimicrobial activity. Using transposon mutagenesis, gene cluster engineering, feeding experiments, LC-MS and NMR analyses we have proposed the biosynthetic pathway for gromomycins, which are the first bacterial triterpenes synthesized independently of the squalene pathway. Besides, they exhibit a so far unprecedented cyclization route that utilizes a hexaprenylguanidine linear precursor (Publication I).

The **second chapter (2.2)** is dedicated to the characterization of new BGCs of gromomycin family and consequently new bioactive gromomycin derivatives, deepening our understanding their distribution across Bacteria. This chapter provides insights into gromomycin mode of action. Mechanistic studies demonstrate that these antibiotics exert potent bactericidal activity against *Staphylococcus aureus* by directly targeting and disrupting the bacterial cytoplasmic membrane. This membrane-centric mechanism, characterized by ion leakage, pore formation, and cell lysis, is further supported by lipid-dependent activity neutralization, inability to develop resistance, and their toxic effects on eukaryotic cells (Publication II).

The **third chapter (2.3)** demonstrates the utility of the genome-mining approach, which led to the discovery of novel guanidine-bearing sesterterpenoids, named darumycins. The darumycin BGC was identified in the *Micromonospora* genus, and heterologously produced in the *Streptomyces* chassis strains. Gene cluster engineering allowed to generate a number of new bioactive darumycin derivatives, enriching the chemical space of the rare sesterterpene class. This, combined with LC-MS, NMR analyses and *in vitro* enzymatic studies, structural and biochemical insights of darumycin tailoring methyltransferases, allowed us to propose the biosynthetic pathway of darumycin. (Publication III).

Each chapter is accompanied by supplementary information containing additional experimental details, datasets and figures.

2. Results and Discussion

2.1. Gromomycins: An Unprecedented Class of Triterpene Antibiotics Produced by a Novel Biosynthetic Pathway

This chapter reproduces, with minor formatting adjustments, the text of the published acticle:

S. Tistechok‡, **D. Bratiichuk‡**, H. Sucipto, N. Gummerlich, M. Stierhof, O. Gromyko, F. Fries, V. Fedorenko, R. Müller, J. Zapp, M. Myronovskyi, A. Luzhetskyy*. Gromomycins: An Unprecedented Class of Triterpene Antibiotics Produced by a Novel Biosynthetic Pathway. *Angew. Chem. Int. Ed.* **2025**, 64, e202422270. https://doi.org/10.1002/anie.202422270.

‡ authors contributed equally.

*****corresponding author.

Contributions and Acknowledgements

Author's Contribution:

The author made significant contributions to the methodology and experimental work of this study, designed and conducted biological experiments, analyzed and visualized the resulting data. Experimental work comprised biotechnological and bioinformatic approaches, including genome mining, cluster cloning, heterologous expression, compound dereplication, and isolation. The author conceived and wrote the respective parts in the original draft of the manuscript.

Contributions by Others

S. Tistechok performed biotechnological and bioinformatic work, including the discovery of first gromomycins, BGC cloning, heterologous expression and dereplication, feeding experiments, and transposon muragenesis. Furthermore, he was responsible for writing the respective parts of the manuscript. N. Gummerlich, M. Stierhof and J. Zapp performed analytics and carried out structure elucidation. H. Sucipto carried transposon mutagenesis and heterologous expression. F. Fries and R. Müller designed and performed bioactivity and toxicity studies, wrote the respective part in the manuscript. O. Gromyko. and V. Fedorenko isolated a gromomycin producer strain. M. Myronovskyi and A. Luzhetskyy conceived and designed the study, provided supervision. S. Tistechok, D. Bratiichuk, J. Zapp, M. Myronovskyi, and A. Luzhetskyy prepared the manuscript. All coauthors proofread and corrected the manuscript.

2.1.2. Abstract

The current situation with drug-resistant microbial pathogens is critical, dictating an acute need for novel efficient antibiotics. Herein, we report a new class of antibiotics entitled gromomycins with significant activity especially against drug-resistant Gram-positive pathogens including methicillin- and daptomycin-resistant *Staphylococcus aureus*. Gromomycins are pentacyclic triterpenes with a cyclic guanidino group forming the fifth six-membered ring. We have used transposon mutagenesis to identify the gromomycin biosynthetic gene cluster since it could not be assigned by any available bioinformatics tools, highlighting its unique biosynthetic route. Using gene cluster engineering, feeding experiments, LC-MS and NMR analyses we have proposed the biosynthetic pathway for gromomycins, which are the first bacterial triterpenes synthesized independently of the squalene pathway. They also exhibit a so far unprecedented cyclization route that utilizes a hexaprenylguanidine linear precursor. Leveraging our understanding of their biosynthesis, we have identified additional gromomycin producers, resulting in the isolation of novel bioactive derivatives.

2.1.3. Introduction

Natural products produced by living organisms, such as bacteria, fungi, plants, and marine organisms have been a valuable and fruitful reservoir for drug discovery, including antibiotics.[3-4, 228-230] Traditional antibiotics, like penicillin and tetracycline, have been derived from natural products and served as the foundation for many successful treatments.[231-233] However, with the emergence of antibiotic resistance, there is a growing need for innovative antibiotics with novel chemical structures to combat multidrug-resistant (MDR) pathogens.[234-235] Novel chemical scaffolds are more likely to target different bacterial vulnerabilities than conventional antibiotics, thereby overcoming existing resistance mechanisms and providing new options for treating infections that were previously difficult to manage.[79-80]

Actinomycetes are a group of Gram-positive bacteria that are known to produce a diverse array of bioactive compounds including antibiotics.[236-237] These bacteria are widely distributed in the soil and have been a rich source of lead structures for drug development, particularly in the field of antibiotics.[238-239] Many important antibiotics used in modern medicine, such as streptomycin, tetracycline, and erythromycin, were originally derived from actinomycetes.[240] Recent advances in technology, such as genomics, transcriptomics, metabolomics and synthetic biology, have enabled researchers to more efficiently screen for and identify new compounds.[241-243] These approaches have already led to the discovery of

several new antibiotics such as teixobactin, which was discovered using a novel cultivation technique.[244]

While bioactivity screening of extracts from various sources is a standard approach in antibiotic discovery, focusing solely on bioactivity may lead to missed opportunities and limited success.[245] The intricate composition of the extract can hinder the recognition of prospective antibiotic compounds through masking their activity within the complex mixtures.[246] Looking into chemical diversity enables the exploration of a vast array of novel, potentially bioactive chemical structures that might otherwise be overlooked within the complex extract mixtures.[2] In recent years modern methods have shifted towards the heterologous expression of cryptic biosynthetic gene clusters (BGCs).[247] This technique involves transferring BGCs from their native organisms into well-characterized host organisms to produce new compounds. This approach holds significant promise, particularly for unlocking the potential of "silent" or "cryptic" BGCs that are not expressed under standard laboratory conditions.[248]

However, a significant challenge remains - identifying novel BGCs that have not been previously described. The current methods often rely on sequence homology to known BGCs, [249-250] which means that truly novel biosynthetic pathways might be overlooked if they do not resemble any known sequences. Consequently, this could lead to the inadvertent omission of unique natural products with potentially strong antibiotic properties. Herein, we describe the identification of a novel class of triterpenoid antibiotics, entitled gromomycins, by adopting a strategy focused on chemical diversity rather than solely on bioactivity, which has proven effective in discovering novel antibiotic structures. Structure elucidation via NMR revealed a novel chemical scaffold comprised of a pentacycle featuring a cyclic guanidino group. The only similar terpenoids, cybastacines, containing a guanidine group, have been isolated from cyanobacteria and belong to the sesterterpene family of natural products.[89]

Furthermore, we propose a so far unprecedented biosynthetic pathway that is independent of the squalene pathway[251] and report the discovery of methylated gromomycin derivatives via a genome mining approach. Notably, we conducted initial activity and toxicity studies and found gromomycins to exhibit promising antibacterial activity against drug-resistant pathogens.

2.1.4. Results and Discussion

2.1.4.1. Isolation, Identification and Structure Elucidation of Gromomycins

The strain *Streptomyces* sp. Je 1-332, sourced from the rhizosphere soil of *Juniperus excelsa* M.-Bieb.,[252] yielded several distinct peaks in its crude extract (**Figure S70**). Mass spectral analysis of these peaks identified molecular ions [M+H$^+$] with masses such as 496.39 Da, 494.37 Da, 494.42 Da, 480.38 Da or 478.38 Da. Dereplication against the Dictionary of Natural Products (DNP)[16, 253] database revealed no corresponding entries, suggesting these compounds are novel.

To elucidate their structures, strain 1-332 was cultivated in 10 liters of DNPM medium, and the metabolites were extracted from the culture supernatant using ethyl acetate. A total of nine compounds were isolated, yielding a couple of milligrams each, after a three-step purification process. Compound **1** (496.39 Da) proved unstable, degrading to **2** (478.38 Da) during the purification process. This degradation, evidenced by an 18 Da mass difference, indicated the likely loss of H_2O. We therefore initially focused on the structure of **2**. Its molecular formula was determined by HRESIMS (*m/z* 478.3804 ([M+H]$^+$) as $C_{31}H_{47}N_3O$ with 10 degrees of unsaturation (DU). Its NMR data (**Table S1**) in CD_3OD revealed seven methyls, eight methylenes, six methines and ten quaternary carbons. Eight olefinic signals (DU=4) appeared in the low field part of the ^{13}C NMR together with a quaternary carbon at δ 152.53, which would fit very well with a guanidine unit (DU=1). In addition, an alcohol function could be deduced from the signal at δ 79.78.

Based on these considerations, the remaining five degrees of unsaturation accounted for rings structures in the molecule. The ^1H-NMR showed seven singlet methyl resonances, two of them with a double bond shift (δ 1.54 and δ 1.64). Furthermore, four olefinic double bonds (δ 5.99, δ 5.85, δ 5.75 and δ 4.99) and a secondary alcohol (δ 3.66) were identified. HHCOSY correlations revealed a 2-methyl-pent-2-en-5-yl side chain together with several smaller C-2 and C-3 ring fragments, all located between quaternary carbons. After analyzing their correlations in the corresponding HMBC, these fragments could be linked with the quatenary carbons and the remaining five methyl groups to form four fused, six-membered carbon rings A-D, whose ring D bore the side chain and whose ring A should have fused with the remaining guanidine to form a 3,4-dihydropyrimidin-2(1H)-imine ring (**Figure 1a**).

To learn more about the nature of this guanidine moiety, we repeated the NMR measurements in DMSO-d_6/TFA (**Table S2**). Its ^1H-NMR revealed signals for the NH protons at δ 9.15 (dd, *J=5.0* and *2.0 Hz*, N_1-H), δ 7.92 (d, *J=2.0 Hz*, N_2-H) and δ 7.04 (s, 2H, N_3-H).

For proton N_1-H, a vicinal coupling with the olefinic hydrogen H-1 was observed, which, in contrast to the spectrum in CD_3OD, now appeared as a doublet (δ 5.86, *J=5.0 Hz*). ^1H-^{13}C HMBC (C-3/N2-H, C-2/N1-H, C-2/N2-H) as well as ^1H-^{15}N HMBC correlations (N_1/H-1, N_2/H-25) proved the cyclic guanidine group. The relative stereochemistry of **2** was determined in CD_3OD by analyzing the coupling patterns and evaluating the NOE effects of selected protons. In contrast to H-4 (dd, *J=12* and *4.5 Hz*), the signals of H-5a, H-5b and H-6 were superimposed by other proton resonances. But with the help of a 1D selective TOCSY, they could be displayed separately, and their coupling constants could be analyzed (**Figure S7a**).

Based on a vicinal coupling constant of 12 Hz for $J_{H\text{-}4/H\text{-}5b}$ and $J_{H\text{-}5b/H\text{-}6}$, an axial position could now be derived for each of the protons involved. The spatial orientations of the ring-bound methyl groups were of particular interest for the relative configuration of **2**. Selective 1D NOESY spectra (**Figure S7b**) revealed NOE interactions between Me-25, Me-26, Me-28 and H-5b indicating that these protons are on the same side of the molecule in axial positions. This also meant that H-6 and Me-26, both in axial position, were located on different sides of the ring system, which required trans-fused rings A and B (**Figure 1b**). NOE interactions between Me-27 and Me-28 suggested cis-fused rings B and C. Only the stereochemistry at C-19 could not yet be determined at this time. Neither the protons of the angular methyl group H-29 and those from the side chain H-21 - H-24 nor those of ring C and D provided useful NOE effects here. Compound 2 (Fig. 3), was named gromomycin A.

The high-resolution mass spectrum of gromomycin B (**3**) with *m/z* = 494.3752 for the ($[M+H]^+$ ion peak provided an additional oxygen atom in the molecular formula, $C_{31}H_{47}N_3O_2$, when compared to **2**. A detailed examination of the NMR data (**Table S3**) revealed that all structural changes were restricted to ring D. According to the ^{13}C NMR, the 14,16-diene function had changed to a conjugated 15-en-17-one. In the ^1H-NMR, the resonances at δ 6.15 for the double bond proton H-16 and those of the doublets at δ 2.54 and 2.11 of the isolated

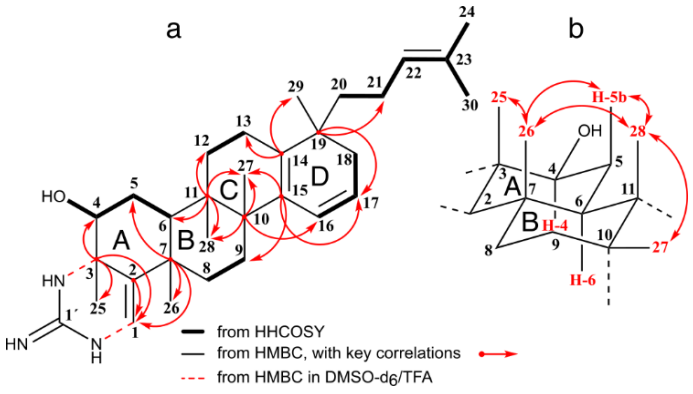

Figure 1. Structural features of Gromomycin A (**2**). a) Significant HHCOSY and HMBC correlations. b) Selected NOEs in ring A and B.

methylene C-18 (2.54 and 2.11) stood out.

However, the proton resonance of the newly formed stereocenter methine C-14 at δ 2.84 ppm proved to be particularly valuable, as it could be used to clarify the stereochemistry at C-19. 1D selective NOESY spectra (**Figure S20**) were particularly helpful in this respect. Excitation of H-14 showed an enhancement of H-6 and H-18a, which therefore must be on the same side of the molecule. Similarly, the NOE interactions between H-18b and methyl-H-29 proved their localisation on the side of the molecule facing away from H-18a (**Figure 2a**). The strong NOE between H-6 and H-14 was not easy to understand at first glance but could be explained with the help of a 3D model. If we assume that rings A and B are in chair conformation and ring C is in boat conformation both atoms are in close proximity to each other (**Figure 2b**). As the verification of the relative stereochemistry for the stereocenters already known from 2 did not lead to any changes, we were now able to determine the relative stereochemistry for the whole molecule. In addition, a well-founded proposal for the spatial position of Me-29 in gromomycin A (**2**) could also be made.

The Mosher´s ester method was used to determine the absolute stereochemistry of C-4 and by interference, the rest of the stereogenic centers in the entire molecule. Treatment of **3** with the (*R*)- and (*S*)-MTPA chloride [α -methoxy- α -trifluoromethylphenylacetyl chloride] in dry pyridine gave the (*S*)- and (*R*)-MTPA esters in reasonable yields (see Experimental Section).

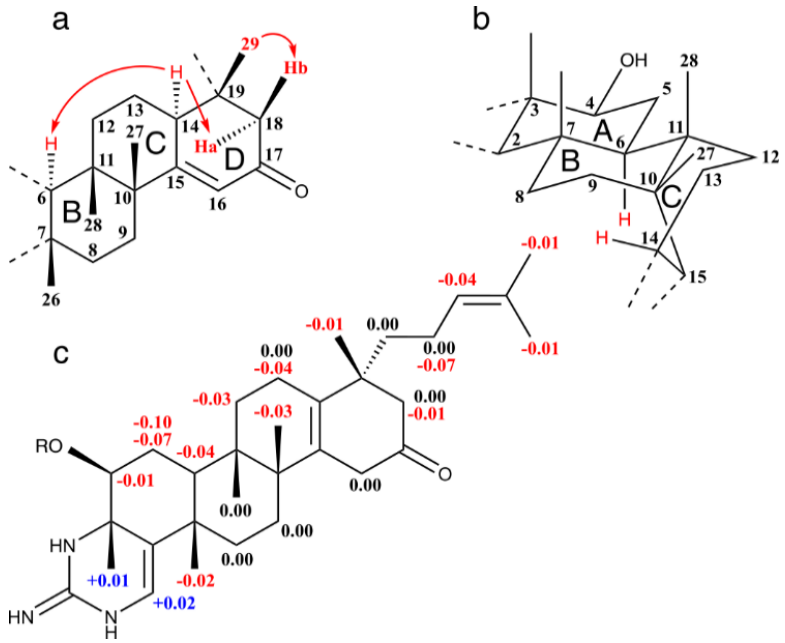

Figure 2. Structural features of Gromomycin B (**3**). a) Selected NOEs in Ring B-D. b) Conformations of ring A, B (both chair) and ring C (boat). c). ΔδS-R values for MTPA derivatives derived from **3**.

This process also led to a migration of the double bond from C-15/C-16 to C-14/C-15 for both products, which was confirmed by a careful analysis of their ^{1}H NMR, HHCOSY and HSQC spectra (**Figures S57-S62**). The ^{1}H NMR data of the mosher ester derivatives (**Table S11**) led to the calculation of the $\Delta\delta_{S-R}$ values (**Figure 2c**) and established the (*S*)-configuration at C-4, thus allowing the full absolute configuration of (3*S*,4*S*,6*S*,7*S*,10*R*,11*S*,14*S*,19*R*) to be assigned for gromomycin B (**3**). Gromomycin C (**4**) displayed a ($[M+H]^+$ ion peak at *m/z* 480.3953 in the HRESIMS corresponding to a molecular formula of $C_{31}H_{49}NO$. As already described for gromomycin B (**3**), a trisubstituted double bond between C-15 (δ 143.48) and C-16 (δ 120.27) could also be detected here. However, their resonances were shifted upfield and the signal for a keto group was completely missing in the 13C NMR (**Table S4**). It was therefore assumed that gromomycin C (**4**) is the 17-deoxo derivative of **3**, which was confirmed by extensive 2D NMR measurements.

Gromomycin D (**5**) was obtained as a white powder. Its HRESIMS was identical to that of **3** and its NMR data (**Table S5**) proved that its structure was the same as that of the double bond isomer formed in the Mosher reaction of 3 with *R*- and *S*-MTPA chloride. Gromomycin E (**6**, **Figure 3**) had a molecular formula of $C_{32}H_{49}N_3O$ as determined by HRESIMS (*m/z* 492.3950 $[M+H]^+$). Its NMR data (**Table S6**) were very close to those of Gromomycin A (**2**), especially for the resonances of ring A-D and the guanidine moiety.

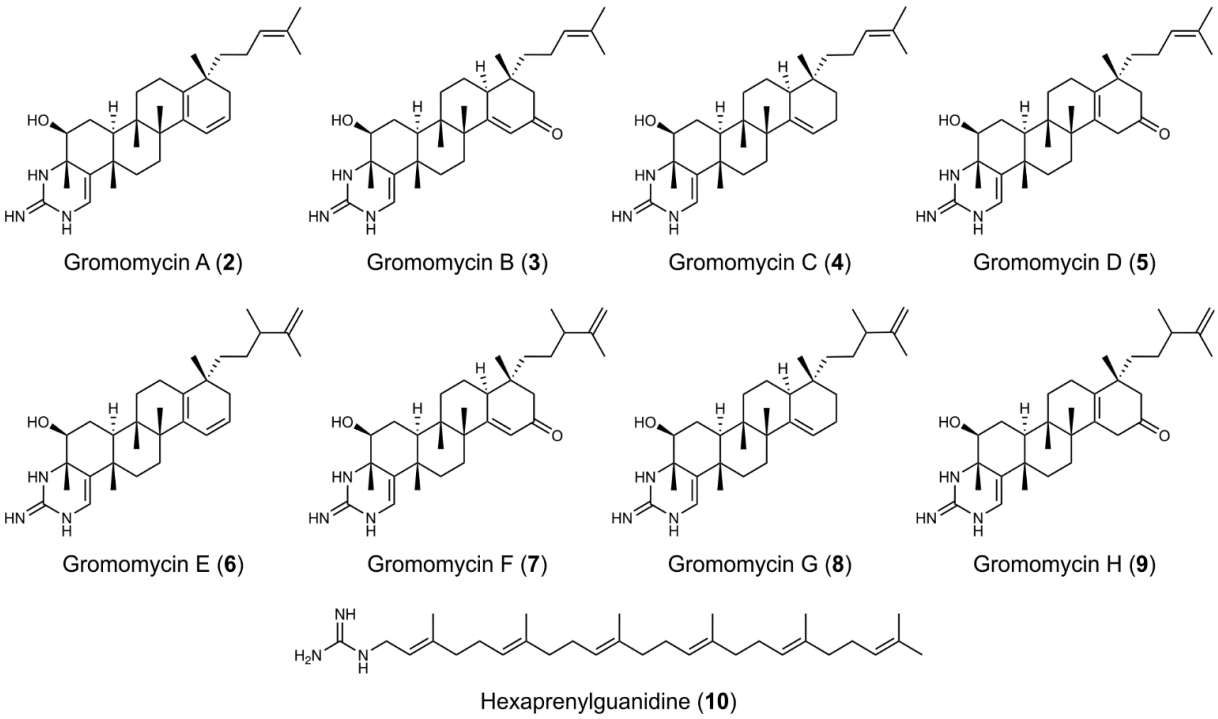

Figure 3. Structures of gromomycins A-H and hexaprenylguanidine.

However, differences could be observed for the side chain. Here, the double bond has been moved from C-22 to C-23 at the end of the side chain and C-22 now bore an additional methyl group C-31. HHCOSY and HMBC correlations supported the 2,3-dimethyl-pent-1-en-5-yl side chain for gromomycin E. HRESIMS data of **7-9** (see analytical data **SI**, p.12) showed that these compounds were also methylated gromomycins. Careful analysis of their NMR data (**Table S7-S9**) revealed the same side chain for them as found for **6** and identical ring structures A-D to those of **3-5**. However, due to the high flexibility of the side chain the stereochemistry of the newly formed stereocenter at C-22 could not be established.

The molecular formula of **10** was calculated as $C_{31}H_{53}N_3$ with **7** degrees of unsaturation based on its ESIMS with *m/z* 468.4355 $[M+H]^+$. The NMR data (**Table S10**) revealed an acyclic structure with six trisubstituted double bonds, bearing six protons (δ 5.06, 5H and 5.19, 1H), seven singlet methyls (δ 1.63, 5 Me and 1.55, 2 Me) and ten methylene groups (δ 1.93-2.02, 20H) similar to those of squalene. The resonance for a methylene group at δ 3.66 (2H) gave hint to an additional polar substituent. Its composition, CH_4N_3, was deduced from the difference between parts of the 1H (δ 7.79, brs, 3H and 8.61, t, 1H) and ^{13}C NMR the molecular formula of 10 and that of the triterpene unit, $C_{30}H_{49}$. The signals of this guanidyl moiety could be found in the lowfield (δ 157.29) spectra. 2D HHCOSY and HMBC proved the terminal position of the guanidyl residue in the polyprenyl chain but raised doubt about the squalene moiety. In contrast to a hypothetical 1-guanidylsqualene, the methylene protons H-1 showed vicinal correlations with the NH proton at δ 8.61 and the proton at δ 5.19 of the neighboured double bond proton.

Therefore, the terpene moiety was formed by six head-tail-linked isoprene units leading to the structure of 1-((2E,6E,10E,14E,18E)-3,7,11,15,19,23-hexamethyltetracosa 2,6,10,14,18,22-hexaen-1-yl) guanidine that we named **hexaprenylguanidine** (**Figure 3**).

2.1.4.2. Identification of the Gromomycin Biosynthetic Gene Cluster

To identify the gromomycin biosynthetic gene cluster (BGC) within *Streptomyces* sp. Je 1-332, we sequenced its genome and conducted an analysis using antiSMASH 6.0.[250] The analysis via antiSMASH revealed 21 potential BGCs. Considering the terpene-like core of gromomycins we have focused on five BGCs for terpene synthesis. Notably, two of these (antiSMASH Regions 14 and 15 (**Table S17**)) displayed low homology to known terpenes, suggesting they might be involved in gromomycin production.

To investigate this hypothesis, we employed homologous recombination to replace the terpene cyclase genes in these regions with apramycin resistance cassettes. HPLC-MS analysis of the resulting strains did not show any changes in gromomycin production, indicating these clusters were not responsible for its biosynthesis. Therefore, we have adopted the Tn5 and Himar1 transposon mutagenesis as our subsequent approach to uncover the elusive gromomycin BGC (**Figure S74**). Over 1500 *Streptomyces* sp. Je 1-332 transposon mutants were screened for their ability to produce gromomycin by HPLC-MS. Within this pool of transposon mutants, we found five mutants lacking gromomycin production (**Figure S69b**) and identified their transposon insertion sites. In the two mutants, Tn5_mut_148 and Tn5_mut_355, the insertions were found close to and surrounded by a gene that encodes for a putative farnesyl diphosphate synthase (*fdps*) (**Figure S69a**), which is identified as a *groD* gene in **Fig. 4**.

The *fdps* gene was replaced by an apramycin resistance marker within the chromosome of *Streptomyces* sp. Je 1-332 to investigate its role in gromomycin biosynthesis. HPLC-MS analysis indicated that the deletion of the *fdps* (*groD*) gene ceased gromomycin production. Consequently, we conducted additional deletions to confirm that this region harbours the gromomycin BGC. These deletions encompassed a gene annotated as a putative enduracidin beta-hydroxylase (*groE*), a hypothetical protein (*groF*), a PAP2 superfamily protein (*groG*), another hypothetical protein (*groH*), and a cytochrome P450 (*groI*), and two genes annotated as putative aminopyrrolnitrin oxygenases (*groB* and *groC*). All resulting deletion mutants either failed to produce gromomycin or produced its derivatives (**Figure S71**). This led us to hypothesize the presence of a gromomycin BGC within the identified genome region (5778465 – 5804255 bp). The corresponding region carrying gromomycin biosynthetic genes has been cloned into a cosmid pHSU-STS10 and transferred into the heterologous host strains *S. albus* Del14[254] and *S. lividans* Del8[255] via conjugation. We analyzed the metabolic profile of the resultant strains, *S. albus* STS10 and *S. lividans* STS10, using HPLC-MS. Gromomycin production was detected in extracts from both heterologous host strains (**Figure S65**), confirming the identification of a gromomycin BGC through random transposon mutagenesis followed by HPLC MS screening of the corresponding mutant library.

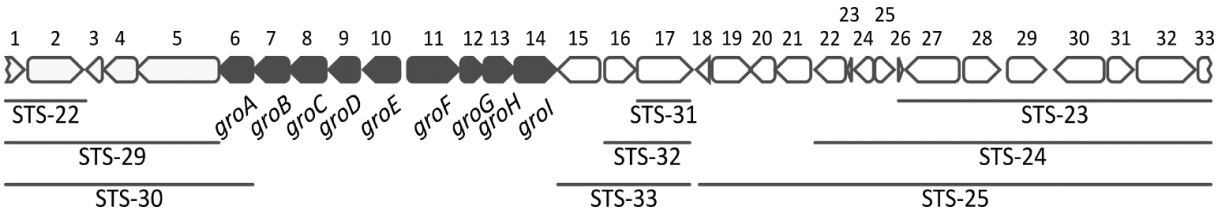

Figure 4. Diagram of the DNA segment containing the gromomycin biosynthetic gene cluster, depicted in black. The lines indicate the individual deletions that were made.

Table 1. Proposed function of genes in gromomycin gene cluster.

Gene	Proposed function
groA	Rieske 2Fe-2S domain-containing protein *S. azureus*
groB	Rieske 2Fe-2S domain-containing protein *S. azureus*
groC	Rieske 2Fe-2S domain-containing protein *S. azureus*
groD	Polyprenyl synthetase (Farnesyl diphosphate synthase)
groE	Reductase
groF	Hypothetical protein (cyclase)
groG	Phosphatase PAP2
groH	Hypothetical protein (prenyl transferase, guanidinatransferase)
groI	Cytochrome P450 107B1 (Monooxygenase/Oxidoreductase)

The vector pHSU-STS10, used for heterologous expression in *S. albus* Del14 and *S. lividans* Del8, harbors a 35.6 kb chromosomal fragment from *Streptomyces* sp. Je 1-332. This particular fragment, not recognized as a putative biosynthetic gene cluster (BGC) by the antiSMASH program, encompasses 33 open reading frames (ORFs) (**Figure 4**). To identify the minimal set of genes essential for gromomycin biosynthesis, we executed a series of gene deletion experiments. The genes previously deleted in the native gromomycin producer strain *Streptomyces* sp. Je 1-332, which demonstrated a significant impact on gromomycin production, were located at positions 6 to 14 and served as the focal point for systematic deletions. To ascertain all the specific genes essential for gromomycin biosynthesis, we initiated six deletions—STS22, STS29, and STS30 on the left arm, and STS23, STS24, and STS25 on the right arm (**Figure 4**). These deletions were generated using the *bla* marker to replace the desired fragment through RedET recombination. Subsequently, the *bla* marker was excised using the PmeI restriction enzyme to avoid a possible polar effect. The deletions STS22, STS23, STS24, and STS25 did not affect gromomycin production, indicating that genes 1, 2, and 18-33 are dispensable for its synthesis. However, the STS29 deletion resulted in a marked reduction in gromomycin levels, whereas the STS30 deletion completely halted production (**Fig. S72**). The difference between STS29 and STS30 is the absence of gene 6 in the latter, suggesting that gene 6 encodes an enzyme crucial for gromomycin synthesis.

To pinpoint the genes that suppress gromomycin production in the STS29 deletion strain, we deleted genes 3-5 individually and assessed the effects. Deletions of genes 3 and 4 were associated with a substantial decrease in gromomycin levels, while deletion of gene 5 had no discernible impact, suggesting regulatory roles for genes 3 and 4. Additionally, to delineate the boundary of the gene cluster downstream of genes 6-14, we performed three more

deletions—STS31, STS32, and STS33. No variation in gromomycin production was observed among *S. albus* STS31, STS32, and STS33 strains (**Figure S72**). Hence, we deduced that the minimal set of genes responsible for gromomycin synthesis encompasses genes 3 to 14. Within this range, it is probable that genes 6 to 14 are structural, designated *groA* to *groI*, while genes 3 to 5 likely play a regulatory role.

2.1.4.3. Establishing Pyruvate and L-ariginine as Gromomycin Biosynthetic Precursors

To uncover the precursors involved in gromomycin biosynthesis, we conducted a series of feeding experiments with [2-^{13}C]- and [3-^{13}C]-labeled sodium pyruvate. We utilized the heterologous host strain *S. albus* STS10 to produce gromomycin. As the *S. albus* Del14 strain is devoid of the mevalonate pathway, we anticipated that the synthesis of isoprene units would occur through the non-mevalonate (MEP) pathway. Following the feeding with [2-^{13}C]-sodium pyruvate, we isolated 0.9 mg of labeled gromomycin, and from the [3-^{13}C]-sodium pyruvate feeding, we isolated 1.2 mg. We employed ^{13}C NMR spectroscopy to pinpoint the positions of the incorporated labeled carbons (**Tables S12** and **S13**; **Figures S63** and **S64**). The experiments revealed that each feeding resulted in the incorporation of six ^{13}C atoms into the gromomycin molecule, confirming the use of these labeled precursors in its biosynthesis and establishing the art of incorporation.

Furthermore, to clarify the origin of the intriguing guanidine moiety in the structure of gromomycin, we conducted feeding experiments using variously labeled arginines. Specifically, we utilized arginine labeled on all carbon and nitrogen atoms, as well as arginine labeled solely on nitrogen atoms. When arginine labeled on both carbons and nitrogens was fed, a uniform mass increase of +4 was detected across all identified peaks. Conversely, when we fed the strain arginine labeled only on nitrogen, we observed a mass increase of +3 in the peaks. These observations lead us to propose that the guanidine moiety of gromomycin is directly derived from arginine (**Figure S66**).

2.1.4.4. Proposed Biosynthetic Pathway of Gromomycin

The postulated minimal gene cluster for gromomycin synthesis comprises 12 open reading frames, spanning from *gro3* to *groI*. We conducted several gene inactivation experiments to elucidate their roles in gromomycin biosynthesis. BLAST analysis did not offer a clear function for these genes, except for *groD* and *groI* encoding a polyprenylsynthase and CYP450 monooxygenase, respectively (**Table 1**).

Genes *groA* to *groC* and *groF* to *groI* were deleted in-frame to avoid any polar effect. Gromomycin production in these modified strains was assessed using HPLC-MS and produced derivatives and precursors have been purified and their structures elucidated with NMR. The deletion of the *groD* gene have been shown to completely abolish gromomycin synthesis. The GroD enzyme shows strong similarity to the class I terpene synthases having two conserved DDxD and DTE motifs for binding of Mg^{2+} ions that in turn binds the substrate's diphosphate. These enzymes synthesize various chain length (C10, C15, C20, C25, C30, C35, C40, C45, and C50) linear isoprenyl diphosphates from precursors, isopentenyl diphosphate (IPP) and dimethylallyl diphosphate (DMAPP). We suggest GroD combines six prenyl groups, forming a hexyprenyl diphosphate, a crucial intermediate in gromomycin biosynthesis.

The deletion of the *groH* gene completely abolished the gromomycin production, suggesting its involvement in the early biosynthetic stages. In-depth analysis of the GroH protein, utilizing Swiss-Prot for structure homology modeling (https://swissmodel.expasy.org), revealed its resemblance to several terpene synthases and a notable similarity to prenyltransferases. We propose that GroH transfers the hexaprenyl moiety to arginine, followed by the release of proline through the nucleophilic attack of the alpha amino group on the imino carbon of the guanidine moiety, forming hexaprenylguanidine (**Figure 5**). Inactivating the groF gene, identified as a hypothetical protein, led to a derivative with a mass of $[M+H^+]$ 468.38 Da. Following purification and structural analysis (**Table S10** and **Figures S51 – S56**), this compound was identified as **hexaprenylguanidine** (**10**), a linear precursor to gromomycins (**Figure 3**). It is characterized by a unique C1-C4′ bond between two farnesyl groups, a feature unprecedented in bacterial triterpenes.

Advanced analysis of the GroF protein, using Swiss-Prot for structure homology modeling, showed that it contains a terpene cyclase domain, similar to the TvTS cyclase from *Talaromyces verruculosus*[256-257] and the FlvF cyclase-like protein from *Aspergillus flavus*.[258] Coupled with the isolation of the linear hexaprenylguanidine precursor, these findings suggest that GroF likely serves as a gromomycin cyclase. The protonation of C-19 in hexaprenylguanidine by GroF cyclase likely follows a mechanism similar to that of squalene-hopene cyclase (SHC) in bacteria.

In SHC, an aspartate-rich DXDDTA motif initiates the polycyclization reaction by facilitating proton donation from aspartate.[259] In GroF, we have identified a DLADPD motif, which is highly enriched in aspartates and may fulfill a comparable catalytic function. Upon protonation, the polycyclization reaction progresses through a sequence of rigidly held carbocation intermediates. Finally, the highly nucleophilic amino group of the guanidine moiety

may attack the last C-3 carbocation in the cascade, resulting in the formation of the cycloguanidine ring.

Inactivating the *groA*, *groB*, and *groC* genes, which are annotated as putative Rieske non-heme iron oxygenases, also resulted in the accumulation of hexaprenylguanidine, a linear precursor to gromomycin. This suggests their involvement in the cyclization process of gromomycins. The C4-OH group is most likely introduced by one of the Rieske oxygenases (GroA, GroB, or GroC), as these enzymes are known to catalyze hydroxylation reactions. Similar mechanisms have been described for the Rieske-type oxygenases KshAB in *Mycobacterium tuberculosis*, which play a key role in cholesterol catabolism.[260]

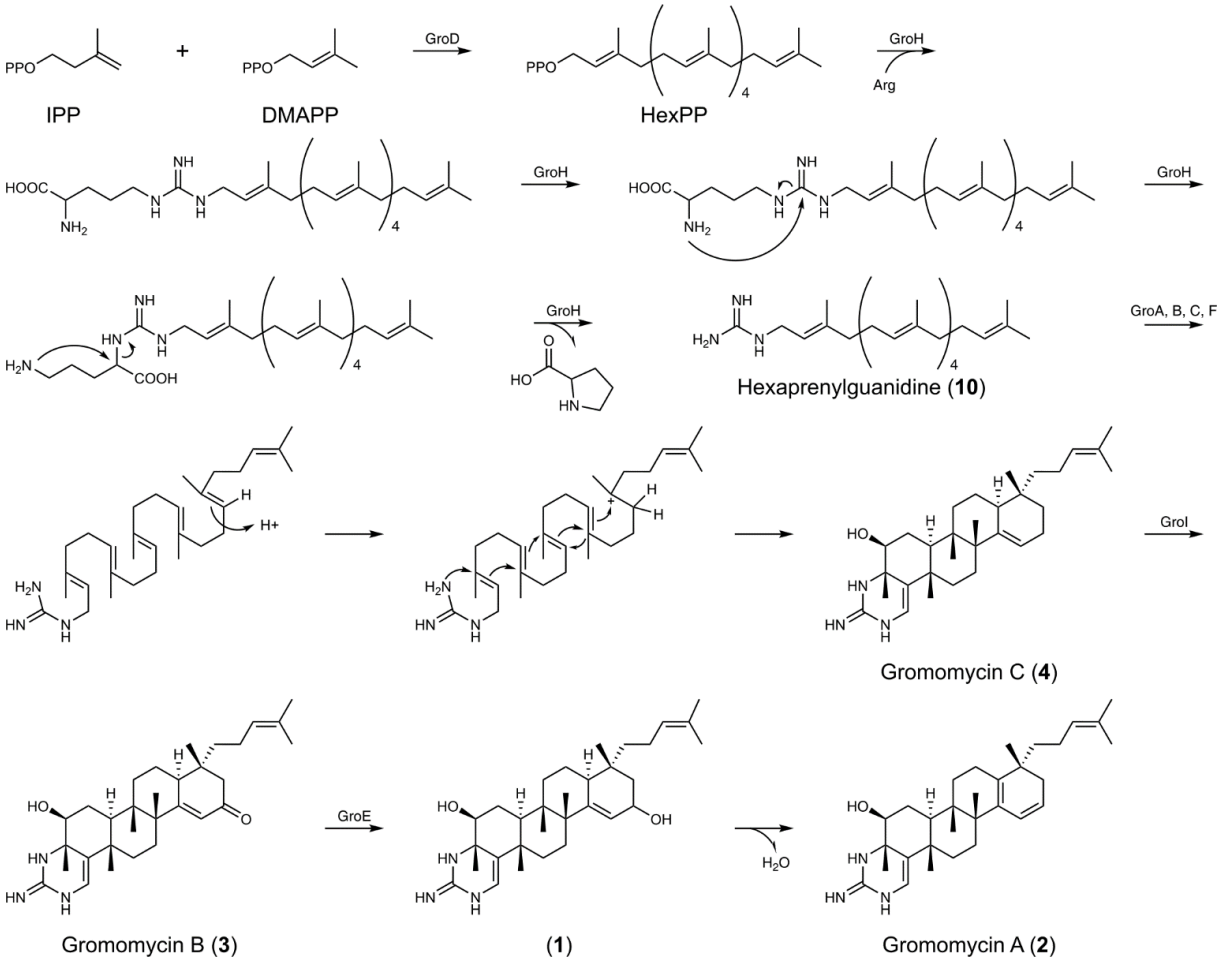

Figure. 5. Proposed biosynthetic pathways of gromomycins. IPP, Isopentenyl diphosphate; DMAPP, Dimethylallyl diphosphate; HexPP, hexaprenyl diphosphate, Arg, L-ariginine.

Additionally, the formation of C1-C2 and C15-C16 double bonds may also be catalyzed by one of the three Rieske oxygenases, as these enzymes are known to introduce double bonds. A well-documented example is the Rieske enzyme DAF-36, which catalyzes the conversion of cholesterol to 7,8-dehydrocholesterol, potentially via a monohydroxylated intermediate that subsequently undergoes dehydration.

The inactivation of the *groI* gene led to the synthesis of a compound, possessing a mass of [M+H$^+$] 480.44 Da. This substance was subsequently isolated, and its structure, confirmed through NMR spectroscopy appears to be gromomycin C (**4**) (**Figure 3**, **Table S4** and **Figures S21 – S26**). Given the absence of a hydroxy group in the fifth ring of gromomycin C (**4**) and the high similarity of the *groI* gene to genes encoding CYP450-dependent oxygenases, we propose that the associated enzyme is responsible for incorporating a keto group at C-17 of gromomycins, leading to the formation of gromomycin B (**3**). The *groE* gene mutants accumulated gromomycin B (**3**) suggesting that the *groE* gene product reduces the keto group to a hydroxyl group at position C-17 leading to the hydroxylated gromomycin **1**, which we could not isolate due to its instability. This compound degrades to gromomycin A (**2**) during the purification process (**Figure 5**).

2.1.4.5. Genome-Guided Isolation of New Gromomycins

After delineating the biosynthetic pathway of gromomycin, we adopted a genome mining approach to understand how widely is the novel gromomycins-like BGCs distributed and to identify new derivatives. This method hinges on the concept that genes dictating the core chemical structure of gromomycin, in our instance *groD*, *groH* and *groF*—serve as "hooks" for genome mining, guiding the search for related analogs. By utilizing technique, we can expand the structural series of compounds, enhancing our understanding and potential optimization of the structure-activity relationships. Prior research has shown that deleting these genes is critical for gromomycin production. We utilized the nucleotide sequences of these genes as probes in the NCBI protein BLAST database to identify new gromomycin-like clusters. Our objective was to find clusters harboring these three genes in close proximity within the genome.

This search revealed seven *Streptomyces* and three rare actinobacteria strains — *Actinoplanes xinjiangensis*, *Saccharopolyspora phatthalungensis*, and *Frankia casuarinae* with all three genes situated closely together in their genomes. Further examination showed that three strains (*S. azureus*, *S. termitum*, and *S. albulus*) possess gromomycin-like clusters nearly identical to the original. Meanwhile, two strains (*S. tendae* and *S. parvulus*) include an extra

gene encoding a protein with a methyltransferase domain. Additionally, *S. pilosus* and *S. flavoviridis* feature gromomycin-like clusters with a type II methyltransferase, absent in the original gromomycin cluster.

We constructed a cosmid library for the *S. flavoviridis* JCM 4372 strain and identified a gromomycin-like biosynthetic gene cluster (BGC) on cosmid P03_G02 through PCR. This BGC was then introduced into the heterologous host strains *S. lividans* Del8 and *S. albus* Del14. High-resolution HPLC-MS analysis of both *S. albus* Del14 and *S. lividans* Del8 strains, containing the P03_G02 cosmid, revealed six distinct peaks (**Figure S67**). The mass spectra analysis showed molecular ions [M+H$^+$] with masses of 458.37 Da, 482.45 Da, 492.39 Da, 494.41 Da, 496.43 Da and 508.39 Da. To determine the structure of the identified compounds, strain *S. albus* Del14 with *S. flavoviridis* gromomycin-like cluster was grown in 10 L of DNPM medium and metabolites were extracted from the supernatant with ethyl acetate.

New gromomycins corresponding to the identified molecular ions [M+H$^+$] with the masses 492.39 Da (gromomycin E (**6**)), 494.41 Da (gromomycin G (**7**)) and 508.39 Da (gromomycins F (**8**) and H (**9**)) were successfully purified from the extract and their structures have been determined by NMR (**Tables S6-S9** and **Figures S36-S50**). Their structures and names, along with the position of the methyl group at C-22, are shown in **Figure 3**. Noteworthy, careful analysis of the extracts of *S. albus* Del14 with gromomycin-like cluster from *S. flavoviridis* led to the identification of a linear methylated hexaprenylguanidine with a mass of 482.45 Da suggesting that methylation occurs prior to cyclization (**Figure S68**).

2.1.4.6. Bioactivity Profiling of Gromomycins

In an effort to study the biological activity of gromomycins we screened derivatives gromomycins A and B against a preliminary panel of bacteria and fungi and found that they possess antibacterial activity in particular against Gram-positive species with minimum inhibitory concentrations (MICs) in the low one-digit μg mL^{-1} range. Consequently, we assessed the activities of gromomycins including the new methylated derivatives gromomycins F and G using a broad panel of high-priority (according to the WHO priority list[261] and ESKAPE (*Enterococcus faecium*, *Staphylococcus aureus*, *Klebsiella pneumoniae*, *Acinetobacter baumannii*, *Pseudomonas aeruginosa*, *Enterobacter* spp.)) pathogens (**Table 2**). All tested compounds except for gromomycin G showed remarkable activity against Gram-positive bacteria. Gromomycins were not only active on the methicillin-susceptible *S. aureus* strains Newman and Cowan 1, but also showed very promising activity against methicillin-

resistant *S. aureus* N315, the vancomycin-intermediate (VISA) strain Mu50 and a laboratory daptomycin-resistant *S. aureus*, indicating an absence of cross-resistance to first-line agents for MRSA treatment.[262] Furthermore, gromomycins were active on penicillin-resistant *Streptococcus pneumoniae* and exhibited substantial activity on *M. tuberculosis* and A. *baumannii*. Interestingly, gromomycin A shows the most potent activity against *A. baumannii*, while its methylated side-chain variant, gromomycin E, completely loses activity. In general, the presence of a methyl group in the side chain of gromomycins appears to reduce activity in most cases. The remaining panel of Gram-negative pathogens revealed only moderate activity against species from the Enterobacteriaceae.

Notably, gromomycins display higher activity against *E. coli* WO153, which lacks the outer membrane porin TolC of the AcrAB-TolC tripartite efflux pump, and which has an impaired penetration barrier due to decreased amounts of lipopolysaccharide (LPS) in its outer membrane.[263] Besides, we observed enhanced activities in the presence of sub-inhibitory concentrations of the outer membrane permeabilizing agent polymyxin B nonapeptide (PMBN); thus, indicating that limited activity against Gram-negative bacteria is mostly due to impaired penetration into the bacterial cell and to some extent also due to efflux, rather than the absence of the target. Interestingly, the activity against *E. coli* ΔtolC and *K. pneumoniae* strongly correlates with the presence of a keto group at position C-17, with Gromomycin B, F, andH being the most active.

Triterpenes often pose the risk of cytotoxicity. Thus, we performed thorough safety profiling and found that gromomycin derivatives gromomycins A, E and H exert cytotoxic effects in vitro on HepG2 (IC50 2.2 to 19.4 μg mL^{-1}) and CHO-K1 cells (IC50 4.1 to 23.9 μg mL^{-1}), whereas other derivatives showed no toxic effects up to concentrations of 37 μg mL^{-1}. By contrast, we observed toxicity for every tested derivative in the highly sensitive zebrafish embryo model (**Table S18** and **Figure S73**), which is more predictive of toxic effects as compared to standard cell culture systems.

Strikingly, the maximum tolerated concentrations (MTCs) determined in zebrafish embryos correlate with the antibacterial activity, hinting towards a target that is universally conserved amongst prokaryotes and eukaryotes. Considering the high toxicity correlated with their activity, gromomycins are unlikely to be further developed as antibiotics. However, they could be valuable tools for studying bacterial resistance mechanisms, understanding biosynthetic pathways, mechanisms, or serving as lead structures for the development of modified derivatives with improved therapeutic potential.

Table 2. Antimicrobial activity spectrum of gromomycin derivatives.

Classification	Organism	MIC [µg mL^{-1}]						
		Grom A	Grom B	Grom E	Grom F	Grom G	Grom H	REF[d]
Gram-positive	*S. aureus* ATCC29213	2	4	4	4	> 64	4	VAN: 2
	S. aureus Newman	2	4	4	4	16	4	VAN: 2
	S. aureus Cowan 1	2	4	4	4	> 64	8	VAN: 2
	S. aureus N315	2	4	4	4	> 64	8	VAN: 2, AMP: > 64
	S. aureus Mu50	2	16	4	8	16	8	VAN: 8, AMP: > 64
	S. aureus HG001 WT	2	4	4	4	> 64	4	DAP: 1
	S. aureus HG001 Dap^{R}	2	4	4	4	16	4	DAP: 64
	S. pneumoniae DSM11865	2	4	4	4	16	nd [b]	RIF: 0.03
	E. faecalis ATCC29212	2	8	4	8	16	8	RIF: 0.5
	B. subtilis DSM10	2	4	4	4	16	4	VAN: 1
Myco-bacteria	*M. smegmatis* mc^{2}155	16	8	16	16	64	nd [b]	RIF: 32
	M. tuberculosis H37Ra	8	16	8	16	32	8	RIF: 0.02
Gram-negative	*E. coli* BW25113	> 64	32	> 64	64	> 64	64	CIP: 0.03
	E. coli K12 Δ*tolC*[a]	64	8	> 64	16	> 64	16	CIP: 0.01
	E. coli K12 Δ*tolC*[a] + PMBN[c]	2	4	8	4	> 64	nd [b]	CIP: 0.01
	E. coli WO153	2	8	8	4	> 64	nd [b]	CIP: 0.01
	S. enterica DSM5569	> 64	32	> 64	64	> 64	64	CIP: 0.02
	C. freundii DSM30039	> 64	32	> 64	64	> 64	64	CIP: 0.02
	K. pneumoniae DSM681	32	8	> 64	16	> 64	16	CIP: 0.01
	A. baumannii DSM30007	8	32	> 64	16	> 64	64	CIP: 2
	A. baumannii DSM30008	8	32	> 64	16	> 64	64	CIP: 0.5
	A. baumannii NCTC13301	16	32	> 64	32	> 64	64	CIP: > 64, COL: 1
	P. aeruginosa PA14	> 64	> 64	> 64	> 64	> 64	> 64	CIP: 0.25

[a] Keio collection mutant; efflux-deficient. [b] Not determined (nd) due to limited compound availability. [c] 3 µg mL^{-1} polymyxin B nonapeptide (PMBN). [d] Reference antibiotics: AMP, ampicillin; CIP, ciprofloxacin; COL, colistin; DAP, daptomycin; RIF, rifampicin; VAN, vancomycin. [R] Daptomycin resistance.

2.1.4.7. Conclusion

In this work, we report a new class of antibiotics entitled gromomycins. The discovery of gromomycins marks a significant advancement in the fight against antibiotic-resistant bacteria. Our newly identified natural compounds, derived from *Streptomyces* bacteria, offer potent activity against some of the most challenging pathogens, including methicillin-resistant *Staphylococcus aureus* (MRSA) and *Mycobacterium tuberculosis*, the bacteria responsible for tuberculosis. What makes gromomycins particularly exciting is their unique biosynthesis, which follows a previously unknown pathway not linked to typical triterpene production pathways. Additionally, the gromomycin biosynthetic gene cluster was identified through transposon mutagenesis, as bioinformatics tools failed to detect it, emphasizing its novel biosynthetic pathway. This opens the door to new ways of understanding and developing antibiotics. As drug resistance continues to rise worldwide, new antibiotics like gromomycins are urgently needed to ensure effective treatment options. By mining bacterial genomes, we also found additional gromomycin variants, increasing the potential diversity and strength of this new class of antibiotics. This discovery not only enhances our understanding of triterpene diversity but also paves the way to a number of promising bioactive triterpenes.

2.1.5. Materials and Methods

Bacterial Strains, Plasmids and Culture Conditions

All strains and plasmids used in this work are listed in Supplementary Tables 14 and 15. *Streptomyces* sp. strain Je 1-332 was isolated from the rhizosphere soil of *Juniperus excelsa*.[252] *S. albus* Del14[254] and *S. lividans* Del8[255] were used as hosts for heterologous expression of the gromomycin biosynthetic gene clusters. *E. coli* strains were grown in Luria-Bertani (LB) broth (Sigma-Aldrich, St. Louis, MO, USA). *Streptomycetes* strains were grown on MS agar medium (Soy flour 20 g, Mannitol 20 g, tap water 1 l, pH 7.2 prior autoclaving) and in liquid tryptic soy broth medium (TSB; Sigma-Aldrich, St. Louis, MO, USA). If necessary, the following antibiotics were added: apramycin (50 μg ml^{-1}), hygromycin (120 μg ml^{-1}), chloroamphenicol (12.5 μg ml^{-1}), phosphomycin (100 μg ml^{-1}), thiostrepton (0.5 μg ml^{-1}), kanamycin (50 μg ml^{-1}) and nalidixic acid (50 μg ml^{-1}) (Sigma-Aldrich, St. Louis, MO, USA; Roth, Karlsruhe, Germany). X-gluc (5-bromo-4-chloro-3-indolyl-beta-D-glucuronic acid) (ThermoFisher scientific, Waltham, MA, USA) at a concentration of 50 μg ml^{-1} was used to determine β-glucuronidase activity. For conjugation, the *Streptomycetes* strains were grown on MS agar for sporulation. For gromomycins production, S*treptomyces* strains were grown in liquid DNPM

medium (40 g l^{-1} dextrin, 7.5 g l^{-1} soytone, 5 g l^{-1} baking yeast, and 21 g l^{-1} MOPS, pH 7.2), SG (20 g l^{-1} glucose, 10 g l^{-1} soy peptone, and 2 g l^{-1} $CaCO_3$, pH 7.2), ISP-2 (4 g l^{-1} yeast extract, 10 g l^{-1} malt extract, 4 g l^{-1} dextrose, pH 7.2) and minimal medium (MM). For feeding experiments, a MM was used.

Metabolite Extraction and Analysis

Streptomyces sp. Je 1-332 or *S. albus* strains were cultivated in 25 ml TSB medium for 48 h at 28 °C to obtain a pre-culture. The main cultures containing 100 ml of DNPM, SG or MM were inoculated with 1 ml of pre-culture. After 7 days of cultivation at 28 °C, the gromomycins were extracted with ethyl acetate from the supernatant, followed by solvent evaporation. One µl of sample was separated using a Dionex Ultimate 3000 UPLC (Thermo Fisher Scientific, Waltham, MA, USA), a 10-cm ACQUITY UPLC® BEH C18 column, 1.7 µm (Waters, Milford, MA, USA) and a linear gradient 5% to 95% of 0.1% formic acid (FA) solution in acetonitrile versus 0.1% FA solution in water for 18 min at a flow rate of 0.6 ml min^{-1} and 45 °C. Samples were analyzed using an amaZon speed mass spectrometer or maXis high-resolution LC-QTOF system (Bruker, USA). Data were collected and analyzed with the Bruker Compass Data Analysis software, version 4.2 (Bruker, Billerica, MA, USA).

Isolation and Purification of Gromomycins

For gromomycins production, cultures were grown in 10 L of DNPM or SG medium 7 days at 28 °C with stirring at 180 rpm. Gromomycins were extracted with ethyl acetate from the culture supernatant and with a mixture of methanol acetone at a 1:1 ratio from the biomass. The obtained extracts were dissolved in methanol and used for purification of the gromomycin an Isolera™ One flash purification system (Biotage, Uppsala, Sweden). For this purpose, SNAP Ultra 50 g (Biotage, Uppsala, Sweden) was used as stationary phase and n-hexane (A)/ chloroform (B)/ ethyl acetate (C)/ methanol (D) as mobile phase in a linear gradient A/B 10 column volumes (CV), B/C 15 CV, C/D 15 CV at a flow rate of 100 ml min^{-1}. The fractions containing gromomycins were pooled together, concentrated and used for the Size-Exclusion Chromatography on the Sephadex LH-20 column (Sigma-Aldrich, Louis, MO, USA) with methanol as a mobile phase. Fractions were collected every 10 min at a flow rate of 0.8 ml min^{-1}. The fractions containing gromomycins were pooled together, concentrated and dissolved in methanol. The second purification stage was Reversed Phase (RP) HPLC (Waters AutoPurufication™ System), separation on preparative C18 column Nucleodur HTec, 5 µm, 250 mm x 21 mm (Macherey-Nagel, Germany) using a water solution containing 0.1%(v/v)

formic acid (solvent A), and an acetonitrile solution containing 0.1% (v/v) formic acid (solvent B) as a mobile phase. The following gradient at a flow rate of 20 mL/min was used for compounds separation: 0 min—5% B, 0.5 min—5%, 12 min—65% B, 25 min—65%B, 27 min—95% B, 28 min—95% B, 29 min—5% B, 31 min—5% B. The fractions were collected using MS detector (WatersTM SQ Detector 2). The gromomycin-containing fractions were pooled together, evaporated and used for the last purification step.

The last purification stage was reversed-phase High performance liquid chromatography (HPLC) separation on Agilent 1100 or Thermo Scientific Dionex UltiMate 3000 system with semipreparative C18 column SynergiTM 4 μm Fusion-RP 80 Å 250×10 (Phenomenex, Torrance, CA, USA) using water + 0.1% formic acid (A) and acetonitrile + 0.1% formic acid (B) as a mobile phase. The following gradient at a flow rate of 4 mL/min was used for separation: 0 min – 5% B, 0.5 min – 5%, 10 min – 65%, 12 min – 65%, 15 min – 95%, 17 min – 95% B, 18 min – 5% B. Fractions containing pure compound were pooled together and evaporated.

Sequencing and analysis of *Streptomyces* sp. Je 1-332 genome

Genomic DNA of *Streptomyces* sp. Je 1-332 was isolated from 50 ml culture grown in TSB medium at 28°C on a rotary shaker (180 rpm) for 72 hours. The salting out procedure was used to obtain total DNA, followed by RNAse treatment.[264] The purity and concentration of genomic DNA were determined using 1% agarose gel electrophoresis and a Nanodrop 2000 spectrophotometer (Thermo Fisher Scientific, USA). The Illumina paired-end sequencing library (TruSeq sample preparation kit; Illumina, USA) was created for genome sequencing according to the manufacturer's protocol. The genome sequence of *Streptomyces* sp. Je 1-332 was obtained on the Illumina MiSeq system in rapid run mode (2x250 nt) with a pair spacing of about 500 bp. After sequencing and processing the obtained data, a *de novo* assembly was performed using the SPAdes Assembler program (version 3.8.1) with default settings.[265] Genome annotation was performed using the prokka v1.11 platform and GenDB 2.0.[266-267] AntiSMASH 6.0 was used to identify clusters of secondary metabolites.[250] The assembled and annotated sequence of the *Streptomyces* sp. Je 1-332 was deposited in the GenBank database under accession number NZ_CP160402.1.

Cosmid Library Construction

A cosmid libraries of streptomycetes were prepared using the EpiCentre CopyControl™ Fosmid Library Production Kit in pCos15A_gusA or pCos15A_AmInt vectors by adapting the protocol from Lucigen. A library of 30−40 kb fragments was constructed according to the

manufacturer's protocol using genomic DNA partially digested with MssI. The purified genomic DNA fragments were ligated into linearized pCos15A_gusA or pCos15A_AmInt vectors. The ligation reactions were packaged into λ phage for *E.coli* EPI300 infection. The packaged library was plated on LB agar plates containing 12.5 μg ml^{-1} chloroamphenicol, and grown overnight at 37 °C. Approximately 1800 single colonies were picked and inoculated into individual wells of 96-well plates. This arrayed cosmid library was stored with 20% glycerol and kept at −80 °C.

Transposon mutagenesis in *Streptomyces* sp. Je 1-332

Spores of *Streptomycetes* exconjugants transformed with a pTNM plasmid,[268] that contains Tn5 transposon were scraped from the MS agar plate by sterile MQ water. One ml of the spores transferred in 100 ml Erlenmeyer shake flask containing 20 ml TSB medium with 200 μg ml^{-1} of phosphomycin and 25 μg ml^{-1} of apramycin for a plasmid selection. After 24 hours of cultivation, 0.5 μg ml^{-1} of thiostrepton was added to induce Tn5 through the thiostrepton-induced promoter. After reaching the stationary phase, 1 ml of culture was transferred into a 100 ml Erlenmeyer flask with 20 ml of TSB medium and phosphomycin and incubated at 37 °C, 180 rpm until the stationary phase was reached. This step was repeated twice. After three passages, 1 ml of the transposon mutant's culture was plated on MS agar plate with phosphomycin and an apramycin. The spores were collected, and serial dilutions were made. 1 ml of each dilution, starting from 10^{-6}, was plated on MS agar plate and incubated for 5-7 days at 28 °C. The obtained colonies were selected for plasmid loss testing.

To generate rescue plasmids, genomic DNAs of strains *Streptomyces* sp. Je 1-332 with Tn5 transposon were isolated and digested with SacII restriction enzyme (Thermo Fisher Scientific, Waltham, MA, USA) for overnight at 37°C, then the chromosomal DNA was precipitated with ethanol, dissolved in 16 μl of MQ water and, after 2 μl of ligation buffer and 2 μl of T4-DNA ligase (Thermo Fisher Scientific, Waltham, MA, USA) were added, selfligated overnight at 16 °C. 3, 5 or 7 μl of selfligated DNA was transformed into the *E. coli* TransforMaxTM EC100DTM pir-116 electrocompetent cells and plated on selective LB medium. The rescue plasmids were isolated and sequenced by GATC-Biotech or by Genewiz using the sequencing primers pMODseq-f and pMODseq-r (Supplementary Table 16).

Genes deletion in *Streptomyces* sp. Je 1-332

Red/ET recombination was used to delete the desired genes in the genome of *Streptomyces* Je 1-332 strain. A linear DNA fragment containing the apramycin resistance and origin of transfer (*oriT*) flanked by suitable homology arms was generated by PCR using specific primers. The

primers used for the deletions are listed in the Supplementary Table 16. PCR was carried out with Dream Taq DNA polymerase (Thermo Fisher Scientific, Waltham, MA, USA), according to the manufacturer's protocol. The respective cosmids containing the appropriate gene for deletion were transformed together with the amplified cassette into the *E. coli* GB05-red strain. Transformants were selected for resistance to apramycin and chloramphenicol. Correct transformants were verified by the restriction analysis and sequencing of the isolated cosmid DNA using the specific primers.

The cosmids with gene deletion was transferred from *E. coli* ET12567 pUB307 cells into *Streptomyces* sp. Je 1-332 cells by means of conjugation.[264] Transconjugants were selected for resistance to apramycin and glucuronidase activity. For the generation of the *Streptomyces* sp. Je 1-332 deletion mutants, single-crossover apramycin and blue mutants were screened for the loss of glucuronidase activity (blue pigmentation) as the result of a double-crossover event. The replacement of the genes was confirmed by PCR using the specific primer pair (Table S16).

Heterologous expression of gromomycin gene cluster and systematic gene deletion

The constructs used in this study for gene disruption and heterologous expression are summarized in the Supplementary Table 15. The constructs were introduced into *S. albus* Del14 and *S. lividans* Del8 by conjugation using donor strain E. coli ET12657/pUB307 on MS plates. After incubating at 30°C for 16 hours, exconjugants were selected with 50 μg ml^{-1} apramycin and and 30 μg ml^{-1} nalidixic acid. Single colonies from this plate were patched onto MS plates 50 μg ml^{-1} apramycin. Candidate colonies were used for further identification by PCR analysis.

The antibiotic cassette apramycin together with *oriT* and integrase genes were amplified by PCR with primers OTC60 and OTC61 using pCos15A_gus_AmInt plasmid as template. Utilizing PCR-based λ-red recombination technique, the amplified cassettes was integrated into cosmid P04_E01 forming pHSU-STS10. pHSU-STS10 was subsequently introduced into *S. albus* Del14 by conjugation and was selected for apramycin resistance. The cluster integration was confirmed by PCR using primers STS40 and STS41, and the resulting strain is named *S. albus* STS10.

To define the minimal gene cluster of gromomycin, a systematic genes deletion was conducted from the downstream and upstream of the pHSU-STS10. In general, the genes that were intended to be deleted were initially replaced by ampicillin resistance (amp^R) cassette using RedET recombination. For the construction of the pHSU-STS22, pHSU-STS23, pHSU-STS24, pHSU-STS25, pHSU-STS29 and pHSU-STS30 the amp^R cassette was amplified with the pairs of primers STS51 and STS52, STS47 and STS49, STS48 and STS49, STS50 and STS49, STS51 and STS72, respectively. For the construction of the pHSU-STS31, pHSU-

STS32 and pHSU-STS33 the *amp*^{R} cassette was amplified with the pairs of primers STS67 and STS68, STS69 and STS68, STS70 and STS68, respectively. Subsequently, the *amp*^{R} was removed by digestion using PmeI or SnaBI and religated to generate appropriate constructs. STS40 and STS41 primers were used to test for mutant integration by PCR.

To determine the role of the genes in the identified gromomycin gene cluster, a series of gene inactivations were performed using the pHSU-STS33 vector. The derivatives of pHSU-STS33 with gene deletions were constructed using the RedET approach. For this, the antibiotic resistance marker was amplified by PCR with primers harbouring overhang regions complementary to the boundaries of the DNA to be deleted. The amplified fragment was used for recombineering of the pHSU-STS33. The recombinant BACs were analysed by PCR. The primers used for recombineering purposes are listed in Supplementary Table 16. For the construction of the pHSU-STS33_KOgroA, pHSU-STS33_KOgroB, pHSU-STS33_KOgroC, pHSU-STS33_KOgroD, pHSU-STS33_KOgroE, pHSU-STS33_KOgroF, pHSU-STS33_KOgroG, pHSU-STS33_KOgroH and pHSU-STS33_KOgroI, the hygromycin marker from phygattB[254] was amplified with the primers KO_groA_F/KO_groA_R, KO_groB_F/KO_groB_R, KO_groC_F/KO_groC_R, KO_groD_F/KO_groD_R, KO_groE_F/KO_groE_R, KO_groF_F/KO_groF_R, KO_groG_F/KO_groG_R, KO_groH_F/KO_groH_R and KO_groI_F/KO_groI_R, respectively. Next, the antibiotic resistance gene was excised with the AscI restriction enzyme to yield marker-free mutants. The marker excision was verified using the appropriate primers listed in Supplementary **Table 16**.

Feeding experiment with labeled L-arginine for LC-MS analysis

Feeding experiments for LC-MS analysis were performed using 1 mM of L-[$^{13}C_6$, $^{15}N_4$]-Arg (Sigma-Aldrich) and L-[$^{15}N_4$]-Arg (Sigma-Aldrich) in 100 mL liquid culture. Precursors were dissolved in 1 ml MQ H_2O and added to the culture in 4 portions (53.65 µl) at 24, 48, 72 and 96 h after inoculation of preculture. Supernatant was separated from culture biomass by centrifugation and extracted with ethyl acetate. Solvent was removed under vacuo, resuspended in 500 µl methanol and resulting crude extract was analyzed by LC-MS.

Feeding experiments with ^{13}C-labeled pyruvates

Feeding experiments were performed using 10mM of [2-^{13}C]-, [3-^{13}C] sodium pyruvate (Sigma-Aldrich) in total of 3 l liquid culture. In all cases, 3.3 g precursors were dissolved in 14 mL sterile water. A 100 µl aliquot was fed to 100 ml growing culture (total 30 flasks) at 24, 48, 72 and 96 h after inoculation. The fermentation continued for six days, and the culture was

extracted as described above. Purification of carbon enriched gromomycin was performed as described above. ^{13}C-NMR data of individual compounds have been acquired.

Genome-quided Identification of new gromomycins

Three genes involved in the biosynthesis of gromomycins were used for genome-wide quantitative screening of new gromomycins: gene 5 (*groD*), gene 7 (*groF*) and gene 9 (*groH*). The nucleotide sequences of these genes were used as probes in the NCBI protein BLAST database to identify new gromomycin-like clusters.[269] The strains with all three of these genes identified in the genome were selected. In this way, several actinomycetes strains were identified, including *S. flavoviridis* strain ISP-5153 (GenBank accession number ASM1464951v1). The new gromomycin-like cluster was isolated from the genome of the *S. flavoviridis* ISP-5153 strain through the cosmid library construction according to the manual (CopyControl™ Fosmid Library Production Kit). Cosmid P03_G02 containing the whole gromomycin-like cluster was identified by pool PCR with two pairs of primers (Left_flavoridis_F/ Left_flavoridis_R and Right_flavoridis_F/ Right_flavoridis_R) designed to amplify regions to the left or right side of the cluster. The P03_G02 cosmid was transferred to *S. albus* Del14 and *S. lividans* Del8 strains for heterologous expansion. The ability of heterologous strains to produce gromomycin was determined by HPLC.

Antibiotic activity (minimum inhibitory concentrations)

Gromomycin stock solutions were prepared in dimethyl sulfoxide (DMSO). All microorganisms used in this study were obtained from the German Collection of Microorganisms and Cell Cultures (DSMZ), the American Type Culture Collection (ATCC), the Coli Genetic Stock Center, or were part of our internal strain collection. *Staphylococcus aureus* strains Newman, N315, Mu50 and Cowan 1 were obtained from M. Bischoff, Saarland University Hospital, Homburg. *S. aureus* wild type and Dap^R HG001[270] were provided by T. Schneider, University of Bonn. *E. coli* WO153 was provided by K. Lewis, Northeastern University, Boston, USA. Minimum inhibitory concentrations (MICs) were determined using the broth microdilution method according to EUCAST guidelines (ISO 20776-1:2019). In short, serial two-fold dilutions of gromomycins (0.03125 to 64 μg/mL) were prepared in 75 μL of cation-adjusted Mueller-Hinton broth (MHB2) in sterile 96-well plates. Equal volume of the bacterial suspension was added and the plates were incubated at 37 °C for 18 h. For *Streptococcus pneumoniae*, MHF broth (MHB2 supplemented with 5% lysed horse blood and 20 mg/L β-NAD) was used and plates were incubated at 37 °C with 5% CO_2. The MIC was defined as the lowest concentration of the antibiotic causing complete inhibition of visible

growth of the microorganism. The same method was used for testing *Mycobacterium smegmatis*, but with the use of Middlebrook 7H9 complete medium supplemented with oleic acid, albumin, dextrose and catalase (OADC, 10%). *M. smegmatis* plates were incubated for 48 h at 37 °C. For assessing activity against *Mycobacterium tuberculosis*, an adapted resazurin microtitre assay (REMA) was performed as previously described.[271] In short, *M. tuberculosis* single cells were prepared and added to compound dilutions in M7H9. Plates were incubated for 6 d at 37 °C, followed by addition of 50 µL of resazurin and incubation for another day at 37 °C. The MIC was determined visually and additionally confirmed by measuring fluorescence (excitation at 530 nm, emission at 590 nm).

Cytotoxic activity (IC50)

HepG2 cells (human hepatoblastoma cell line; ACC 180) and CHO-K1 (chinese hamster ovary cells; ACC 110) were obtained from the German Collection of Microorganisms and Cell Cultures (DSMZ) and cultured under the conditions recommended by the depositor. Cells were propagated in Roswell Park Memorial Institute (RPMI) 1640 medium and Ham's F12 medium, respectively, supplemented with 10% fetal bovine serum (FBS), and seeded at 6×10^3 cells per well of 96-well plates in 120 µL of complete medium. After 2 h of equilibration (37 °C, 5% CO_2), the cells were treated with a serial dilution of gromomycins. Gromomycins, doxorubicin as reference, as well as the solvent control (DMSO) were tested as duplicates in two independent experiments. After 5 d of incubation (37 °C, 5% CO_2), a total of 20 µL of 5 mg/ml MTT (thiazolyl blue tetrazolium bromide) in phosphate-buffered saline (PBS) were added to each well and the cells were further incubated for 2 h at 37 °C before the supernatant was discarded. Subsequently, the cells were washed with 100 µL of PBS and treated with 100 µl of 2-propanol/10 N HCl (250:1) to dissolve formazan granules. Cell viability was measured as a percentage relative to the respective solvent control by measuring the absorbance at 570 nm using a microplate reader (Tecan Infinite M200Pro). GraphPad Prism (version 10.0.3, GraphPad, Boston, MA, USA) was used for sigmoidal curve fitting to determine the IC_{50} values.

Maximum tolerated concentration

Husbandry of adult zebrafish was performed according to internal guidelines set out in the German Animal Welfare Act (§11 Abs. 1 TierSchG). Experiments were carried out with wild type AB (obtained from the European Zebrafish Resource Center at Karlsruhe Institute of Technology) embryos within the first 120 hours post fertilization (hpf) as these early life stages are not considered as animal experiments according to the EU Directive 2010/63/EU.[272] Embryos were maintained in fresh 0.3x Danieau's (17.4 mM NaCl, 0.21 mM KCl, 0.12 mM

$MgSO_4$, 0.18 mM $Ca(NO_3)_2$, 1.5 mM HEPES, 1.2 µM methylene blue, pH 7.1-7.3) at 28 °C. At a maximum of 120 hpf, embryos were euthanized by submersion in ice water for at least 12 h.

For evaluation of the maximum tolerated concentration (MTC), embryos were dechorionated at 30 hpf using 1 mg/mL pronase and placed in a flat-bottom 96-well plate with one embryo per well. Excess medium was removed and 150 µL of gromomycin dilutions (in 0.3x Danieau's, maximum of 1% DMSO) and of the solvent control (1% DMSO in 0.3x Danieau's) were added. Ten embryos were used per condition. Exposed embryos were maintained at 28 °C until 120 hpf and they were monitored daily under a stereo microscope (Stemi 508, Zeiss) in order to record survival as well as anomalies, pigmentation, heartbeat and locomotor responses. An embryo was considered dead when no heartbeat could be observed. The maximum tolerated concentration (MTC) was defined as the highest concentration of the antibiotic with more than 90% survival of zebrafish embryos. Kaplan-Meier curves were generated using GraphPad Prism (version 10.0.3, GraphPad, Boston, MA, USA).

2.1.6. Supplementary Information for Chapter 2.1

Gromomycins: An Unprecedented Class of Triterpene Antibiotics Exhibiting Biosynthetic Uniqueness

Structure elucidation

General

Chiroptical measurements ($[\alpha]_D^{20}$) were obtained on a Perkin Elmer (Model 341) polarimeter in a 100 × 2mm cell at 20°C. NMR spectra were obtained for Gromomycin A on a Bruker AVANCE III 700 MHz spectrometer equipped with a helium cooled cryoprobe and for all the other compounds on a Bruker AVANCE NEO 500 spectrometer equipped with a nitrogen cooled cryoprobe system (Bruker Biospin GmbH, Germany), in the solvents indicated and referenced to residual ^{1}H signals in deuterated solvents.

Isolated compounds and their analytical data

Gromomycin A (**2**) (3*S*, 4*S*, 6*S*, 7*S*, 10*R*, 11*S*, 19*R*) white powder, $[\alpha]_D^{20}$ +9° (c 0.20, MeOH). For NMR see Table S1 (700 MHz, CD3OD) and S2 (700 MHz, DMSO-d_6). HRESIMS *m/z* 478.3804 $[M+H]^+$, (calcd for $C_{31}H_{48}N_3O$, 478.3792).

Gromomycin B (**3**) (3*S*, 4*S*, 6*S*, 7*S*, 10*R*, 11*S*, 14*S*, 19*R*) white powder, $[\alpha]_D^{20}$ -28° (c 0.20, MeOH). For NMR see Table S3 (500 MHz, CD_3OD). HRESIMS *m/z* 494.3752 $[M+H]^+$, (calcd for $C_{31}H_{48}N_3O_2$, 494.3741).

Gromomycin C (**4**) (3*S*, 4*S*, 6*S*, 7*S*, 10*R*, 11*S*, 14*S*, 19*R*) white powder, $[\alpha]_D^{20}$ -14° (c 0.64, MeOH). For NMR see Table S4 (500 MHz, DMSO-d_6). HRESIMS *m/z* 480.3953 $[M+H]^+$, (calcd for $C_{31}H_{50}N_3O$, 480.3948).

Gromomycin D (**5**) (3*S*, 4*S*, 6*S*, 7*S*, 10*R*, 11*S*, 19*R*) white powder, $[\alpha]_D^{20}$ -23° (c 0.11, MeOH). For NMR see Table S5 (500 MHz, CD_3OD). HRESIMS *m/z* 494.3751 $[M+H]^+$, (calcd for $C_{31}H_{48}N_3O_2$, 494.3741).

Gromomycin E (**6**) (3*S*, 4*S*, 6*S*, 7*S*, 10*R*, 11*S*, 19*R*, 22*R*) white powder, $[\alpha]_D^{20}$ -1° (c 0.27, MeOH). For NMR see Table S6 (500 MHz, CD_3OD). HRESIMS *m/z* 492.3950 $[M+H]^+$, (calcd for $C_{32}H_{50}N_3O$, 492.3948).

Gromomycin F (**7**) (3*S*, 4*S*, 6*S*, 7*S*, 10*R*, 11*S*, 14*S*, 19*R*, 22*R*) white powder, $[\alpha]_D^{20}$ -39° (c 0.16, MeOH). For NMR see Table S7 (500 MHz, CD_3OD). HRESIMS *m/z* 508.3895 $[M+H]^+$, (calcd for $C_{32}H_{50}N_3O_2$, 508.3898).

Gromomycin G (**8**) (3*S*, 4*S*, 6*S*, 7*S*, 10*R*, 11*S*, 14*S*, 19*R*, 22*R*) white powder, $[\alpha]_D^{20}$ 0°(c 0.20, MeOH) . For NMR see Table S8 (500 MHz, CD_3OD). HRESIMS *m/z* 494.4105 $[M+H]^+$, (calcd for $C_{32}H_{52}N_3O$, 494.4105).

Gromomycin H (**9**) (3*S*, 4*S*, 6*S*, 7*S*, 10*R*, 11*S*, 19*R*, 22*R*) white powder, $[\alpha]_D^{20}$ -13° (c 0.21, MeOH). For NMR see Table S9 (500 MHz, CD_3OD). HRESIMS *m/z* 508.3899 $[M+H]^+$, (calcd for $C_{32}H_{50}N_3O_2$, 508.3898).

Hexaprenylguanidine (**10**): 1-((2*E*, 6*E*, 10*E*, 14*E* ,18*E*) - 3, 7, 11, 15, 19, 23 - hexamethyltetra-cosa-2,6,10,14,18,22-hexaen-1-yl) guanidine. White powder. For NMR see Table S10 (500 MHz, DMSO-d_6). HRESIMS *m/z* 468.4355 $[M+H]^+$, (calcd for $C_{31}H_{54}N_3$, 468.4318).

Mosher Analysis of Gromomycin B

The absolute stereochemistry was determined according to Mosher et al.[273] In brief, two glass vials with 500 µg dried Gromomycin B in 100 µL dry CDCl3, 10 µL dry pyridine and 10 µL *R*-MTPA-Cl or *S*-MTPA-Cl, respectively, were prepared. The vials were flushed with nitrogen, closed airtight and were incubated with occasional shaking at room temperature while the reaction progress was monitored by LC-MS analysis by a Bruker Amazon Ion trap. Full conversion to the Mosher conjugate (*m/z* 710.44, **Figure below**) was observed after 45 min. Subsequently, the samples were dried, dissolved in methanol and purified by HPLC using an Agilent 1100 system equipped with a Phenomenex Synergi C18 column and a 15 min gradient of 40-95% acetonitrile/water containing 0.1% formic acid. The purified samples were dissolved in CD_3OD and NMR spectroscopy was performed.

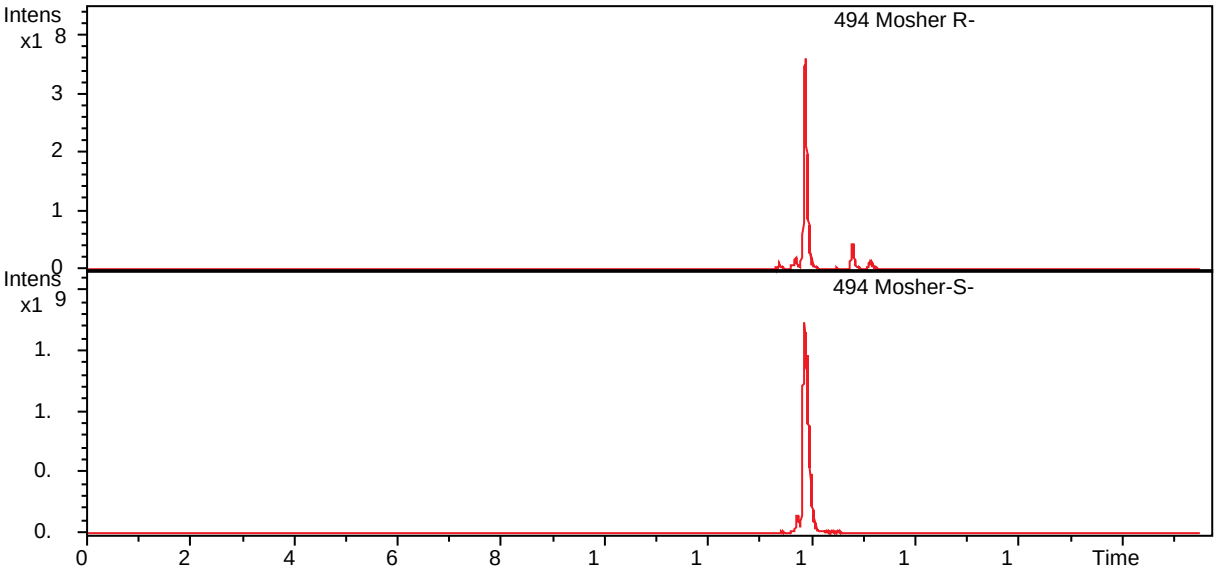

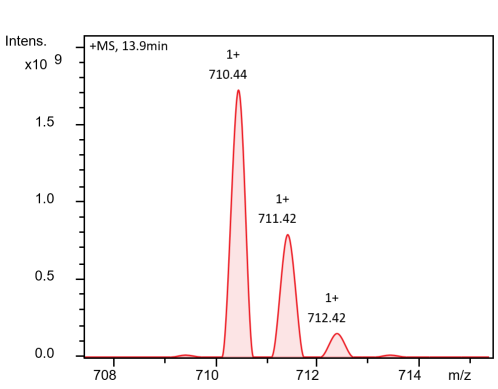

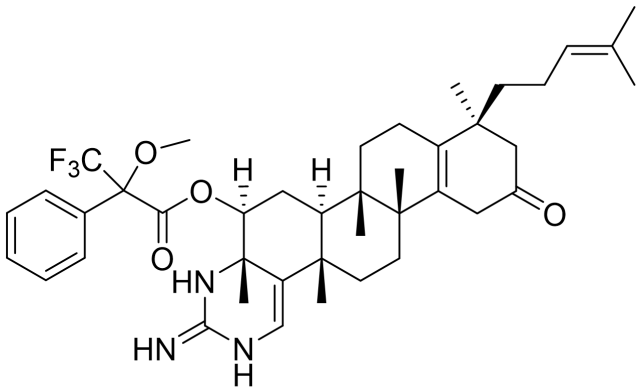

Structure of the Mosher conjugate (m/z 710.44).

Isotopic enrichment of 13C-labelled gromomycin B

Distribution of the isotopic label was determined by comparing ^{13}C NMR spectra of the enriched and natural abundance gromomycin B. All compounds were recorded under identical experimental conditions (zgpr pulse program from Bruker pulse library with D1=3) corresponding to identical nuclear Overhauser effects and relaxation times for both measurements. As it was impossible to work with identical concentrations for the unlabelled reference and the biosynthetically labelled compounds, the spectra were normalized with reference to the signal of DMSO-d_6 as internal standard.

List of Tables

Table S1. NMR Data for Gromomycin A (**2**) in CD_3OD.

Nr.	δ_C	δ_H (*J* in Hz)	HHCOSY	HMBC (C→H)	NOESY Key Correlations
1	116.07 CH	5.85 br s			8ab,
2	132.32 C			1, 25, 26	
3	59.74 C			1, 4, 5ab, 25	
4	79.78 CH	3.66 dd (*12, 4.5*)	5ab, 6	5ab, 6, 25	
5	29.15 CH_2	a: 1.73 dd* (*12, 4.5*)	4, 6	4, 6	
6	41.55 CH	1.67 d (*12*)	5ab	4, 5ab, 12ab, 26, 27, 28	
7	38.54 CH			26	
8	35.14 CH_2	a: 1.45 m	8b, 9ab	9ab	
9	29.02 CH_2	a: 1.77 m	9b, 8ab	8ab, 27	
10	41.56 C			27, 28	
11	38.11 C			6, 13a, 7, 27, 28	
12	31.15 CH_2	a: 1.60 m	12b,13ab	6, 13ab, 28	
13	22.89 CH_2	a: 2.04 dd (*19.0, 5.5*)	13b,12ab, 18a	12ab,	
14	137.80 C			12a, 13a, 16, 17, 18ab, 20ab, 29	
15	133.81 C			9b, 13ab, 17, 27	
16	124.69 CH	5.99 d (*9.5*)	17, 18ab	18b	9a, 17, 27
17	125.34 CH	5.75 dt (*9.5, 4.5*)	16, 18ab	18b	16, 18ab
18	36.25 CH_2	a: 2.20 dt (*17.0, 3.0*)	13ab, 16,17, 18b	17, 20ab, 29	17, 20ab, 29
19	38.57 C			18b, 29	
20	39.91 CH_2	a: 1.44 m	21ab, 22	18b, 29	18
21	25.28 CH_2	a: 1.99 m	20ab, 22	20ab	
22	126.39 CH	4.99 tsept (*6.0, 1.2*)	20ab, 21ab, 24, 30	20ab, 24, 30	20ab, 21ab, 24

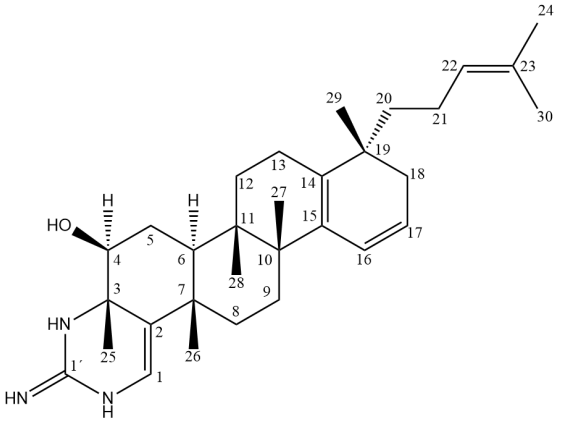

23	131.95	C			24, 30	
24	25.92	CH_3	1.64 s (3H)	20ab, 21ab, 22, 24	30	22, 30
25	23.73	CH_3	1.39 s (3H)		1, 4	5b, 26,
26	24.91	CH_3	1.20 s (3H)		1, 6	5b, 8a, 25, 28
27	24.70	CH_3	0.92 s (3H)			9a, 13a, 28
28	20.68	CH_3	0.88 s (3H)		6, 12a	5b, 2ab, 26, 27
29	24.32	CH_3	0.90 s (3H)		18b, 20ab	18, 26
30	17.90	CH_3	1.54 s (3H)	20ab, 21ab, 22, 30	24	24
1′	152.53	C	------			

*Coupling pattern taken from selective 1D TOCSY (fig S7)

Table S2. NMR Data for Gromomycin A (**2**) in DMSO-d6 + 1 drop TFA.

Nr.	δ_C	δ_H (*J* in Hz)	HHCOSY	HMBC (C→H)	NOESY Key Correlations
1	115.07 CH	5.86 d (*5.0*)	N_1-H		8ab, NHa
2	130.11 C			1, 25, 26, N_1-H, N_2-H	
3	57.86 C			1, 4, 5ab, 25, N_2-H	
4	78.05 CH	3.50 m	5ab	5ab, 6, 25	6, OH
5	28.00 CH_2	a: 1.60 m	4,6	4, 6	
6	40.07 CH	1.48 m	5a	4, 5ab, 12ab, 26	4
7	37.09 C			1, 5ab, 26	
8	33.87 CH_2	a: 1.39 m	8b, 9ab	6, 9ab, 26	1
9	27.71 CH_2	a: 1.67 m	9b, 8ab	8a, 27, 28	16
10	40.22 C			16, 27, 28	
11	36.67 C			6, 9a, 12b, 13b, 27,28	
12	29.92 CH_2	a: 1.49 m	12b, 13ab	13ab, 28	
13	21.58 CH_2	a: 1.98 dd (*19.0, 6.0*)	13b, 12ab	12ab, 28	
14	136.33 C			12ab, 13ab,16, 17, 18ab, 29	
15	132.20 C			9b, 13ab, 17, 27	
16	123.70 CH	5.96 d (*10.0*)	17, 18ab	13a, 18ab	9a, 17, 27
17	124.10 CH	5.71 dt (*10.0, 4.5*)	16, 18ab	18ab	16, 18ab
18	34.87 CH_2	a: 2.12 dt (*17.0, 2.5*)	16,17	16, 17, 20ab, 29	17,
19	37.27 C			13b, 17, 21b, 29	
20	38.53 CH_2	a: 1.37 m	21ab	18a, 21ab, 22, 29	
21	23.77 CH_2	a: 1.90 m	20ab, 22	20ab, 29	
22	125.30 CH	4.95 tsept (*6.5, 1.2*)	21ab, 24, 30	20ab, 21ab, 24, 30	24
23	130.72 C			21, 24, 30	
24	25.55 CH_3	1.60 s (3H)	22	22, 30	22, 30
25	23.42 CH_3	1.26 s (3H)		4	5b, 26
26	24.19 CH_3	1.10 s (3H)		6	5b, 25, 28
27	24.26 CH_3	0.86 s (3H)			
28	20.14 CH_3	0.80 s (3H)		6, 12a	5b, 26

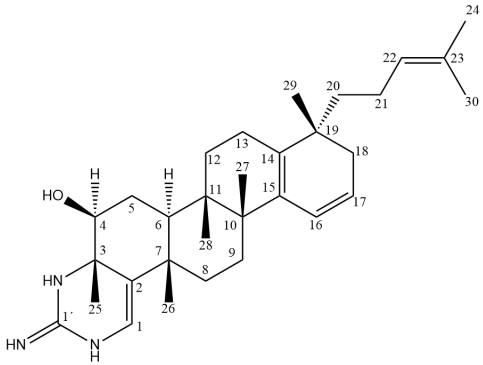

29	23.79	CH_3	0.85 s (3H)			
30	17.55	CH_3	1.48 s (3H)	22	22, 24	24
1′	150.88	C			1	
OH			5.43 d (*5.0*)			4

Nr.	δ_N	δ_H (*J* in Hz)	^{15}N-HMBC (N→H)	NOESY Key Correlations
N_1	96.2*	9.15 dd (*5.0, 2.0*)	1, N_2-H,	1
N_2	101.7*	7.92 d (*2.0*)	25	
N_3	72.6*	7.04 s (2H)		

* taken from the ^{1}H-^{15}N HSQC

Table S3. NMR Data for Gromomycin B (**3**) in CD_3OD.

Nr.	δ_C	δ_H (*J* in Hz)	HHCOSY	HMBC (C→H)	NOESY Key Correlations
1	116.52 CH	5.89 s			8ab
2	131.98 C			1, 25, 26	
3	59.71 C			1, 4, 25	
4	79.54 CH	3.70 dd (*11.8, 4.5*)	5ab	5b, 6, 25	6
5	29.32 CH_2	a: 1.86 m	4, 6	6	
6	47.70 CH	1.39 m	5ab	12b, 26, 28	4, 14
7	38.68 C			1, 6, 26, 27, 28	
8	35.16 CH_2	a: 1.57 m	8b, 9ab	26	
9	33.10 CH_2	a: 1.99 m	9b, 8ab	27	
10	45.98 C			27, 28	
11	38.68 C			6, 26, 27, 28	
12	33.50 CH_2	a: 1.75 m	12b, 13ab	28	
13	19.50 CH_2	a: 1.72 m	12ab, 14		
14	43.74 CH	2.84 td (*8.5, 2.5*)	13ab	12a, 13a, 18b, 29	6, 13a, 18a
15	176.67 C			27	
16	126.77 CH	6.15 d (*2.5*)	14, 18b	18b	9b, 27
17	202.84 C			16, 18ab	
18	50.58 CH_2	a: 2.54 d (16.3)	18b, 29	29	14, 18b
19	42.57 C			18ab, 29	
20	41.07 CH_2	a: 1.49 m	21ab	18a, 29	
21	23.57 CH_3	a: 2.01 m	22, 20ab		
22	125.44 CH	5.11 t (7.3)	21ab, 24, 30	24, 30	24
23	132.47 C			24, 30	
24	17.81 CH_3	1.61 s (3H)		30	22
25	23.66 CH_3	1.41 s (3H)			26
26	25.01 CH_3	1.24 s (3H)			5b, 25; 28
27	28.18 CH_3	1.14 s (3H)		28	28
28	21.95 CH_3	0.94 s (3H)		6	5b, 21a, 26, 27, 29
29	19.23 CH_3	0.82 s (3H)	18a	18a	12a, 13b, 18b, 20b, 28
30	25.89 CH_3	1.67 s (3H)		24	
1′	152.5 C			1	

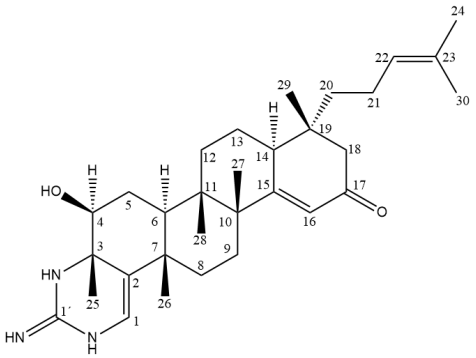

Table S4. NMR Data for Gromomycin C (**4**) in DMSO-d_6.

Nr.	δ_C	δ_H (*J* in Hz)	HHCOSY	HMBC (C→H)	NOESY Key Correlations
1	115.34 CH	5.82 s			8ab
2	129.87 C			1, 6. 25, 26	
3	57.66 C			1, 4, 5ab, 25	
4	78.03 CH	3.55 dd (*11.0, 4.3*)	5ab, 6	5ab, 6, 25	6
5	27.85 CH_2	a: 1.61 m	4, 6	4, 6	
6	45.34 CH	1.37 m	4, 5ab	4, 5ab, 8a, 12ab, 26, 28	4
7	36.94 C			1, 5ab, 26	
8	33.58 CH_2	a: 1.43 m	8b, 9ab	6,, 9ab, 26	
9	32.59 CH_2	a: 1.73 m	9b, 8ab	27	
10	42.04 C			8a, 9b, 12ab, 16, 27, 28	
11	37.26 C			27,28	
12	32.13 CH_2	a: 1.54 m	12b, 13ab	13ab, 28	
13	18.76 CH_2	a: 1.45 m	12ab, 14	12ab, 28	
14	40.02 CH	2.25 m	13ab	12a, 13a, 16, 18b, 20ab	6, 20ab, 21ab
15	143.48 C			9ab, 13a, 17, 27	
16	120.27 CH	5.60 q (*2.5*)	13ab, 14, 17ab	14, 17, 18ab	9ab,17ab, 27
17	22.98 CH_2	2.04 m (2H)	14, 18ab	16, 18ab	
18	32.77 CH_2	a: 1.39 m	17ab	16, 17ab, 20ab, 29	
19	34.80 C			13b, 20ab, 21ab, 29	
20	40.61 CH_2	1.22 m (2H)	21ab	21, 22, 29	
21	21.72 CH_2	1.85 q (*7.5*, 2H)	20ab, 22		
22	125.10 CH	5.07 t (*7.5*)	21ab, 24, 30	20ab 21ab, 24, 30	24, 21ab
23	130.21 C			21ab, 24, 30	
24	17.44 CH_3	1.53 br s (3H)	22, 30	22,30	21ab, 30
25	23.31 CH_3	1.25 s (3H)		1, 4	5b, 26,
26	24.36 CH_3	1.10 s (3H)		1, 6	5b, 8a, 9a, 25, 28
27	21.64 CH_3	0.76 s (3H)		9ab, 16	12ab, 28,
28	29.14 CH_3	0.96 s (3H)			5b, 9ab, 26, 27

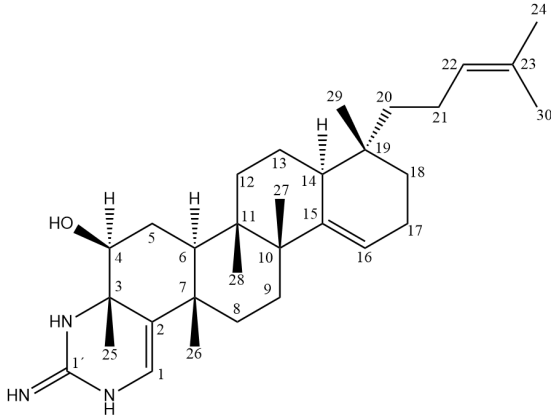

29	18.04	CH_3	0.68 s (3H)	14, 18ab	13ab, 20ab, 18b, 21ab
30	25.50	CH_3	1.62 br s (3H)	22, 24	24
1′	151.71*	C		1	
OH			5.47 br s		
N_1-H			11.30 br s		
N_2-H			8.74 br s		
N_3-H			8.06 br s		

* taken from the ^{1}H-^{13}C HMBC

Table S5. NMR Data for Gromomycin D (**5**) in CD_3OD.

Nr.	δ_C		δ_H (*J* in Hz)	HHCOSY	HMBC (C→H)
1	116.25	CH	5.91 s		
2	132.15	C			1, 25, 26
3	59.73	C			1, 4, 5a, 25
4	79.65	CH	3.68 m	5ab	5ab, 25
5	29.01	CH_2	a: 1.76 m	4	4, 6
6	41.94	CH	1.64 m		5ab, 26, 28
7	38.33	C			1, 8a, 9a, 26
8	35.58	CH_2	a: 1.59 m		26
9	28.33	CH_2	a: 1.69 m		27
10	42.94	C			6, 8a, 12ab, 27, 28
11	38.64	C			27, 28
12	30.85	CH_2	a: 1.65 m		28
13	23.18	CH_2	a: 2.09 m		
14	137.10	C			12a, 18ab, 20b, 29
15	133.23	C			18b, 27
16	41.14	CH_2	a: 2.94 dd (*20.0*, *2.5*)	13a, 16ab, 18a	18ab
17	214.05	C			18ab
18	52.00	CH_2	a: 2.63 d (*13.5*)	16a, 18b,	29
19	44.60	C			18ab, 29
20	41.32	CH_2	a: 1.58 m	20b, 21ab	18ab, 29
21	25.22	CH_2	a: 1.98 m	20ab, 21b	
22	125.35	CH	4.99 t (*6.0*)	21ab, 24, 30	20b, 21a, 24, 30
23	132.76	C			24, 30
24	17.98	CH_3	1.54 s (3H)		22, 30
25	23.72	CH_3	1.40 s (3H)		4
26	24.97	CH_3	1.22 s (3H)		
27	23.72	CH_3	0.95 s (3H)		
28	20.94	CH_3	0.90 s (3H)		6
29	27.52	CH_3	1.00 s (3H)		18ab
30	25.87	CH_3	1.64 s (3H)		22
1′	152.50	C			1

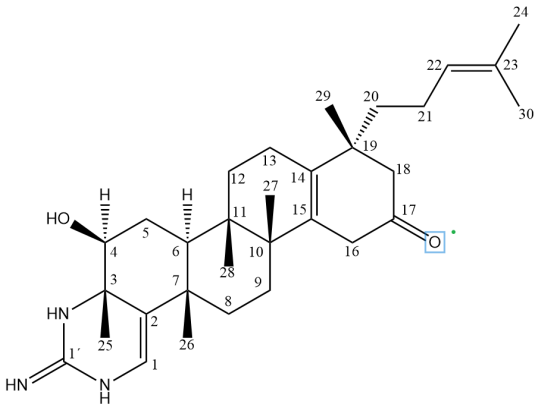

Table S6. NMR Data for Gromomycin E (**6**) in CD_3OD.

Nr.	δ_C		δ_H (*J* in Hz)	HHCOSY	HMBC (C→H)
1	116.18	CH	5.85 s		
2	132.30	C			1, 6, 25,26
3	59.78	C			1, 4, 5ab, 25
4	79.72	CH	3.71 dd (*11.0, 4.5*)	5ab	5ab, 6, 25
5	29.16	CH_2	a: 1.74 m	4	4, 6
6	41.77	CH	1.63 m		26, 28
7	38.57	C			1, 26
8	35.26	CH_2	a: 1.47 m	8b, 9ab	
9	29.01	CH_2	a: 1.73 m	9b, 8ab	6, 27
10	41.66	C			8b, 9ab, 27, 28
11	38.12	C			27
12	31.26	CH_2	a: 1.61 m	12b, 13ab	
13	22.59	CH_2	a: 2.04 m	13b, 12b	12ab
14	138.00	C			12a, 13ab, 16, 17, 18ab, 29
15	133.60	C			13ab, 16, 17, 18ab, 27
16	124.76	CH	5.99 d (*9.5*)	17, 18ab	18ab
17	125.32	CH	5.73 dt (*9.5, 4.5*)	16, 18ab	18ab
18	35.75	CH_2	a: 2.21 dd (*17.0, 5.0*)	16, 17, 18b,	16, 17, 20ab
19	38.23	C	--------		18ab
20	37.35	CH_2	a: 1.38 m		18b, 21ab, 22
21	31.89	CH_2	a: 1.38 m	22	20ab, 22, 31
22	43.58	CH	2.01 m	21ab, 31	21ab, 24ab, 30, 31
23	150.97	C			22, 24ab, 30, 31
24	110.20	CH_2	4.63 s	24b	22, 30
25	23.96	CH_3	1.40 s (3H)		3
26	24.91	CH_3	1.20 s (3H)		6
27	24.82	CH_3	0.91 s (3H)		
28	20.75	CH_3	0.87 s (3H)		
29	20.75	CH_3	0.87 s (3H)		
30	18.98	CH_3	1.59 s (3H)		24ab
31	20.47	CH_3	0.98 d (7.0, 3H)	22	21ab, 22
1′	152.57	C			1

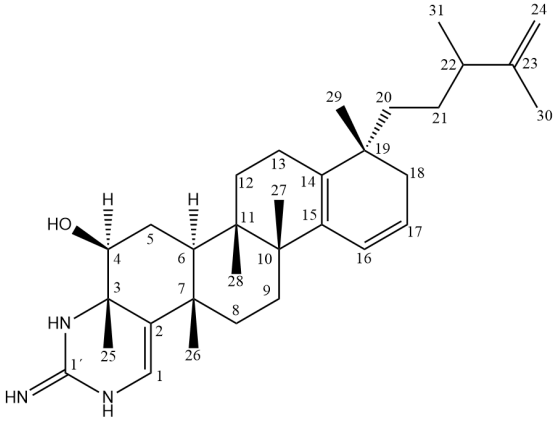

Table S7. NMR Data for Gromomycin F (**7**) in CD_3OD.

Nr.	δ_C		δ_H (*J* in Hz)	HHCOSY	HMBC (C→H)	NOESY Key Correlations
1	116.58	CH	5.89 s			8ab
2	131.93	C			1, 25, 26	
3	59.73	C			1, 4, 5a, 25	
4	79.60	CH	3.70 dd (*12.0, 4.3*)	5ab	5ab, 6, 25	6
5	29.32	CH_2	a: 1.86 m	4, 6	6	
6	47.76	CH	1.39 m	5ab	12b, 26, 28	4, 5a, 14, 26
7	38.71	C			1, 6, 26, 27, 28	
8	35.15	CH_2	a: 1.56 m	8b, 9ab	26	
9	33.08	CH_2	a: 1.97 m	9b, 8ab	27	
10	45.97	C			12a, 16, 27, 28	
11	38.70	C			6, 26, 27, 28	
12	33.54	CH_2	a: 1.75 m	12b, 13ab	13ab, 28	
13	19.50	CH_2	a: 1.68 m	12ab, 13b, 14		13b, 20a, 21b
14	44.13	CH	2.81 td (*8.5, 2.7*)	13ab, 14	12ab, 13ab, 16,18b, 29	6, 13a, 18a
15	176.64	C			9a, 13a, 14, 27	
16	121.57	CH	6.14 d (*2.5*)	14, 18a		9a, 27
17	202.85	C			18ab	
18	50.58	CH_2	a: 2.46 d (*16.5*)	18b, 29	16, 29	14, 18b, 20
19	42.32	C			14, 18ab, 29	
20	39.07	CH_2	a: 1.38 m		18ab, 29	18a, 2
21	29.75	CH_2	a: 1.38 m		20a, 22, 31	
22	43.00	CH	2.10 m	21ab, 31	24ab, 30, 31	24b, 31
23	150.83	C			23, 31	
24	110.53	CH_2	a: 4.69 br s	30	31	30
25	23.65	CH_3	1.41 s (3H)		4	5b, 26
26	25.04	CH_3	1.23 s (3H)		6	5b, 25, 28
27	28.18	CH_3	1.13 s (3H)		12b	12b, 28
28	21.94	CH_3	0.94 s (3H)		6	27, 29
29	19.01	CH_3	0.80 s (3H)	18a	18ab	13b, 18b, 20b, 28
30	18.92	CH_3	1.64 s (3H)	24ab	24ab	24a
31	20.43	CH_3	1.03 d (*7*, 3H)	22		22
1´	152.65	C				

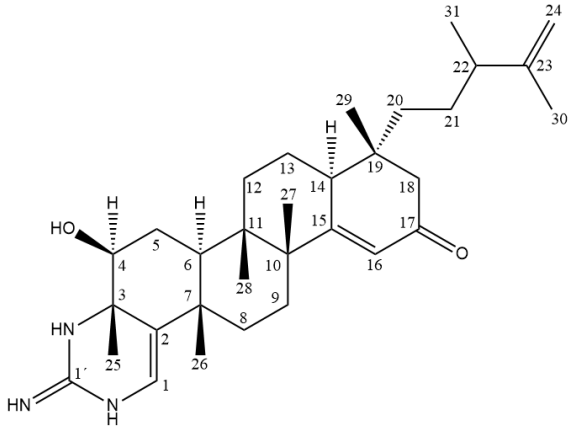

Table S8. NMR Data for Gromomycin G (**8**) in CD_3OD.

Nr.	δ_C		δ_H (*J* in Hz)	HHCOSY	HMBC (C→H)
1	116.19	CH	5.91 s		
2	132.70	C			1, 25, 26
3	59.80	C			1, 4, 5a, 25
4	80.03	CH	3.65 m	5ab, 6	5a, 6, 25
5	29.47	CH_2	a: 1.85 m	4, 5b, 6	6
6	47.13	CH	1.57 m	4, 5ab	5ab, 12b, 26, 28
7	38.73	C		8	1, 5a, 6, 26
8	35.06	CH_2	1.49 m (2H)	7	26
9	34.15	CH_2	a: 1.82 m	8, 9b	27
10	43.54	C			27, 28
11	39.02	C			27, 28
12	33.38	CH_2	a: 1.65 m	13a	28
13	20.15	CH_2	a: 1.50 m	12a,	12ab
14	41.78	CH	2.32 m	13ab	13ab
15	145.00	C			
16	122.41	CH	5.65 m	17, 18b	
17	24.44	CH_2	2.08 m (2H)	16, 18a	
18	34.57	CH_2	a: 1.41 m	17	
19	35.97	C			29
20	39.87	CH_2	1.19 m (2H)		20
21	29.67	CH_2	a: 1.31 m	21b	
22	43.23	CH	2.04 m	31	24ab, 30, 31
23	151.28	C			30, 31
24	110.12	CH_2	a: 4.66 br s	24b	
25	23.66	CH_3	1.40 s (3H)		6
26	25.07	CH_3	1.20 s (3H)		
27	29.56	CH_3	1.02 s (3H)		
28	22.28	CH_3	0.84 s (3H)		6
29	18.88	CH_3	0.73 s (3H)		
30	18.96	CH_3	1.63 s (3H)		22, 24a
31	20.44	CH_3	0.99 d (*7*, 3H)	22	22
1′	152.67	C			1

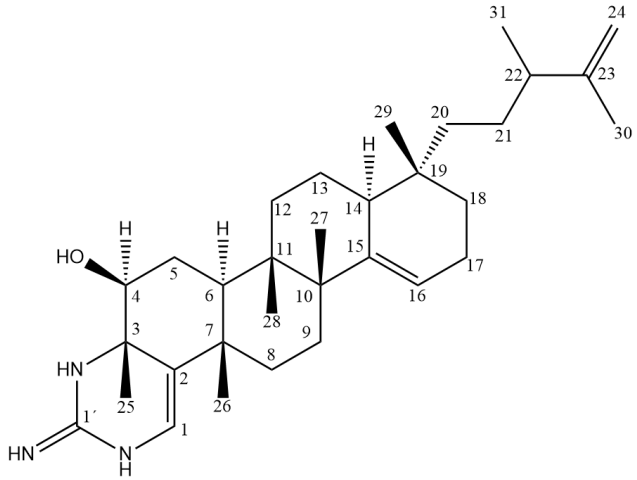

Table S9. NMR Data for Gromomycin H (**9**) in CD_3OD.

Nr.	δ_C	δ_H (*J* in Hz)	HHCOSY	HMBC (C→H)
1	116.27 CH	5.92 s		
2	132.16 C			1, 25, 26
3	59.77 C			1, 4, 5a, 25
4	79.65 CH	3.73 dd (*11.5*, *4.3*)	5ab, 6	5ab, 25
5	29.03 CH_2	1.77 m	4, 5a, 6	6
6	42.13 CH	1.59 m	4, 5a, 6	5ab, 26, 28
7	38.38 C			1, 26
8	35.57 CH_2	1.60 m	9a	9a, 26
9	28.32 CH_2	1.70 m	8ab	27
10	42.93 C			12b,27, 28
11	38.65 C			27, 28
12	30.87 CH_2	1.68 m		28
13	22.90 CH_2	2.09 m	12b	12ab, 28
14	137.12 C			12a, 18ab, 29
15	132.88 C			9a, 16ab, 27
16	41.16 CH_2	2.91 br d (*20.0*)	13b, 16b, 18b	18b, 27
17	214.11 C			16ab, 18ab
18	51.80 CH_2	2.61 d (*13.5*)	18b, 29	20a, 29
19	43.24 C			
20	39.42 CH_2	1.45 m	21a	18ab, 29
21	31.62 CH_2	1.32 m	20a, 22	22, 31
22	43.25 CH	2.07 m	21ab, 31	24ab, 30, 31
23	150.54 C			30, 31
24	110.51 CH_2	4.65 br s	30	21. 30
25	23.79 CH_3	1.41 s (3H)		
26	25.03 CH_3	1.23 s (3H)		6
27	23.86 CH_3	0.95 s (3H)		
28	21.07 CH_3	0.90 s (3H)		6, 12ab
29	27.90 CH_3	0.99 s (3H)	18a	18ab
30	18.91 CH_3	1.59 s (3H)	24ab	24ab
31	20.62 CH_3	0.98 d (*7.0*, 3H)	22	22
1´	152.54 C	-----		1

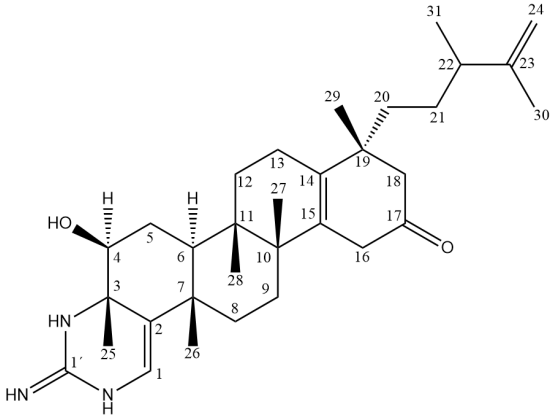

Table S10. NMR Data for Hexaprenylguanidine (**10**) in DMSO-d_6.

Nr.	δ_C		δ_H (*J* in Hz)	HHCOSY	HMBC (C→H)
1	38.62	CH_2	3.66 t* (*5.7*, 2H)	H-N_a, H-2	
2	119.17	CH	5.19 t (*6.5*)	H-1, H-25,	H-1, H-4, H-25
3	138.91	C			H-1, H-4, H-5, H-25
4	38.97	CH_2	1.99 m (2H)		
5	26.21	CH_2	2.05 m (2H)		
6	124.13	CH	5.06 m		
7	134.67	C			
8	39.00	CH_2	1.93 m (2H)		
9	26.08	CH_2	2.02 m (2H)		
10	124.00	CH	5.06 m		
11	134.30	C	-----		
12	39.00	CH_2	1.93 m (2H)		
13	26.04	CH_2	2.02 m (2H)		
14	123.97	CH	5.06 m		
15	134.30	C			
16	39.00	CH_2	1.93 m (2H)		
17	26.00	CH_2	2.02 m (2H)		
18	123.92	CH	5.06 m		
19	134.24	C			
20	39.00	CH_2	1.93 m (2H)		
21	25.94	CH_2	2.02 m (2H)		
22	123.67	CH	5.06 m		
23	130.65	C			
24	25.53	CH_3	1.63s (3H)		
25	16.17	CH_3	1.63 s (3H)	H-1, H-2	H-2, H-4
26	15.80	CH_3	1.55 s (3H)		
27	15.80	CH_3	1.55 s (3H)		
28	15.80	CH_3	1.55 s (3H)		
29	15.80	CH_3	1.55 s (3H)		
30	17.57	CH_3	1.55 s (3H)		
1′	157.29	C			H-1
	δ_N				
N_a	85.5**		8.61 t (5.0)	H-1	
$N_{b,c}$	75.5**		7.79 br s (3H)		

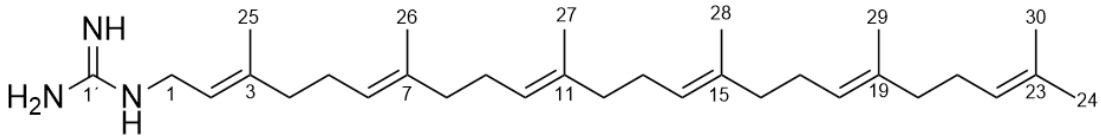

*t= pseudo triplet; formed by two doublets with $J_{HNa,H-1}$ =5.0 Hz and $J_{H-1,H-2}$ =6.5 Hz

**= taken from the ^{15}N HSQC

Table S11. ^{1}H NMR ($CDCl_3$) data of S-MTPA ester (5a) and R-MTPA ester (5b) derived from Gromomycin B (**3**) and their $\Delta\delta_{S-R}$ values.

	5a	**5b**	$\Delta\delta_{S-R}$
1	5.93 s	5.91 s	+0.02
4	4.83 dd (*11.8, 4.4*)	4.84 dd (*11.8, 4.4*)	- 0.01
5	1.93 m	2.03 m	- 0.10
6	1.69 d (*12.5*)	1.73 d (*12.5*)	- 0.04
8	1.54 m	1.54 m	0.00
9	1.57 m (2H)	1.57 m (2H)	0.00
12	1.50 m (2H)	1.53 m (2H)	- 0.03
13	2.06 m	2.06 m	0.00
16	2.83 d (*20.0*)	2.83 d (*20.0*)	0.00
18	2.65 d (*13.0*)	2.66 d (*13.0*)	- 0.01
20	1.63 m	1.63 m	0.00
21	2.03 m	2.03 m	0.00
22	5.05 t (*6.3*)	5.09 t (*6.3*)	- 0.04
24	1.53 s (3H)	1.54 s (3H)	- 0.01
25	1.36 s (3H)	1.35 s (3H)	+0.01
26	1.15 s (3H)	1.17 s (3H)	- 0.02
27	0.82 s (3H)	0.85 s (3H)	- 0.03
28	0.99 s (3H)	0.99 s (3H)	0.00
29	0.91 s (3H)	0.92 s (3H)	- 0.01
30	1.64 s (3H)	1.65 s (3H)	- 0.01

Table S12. Incorporation of [2-13C] pyruvate in gromomycin B (**3**).

Nr.	Isotopic enrichment in %
3	8
7	8
11	8
15	7
19	11
23	8

All positions which are not mentioned in this table were not labelled, with the exception of C-20, which showed an moderate enrichment of 3%

Table S13. Incorporation of [3-13C] pyruvate in gromomycin B (**3**).

Nr.	Isotopic enrichment in %
25	5
26	5
27	6
28	6
29	10
30	7

All positions which are not mentioned in this table were not labelled

Table S14. Bacterial strains used in this work.

Strains	Description	Reference or Source
Streptomyces sp. Je 1-332	Gromomycin producing wild-type strain	This work
S. flavoviridis NRRL ISP-5153	Type strain	Agricultural Research Service Culture Collection (NRRL)
S. albus Del14	Cluster-free heterologous host strain	[254]
S. lividans Del8	Cluster-free heterologous host strain	[255]
Streptomyces sp. Je 1-332_Tn5_mut_148	Tn5 transposon mutant of *Streptomyces* sp. Je 1-332, no gromomycin producing strain	This work
Streptomyces sp. Je 1-332_Tn5_mut_355	Tn5 transposon mutant of *Streptomyces* sp. Je 1-332, no gromomycin producing strain	This work
Streptomyces sp. Je 1-332del_ fdps	Strain *Streptomyces* sp. Je 1-332 with the deletion of the farnesyl diphosphate synthase gene	This work
Streptomyces sp. Je 1-332del_ mppO	Strain *Streptomyces* sp. Je 1-332 with the deletion of the putative enduracidin beta-hydroxylase gene	This work
Streptomyces sp. Je 1-332del_hypprot	Strain *Streptomyces* sp. Je 1-332 with the deletion of the hypothetical protein gene downstream to mppO gene	This work
Streptomyces sp. Je 1-332del_PAP2-hypprot-P450	Strain *Streptomyces* sp. Je 1-332 with the deletion of the three genes (a PAP2 superfamily protein, hypothetical protein, and a cytochrome P450)	This work
Streptomyces sp. Je 1-332del_PrnD3-2	Strain *Streptomyces* sp. Je 1-332 with the deletion of the two genes annotated as putative aminopyrrolnitrin oxygenases PrnD	This work
S. albus STS10	S. *albus* strain Del14 containing the pHSU-STS10 vector	This work
S. lividans STS10	*S. lividans* Del8 containing the pHSU-STS10 vector	This work
S. albus STS-22	S. *albus* strain Del14 containing the pHSU-STS22 vector	This work
S. albus STS-23	S. *albus* strain Del14 containing the pHSU-STS23 vector	This work
S. albus STS-24	S. *albus* strain Del14 containing the pHSU-STS24 vector	This work

S. albus STS-25	S. *albus* strain Del14 containing the pHSU-STS25 vector	This work
S. albus STS-29	S. *albus* strain Del14 containing the pHSU-STS29 vector	This work
S. albus STS-30	S. *albus* strain Del14 containing the pHSU-STS30 vector	This work
S. albus STS-31	S. *albus* strain Del14 containing the pHSU-STS31 vector	This work
S. albus STS-32	S. *albus* strain Del14 containing the pHSU-STS32 vector	This work
S. albus STS-33	S. *albus* strain Del14 containing the pHSU-STS33 vector	This work
S. albus STS-33delgroA	S. *albus* strain Del14 containing the pHSU-STS33_KOgroA vector	This work
S. albus STS-33delgroB	S. *albus* strain Del14 containing the pHSU-STS33_KOgroB vector	This work
S. albus STS-33delgroC	S. *albus* strain Del14 containing the pHSU-STS33_KOgroC vector	This work
S. albus STS-33delgroD	S. *albus* strain Del14 containing the pHSU-STS33_KOgroD vector	This work
S. albus STS-33delgroE	S. *albus* strain Del14 containing the pHSU-STS33_KOgroE vector	This work
S. albus STS-33delgroF	S. *albus* strain Del14 containing the pHSU-STS33_KOgroF vector	This work
S. albus STS-33delgroG	S. *albus* strain Del14 containing the pHSU-STS33_KOgroG vector	This work
S. albus STS-33delgroH	S. *albus* strain Del14 containing the pHSU-STS33_KOgroH vector	This work
S. albus STS-33delgroI	S. *albus* strain Del14 containing the pHSU-STS33_KOgroI vector	This work
E. coli ET12567 pUB307	Donor strain for intergeneric conjugation	[274]
E. coli GB05-red	Strain used for Red/ET	[275]
E. coli TransforMax EC100D pir-116	Strain used for high-copy propagation of rescue plasmid copies	Lucigen
E.coli EPI300-T1R	Strain used for Construction of inducible-copy-number genomic libraries using the CopyControl™ Cloning System, with clones that are resistant to contaminating phage T1 and T5	Lucigen

Table S15. Plasmids used in this work.

Plasmids	Description	Reference or Source
pTNM	*ts*-orip^{SG5} *aac(3)IV* (Amr) *hygB* (Hyr), carries synthetic gene *tnp(a)* of Tn5 transposase, apramycin resistance *gene aac(3)IV* flanked with mosaic ends for Tnp(a)	[268]
pCos15A_gusA	Cloning vector	Lucigen
pCos15A_gus_AmInt	pCos15A_gusA, which contains the *oriT* and integrase genes	This work
pCos15A_AmInt	pCos15A_gus_AmInt, where *gus* gene was deleted	This work
patt-saac-oriT	Resistance cassette plasmid containing a synthetic fragment with *aac(3)IV*, *oriT*, B-CC, P-GG and loxP sites	[276]
phygattB	Resistance cassette plasmid containing hygromycin resistance marker flanked with MssI restriction sites and attB sequence	[254]
pHSU-STS2	Cosmid P05_A07 containing gene cluster (antismash Region 14) in which T-muurolol synthase gene is replaced by *aac(3)IV* and *oriT*	This work
pHSU-STS3	Cosmid P10_C04 containing gene cluster (antismash Region 15) in which Squalene-hopene cyclase gene is replaced by aac(3)IV and oriT	This work
pHSU-STS6	Cosmid P05_A10 in which farnesyl diphosphate gene is replaced by *aac(3)IV* and *oriT*	This work
pSTS-del-mppO	Cosmid P05_A10 in which the putative enduracidin beta-hydroxylase gene is replaced by *aac(3)IV* and *oriT*	This work
pSTS-del-hypprot	Cosmid P05_A10 in which the hypothetical protein gene is replaced by *aac(3)IV* and *oriT*	This work
pSTS-del-PAP2-hypprot-P450	Cosmid P05_A10 in which the PAP2 superfamily protein, hypothetical protein, and a cytochrome P450 genes are replaced by *aac(3)IV* and *oriT*	This work
pSTS-del-PrnD3-2	Cosmid P05_A10 in which putative aminopyrrolnitrin oxygenases (PrnD) genes are replaced by *aac(3)IV* and *oriT*	This work
pHSU-STS10	Cosmid P04_E01 containing putative gromomycin gene cluster with *aac(3)IV*, *oriT*, and integrase	This work
pHSU-STS22	The construct based on the pHSU-STS10 plasmid for deletion 1 and 2 genes upstream to putative gromomycin gene cluster	This work
pHSU-STS23	The construct based on the pHSU-STS10 plasmid for deletion 26 – 33 genes downstream to putative gromomycin gene cluster	This work

pHSU-STS24	The construct based on the pHSU-STS10 plasmid for deletion 22 – 33 genes downstream to putative gromomycin gene cluster	This work
pHSU-STS25	The construct based on the pHSU-STS10 plasmid for deletion 18 – 33 genes downstream to putative gromomycin gene cluster	This work
pHSU-STS29	The construct based on the pHSU-STS10 plasmid for deletion 1-5 genes upstream to putative gromomycin gene cluster	This work
pHSU-STS30	The construct based on the pHSU-STS10 plasmid for deletion 1-6 genes upstream to putative gromomycin gene cluster	This work
pHSU-STS31	The construct based on the pHSU-STS25 plasmid for deletion 17 gene downstream to putative gromomycin gene cluster	This work
pHSU-STS32	The construct based on the pHSU-STS25 plasmid for deletion 16 and 17 genes downstream to putative gromomycin gene cluster	This work
pHSU-STS33	The construct based on the pHSU-STS25 plasmid for deletion 15 – 17 genes downstream to putative gromomycin gene cluster	This work
pHSU-STS33_KOgroA	The construct based on the pHSU-STS33 plasmid for deletion *groA* gene	This work
pHSU-STS33_KOgroB	The construct based on the pHSU-STS33 plasmid for deletion *groB* gene	This work
pHSU-STS33_KOgroC	The construct based on the pHSU-STS33 plasmid for deletion *groC* gene	This work
pHSU-STS33_KOgroD	The construct based on the pHSU-STS33 plasmid for deletion *groD* gene	This work
pHSU-STS33_KOgroE	The construct based on the pHSU-STS33 plasmid for deletion *groE* gene	This work
pHSU-STS33_KOgroF	The construct based on the pHSU-STS33 plasmid for deletion *groF* gene	This work
pHSU-STS33_KOgroG	The construct based on the pHSU-STS33 plasmid for deletion *groG* gene	This work
pHSU-STS33_KOgroH	The construct based on the pHSU-STS33 plasmid for deletion *groH* gene	This work
pHSU-STS33_KOgroI	The construct based on the pHSU-STS33 plasmid for deletion *groI* gene	This work

Table S16. Primers used in this work.

Primer name	Sequence (5'-3')	Description	Source
pMODseq-f pMODseq-r	GCCAACGACTACGCACTAGCCAAC GAGCCAATATGCGAGAACACCCGA GAA	For Tn5 insertion loci identification	[254]
OTC60	TGCTTAATGAATTACAACAGTACTG CGATGAGTGGCAGGGCGGGGCGTA AGGTTCATGTGCAGCTCCA	Amplification of apramycin-oriT-Integrase cassettes from pCos15A_gus_AmInt	This work
OTC61	CTGTCGTTTCCTTTCTCTGTTTTTGTC CGTGGAATGAACAATGGAAGTCCCT ACGCCGCTACGTCTTC		
STS3	CGTGACTCATCCCTCATTCCTCATCC TTGCGCCGGAAGGTGTGTGCCGCCT TCCGGGGATCCGTCGACCC	For T-muurolol synthase deletion (antismash Region 14)	This work
STS4	GGGCGAGGACGGCCTCTGGTGGGC GGTGGATCTGGCCGCGCCCCGATGA GTGTAGGCTGGAGCTGCTTCG		
STS13	GGCCGACGGCGGACCCACAGCAGA GAAGACGACTGCACGAAGGGGAAG CCTTCCGGGGATCCGTCGACCC	For squalene-hopene cyclase deletion (antismash Region 15)	This work
STS14	GCAGGCGATCAGCAGCGGCGCGGG GCCCGGCACGGCCGGGGTCCTCTCC ATGTAGGCTGGAGCTGCTTCG		
STS21	AGCCGAGGCGGGGACGGTGTGCAC GTCCTCCTGGGAGCCGTCCGCGCCG ATTCCGGGGATCCGTCGACCC	For farnesyl diphosphate deletion	This work
STS22	TGTCTTTCGCGATTGACAACACCCA AGCAGAAACAGACTTTCCGGTTCCG TGTAGGCTGGAGCTGCTTCG		
Fdps_del_chk_F Fdps_del_chk_R	GTTCCAGGCGCCCATCGCAT ATCCGCACCGTCCAGGCTTG	To test for farnesyl diphosphate and *groE* genes deletion	This work
Del_mppO_F	GAGACTGCAGAGATGACGACAGGT GGATCGCGGTGCGTCAGTGGATCCG GTGTAGGCTGGAGCTGCTTCG	For putative enduracidin beta-hydroxylase gene deletion	This work
Del_mppO_R	ACTGCTCTTCGCGGCTTCGATCTTGT CCGACCAACCACGGGGGACTCGCAT TCCGGGGATCCGTCGACCC		
mppO_del_chk_F mppO_del_chk_R	GCTCTTGATCGCGGCATA GTCTCTAATTCGTCGCCG	To test for mppO and *groD* genes deletion	This work

Del_hupprot_F Del_hupprot_R	ACGGGTCTGACGCACTGTGCGGGGC TCGGCTCTAGGAGACTGGATTGAGC TTCCGGGGATCCGTCGACCC CTTCCTGACGTGCGAGCGCGGACCG CGGCCCCGCTGCGGAGCGGAGATGC TGTAGGCTGGAGCTGCTTCG	For hypothetical protein gene deletion	This work
Hp_del_chk_F Hp_del_chk_R	AGCCTGGACGGTGCGGATCA GCGGATCCGAGGAGATGCCG	To test for hypothetical protein gene deletion	This work
Del_pap2-p450_F Del_pap2-p450_R	GCTCCGCAGCGGGGCCGCGGTCCGC GCTCGCACGTCAGGAAGGAGAGGT GTTCCGGGGATCCGTCGACCC TCGCGGTTCCGGAGTTCCGCTGCCC CGGAGGCCCGCGCCGCGTACGACG GTGTAGGCTGGAGCTGCTTCG	For PAP2 superfamily protein, hypothetical protein, and a cytochrome P450 genes deletion	This work
Pap2-P450_del_chk_F Pap2-P450_del_chk_R	TACTGCGTGCTGCTCCACCG TCGACCTGGACGACGGCGAG	To test for PAP2 superfamily protein, hypothetical protein, and a cytochrome P450 genes deletion	This work
Del_prnD3-prnD2_F Del_prnD3-prnD2_R	CTCCTCCCGAACACTCCGCTGCCGT TCGTGCGCTGCCCTCGGTCGGTCTCT GTAGGCTGGAGCTGCTTCG CGGCTCCCAGGAGGACGTGCACACC GTCCCCGCCTCGGCTGCTCCGCCGA TTCCGGGGATCCGTCGACCC	For putative aminopyrrolnitrin oxygenases (PrnD) genes deletion	This work
prnD3-prnD2_del_chk_F prnD3-prnD2_del_chk_R	CCCGAGGCGAGGTTCGTGGT CGGACTGATCACGCAGGCAG	To test for putative aminopyrrolnitrin oxygenases (PrnD) genes deletion	This work
STS40 STS41	GTCCACGAGCTGATCACC CTGCCAGGAGATCGAGTAC	For verification of heterologous constructs integration	This work
STS51 STS52	CCGGCAAGGAGCTGCGCAAGCTCAT GTCGTGGGTGAACGAAGAGGCCTG AGATACAGTTTAAACTTCAAATATG TATCCGCTCA GGCGAACTCGGCGGAGCCGGTGAT GACCGGCAGCCGAAGCCGCGGGGT TATCTATGGTTTAAACTTACCAATG CTTAATCAGTGAG	For construction pHSU-STS22	This work

STS47	CGTGCCCCGCTGCGGGCGTCGGCCC GTAGCGCCGGGCCTCGTACGTACCC GATACAGTTTAAACTTCAAATATGT ATCCGCTCA	For construction pHSU-STS23	This work
STS49	GTCGACGTCGATGGAGCCGGTGCGG GAGTTGAGCCGCAGGTCGGCGGGG CTCTATGGTTTAAACTTACCAATGCT TAATCAGTGAG		
STS48	GTGGGGGAGTCTCGCAGTACATCCT TTTTCCCTCAAGGAGTGGATCTCCC GATACAGTTTAAACTTCAAATATGT ATCCGCTCA	For construction pHSU-STS24	This work
STS49	GTCGACGTCGATGGAGCCGGTGCGG GAGTTGAGCCGCAGGTCGGCGGGG CTCTATGGTTTAAACTTACCAATGCT TAATCAGTGAG		
STS50	GGCCATGCCGGCGAGGCCCCGCCCC GCAGACGAAGCGGTTCCGCCCGGCA GATACAGTTTAAACTTCAAATATGT ATCCGCTCA	For construction pHSU-STS25	This work
STS49	GTCGACGTCGATGGAGCCGGTGCGG GAGTTGAGCCGCAGGTCGGCGGGG CTCTATGGTTTAAACTTACCAATGCT TAATCAGTGAG		
STS51	CCGGCAAGGAGCTGCGCAAGCTCAT GTCGTGGGTGAACGAAGAGGCCTG AGATACAGTTTAAACTTCAAATATG TATCCGCTCA	For construction pHSU-STS29	This work
STS71	GCCGAGGCCGCGGACCTGCCCGTCG AACGGGTGGGGGGCAAGGCCAAGG GTCTATGGTTTAAACTTACCAATGC TTAATCAGTGAG		
STS51	CCGGCAAGGAGCTGCGCAAGCTCAT GTCGTGGGTGAACGAAGAGGCCTG AGATACAGTTTAAACTTCAAATATG TATCCGCTCA	For construction pHSU-STS30	This work
STS72	CGACCGAGGGCAGCGCACGAACGG CAGCGGAGTGTTCGGGAGGAGGCC GGTCTATGGTTTAAACTTACCAATG CTTAATCAGTGAG		
STS67	ATGGACGCCGTCACCCAGGTCCCCG CGCCGGTCAACGAGCCGGTGCACGG	For construction pHSU-STS31	This work

STS68	GATACAGTTTAAACTTCAAATATGT ATCCGCTCA TCAGCCCATGTGCGGGTACGCGTAG TCCGTCGGCGAGACCAGCGTCTCCT TCTATGGTTTAAACTTACCAATGCTT AATCAGTGAG		
STS69 STS68	GTTTCGCATATCCAGGTACGGCCCT GTTTCTACTCTCCGTGGAGGTGCCC GATACAGTTTAAACTTCAAATATGT ATCCGCTCA TCAGCCCATGTGCGGGTACGCGTAG TCCGTCGGCGAGACCAGCGTCTCCT TCTATGGTTTAAACTTACCAATGCTT AATCAGTGAG	For construction pHSU-STS32	This work
STS70 STS68	TACGCGGCGCGGGCCTCCGGGGCAG CGGAACTCCGGAACCGCGAATGCTC GATACAGTTTAAACTTCAAATATGT ATCCGCTCA TCAGCCCATGTGCGGGTACGCGTAG TCCGTCGGCGAGACCAGCGTCTCCT TCTATGGTTTAAACTTACCAATGCTT AATCAGTGAG	For construction pHSU-STS33	This work
KO_groA_F KO_groA_R	ATGAGGCGCAGTACGTCTGAGCGGA TCGCTGCGTCCGCGAGGCCGACCAG GCGCGCCAATACTTGACATATCACT GT TCAGCCATGCTCTGCCACCTCCACC CACTGCTGATAGAAACGCCGGAATC GTCAGGCGCCGGGGGCGGTGT	For construction pHSU-STS33_KOgroA	This work
KO_groB_chk_F KO_groB_chk_R	ACCAGGTCCTCACCTTCG TACGGGAAATCCCGCTGC	To test for *groA* gene deletion	To test for *groA* gene deletion
KO_groB_F KO_groB_R	ATGAGTCTCGCGCCGGTACGAGGGC AGCCTCCCCTCGATCTCGAACCGCG GCGCGCCAATACTTGACATATCACT GT TCACGTGTCCCCCCGCCCCGTCCAA CGGCGATGGAACTGGCGGAATCGC AGGGCGCGCCTCAGGCGCCGGGGG CGGTGT	For construction pHSU-STS33_KOgroB	This work

KO_groB_chk_F KO_groB_chk_R	AGGTGATCATGGGCATCGTC AAGACACATGCTCCGGACTC	To test for *groB* gene deletion	To test for *groB* gene deletion
KO_groC_F	ATGATCGGCGCGGACGGCTCCCAGG AGGACGTGCACACCGTCCCCGCCTG GCGCGCCAATACTTGACATATCACT GT	For construction pHSU-STS33_KOgroC	This work
KO_groC_R	TCATCGGCCGACCTTTCCGTCTCCCG CGGCGCGGTCGACCCATGACTGGTA GGCGCGCCTCAGGCGCCGGGGGCG GTGT		
KO_groC_chk_F KO_groC_chk_R	GAAGGACGACATAGCCCACC ACATCCCGTCACTGTCGAAC	To test for *groC* gene deletion	This work
KO_groD_F	ATGGAAGAGTTCCGTCGCCAGGTCA ACGAAAGACTGCGCTCCTCCATCGG GCGCGCCAATACTTGACATATCACT GT	For construction pHSU-STS33_KOgroD	This work
KO_groD_R	TCATGCCGCCGCCCGGCCGTGAACC ACCTGCGCCGCCCAGCGAAGCATCG CGGCGCGCCTCAGGCGCCGGGGGC GGTGT		
KO_groE_F	ATGGACGTCTTATTAGGGCACTCTC CGTCTGTTCTGGGATGCGTTCTGTG GCGCGCCAATACTTGACATATCACT GT	For construction pHSU-STS33_KOgroE	This work
KO_groE_R	TCAGATCGTCCGTACCCGCGCGTCC GCGCCGGGCATCGTCGTGGACAGCG GGGCGCGCCTCAGGCGCCGGGGGC GGTGT		
KO_groF_F	ATGCGGCGAAATCTCAGGCTGGCGG CTTCTCAACGCGCCAAACGGTTGTG GCGCGCCAATACTTGACATATCACT GT	For construction pHSU-STS33_KOgroF	This work
KO_groF_R	TCAGAGCCGGCGCCAAGGCGACAT ACCGGCGGCCTTGAGGGAGCGGTG GAGGGCGCGCCTCAGGCGCCGGGG GCGGTGT		
KO_groF_chk_F KO_groF_chk_R	CAGAACAGACGGAGAGTGCC CACCAGTACGCCGAGGAC	To test for *groF* gene deletion	This work

KO_groG_F	GTGAACGTGCCCAGCCAACAGGAC GCCGACCACGCCGTGACCGGCGCCG GGCGCGCCAATACTTGACATATCAC TGT	For construction pHSU-STS33_KOgroG	This work
KO_groG_R	TCATCGGGTTTCCCTTCCAGAGGAG TGCGGGGGCCCGGCGTCGACACGCC AGGCGCGCCTCAGGCGCCGGGGGC GGTGT		
KO_groG_chk_F	CTCAAGATGCTGGAGGACCG	To test for *groG* gene deletion	This work
KO_groG_chk_R	ACATCGTCGTTCCATGCTCC		
KO_groH_F	ATGAACAGCTTGGCCCGCCTGGCGG AGACCCCGTTGTGGAAGGCGGCGG GGCGCGCCAATACTTGACATATCAC TGT	For construction pHSU-STS33_KOgroH	This work
KO_groH_R	TCATGCGGTGTGTCCTCTCGTCTTGC GAAGCGATGAAGGGGTGCGCGAGG GGGCGCGCCTCAGGCGCCGGGGGC GGTGT		
KO_groH_chk_F	CGACTCCGGGTACAGCTTC	To test for *groH* gene deletion	This work
KO_groH_chk_R	GAGACGAGTTTGCGCAACC		
KO_groI_F	ATGAGCAGCGCGATGCGCCCCACCC CCGTCATGTTCAACCCGCTCTCCGG GCGCGCCAATACTTGACATATCACT GT	For construction pHSU-STS33_KOgroI	This work
KO_groI_R	TCAGACGTGGACGGGAAGGTGAGT GGCCCCGCGCAGGCTCAGAAGGCC GTTGGCGCGCCTCAGGCGCCGGGGG CGGTGT		
KO_groI_chk_F	TCTTCGTGAAGCTCTACGGC	To test for *groI* gene deletion	This work
KO_groI_chk_R	TGAATCAGGCGCCTTAGACC		
9_flavoviridis_F	GTAGTGGCGGAGGTCGTTG	To test for *groH* homolog gene presence	This work
9_flavoviridis_R	GTCCTGGTGCTCCTGCTG		
Left_flavoviridis_F	CGCAGTCTTCGGGGAGAC	To identify the cosmid containing whole gromomycin-like cluster	This work
Left_flavoviridis_R	GGTCCACTCCGTCGTTGG		
Right_flavor_F	GTTCCAGCAGGACGTCGAA		
Right_flavor_R	GACCATCATCGGCACCATGA		
cosmid-chk-For_DB	GATCTCCATCGACTAAACGT	To sequence the insert containing gromomycin-like cluster from the left of right side	This work
cosmid-chk-rev_DB	GTTAACTGCGGTCAAGATAT		

Table S17. Clusters of secondary metabolism genes identified in the genome of *Streptomyces* sp. strain Je 1-332 by the type of biosynthesis and corresponding profile using antiSMASH 6.0 software.

antiSMASH region	**Type**	**Most similar known cluster/MIBiG BGC-ID**	**Similarity (%)**
1	Other	A-503083/ BGC0000288	7
2	T1PKS	Salinomycin/ BGC0000144	12
3	Ectoine	Ectoine/ BGC0000853	100
4	Lanthipeptide class III	AmfS/BGC0000496	80
5	Siderophore	Desferrioxamin B/ BGC0000940	83
6	NRPS	Friulimicin A/ BGC0000354	78
7	Butyrolactone	Granaticin/ BGC0000227	10
8	T1PKS, Butyrolactone, Ectoine	Streptazone E/ BGC0001296	91
9	Melanin	Melanin/ BGC0000910	100
10	Terpene	Albaflavenone/ BGC0000660	100
11	T3PKS, T1PKS, siderophore	RK-682/ BGC0000140	45
12	RiPP-like	-	-
13	NRPS-terpene	Griseobactin/ BGC0000368	52
14	Terpene	-	-
15	Terpene	Hopene/ BGC0000663	92
16	T3PKS	BE-14106/ BGC0000029	17
17	Siderophore	-	-
18	RiPP-like	-	-
19	Terpene	2-methyllisoborneol/ BGC0000658	100
20	Terpene	Isorenieratene/ BGC0000664	100
21	T3PKS	Alkylresorcinol/ BGC0000282	100

Table S18. Toxicity assessment of gromomycin derivatives. *In vitro* cytotoxicity was evaluated performing a MTT assay (half maximal inhibitory concentration IC50 ± standard deviation). *In vivo* toxicity was assessed by determination of the maximum tolerated concentration (MTC) in zebrafish (*Danio rerio*) embryos. Kaplan-Meier curves of embryos exposed to gromomycins can be found in Supplementary Figure 68. CHO: chinese hamster ovary.

Gromomycin derivative	***In vitro* IC_{50} [µg mL^{-1}]**		***In vivo* MTC [µg mL^{-1}]**
	HepG2	**CHO-K1**	***Danio rerio***
Gromomycin A	9.0 ± 6.6	23.9 ± 0.7	1
Gromomycin B	> 37	> 37	5
Gromomycin E	19.4 ± 1.2	31.2 ± 2.5	5
Gromomycin F	> 37	27.0 ± 2.5	5
Gromomycin G	> 37	> 37	10
Gromomycin H	2.2 ± 0.4	4.1 ± 1.1	nd[a]

[a] not determined (nd) due to poor solubility in the incubation medium

List of Figures

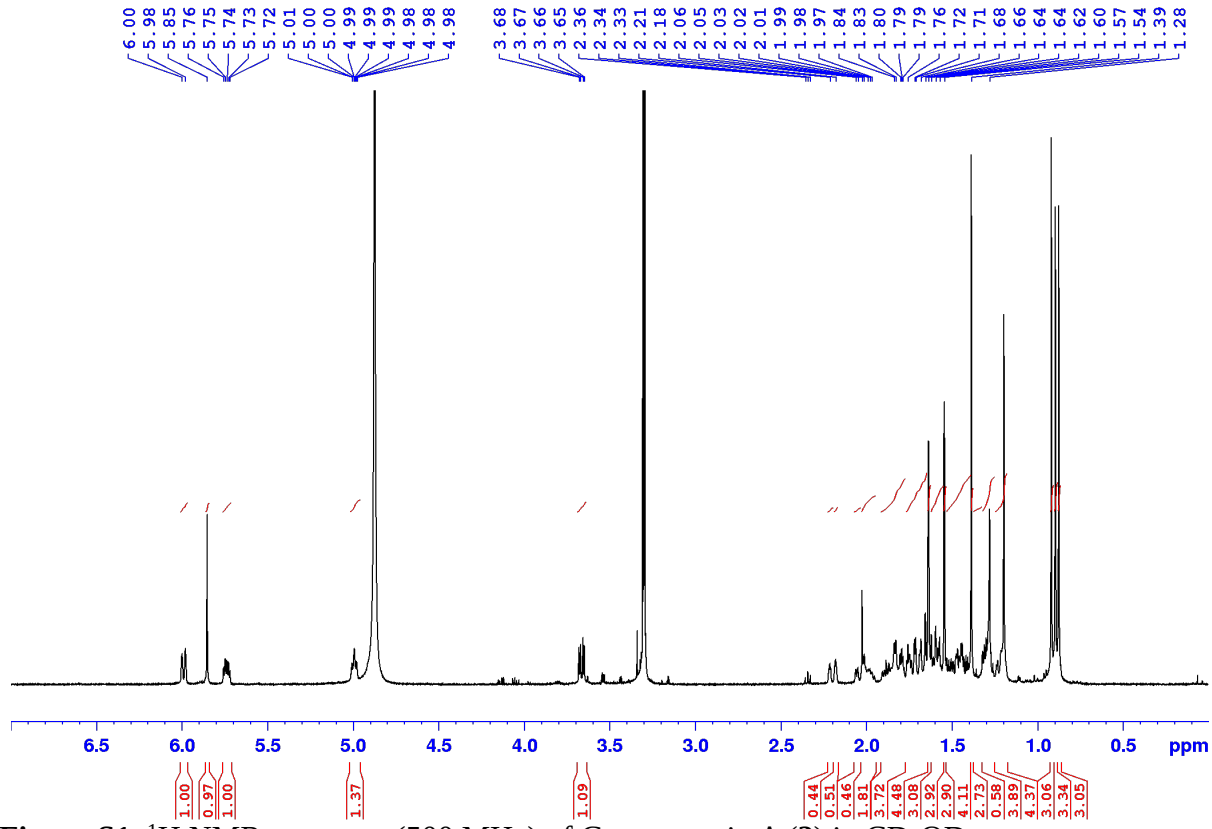

Figure S1. ^{1}H NMR spectrum (500 MHz) of Gromomycin A (**2**) in CD_3OD.

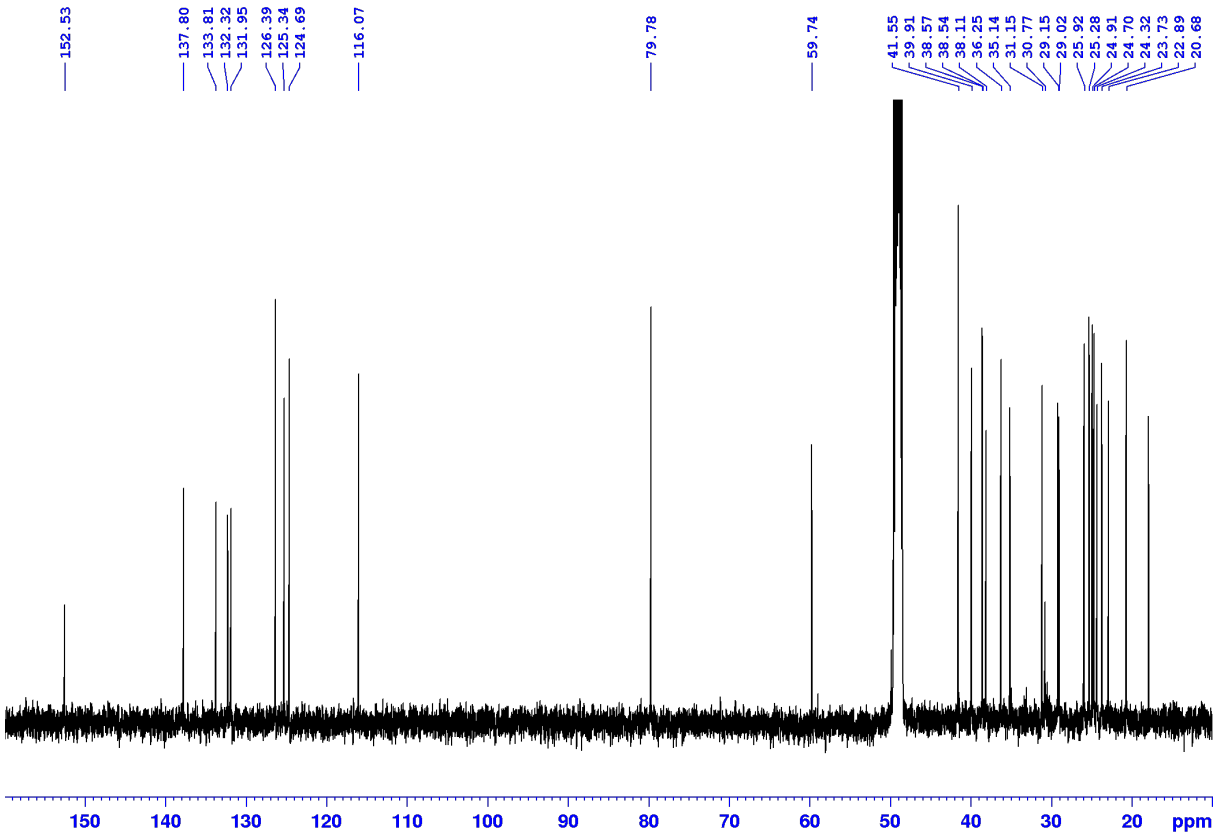

Figure S2. ^{13}C NMR spectrum (125 MHz) of Gromomycin A (**2**) in CD_3OD.

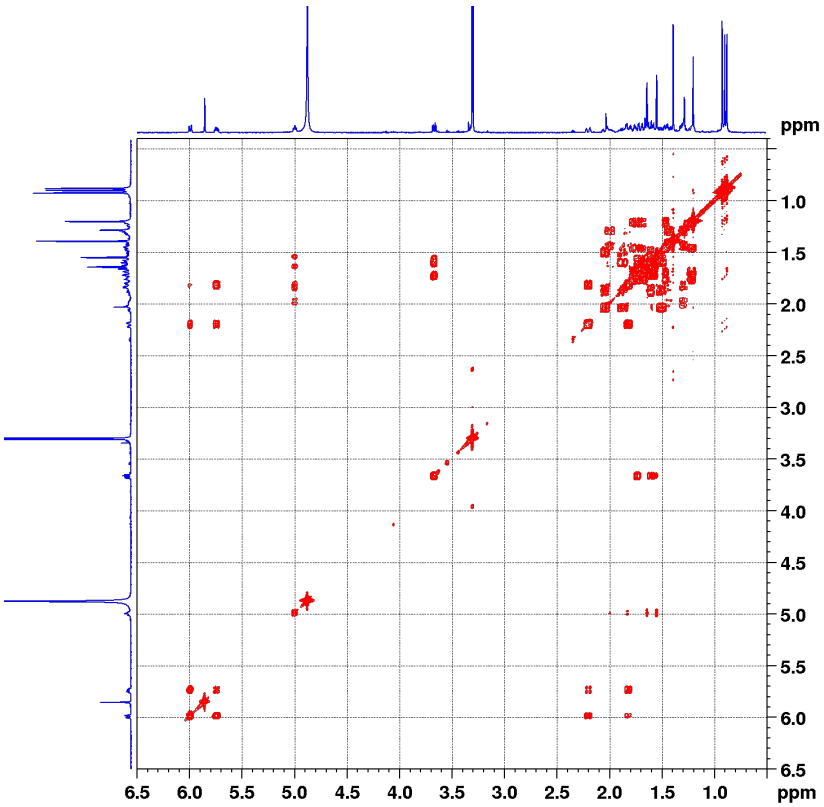

Figure S3. COSY spectrum (500 MHz) of Gromomycin A (**2**) in CD_3OD.

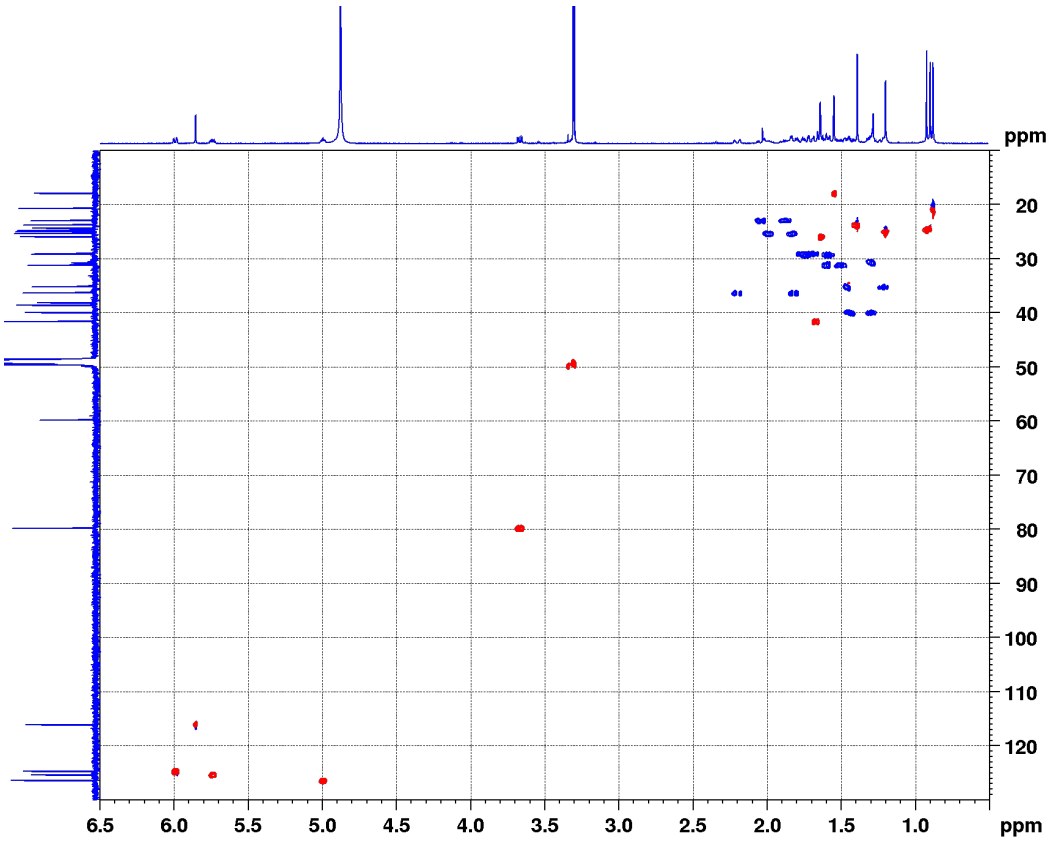

Figure S4. ^{1}H-^{13}C HSQC spectrum (500 MHz) of Gromomycin A (**2**) in CD_3OD.

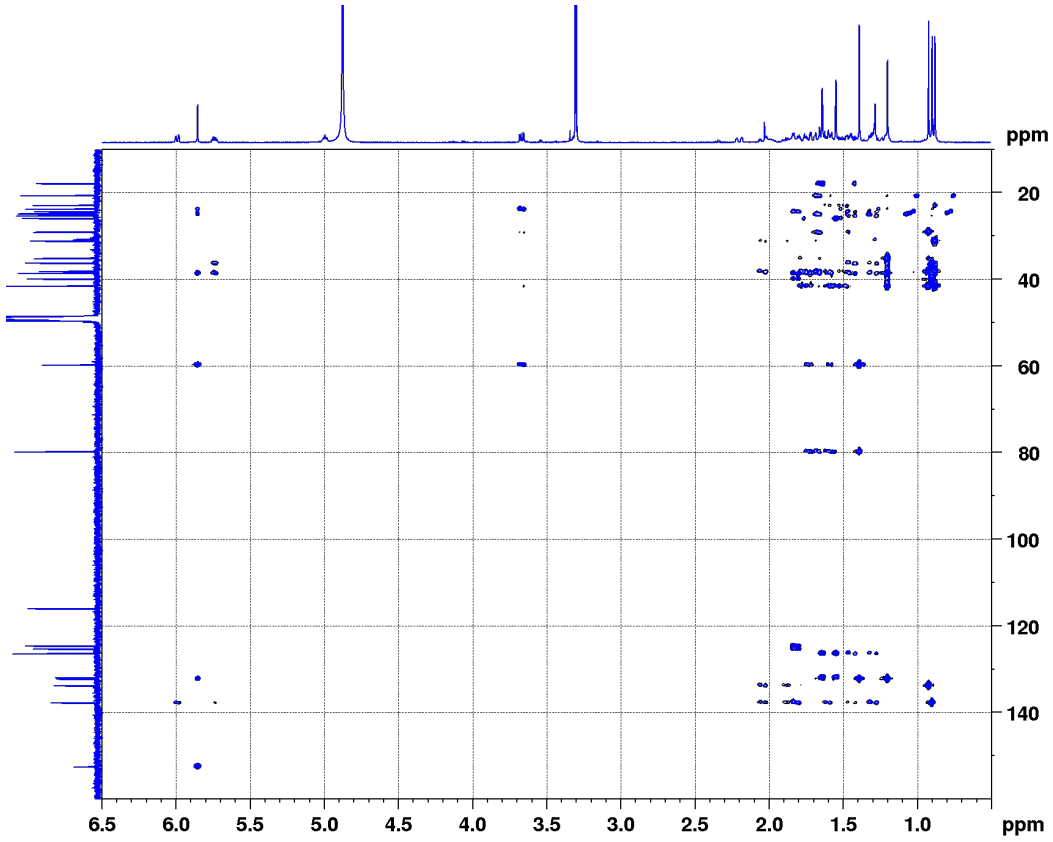

Figure S5. ^{1}H-^{13}C HMBC spectrum (500 MHz) of Gromomycin A (**2**) in CD_3OD.

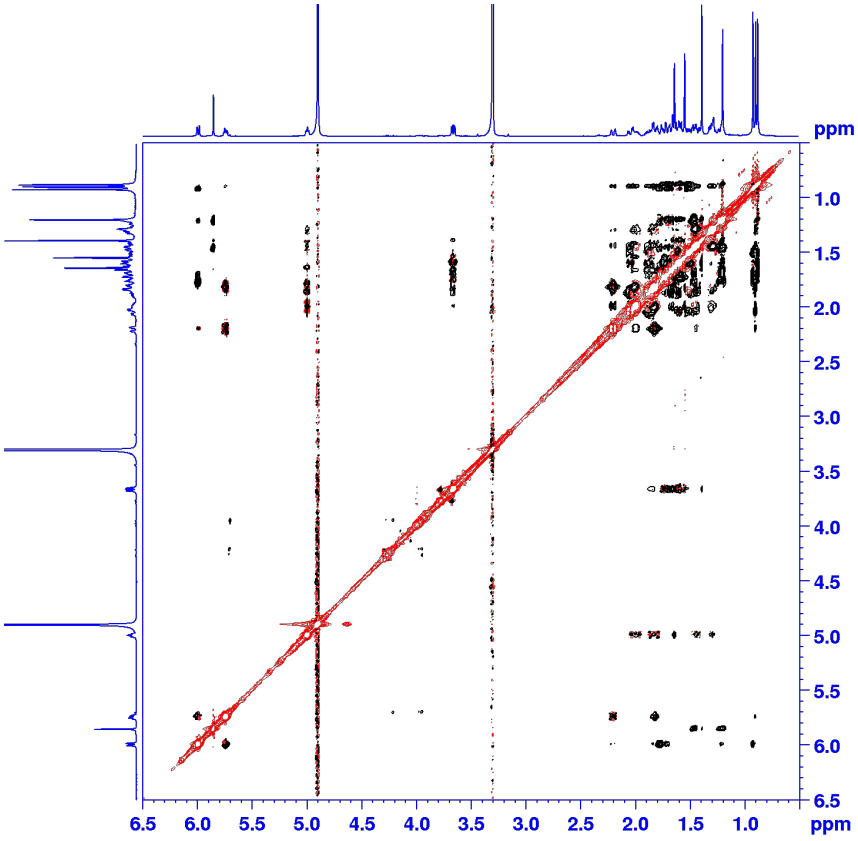

Figure S6. NOESY spectrum (500 MHz) of Gromomycin A (**2**) in CD_3OD.

a)

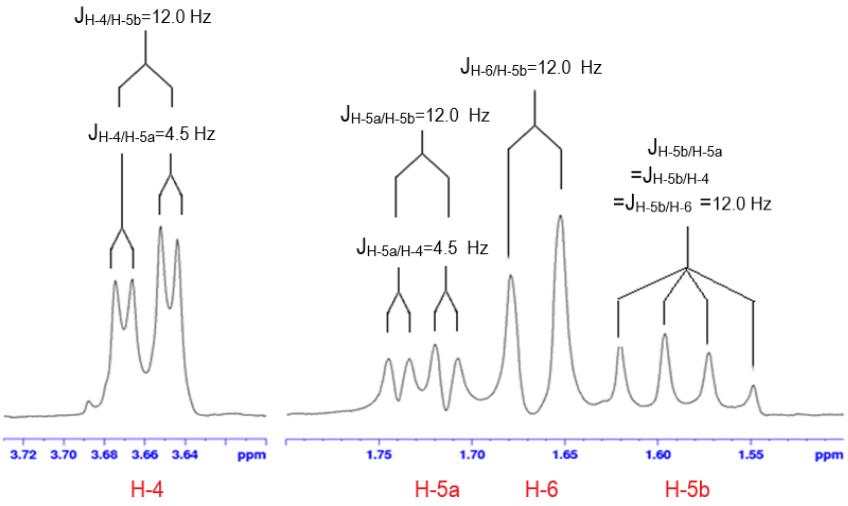

b.)

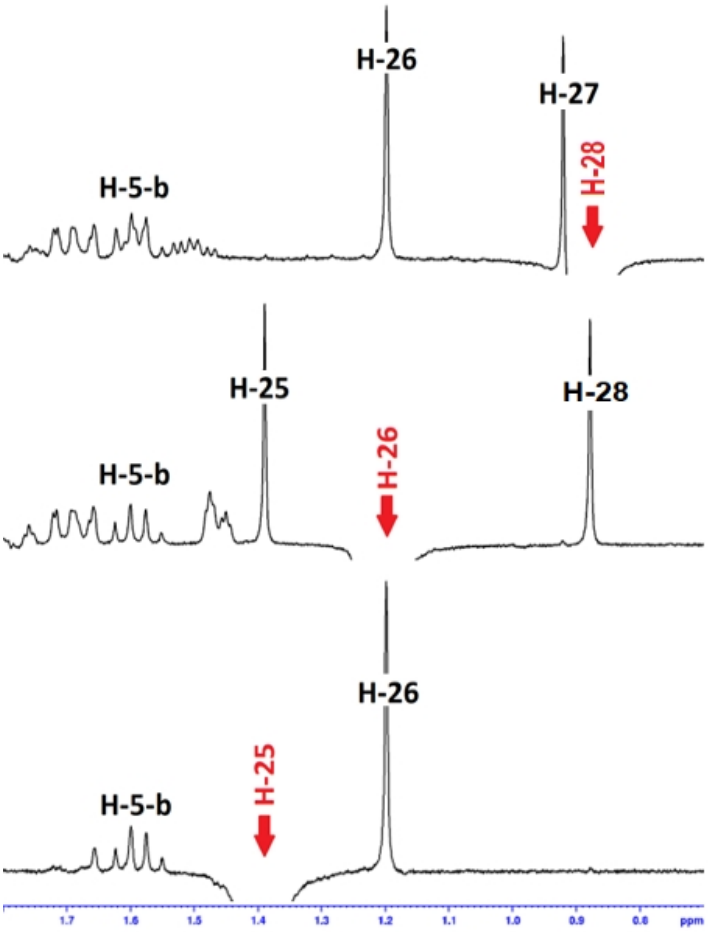

Figure S7. Selective 1D experiments of gromomycin (**2**). a) selective TOCSY with excitation of H-4 (δ_H 3.66). b) 1D selective NOESY´s with excitations of H-25 (δ_H 1.40), H-26 (δ_H 1.20) and H-28 (δ_H 0.88).

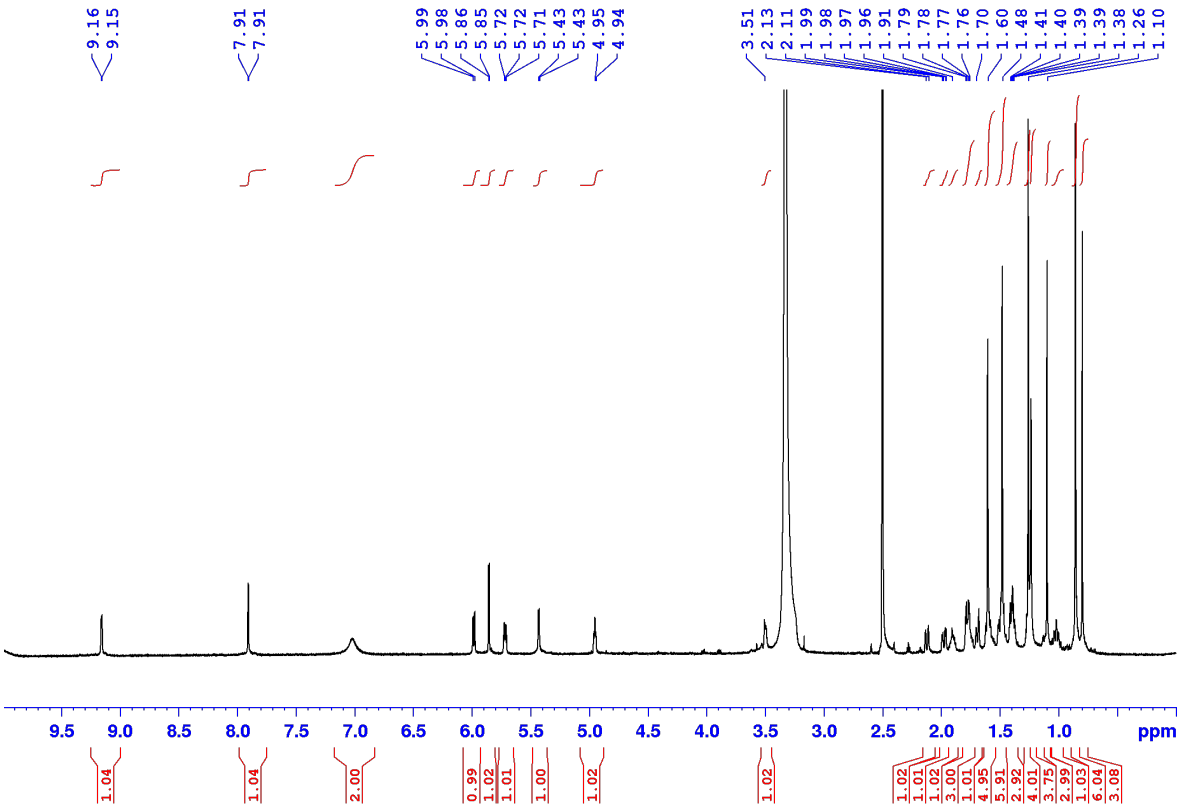

Figure S8. ^{1}H NMR spectrum (700 MHz) of Gromomycin A (**2**) in DMSO-d_6/1 drop TFA-d_1.

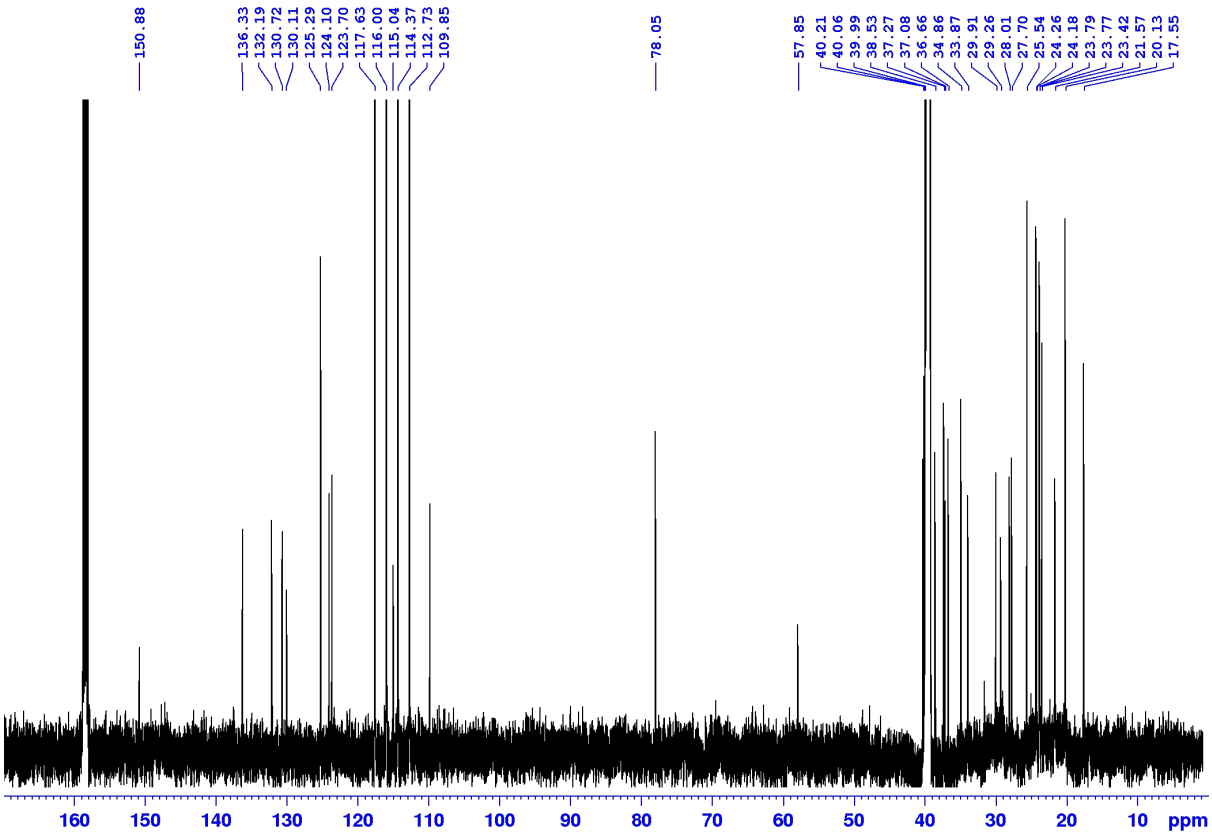

Figure S9. ^{13}C NMR spectrum (175 MHz) of Gromomycin A (**2**) in DMSO-d_6/1 drop TFA.

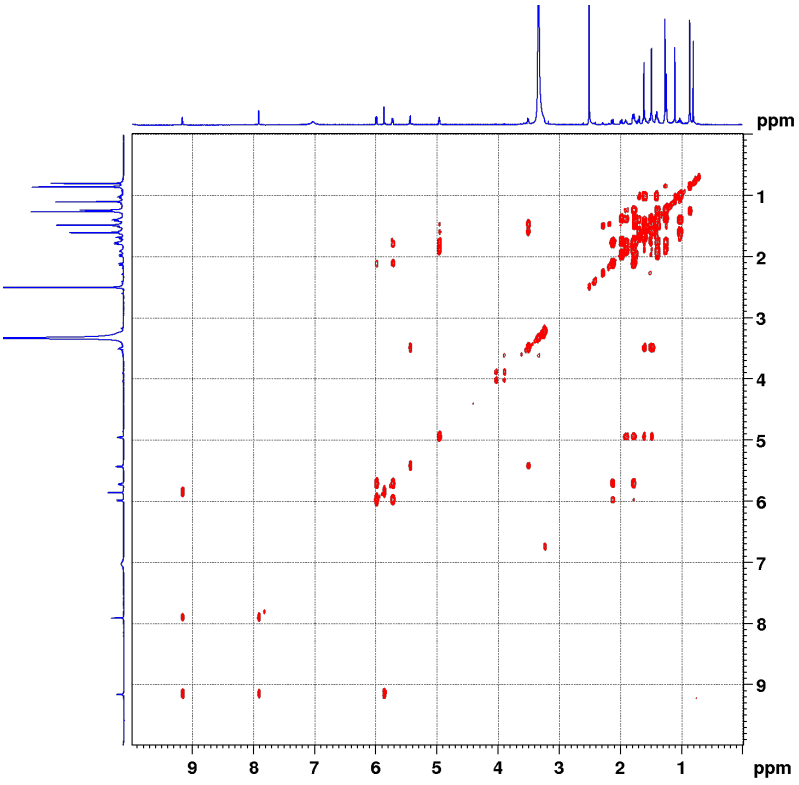

Figure S10. COSY spectrum (700 MHz) of Gromomycin A (**2**) in DMSO-d_6/1 drop TFA.

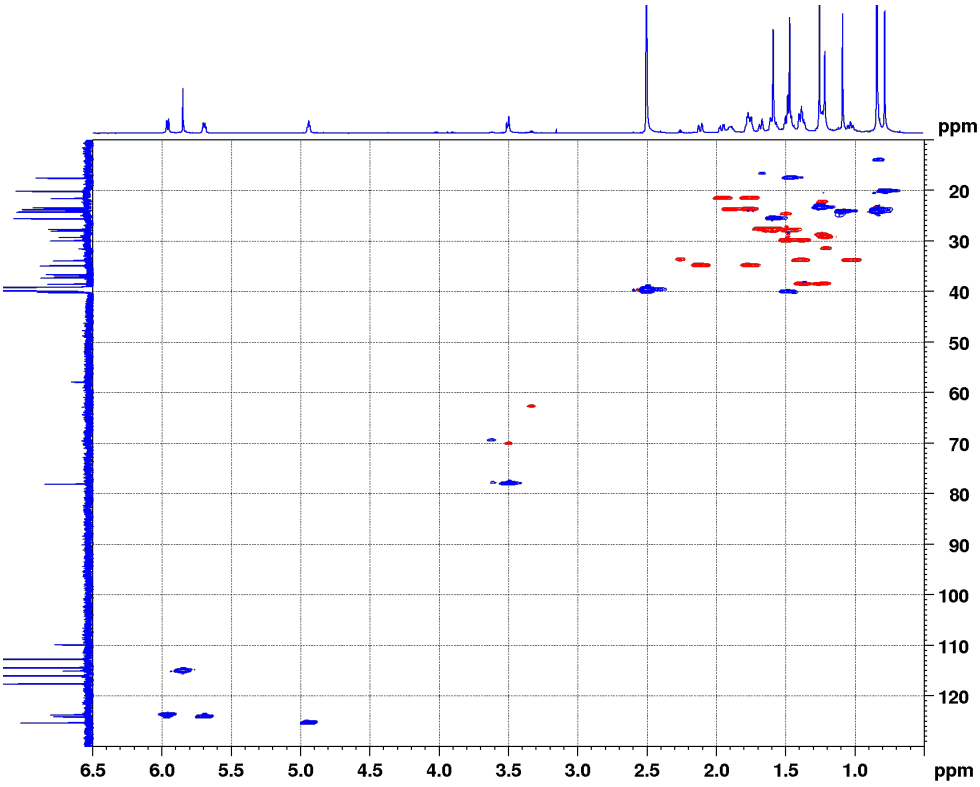

Figure S11. ^{1}H-^{13}C HSQC spectrum (700 MHz) of Gromomycin A (**2**) in DMSO-d_6/1 drop TFA.

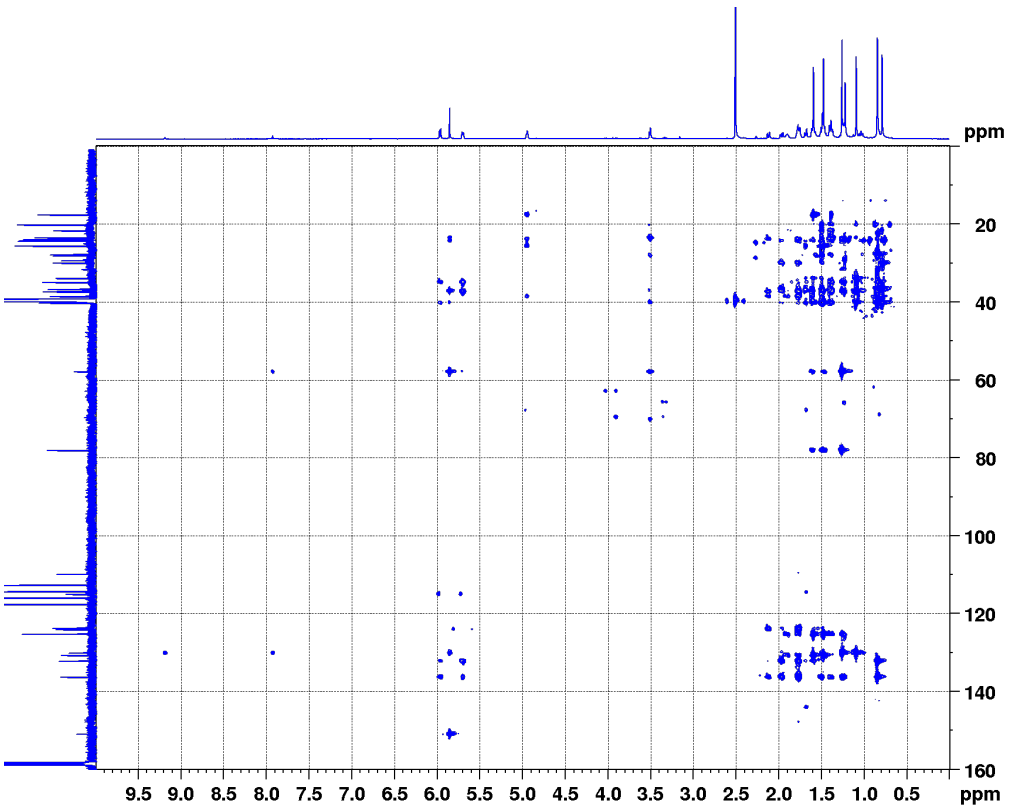

Figure S12. ^{1}H-^{13}C HMBC spectrum (700 MHz) of Gromomycin A (**2**) in DMSO-d_6/1 drop TFA.

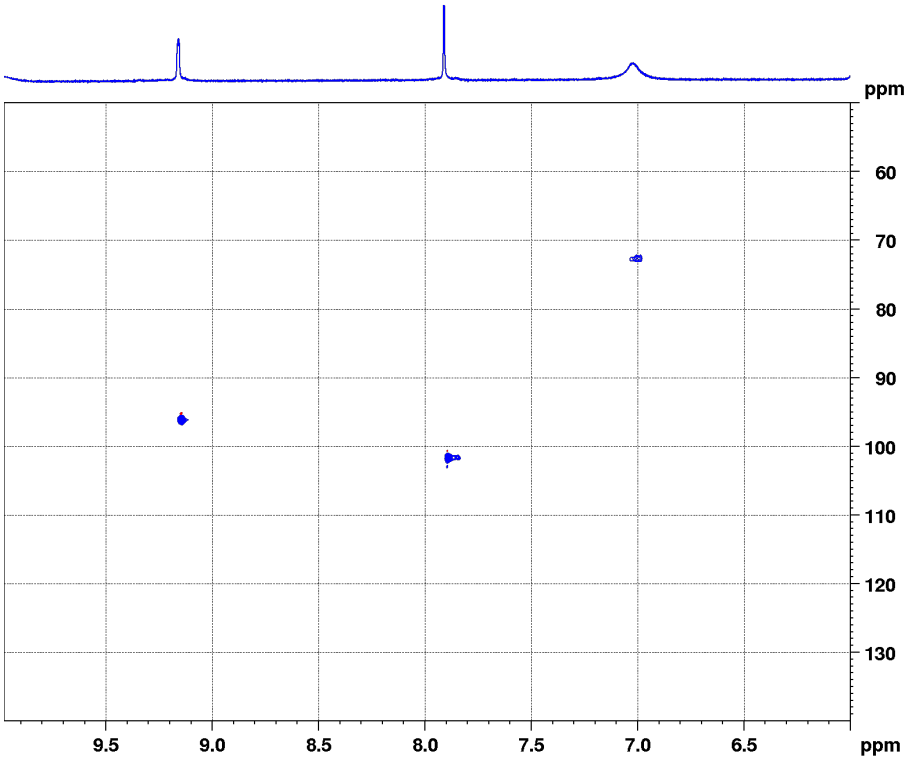

Figure S13. 1H-^{15}N HSQC spectrum of Gromomycin A (**2**) in DMSO-d_6/1 drop TFA.

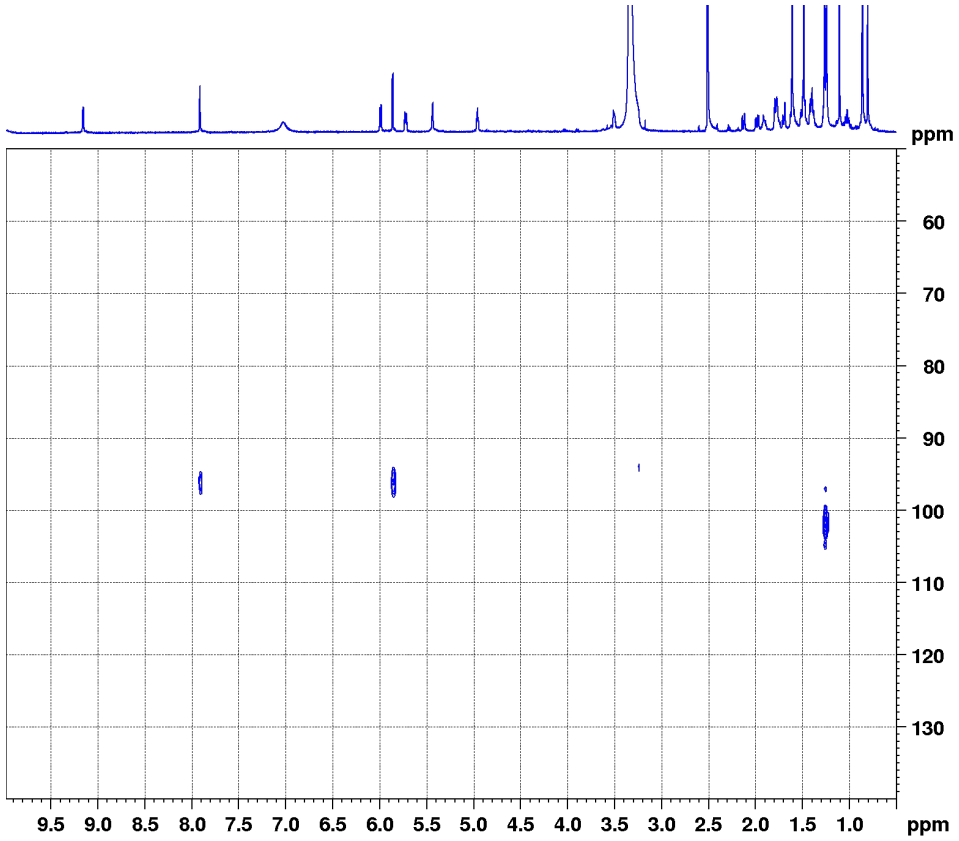

Figure S14. 1H-^{15}N HMBC spectrum of Gromomycin A (**2**) in DMSO-d_6/1 drop TFA.

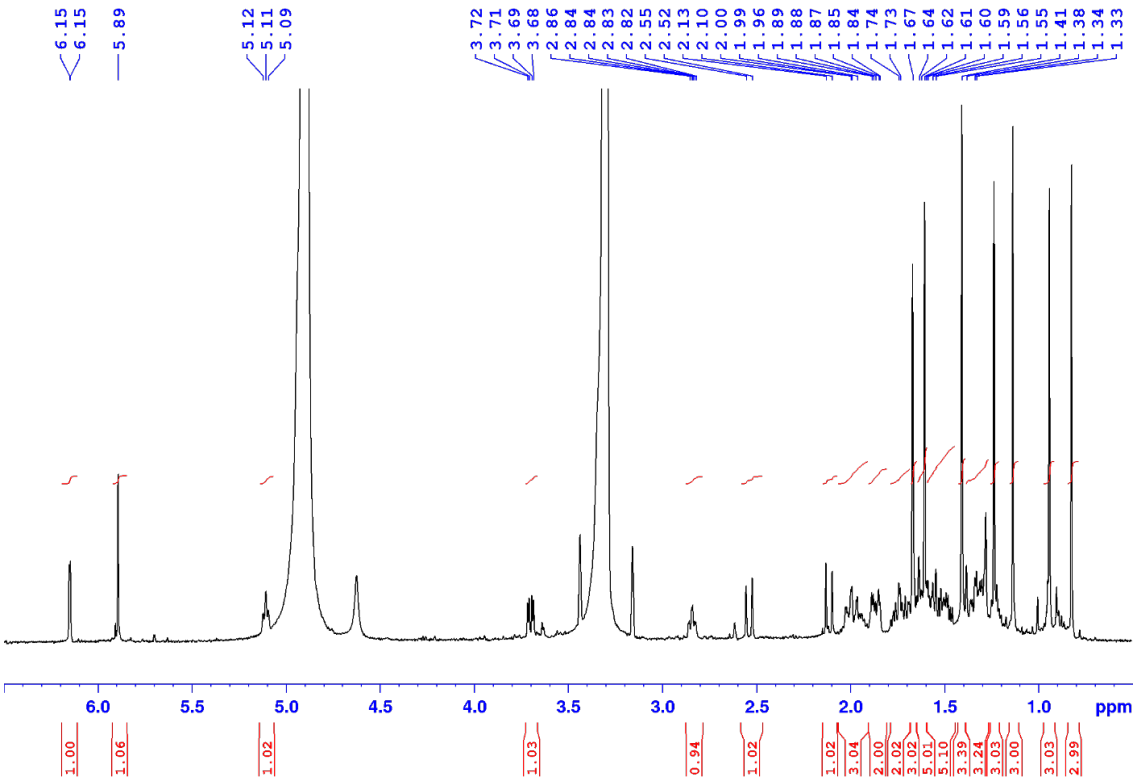

Figure S15. ^{1}H NMR spectrum (500 MHz) of Gromomycin B (**3**) in CD_3OD.

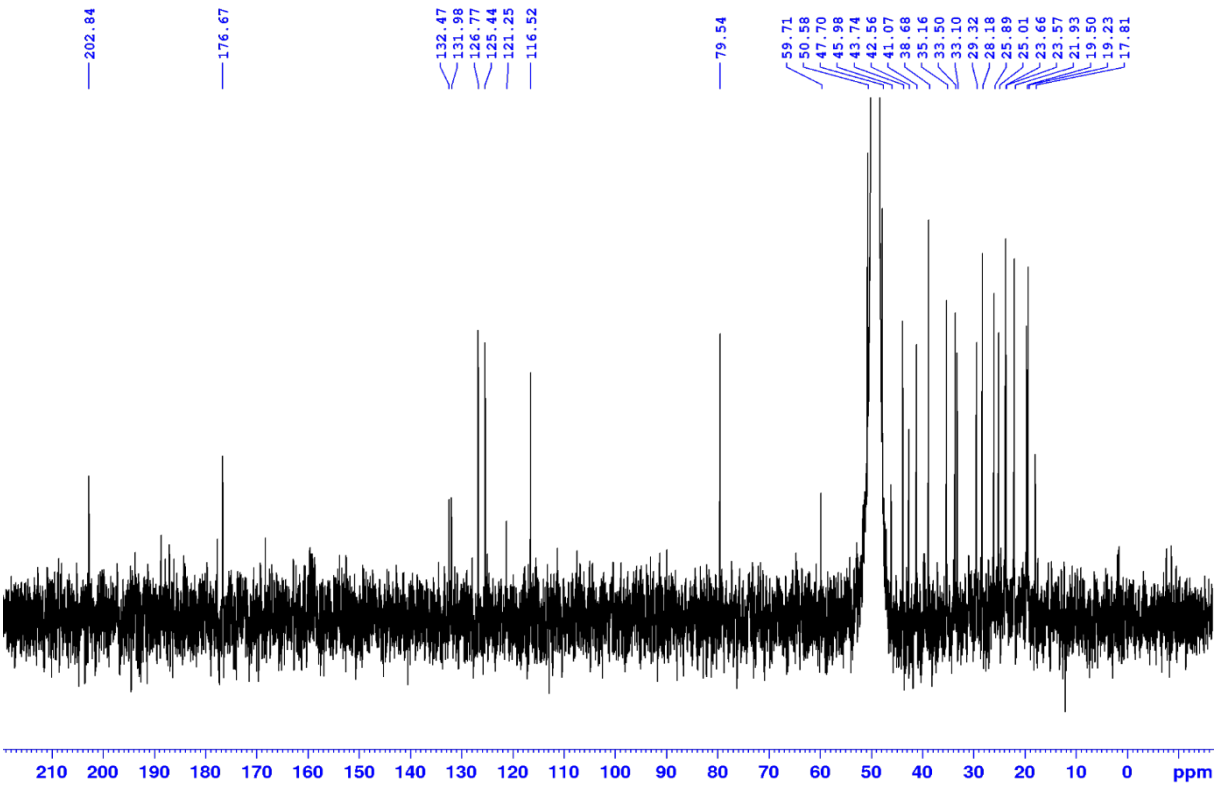

Figure S16. ^{13}C NMR spectrum (125 MHz) of Gromomycin B (**3**) in CD_3OD.

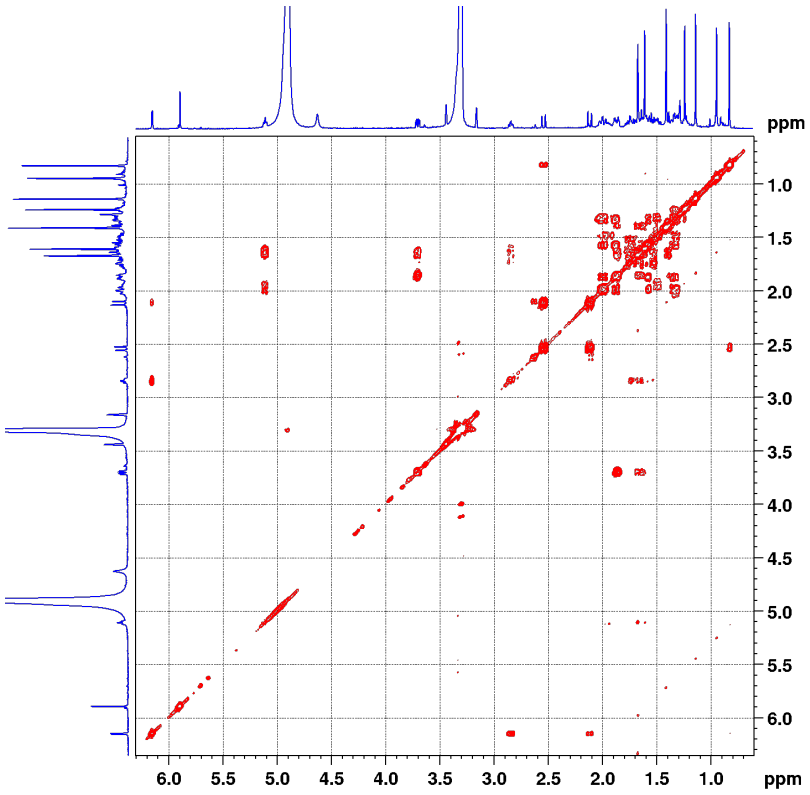

Figure S17. COSY spectrum (500 MHz) of Gromomycin B (**3**) in CD_3OD.

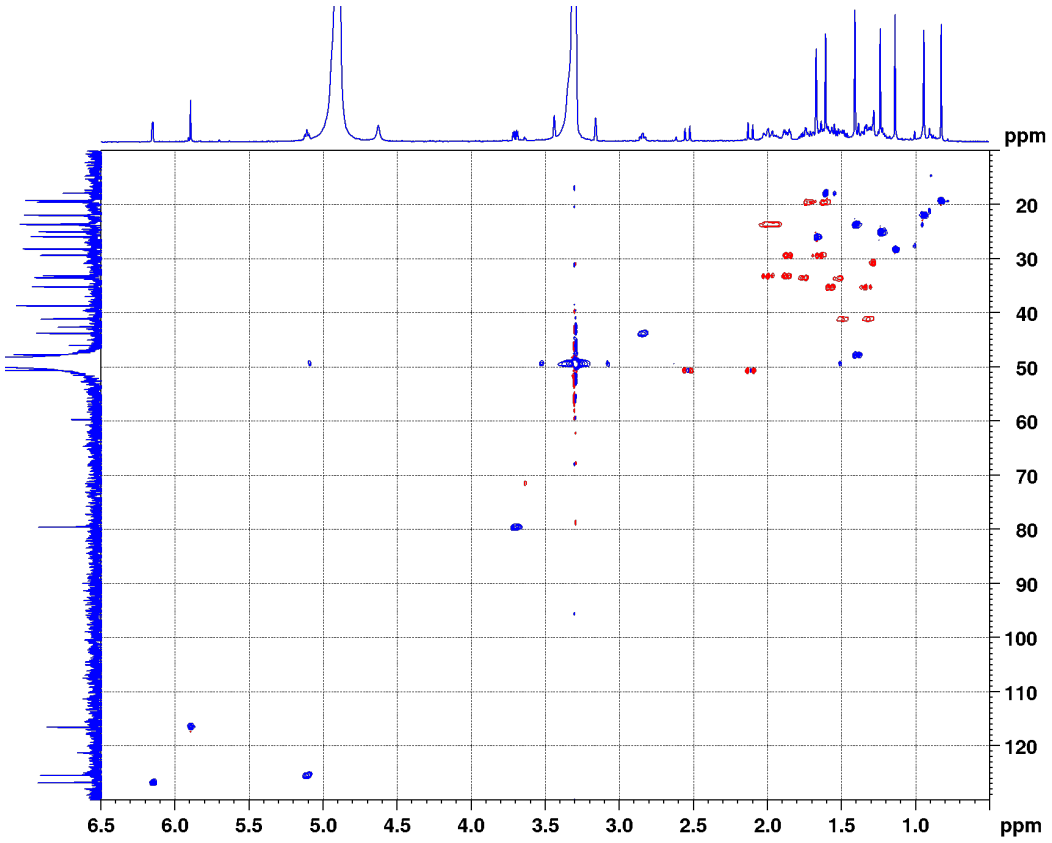

Figure S18. ^{1}H-^{13}C HSQC spectrum (500 MHz) of Gromomycin B (**3**) in CD_3OD.

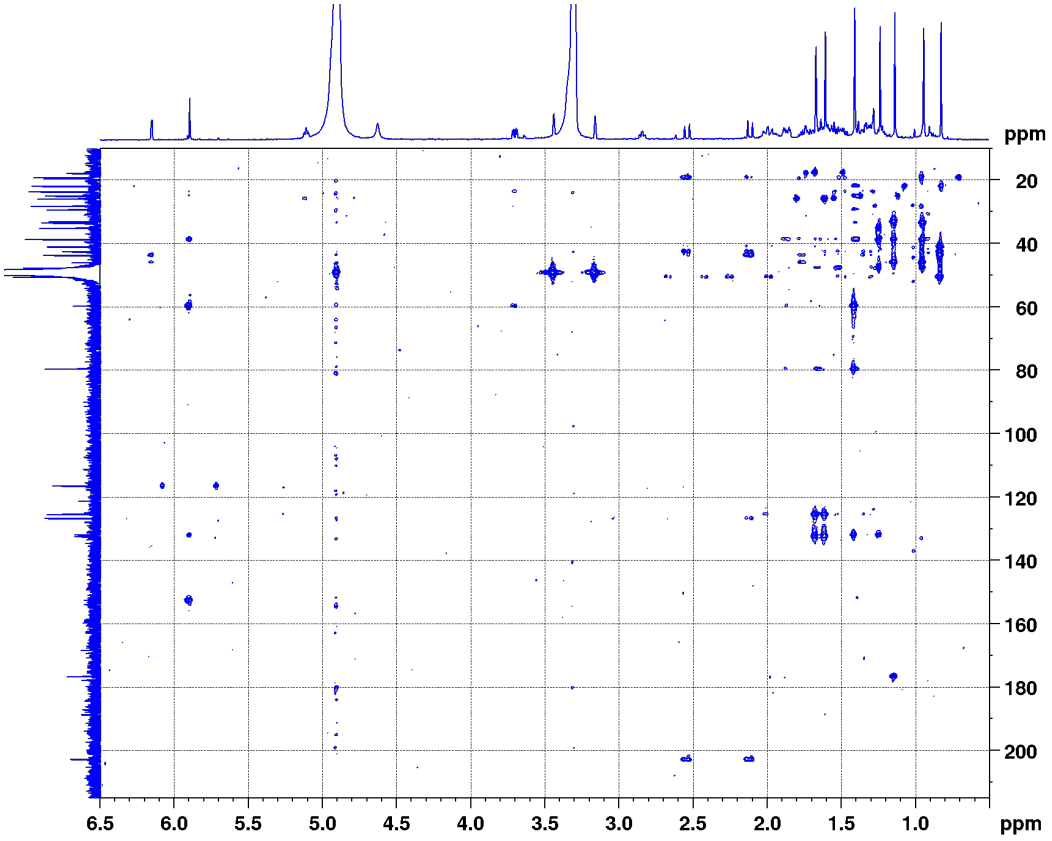

Figure S19. ^{1}H-^{13}C HMBC spectrum (500 MHz) of Gromomycin B (**3**) in CD_3OD.

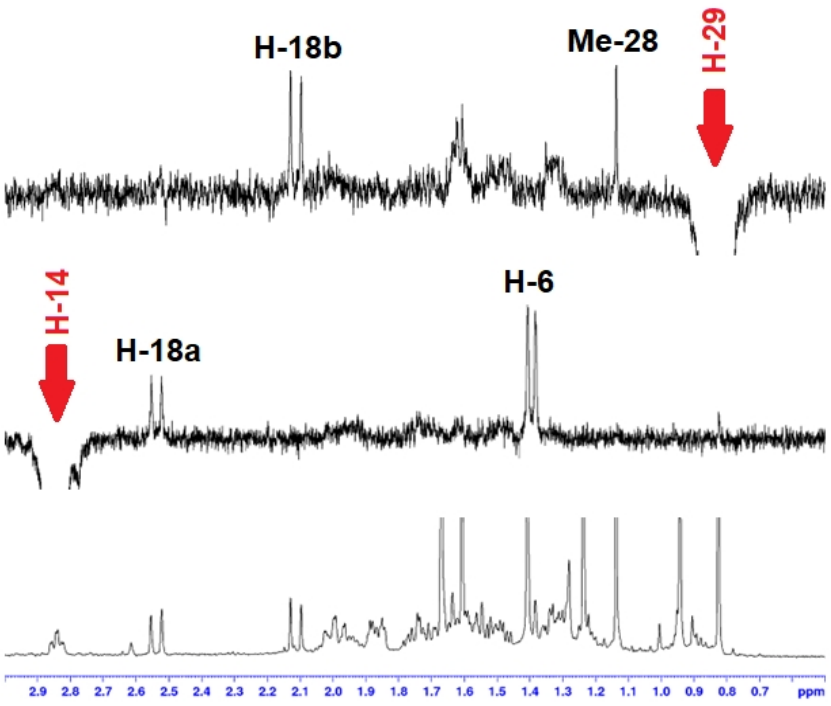

Figure S20. 1D selective NOESY´s of gromomycin B (**3**) with excitations of H-14 (δ_H 2.84) and H-29 (δ_H 0.85).

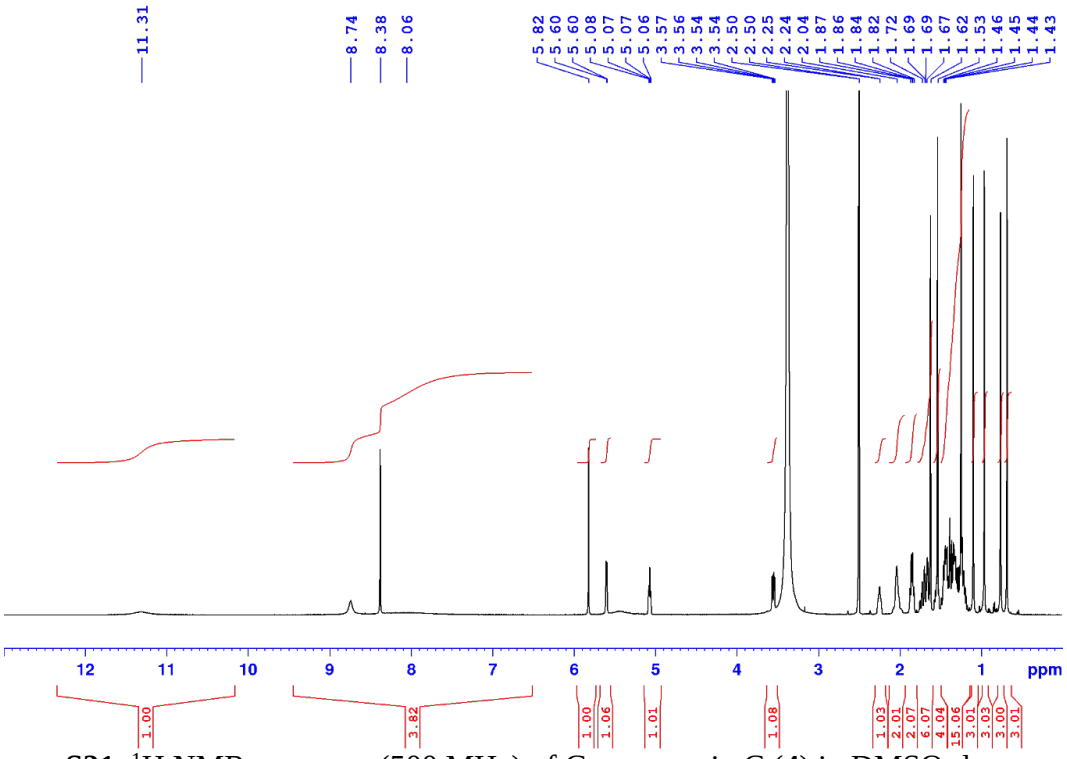

Figure S21. ^{1}H NMR spectrum (500 MHz) of Gromomycin C (**4**) in DMSO-d_6.

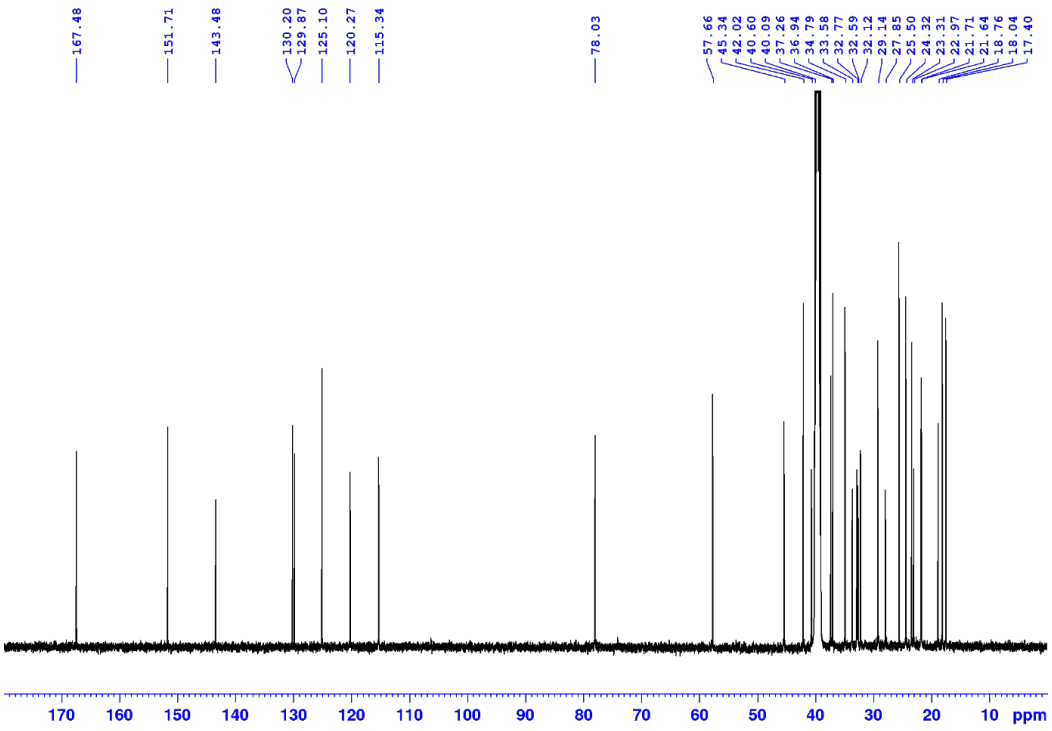

Figure S22. ^{13}C NMR spectrum (125 MHz) of Gromomycin C (**4**) in DMSO-d_6.

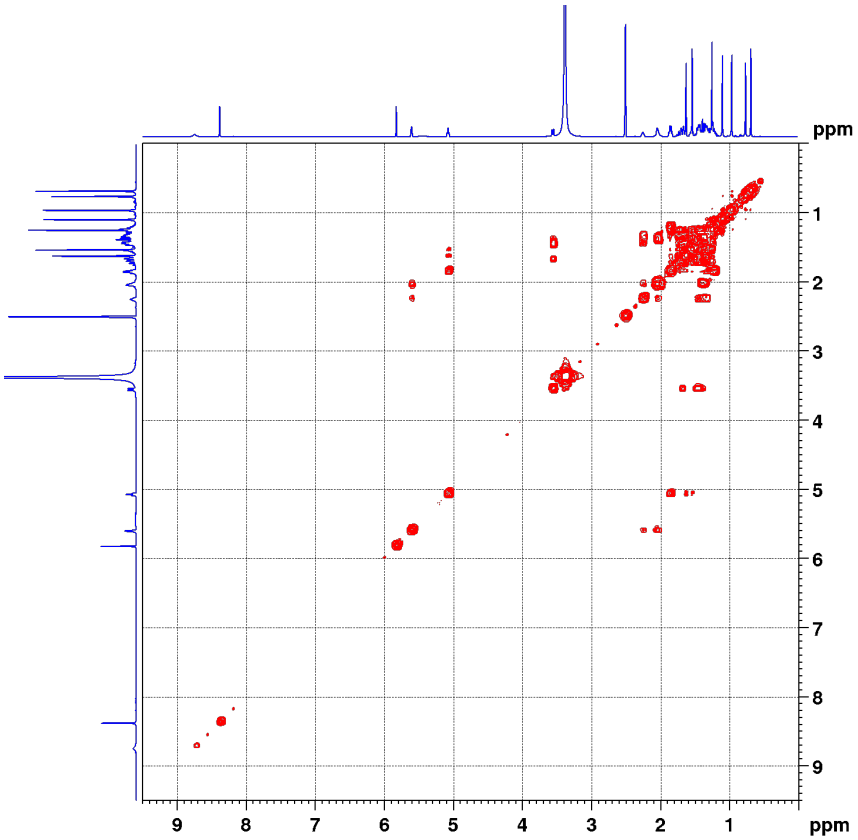

Figure S23. COSY spectrum (500 MHz) of Gromomycin C (**4**) in DMSO-d_6.

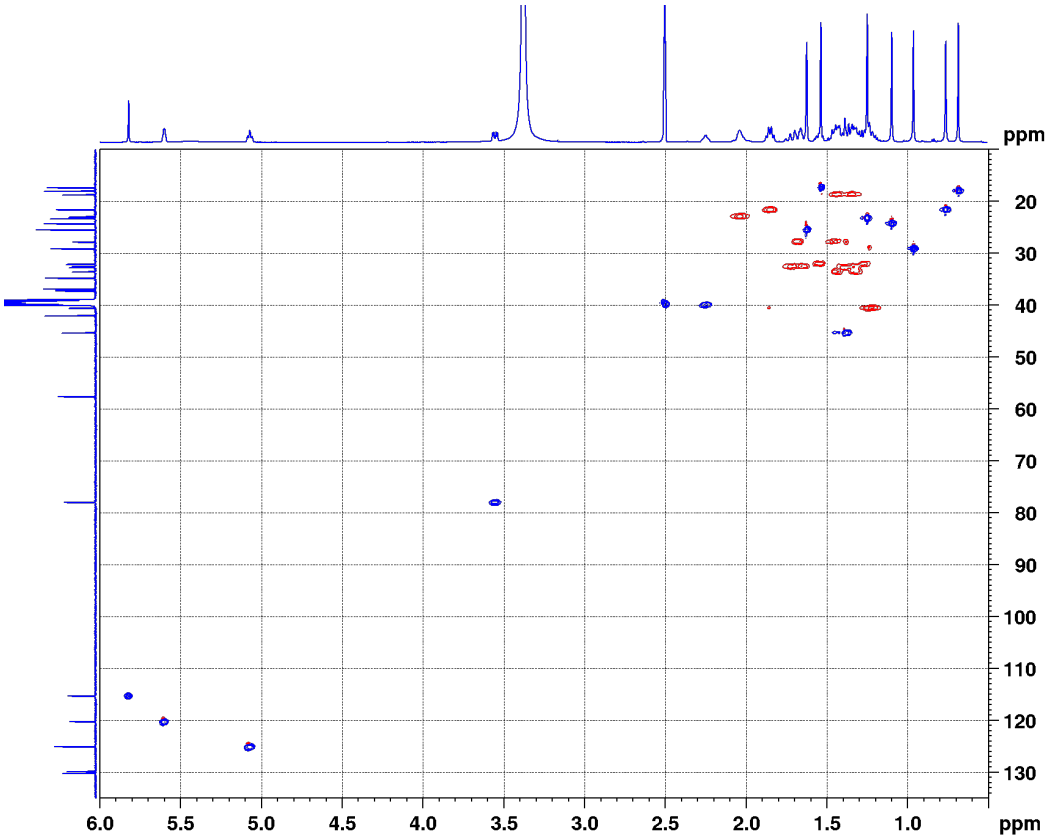

Figure S24. ^{1}H-^{13}C HSQC spectrum (500 MHz) of Gromomycin C (**4**) in DMSO-d_6.

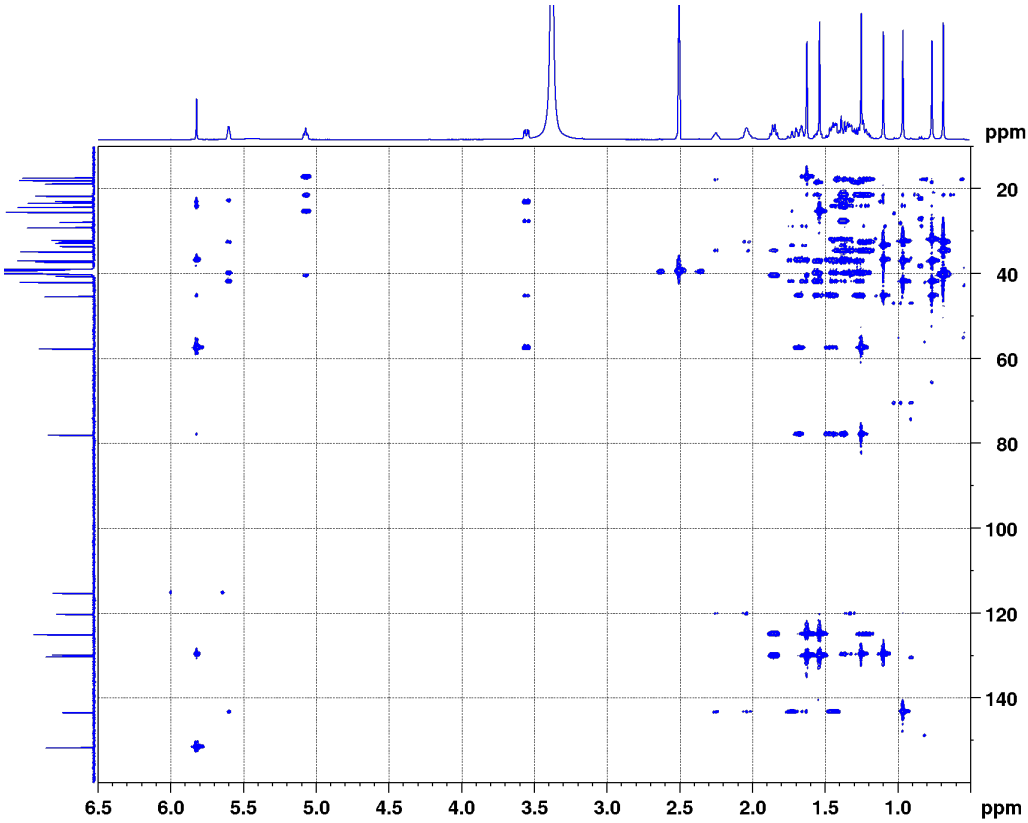

Figure S25. ^{1}H-^{13}C HMBC spectrum (500 MHz) of Gromomycin C (**4**) in DMSO-d_6.

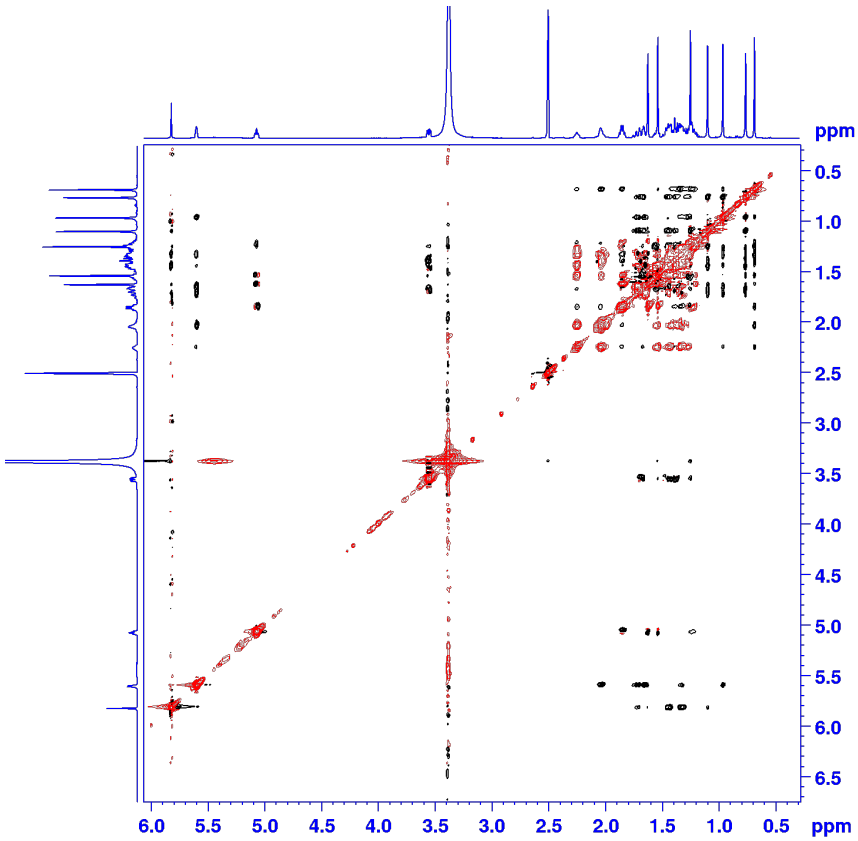

Figure S26. ROESY spectrum (500 MHz) of Gromomycin C (**4**) in DMSO-d_6.

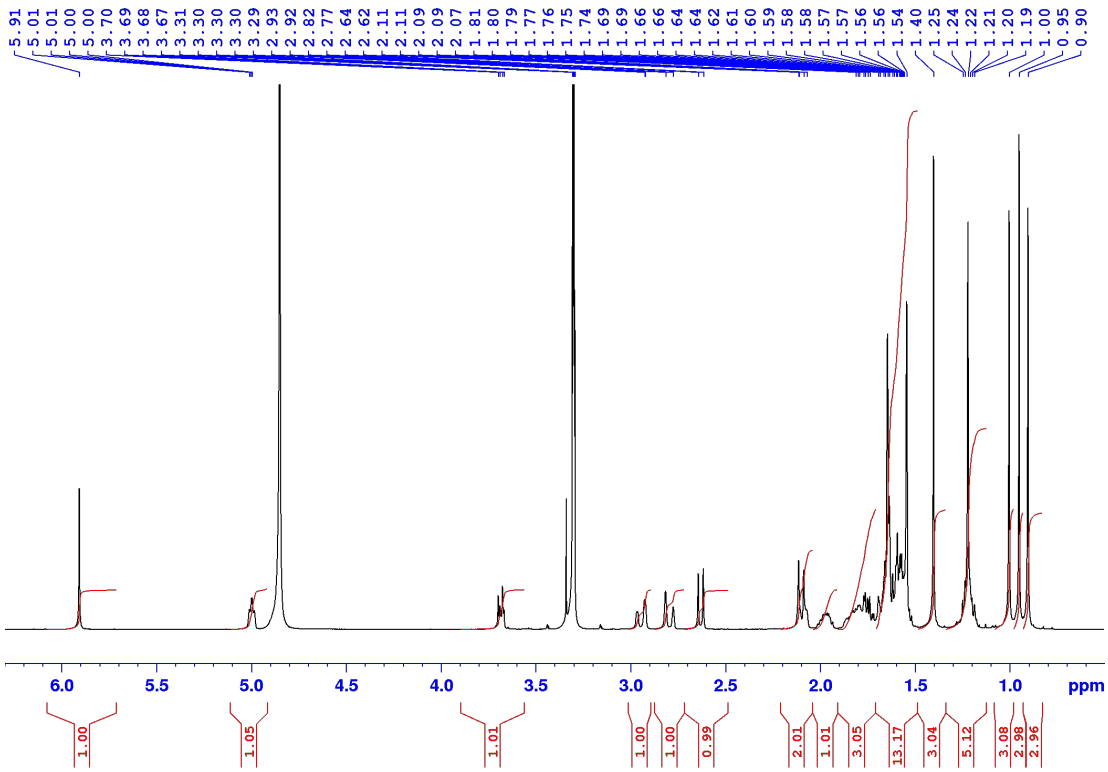

Figure S27. ^{1}H NMR spectrum (500 MHz) of Gromomycin D (**5**) in CD_3OD.

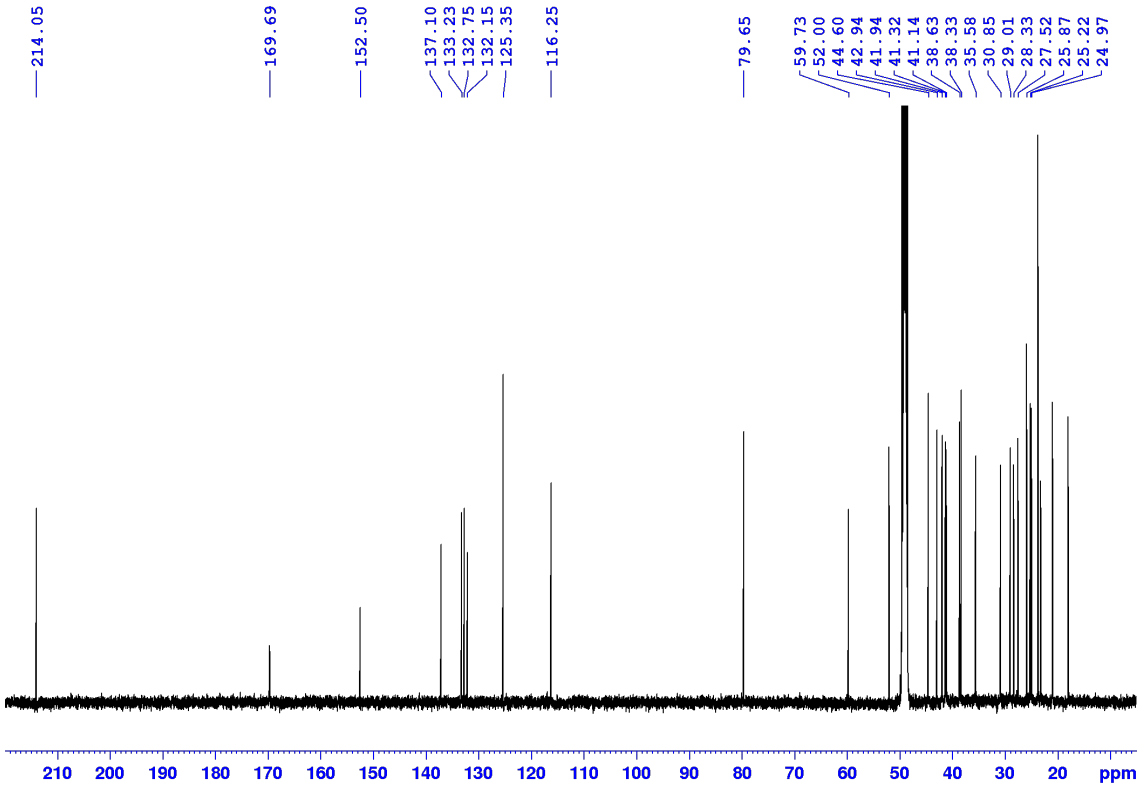

Figure S28. ^{13}C NMR spectrum (125 MHz) of Gromomycin D (**5**) in CD_3OD.

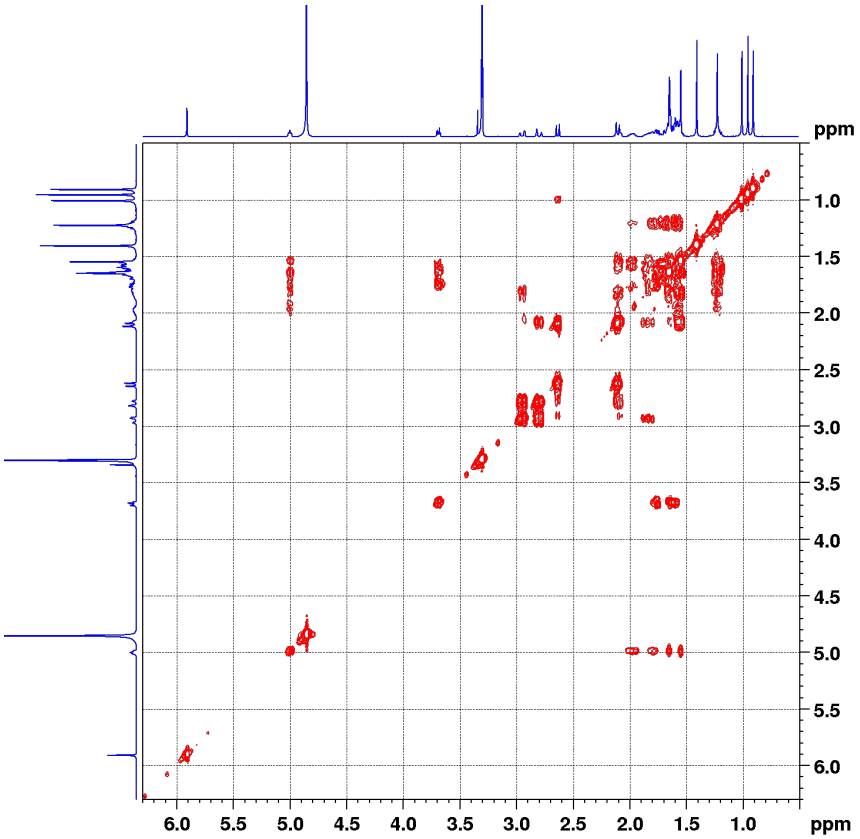

Figure S29. COSY spectrum (500 MHz) of Gromomycin D (**5**) in CD_3OD.

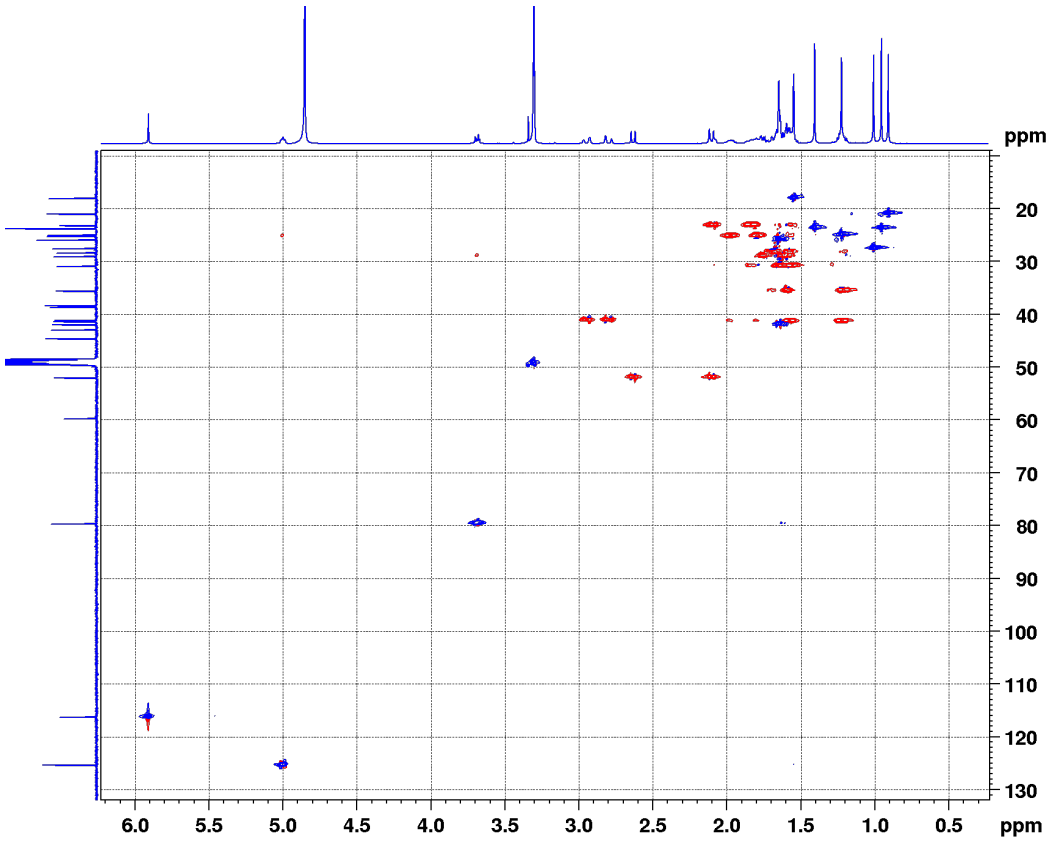

Figure S30. ^{1}H-^{13}C HSQC spectrum (500 MHz) of Gromomycin D (**5**) in CD_3OD.

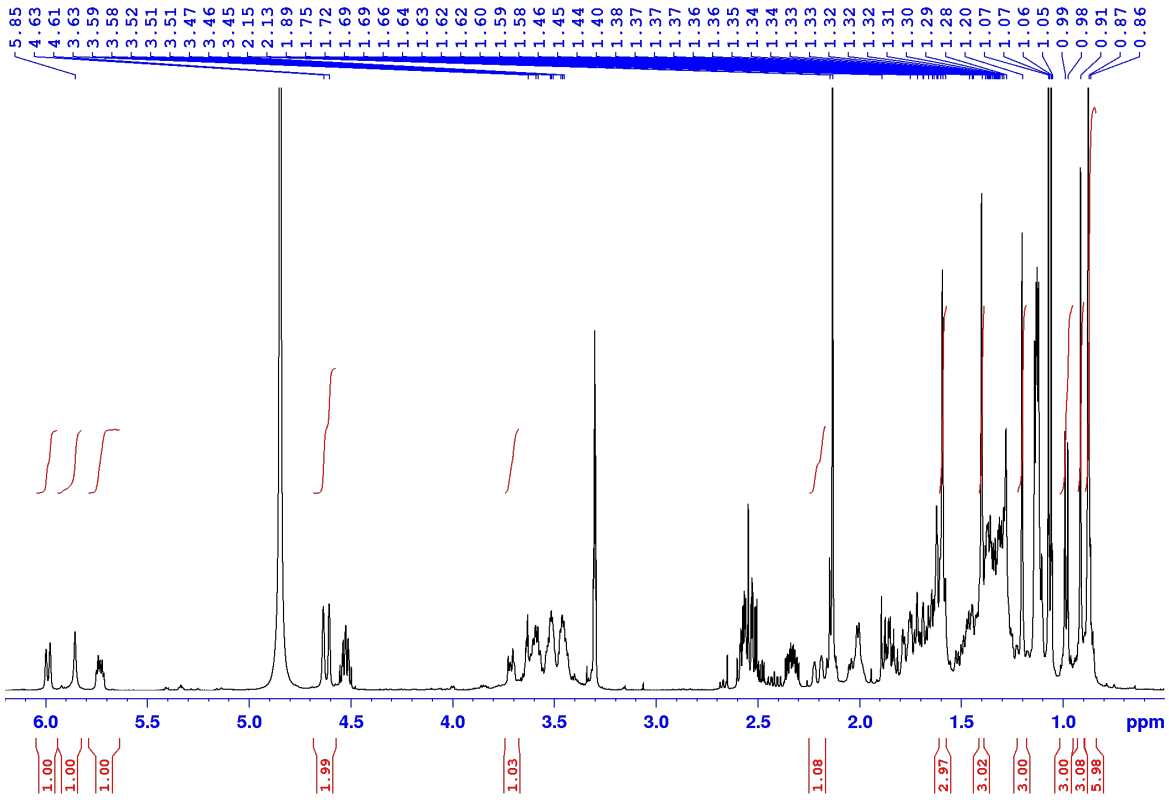

Figure S31. ^{1}H NMR spectrum (500 MHz) of Gromomycin E (**6**) in CD_3OD.

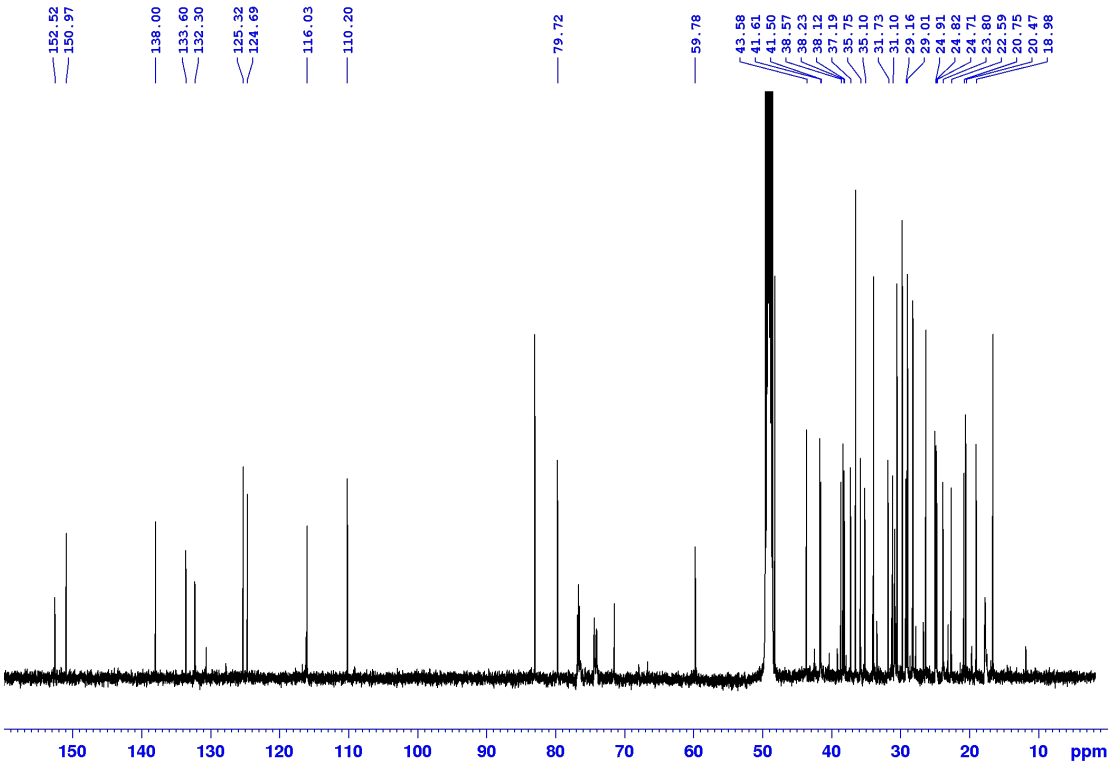

Figure S32. ^{13}C NMR spectrum (125 MHz) of Gromomycin E (**6**) in CD_3OD.

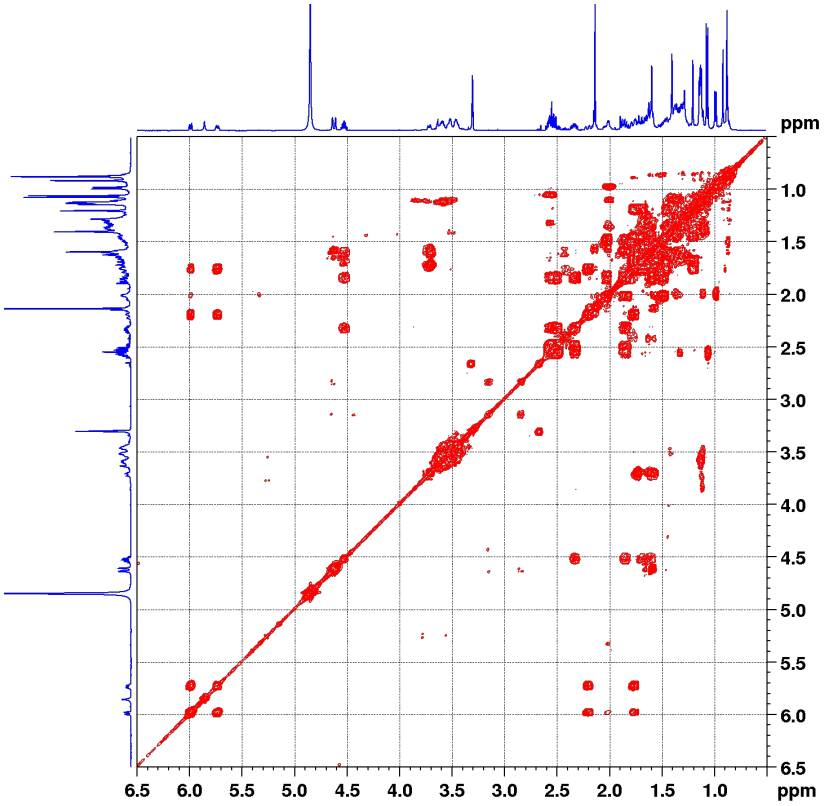

Figure S33. COSY spectrum (500 MHz) of Gromomycin E (**6**) in CD_3OD.

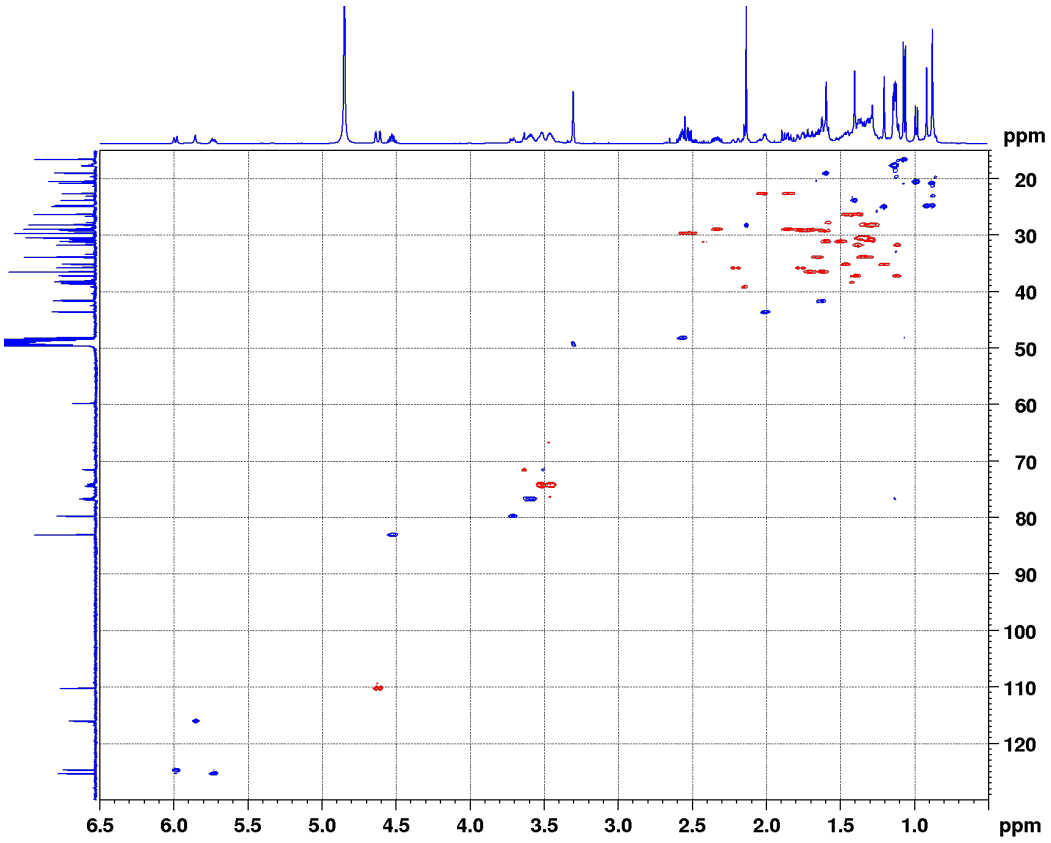

Figure S34. ^{1}H-^{13}C HSQC spectrum (500 MHz) of Gromomycin E (**6**) in CD_3OD.

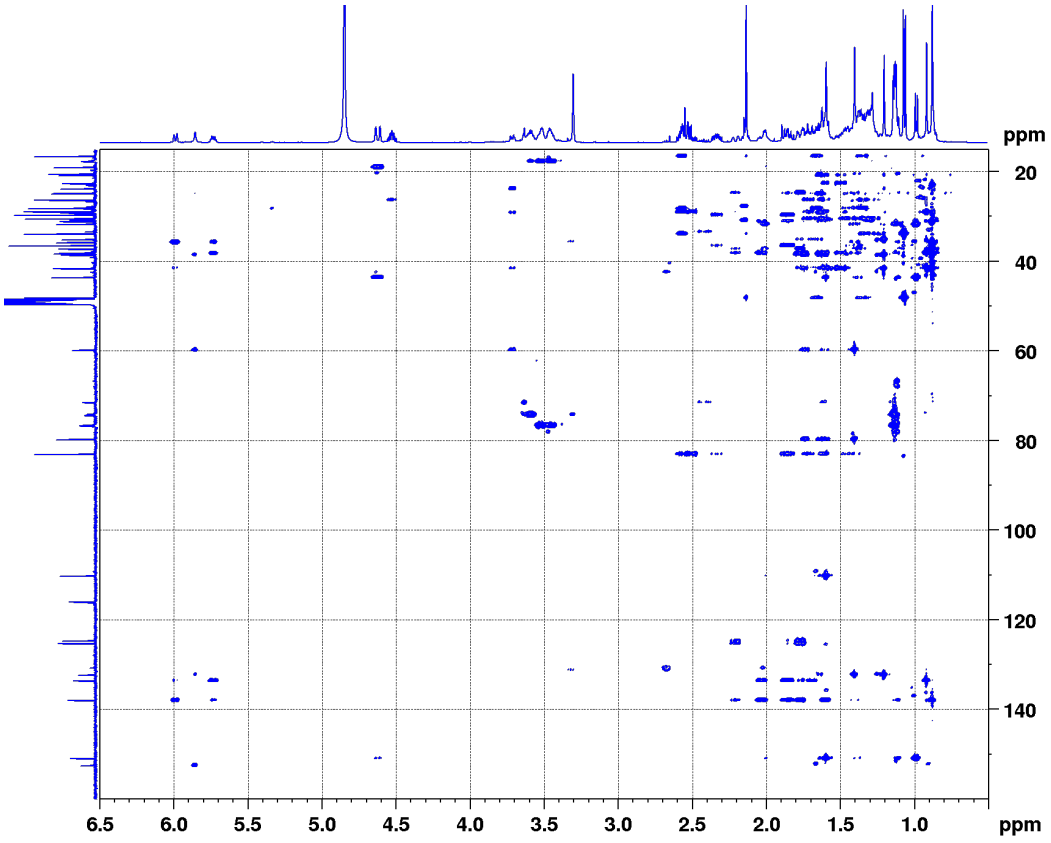

Figure S35. ^{1}H-^{13}C HMBC spectrum (500 MHz) of Gromomycin E (**6**) in CD_3OD.

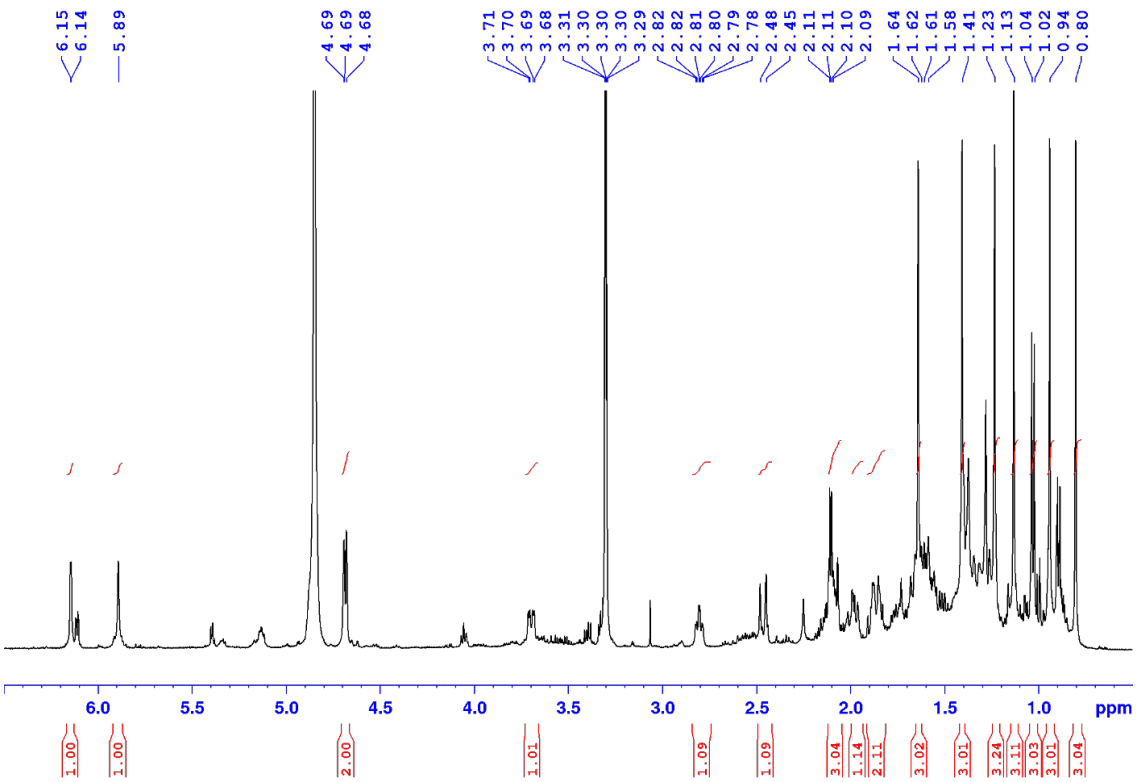

Figure S36. [1]H NMR spectrum (500 MHz) of Gromomycin F (**7**) in CD_3OD.

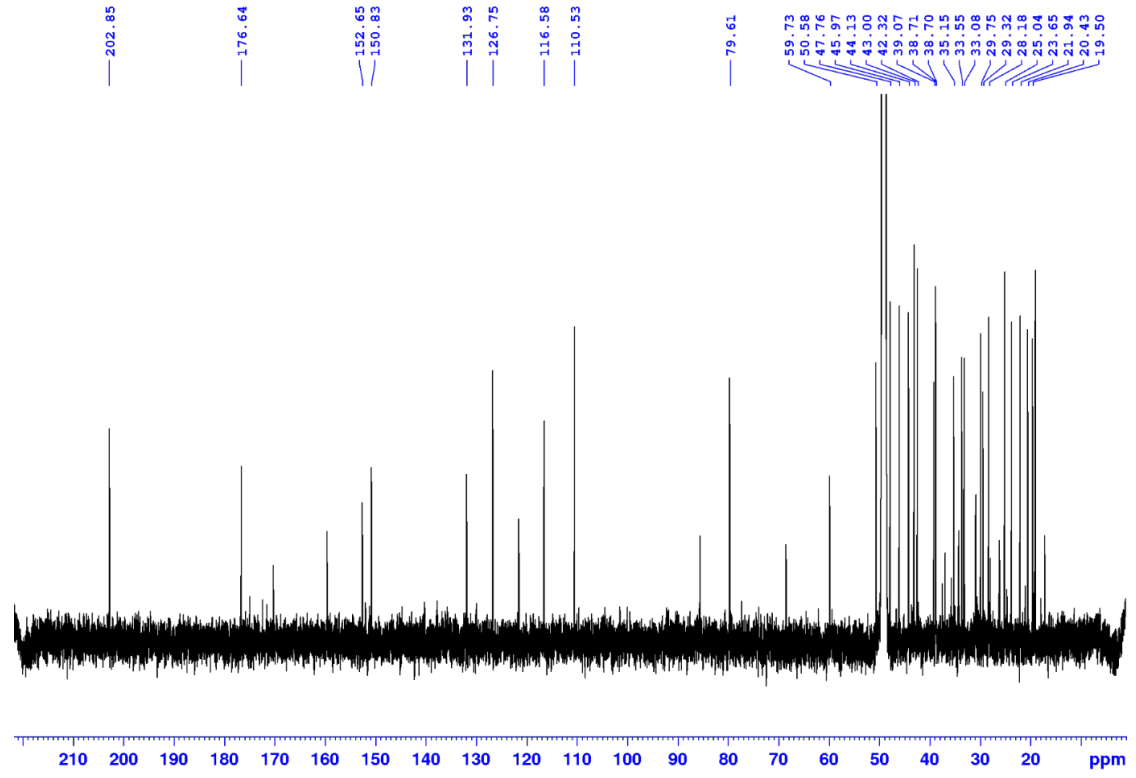

Figure S37. [13]C NMR spectrum (125 MHz) of Gromomycin F (**7**) in CD_3OD.

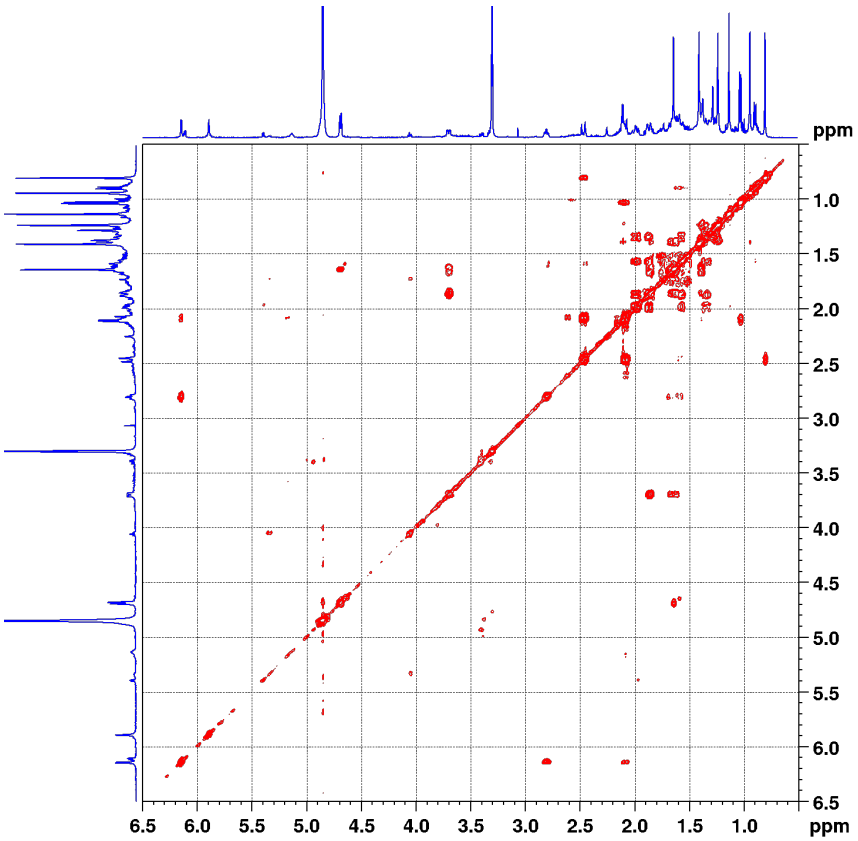

Figure S38. COSY spectrum (500 MHz) of Gromomycin F (**7**) in CD_3OD**.**

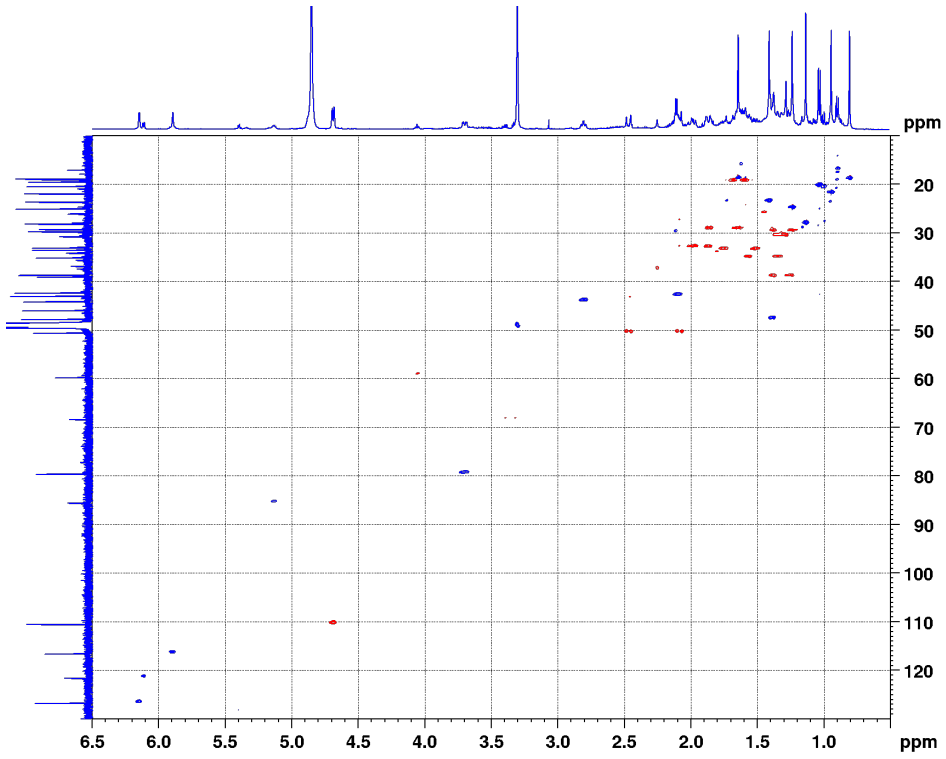

Figure S39. ^{1}H-^{13}C HSQC spectrum (500 MHz) of Gromomycin F (**7**) in CD_3OD.

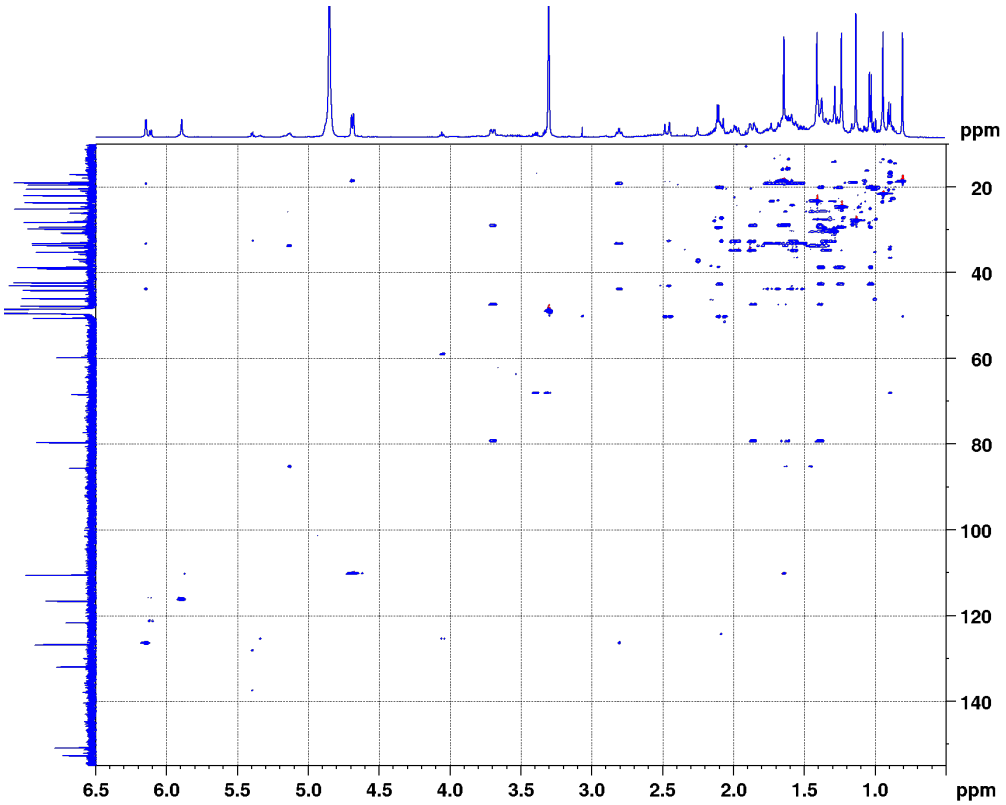

Figure S40. ^{1}H-^{13}C HMBC spectrum (500 MHz) of Gromomycin F (**7**) in CD_3OD.

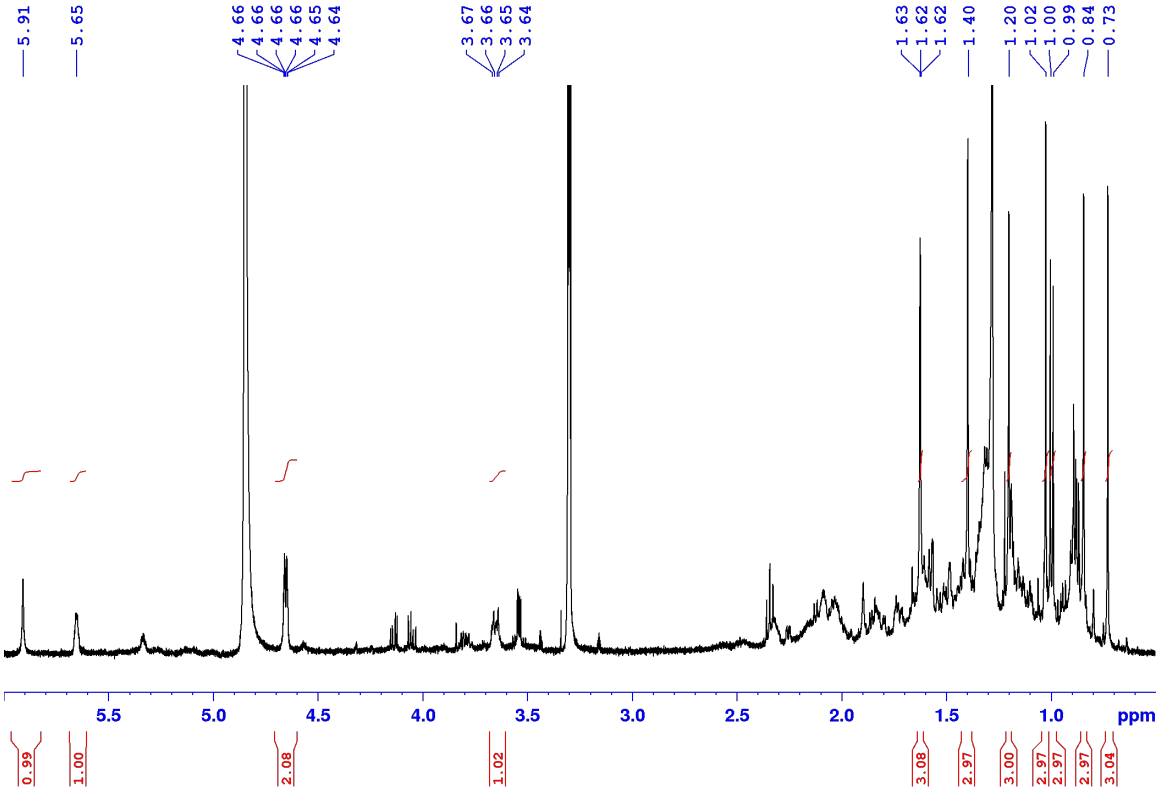

Figure S41. ^{1}H NMR spectrum (500 MHz) of Gromomycin G (**8**) in CD_3OD.

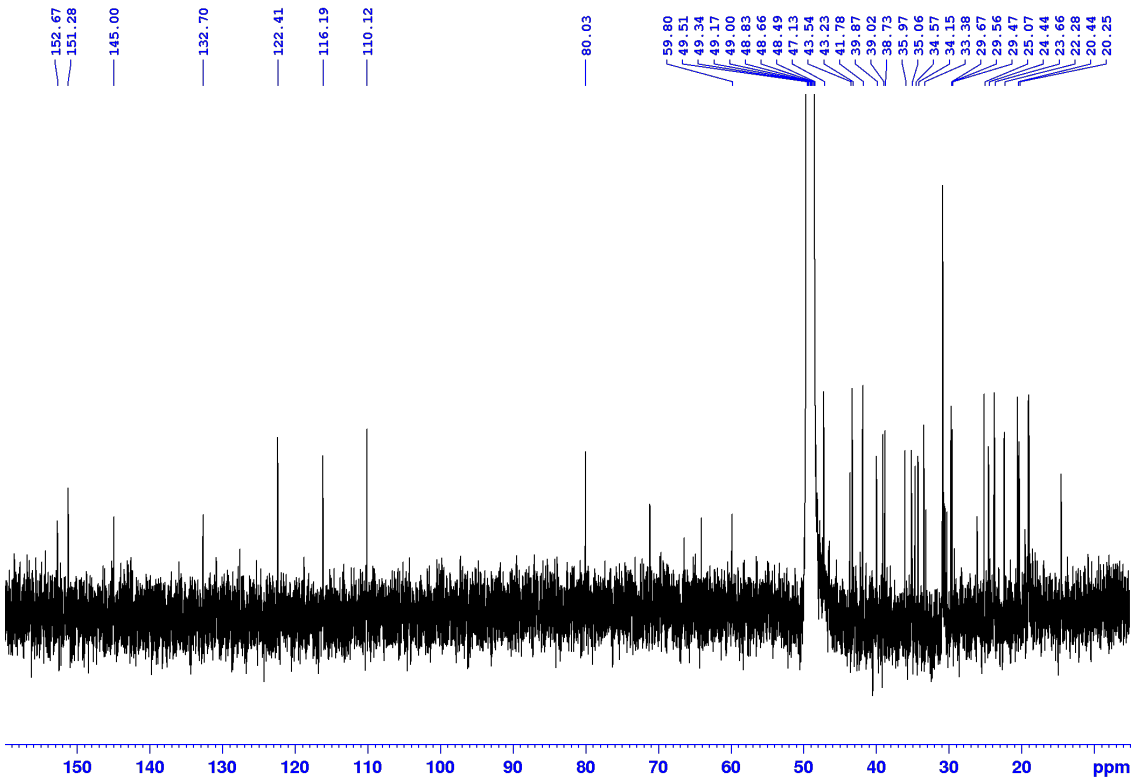

Figure S42. ^{13}C NMR spectrum (125 MHz) of Gromomycin G (**8**) in CD_3OD.

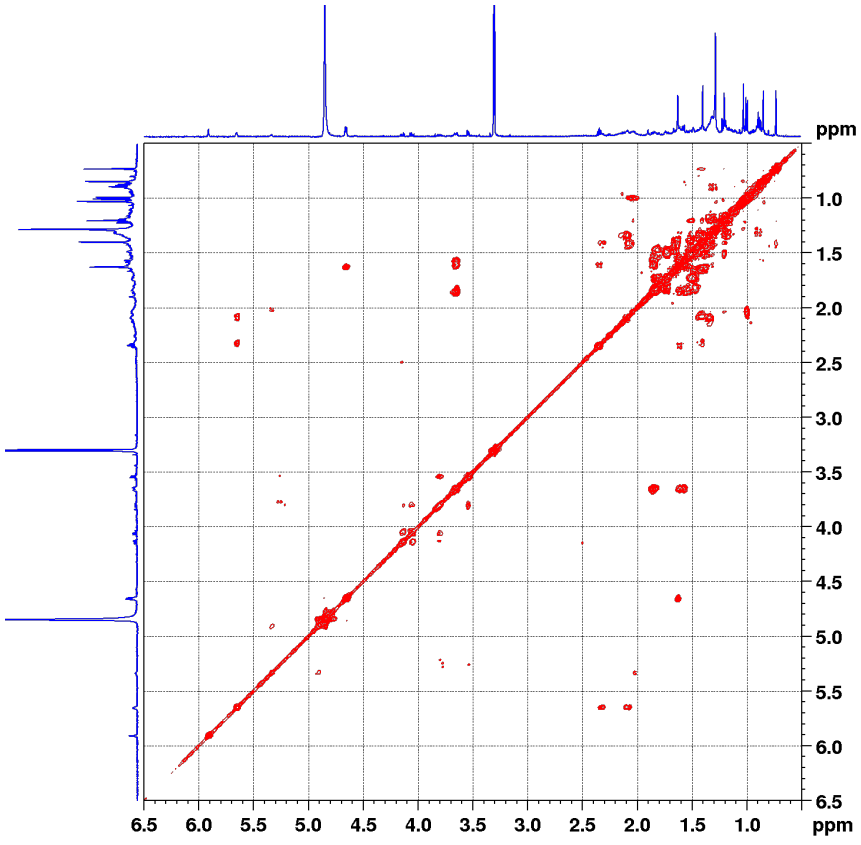

Figure S43. COSY spectrum (500 MHz) of Gromomycin G (**8**) in CD_3OD.

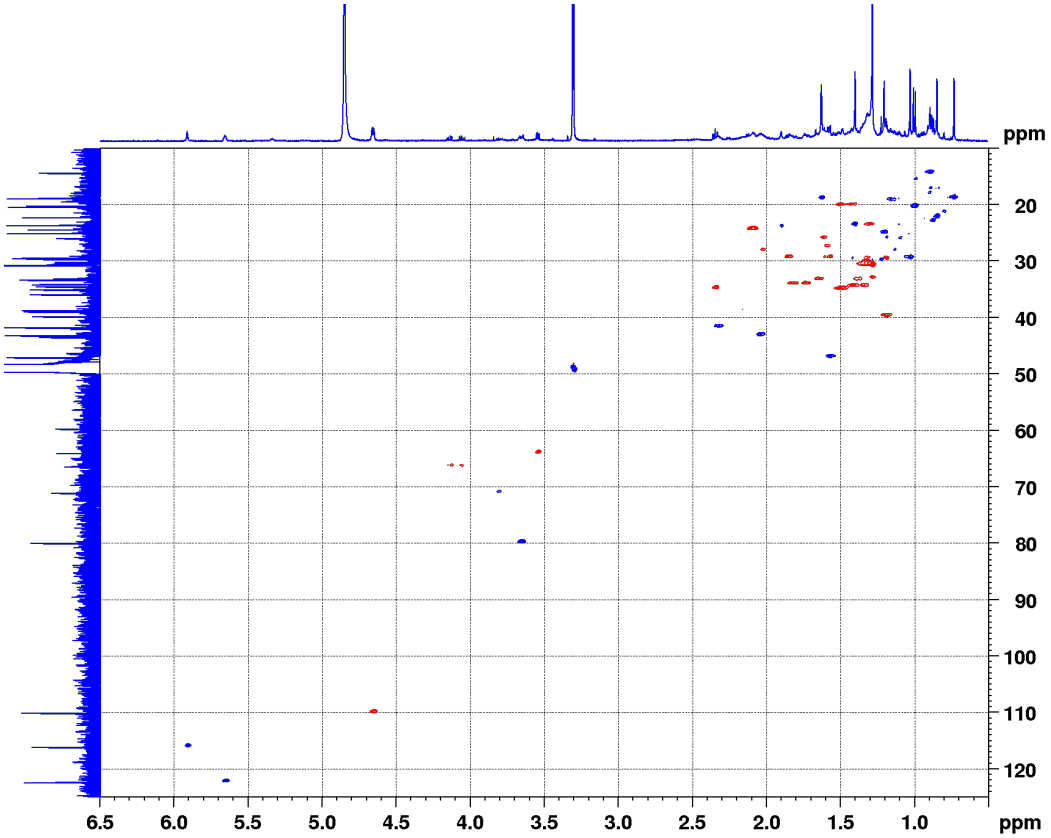

Figure S44. ^{1}H-^{13}C HSQC spectrum (500 MHz) of Gromomycin G (**8**) in CD_3OD.

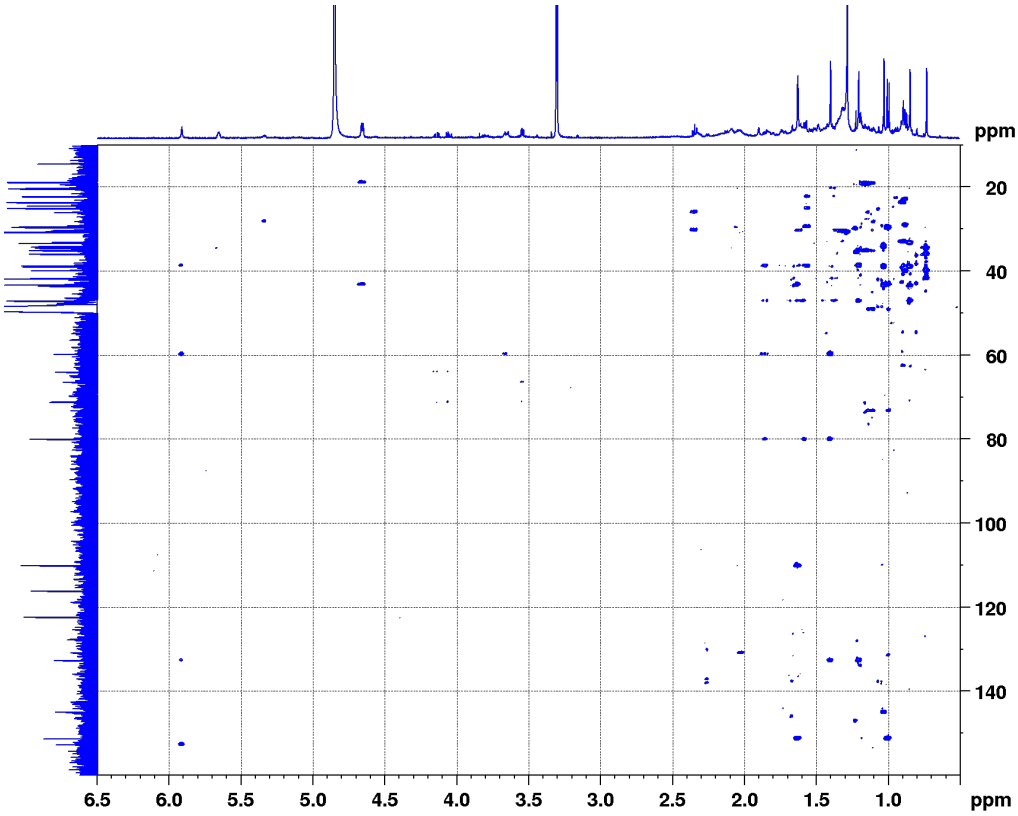

Figure S45. ^{1}H-^{13}C HMBC spectrum (500 MHz) of Gromomycin G (**8**) in CD_3OD.

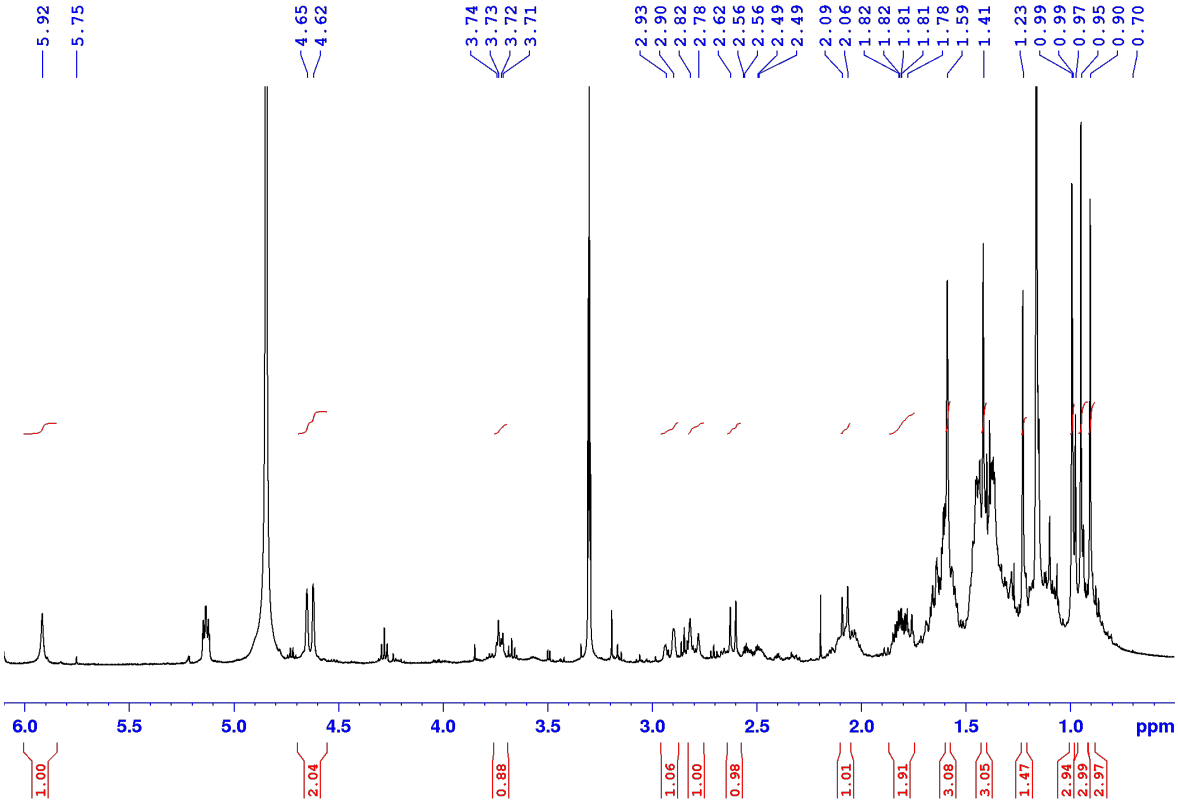

Figure S46. ^{1}H NMR spectrum (500 MHz) of Gromomycin H (**9**) in CD_3OD.

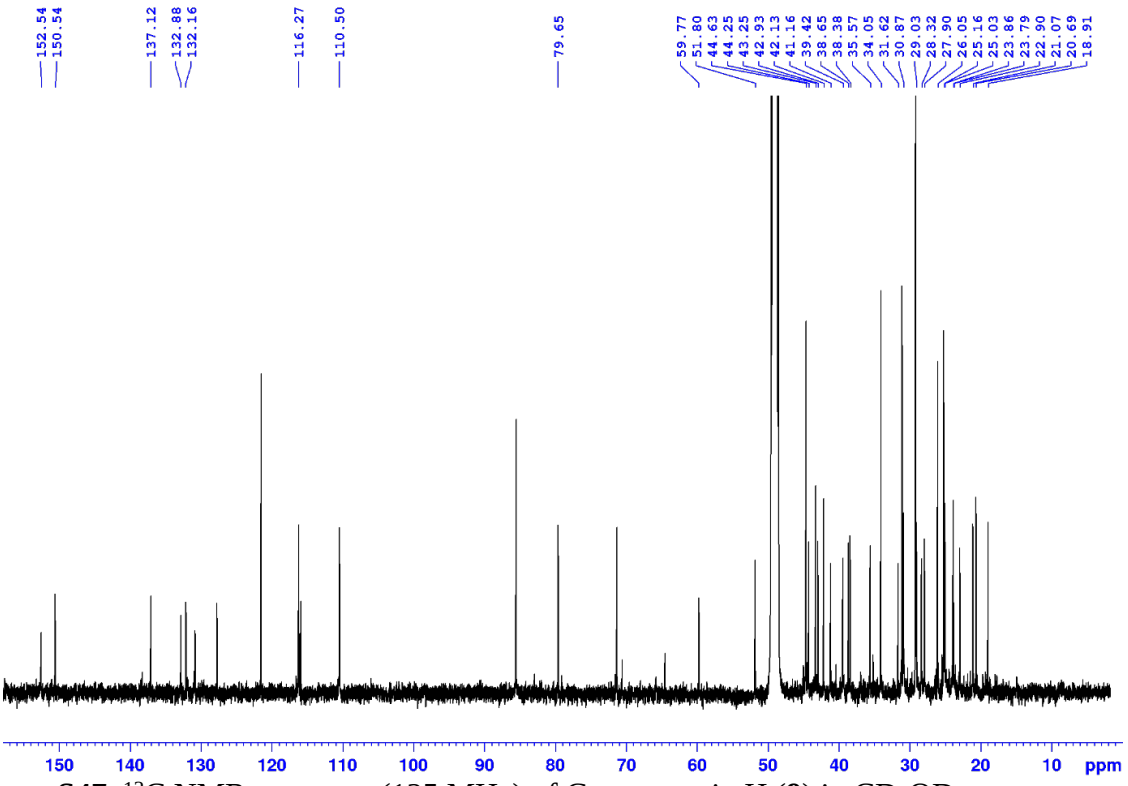

Figure S47. ^{13}C NMR spectrum (125 MHz) of Gromomycin H (**9**) in CD_3OD.

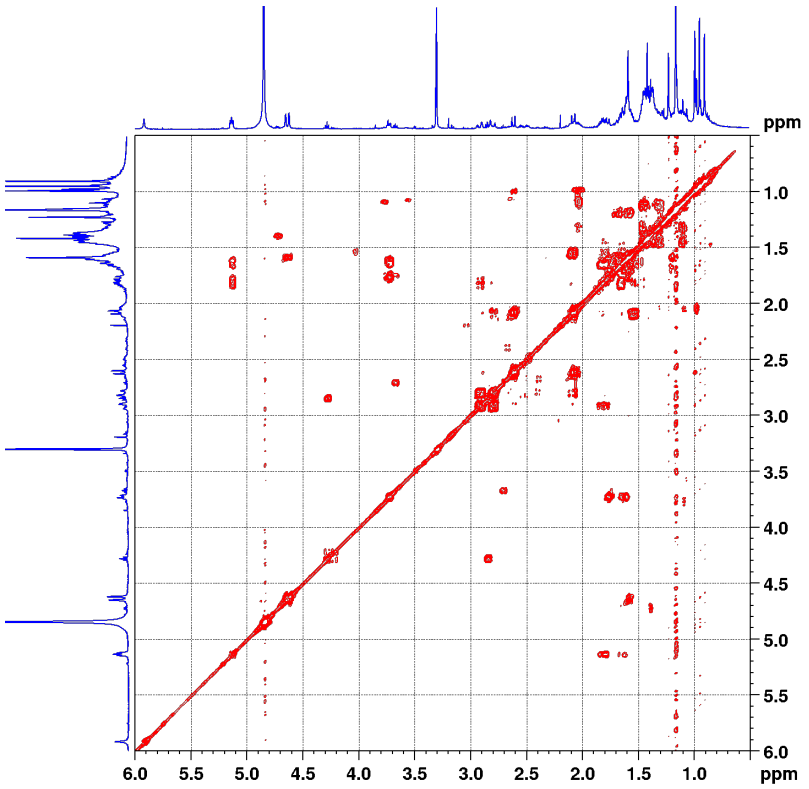

Figure S48. COSY spectrum (500 MHz) of Gromomycin H (**9**) in CD_3OD.

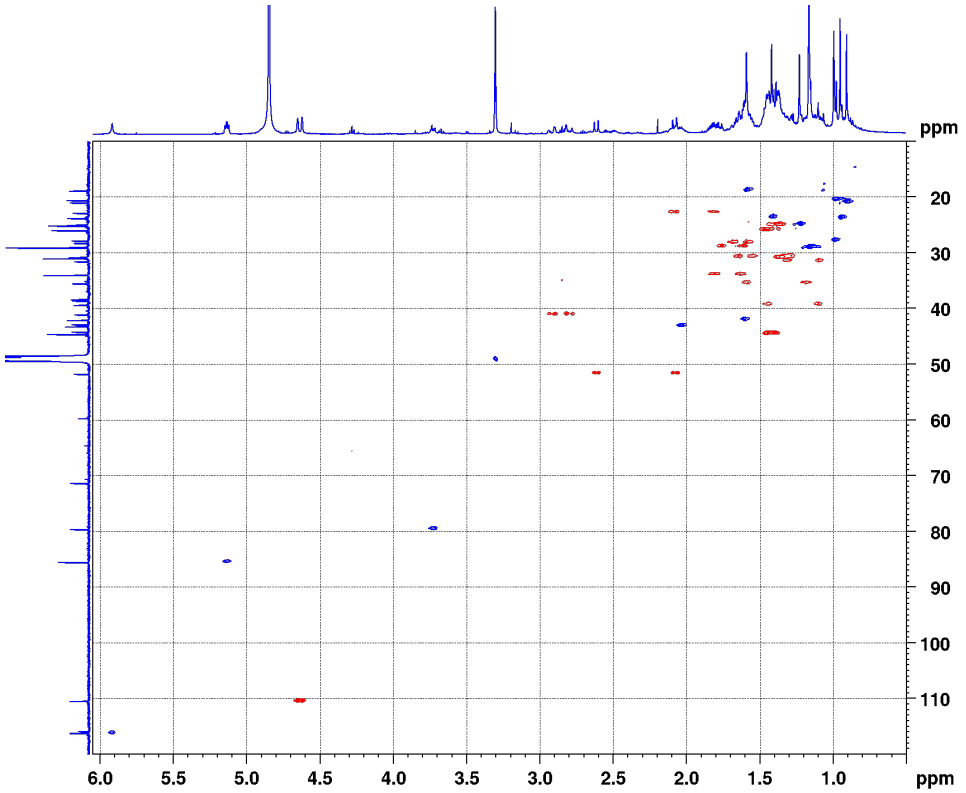

Figure S49. ^{1}H-^{13}C HSQC spectrum (500 MHz) of Gromomycin H (**9**) in CD_3OD.

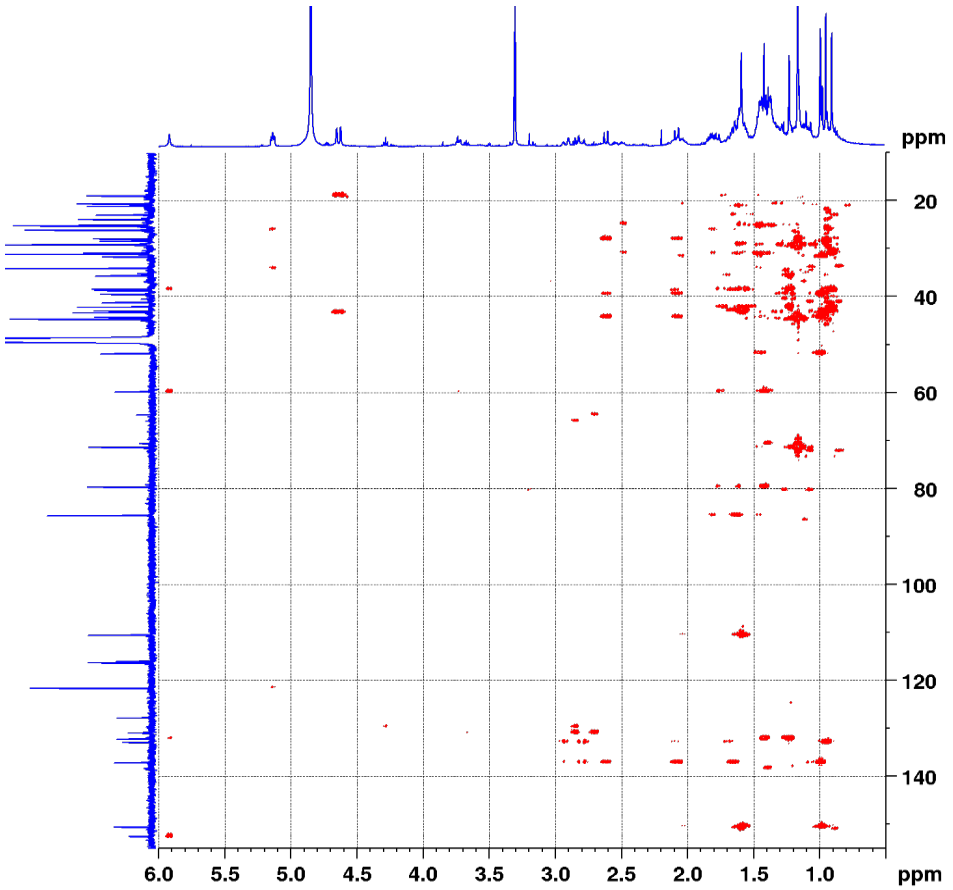

Figure S50. ^{1}H-^{13}C HMBC spectrum (500 MHz) of Gromomycin H (**9**) in CD_3OD.

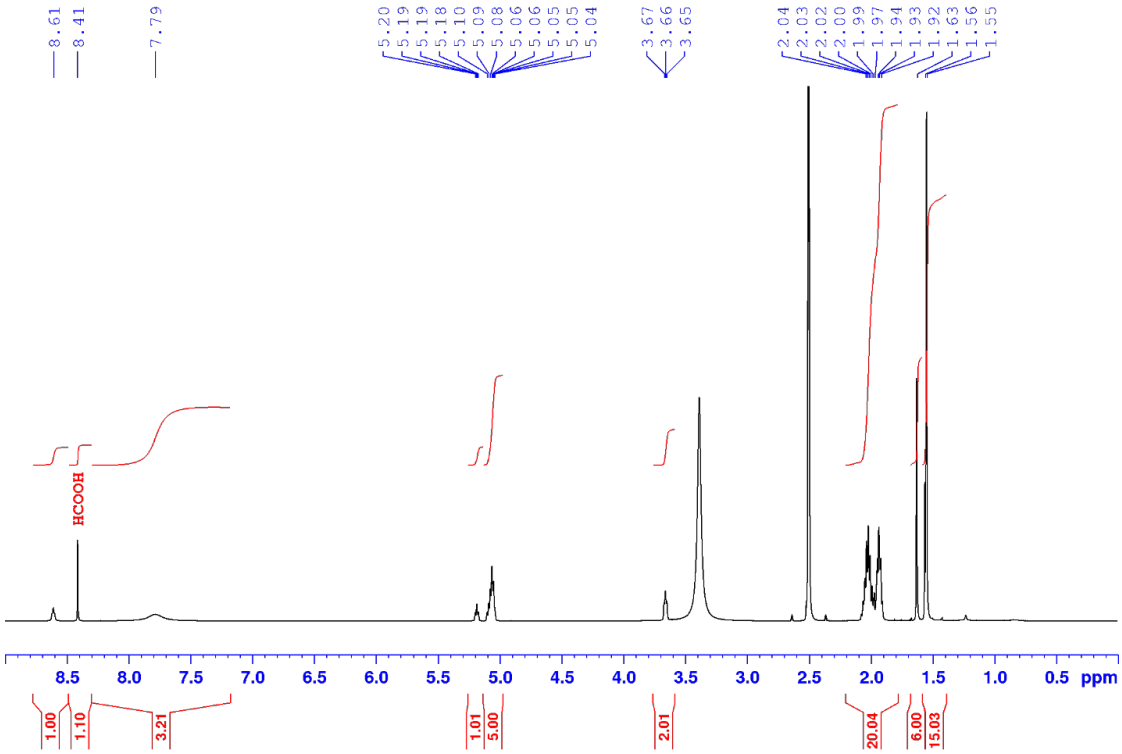

Figure S51. ^{1}H NMR spectrum (500 MHz) of Hexaprenylguanidine (**10**) in DMSO-d_6.

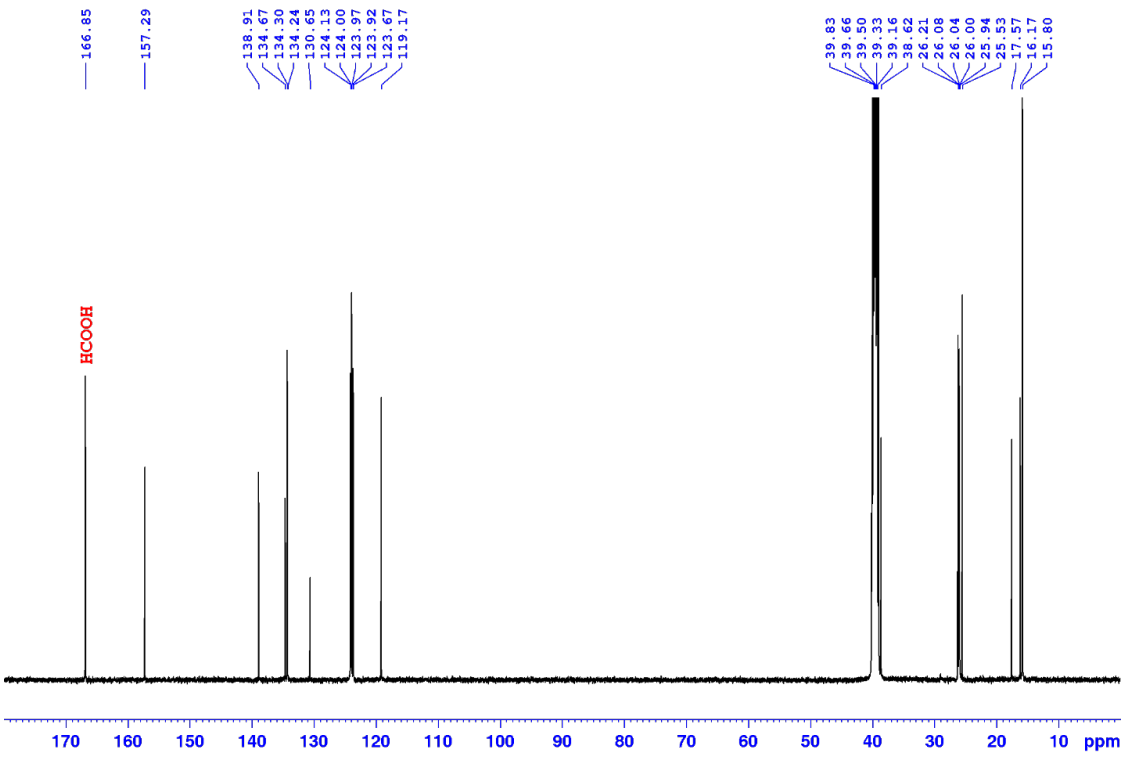

Figure S52. ^{13}C NMR spectrum (125 MHz) of Hexaprenylguanidine (**10**) in DMSO-d_6.

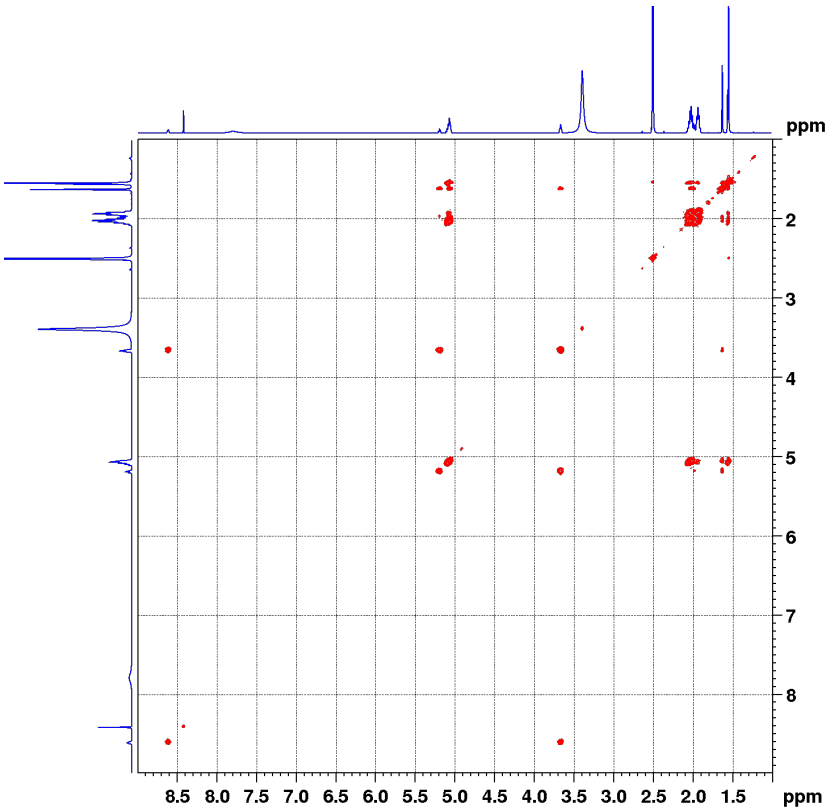

Figure S53. COSY spectrum (500 MHz) of Hexaprenylguanidine (**10**) in DMSO-d_6.

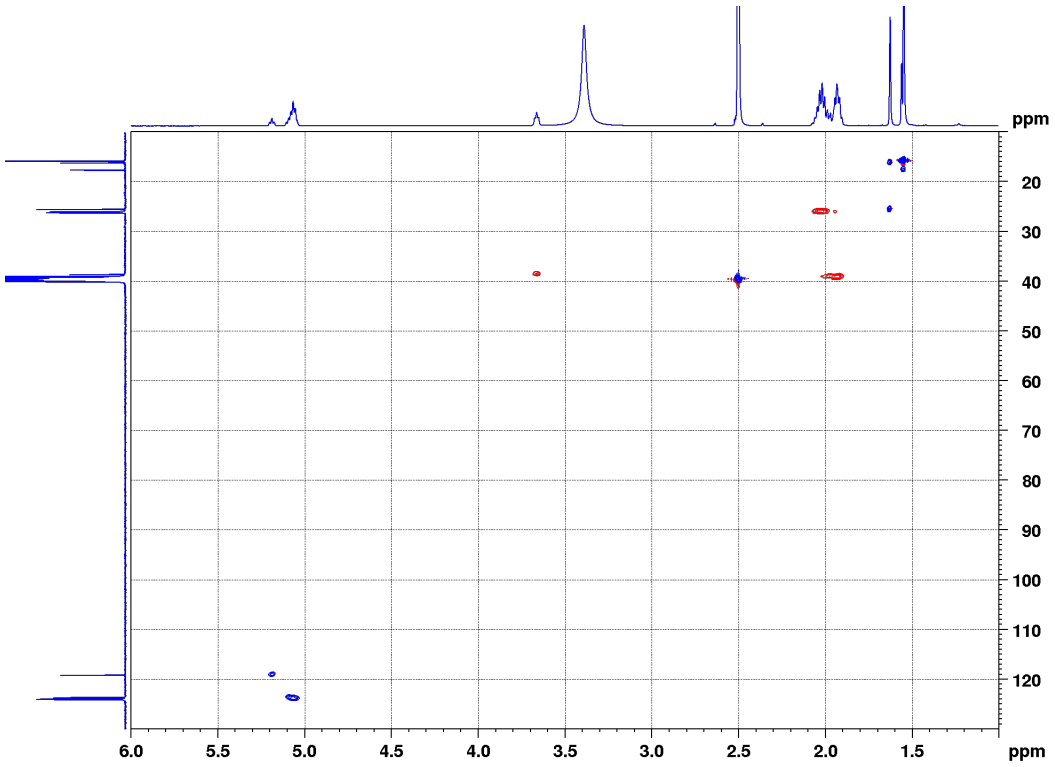

Figure S54. ^{1}H-^{13}C HSQC spectrum (500 MHz) of Hexaprenylguanidine (**10**) in DMSO-d_6.

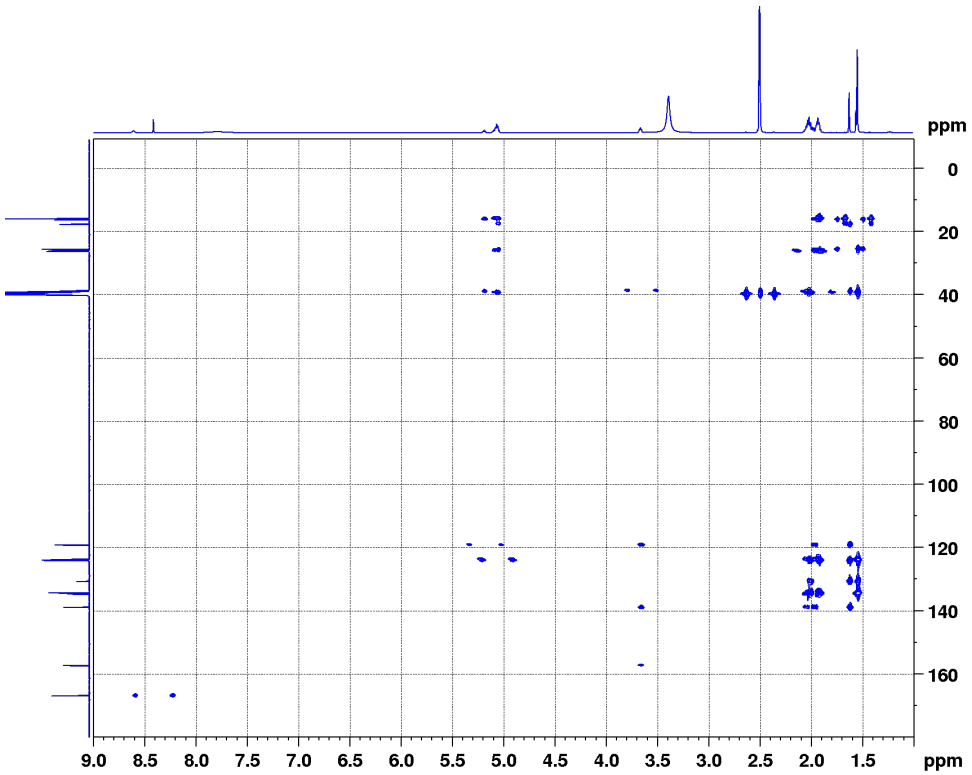

Table S55. ^{1}H-^{13}C HMBC spectrum (500 MHz) of Hexaprenylguanidine (**10**) in DMSO-d_6.

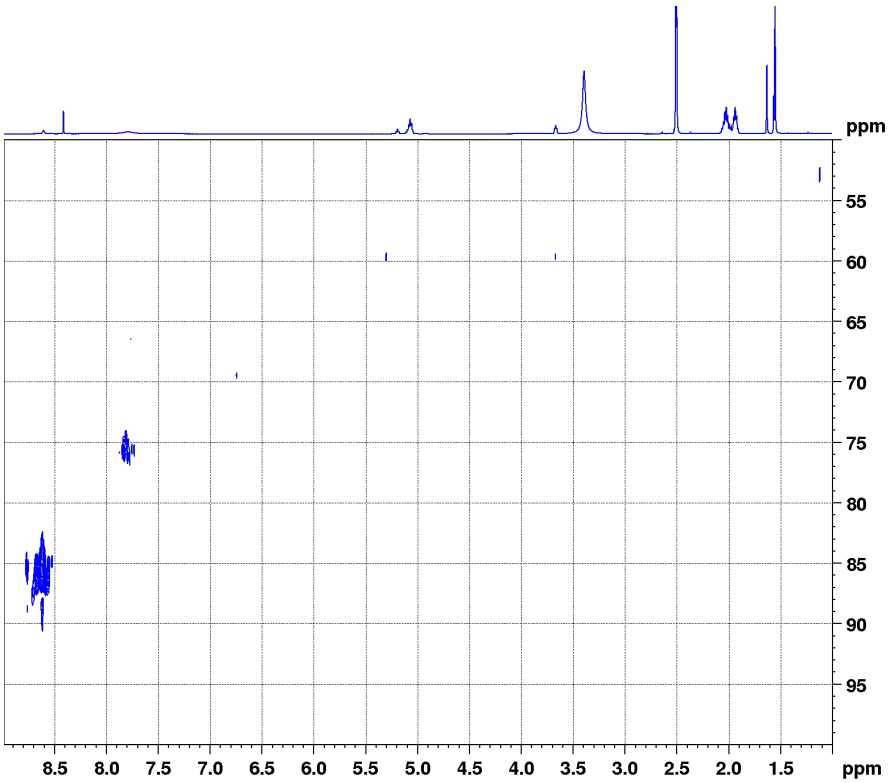

Table S56. ^{1}H-^{15}N HSQC spectrum (500 MHz) of Hexaprenylguanidine (**10**) in DMSO-d_6.

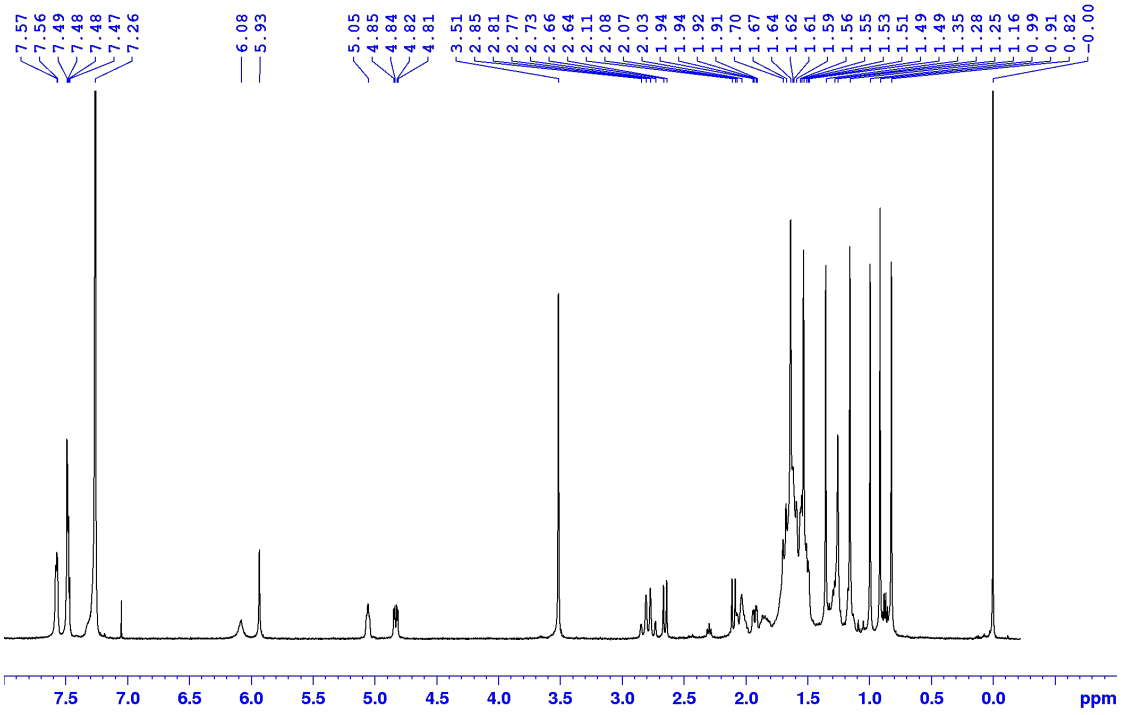

Figure S57. ^{1}H NMR spectrum (500 MHz) of Gromomycin D (*R*)-MTPA ester (5a) in $CDCl_3$.

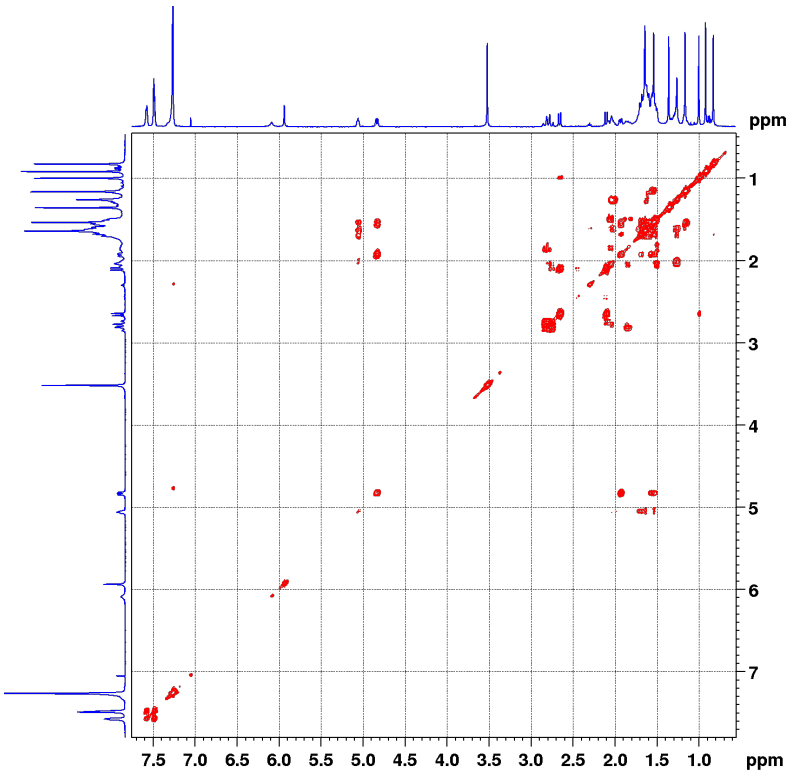

Figure S58. COSY spectrum (500 MHz) of Gromomycin D (*R*)-MTPA ester (5a) in $CDCl_3$.

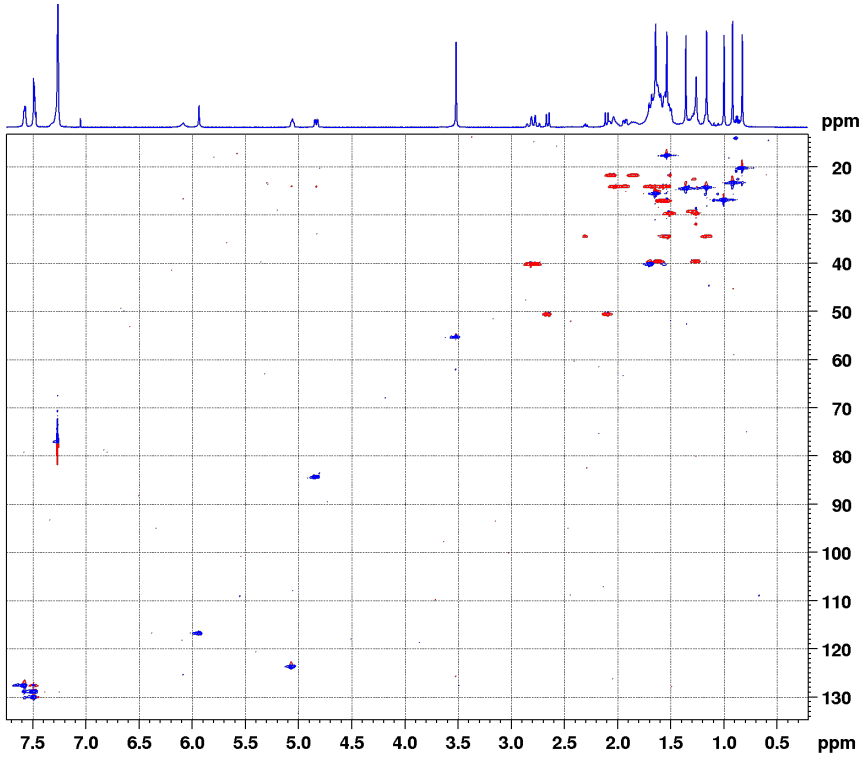

Figure S59. ^{1}H-^{13}C HSQC spectrum (500 MHz) of Gromomycin D (*R*)-MTPA ester (5a) in $CDCl_3$.

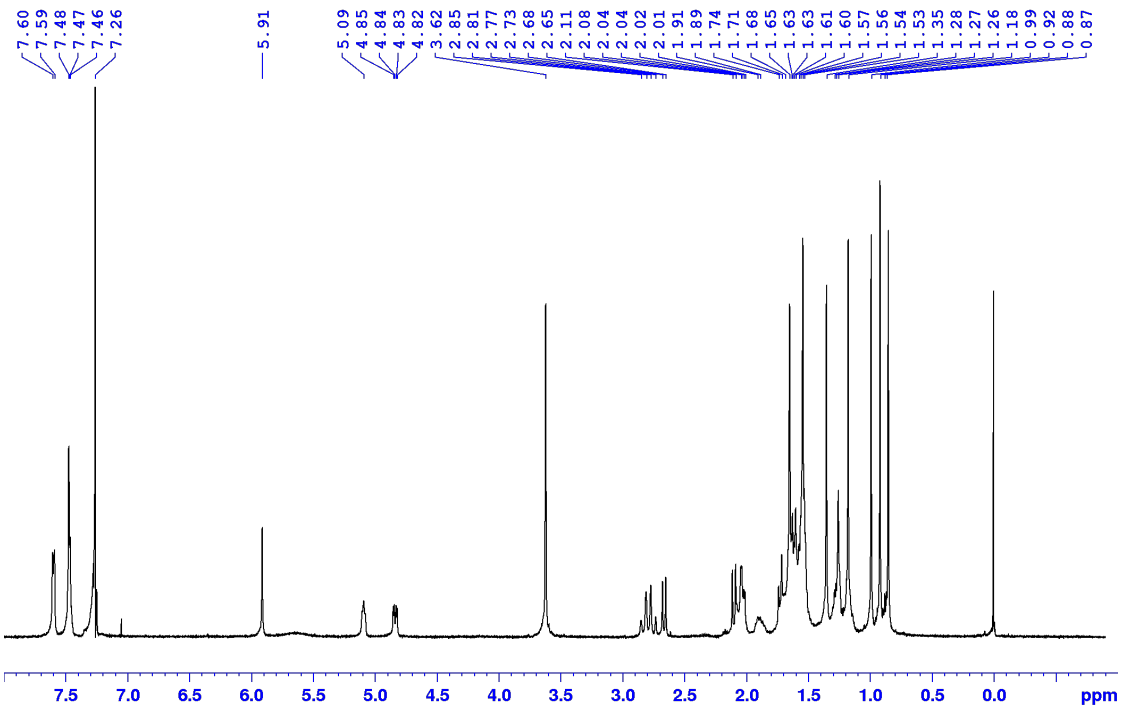

Figure S60. ^{1}H NMR spectrum (500 MHz) of Gromomycin D (*S*)-MTPA ester (5b) in $CDCl_3$.

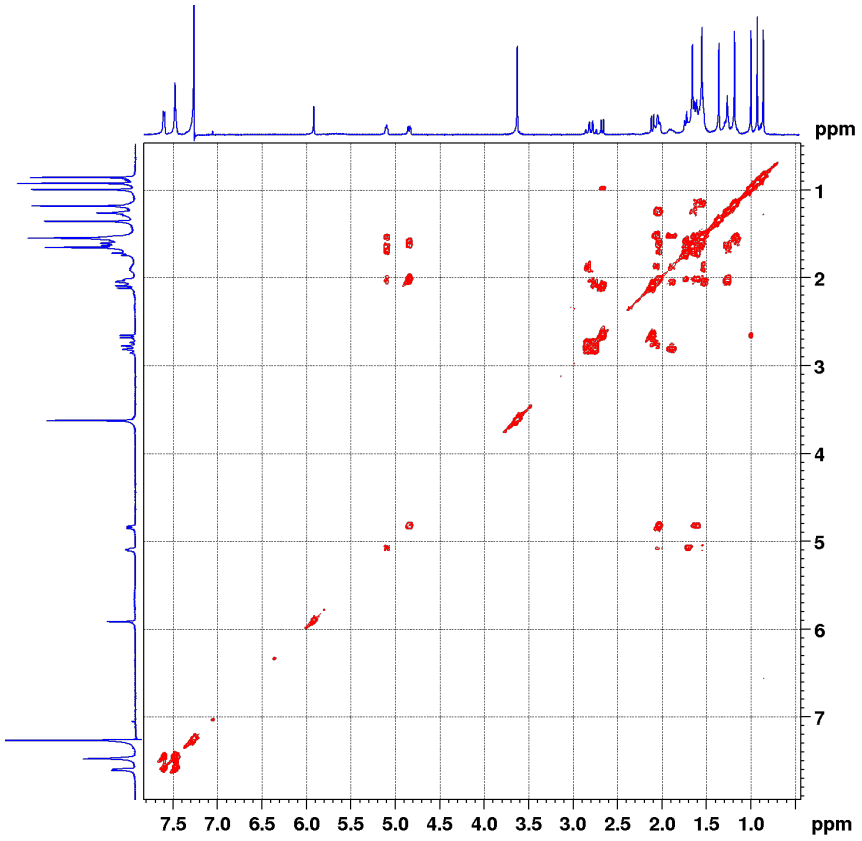

Figure S61. COSY spectrum (500 MHz) of Gromomycin D (*S*)-MTPA ester (5b) in $CDCl_3$.

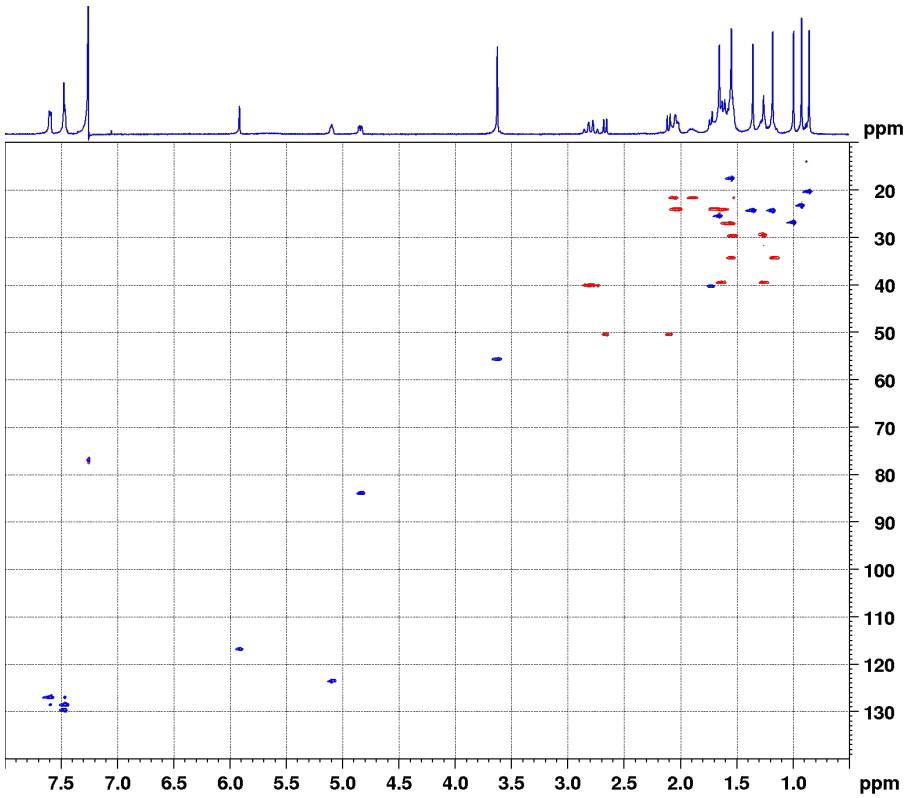

Figure S62. ^{1}H-^{13}C HSQC spectrum (500 MHz) of Gromomycin D (*S*)-MTPA ester (5b) in $CDCl_3$.

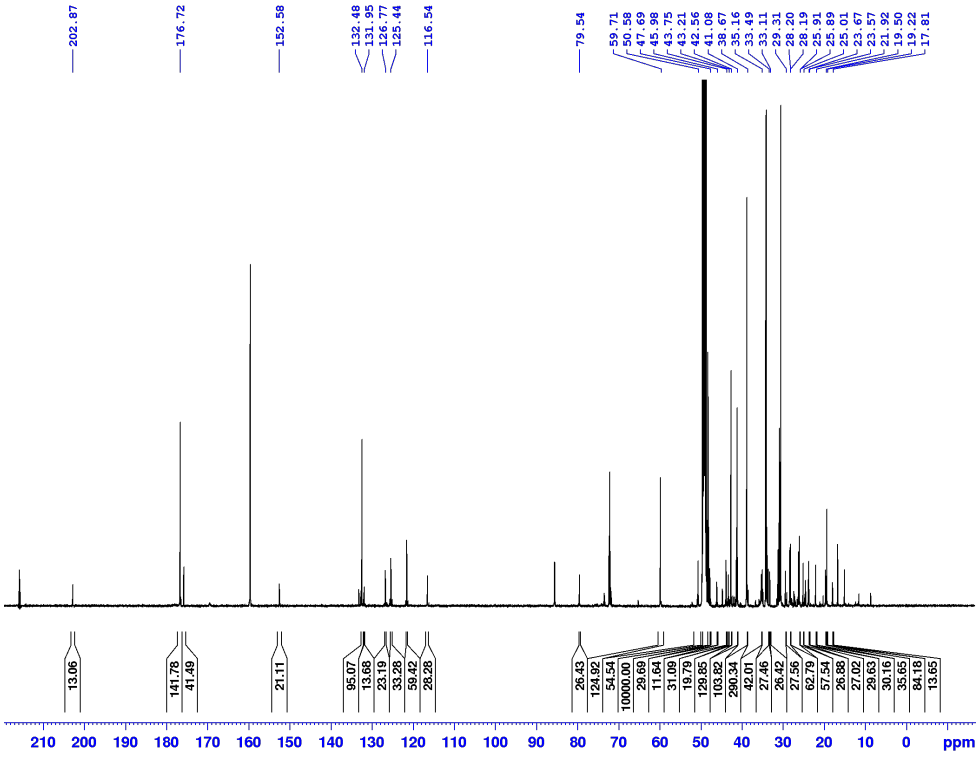

Figure S63. ^{13}C NMR spectrum (125 MHz) of Gromomycin B (**3**) in CD_3OD from feeding experiment with [2-^{13}C] pyruvate.

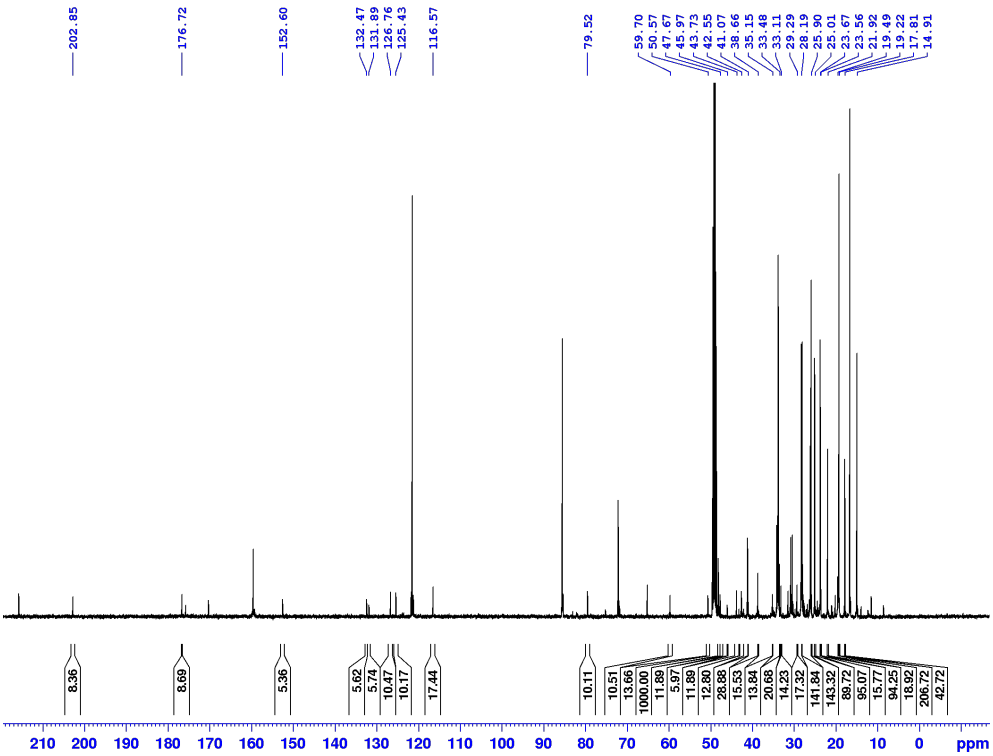

Figure S64. ^{13}C NMR spectrum (125 MHz) of Gromomycin B (3) in CD_3OD from feeding experiment with [3-^{13}C] pyruvate.

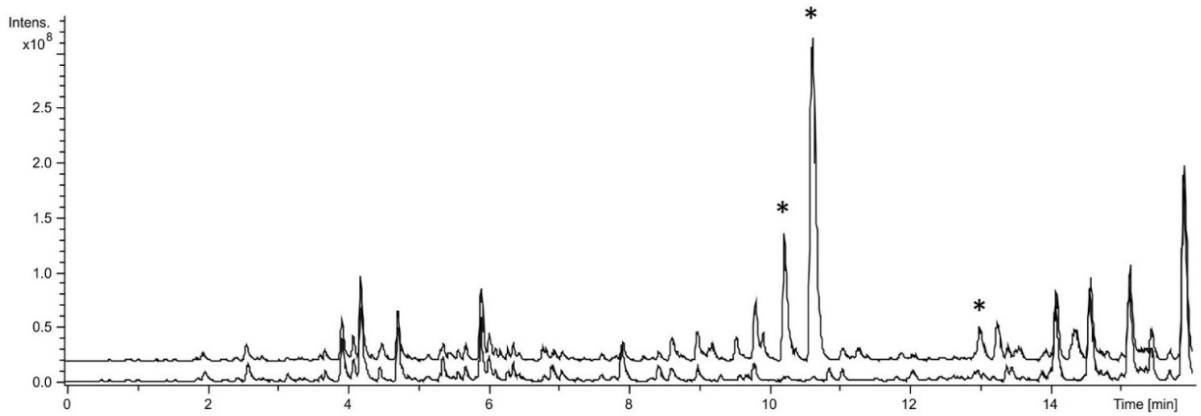

Figure S65. Heterologous expression of the cosmid P04_E01 with gromomycin cluster into *S. albus* Del14. Peaks induced by gromomycin are indicated by asterisks.

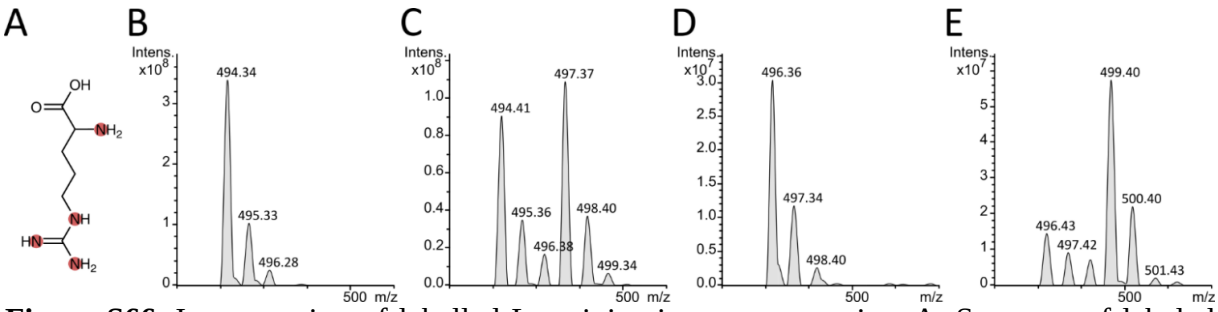

Figure S66. Incorporation of labelled L-arginine into gromomycins. A, Structure of labeled arginine (the labeled nitrogen atoms is indicated by the red circle). B, C, D, E Mass peaks of gromomycins without (B, D) and with (C, E) feeding of labelled L-arginine.

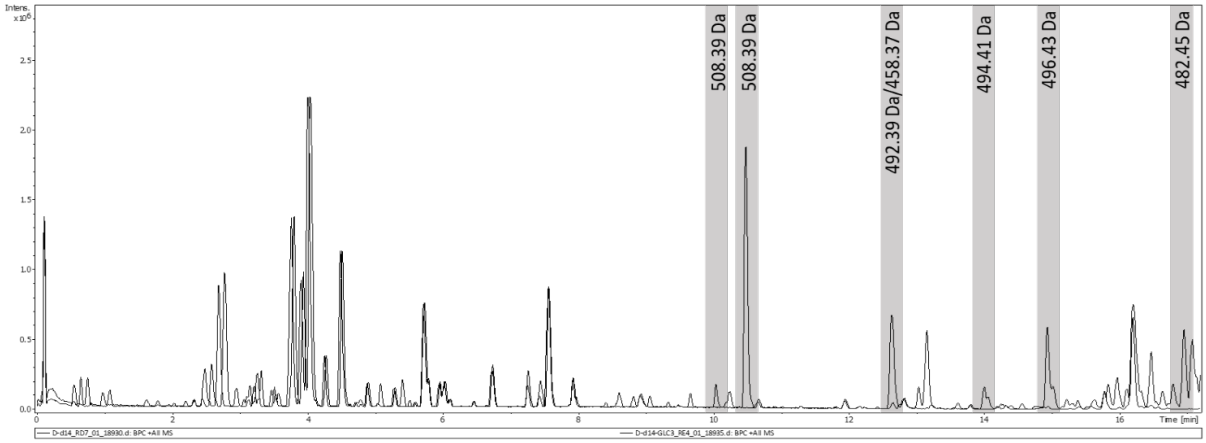

Figure S67. Heterologous expression of the P03_G02 cosmid with gromomycin-like cluster into *S. albus* Del14 strain. New methylated gromomycins are indicated by grey rectangles.

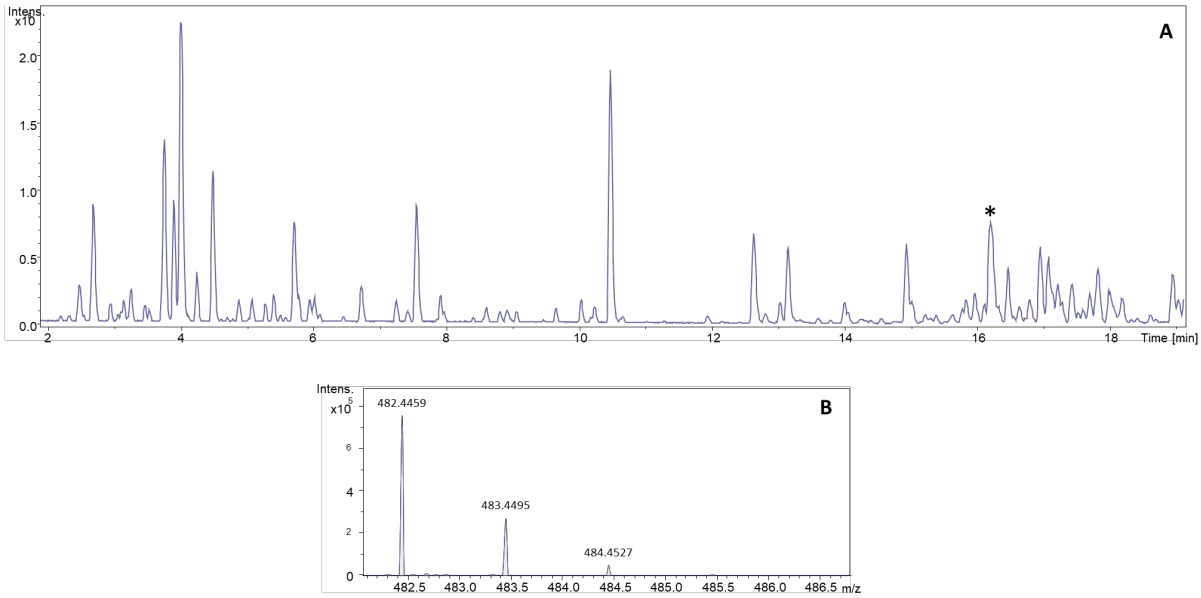

Figure S68. Linear methylated hexaprenylguanidine (marked with asterisks). **A**, chromatogram of extract from *S. albus Del14* with gromomycin-like cluster from *Streptomyces flavoviridis*; **B**, mass range of linear methylated hexaprenylguanidine.

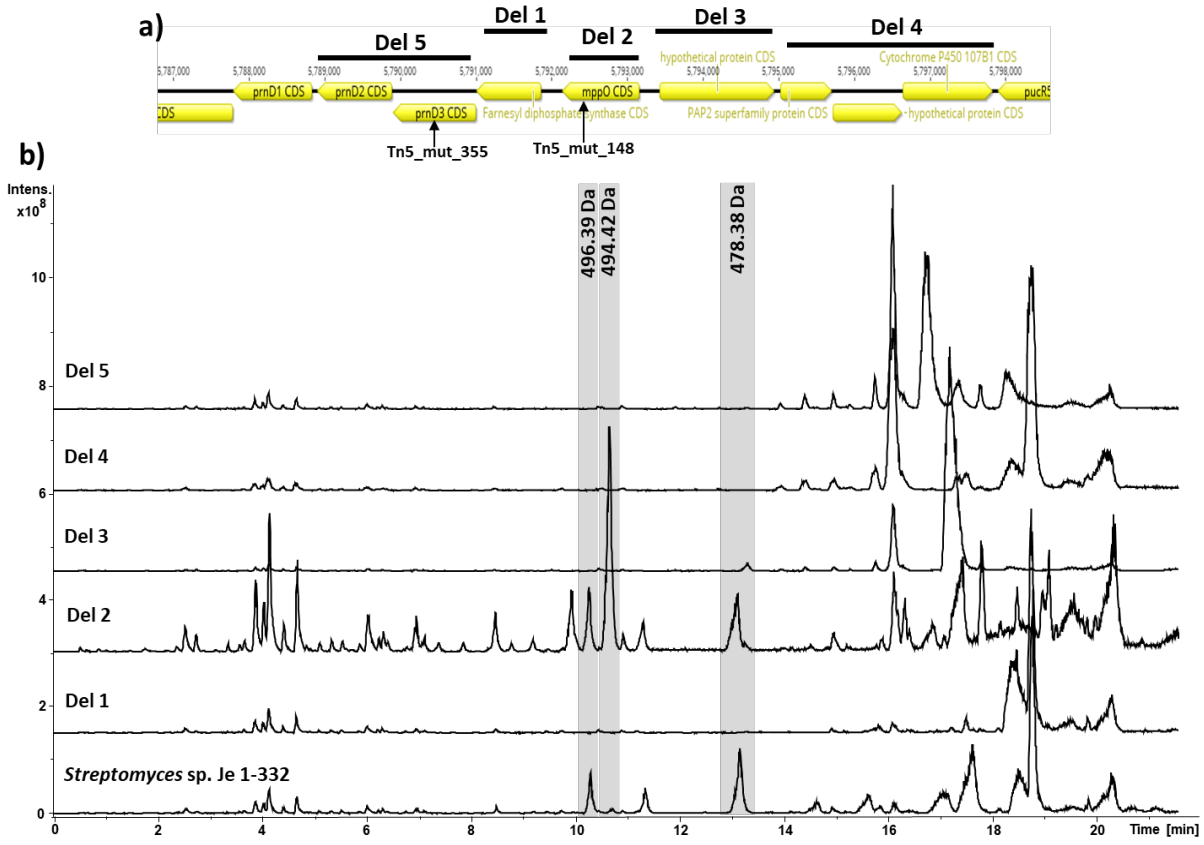

Figure S69. Deletion into *Streptomyces* sp. Je 1-332 strain. a) Deletion scheme into chromosome. b) HPLC-MS chromatograms.

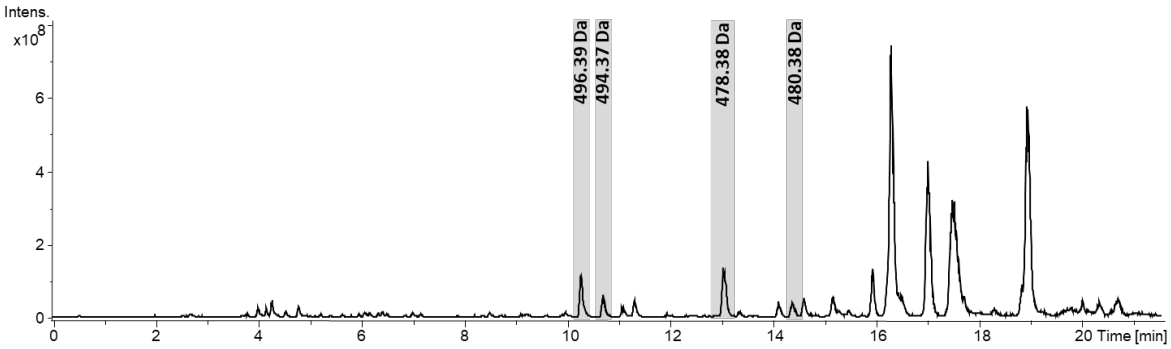

Figure S70. HPLC-MS chromatogram of crude extract of *Streptomyces sp.* Je 1-332 strain.

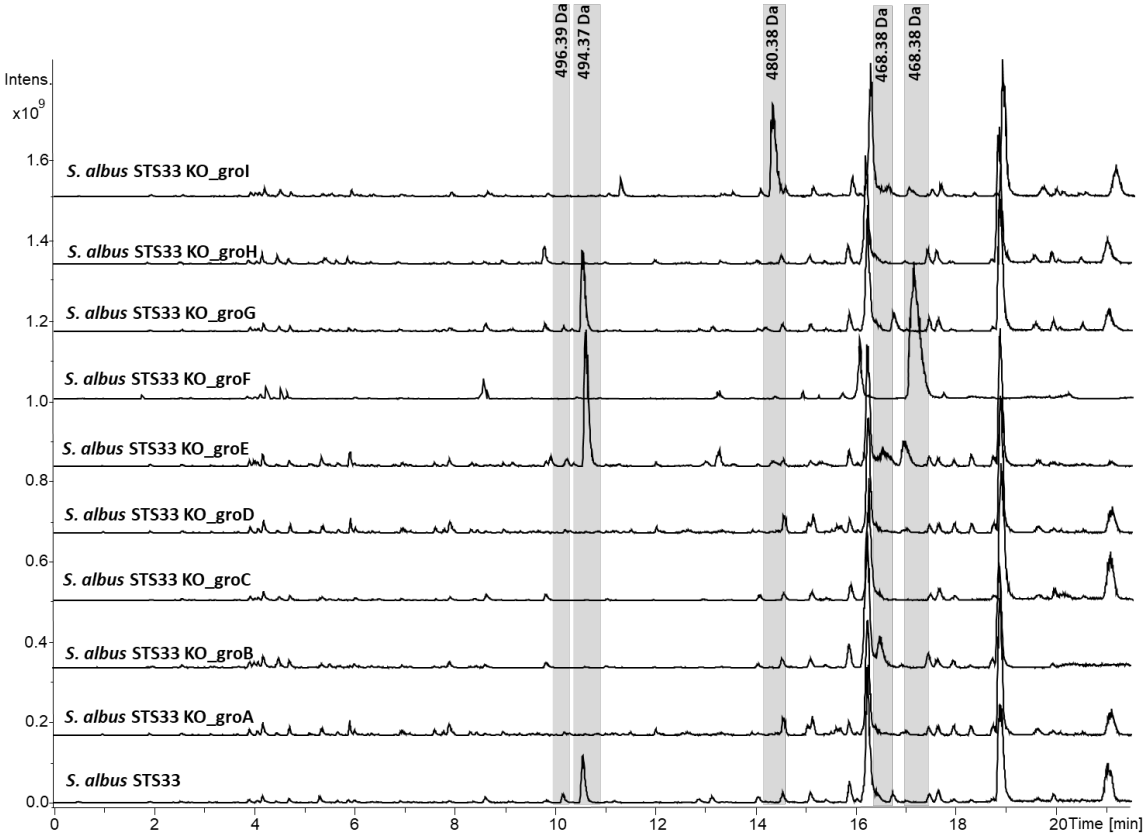

Figure S71. HPLC-MS chromatograms of the *S. albus* with the *gro*-gene deletion.

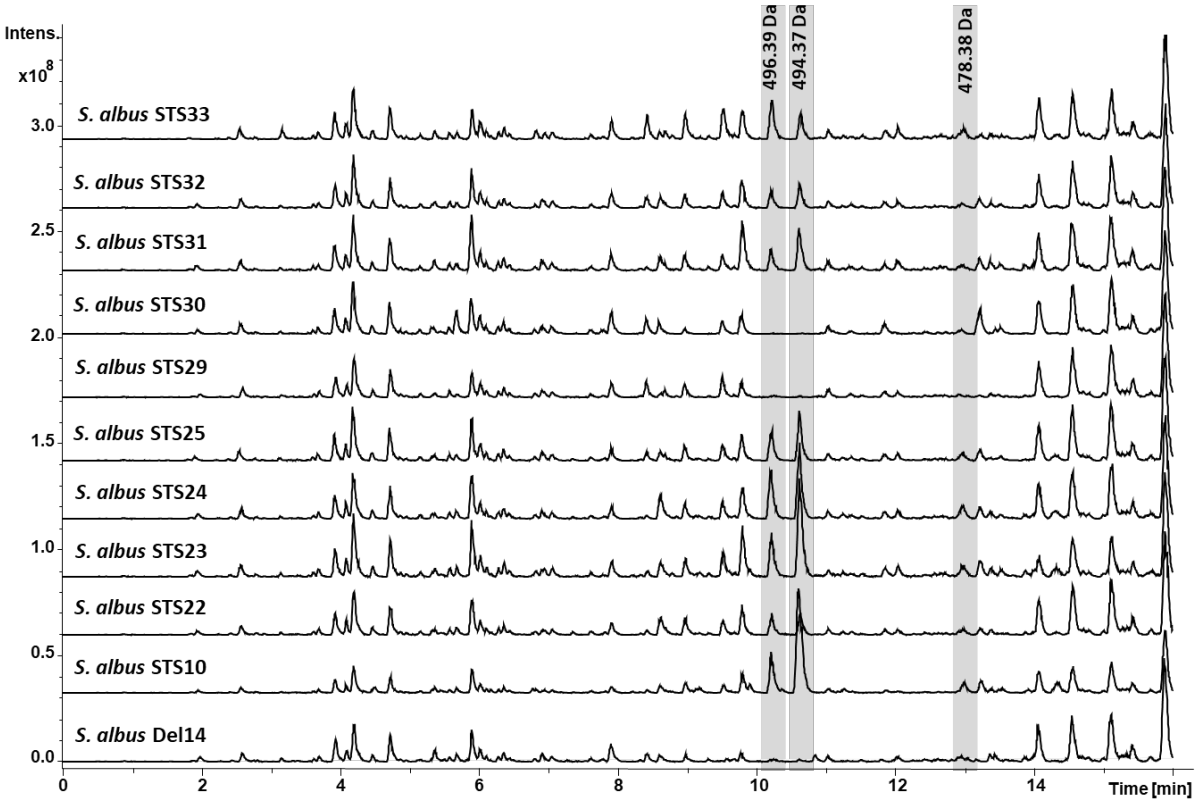

Figure S72. HPLC-MS chromatograms of the deletion mutants which are shown in **Figure 4**.

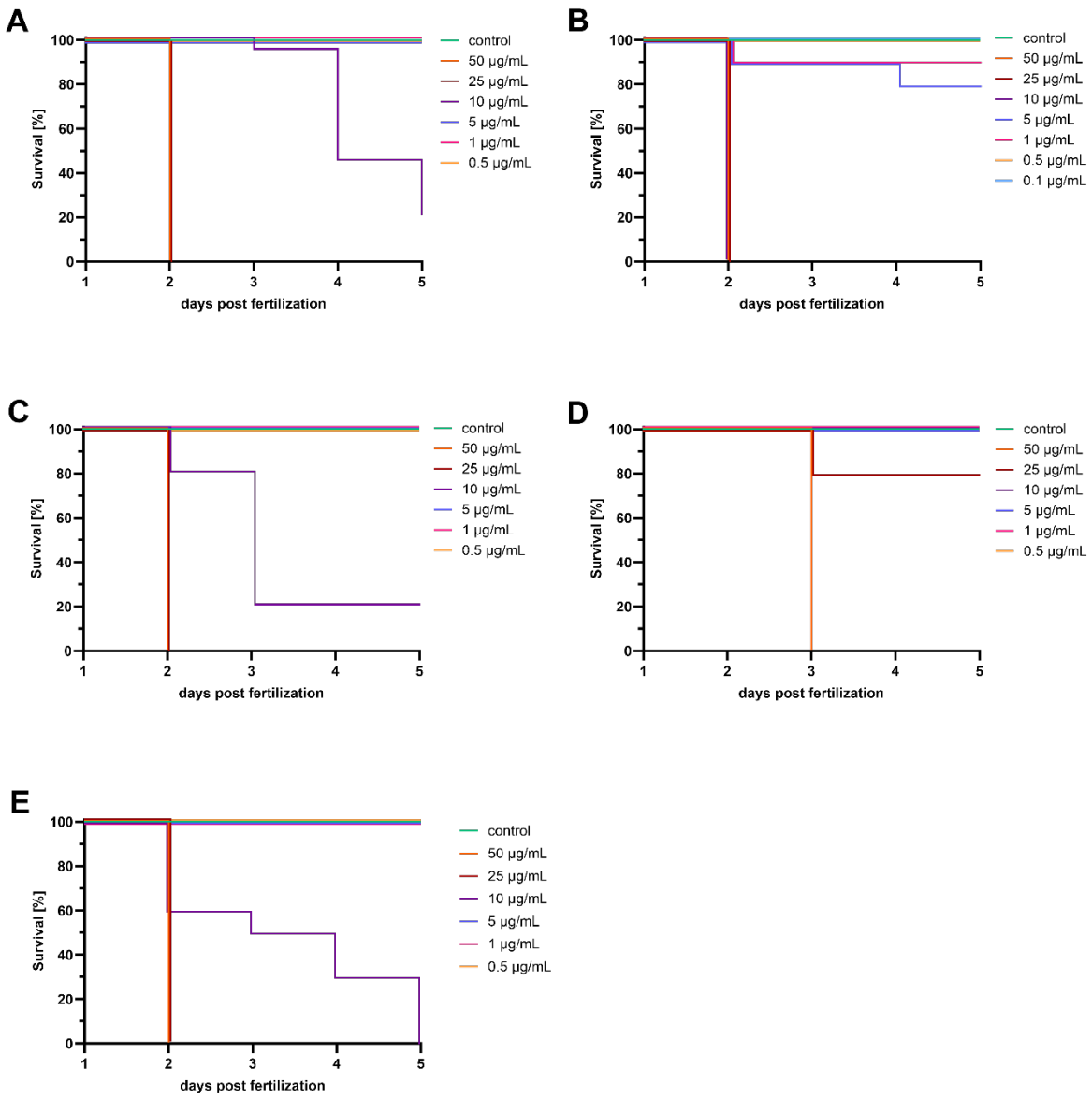

Figure S73. Kaplan-Meier curves of zebrafish embryos exposed to different concentrations of gromomycin B (A), gromomycin A (B), gromomycin F (C), gromomycin G (D) and gromomycin E (E). Zebrafish embryos (n = 10) were treated with a series of concentrations of different gromomycin derivatives (aquatic exposure) and were monitored daily until 5 days post fertilization (dpf). Embryos exposed to the solvent (1% DMSO in 0.3x Danieau's) served as control. Kaplan-Meier curves were generated using GraphPad Prism.

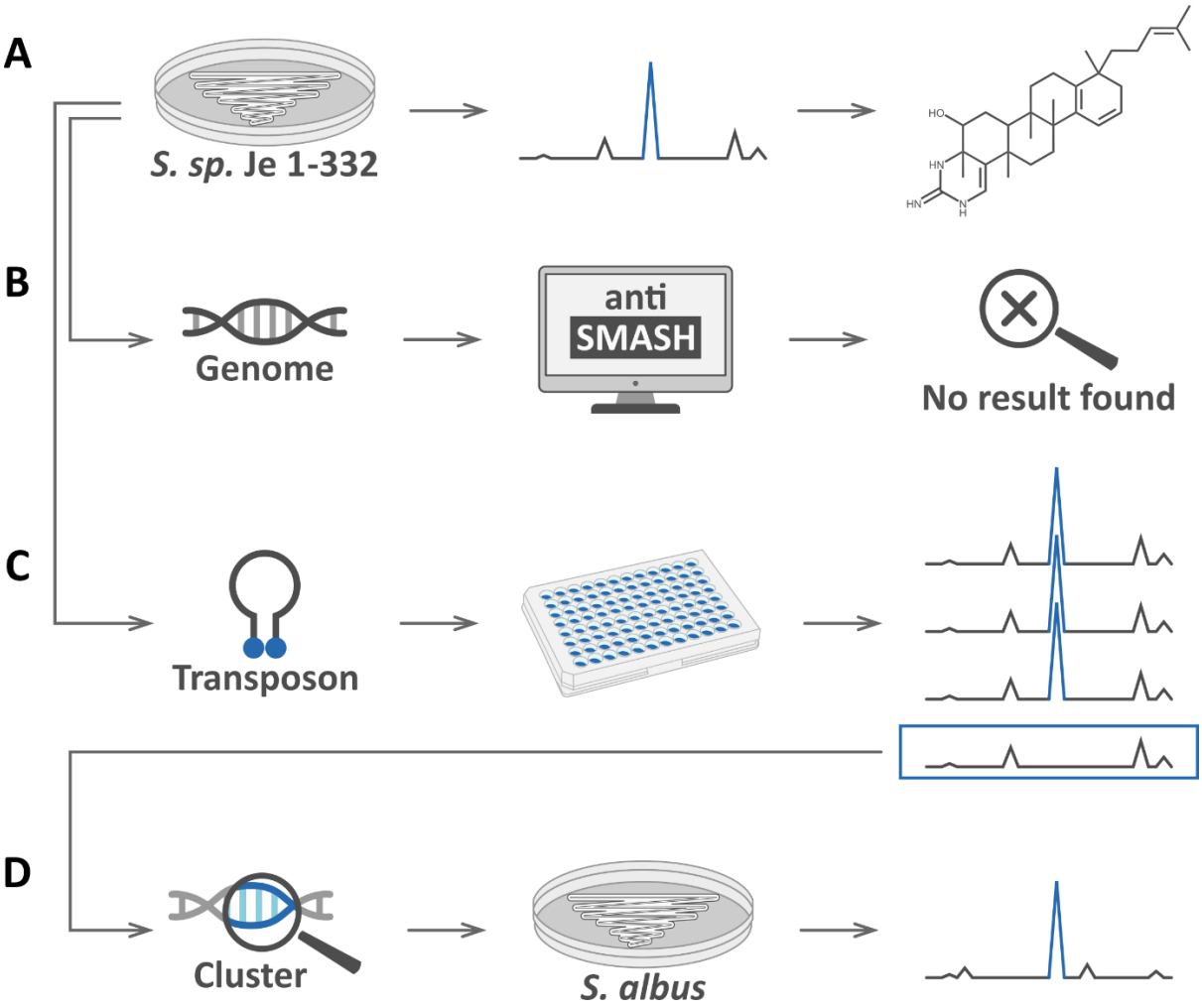

Figure S74. Scheme for identifying gene cluster involved in gromomycin biosynthesis. A, Chemical screening of crude extract. B, C, Identification of biosynthetic gene clusters using bioinformatics tools (B) and transposon mutagenesis (C). D, Validation and heterologous expression of the identified gene cluster.

2.2. Genome Mining–Driven Isolation of New Gromomycins and Insights into Their Mode of Action

This chapter reproduces, with minor formatting adjustments, the text of the submitted manuscript:

Dmytro Bratiichuk‡, Franziska Fries‡, Marc Stierhof, Leon Morguet, Josef Zapp, Mathias Müsken, Yuriy Rebets, Maksym Myronovskyi, Rolf Müller, Jennifer Herrmann*, Andriy Luzhetskyy*. Genome Mining – Driven Isolation of New Gromomycins and Insights into Their Mode of Action. *Submitted to* ***ACS Chemical Biology***. 2025.

‡ D.B. and F.F. contributed equally to this paper.

*corresponding authors.

Contributions and Acknowledgements

Author's Contribution

The author made significant contributions to the methodology and experimental aspects of this study. The author designed and conducted biological experiments, analyzed and visualized the resulting data. Experimental work encompassed both biotechnological and bioinformatic approaches, including genome mining, identification of biosynthetic gene clusters, heterologous expression, compound dereplication, and isolation. The author conceived and wrote the respective parts in the original draft of the manuscript.

Contributions by Others

F. Fries designed and performed biological experiments, including bioactivity testing, time-kill assays, resistance analysis, membrane assays, preparation of electron microscopy samples. Furthermore, she was responsible for writing the respective parts of the manuscript. M. Stierhof and J. Zapp aided analytics and carried out structure elucidation. L. Morguet assisted with the mechanism of action studies. M. Müsken performed electron microscopy. Y. Rebets and M. Myronovskyi provided valuable advice and contributed to proofreading the manuscript. R. Müller provided supervision and performed proofreading of the manuscript. J. Herrmann and A. Luzhetskyy provided supervision and designed the research. All coauthors proofread and corrected the manuscript.

2.2.1. Abstract

The growing threat of multidrug-resistant bacterial infections highlights the urgent need for antibiotics with novel mechanisms of action. Gromomycins, a newly identified class of triterpene antibiotics, exhibit potent activity against Gram-positive bacteria, including drug-resistant species, through a previously uncharacterized mode of action. Here, we report the discovery of a gromomycin-like biosynthetic gene cluster in the *Actinoplanes* genus through a genome mining approach, leading to the isolation and characterization of new bioactive derivatives that overcome resistance to clinically used drugs in vancomycin-resistant enterococci. Mechanistic studies revealed that gromomycins induce rapid potassium ion leakage and depolarization of the bacterial membrane, resulting in bactericidal activity against *Staphylococcus aureus*. Gromomycins disrupt the integrity of the cytoplasmic membrane, as evidenced by large pore formation, leakage of intracellular content, and subsequent cell lysis. Supplementation with membrane lipids and fatty acids neutralized their antibacterial activity, suggesting a direct membrane-targeting mechanism, further supported by the inability to raise gromomycin resistance and their toxic effects on eukaryotic cells. Collectively, these findings deepen our understanding of gromomycin activity and demonstrate the utility of genome mining to uncover structurally novel and biologically active natural products.

2.2.2. Introduction

Actinobacteria have long been recognized as a key provider of many natural products (NPs) throughout the years.[236-239] *Streptomyces*, a highly characterized genus of actinomycetes, is viewed as one of the most essential industrial bacteria due to its significant potential for generating secondary metabolites, including antibiotics, immunosuppressants and anticancer agents.[277-279] However, ongoing studies on *Streptomyces* have made it increasingly challenging to discover new compounds that exhibit strong antibacterial properties from this genus. On the contrary, many non-Streptomycetes belonging to genera, such as *Actinoplanes*, *Micromonospora*, *Saccharopolyspora*, *Nocardia*, *Actinomadura*, *Amycolatopsis*, *Streptoverticilllium* have become potential resources for antibiotic discovery, generating distinct compounds with significant antibacterial activity.[280-285]

The early 2000s marked the emergence of microbial genome mining as a strategy to enhance drug discovery, based on the insight that newly sequenced actinomycete genomes encode a much larger number of secondary metabolite biosynthetic gene clusters (BGCs) than what was anticipated from established secondary metabolomes.[286-288] With the development of

rapid and affordable sequencing technologies, the understanding of this phenomenon has further strengthened.[289-290] The identification and studies of new classes of bacterial NPs and the development of different bioinformatics tools for BGCs identification, such as antiSMASH, PRISM, ClusterFinder, PKMiner, SBSPKS, RiPPER etc., have significantly sped up the discovery of new compounds from bacterial sources.[250, 291-298] At the same time, the majority of these instruments are primarily based on the existing knowledge about biosynthetic principles of known classes of secondary metabolites. This causes certain limitations that these tools are facing – they cannot recognize new types of biosynthesis and thus identify new classes of bacterial NPs.[250, 299]

Recently, we reported the structure, activity and biosynthetic pathway for a new family of bacterial natural products named gromomycins from *Streptomyces* sp. 1-332wt (gromomycins A, B) and *Streptomyces flavoviridis* (gromomycins E, F) (Figure 1A).[300] Gromomycins are pentacyclic triterpenes with a cyclic guanidino group forming the fifth six-membered ring. They represent a new type of biosynthetic logic of secondary metabolism, being the first bacterial triterpenes synthesized independently of the squalene pathway and exhibiting an unprecedented cyclization route that utilizes a hexaprenylguanidine linear precursor. Gromomycins E and F from *Streptomyces flavoviridis* differ from A and B derivatives by the methylation of the side chain, which is performed by an additional gene encoding a protein with a methyltransferase domain in *S. flavoviridis* gromomycin-like BGC (groBGC).[300] On the other hand, these compounds have a pronouncing antimicrobial activity against methicillin-resistant, vancomycin-intermediate (VISA) resistant, daptomycin-resistant *S. aureus* strains, as well as a substantial activity against *M. tuberculosis* and *A. baumannii*.[300] This activity seems to be strongly dependent on the variations in the structure of the side chain of the compound, prompting the search for new gromomycin derivatives. At the same time, the mode of action and thus the cellular target(s) of these compounds remained unclear.

Here, we report the identification of a novel groBGC from the *Actinoplanes* genus, which resulted in the isolation and characterization of new biologically active gromomycin derivatives with potent activity against vancomycin-resistant *Enterococcus faecium* isolates. The use of a new producer strain with a higher yield of compounds than in the case of *Streptomyces* sp. 1-332wt resulted in better access to these antibiotics and thus allowed mode of action studies. In-depth mechanistic profiling revealed that gromomycins target the cytoplasmic membrane, which underlies their rapid bactericidal effect, but also accounts for their off-target activity toward eukaryotic cells.

2.2.3. Results and Discussion

2.2.3.1. Identification of New Gromomycin-like BGCs in *Actinoplanes*

Gromomycins are a new class of bacterial natural products with a distinct biosynthetic pathway which previously could not be recognized by the pattern-based BGC prediction tools. Elucidation of the gromomycin biosynthetic pathway laid the foundation for a genome mining approach, which was used to explore the distribution of groBGCs and to identify new derivatives.[300] The core part of the gromomycin BGC is represented with three genes: farnesyl diphosphate synthase (*groD*), prenyltransferase (*groH*), and cyclase (*groF*) (**Figure 1B**). We used the nucleotide sequences of these genes as probes to search for the related BGCs within the genomes of *Actinobacteria* deposited in the NCBI GenBank database. Since the enzymes involved in the gromomycin assembly are highly abundant within bacterial genomes and are involved in different processes, the ultimate search criteria was the proximity of all three genes.

The search revealed a number of *Streptomyces* and non-*Streptomyces* Actinobacteria harboring groBGC homologues within their genomes (**Figure 1B**). Further examination showed that the strains *Streptomyces lunalinharesii*, *Streptomyces* sp. JJ66, *Streptomyces sp*. NPDC008137 and *Streptomyces* sp. NPDC001584 all possess gromomycin BGC almost identical to the *Streptomyces* sp. Je 1–332. At the same time, six strains (*Streptomyces* sp. CS090A, *Streptomyces cyaneofuscatus*, *Streptomyces* sp. RS2, *Streptomyces* sp. NPDC050388, *Streptomyces* sp. NPDC005549, *Streptomyces* sp. NPDC020571) include an additional gene encoding a protein with a methyltransferase domain. Additionally, *Streptomyces noursei* harbors a groBGC with an additional class I SAM-dependent methyltransferase, whereas the cluster from *Streptomyces* sp. MH60 contains a gene annotated as 27-O-demethylrifamycin SV methyltransferase. These seven groBGCs encompass a set of genes similar to the previously found in *S. flavoviridis*, which is known to produce methylated gromomycins (**Figure 1A**).[300] Noteworthy, the strain *Streptomyces* sp. NPDC021212 was found to contain a groBGC carrying two additional genes, encoding for putative FAD-dependent oxidoreductase and uroporphyrinogen decarboxylase. These enzymes might be involved in the new tailoring modifications during gromomycin biosynthesis and the generation of novel derivatives.

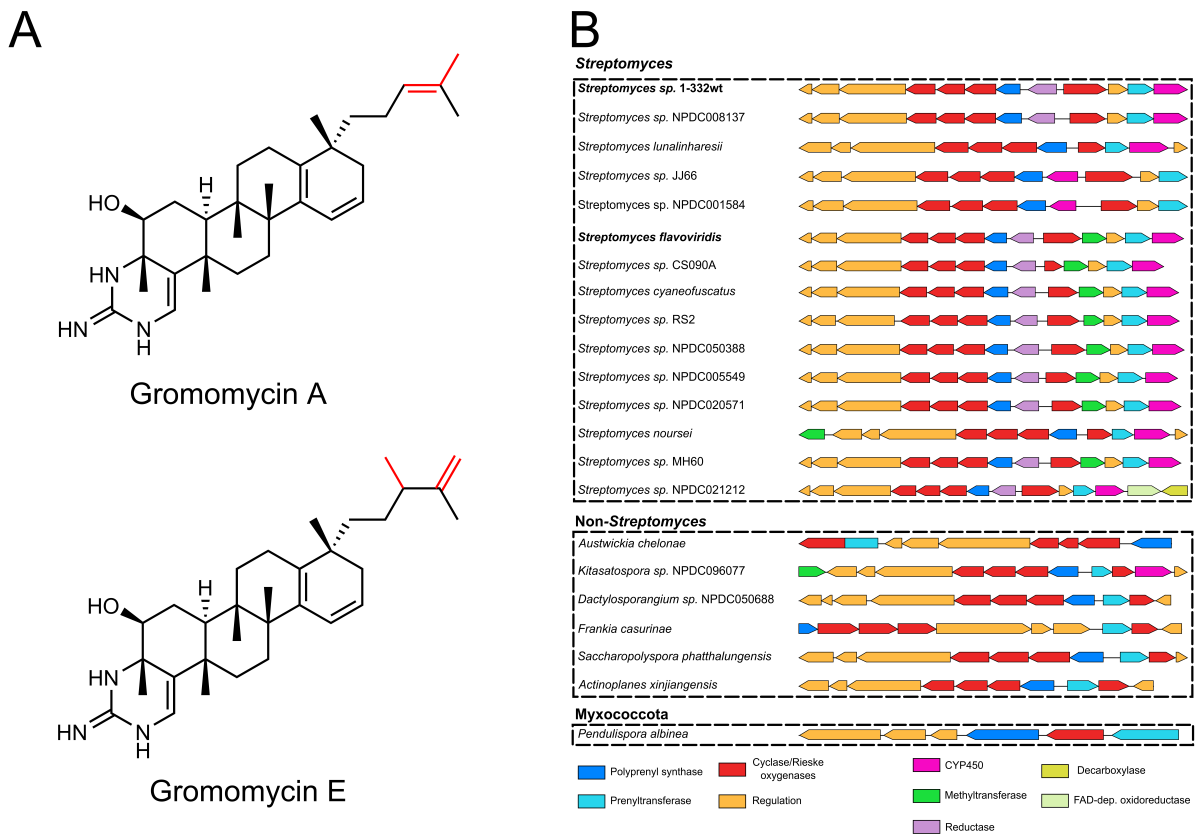

Figure 1. A. Structures of gromomycins A and E (methylated). **B.** Gromomycin BGC and its homologues.

Meanwhile, the groBGCs were found within the genomes of rare actinobacterial strains, such as *Austwickia chelonae*, *Kitasatospora* sp. NPDC096077, *Dactylosporangium* sp. NPDC050688, *Frankia casurinae*, *Saccharopolyspora phatthalungensis* and *Actinoplanes xinjiangensis*. A detailed analysis revealed that *Kitasatospora* sp. NPDC096077 cluster is virtually identical to the *S. flavoviridis* gromomycin BGC, while the clusters of the other five strains differ by the absence of several biosynthetic genes. In particular, the BGC from *A. xinjiangensis* strain lacks *groI* and *groE* which are encoding CYP450 monooxygenase and reductase tailoring enzymes, involved in the incorporation of a keto group at C-17 of gromomycins, and its subsequent reduction a hydroxyl group, which, in turn, degrades, generating gromomycin A.[300]

It is noteworthy that groBGCs were identified within the genomes of other than Actinomycetota phylum, including Myxococcota species, and particularly *Pendulispora albinea* strain. Its groBGC contains only homologues of the core genes *groD*, *groH*, and *groF* while lacking genes encoding other enzymes, suggesting the potential to produce novel and intriguing derivatives.

2.2.3.2. Heterologous Expression of *A. xingiangensis* groBGC and Isolation of New Derivatives

A genome library of the *Actinoplanes xinjiangensis* DSM 45184 strain was constructed, using the φC31-based integrative cosmid vector cos15AAmInt. The library was end-sequenced and mapped to the genome of the *A. xinjiangensis* DSM 45184 (GenBank Ref GCF_003148685.1). The cosmid clone P19-C01 was found to carry a 31.7 kb fragment of *A. xinjiangensis* chromosome with groBGC. The cosmid was additionally confirmed by PCR. The P19-C01 cosmid was introduced into *S. albus* Del14 and *S. lividans* ΔYA9 strains.[254-255] Obtained transconjugants were cultured in SG, DNPM or GYM media and metabolites were extracted with ethyl acetate. The high-resolution LC-MS analysis of extracts of both *S. albus* Del14 and *S. lividans* ΔYA9 strains, containing the P19-C01 cosmid, revealed several distinct peaks (**Figure 2A**). The mass spectra analysis showed molecular ions with *m/z* of 480.39 $[M+H]^+$ (480A1), 480.39 $[M+H]^+$ (480A2), 482.41 $[M+H]^+$ (482A) (**Figure S19**). To determine the structures of the identified compounds, strain *S. albus* Del14-P19-C01 was grown in 10 L of SG medium, and metabolites were extracted from the supernatant with ethyl acetate.

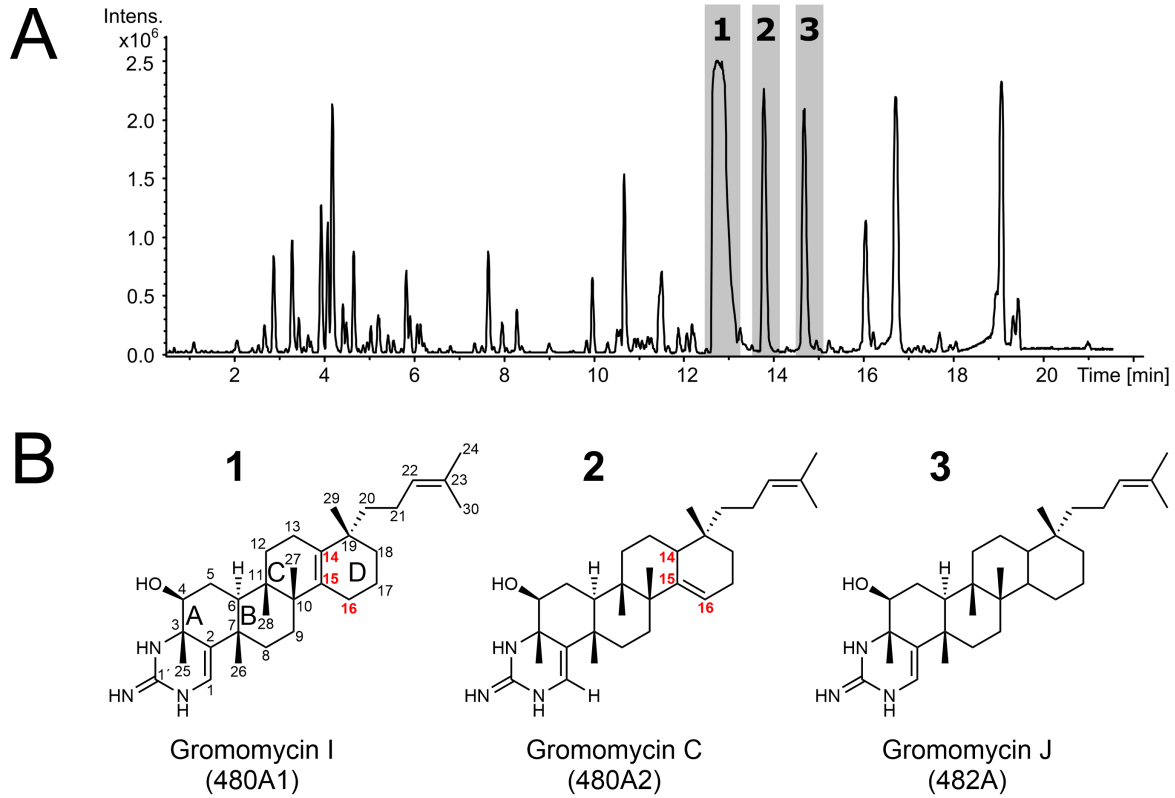

Figure 2. A. Heterologous expression of the cosmid P19-C01 with groBGC into *S. albus* Del14. Peaks induced by cluster are marked by numbers: 1. Gromomycin I (480A1), 2. Gromomycin C (480A2), and 3. Gromomycin J (482A). B. Structures of gromomycins I, C, and J.

Compounds 480A1, 480A2 and 482A were purified, and their structures were determined by NMR (**Figure 2B**, **Figures S1-S16**, **Table S1**). Compounds 480A1 (1) and 480A2 (2) (**Figure 2**) share the same molecular formula, $C_{31}H_{49}N_3O$, identical to that of gromomycin C, which is a key intermediate in the gromomycin biosynthesis.[300] Comparison of the ^{1}H and ^{13}C NMR data of 480A2 with those of gromomycin C confirmed that these two compounds are structurally identical. In contrast, the same mass but different retention time of the compound 480A1 indicates that it is a structural isomer of gromomycin C. Full assignment of the structure using HMBC correlations from CH_3-29 to C-14 and from CH_3-27 to C-15 revealed that the double bond in ring D, originally located at C-15/C-16 in gromomycin C, had shifted to C-14/C-15 in 480A1 (**Figure 2B**, **Figures S1**, **S6** and **S11**). This new derivative was named gromomycin I. Compound 482A (**3**) has a calculated molecular formula of $C_{31}H_{51}N_3O$, indicating the loss of one double bond. This was supported by COSY and HMBC correlations, which showed that ring D is fully saturated (**Figure 2B**). The origin of this derivative, designated as gromomycin J, remains unclear.

Since there are no respective genes on the P19-C01 cosmid that could explain the reduction of C=C bond of gromomycin, we anticipate that it may be a shunt product arising during the cyclization of the linear precursor. Based on the previously postulated minimal gene cluster for gromomycin synthesis, we have bioinformatically identified the borders of *A. xinjiangensis* groBGC spanning from gene 6 to gene 15 (**Figure 3**, **Table 1**).

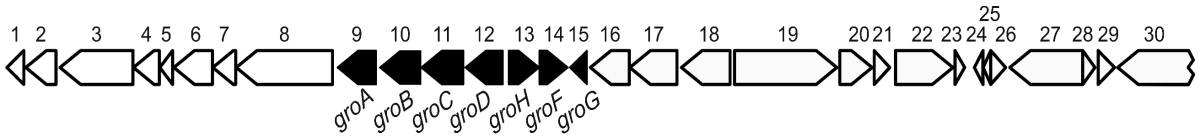

Figure 3. Diagram of the DNA segment containing the *A. xinjiangensis* groBGC depicted in black.

Table 1. Proposed function of genes in *A. xingiangensis* groBGC.

Gene	Proposed function
9 (groA)	Rieske-like 2Fe-2S protein
10 (groB)	Phenylpropionate dioxygenase-like ring-hydroxylating dioxygenase large terminal subunit
11 (groC)	Rieske-like 2Fe-2S protein
12 (groD)	Farnesyl-diphosphate synthase
13 (groH)	Hypothetical protein (prenyl transferase, guanidinatransferase)
14 (groF)	Hypothetical protein (cyclase)
15 (groG)	Protein-tyrosine-phosphatase

Within this range, we propose that genes 9 to 14 are structural (designated as *groA* to *groF*), whereas genes 6 to 8 and 15 are likely to be regulatory genes (designated as *gro6* to *gro8* and *gro15*). The functions of structural genes in *A. xinjiangensis* groBGC could be assigned based on proposed gromomycin assembly pathway in *Streptomyces* sp. Je 1-332.[300] *GroD* is coding for polyprenyl synthetase family protein. It is performing the condensation of six isoprenoid precursors, forming a hexaplenyl pyrophosphate. Gene 13, homologue of *groH*, is encoding a prenyltransferase, which is responsible for the hexaprenylguanidine formation. Gene 14, as its homologue of *groF*, is coding for a hypothetical protein which serves as a gromomycin cyclase. While the genes 9, 10 and 11 are annotated as Rieske non-heme iron oxygenases, as their *groA*, *groB* and *groC* homologues, they are also involved in the cyclisation process by introduction of the C4-OH group, and the formation of C1-C2 and C15-C16 double bonds.[300]

The groBGC of *A. xinjiangensis* lacks two genes, *groI* and *groE* involved in tailoring modifications of gromomycin. The GroI cytochrome P450 monooxygenase introduces the keto group of C17 position of the gromomycin C.[300] While the GroE reductase catalyses the reduction to a hydroxyl group, which, in turn, degrades generating gromomycin A. Thus, we anticipate that the final products of the *A. xinjiangensis* groBGC are gromomycins I (480A1) and C (480A2). These derivatives are structurally similar, with the difference of the double bond position at C14-C15 for gromomycin I and at C15-C16 for gromomycin C (**Figure 2B**). We propose that both derivatives could arise during gromomycin cyclization, as terpene synthases (or cyclases) are known to facilitate carbocation-driven rearrangements, including intramolecular allylic rearrangements and double bond migration as part of their catalytic mechanisms.[47, 301] A similar mechanism is described during the cyclisation reaction of a tetracyclic triterpene Euphol. An euphol-producing OSC enzyme (EtOSC5) is reported to produce two euphane and two tirucallane triterpenoids. Both euphane (euphol and eupha-7,24-dien-3β-ol, 20*R* epimers) and triturcallane (tirucallol and tirucalla-7,24-dien-3β-ol, 20*S* epimers) derivatives are structural isomers distinguished by the double bond position at C7-C8 or C8-C9.[302]

2.2.3.3. Bioactivity Testing

We have previously reported that gromomycins display broad-spectrum activity against Gram-positive bacteria, including drug-resistant strains.[300] Bioactivity testing of *A. xinjiangensis*-derived gromomycin derivatives revealed comparable antibacterial potencies with gromomycins I and C being more active against the gram-positive pathogens (2-4 μg/mL) than gromomycin J (16-32 μg/mL) (**Table S5**). Interestingly, while the position of the double

bond in gromomycin C and gromomycin I do not appear to significantly influence antibacterial activity, its complete absence, as exemplified for gromomycin J, results in reduced activity. It is worth mentioning that similar to previously described gromomycin derivatives, we observed a discrepancy between cell-based toxicity assays and the zebrafish embryo model. The zebrafish embryo model proved more sensitive toward gromomycin activity, with maximum tolerated concentrations (MTCs) closely mirroring antibacterial activity (**Table S6**). This discrepancy is likely due to binding to fetal bovine serum proteins present in cell culture medium, which partly masks gromomycin toxicity (**Table S7**).

The promising activity of gromomycins prompted us to investigate their antibacterial potential further. Specifically, we tested one representative of this compound class, gromomycin I, against 89 vancomycin-resistant *Enterococcus faecium* (VRE) isolates, which also carry resistance determinants to multiple other antibiotics, underscoring their clinical relevance. Gromomycin I exhibited a unimodal distribution of MIC values with MIC50 and MIC90 of 2 μg/mL (**Table 2**), respectively, highlighting its ability to overcome resistance to conventional antibiotics.

In addition, we assessed the killing kinetics of gromomycin I against *S. aureus* ATCC29213, which served as model strain for subsequent mode of action studies. Gromomycin I demonstrated time- and concentration-dependent bactericidal activity. While 1x MIC led to a 2-log10 reduction in colony-forming units (CFUs) - likely attributable to the higher starting inoculum compared to that used in standard MIC assays - supra-MIC resulted in a > 5-log10 reduction within only 30 min, indicating a potent and rapid bactericidal effect. Notably, recovery of cells was observed across all tested concentrations approximately 7 h post-treatment (**Figure 4A**). However, this resurgence was not attributable to the development of spontaneous resistance as isolated colonies remained susceptible to gromomycins. Indeed, gromomycins appear to have a low risk of resistance development. Attempts to select for gromomycin resistance in *S. aureus* ATCC29213 by plating high bacterial inocula on agar containing different doses of gromomycin I were unsuccessful. In addition, 30 days of continuous serial passaging in the presence of sub-MIC levels of gromomycin also failed to produce resistance. Similar results were obtained with the glycopeptide vancomycin, which targets the D-Ala-D-Ala motif of the bacterial peptidoglycan. In contrast, antibiotics with well-defined protein targets, such as rifampicin and ciprofloxacin, rapidly induced resistance within a few days of exposure (**Figure 4B**). The inability to select for gentamicin-resistant mutants strongly suggests a non-specific mode of action and/or the absence of a conventional protein target.[303]

2.2.3.4. Mode of Action Studies

These findings, combined with the non-selective activity of gromomycins (**Table S6**) and their amphiphilic nature, point towards an interaction with the bacterial cell envelope. To test this hypothesis, we utilized the fluorescent dye 3,3'-diethyloxacarbocyanide iodide (DiOC2(3)) which serves as an indicator of membrane potential.37 In healthy polarized cells, DiOC2(3) emits red fluorescence, which shifts toward green fluorescence upon membrane depolarization. The addition of gromomycin I to DiOC2(3)-stained *S. aureus* cells induced bacterial membrane depolarization as evidenced by a reduction in the red/green fluorescence ratio. Notably, this effect was observed at sub-MIC concentrations as low as 0.5-1 μg/mL (0.25-0.5x MIC), and increased gradually with rising concentration, ultimately reaching depolarization levels comparable to those induced by the protonophore carbonyl cyanide m-chlorophenyl hydrazone (CCCP) (5 μM). Importantly, the MIC-dependent depolarization of the molecule closely mirrors the bactericidal activity observed in the killing kinetics. A significant drop in membrane potential was observed between 2 μg/mL (1x MIC) and 4 μg/mL (2x MIC), corresponding with the onset of its bactericidal action (**Figure 4A and C**).

To investigate whether gromomycins enhance the ion permeability of the bacterial membrane, we measured the extracellular potassium concentration [K^+] following gromomycin exposure using a K^+-selective electrode. Addition of 20 μg/mL gromomycin I resulted in a rapid increase in extracellular [K^+], reaching a maximum of 80% K^+ release compared to the bee venom melittin, within approximately 2 min (**Figure 4D**). It is worth mentioning that the usage of high compound concentrations in this assay was necessary due to the high cell density (OD600 of 3) required to achieve detectable [K^+]. The rapid onset of leakage, correlating with the fast depolarization and killing kinetics, prompted us to check for large pore formation. Indeed, we were able to confirm a pore-forming activity by performing a propidium iodide influx assay. Propidium iodide is a fluorescent dye that enters the cells through large membrane pores and is thus indicative for membrane disruption. A strong increase in fluorescence was observed at concentrations starting 8 μg/mL (4x MIC). In contrast to melittin, which promotes fluorescence immediately after 5 min, maximum values for gromomycin I were only observed after 30 min (**Figure 4E**). Consistent with these findings, we found that gromomycin I induces lysis of S. aureus cells at concentrations of 8 μg/mL (**Figure 4F**). However, pore formation and subsequent lysis occurred only at higher concentrations and were too slow to account for the much faster membrane depolarization, suggesting that these are secondary effects of gromomycin action.

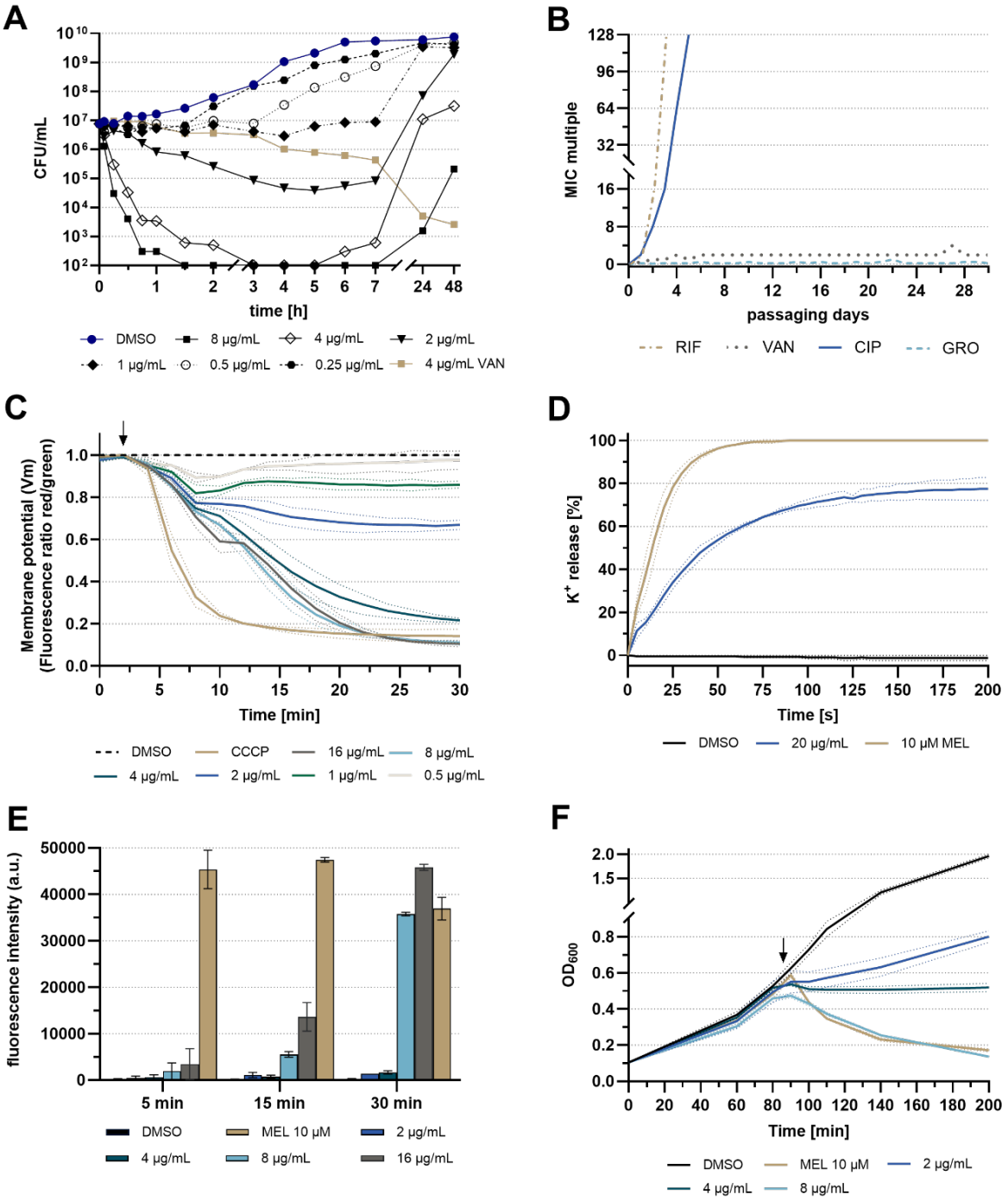

Figure 4. Gromomycin causes depolarization of the bacterial membrane and rapid cell lysis with bactericidal consequences for *Staphylococcus aureus*. A Time- and concentration-dependent killing of *S. aureus* by gromomycin I. Limit of detection is 102 CFU/mL. Vancomycin was used as positive control. B Resistance development through serial passaging in the presence of sub-MIC levels of antibiotics. The y axis represents the highest concentration with visible growth. C Membrane depolarization assay using DiOC2(3). The protonophore CCCP (5 µM) served as positive control. Mean ± SD of two biological replicates (n = 2). Black arrow indicates time point of compound addition. D Potassium release from whole cells. Potassium concentrations were measured using an ion-selective electrode. Leakage is expressed relative to the total amount of potassium release induced by the addition of 10 µM melittin. Mean ± SD of two biological replicates (n = 2). E Propidium iodide influx as an indicator for the presence of large membrane pores. The bee venom melittin is a membrane-disrupting peptide and was used as positive control. Mean ± SD of two biological replicates (n = 2). F Impact of gromomycin I on growth of S. aureus. A decrease in OD_{600} represents lysis of bacterial cells. Black arrow indicates time point of compound addition. Mean ± SD of two technical replicates. A representative curve of two biological replicates is shown (n = 2). CIP, ciprofloxacin; GRO, gromomycin I; MEL, melittin; RIF, rifampicin; VAN, vancomycin.

Utilizing scanning and transmission electron microscopy (SEM and TEM), we investigated the impact of gromomycins on the morphology and intracellular structures of S. aureus. In control SEM samples, *S. aureus* cells appeared healthy with no visible damage. In contrast, after 15 min of exposure to supra-MIC doses of gromomycin I, cells started exhibiting signs of intracellular leakage, suggesting compromised membrane integrity (**Figure S17**). This effect became more apparent after 30 min. with almost all cells showing any form of membrane damage. *S. aure*us cells show membrane blebs, furrows and dents, and even large pores are visible from which intracellular material is leaking (**Figure 5A**). TEM analysis provided further insights, revealing the presence of double-layered mesosomes and other aberrant membranous structures, along with numerous spherical, non-membrane-enclosed vesicles in gromomycin-treated cells, which were not observed in control samples (**Figure 5B**). Mesosome-like structures arise from invaginations of the cytoplasmic membrane and can occur during fundamental bacterial processes such as cell division. Although it is known that chemical fixation is a relevant factor for mesosomes, their formation has also been reported in response to antibiotic exposure.[304-305] For example, lateral expansion of the lipid bilayer, driven by molecule insertion and subsequent displacement of lipids, may result in the emergence of mesosome-like structures. Similar effects have been observed with the antimicrobial peptide gramicidin S, which is known to disrupt the lipid bilayer through interaction with membrane lipids. Interestingly, gramicidin S also promotes the emergence of inclusion bodies, likely composed of peptidoglycan precursors.[306] Another explanation could be that these inclusion bodies are composed of lipids, potentially serving to compensate for the increased surface area of the bacterial cell membrane.

We next sought to investigate whether the compound's effect on the bacterial cell envelope stems from a direct interaction with membrane lipids. To this end, we conducted MIC assays in the presence of representatives of fatty acids and lipids, monitoring for activity neutralization as a surrogate for lipid binding. MIC values shifted by up to 32-fold in a concentration-dependent manner, with the most significant changes induced by unsaturated fatty acids, such as palmitoleic acid, and negatively charged phosphatidylglycerols (PGs), including POPG (1-palmitoyl-2-oleoyl-sn-glycero-3-phosphatidylglycerol) and DOPG (1,2-dioleoyl-sn-glycero-3-phosphatidylglycerol). Neutral lipids resulted in a less pronounced shift (4- to 8-fold), and the cationic lipid DOTAP (1,2-dioleoyl-3-trimethylammonium propane) did not alter MIC values at all, likely due to electrostatic repulsion between this lipid and the positively charged gromomycin (**Figure S18**). To rule out the possibility that the observed effect is merely due to gromomycin's positive charge, we included gentamicin, a positively charged antibiotic with an intracellular target, as a control. Notably, gentamicin's activity remained

unaffected in the presence of PGs and even increased upon addition of fatty acids, suggesting a potential synergistic effect (**Figure S18B**).

Taken together, these results suggest that the antimicrobial activity of gromomycins primarily arises from membrane depolarization, driven by nonspecific interactions with

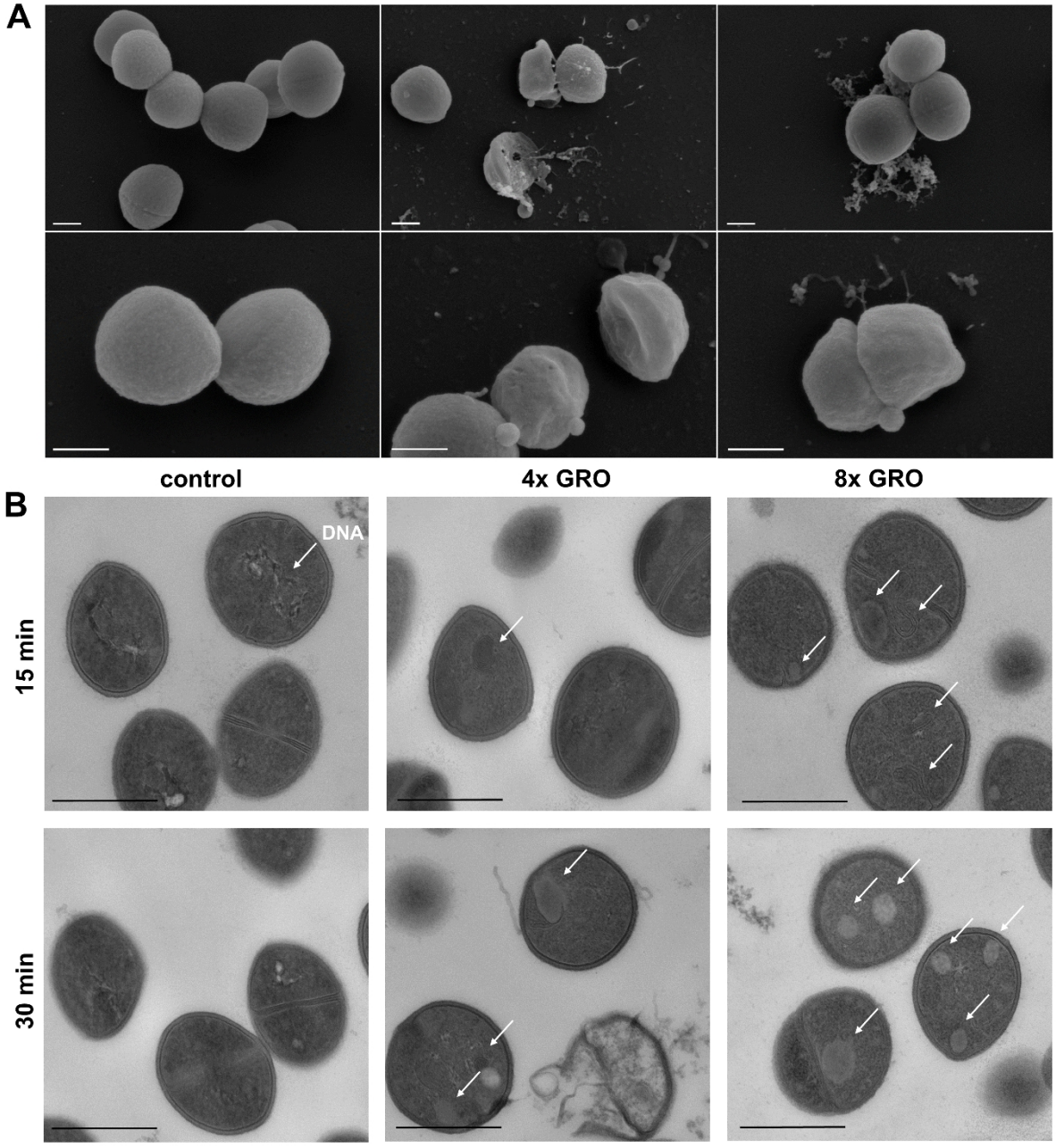

Figure 5. Ultrastructural analysis of *Staphylococcus aureus* exposed to gromomycin I. A Scanning electron microscopy (SEM) of S. aureus treated with 4- and 8-fold MIC of gromomycin I (T = 30 min). Scale bars are 300 nm. B Transmission electron microscopy (TEM) of S. aureus treated with 4- and 8-fold MIC of gromomycin I for 15 min and 30 min, respectively. Arrows indicate irregularities induced by the compound that are not present in control samples. Scale bars are 500 nm. The control represents S. aureus cells exposed to DMSO. GRO, gromomycin I.

membrane lipids and subsequent disruption of ion homeostasis. We postulate that gromomycins integrate into the membrane, a process facilitated by their amphiphilic scaffold: the cyclic hydrophobic part of the molecule likely interacts with the acyl chains of membrane lipids, while the positively charged guanidino group associates with the polar head groups. Electrostatic interactions between the guanidino moiety and anionic components of the cell envelope of Gram-positive bacteria – such as teichoic acids – likely contribute to the initial attraction to the bacterial surface.[307] While it remains unclear whether gromomycins form an actual ion channel, we speculate that, upon reaching a critical concentration, additional molecules insert into the membrane or oligomerize to form transient pores. This leads to disruption of membrane integrity and ultimately results in cell lysis.

2.2.3.5. Conclusion

The genome-mining approach has demonstrated impressive efficiency in the identification of novel gromomycin-like clusters, thereby highlighting their diversity among various bacterial taxa. This approach has resulted in the identification of a new groBGC from the *Actinoplanes* species and the isolation of new bioactive gromomycin derivatives, highlighting the significant untapped potential of underexplored actinobacteria in the field of antibiotic discovery. Mode of action studies have demonstrated that gromomycins act on the bacterial cell envelope. Targeting bacterial membranes has proven to be a highly effective antimicrobial strategy; however, it also raises concerns regarding toxicity toward eukaryotic cells. Due to the largely nonspecific nature of their interactions with lipid bilayers, membrane-active compounds can also disrupt eukaryotic cell membranes.[308-310] Indeed, also in the case of gromomycins, the cytotoxicity is closely mirroring their antibacterial activity. This off-target toxicity poses a major challenge in the clinical development of membrane-disrupting agents, calling for careful optimization of their selectivity index.[311] Nevertheless, FDA-approved drugs such as gramicidin and colistin illustrate the clinical potential of this potent mechanism of action. Although gramicidin is limited to topical use due to its hemolytic activity,[312] and colistin is reserved as a last-resort treatment for multidrug-resistant (MDR) infections due to its nephro- and neurotoxicity,[313] both compounds demonstrate that membrane-targeting agents can be successfully translated into clinical practice under carefully controlled conditions.

2.2.4. Materials and Methods

Bacterial strains and growth media

All strains and plasmids and primers used in this work are listed in **Tables S2-S4**. *A. xinjiangensis* DSM 45184 strain (Leibniz Institute DSMZ-German Collection of Microorganisms and Cell Cultures) was used for as a source of DNA for cosmid library construction. *S. albus* Del14 and *S. lividans* ΔYA9 were utilized as hosts for heterologous expression of the new groBGC. *E. coli* EPI300-T1R cells were used for DSM 45184 cosmid library preparation. *E. coli* ET12567 pUB307 was used as a donor strain for intergeneric conjugations. *E. coli* strains were grown in Luria-Bertani (LB) broth (Sigma-Aldrich, St. Louis, MO, USA). *Streptomyces* strains were grown on MS agar medium (Soy flour 20 g, Mannitol 20 g, tap water 1 L, pH 7.2) and in liquid tryptic soy broth medium (TSB; Sigma-Aldrich, St. Louis, MO, USA). For genomic DNA isolation *A. xinjiangensis* strain was cultivated in liquid TSB medium. For conjugation, the *Streptomyces* strains were cultivated on MS agar for sporulation. Where necessary, the following antibiotics were applied: apramycin (50 μg/ml), kanamycin (50 μg/ml) and nalidixic acid (50 μg/ml) (Sigma-Aldrich, St. Louis, MO, USA; Roth, Karlsruhe, Germany). For compounds production, S*treptomyces* strains were grown in liquid SG medium (20 g glucose, 10 g soy peptone, and 2 g $CaCO_3$, distilled water 1 L, pH 7.2).

Metabolite Extraction and Analysis

S. albus or *S. lividans* recombinant strains along with *A. xinjiangensis* control were cultivated in 50 ml TSB medium for a period of 48 h at 28 °C yielding a pre-culture. The main cultures containing 100 ml of SG, DNPM (40 g dextrin, 7.5 g soy peptone, 5 g baking yeast, and 21 g MOPS, distilled water 1 L, pH 6.8), or GYM (4 g glucose, 4 g yeast extract, 10 g malt extract and 2 g CaCO3, distilled water 1 L, pH 7.2) were inoculated with 1 ml of pre-culture. Following a six-day cultivation period at 28°C, the extraction of compounds was conducted using ethyl acetate from the clarified medium, followed by a solvent evaporation. One μl of sample was measured using a Dionex Ultimate 3000 UPLC (Thermo Fisher Scientific, Waltham, MA, USA), a 10-cm ACQUITY UPLC® BEH C18 column, 1.7 μm (Waters, Milford, MA, USA) and a linear gradient 5% to 95% of 0.1% formic acid (FA) solution in acetonitrile versus 0.1% FA solution in water for 18 min at a flow rate of 0.6 ml min^{-1} and 45 °C. Samples were analyzed using an amaZon speed mass spectrometer or maXis high-resolution LC-QTOF system (Bruker, USA). Data was collected and analyzed with the Bruker Compass Data Analysis software, version 5.2 (Bruker, Billerica, MA, USA).

Isolation and Purification of New Gromomycins

For production, the recombinant strain was grown in 10 L of SG medium 6 days at 28 °C with agitation at 180 rpm. New derivatives were extracted with ethyl acetate from the culture supernatant. The obtained extracts were dissolved in methanol and subsequently subjected to a purification process via size-exclusion chromatography on a Sephadex LH-20 column (Sigma-Aldrich, Louis, MO, USA) with methanol as a mobile phase. Fractions were collected every 10 min at a flow rate of 0.6 ml min^{-1}. The fractions containing pure compounds were pooled together, concentrated and dissolved in methanol. The second purification stage was performed using a Reversed Phase (RP) HPLC (Waters AutoPurufication™ System), separation on preparative C18 column Nucleodur HTec, 5 μm, 250 mm x 21 mm (Macherey-Nagel, Germany) using a water solution containing 0.1%(v/v) formic acid (solvent A), and an acetonitrile solution containing 0.1% (v/v) formic acid (solvent B) as a mobile phase. The fractions were collected using an MS detector (Waters™ SQ Detector 2). For compounds separation we used the following gradient at a flow rate of 20 mL/min: 0 min—5% B, 1 min—5% B, 2 min—5% B, 4 min—50% B, 25 min—50.5 % B, 27 min—66% B, 29 min—69% B, 30 min—95% B, 31 min—5% B. Gromomycin-containing fractions were pooled together, evaporated and used for the final purification step. The final purification stage was reversed-phase High performance liquid chromatography (HPLC), separation on semipreparative C18 column Synergy™ 4 μm Fusion-RP 80 Å 250×10 (Phenomenex, Torrance, CA, USA) using water + 0.1% formic acid (A) and acetonitrile + 0.1% formic acid (B) as a mobile phase. Fractions containing pure compound were pooled together and evaporated.

Gromomycin C white powder [11.4 mg], $[\alpha]_D^{20}$ -15° (c 0.53, MeOH). For NMR see Table S1 (500 MHz, CD_3OD). HRESIMS *m/z* 480.39 $[M+H]^+$, (calcd for $C_{31}H_{50}N_3O$, 480.3948).

Gromomycin I white powder [34.7 mg], $[\alpha]_D^{20}$ -41° (c 0.64, MeOH). For NMR see Table S1 (500 MHz, CD_3OD). HRESIMS *m/z* 480.39 $[M+H]^+$, (calcd for $C_{31}H_{50}N_3O$, 480.3948).

Gromomycin J white powder [9.6 mg], $[\alpha]_D^{20}$ n.a. For NMR see Table S1 (500 MHz, CD_3OD). HRESIMS *m/z* 482.41 $[M+H]^+$, (calcd for $C_{31}H_{52}N_3O$, 482.4105).

NMR Spectroscopy and Optical Rotations Measurements

The chemical structures of gromomycins were determined via multidimensional NMR analysis. ^{1}H-NMR, ^{13}C-NMR, and 2D spectra were recorded at 500 MHz (^{1}H) and 126 MHz (^{13}C),

conducted in the Bruker Avance Neo 500 MHz, equipped with a Prodigy Cryo-probe. Gromomycins were dissolved in deuterated methanol-d_4. All 2D experiments were measured using standard experiments from Bruker Topspin software 4.3.0 and non-uniform sampling (NUS). Chemical shifts are reported in ppm relative to tetramethylsilane; the solvent was used as the internal standard. Chiroptical measurements of all the compounds in H_2O ($[\alpha]_D^{20}$) were obtained on a model Jasco P-2000 Automatic Digital Polarimeter (JASCO, Easton, MD, USA) in a 3.5 x 50mm cell at 20 °C.

Cosmid Library Construction

A cosmid libraries of actinomycetes were prepared using the EpiCentre CopyControl™ Fosmid Library Production Kit in pCos15AAmInt vector by adapting the protocol from Lucigen. A library of 30–40 (kb) was constructed according to the protocol established by the manufacturer. Genomic DNA was isolated using the NucleoSpin Microbial DNA Mini kit (MACHEREY-NAGEL GmbH & Co. KG, Germany) for DANN isolation from microorganisms. Purified genomic DNA fragments were then ligated into linearized cos15AAmInt vector. The ligation reactions were packaged into λ phage for *E.coli* EPI300 infection. The packaged library was plated on LB agar plates containing 50 μg ml^{-1} apramycin, and grown overnight at 37 °C. Approximately 1800 single colonies were picked and inoculated into individual wells of 96-well plates. The library was stored with 20% glycerol and kept at −80 °C.

Genome-Guided Identification of New Gromomycin-Like Clusters

A genome-wide quantitative screening of new gromomycins was conducted using three genes involved in the biosynthesis of gromomycins: *groD*, *groF* and *groH*. The nucleotide sequences of these genes were used as probes in the NCBI protein BLAST database to identify new groBGCs. The strains where all three of these genes were found in close proximity in the genome were selected. As a result, many actinomycetes strains were identified, including *A. xinjiangensis* strain. The new groBGC was isolated from the genome of the *A. xinjiangensis* strain through the cosmid library construction according to the manual (CopyControl™ Fosmid Library Production Kit). The cosmid P19-C01 sample, which contained the entire cluster, was identified through a combination of end sequencing and PCR with two pairs of primers designed to amplify regions on the left or right side of the cluster.

Heterologous Expression of the New Gromomycin-Like BGC

The cosmid 19_C01 harboring a novel *gro*BGC was introduced into *S. albus* Del14 and *S. lividans* ΔYA9 by a standard intergeneric mating protocol[264] using donor strain *E. coli* ET12657 pUB307 on MS plates. After incubating at 29°C for 15 hours, plates were overlaid with 1 mL of sterile distilled water containing 50 μg ml^{-1} apramycin and 50 μg ml^{-1} nalidixic acid. Antibiotic-resistant transconjugants were patched onto MS plates containing 50 μg ml^{-1} apramycin. The ability of heterologous strains to generate novel derivatives was assessed through HPLC analysis.

Antibiotic Activity (Minimum Inhibitory Concentrations)

Gromomycin stock solutions were prepared in dimethyl sulfoxide (DMSO). All microorganisms used in this study were obtained from the German Collection of Microorganisms and Cell Cultures (DSMZ), the American Type Culture Collection (ATCC), the Coli Genetic Stock Center, or were part of our internal strain collection. *Staphylococcus aureus* strains Newman, N315, Mu50 and Cowan 1 were obtained from M. Bischoff, Saarland University Hospital, Homburg. *S. aureus* wild type and Dap^R HG001 were provided by T. Schneider, University of Bonn.[270] *E. coli* WO153 was provided by K. Lewis, Northeastern University, Boston, USA. *E. faecium* clinical isolates were collected between 2019 and 2024 and were provided by Stefano Mancini, Institute of Medical Microbiology, Zürich, Switzerland. Minimum inhibitory concentrations (MICs) were determined using the broth microdilution method according to EUCAST guidelines (ISO 20776-1:2019). In short, serial two-fold dilutions of gromomycins (0.03125 to 64 μg/mL) were prepared in 75 μL of cation-adjusted Mueller-Hinton broth (MHB2) in sterile 96-well plates. Equal volume of the bacterial suspension was added, and the plates were incubated at 37 °C for 18 h. For *Streptococcus pneumoniae,* MHF broth (MHB2 supplemented with 5% lysed horse blood and 20 mg/L β-NAD) was used and plates were incubated at 37 °C with 5% CO_2. The MIC was defined as the lowest concentration of the antibiotic causing complete inhibition of visible growth of the microorganism. The same method was used for testing *Mycobacterium smegmatis,* but with the use of Middlebrook 7H9 complete medium supplemented with oleic acid, albumin, dextrose and catalase (OADC, 10%). *M. smegmatis* plates were incubated for 48 h at 37 °C. For assessing activity against *Mycobacterium tuberculosis,* an adapted resazurin microtitre assay (REMA) was performed. In short, *M. tuberculosis* single cells were prepared and added to compound dilutions in M7H9. Plates were incubated for 6 d at 37 °C, followed by addition of 50 μL of resazurin and incubation for another day at 37 °C. The MIC was determined visually and additionally confirmed by measuring fluorescence (excitation at 530 nm, emission at 590 nm).

Cytotoxic Activity (IC50)

HepG2 cells (human hepatoblastoma cell line; ACC 180) and CHO-K1 (chinese hamster ovary cells; ACC 110) were obtained from the German Collection of Microorganisms and Cell Cultures (DSMZ) and cultured under the conditions recommended by the depositor. Cells were propagated in Roswell Park Memorial Institute (RPMI) 1640 medium and Ham's F12 medium, respectively, supplemented with 10% fetal bovine serum (FBS), and seeded at 6×10^3 cells per well of 96-well plates in 120 µL of complete medium. After 2 h of equilibration (37 °C, 5% CO_2), the cells were treated with a serial dilution of gromomycins. Gromomycins, doxorubicin as reference, as well as the solvent control (DMSO) were tested as duplicates in two independent experiments. After 5 d of incubation (37 °C, 5% CO_2), a total of 20 µL of 5 mg/ml MTT (thiazolyl blue tetrazolium bromide) in phosphate-buffered saline (PBS) were added to each well and the cells were further incubated for 2 h at 37 °C before the supernatant was discarded. Subsequently, the cells were washed with 100 µL of PBS and treated with 100 µl of 2-propanol/10 N HCl (250:1) to dissolve formazan granules. Cell viability was measured as a percentage relative to the respective solvent control by measuring the absorbance at 570 nm using a microplate reader (Tecan Infinite M200Pro). GraphPad Prism (version 10.0.3, GraphPad, Boston, MA, USA) was used for sigmoidal curve fitting to determine the IC_{50} values.

Maximum Tolerated Concentration

Husbandry of adult zebrafish was performed according to internal guidelines set out in the German Animal Welfare Act (§11 Abs. 1 TierSchG). Experiments were carried out with wild type AB (obtained from the European Zebrafish Resource Center at Karlsruhe Institute of Technology) embryos within the first 120 hours post fertilization (hpf) as these early life stages are not considered as animal experiments according to the EU Directive 2010/63/EU. Embryos were maintained in fresh 0.3x Danieau's (17.4 mM NaCl, 0.21 mM KCl, 0.12 mM $MgSO_4$, 0.18 mM Ca $(NO_3)_2$, 1.5 mM HEPES, 1.2 µM methylene blue, pH 7.1-7.3) at 28 °C. At a maximum of 120 hpf, embryos were euthanized by submersion in ice water for at least 12 h. For evaluation of the maximum tolerated concentration (MTC), embryos were dechorionated at 30 hpf using 1 mg/mL pronase and placed in a flat-bottom 96-well plate with one embryo per well. Excess medium was removed and 150 µL of gromomycin dilutions (in 0.3x Danieau's, maximum of 1% DMSO) and of the solvent control (1% DMSO in 0.3x Danieau's) were added. Ten embryos were used per condition. Exposed embryos were maintained at 28 °C until 120 hpf and they were monitored daily under a stereo microscope (Stemi 508, Zeiss) in order to record survival as well as anomalies, pigmentation, heartbeat and locomotor responses. An

embryo was considered dead when no heartbeat could be observed. The maximum tolerated concentration (MTC) was defined as the highest concentration of the antibiotic with more than 90% survival of zebrafish embryos. Kaplan-Meier curves were generated using GraphPad Prism (version 10.0.3, GraphPad, Boston, MA, USA).

Time-Kill Kinetics

An overnight culture of *S. aureus* ATCC29213 was diluted 1:100 in MHB2 and incubated at 37 °C until log-phase was reached. The bacteria were adjusted to reach approximately 10^7 CFU/mL, distributed to test tubes and challenged with different concentrations of gromomycins I. DMSO was used as a negative control and 2x MIC of vancomycin was used as a positive control. The bacteria were incubated at 37 °C and 300 rpm, and at designated time points, an aliquot of the samples was taken, and appropriate dilutions were plated on CASO agar. Agar plates were incubated at 37 °C overnight and colonies were counted to calculate CFU/mL.

Resistance Studies

For single-step resistance, CASO agar plates containing 4x and 8x MIC of gromomycin I were prepared. $5x10^9$ and $5x10^8$ CFU (*S. aureus* ATCC29213) were plated on selective agar plates, and appropriate dilutions of the inoculum were plated on non-selective agar to determine the proper count. Plates were incubated for 48 h at 37 °C. For resistance development by serial passaging, an overnight culture of *S. aureus* ATCC29213 was diluted 1:200 in fresh MHB2 containing different compound concentrations (0.25x to 4x MIC). Test tubes were incubated at 37 °C overnight and the next day, the highest concentration with visible growth was used to inoculate (1:200) the next series of concentrations based on the growth results from the previous day. Rifampicin, ciprofloxacin and vancomycin were used as reference compounds. This procedure was repeated until a significant level of resistance was reached or terminated after 30 days. Resistance was confirmed by broth microdilution method.

Electron Microscopy

An overnight culture of *S. aureus* ATCC29213 was sub-cultured 1:100 in fresh MHB2 and re-incubated until OD_{600} 0.5 was reached. The culture was divided into 2 mL samples and exposed to 4x and 8x MIC of gromomycin I, or DMSO (control). Samples were incubated for 15 min and 30 min at 37 °C and 300 rpm, respectively. Cells were fixed by incubating with 2% glutaraldehyde and 5% paraformaldehyde (final concentrations) for 30 min. Samples for both scanning electron microscopy (SEM) and transmission electron microscopy (TEM) were processed as previously described.[314] For TEM, samples were further treated with osmium

tetroxide, dehydrated in a graded series of ethanol on ice, and embedded in LR White resin. 50-70 nm thick, ultrathin sections were counterstained with 4% aqueous uranyl acetate and lead citrate and analysed with a Libra 120 Plus (Zeiss, Oberkochen, Germany) operating at an acceleration voltage of 120 kV and with the image analysis software ITEM (Olympus). For SEM, bacteria were fixed to 12 mm, round, poly-L-lysine pre-treated cover slips and dehydrated in a graded series of acetone on ice, critical-point dried with liquid CO_2 (CPD 300, Leica Microsystems, Wetzlar) and sputter coated with a gold-palladium film (SCD 500, Bal-Tec, Lichtenstein). Image acquisition was performed with a field-emission scanning-electron microscope Zeiss Merlin (Oberkochen, Germany) using Everhart Thornley and the inlens SE detectors at an acceleration voltage of 5 kV.

Membrane Potential Assay

The assay was performed as previously described. An overnight culture of *S. aureus* ATCC29213 was diluted 1:100 in fresh LB medium supplemented with 0.1% glucose and incubated at 37 °C until log-phase was reached. Cells were pelleted (4000 rpm, 4 °C, 5 min) and resuspended in PBS supplemented with 0.1% glucose to an OD_{600} of 0.5. Cells were incubated with 30 µM 3,3'-diethyloxacarbocyanine iodide ($DiOC_2(3)$) for 15 min in the dark. $DiOC_2(3)$-treated cells were transferred to a black-bottom 96-well plate with 100 µL/well, and a baseline measurement was recorded for 4 min at an excitation wavelength of 485 nm and emission wavelengths of 530 nm (green) and 630 nm (red). The measurement was stopped and a concentration series of gromomycin I (1 µL of 100x stocks) was added, after which the measurement was continued for a total of 30 min. Carbonylcyanide-*m*-chlorphenylhydrazone (5 µM, CCCP) was used as positive control, while 1% DMSO served as negative control. Experiments were performed in technical and biological duplicates.

Potassium Release from Whole Cells

Potassium release was measured using a potassium-selective electrode as recently described with a few modifications.[315] An overnight culture of *S. aureus* ATCC29213 was diluted 1:100 in fresh MHB2 and incubated at 37 °C until early stationary phase (OD_{600} 1.2) was reached. Cells were pelleted (4000 rpm, 4 °C, 20 min) and washed with 10 mM Tris-HCl, 100 mM NaCl, pH 7.4, adjusted with ionic strength adjuster (2 mL/100 mL buffer). The cell suspension was pelleted again, and the pellet was resuspended in the aforementioned buffer to reach an OD_{600} of 30. The bacteria were kept on ice and used within 30 min. The potassium electrode was calibrated with standard solutions containing 10, 100 and 1000 mg/L K^+, respectively. For each measurement, the bacteria were diluted 1:10 with buffer and the baseline potassium

concentration was measured ($[K^+]_{init}$). Then, 10x MIC of gromomycin I (20 µg/mL) or 10 µM melittin was added and potassium release was measured every 5 s until the potassium value remained stable ($[K^+]_{meas}$). DMSO was used as negative control. Experiments were performed in biological duplicates. Leakage is expressed relative to the total amount of potassium release induced by the addition of 10 µM melittin ($[K^+]_{tot/MEL}$).

$$K^+ \text{ release } [\%] = \frac{[K^+]_{meas} - [K^+]_{init}}{[K^+]_{tot/MEL} - [K^+]_{init/MEL}} \cdot 100$$

Propidium Iodide Influx Assay

An overnight culture of *S. aureus* ATCC29213 was sub-cultured 1:100 in fresh MHB2 and re-incubated until OD_{600} 0.5 was reached. Bacteria were treated with 1x, 2x, 4x or 8x MIC of gromomycins I, 10 µM melittin (positive control) or DMSO in test tubes in a total volume of 500 µL. Samples were incubated at 37 °C and 300 rpm, and after 5, 15 and 30 min 100 µL aliquots were taken and stained with 10 µg/mL propidium iodide for 5 min in the dark (37 °C, 300 rpm). Stained bacteria were pelleted (maximum speed, 2 min, 4 °C) and washed twice with 100 µL PBS. The pellet was resuspended in PBS, and cells were dispensed in a black flat-bottom 96-well plate. Fluorescence was measured at an excitation wavelength of 535 nm and an emission wavelength at 617 nm. Experiments were performed in technical triplicates and biological duplicates.

Lysis Assay

An overnight culture of *S. aureus* ATCC29213 was sub-cultured 1:100 in fresh MHB2 and re-incubated until OD_{600} of 0.5 was reached. Bacteria were diluted to an OD_{600} of 0.1 and distributed into test tubes, after which they were grown to mid-log phase. Subsequently, 1x, 2x or 4x MIC of gromomycins I, 10 µM melittin (positive control) or DMSO (negative control) were added. OD_{600} was measured until 120 min after compound addition. Experiments were performed in technical and biological duplicates.

2.2.5. Supplementary Information for Chapter 2.2

Genome Mining–Driven Isolation of New Gromomycins and Insights into Their Mode of Action

Structure elucidation

List of Tables

Table S1: NMR data (500MHz, MeOD4) of gromomycin C, gromomycin I and gromomycin J.

	gromomycin C (480A2)*		gromomycin I (480A1)		gromomycin J (482A)	
No	$\delta(^{13}C)$ [ppm], type	$\delta(^{1}H)$ [ppm], mult(J)	$\delta(^{13}C)$ [ppm], type	$\delta(^{1}H)$ [ppm], mult(J)	$\delta(^{13}C)$ [ppm], type	$\delta(^{1}H)$ [ppm], mult(J)
1	116.4, CH	5.92, s	116.1, CH	5.89, s	116.3, CH	5.92, s
2	132.7, C	-	132.3, C	-	132.5, C	-
3	59.9, C	-	59.9, C	-	59.9, C	-
4	80.0, CH	3.68, dd (10.7, 4.0)	79.6, CH	3.70, dd (11.3, 4.5)	79.5, CH	3.68, dd (11.7, 4.5)
5	29.6, CH_2	1.60, m 1.86, m	29.2, CH_2	1.73, m 1.59, m	27.8, CH_2	1.82, m 1.52, m
6	47.4, CH	1.57, m	41.8, CH	1.64, m	56.9, CH	1.06, m
7	38.0, C	-	38.4, C	-	39.0, C	-
8	35.2, CH_2	1.51, m	35.8, CH_2	1.53, m 1.24, m	40.9, CH_2	1.87, m 1.37, m
9	34.2, CH_2	1.82, m 1.74, m	28.1, CH_2	1.70, m 1.58, m	41.0, CH_2	1.72, m 0.81, m
10	43.7, C	-	43.4, C	-	39.2, C	-
11	39.2, C	-	38.6, C	-	38.8, C	-
12	33.6, CH_2	1.39, m 1.66, m	31.3, CH_2	1.56, m 1.49, m	42.9, CH_2	1.83, m 0.95, m
13	20.5, CH_2	1.46, m 1.54, m	22.5, CH_2	1.93, m 1.69, m	18.5, CH_2	1.67, m 1.50, m
14	41.8, CH	2.35, m	135.4, C	-	54.7, CH	0.93, m
15	145.1, C	-	136.5, C	-	62.7, CH	0.82, m
16	122.6, CH	5.67, m	27.7, CH_2	2.09, m 1.82, m	19.6, CH_2	1.47, m 1.69, m
17	24.6, CH_2	2.1, m	21.3, CH_2	1.52, m 1.69, m	19.1, CH_2	1.48, m
18	34.6, CH_2	1.47, m 1.38, m	36.5, CH_2	1.61, m 1.27, m	38.5, CH_2	1.30, m
19	36.4, C	-	39.5, C	-	36.7, C	-
20	42.3, CH_2	1.28, m	41.8, CH_2	1.56, m 1.08, m	45.5, CH_2	1.25, m 1.10, m
21	23.4, CH_2	1.91, m	24.9, CH_2	2.02, m 1.56, m	23.1, CH_2	1.87, m
22	126.5, CH	5.09, m	126.5, CH	5.02, m	126.4, CH	5.08, m
23	131.8, C	-	132.0, C	-	131.8, C	-
24	17.9, CH_3	1.59, s	18.1, CH_3	1.54, s	26.1, CH_3	1.67, s
25	23.8, CH_3	1.40, s	24.0, CH_3	1.39, s	23.7, CH_3	1.39, s
26	25.3, CH_3	1.21, s	25.0, CH_3	1.20, s	26.1, CH_3	1.18, s
27	29.8, CH_3	1.03, s	24.1, CH_3	0.92, s	17.4, CH_3	0.91, s
28	22.5, CH_3	0.85, s	21.3, CH_3	0.86, s	18.4, CH_3	0.92, s
29	19.1, CH_3	0.76, s	28.9, CH_3	1.02, s	21.6, CH_3	0.83, s

30	26.1, CH_3	1.66, s		26.1, CH_3	1.66, s	17.8, CH_3	1.59, s
1'	152.9, C	-		152.6, C	-	152.8, C	-

*The literature data of gromomycin C were measured in DMSO-d_6. For better comparability, a small sample of A480A2 was also measured in DMSO-d_6. The ^{1}H and HSQC data obtained were consistent with the literature data.

Table S2. Bacterial strains used in this work.

Strains	Description	Reference or Source
Actinoplanes xinjiangensis DSM 45184	Type strain	DSMZ-German Collection of Microorganisms and Cell Cultures
S. albus Del14	Cluster-free heterologous host strain	[254]
S. lividans ΔYA9	Cluster-free heterologous host strain	[255]
S. albus Del14 cos15AAmInt-19C01	S. *albus* strain Del14 containing the cos15AAmInt-19C01 vector	This work
S. lividans ΔYA9 cos15AAmInt-19C01	*S. lividans* ΔYA9 containing the cos15AAmInt-19C01 vector	This work
E. coli ET12567 pUB307	Donor strain for intergeneric conjugation	[274]
E.coli EPI300-T1R	Strain used for Construction of inducible-copy-number genomic libraries using the CopyControl™ Cloning System, with clones that are resistant to contaminating phage T1 and T5	Lucigen

Table S3. Plasmids used in this work.

Plasmids	Description	Reference or Source
pCos15A_AmInt	pCos15A_gus_AmInt, where *gus* gene was deleted	[300]
Cos15AAmInt-19C01	Cosmid 19C01 containing gromomycin-like gene cluster with *aac(3) IV*, *oriT*, and integrase	This work

Table S4. Primers used in this work.

Primer name	Sequence (5'-3')	Description	Source
actino_7_ F actino_7_R	CTGCGTCCTGTTCTGGATGA CACGGGTTCTTTCCCTCGG	To test for *groF* homolog gene presence	This work
Left_actino_F Left_actino_R	GAGACGATCAGCACCTCCG GACAACGGCCGCTCCTAC	To sequence the insert containing gromomycin-like cluster from the left side of the cluster	This work
Right_actino_F Right_actino_R	CTGGCAACTGCTCCATGAG GGAACGGTGGATAGTCGTCG	To sequence the insert containing gromomycin-like cluster from the right side of the cluster	This work

Table S5. Antimicrobial activity spectrum of gromomycin derivatives.

Classification	Organism	MIC [µg/mL]			
		Gromomycin I	Gromomycin C	Gromomycin J	REF[c]
Gram-positive	*S. aureus* ATCC29213	2	4	32	VAN: 2
	S. aureus Newman	2	2	16-32	VAN: 2
	S. aureus Cowan 1	2	4	32	VAN: 2
	S. aureus N315	2	4	32	VAN: 2, AMP: > 64
	S. aureus Mu50	2	4	16	VAN: 8, AMP: > 64
	S. aureus HG001 WT	2	4	32	DAP: 1
	S. aureus HG001 Dap^R	2	2	8	DAP: 64
	S. pneumoniae DSM11865	2	2	8	RIF: 0.03
	E. faecalis ATCC29212	2	4	32	RIF: 0.5
	B. subtilis DSM10	2	2	32-64	VAN: 1
Mycobacteria	*M. smegmatis* mc^{2}155	16	16	16	RIF: 32
	M. tuberculosis H37Ra	4	4	4-8	RIF: 0.02
Gram-negative	*E. coli* BW25113	> 64	> 64	> 64	CIP: 0.03
	E. coli K12 Δ*tolC*[a]	> 64	> 64	> 64	CIP: 0.01
	E. coli K12 Δ*tolC*[a] + PMBN[b]	4	4	64	CIP: 0.01
	E. coli WO153	4	32	32	CIP: 0.01
	S. enterica DSM5569	> 64	> 64	> 64	CIP: 0.02
	C. freundii DSM30039	> 64	> 64	> 64	CIP: 0.02
	K. pneumoniae DSM681	64	> 64	> 64	CIP: 0.01
	A. baumannii DSM30007	16	> 64	> 64	CIP: 2
	A. baumannii DSM30008	16	> 64	> 64	CIP: 0.5
	A. baumannii NCTC13301	16-32	> 64	> 64	CIP: > 64, COL: 1
	P. aeruginosa PA14	> 64	> 64	> 64	CIP: 0.25

[a] Keio collection mutant; efflux-deficient [b] 3 µg mL^{-1} polymyxin B nonapeptide (PMBN) [c] Reference antibiotics: AMP, ampicillin; CIP, ciprofloxacin; COL, colistin; DAP, daptomycin; RIF, rifampicin; VAN, vancomycin
[R] Daptomycin resistance.

Table S6. Toxicity profile of gromomycin derivatives. *In vitro* cytotoxicity was evaluated performing a MTT assay (half maximal inhibitory concentration IC_{50} ± standard deviation). *In vivo* toxicity was assessed by determination of the maximum tolerated concentration (MTC) in zebrafish (*Danio rerio*) embryos. CHO: chinese hamster ovary.

Gromomycin derivative	***In vitro* IC_{50} [µg/mL]**		***In vivo* MTC [µg/mL]**
	HepG2	**CHO-K1**	***Danio rerio***
Gromomycin I	24.5 ± 8.3	25.4 ± 3.3	1
Gromomycin C	22.7 ± 0.2	24.3 ± 1.3	1
Gromomycin J	22.7 ± 2.0	> 37	nd[a]

[a] not determined (nd) due to poor solubility in the incubation medium

Table S7. Gromomycin I binds to plasma proteins. Minimum inhibitory concentrations (MICs) of gromomycin I and daptomycin in the presence of different plasma protein constituents. MICs were determined in MHB2 adjusted to 1.25 mM Ca^{2+} and 0.8 mM Mg^{2+} (physiological concentration). BSA: bovine serum albumin; FBS: fetal bovine serum.

Condition	**MIC [µg/mL]**	
	Gromomycin I	**Daptomycin**
MHB2 (no addition)	2	1
6% (*w/v*) BSA	32	16
25% (*v/v*) FBS	8	1
50% (*v/v*) FBS	8	1
25% (*v/v*) human serum	32	2
50% (*v/v*) human serum	64	4

List of Figures

Figure S1. Structures of gromomycins C, I and J, showing COSY correlations and key HMBC correlations crucial for the assignment of ring D.

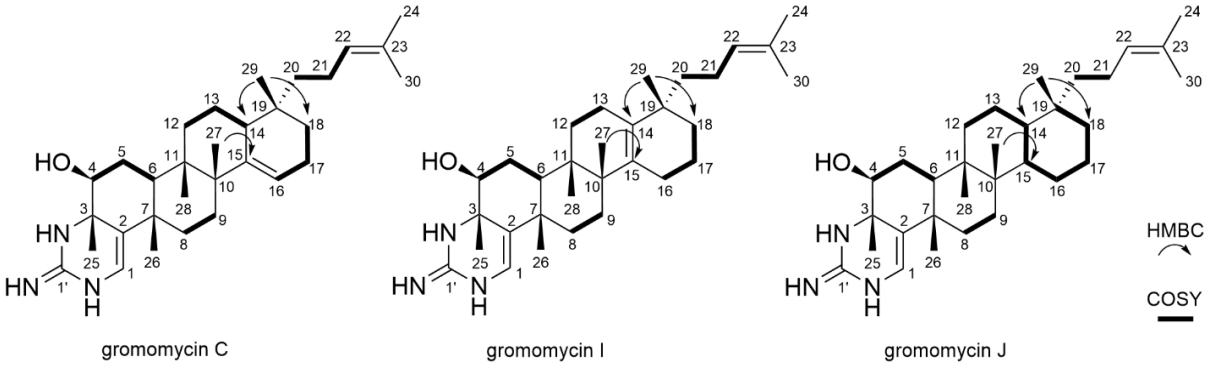

gromomycin C gromomycin I gromomycin J

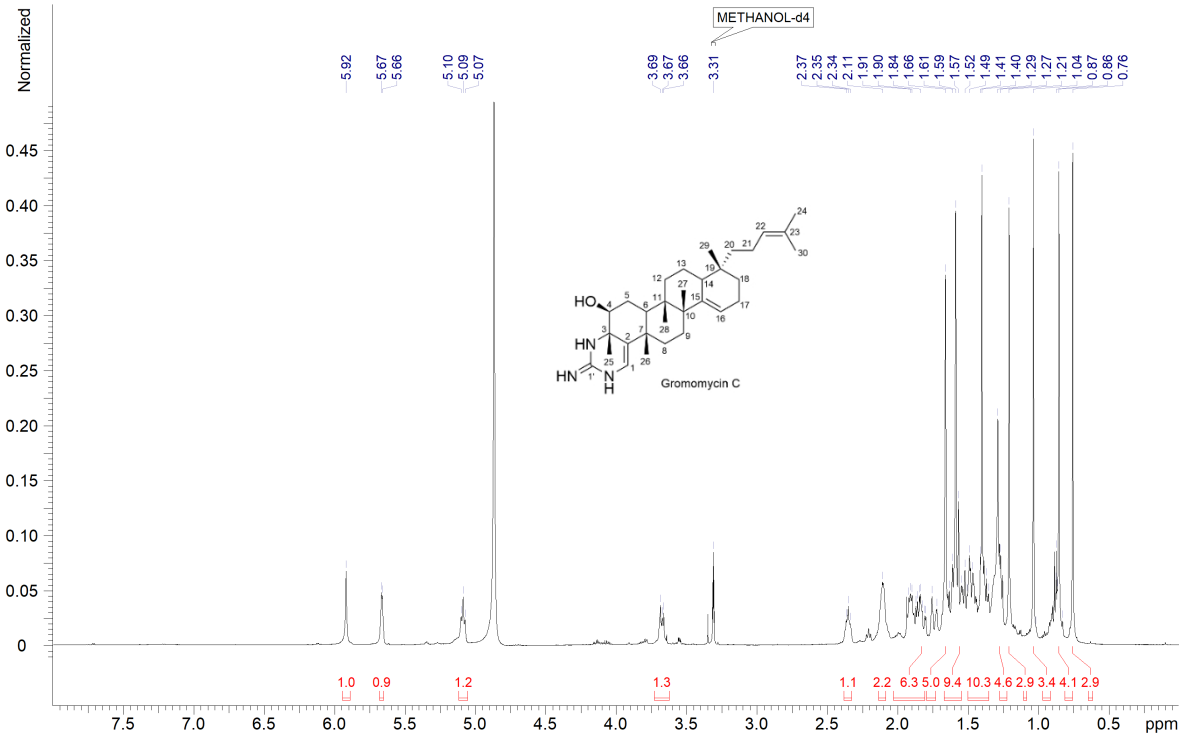

Figure S2. ^{1}H-NMR spectrum (500 MHz, $MeOD_4$) of gromomycin C (480A2).

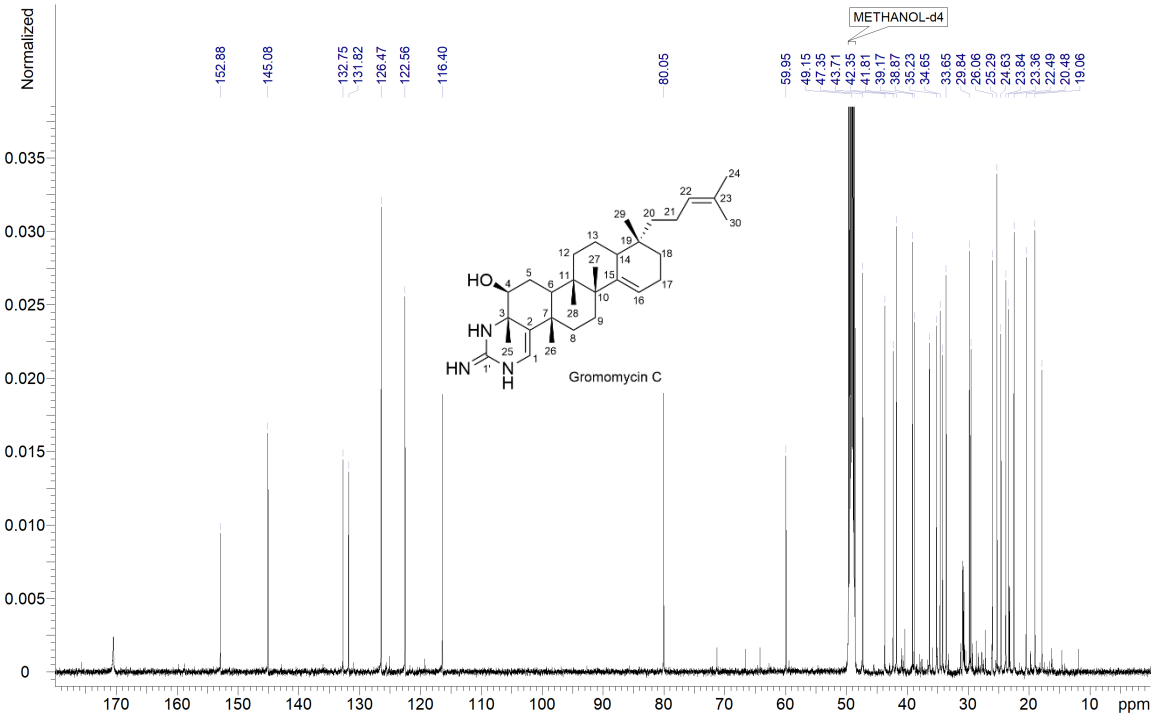

Figure S3. ^{13}C-NMR spectrum (125 MHz, $MeOD_4$) of gromomycin C (480A2).

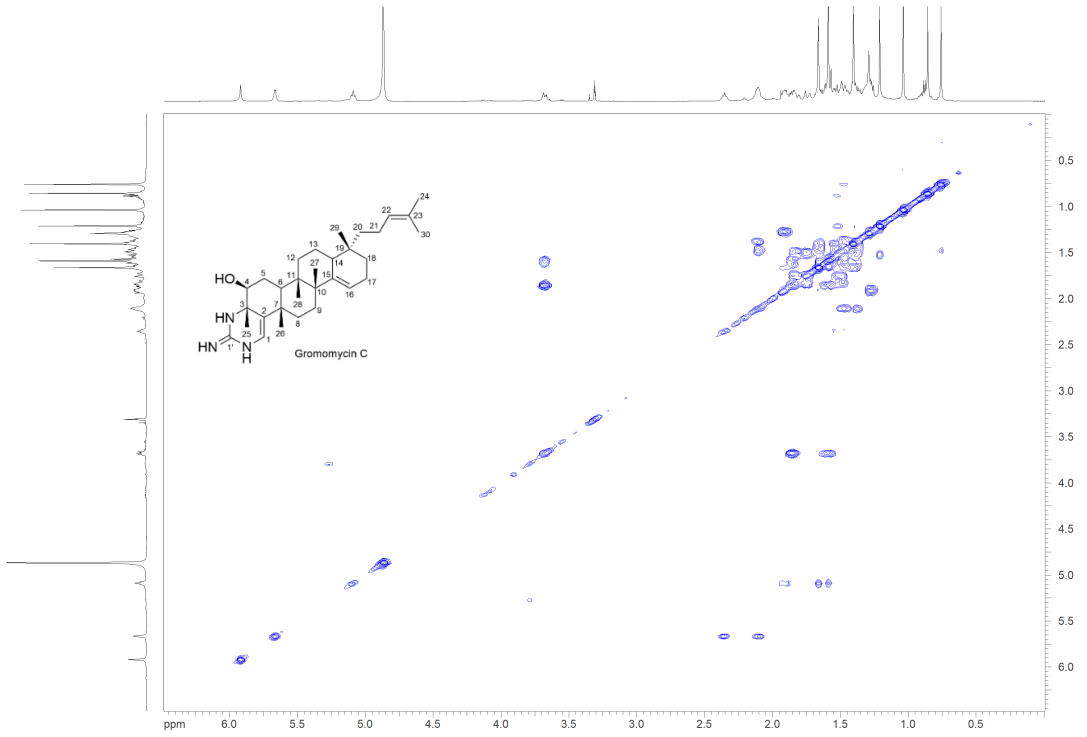

Figure S4. COSY spectrum ($MeOD_4$) of gromomycin C (480A2).

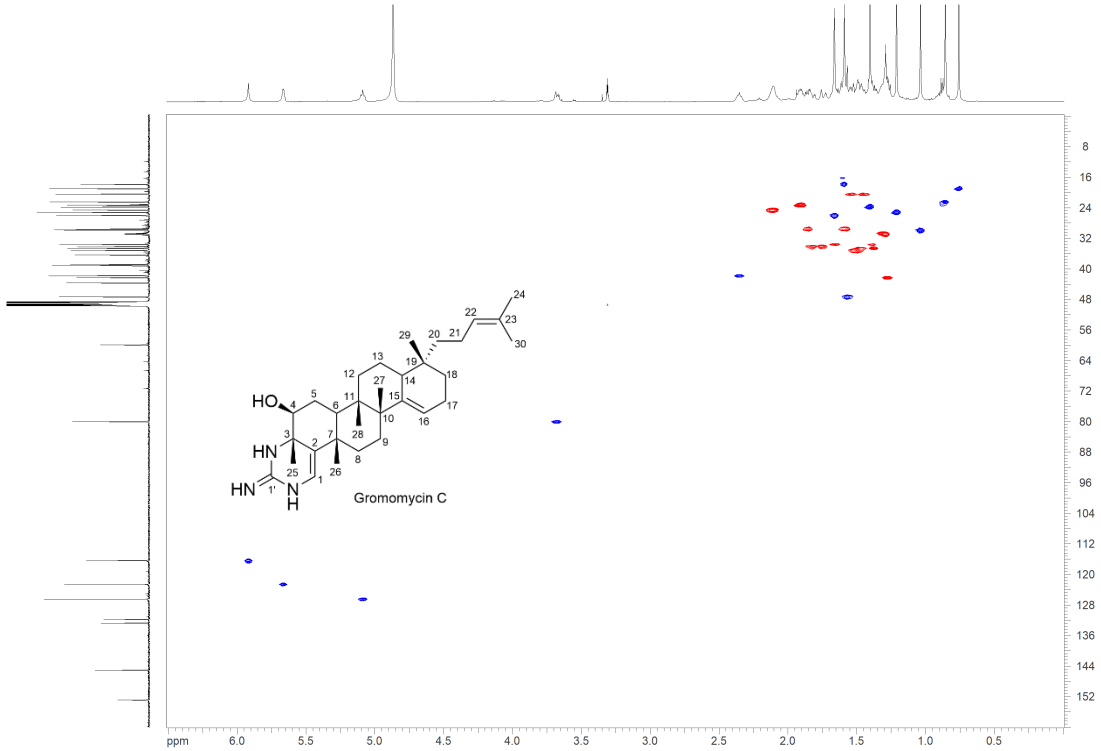

Figure S5. HSQC spectrum ($MeOD_4$) of gromomycin C (480A2).

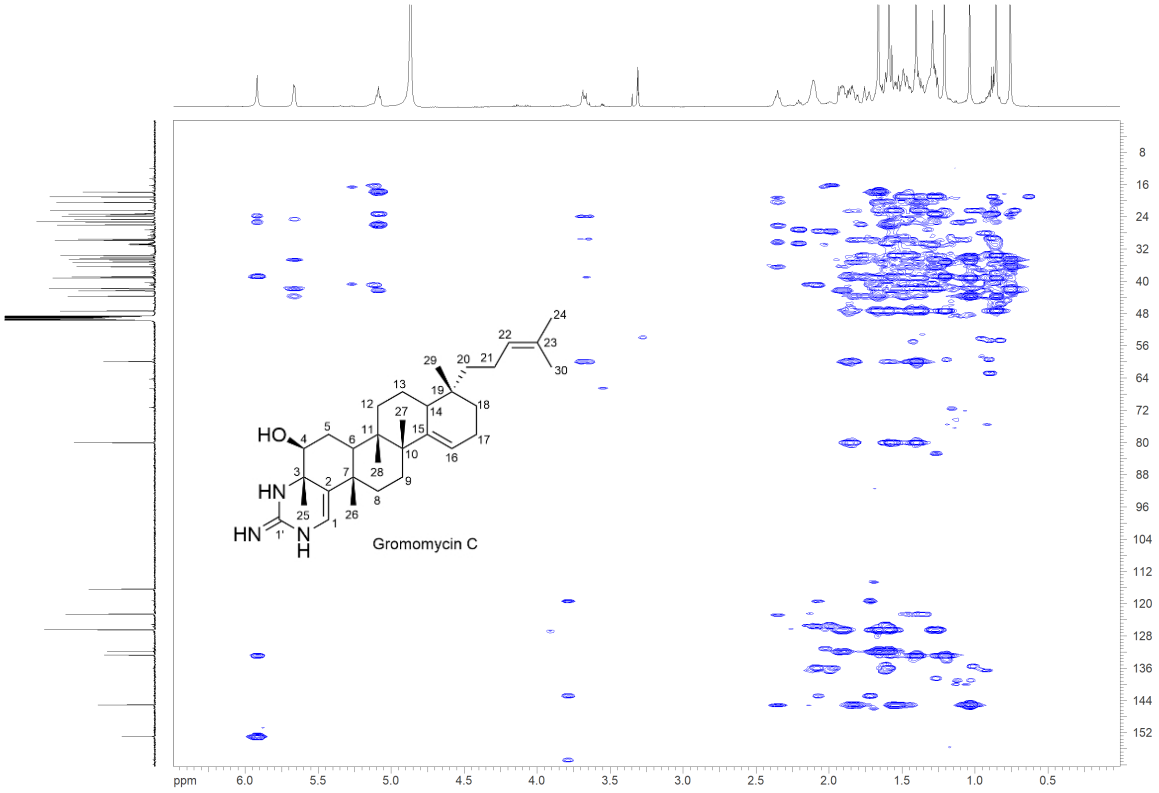

Figure S6. HMBC spectrum ($MeOD_4$) of gromomycin C (480A2).

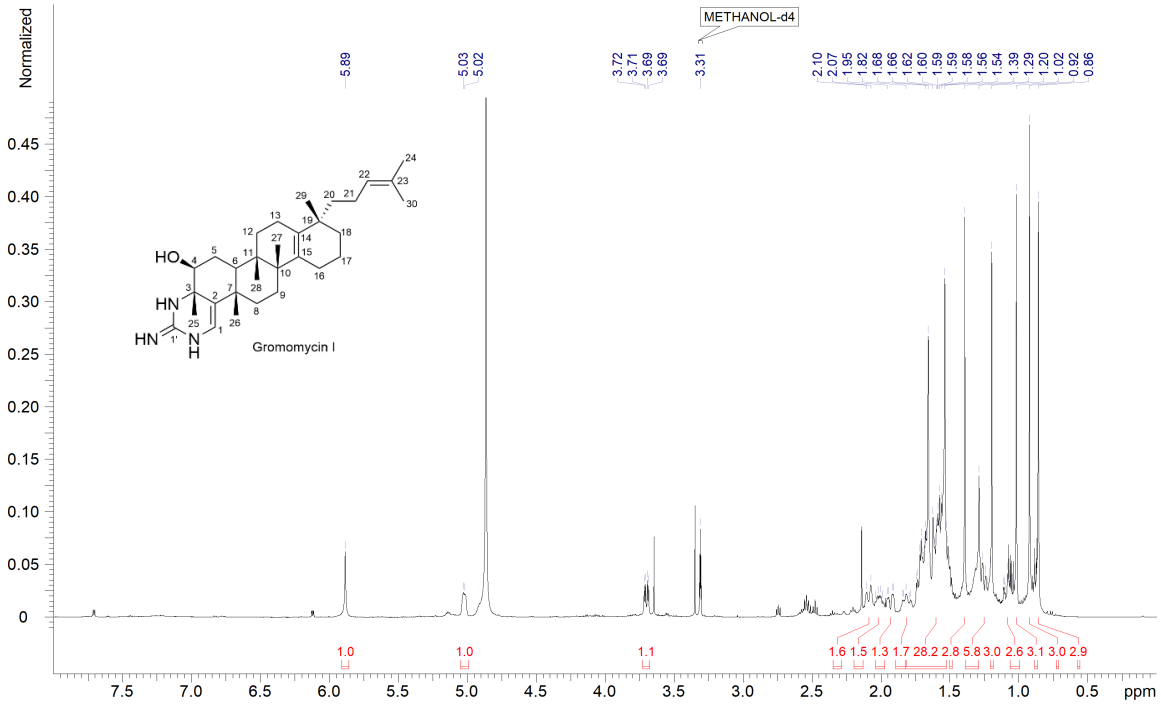

Figure S7. ^{1}H-NMR spectrum (500 MHz, $MeOD_4$) of gromomycin I (480A1).

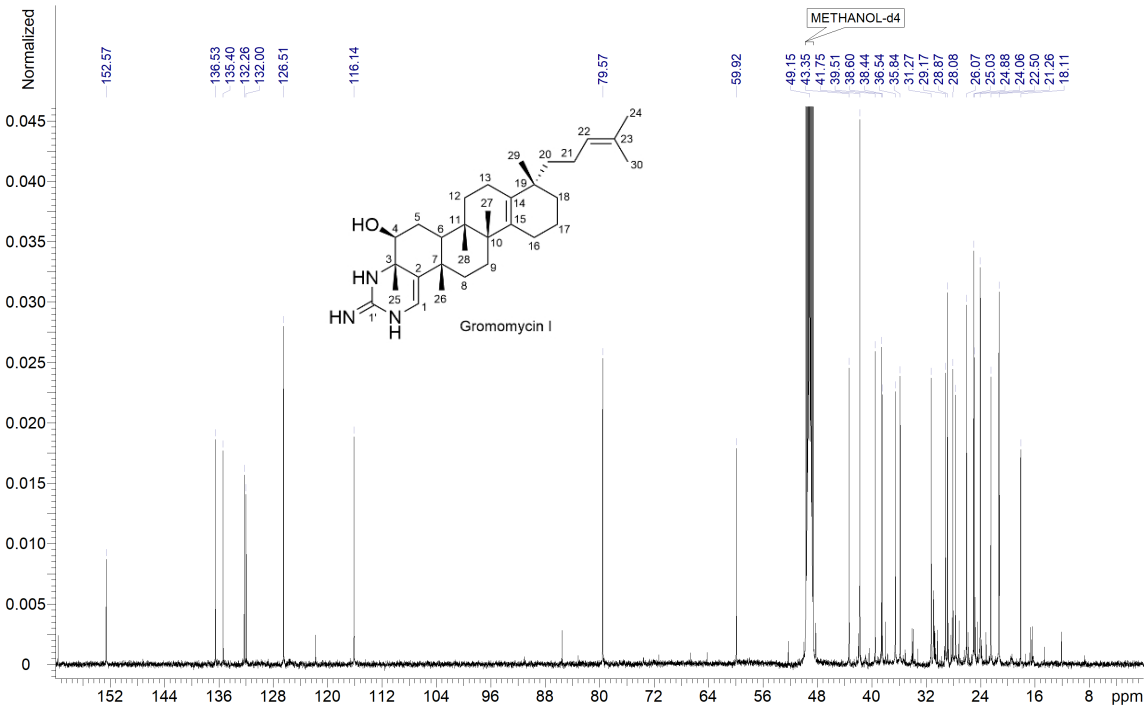

Figure S8. ^{13}C-NMR spectrum (125 MHz, $MeOD_4$) of gromomycin I (480A1).

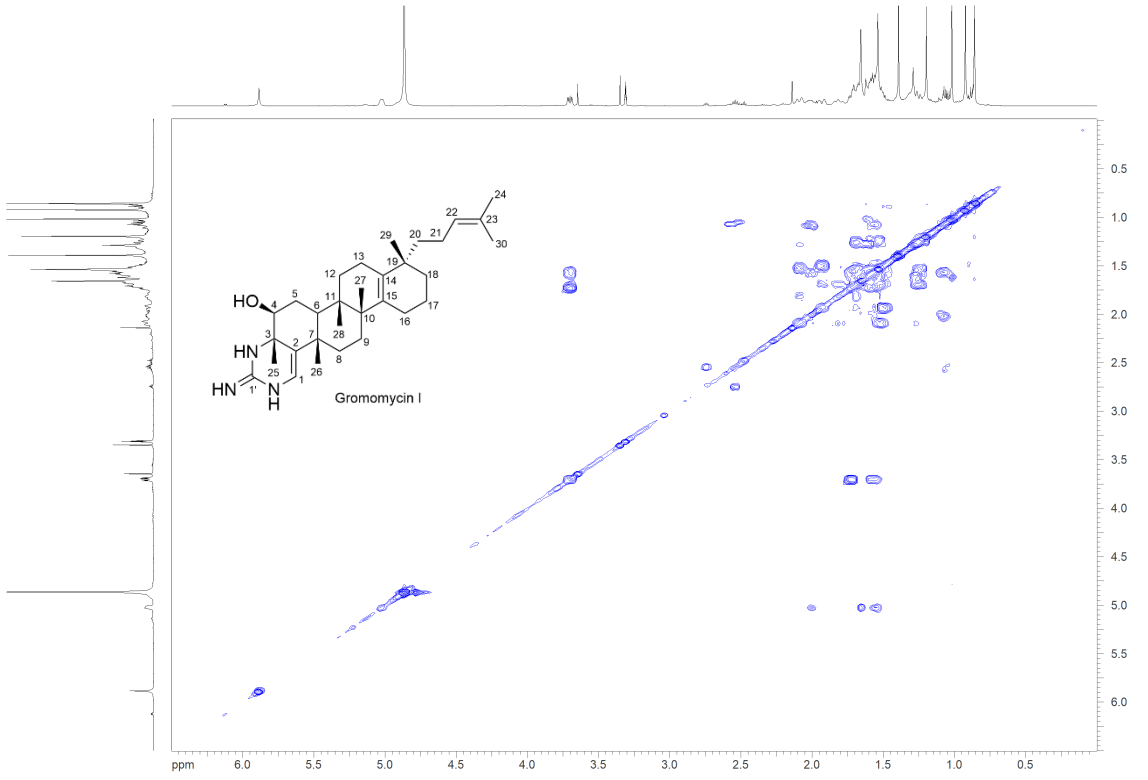

Figure S9. COSY spectrum (500 MHz, $MeOD_4$) of gromomycin I (480A1).

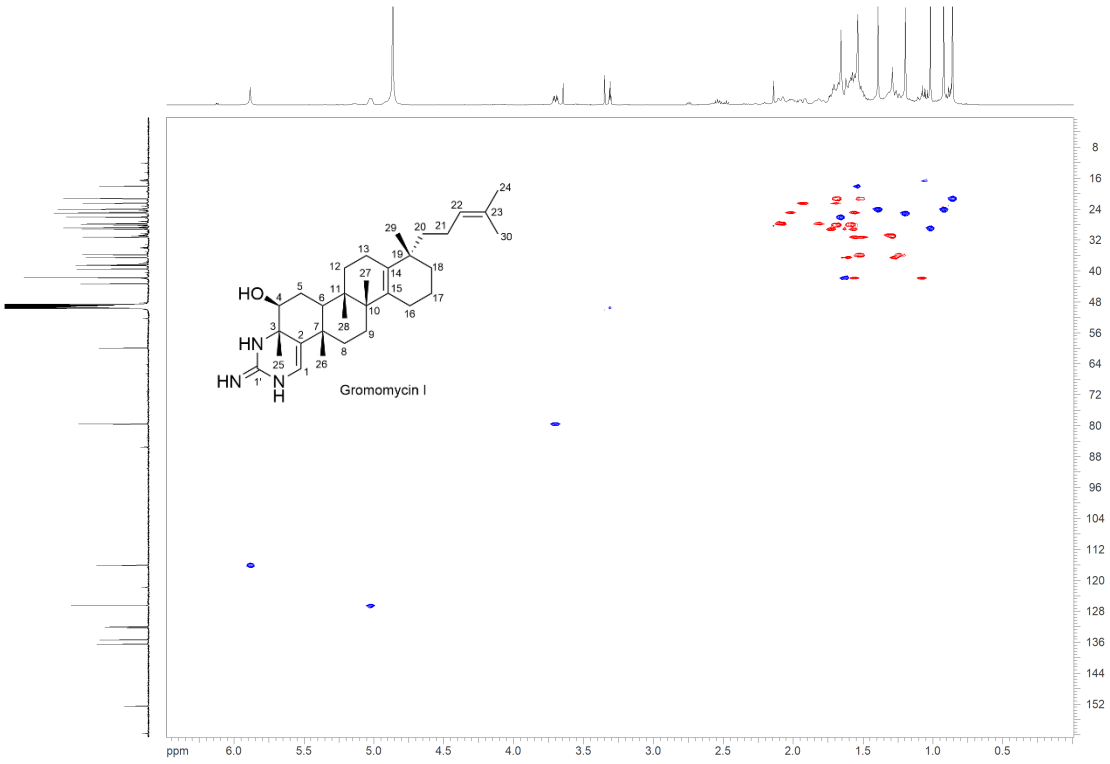

Figure S10. HSQC spectrum ($MeOD_4$) of gromomycin I (480A1).

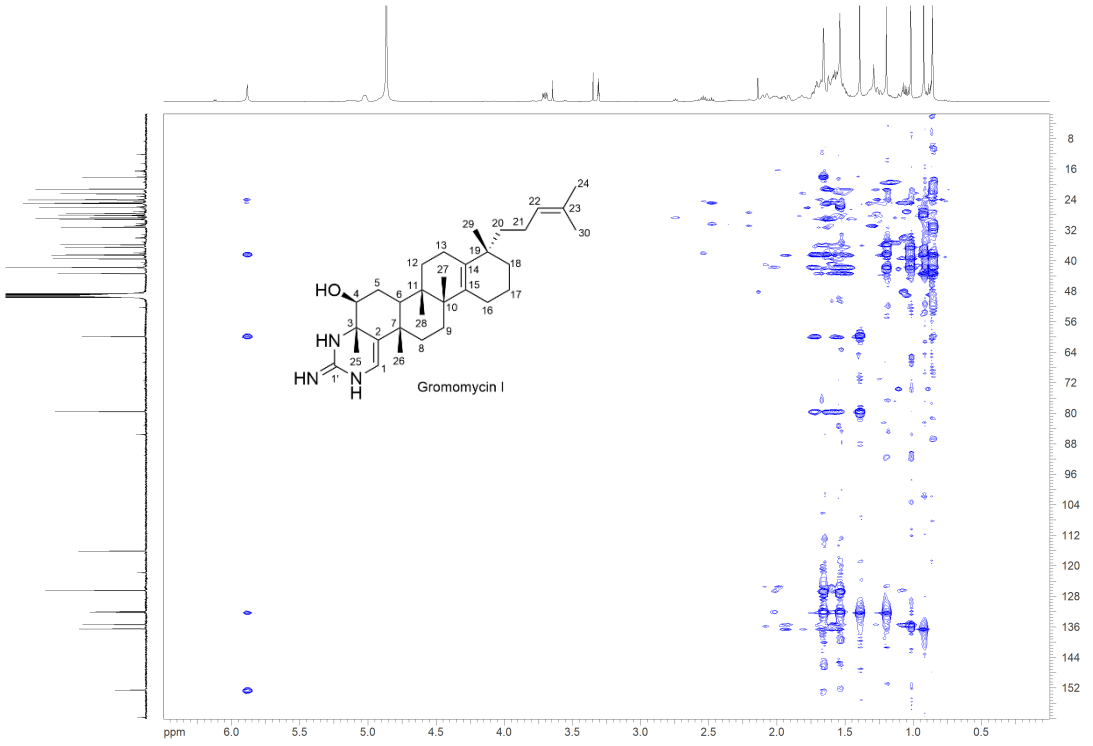

Figure S11. HMBC spectrum ($MeOD_4$) of gromomycin I (480A1).

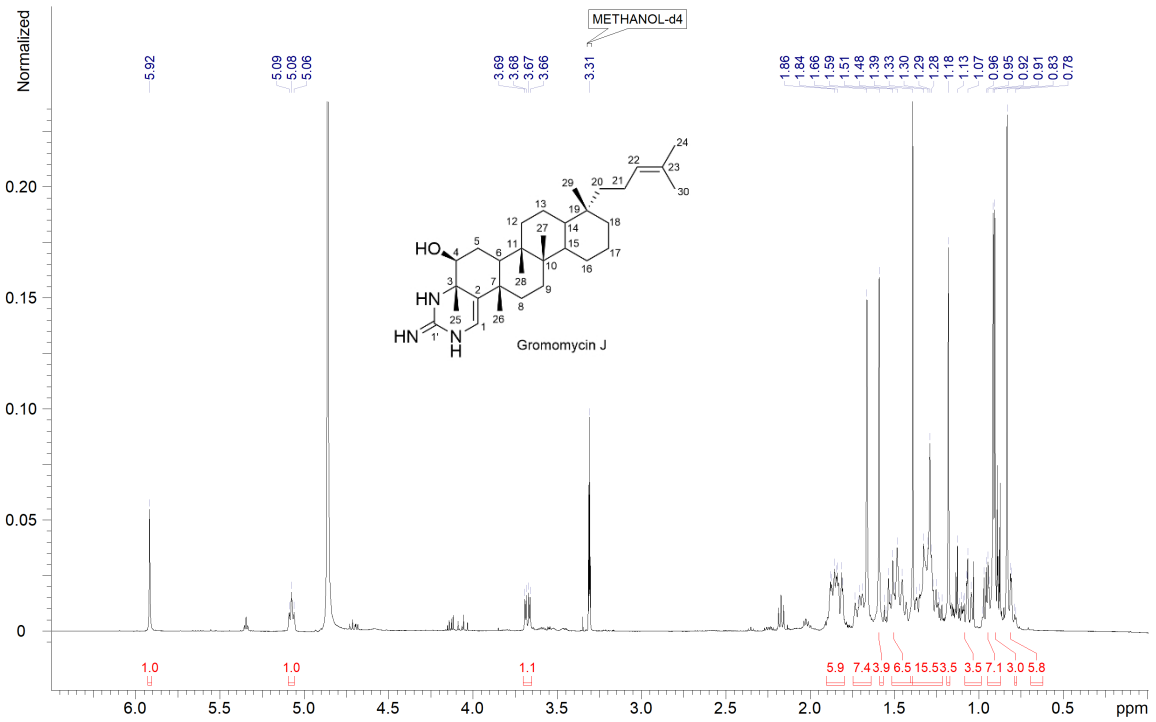

Figure S12. ^{1}H-NMR spectrum (500 MHz, $MeOD_4$) of gromomycin J (482A).

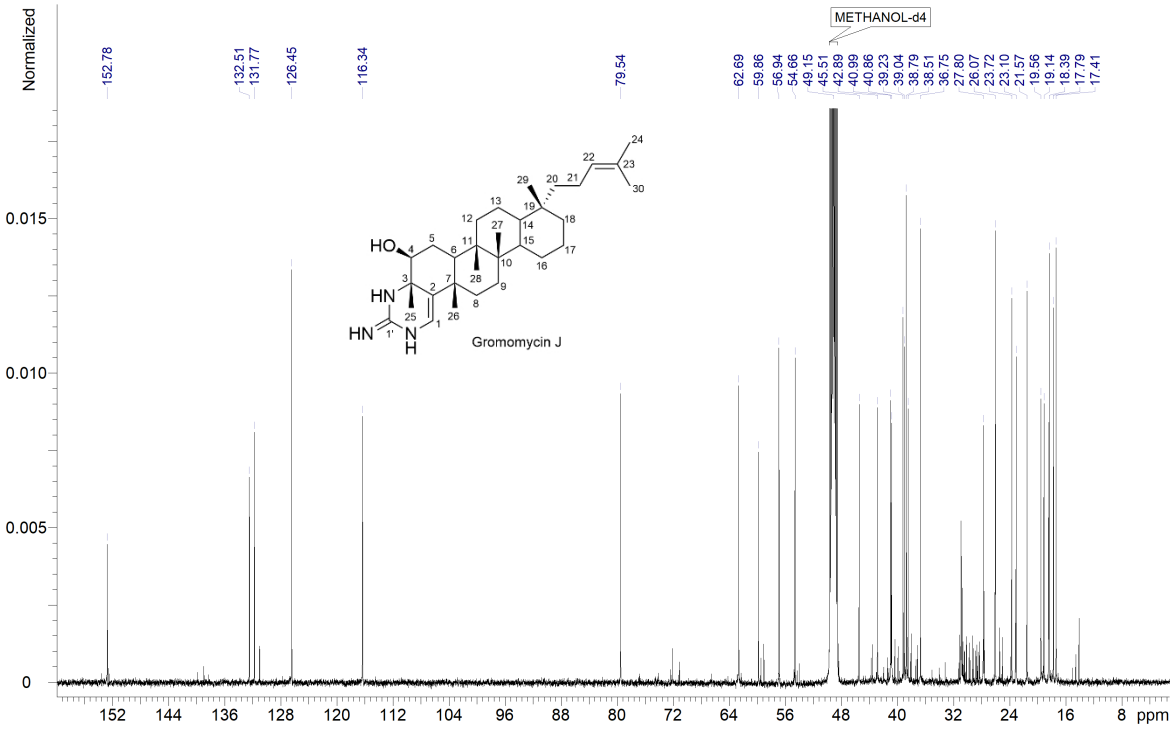

Figure S13. ^{13}C-NMR spectrum (125 MHz, $MeOD_4$) of gromomycin J (482A).

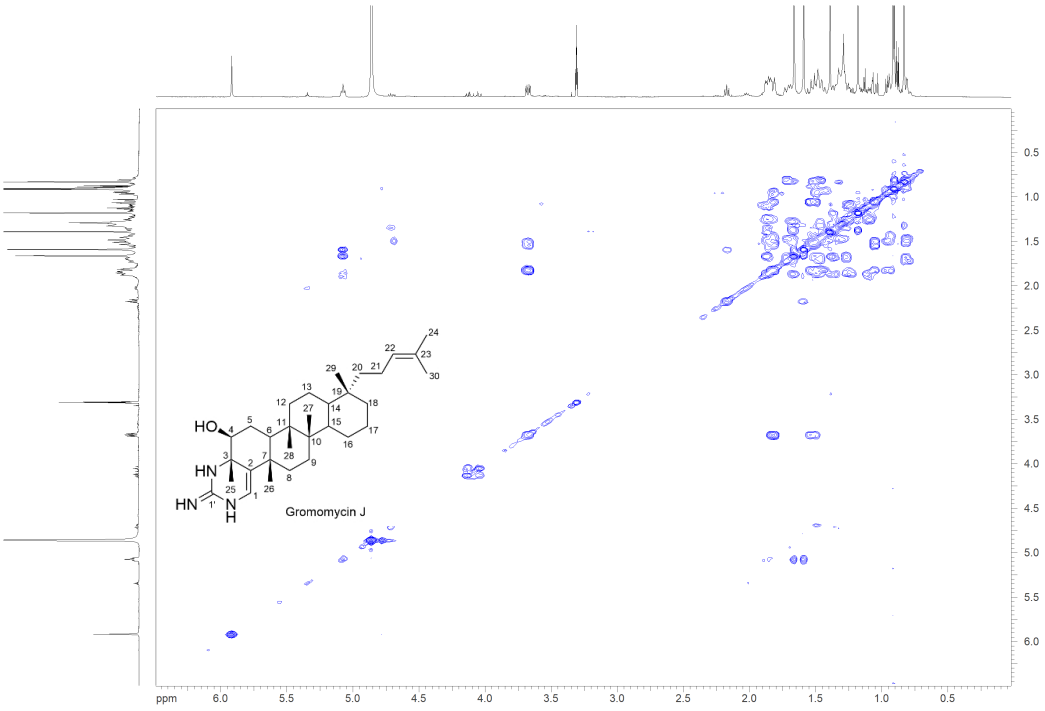

Figure S14. COSY spectrum ($MeOD_4$) of gromomycin J (482A).

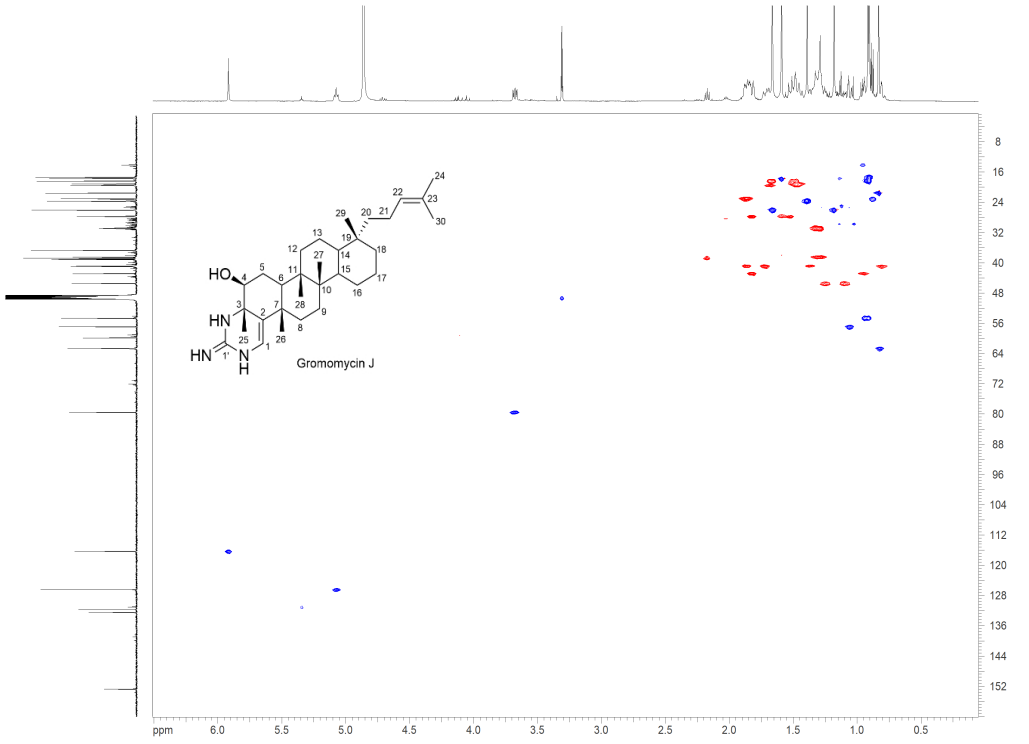

Figure S15. HSQC spectrum ($MeOD_4$) of gromomycin J (482A).

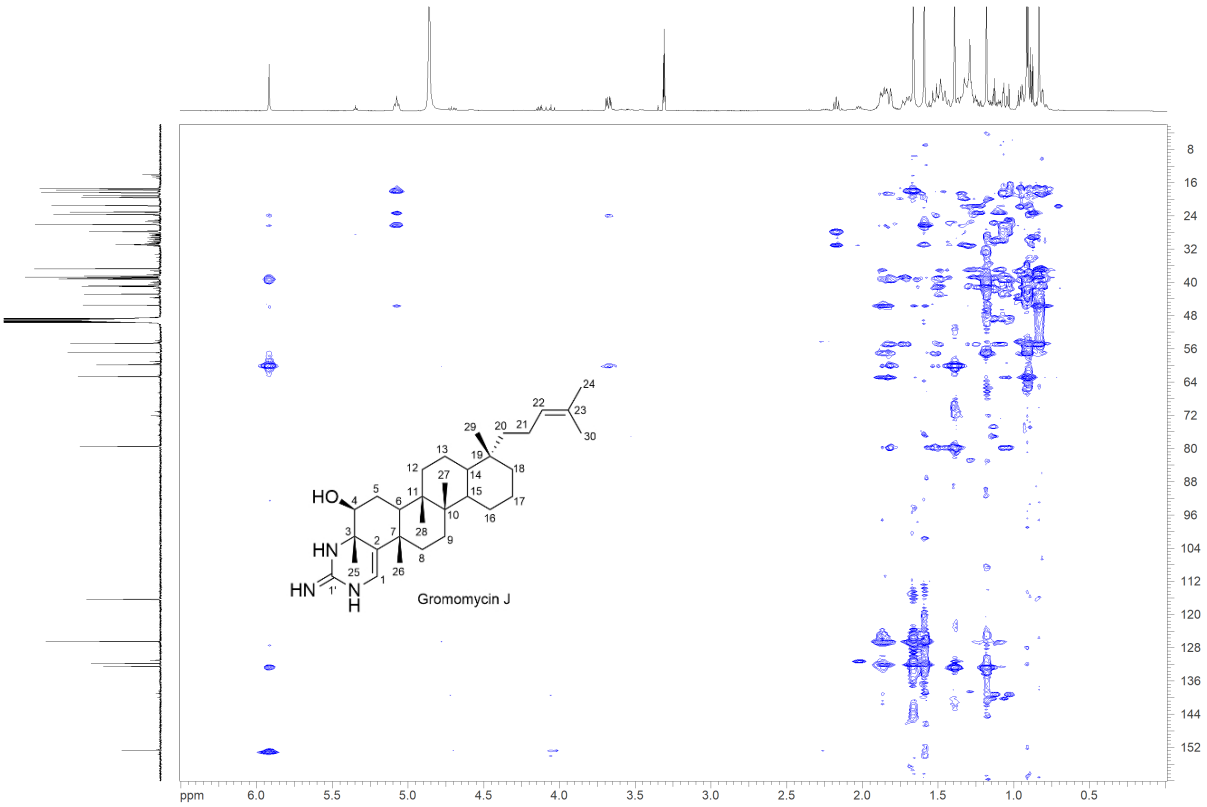

Figure S16. HMBC spectrum ($MeOD_4$) of gromomycin J (482A).

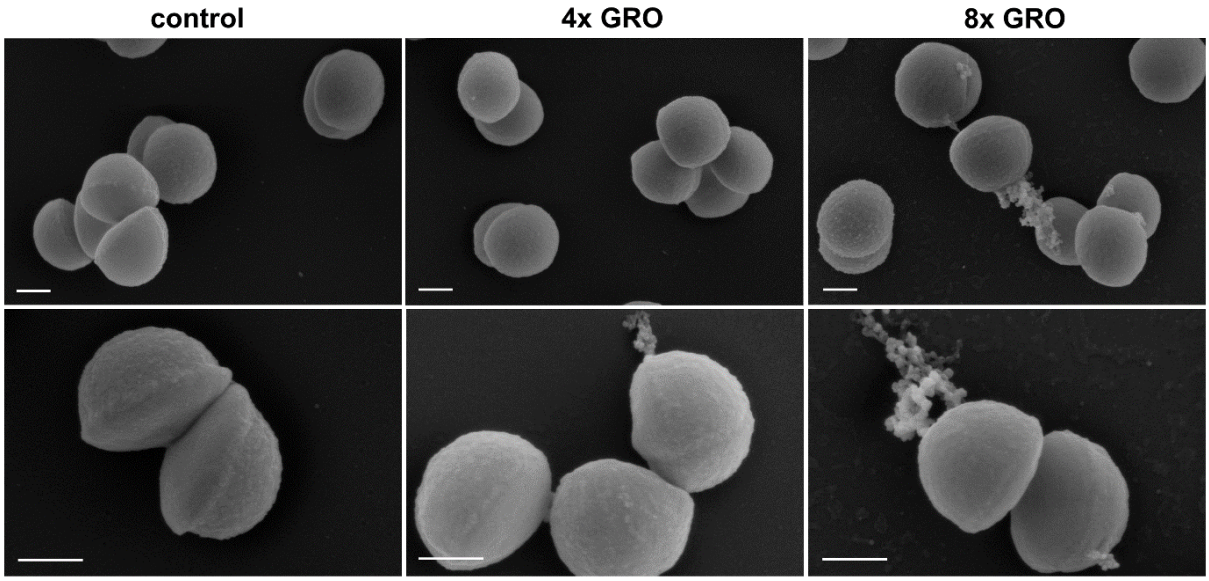

Figure S17. Bacterial phenotyping by scanning electron microscopy (SEM) imaging. SEM micrographs of *S. aureus* treated with 4- and 8-fold MIC of gromomycin I (T = 15 min). The control represents *S. aureus* cells exposed to DMSO. Scale bars are 300 nm. GRO, gromomycin I.

A

Condition	MIC [µg/mL] GRO	MIC fold change
MHB2	2	-
+ DOPG (negative)	64	32
+ POPG (negative)	64	32
+ POPS (negative)	32	16
+ POPC (neutral)	16	8
+ POPE (neutral)	8	4
+ DOTAP (positive)	2	-
+ lauric acid (C12:0)	16	8
+ myristic acid (C14:0)	32	16
+ pentadecanoic acid (C15:0)	16	8
+ palmitic acid (C16:0)	8	4
+ palmitoleic acid (C16:1)	64	32
+ stearic acid (C18:0)	8	4
+ linoleic acid (C18:2)	64	32

B

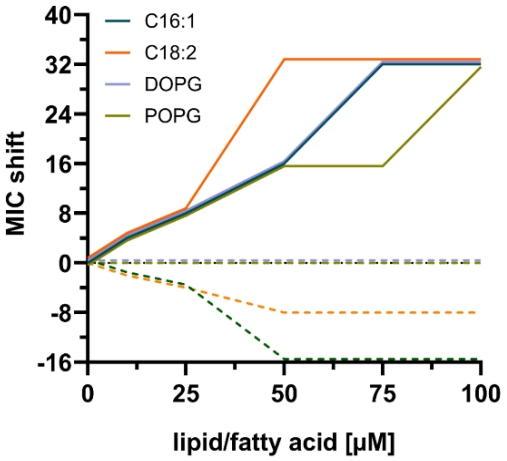

Figure S18. Gromomycin activity is impaired in the presence of fatty acids and phospholipids. A MIC values of gromomycin I against *S. aureus* ATCC29213 in the presence of different fatty acids and (phospho-) lipids. Lipids and fatty acids were used at 100 µM concentration. **B** Concentration dependency of activity neutralization (gromomycin: solid line, gentamicin: dashed line). GRO, gromomycin I.

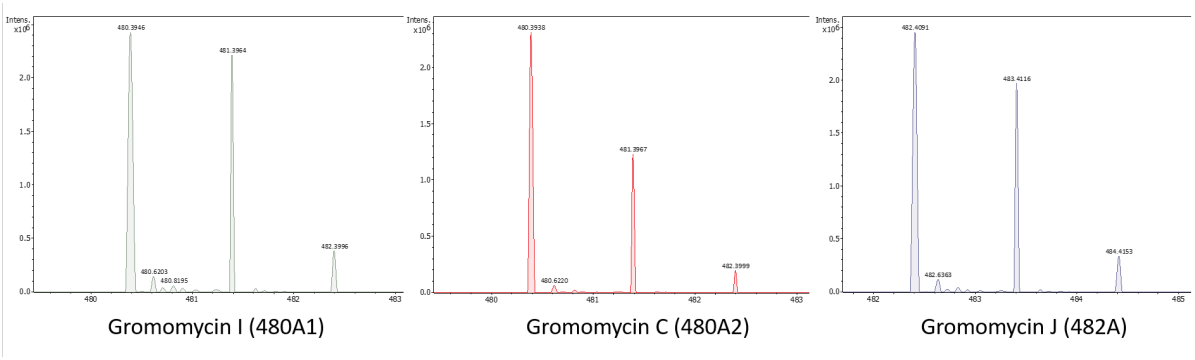

Figure S19. Mass spectra analysis (*m/z*) of Gromomycins I, C, J.

2.3. Expanding the Chemical Space of Sesterterpene Antibiotics: Discovery and Characterization of Darumycins

This chapter reproduces, with minor formatting adjustments, the text of the manuscript to be submitted:

Dmytro Bratiichuk, Irma Redzic, Dominik Kolling, Marc Stierhof, Franziska Fries, Josef Zapp, Rolf Müller, Jesko Köhnke, Maksym Myronovskyi and Andriy Luzhetskyy*. Expanding the Chemical Space of Sesterterpene Antibiotics: Discovery and Characterization of Darumycins. *To be submitted*.

Contributions and Acknowledgements

Author's Contribution

The author made substantial contributions to the methodology and experimental design of the study, performed the biological experiments, and carried out data analysis and visualization. The experimental work combined bioinformatic and biotechnological methods, including genome mining, cluster cloning, gene knockouts, heterologous expression, compound dereplication, and isolation. The author conceived and wrote the corresponding sections in the original draft of the manuscript.

Contributions by Others

I. Redzic performed gene knockouts, heterologous expression, and compound isolation. M. Stierhof and J. Zapp aided analytics and carried out structure elucidation. D. Kolling and J. Köhnke designed and performed in vitro studies and protein characterization. F. Fries and R. Müller designed and performed bioactivity and toxicity assay. M. Myronovskyi and A. Luzhetskyy provided supervision and designed the research. D. Bratiichuk, I. Redzic, M. Stierhof, J. Zapp, D. Kolling, and F. Fries conceived and wrote the respective parts in the manuscript. All authors contributed to proofreading of the manuscript.

2.3.1. Abstract

The global rise of antibiotic resistance presents a critical health challenge, emphasizing the urgent need for antibiotics with new chemical scaffolds and mechanisms of action. Herein, we report the discovery and characterization of new sesterterpene antibiotics, named darumycins, with potent activity against high-priority gram-positive pathogens and mycobacteria. Darumycins are pentacyclic sesterterpenoids containing a guanidine group. The darumycin biosynthetic gene cluster was identified through genome mining in *Micromonospora rubida*, followed by heterologous expression in *Streptomyces* chassis strains. Utilizing gene cluster engineering, we have generated new structural analogues, expanding the chemical diversity of actinobacterial natural products by introducing new members to the rare sesterterpene class. Targeted gene deletions, combined with LC-MS, NMR analyses, and in vitro enzymatic studies, allowed us to propose the biosynthetic pathway for darumycin. Furthermore, in vitro characterization of darumycin methyltransferases demonstrated their site-specific catalytic function. Additionally, the crystal structure of DarM methyltransferase revealed distinct architecture compared to canonical classes of known *O*- or *C*- metyltransferases.

2.3.2. Introduction

Since the mid-20th-century golden age of antibiotics, natural products NPs have played a vital role in combating pathogenic bacteria and have formed the basis for numerous effective treatments.[316-318] Actinomycetes stand out as the most potent and fruitful organisms in the world of NPs, recognized for their unique biology, ecological significance, and production of secondary metabolites with high commercial and pharmaceutical potential.[319-321] Since the sequencing of the first genome of *Streptomyces* species[286], the field of NPs discovery has experienced a consequential transformation.[322-323] It was revealed, that there are far more biosynthetic gene clusters (BGCs) encoding secondary metabolites than the number of compounds previously isolated through traditional laboratory culture methods.[324] Genome mining has become a critical approach, facilitating the identification and prediction of BGCs responsible for producing novel compounds directly from genomic data.[325-326]

Despite a large number of known bioactive NPs, the emergence and rapid spread of antibiotic-resistant pathogens represent one of the most pressing challenges to global public health in the 21st century.[80, 261, 327] Compared to traditional antibiotics, compounds with novel chemical scaffolds are more likely to target distinct bacterial vulnerabilities, circumventing resistance processes and offering new treatment options for infections that were previously

challenging to control.[80] Our recent discovery of gromomycins,[300] guanidine-containing pentacyclic triterpenoids with an unprecedented non-squalene cyclization pathway and strong activity against drug-resistant pathogens, highlighted the potential of actinomycetes to generate structurally unusual and biologically active terpenes. These unique characteristics prompted us to investigate their distribution and search for new gromomycin analogues.

In this study, we describe the identification and characterization of new guanidine-containing sesterterpene antibiotics, darumycins. These pentacyclic sesterterpenoids exhibit potent antimicrobial activity against a broad spectrum of clinically relevant pathogens, including drug-resistant Gram-positive and mycobacterial species. Darumycins were identified through genome mining in the *Micromonospora rubida* strain, and heterologously produced in *Streptomyces* chassis strains. Darumycins Performing targeted gene deletions within the darumycin BGC enabled the generation of several new derivatives, which, combined with in vitro biosynthetic studies and protein characterization, provided key insights into darumycin biosynthesis. Biochemical characterization of darumycin methyltransferases demonstrated their site-specific catalytic function. Furthermore, the crystal structure of DarM methyltransferase has revealed its distinct architecture compared to canonical classes of known *O*- or *C*-metyltransferases, consistent with its low sequence homology to previously characterized enzymes.

2.3.3. Results and Discussion

2.3.3.1. Identification of Darumycin BGC in *Micromonospora rubida*

Gromomycins represent a new class of bacterial triterpene antibiotics, with guanidine-containing pentacyclic scaffold.[300] These compounds are synthesized independently of the canonical squalene pathway and assembled through an unprecedented cyclization route, involving a hexaprenylguanidine precursor. Notably, the gromomycins biosynthetic pathway could not be identified by any pattern-based BGC prediction tools. Together, these distinctive structural and biosynthetic features, together with their activity against drug-resistant pathogens, motivated further investigation of gromomycins and search for new analogues. The core part of the gromomycin BGC comprises three genes: *groD* (encoding a farnesyl diphosphate synthase), *groH* (a prenyltransferase), and *groF* (a cyclase). To uncover microbial producers harboring BGCs homologous to the gromomycin BGC,[300] we employed a genome mining approach. Utilizing the nucleotide sequences of these three genes as probes, we conducted homology search using NCBI protein BLAST to identify new gromomycin-like BGCs (*gro*BGCs) in which the three genes are clustered.

The search yielded a substantial number of actinobacterial strains, most of which were classified within the genus *Streptomyces*, along with a selected number of non-*Streptomycetes* bacteria from *Kitasatospora*, *Lentzea*, *Dactylosporangium*, and *Micromonospora* genera. As the majority of *Streptomyces*-derived clusters appeared to be identical to already known *gro*BGCs, the other bacteria, especially those from the *Lentzea* and *Micromonospora* genera, were of particular interest due to the presence of *gro*BGCs harboring additional genes. For instance, the clusters from strains *Lentzea rhizosphaerae*, *Micromonospora sp.* CA-111912, *Micromonospora sp.* NPDC002296 and *Micromonospora sp.* NPDC001898, *Micromonospora sp.* NBC_01405 and *Micromonospora rubida* JCM 32386 all contain *gro*BGCs with two genes encoding methyltransferase domain-containing protein. Subsequently, the *M. rubida* strain[328] (Japan Collection of Microorganisms, RIKEN BRC) was selected as a source to isolate the new *gro*BGC.

2.3.3.2. Heterologous Expression and Identification of Darumycins

Using the φC31-based integrative cosmid vector cos15AAmInt, a cosmid library of the *M. rubida* strain was constructed. Following, via PCR we identified the cosmid P05-E12, which harbors a 39.2kb chromosomal fragment from *M. rubida* genome (RefSeq GCF_009908295.1) containing the novel *gro*BGC.

Noteworthy, the previously described gromomycins, such as gromomycins A and E, possess molecular formulae of $C_{31}H_{47}N_3O$ and *m/z* 478.38 $[M + H]^+$ (gromomycin A), or $C_{32}H_{49}N_3O$ and *m/z* 492.39 $[M + H]^+$ (methylated gromomycin E).[300] Given the presence of two methyltransferases in the *M. rubida gro*BGC, it was expected that the potential new derivative would have a molecular formula proposed as $C_{33}H_{51}N_3O$, and *m/z* 506.40 $[M + H]^+$. This cluster was subsequently introduced into *S. albus* Del14[254] and *S. lividans* DelYA9[255] heterologous host strains.

HPLC-MS dereplication analysis revealed two new peaks with molecular ions of *m/z* 470.34 and 486.33 $[M+H]^+$ in both heterologous host strains containing the P05-E12 cosmid (**Figures S57**, **S65)**. Surprisingly, the obtained masses deviated from our predictions, suggesting that the new compounds do not belong to the triterpene class, like gromomycins, but are sesterterpenes. For structure elucidation, the strain *S. albus* Del14 with *M. rubida gro*BGC was cultivated in 10 liters of DNPM medium, followed by ethyl acetate extraction and a three-step purification process, resulting in the isolation of two new compounds.

The first compound with *m/z* 470.34 $[M+H]^+$ has a calculated molecular formula of $C_{28}H_{44}N_3O_3$ with 9 levels of unsaturation. Analysis of 1D and 2D NMR spectra (**Table S1, Figures S3-S9**) revealed a similar peak profile in the ^{1}H proton NMR as previously reported for gromomycins. ^{1}H proton and HSQC spectra revealed a CH group at δ_{CH} 117.4, 5.97 ppm with ^{13}C-HMBC correlations to four quaternary carbons C-1' (δ_C 153.0), C-2 (δ_C 131.9), C-3 (δ_C 59.0) and C-7 (δ_C 38.3), which is highly similar to gromomycins, indicating a similar ring structure containing a guanidine group. This was further confirmed by ^{15}N-HMBC data showing a correlation from H-1 to N1 (δ_{N1} 94.7). Interpretation of COSY, and ^{13}C-HMBC

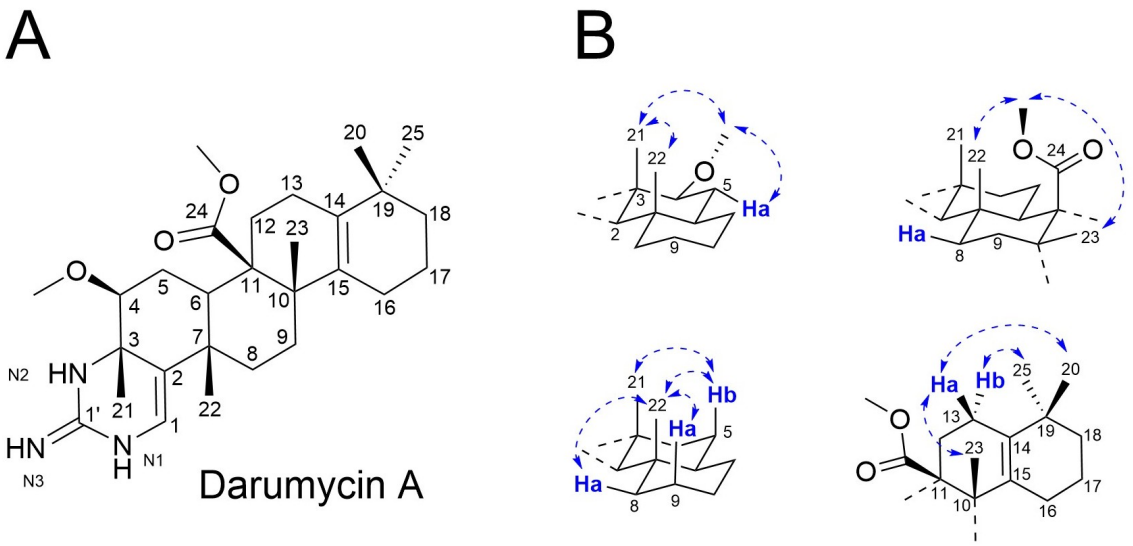

Figure 1. A) Structure of darumycin A. **B**) NOESY correlations for assignment of the relative stereochemistry.

correlations revealed the same carbon scaffold consisting of 5 annealed rings with identical methylation pattern but lacking the prenyl moiety on ring D, confirming that the compound is not a triterpene but belongs to the class of sesterterpenes **(Figure 1A**). Unlike gromomycins, the carbon scaffold of the new compound is showing several modifications. Methyl group at C-24 was fully oxidized to a carboxyl group and decorated with an *O*-methyl group, resulting in a methyl ester. Further modifications include an *O*-methylation at C-4 resulting in a methoxy group and a double bond in ring D between C14 and C-15. Stereochemical assignment was established by interpretation of NOESY correlation (**Figure 1B**) and revealed the same relative configuration as gromomycins. Given the structural novelty, the new compound was named darumycin A (**1**), and the *M. rubida gro*BGC was renamed to darumycin BGC.

Compound with *m/z* 468.32 $[M+H]^+$ showed a molecular formula of $C_{28}H_{42}N_3O_3$ with 10 levels of unsaturation. 1D and 2D NMR data evaluation (**Table S7**, **Figures S41-46**) revealed the same molecular scaffold as darumycin A but containing a different double bond configuration in ring C/D at position C-13/C-14 and C-15/C-16 as indicated by the levels of unsaturation and assigned be COSY and ^{13}C-HMBC correlations. The compound was later named darumycin G (**7, Figure 3**).

2.3.3.3. Functional Characterization of the Darumycin BGC

The general organization of the genes of darumycin BGC shows high similarity to the gromomycin BGC, suggesting that both share common biosynthetic logic, but differ in the number of isoprene polymerization steps and tailoring modifications. Guided by this structural similarity, we have bioinformatically identified the borders of the darumycin BGC on cosmid P05-E12. The proposed minimal gene cluster for darumycin biosynthesis consists of 13 genes, spanning from *darA* to *darM* (**Figure 2, Table 1)**, most of which show clear homology to their gromomycin counterparts (**Table 2**). For instance, genes darD, darB and darA are homologous to groD, groH and groF, respectively. This suggests their roles as a darumycin polyprenyl (C_{25}) synthetase (DarD), prenyltransferase (DarB) and cyclase (DarA). In addition, genes *darE*, *darF*, and *darI* are annotated as putative Rieske 2Fe-2S oxygenases, alligning with their gromomycin homologs (*groA*, *groB*, and *groC*).

However, a distinct feature of the darumycin BGC is the presence of several other genes, absent in the gromomycin BGC. These include *darG* and *darM*, both encoding proteins with methyltransferase domains, suggesting their roles as darumycin methyltransferases at hydroxy

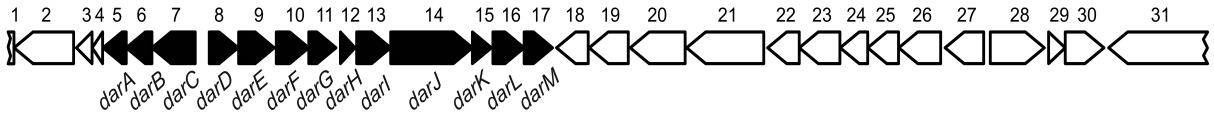

Figure 2. Diagram of the DNA segment containing the darumycin biosynthetic gene cluster, depicted in black.

Table 1. The proposed function of genes in darumycin cluster.

Gene	Proposed function
darA	Hypothetical protein (cyclase)
darB	Hypothetical protein (prenyl transferase)
darC	Cytochrome P450 oxygenase
darD	Polyprenyl synthetase family protein
darE	Rieske 2Fe-2S domain-containing protein
darF	Rieske 2Fe-2S domain-containing protein
darG	Methyltransferase domain-containing protein
darH	Protein phosphatase
darI	Rieske 2Fe-2S domain-containing protein
darJ	Phosphoenolpyruvate synthase
darK	Hypothetical protein
darL	UPF0104 family protein
darM	Methyltransferase domain-containing protein

Table 2. The proposed function of genes in gromomycin cluster.[300]

Gene	Proposed function
groA	Rieske 2Fe-2S domain-containing protein
groB	Rieske 2Fe-2S domain-containing protein
groC	Rieske 2Fe-2S domain-containing protein
groD	Polyprenyl synthetase (farnesyl diphosphate synthase)
groE	Reductase
groF	Hypothetical protein (cyclase)
groG	Phosphatase PAP2
groH	Hypothetical protein (prenyl transferase)
groI	Cytochrome P450 107B1 (Monooxygenase/Oxidoreductase)

C-4 and carboxy group C-24 of darumycin. (**Figure 1**). In addition, a cytochrome P450 oxygenase encoded by *darC*, likely catalyses the oxidation of the C-24 methyl group, generating a carboxyl group. To invertigate the roles of these, and several other genes from the cluster, we performed respective targeted gene deletions on the P05-12 cosmid, using the *bla* marker to replace the desired gene via Red/ET recombination. Subsequently, the *bla* marker was excised using the PmeI restriction enzyme to avoid a possible polar effect. This resulted in 8 new cosmids each containing single or double gene knockouts (**Table S11**). The cosmids were then introduced into *S. albus* Del14 and *S. lividans* DelYA9 heterologous host strains (**Table S10**), followed by strains cultivation, solvent extraction and analysis.

Single and double knockouts of both *darG* and *darM* genes led to new derivatives with *m/z* 456.32, 456.32 and 442.31 $[M+H]^+$, indicating the absence of one or both methyl groups (**Figures S58-S60**). Analysis of 1D and 2D NMR data (**Tables S2**, **S5 and S6**, **Figure S10-15**, **S28-33**, **S 34-39**) revealed darumycin derivatives lacking the methyl groups on the oxygen on C-4 and/or the carboxyl group C-24 (**Figure 3**). The exact location of the missing methyl groups was determined by analysing ^{13}C-HMBC correlations. The *darG* gene deletion led to the derivative lacking a mehthyl group on the hydroxy group at C-4, darumycin F (**6**). The deletion of the *darM* gene resulted in the formation of darumycin B (**2)**, with an unmethylated carboxyl group. Whereas the double knockout of *darG* and *darM* generated the darumycin E (**5**) derivative, in which both functional groups are free. Analysis of stereochemistry led to the same stereochemical assignments as described for the gromomycins. While the relative configuration could be determined by interpreting the NOESY correlations (**Figure 2B**), the absolute configuration was deduced from Mosher analysis of the darumycin F (**6**) (see SI, **Table S9**, **Figures S1-2** and **S53–S56**).

Next, *darC* gene deletion (**Figure S61**) led to a new derivative with *m/z* 426.35 $[M+H]^+$, and a calculated molecular formula of $C_{27}H_{44}N_3O$. Full assignment using 1D and 2D NMR data (**Table S3**, **Figure S16-21**) revealed a loss of the *O*-methylated carboxyl group, as indicated by

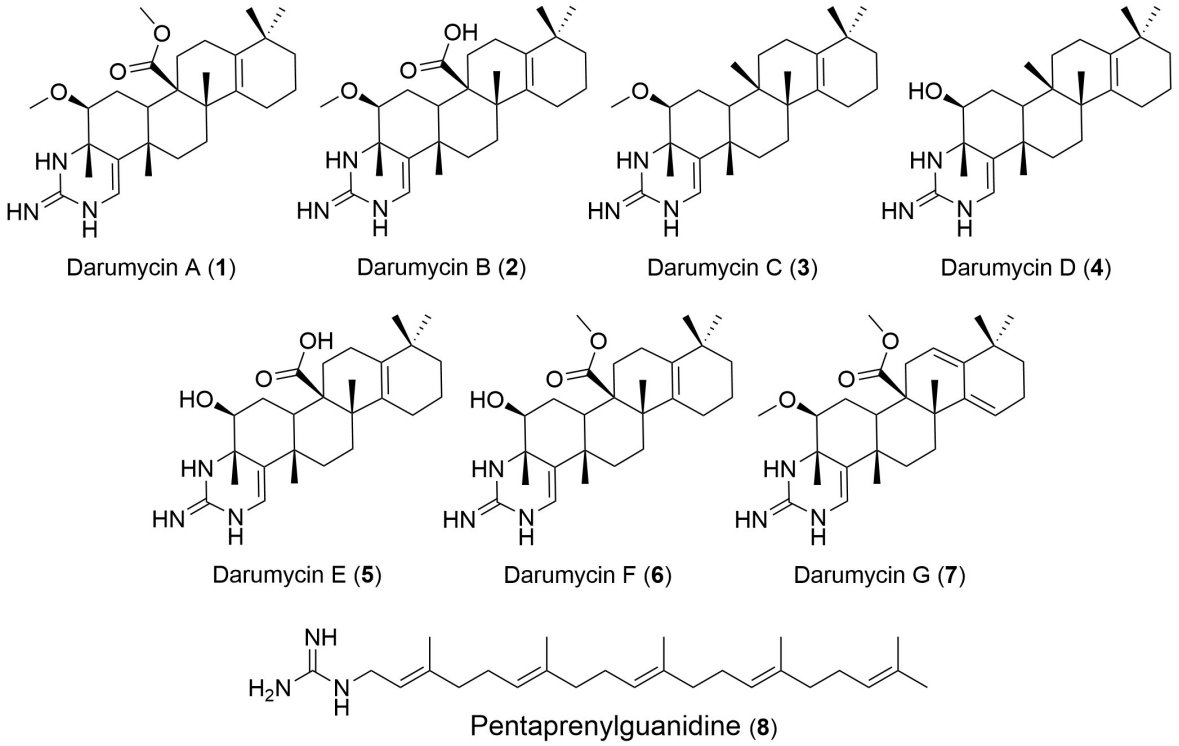

Figure 3. Structures of darumycins A-G and pentaprenylguanidine.

the molecular formula, resulting in darumycin C (**3, Figure 3**).

It is noteworthy that while the darumycin C (**3**) derivative is missing the carboxyl group, it still undergoes methylation at the C4-OH group. To obtain its unmethylated derivative, we have generated a double knockout of the *darC* and *darG* genes. This resulted in a new derivative with *m/z* 412.33 $[M+H]^+$ (**Figure S62)** and a calculated molecular formula of $C_{26}H_{42}N_3O$. Full assignment using 1D and 2D NMR data (**Table S4**, **Figure S13-27**) revealed darumycin D (**4, Figure 3**) which is lacking both the *O*-methylated carboxyl group and the methyl group on oxygen C-4, both confirmed by HMBC correlation experiments. These results also suggest that methylation of the hydroxyl group might occur prior to carboxylation by the DarC oxygenase.

In addition, we deleted the *darA* gene, to confirm its function as darumycin cyclase. This led to the accumulation of a compound with *m/z* 400.37 $[M+H]^+$ (**Figure S66**), following by its purification and structural elucidation. Analyses of ^{1}H-proton and HSQC (**Table S8**, **Figures S47-52**) revealed 5 olifinic methine and 6 methyl groups, indicating a scaffold with 5 isoprene units. Methine signal at δ_H 5.20, 119.2 showed ^{13}C HMBC correlation to δ_{CH} 158.7 indicating a guanidine group. Full assignment was achieved by MS, ACD labs shifts prediction, COSY and HMBC correlations revealing pentaprenylguanidine (**8**, **Figure 3**), the proposed darumycin linear precursor. Combined, these results suggest the role of DarA as darumycin cyclase, analogous to the GroF cyclase.

The darumycin cluster also contains several genes which do not seem to be involved directly in biosynthesis, but their functions are not fully understood. These include the *darK*, *darL*, and *darH*. While the deletion of the gene *darL* had no visible impact, the deletion of the *darK* resulted in a significant reduction in Darumycin production (**Figures S64** and **S63**, respectively). Conversely, BLAST analysis of DarK did not suggest a clear function for this gene, while its in-depth analysis, utilizing Swiss-Prot for structure homology modeling, revealed its resemblance to the RNA polymerase sigma factor RpoN.[329] We suggest that DarK is involved in the process of transcription regulation, thereby impacting darumycin production.

The next gene, *darH*, is annotated as protein–tyrosine phosphatase and shows high similarity to the *gro3* gene from the gromomycin cluster.[300] Protein-tyrosine phosphatases (PTPs) are generally known to be involved in the regulation of protein tyrosine phosphorylation, a key mechanism for controlling cellular functions in bacteria.[330] Moreover, these regulatory enzymes can modulate secondary biosynthesis indirectly through dephosphorylation of transcription factors or biosynthetic enzymes.[331] For example, in *Streptomyces coelicolor*, the protein phosphatase SppA dephosphorylates AfsK, which can lead to a decrease in the

phosphorylation of AfsR, a transcriptional regulator.[332] AfsR is involved in the production of some secondary metabolites (such as actinorhodin and undecylprodigiosin), and is also phosphorylated by AfsK in in vitro assays.[333-335] In addition, the deletion of its homologue from the gromomycin cluster, gene *gro3* (encoding protein-tyrosine phosphatase), was associated with a substantial decrease in gromomycin levels.[300] Thus, we suggest that DarH might be involved in darumycin biosynthesis regulation.

2.3.3.4. In vitro Characterization of Darumycin Methyltransferases

To elucidate the substrate specificity and the catalytic function of the two methyltransferases encoded in the darumycin biosynthetic gene cluster, DarM and DarG were heterologously expressed in *E. coli* and purified to homogeneity. The activity of each enzyme was assayed in vitro using S-adenosyl-L-methionine (SAM) as methyl donor and a set of biosynthetic intermediates obtained from dene deletion experiments were used as substrates (**Figure 4**). Intermediates included compounds darumycin B (**2**), darumycin F (**6**) each lacking a single methyl group; darumycin E (**5**), a double demethylated derivative; and darumycin D (**4**), a demethylated precursor lacking the carboxyl group.

Both DarM and DarG exhibited SAM-dependent methyltransferase activity, as product formation was observed only in presence of both enzymes and SAM, while no turnover occurred in control reactions lacking enzyme or cofactor. The distinct substrate preferences were revealed for each enzyme. DarG catalyzed the methylation of darumycin F (**6**) to yield the fully methylated natural product darumycin A (**1**) (**Figure 4, B1**), whereas DarM did not

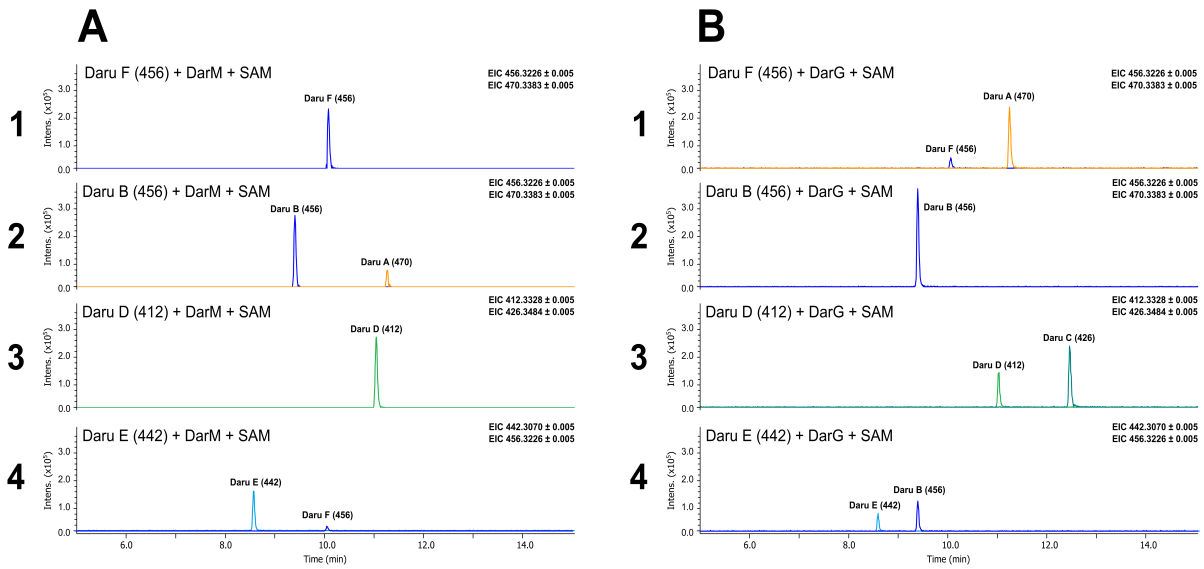

Figure 4. Biochemical characterization of DarM and DarG.

accept darumycin F (**6)** as substrate (**Figure 4, A1)**. Conversely, DarM efficiently converted darumycin B (**2**) to darumycin A (**1**) (**Figure 4, A2**), while DarG showed no detectable activity toward this intermediate (**Figure 4, B2**). These results indicate that DarM and DarG each target a specific methylation site on the darumycin scaffold. The double unmethylated intermediate darumycin E (**5)** was accepted by both enzymes, leading to the formation of the respective singly methylated products (**Figure 4, A4** and **B4**). In contrast, darumycin D (**4**) was converted only by DarG (**Figure 4, B3**) but not by DarM (**Figure 4, A3)**, suggesting that the presence of the terminal carboxyl group is required for substrate recognition by DarM.

Collectively, these data demonstrate that DarM and DarG act in a site-specific but not obligatorily sequential manner in darumycin biosynthesis. Despite their complementary activities, the available biochemical data do not allow an unambiguous determination of the chronological order of the methylation events in vivo.

2.3.3.5. Crystal Structure of DarM Methyltransferase in Complex with SAH

To gain further insight into the molecular basis of substrate recognition, structural studies were performed for both methyltransferases. Crystals suitable for X-ray diffraction could be obtained only for DarM, whose structure in complex with S-adenosyl-L-homocysteine (SAH) was determined at 1.5 A resolution (**Figure 5**). The overall architecture of DarM deviates from the

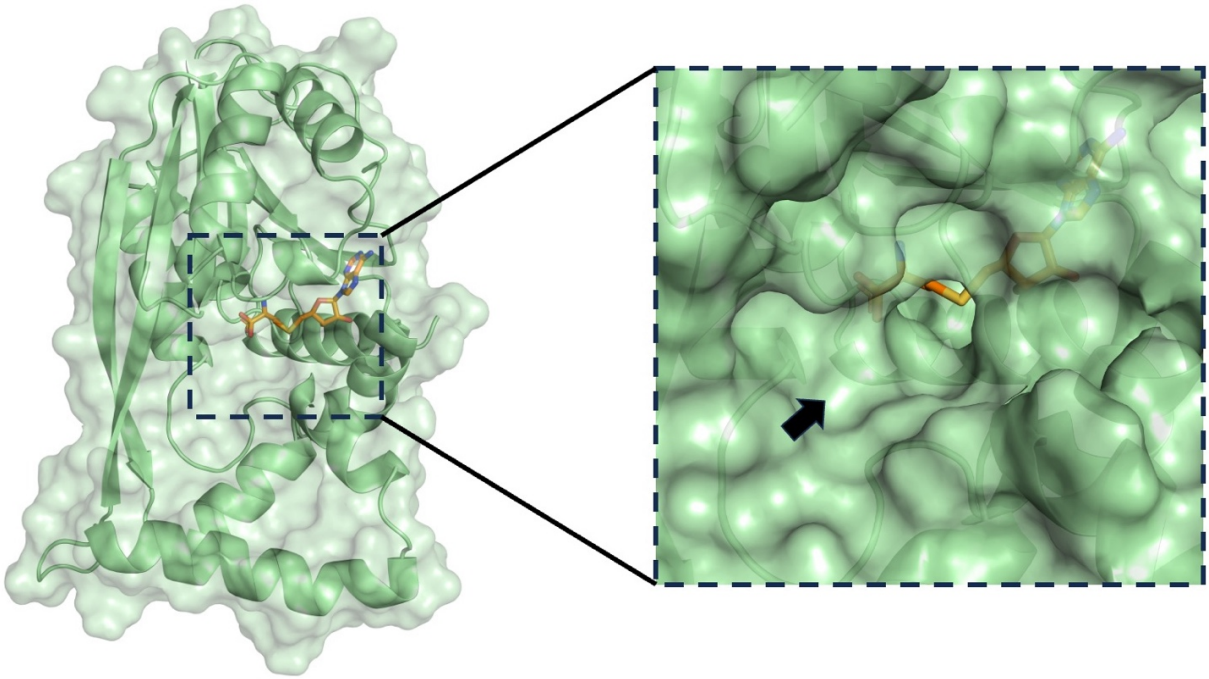

Figure 5. Crystal structure of the methyltransferase DarM in complex (**green**) with SAH (**orange**). The potential substrate binding site is indicated by an arrow.

canonical classes of known *O*- or *C*-methyltransferases, consistent with its low sequence homology to previously characterized enzymes.

The bound SAH defines the active site and reveals a hydrophobic substrate-binding pocket adjacent to the methyl-donor site. This cavity is lined predominantly by nonpolar residues, which are likely to engage in hydrophobic interactions with the terpenoid scaffold of the substrate darumycin B (**2**). The spatial arrangement of these residues is compatible with the highly specific substrate orientation, providing a structural rationale for the observed position-specific methylation and the absence of activity toward the alternative substrate.

2.3.3.6. Proposed Biosynthetic Pathway of Darumycin

Based on the targeted gene deletions, combined with LC-MS, NMR analyses and in vitro enzymatic studies, we have proposed the biosynthetic pathway of darumycin (**Figure 6**). First, the DarD polyprenyl synthetase catalyses the condensation of five isoprenoid precursors, forming a pentaprenyl diphosphate, a crucial intermediate in the biosynthetic pathway. The DarD enzyme shows similarity (48.04%) to the GroD polyprenyl synthetase (protein - protein BLAST), responsible for the synthesis of hexaprenyl pyrophosphate intermediate in gromomycin biosynthesis.

Next, the DarB reveals a high degree of similarity (50.22 %) to GroH, a prenyltransferase responsible for the synthesis of hexaprenylguanidine, the linear precursor of gromomycins. Therefore, we propose that DarB enzyme similarly transfers the pentaprenyl moiety to arginine, followed by the release of proline through the nucleophilic attack of the alpha-amino group on the iminocarbon of the guanidine moiety forming pentaprenylguanidine catalyzes the formation of pentaprenylguanidine (**8**), the linear precursor of darumycins. Following, the DarA showes a significant degree of similarity (53,59 %) to GroF gromomycin cyclase. Furhermore, genes *darE*, *darF*, and *darI*, annotated as putative Rieske 2Fe-2S oxygenases, align with their gromomycin homologs (*groA*, *groB*, and *groC*). In our previous study, the knockout of these three genes led to the accumulation of hexaprenylguanidine, a linear intermediate of gromomycins. Therefore, we suggest their likewise involvement in the darumycin cyclization by introduction of the C4-OH group, and the formation of C1-C2 and C14-C15 double bonds. We propose that DarA cyclase, in combination with DarE, DarF, and DarI Rieske oxygenases catalyze the cyclization of pentaprenylguanidine, resulting in the darumycin D (**4**) as the first cyclic intermediate of darumycins.

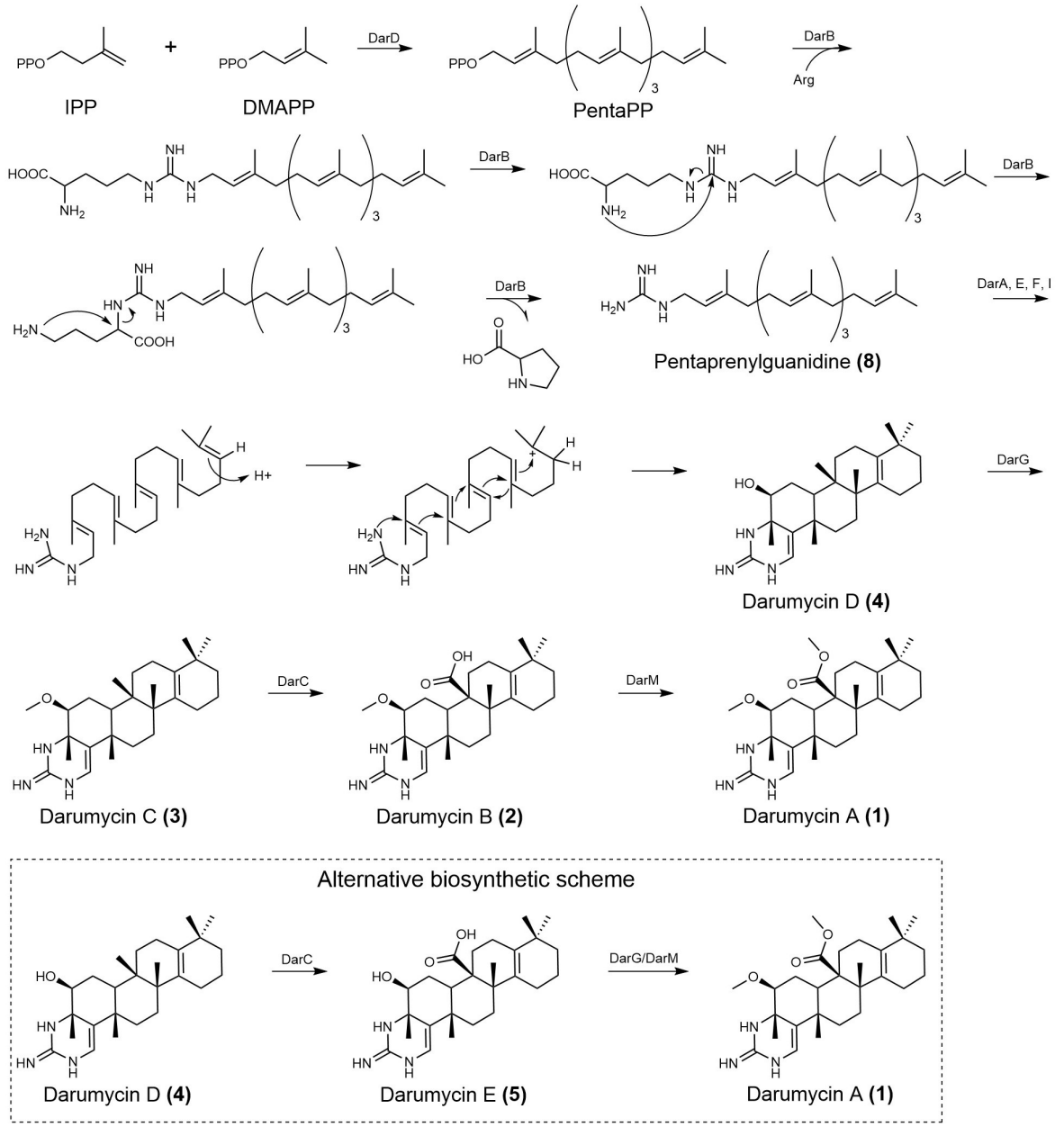

Figure 6. Proposed biosynthetic pathways of darumycins. IPP, Isopentenyl diphosphate; DMAPP, Dimethylallyl diphosphate; PenPP, pentaprenyl diphosphate, Arg, L-ariginine.

Subsequently, the DarG methyltransferase methylates the C4-OH group resulting in the generation of darumycin C (**3**). Then, DarC oxygenase catalyzes the sequential oxidation of the methyl group at position C-24, leading to the formation of darumycin B (**2**). A similar oxidation mechanism has been previously described for a *Streptomyces*-derived cytochrome P450 enzyme, which catalyzes the conversion of a methyl group to a carboxyl group, through diol and aldehyde intermediates in indolosesquiterpene alkaloids, xiamycins.[336] Furthermore, a *Micromonospora*-derived cytochrome P450 monooxygenase RosC, has been reported to catalyze the three-step oxidation reactions, which also leads to the formation of a hydroxyl, formyl, and carboxyl groups during rosamicin biosynthesis.[337] Noteworthy, inactivation of the

gromomycin cytochrome P450, encoded by *groI*, led to the production of the gromomycin C derivative lacking a keto group.[300] Finally, DarM methylates the previous derivative, leading to the accumulation of the final compound, darumycin A (**1**).

However, given the observation that DarM and DarG methyltransferases act in a site-specific but not obligatorily sequential manner during darumycin assembly, an alternative biosynthesis scheme could be proposed (**Figure 6**), suggesting that both methylation events could also occure after the introduction of the carboxyl group. In this case darumycin D (**4**), the first cyclic intermediate serves as a substarte for the DarC oxygenase, resulting in darumycin E (**5**), which is subsequently modified by both DarG and DarM methyltransferases, generating the final darumycin A (**1**) derivative.

Sesterterpenes, comprising five isoprene units, form the rarest group of terpenes discovered to date.[91] Since the initial identification of the first sesterterpene, ophiobolin A,[338-339] natural sources have yielded only around 1,600 structurally and functionally diverse compounds of this class, representing a relatively modest number compared to the other terpene classes.[56] These secondary metabolites are mostly reported from plants,[340] fungi,[341-342] and Spongia,[343-345] but rarely produced by bacteria, with several discovered from Cyanobacteria,[86, 89] and Actinobacteria.[223, 346-348] It should be noted that similar sesterterpene scaffolds containing guanidine moiety have been reported before, represented by scytoscalarol[86] and cybastacines (A and B),[89] both isolated from Cyanobacteria. Scytoscalarol, isolated from *Scytonema* UTEX 1163, possesses a tetracyclic scalarane skeleton with a hydroxy substituent and guanidine moiety. It was the first sesterterpene documented in cyanobacteria, as well as first sesterterpene with a guanidine moiety to be isolated from a natural source.[86] Cybastacines, on the other hand, were isolated from *Noctoc* sp. BEA-0956,[89] and feature a pentacyclic carbon skeleton with an incorporated guanidine group forming one of the rings (**Figure 7**), which differs from the free guanidine moiety found in scytoscalarol.

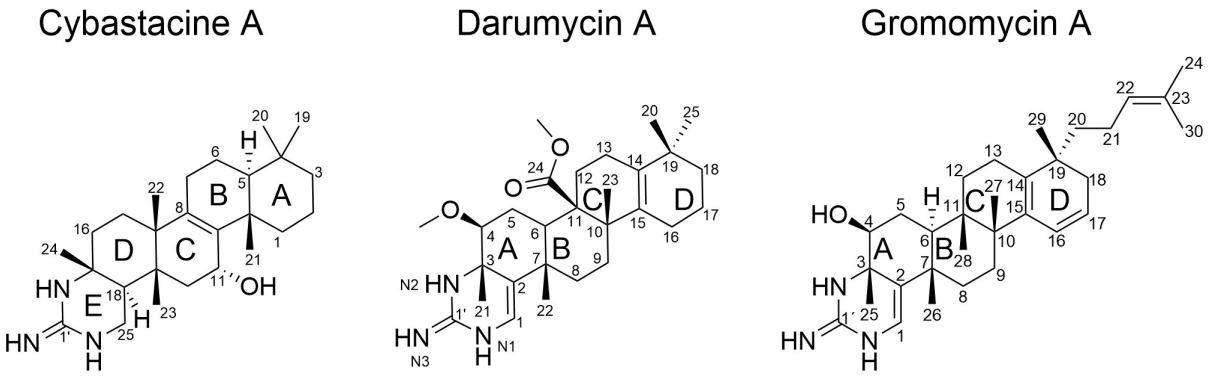

Figure 7. Structures of guanidine-bearing terpenoids: Cybastacine A, Darumycin A and Gromomycin A.

Although at first sight both cybastacine and darumycin are quite similar sharing a guanidine-bearing pentacyclic sesterterpene skeleton (**Figure 7**), they are still distinguished by sevelar features. For instance, the hydroxyl group of cybastacine is located at C-11 of its middle C ring, whereas both darumycin and gromomycin carry the hydroxyl group at C-4 of the A ring. Furthermore, cybastacine's structure shows distinct positions of double bonds and methyl groups compared to darumycin. In addition, both darumycin and gromomycin (**Figure 7**) are distinguished by various tailoring modifications, including methylation, oxidation (the keto group in gromomycins), and carboxylation (darumycins). Ultimately, these modifications play an important role in modulating the antimicrobial activity of different derivatives.

2.3.3.7. Bioactivity Profiling of Darumycins

Darumycins A (**1**) and G (**7**) display an overlapping antibacterial profile with gromomycins,[300] demonstrating potent activity against high-priority Gram-positive pathogens, and mycobacteria (**Table 3**). Similar to gromomycins, activity against Gram-negative pathogens is limited by efflux mechanisms and poor outer membrane penetration.

Interestingly, the precursor pentaprenylguanidine (**8**) exhibits only marginally higher MICs than darumycins A (**1**) and G (**7**), suggesting that cyclization is not crucial for bioactivity but does provide modest enhancement. In contrast, demethylated derivatives show reduced antibacterial activity, particularly darumycin E (**5**), where both hydroxyl and carboxyl groups are unmethylated. The loss of activity appears to result primarily from the free carboxyl group, as evidenced by the activities of the single demethylated derivatives darumycin B (**2**) and darumycin F (**6**). Given the high structural similarity between darumycins and gromomycins, along with their overall similar bioactivity profiles, it appears likely that the sesterpenes also exert their action by targeting the bacterial cell envelope (Bratiichuk D., Fries F. et. al. (2025) *Genome Mining–Driven Isolation of New Gromomycins and Insights into Their Mode of Action* [Manuscript submitted for publication]). This is further supported by the close correlation between antibacterial potency and cytotoxicity (**Table S13**), consistent with unspecific interactions with membrane lipids.

The membrane-targeting mode of action further accounts for the loss of activity observed for darumycin B (**2**) and E (**5**), as the negative charge of the free carboxyl group likely disrupts hydrophobic interactions between the cyclic core and the fatty acid chains of membrane lipids. In contrast, darumycins C (**3**) and D (**4**) are slightly more active than derivatives A (**1**) and G (**7**), owing to the absence of carboxyl moiety and the resulting increase in hydrophobicity.

Table 3. Antimicrobial spectrum of darumycins.

Classification	Organism	MIC [μg/mL]								
		DaruA	DaruB	DaruC	DaruD	DaruE	DaruF	DaruG	Pentaprenylguanidine	REF[c]
Gram-positive	*S. aureus* ATCC29213	2	16	1	1	32	4	2	8	CIP: 0.5
	S. aureus Newman	2	16	2	1	32	8	2	4	CIP: 0.5
	S. aureus Cowan 1	2	16	1	1	32	8	2	8	CIP: 1
	S. aureus N315	2	16	1	1	32	4	2	8	CIP: 1, AMP: > 64
	S. aureus Mu50	4	32	1	2	32	4	4	4	VAN: 8, AMP: > 64
	S. aureus HG001 WT	2	16	2	2	32	4	2	8	DAP: 0.5
	S. aureus HG001 Dap^{R}	2	8	1	1	32	2	2	2	DAP: 32
	S. pneumoniae DSM11865	2	8	1	4	16	4	2	4	CIP: 1
	E. faecalis ATCC29212	2	16	1	2	64	4	2	4	CIP: 2
	B. subtilis DSM10	2	16	1	1	32	4	2	8	CIP: 0.25
Mycobacteria	*M. smegmatis* mc^{2}155	2	16	2	4	32	2	2	4	RIF: 32
	M. tuberculosis H37Ra	4	32	2	8	64	8	4	8	RIF: 0.02
Gram-negative	*E. coli* BW25113	64	> 64	32	16	> 64	16	64	> 64	CIP: 0.03
	E. coli K12 Δ*tolC*[a]	8	16	4	4	16	8	8	> 64	CIP: 0.01
	E. coli K12 Δ*tolC*[a] + PMBN[b]	2	4	1	1	16	2	2	64	CIP: 0.01
	E. coli WO153	2	8	2	2	16	4	2	> 64	CIP: 0.01
	S. enterica DSM5569	> 64	> 64	16	8	> 64	16	> 64	> 64	CIP: 0.02
	C. freundii DSM30039	64	> 64	16	8	> 64	16	64	> 64	CIP: 0.02
	K. pneumoniae DSM681	8	32	4	4	64	8	8	> 64	CIP: 0.01
	A. baumannii DSM30007	16	> 64	4	4	> 64	16	16	> 64	CIP: 1
	A. baumannii DSM30008	16	> 64	4	4	> 64	16	16	> 64	CIP: 0.5
	A. baumannii NCTC13301	16	> 64	8	8	> 64	16	16	> 64	CIP: > 64, COL: 1
	P. aeruginosa PA14	> 64	> 64	> 64	64	> 64	64	> 64	> 64	CIP: 0.25

[a] Keio collection mutant; efflux-deficient

[b] 3 μg/mL polymyxin B nonapeptide (PMBN)

[c] Reference antibiotics: AMP, ampicillin; CIP, ciprofloxacin; COL, colistin; DAP, daptomycin; RIF, rifampicin; VAN, vancomycin

[R] Daptomycin resistant.

2.3.3.8. Conclusion

In this work, we report the discovery of new sesterterpene antibiotics, entitled darumycins, possessing potent activity against high-priority gram-positive pathogens, and mycobacteria. Genome mining enabled identification of the darumycin biosynthetic gene cluster in the *Micromonospora rubida* strain. Performing targeted gene deletions within the darumycin BGC generated several new bioactive derivatives, enriching the chemical space of the rare sesterterpene class. This, combined with LC-MS and NMR analyses, in vitro enzymatic studies, provided critical insights into the biosynthetic pathway of darumycin. Notably, in vitro enzymatic characterization revealed highly site-specific methylation reactions catalyzed by darumycin methyltransferases. In addition, the crystal structure of DarM uncovered a distinct SAM-dependent methyltransferase architecture that diverges from the known canonical *O*- and *C*-methyltransferase classes. These findings expand the known functional and structural diversity of methyltransferases involved in terpene biosynthesis.

2.3.4. Materials and Methods

Bacterial Strains, Plasmids and Culture Conditions

All strains and plasmids used in this work are listed in Supplementary **Tables S10-S12**. The strain *Micromonospora rubida* JCM 32386 was obtained from the Japan Collection of Microorganisms, RIKEN BRC. ISP-1 (656) medium (5 g l^{-1} tryptone, 3 g l^{-1} yeast extract, 2 g l^{-1} $MgSO_4*7H_2O$, pH to 7.0-7.2) or Sucrose-Bennets agar (104) medium (1 g l^{-1} yeast extract, 1 g l^{-1} beef extract, 2 g l^{-1} N-Z amine (type A), 10 g l^{-1} sucrose, 15 g l^{-1} agar, pH 7.3) were used for the *Micromonospora* strain cultivation. *S. albus* Del14 and *S. lividans* DelYA9 were used as hosts for heterologous expression of the darumycin biosynthetic gene cluster. *E. coli* strains were grown in Luria-Bertani (LB) broth (Sigma-Aldrich, St. Louis, MO, USA). *Streptomycetes* strains were grown on MS agar medium (Soy flour 20 g, Mannitol 20 g, tap water 1 l, pH 7.2 prior autoclaving) and in liquid tryptic soy broth medium (TSB; Sigma-Aldrich, St. Louis, MO, USA). If necessary, the following antibiotics were added: apramycin (50 μg ml^{-1}), kanamycin (50 μg ml^{-1}) and nalidixic acid (50 μg ml^{-1}) (Sigma-Aldrich, St. Louis, MO, USA; Roth, Karlsruhe, Germany). For conjugation, the *Streptomyces* strains were grown on MS agar for sporulation. For compounds production, S*treptomyces* strains were grown in liquid DNPM medium (40 g l^{-1} dextrin, 7.5 g l^{-1} soytone, 5 g l^{-1} baking yeast, and 21 g l^{-1} MOPS, pH 6.8), SG (20 g l^{-1} glucose, 10 g l^{-1} soy peptone, and 2 g l^{-1} $CaCO_3$, pH 7.2), GYM (4 g l^{-1} glucose, 4 g l^{-1} yeast extract, 10 g l^{-1} malt extract and 2 g l^{-1} $CaCO_3$, pH 7.2) and MM (minimal medium) (0.5

g l^{-1} L-Aspartic acid, 0.5 g l^{-1} K_2HPO_4, 0.2 g l^{-1} $MgSO_4*7H_2O$, 0.2 g l^{-1} $FeSO_4*7H2O$, 10 g l^{-1} glucose).

Metabolite Extraction and Analysis

S. albus Del14 and *S. lividans* DelYA9 carrying the cluster were grown in 50 mL of TSB medium at 28°C for 2 days to generate the pre-culture. For the main cultures, 100 mL of DNPM, SG, GYM or MM medium was inoculated with 1 mL of the pre-culture. In the fermentation experiments aimed at identifying the most productive medium for darumycin synthesis, *S. albus* Del14, carrying no cluster, and *S. albus* Del14 P05-E12, carrying the intact darumycin cluster, were used as controls. After six days of incubation at 28°C, darumycin derivatives were extracted from the culture supernatant using ethyl acetate, followed by solvent evaporation. Chromatographic analysis was performed by injecting 1 µL of the extracted sample into a Dionex Ultimate 3000 UPLC system (Thermo Fisher Scientific, Waltham, MA, USA) with a 10-cm ACQUITY UPLC® BEH C18 column (1.7 µm, Waters, Milford, MA, USA). Separation followed a linear gradient from 5% to 95% acetonitrile with 0.1% formic acid (FA) against 0.1% FA in water over 25 minutes, at a 0.6 mL/min flow rate and 45°C column temperature. Mass spectrometric analysis was conducted on an amaZon speed mass spectrometer or a maXis high-resolution LC-QTOF system (Bruker, USA). Bruker Compass Data Analysis software (version 6.1, Bruker, Billerica, MA, USA) was used for data collection and processing.

Isolation and Purification of Darumycins

Darumycins were isolated through the strain's cultivation in 10 L of DNPM, SG or GYM medium (depending on the derivative) at 28°C for six days under continuous agitation at 180 rpm. Following fermentation, the compounds were extracted from the culture supernatant using ethyl acetate. The resulting extracts were dried through solvent evaporation, redissolved in methanol, and subjected to purification via size-exclusion chromatography on a Sephadex LH-20 column (Sigma-Aldrich, Louis, MO, USA) with methanol as the mobile phase. Fraction collection was performed at 10-minute intervals at a flow rate of 0.8 mL/min. The fractions containing the desired darumycin derivative were pooled together, concentrated and dissolved in methanol, followed by Reversed-Phase High Performance Liquid Chromatography (RP-HPLC) (Waters AutoPurification™ System) separation on preparative C18 column Nucleodur HTec, 5 µm, 250 mm x 21 mm (Macherey-Nagel, Germany) using a water solution containing 0.1% (v/v) formic acid (solvent A), and an acetonitrile solution containing 0.1% (v/v) formic acid (solvent B) as a mobile phase. For compounds separation by RP-HPLC, the following gradient at a flow rate of 20 mL/min was used: 0 min-5% B, 0.5 min-5%, 12 min-65% B, 25

min-65%B, 27 min-95% B, 28 min-95% B, 29 min-5% B, 31 min-5% B. The fractions were collected using MS detector (Waters™ SQ Detector 2). The darumycin-containing fractions were pooled, evaporated, and subjected to the final purification step. The final purification step involved RP-HPLC using Thermo Scientific Dionex UltiMate 3000 system equipped with a semipreparative Synergy™ 4 μm Fusion-RP C18 column (80 Å, 250 × 10 mm; Phenomenex, Torrance, CA, USA). Separation was achieved with a mobile phase consisting of water with 0.1% formic acid (solvent A) and acetonitrile with 0.1% formic acid (solvent B). Separation was performed using the following gradient at a flow rate of 4 mL/min: 0 min-5% B, 0.5 min-5% B, 10 min-65% B, 12 min-65% B, 15 min-95% B, 17 min-95% B, and 18 min-5% B. Fractions containing the purified compound were collected, pooled, and evaporated.

Cosmid Library Construction

A cosmid library of *M. rubida* JCM 32386 were prepared using the EpiCentre CopyControl™ Fosmid Library Production Kit in pCos15A_AmInt vector by adapting the protocol from Lucigen. A library of 30−40 kb fragments was constructed according to the manufacturer's protocol using genomic DNA isolated with NucleoSpin Microbial DNA Mini kit for DNA from microorganisms (MACHEREY-NAGEL GmbH & Co. KG, Germany). The purified genomic DNA fragments were ligated into linearized pCos15A_AmInt vectors. The ligation reactions were packaged into λ phage for *E. coli* EPI300 infection. The packaged library was plated on LB agar plates containing 50 μg ml^{-1} Apramycin and grown overnight at 37 °C. Approximately 1700 single colonies were picked and inoculated into individual wells of 96-well plates. This arrayed cosmid library was stored with 20% glycerol and kept at −80 °C.

Heterologous Expression of Darumycin Gene Cluster and Systematic Gene Deletion

The constructs used in this study for heterologous expression were introduced into *S. albus* Del14 and *S. lividans* DelYA9 by conjugation using donor strain *E. coli* ET12657/pUB307 on MS plates. After incubating at 29°C for 15 hours, exconjugants were selected with 50 μg ml^{-1} apramycin and and 50 μg ml^{-1} nalidixic acid. Single colonies from this plate were patched onto MS plates 50 μg ml^{-1} apramycin.

Genome Mining-Guided Identification of Darumycin Cluster

Three genes involved in the biosynthesis of gromomycins were used for genome-wide quantitative screening of novel derivatives: *groD*, *groF* and *groH*. The nucleotide sequences of these genes were used as probes in the NCBI protein BLAST database to identify new gromomycin-like clusters. The strains with all three of these genes identified in the genome

were selected. In this way, many actinomycetes strains were identified, including *M. rubida* strain. The new gromomycin like cluster, later renamed to darumycin cluster, was isolated from the genome of the *M. rubida* strain through the cosmid library construction. Cosmid P05-E12 containing whole darumycin cluster was identified by PCR with two pairs of primers designed to amplify regions to the left or right side of the cluster. The P05-E12 cosmid was introduced into *S. albus* Del14 and *S. lividans* DelYA9 strains. The ability of heterologous strains to produce new derivatives was determined by HPLC.

Cloning, Recombinant Expression and Purification of DarG and DarM

The full-length synthetic codon-optimized genes for DarG (accession number: WP_161689877.1) and DarM (accession number: WP_161689883.1) from *Micromonospora rubida* were ordered from GenScript pre-cloned into the expression vector pET-29a(+). A tobacco etch virus (TEV) protease site (ENLYFQG) was inserted upstream of both genes to enable cleavage of the N-terminal His_6-tag during recombinant protein purification. E. coli Lemo21 (DE3) was used for recombinant protein expression, and the two plasmids were transformed using a standard heat shock protocol.

A single colony of *E. coli* Lemo21 harboring the plasmid pET-28a(+)-TEV-DarG or pET-28a(+)-TEV-DarM was used to inoculate a preculture in Luria-Bertani (LB) medium supplemented with 25 μg mL^{-1} Chloramphenicol and 50 μg mL^{-1} Kanamycin and incubated overnight at 37 °C and 180 rpm. At the next day 1 L LB main culture in 2 L buffled flasks was inoculated with 15 mL overnight culture and incubated at 37 °C and 180 rpm until an OD_{600} of 0.8 was reached. Protein expression was induced with 1 mM IPTG, and the culture was incubated at 16 °C and 180 rpm for 16 h. The cells were harvested by centrifugation at 12 800 g and 4 °C for 15 min, and the pellet was flash-frozen and stored at - 80 °C until further use. Both proteins DarG and DarM were purified using the same following conditions. The cell pellet (100 mL lysis buffer per every 25 g wet cell mass) was resuspended in buffer A (50 mM Tris pH 8.0, 500 mM NaCl, 10% glyercol, 20 mM imidazole and 3 mM BME) supplemented with DNAse (0.4 mg g^{-1} wet cell pellet, Sigma) and cOmplete EDTA-free protease inhibitor tablets (Roche). The cells were lysed by passing them twice through a cell disruptor (24.5 kPSI, 4 °C, Constant Systems) and the cell debris was removed by centrifugation at 40 000 g and 4 °C for 30 min. The clarified lysate was subsequently loaded using an ÄKTA go onto a HisTrap HP 5 mL column (Cytiva) pre-equilibrated with buffer A using a flow rate of 5 mL min^{-1} and at 4 °C. After a column wash with 20 CV buffer A, elution was performed using buffer B (50 mM Tris pH 8.0, 500 mM NaCl, 10% glyercol, 300 mM imidazole and 3 mM BME), and protein containing fractions were pooled together. For subsequent removal of the His-tag, the pooled

fractions were desalted into buffer C (50 mM Tris pH 8.0, 500 mM NaCl, 10% glyercol, 20 mM imidazole and 3 mM BME) by passing over a HiPrep 26/10 desalting column (Cytiva) at a flow rate of 10 mL min^{-1} connected to a ÄKTA pure, TEV protease was added in a 1:10 mass ratio and incubated overnight at 4 °C. Undigested protein and His-tagged TEV protease were removed by another Ni affinity chromatography. To further increase protein purity, anion exchange chromatography was performed, whereby DarG- / DarM-containing fractions were buffer-exchanged into buffer D (25 mM Tris pH 8.0, 30 mM NaCl, 5% glycerol and 1 mM DTT) using a HiPrep26/10 column. The desalted sample was loaded onto a HiTrap Q 5 mL column (Cytiva) previously equilibrated with buffer D and both proteins were eluted using a linear gradient with buffer E (25 mM Tris pH 8.0, 1 M NaCl, 5% glycerol and 1 mM DTT). DarG or DarM containing fractions were pooled and the proteins were finally purified by size-exclusion chromatography on a Superdex S75 16/600 column pre-equilibrated with storage buffer F (10 mM Tris pH 8.0, 100 mM NaCl) at a flow rate of 1 mL min^{-1}. The resulting peak was collected and fractions containing purified DarG or DarM were concentrated to 20 mg mL^{-1} and 30 mg mL^{-1} using a 10 kDa cut-off filter (Thermo Fisher Scientific) and flash-frozen in liquid nitrogen. The protein concentration was measured by specific absorption at A280 on a Nanodrop2000 (Thermo Fisher Scientific) and protein purity was assayed using sodium dodecyl-sulfate polyacrylamide gel electrophoresis.

In Vitro Enzyme Assay of DarG and DarM

Biochemical reactions were performed in 10 mM Tris pH 8.0 and 100 mM NaCl in a reaction volume of 50 µL. For DarG reactions a mixture of 100 µM compound (456M1, 456M2, 442 and 412), 1 µM purified enzyme, 1 mM freshly prepared SAM were incubated for 2 h at 37 °C. For DarM reactions a mixture of 100 µM compound (456M1, 456M2, 442 and 412), 10 µM purified enzyme, 1 mM freshly prepared SAM were incubated for 2 h at 37 °C. Proteins were subsequently precipitated by adding 50% acetonitrile and the mixture was flash frozen in liquid nitrogen. The samples were stored at -80 °C at least 2 h prior to LC-MS analysis.

Crystallization of DarM and Structure Determination

Crystallization screening experiments for DarM in complex with SAH were performed using a protein concentration of 10 mg mL^{-1} (stored in gel filtration buffer 10 mM Tris pH 8.0 and 100 mM NaCl) using commercially available screens form Nextal. The screens were pipetted into sitting-drop SwissSCI plates using a Gryphron crystallization robot (Art Robbins Instruments) and incubated at XY K. Diffraction quality crystals of DarM appeared within the next few days in a condition with a well solution of 0.2 M sodium chloride, 0.1 sodium acetate

pH 4.5 and 1.26 M ammonium sulfate. The crystals were cryoprotected using the well solution supplemented with 32% glycerol, mounted into cryo-loops (Hampton Research) and immediately flash-frozen in liquid nitrogen. A dataset for DarM in complex with SAH was collected at ESRF using the beamlines ID-30B at 100 K. Data were processed using POINTLESS and AIMLESS as well as ctruncate implemented in ccp4 (CCP4Interface 8.0.019). The structure was solved in Phenix (phenix.phase) by molecular replacement using a model generated with AlphaFold 2, following by further processing using Phenix.autobild. The resulting structure was manually rebuilt in COOT (Version 0.9.8.93 under Xquartz 11 version 2.8.5) and refined several times using Phenix.refine. Final PDB coordinates were analyzed using MolProbity implemented in Phenix before deposition into the protein database. The coordinated were further used to search for structural homologs utilizing the DALI server. All protein structure images shown in this study were rendered in PyMOL (The PyMOL Molecular Graphics System Version 3.1.6.1, Schrödinger, LLC).

Antibiotic Activity (Minimum Inhibitory Concentrations)

Darumycin stock solutions were prepared in dimethyl sulfoxide (DMSO). All microorganisms used in this study were obtained from the German Collection of Microorganisms and Cell Cultures (DSMZ), the American Type Culture Collection (ATCC), the Coli Genetic Stock Center, or were part of our internal strain collection. *Staphylococcus aureus* strains Newman, N315, Mu50 and Cowan 1 were obtained from M. Bischoff, Saarland University Hospital, Homburg. *S. aureus* wild type and Dap^R HG001 were provided by T. Schneider, University of Bonn. *E. coli* WO153 was provided by K. Lewis, Northeastern University, Boston, USA. Minimum inhibitory concentrations (MICs) were determined using the broth microdilution method according to EUCAST guidelines (ISO 20776-1:2019). In short, serial two-fold dilutions of darumycins (0.03125 to 64 µg/mL) were prepared in 75 µL of cation-adjusted Mueller-Hinton broth (MHB2) in sterile 96-well plates. Equal volume of the bacterial suspension was added, and the plates were incubated at 37 °C for 18 h. For *Streptococcus pneumoniae*, MHF broth (MHB2 supplemented with 5% lysed horse blood and 20 mg/L β-NAD) was used and plates were incubated at 37 °C with 5% CO_2.

The MIC was defined as the lowest concentration of the antibiotic causing complete inhibition of visible growth of the microorganism. The same method was used for testing *Mycobacterium smegmatis*, but with the use of Middlebrook 7H9 complete medium supplemented with oleic acid, albumin, dextrose and catalase (OADC, 10%). *M. smegmatis* plates were incubated for 48 h at 37 °C. For assessing activity against *Mycobacterium tuberculosis*, an adapted resazurin microtitre assay (REMA) was performed. In short, *M. tuberculosis* single cells were prepared

and added to compound dilutions in M7H9. Plates were incubated for 6 d at 37 °C, followed by addition of 50 µL of resazurin and incubation for another day at 37 °C. The MIC was determined visually and additionally confirmed by measuring fluorescence (excitation at 530 nm, emission at 590 nm).

Cytotoxic Activity (IC50)

HepG2 cells (human hepatoblastoma cell line; ACC 180) and CHO-K1 (chinese hamster ovary cells; ACC 110) were obtained from the German Collection of Microorganisms and Cell Cultures (DSMZ) and cultured under the conditions recommended by the depositor. Cells were propagated in Roswell Park Memorial Institute (RPMI) 1640 medium and Ham's F12 medium, respectively, supplemented with 10% fetal bovine serum (FBS), and seeded at 6×10^3 cells per well of 96-well plates in 120 µL of complete medium. After 2 h of equilibration (37 °C, 5% CO_2), the cells were treated with a serial dilution of darumycins. Darumycins, doxorubicin as reference, as well as the solvent control (DMSO) were tested as duplicates in two independent experiments. After 5 d of incubation (37 °C, 5% CO_2), a total of 20 µL of 5 mg/ml MTT (thiazolyl blue tetrazolium bromide) in phosphate-buffered saline (PBS) were added to each well and the cells were further incubated for 2 h at 37 °C before the supernatant was discarded. Subsequently, the cells were washed with 100 µL of PBS and treated with 100 µl of 2-propanol/10 N HCl (250:1) to dissolve formazan granules. Cell viability was measured as a percentage relative to the respective solvent control by measuring the absorbance at 570 nm using a microplate reader (Tecan Infinite M200Pro). GraphPad Prism (version 10.0.3, GraphPad, Boston, MA, USA) was used for sigmoidal curve fitting to determine the IC_{50} values.

Maximum Tolerated Concentration

Husbandry of adult zebrafish was performed according to internal guidelines set out in the German Animal Welfare Act (§11 Abs. 1 TierSchG). Experiments were carried out with wild type AB (obtained from the European Zebrafish Resource Center at Karlsruhe Institute of Technology) embryos within the first 120 hours post fertilization (hpf) as these early life stages are not considered as animal experiments according to the EU Directive 2010/63/EU. Embryos were maintained in fresh 0.3x Danieau's (17.4 mM NaCl, 0.21 mM KCl, 0.12 mM $MgSO_4$, 0.18 mM Ca $(NO_3)_2$, 1.5 mM HEPES, 1.2 µM methylene blue, pH 7.1-7.3) at 28 °C. At a maximum of 120 hpf, embryos were euthanized by submersion in ice water for at least 12 h. For evaluation of the maximum tolerated concentration (MTC), embryos were dechorionated at 30 hpf using 1 mg/mL pronase and placed in a flat-bottom 96-well plate with one embryo per

well. Excess medium was removed and 150 µL of darumycin dilutions (in 0.3x Danieau's, maximum of 1% DMSO) and of the solvent control (1% DMSO in 0.3x Danieau's) were added. Ten embryos were used per condition. Exposed embryos were maintained at 28 °C until 120 hpf and they were monitored daily under a stereo microscope (Stemi 508, Zeiss) to record survival as well as anomalies, pigmentation, heartbeat and locomotor responses. An embryo was considered dead when no heartbeat could be observed. The maximum tolerated concentration (MTC) was defined as the highest concentration of the antibiotic with more than 90% survival of zebrafish embryos. Kaplan-Meier curves were generated using GraphPad Prism (version 10.0.3, GraphPad, Boston, MA, USA).

2.3.5. Supplementary Information for Chapter 2.3.

Expanding the Chemical Space of Sesterterpene Antibiotics: Discovery and Characterization of Darumycins.

Structure elucidation

Nuclear Magnetic Resonance Spectroscopy

The chemical structures of all the compounds were determined *via* multidimensional NMR analysis. ^{1}H-NMR, ^{13}C-NMR, and 2D spectra were recorded at 500 MHz (^{1}H)/ 125 MHz (^{13}C), conducted in the Bruker Avance Neo 500 MHz, equipped with a Prodigy Cryo-probe. Samples were dissolved in methanol-d_4 or memethanol-d_3. Chemical shifts are reported in ppm relative to tetramethylsilane; the solvent was used as the internal standard. Coupling constants are reported in Hertz (Hz). Multiplicity is reported with the usual abbreviations (s: singlet, br s: broad singlet, d: doublet, dd: doublet of doublets, ddd: doublet of doublet of doublets, t: triplet, dt: doublet of triplets, q: quartet, p: pentet, dp: doublet of pentets, m: multiplet).

Isolated Compounds and Their Analytical Data

Darumycin A (*3S, 4S, 6S, 7S, 10R, 11S*): white powder, $[\alpha]_D^{20}$ $+26°$ (c 0.37, MeOH). For NMR see Table S1 (500 MHz, CD_3OH), HRESIMS *m/z* 470.34 $[M+H]^+$, (calcd for $C_{28}H_{44}N_3O_3$, 470.3383).

Darumycin B (*3S, 4S, 6S, 7S, 10R 11S*): white powder, $[\alpha]_D^{20}$ $-19°$ (c 0.50, MeOD). For NMR see Table S2 (500 MHz, CD_3OD), HRESIMS *m/z* 456.32 $[M+H]^+$, (calcd for $C_{27}H_{42}N_3O_3$, 456.3226).

Darumycin C (*3S, 4S, 6S, 7S, 10R, 11S*): white powder, $[\alpha]_D^{20}$ $-60°$ (c 0.70, MeOH). For NMR see Table S3 (500 MHz, CD_3OD), HRESIMS *m/z* 426.35 $[M+H]^+$, (calcd for $C_{27}H_{44}N_3O$, 426.3484).

Darumycin D (*3S, 4S, 6S, 7S, 10R, 11S*): white powder, $[\alpha]_D^{20}$ $-50°$ (c 0.22, MeOH). For NMR see Table S4 (500 MHz, CD_3OD), HRESIMS *m/z* 412.33 $[M+H]^+$, (calcd for $C_{26}H_{42}N_3O$, 412.3328).

Darumycin E (*3S, 4S, 6S, 7S, 10R, 11S*): white powder, $[\alpha]_D^{20}$ $-18°$ (c 0.24, MeOH). For NMR see Table S5 (500 MHz, CD_3OD), HRESIMS *m/z* 442.31 $[M+H]^+$, (calcd for $C_{26}H_{40}N_3O_3$, 442.3070).

Darumycin F (*3S, 4S, 6S, 7S, 10R, 11S*): white powder, $[\alpha]_D^{20}$ -23° (c 0.20, MeOH). For NMR see Table S6 (500 MHz, CD_3OD), HRESIMS *m/z* 456.32 $[M+H]^+$, (calcd for $C_{27}H_{42}N_3O_3$, 456.3226).

Darumycin G (*3S, 4S, 6S, 7S, 10R, 11S*): white powder, $[\alpha]_D^{20}$ +57° (c 0.23, MeOH). For NMR see Table S7 (500 MHz, CD_3OD), HRESIMS *m/z* 468.32 $[M+H]^+$, (calcd for $C_{28}H_{42}N_3O_3$, 468.3226).

Pentaprenylguanidine: white powder, for NMR see Table S8 (500 MHz, CD_3OD), HRESIMS *m/z* 400.37 $[M+H]^+$, (calcd for $C_{26}H_{46}N_3$, 400.3692).

Mosher Analysis of Darumycin F

The absolute stereochemistry was determined according to Mosher et al.[349] In brief, two glass vials with 1 mg dried Darumycin F in 150 µL dry $CDCl_3$, 7 µL dry pyridine and 7 µL R-MTPA-Cl or S-MTPA-Cl, respectively, were prepared. The vials were flushed with nitrogen, closed airtight and were incubated with occasional shaking at room temperature while the reaction progress was monitored by LC-MS analysis by a Bruker Amazon Ion trap. Even after one day, 10% to 25% of unused Darumycin F were still detectable. However, the desired Mosher products with *m/z* =672.41 dominated in both approaches. Subsequently, the reactions were stopped, and the samples were dried and purified by HPLC (Thermo Scientific Dionex UltiMate 3000 system equipped with a Phenomenex Synergi 4µm C18 column 250*10 mm and a 20 min gradient of 50-65% acetonitrile/water containing 0.1% formic acid). This led to 0.6 mg Darumycin F (*R*)-MTPA ester and 0.7 mg Darumycin F (*S*)-MTPA ester (**Figure S2**). The purified samples were dissolved in CD_3OD and NMR spectroscopy was performed.

According to the rules of Mosher analysis, protons H-1 and H-21 (group 1) and the remaining protons (group 2) should be divided into two groups based on the sign of the ΔδS-R values, whereby the type of sign should allow conclusions about the stereochemistry at C-4. (**Figure S1**) Unfortunately, the analysis of the ΔδS-R values did not lead to the desired result. While negative values were found for group 2, the values for group 1 were also negative, which is actually incompatible with the rules of Mosher analysis. MTPA derivatives not always fully meet the specified criteria, which can lead to a loss of confidence in the assignement.[350] Nevertheless, we attribute the strikingly high negative values for H-5a and H-5b, which are spatially very close to the MTPA residue, to an S-configuration at C-4, as was found in the closely related gromomycins.[300]

List of Tables

Table S1. NMR data of Darumycin A (**1**) in CD3OH.

No	δ_C [ppm]	δ_H [ppm], mult (J)	HHCOSY	HMBC (H→C/N)	key-NOESY
1	117.4, CH	5.97, bs		1', 2, 3, 7, N_1	
2	131.9, C				
3	59.0, C				
4	89.5, CH	3.13, dd (11.8,3.9)	5	3, 6, 21, N_2	
5	25.2, CH_2	a: 2.27, m b: 1.47, m	4, 6	3, 4, 6, 7, 11	22
6	41.8, CH	1.85, m	5	2, 4, 5, 7, 8, 12, 24	
7	38.3, C				
8	36.7, CH_2	a: 1.64, m b: 1.25, m	9	6, 7, 10, 22	22
9	28.2, CH_2	a: 2.38, td (14.6, 2.9) b: 1.72, dt (15.3, 3.5)	8	7, 8, 10, 11, 15, 23	22
10	42.8, C				
11	51.0, C				
12	26.4, CH_2	a: 2.25, m b: 1.86, m	13	6, 10, 11, 13, 14, 24	
13	22.4, CH_2	a: 2.10, m b: 1.98, m	12	11, 12, 14, 15, 19	20, 23 25
14	135.9, C				
15	134.6, C				
16	27.0, CH_2	a: 2.09, m b: 1.87, m	17	14, 15, 17	
17	21.2, CH_2	a: 1.68, m b: 1.53, m	16, 18	15, 19	
18	41.0, CH_2	a: 1.50, m b: 1.35, m	17	14, 16, 17, 19, 20, 25	
19	35.5, C				
20	28.1, CH_3	1.02, s		14, 18, 19, 25	H-13a
21	23.7, CH_3	1.34, s		2, 3, 4, N_2	H-5b, 22, 4-OMe,
22	23.3, CH_3	1.07, s		2, 6, 7, 8	21, H-9a, H-8a, H-5b
23	25.4, CH_3	1.18, s		9, 10, 11, 15	24-OMe, H-13a, H-9a
24	177.2, C				
25	29.8, CH_3	0.98, s		14, 18, 19, 20	H-13b
4-OMe	57.5, CH_3	3.47, s		4	H-5a, 21
24-OMe	51.6, CH_3	3.64, s		24	
1'	153.0, C				
N_1	94.7, NH				
N_2	98.6, NH				

Table S2. NMR data of Darumycin B (**2**) in CH_3OD.

No	δ_C [ppm]	δ_H [ppm], mult (J)	HHCOSY	HMBC (H→C)
1	117.1, CH	5.97, s		1', 2, 3, 7
2	132.3, C			
3	59.1, C			
4	89.7, CH	3.15, dd (11.8, 4.0)	5	3, 6, 21, 4-OMe
5	25.3, CH_2	a: 2.30, m b: 1.59, m	4, 6	3, 4, 6, 7
6	41.5, CH	1.83, m	5	2, 4, 5, 7, 8, 11, 22, 24
7	38.6, C			
8	36.9, CH_2	a: 1.64, m b: 1.25, m	9	2, 6, 7, 9, 10
9	28.2, CH_2	a: 2.48, td (14.5, 2.8) b: 1.69, dt (14.8, 3.0)	8	7, 8, 10, 11, 15, 23
10	42.7, C			
11	50.5, C			
12	26.8, CH_2	a: 2.27, m b: 1.86, m	13	6, 10, 11, 13, 14, 24
13	22.5, CH_2	a: 1.99, m b: 2.09, m	12	11, 12, 14, 15, 19
14	135.7, C			
15	134.9, C			
16	27.0, CH_2	a: 1.88, m b: 2.10, m	17	10, 14, 17, 18
17	21.3, CH_2	a: 1.56, m b: 1.69, m	16, 18	15, 19
18	41.1, CH_2	a: 1.35, m b: 1.51, m	17	14, 16, 19, 20, 25
19	35.5, C			
20	29.9, CH_3	0.98, s		14, 18, 19, 25
21	23.8, CH_3	1.36, s		2, 3, 4
22	23.4, CH_3	1.20, s		2, 6, 7, 8
23	25.5, CH_3	1.22, s		9, 10, 11, 15
24	179.4, C			
25	28.1, CH_3	1.03, s		14, 18, 19, 20
4-OMe	57.4, CH_3	3.47, s		4
1'	152.9, C			

Table S3. NMR data of Darumycin C (**3**) in CH_3OD.

No	δ_C [ppm]	δ_H [ppm], mult (J)	HHCOSY	HMBC (H→C)
1	116.3, CH	5.92, s		1', 2, 3, 7
2	133.0, C			
3	59.8, C			
4	80.0, CH	3.60, dd (10.7, 4.1)	5	2, 3, 5, 6, 21
5	29.1, CH_2	a: 1.58, m b: 1.72, m	4, 6	3, 4, 6, 7
6	41.8, CH	1.59, m	5	2, 4, 8, 22, 24
7	38.4, C			
8	36.1, CH_2	a: 1.22, m b: 1.55, m	9	2, 6, 9, 10, 22
9	28.3, CH_2	a: 1.90, m b: 1.70, m	8	7, 11, 15, 23
10	42.9, C			
11	38.6, C			
12	22.6, CH_2	a: 1.88, m b: 1.92, m	13	11, 13, 14, 24
13	31.2, CH_2	a: 1.56, m b: 1.52, m	12	11, 12, 14, 15, 19
14	137.2, C			
15	133.5, C			
16	27.3, CH_2	a: 2.07, m b: 1.86, m	17	14, 15, 17, 18
17	21.3, CH_2	a: 1.67, m b: 1.56, m	16, 18	15, 16, 19
18	41.1, CH_2	a: 1.50, m b: 1.35, m	17	14, 16, 17, 19, 20, 25
19	35.6, C			
20	29.9, CH_3	0.95, s		14, 18 ,19 ,25
21	23.5, CH_3	1.40, s		2, 3, 4
22	25.4, CH_3	1.21, s		2, 6, 7, 8
23	24.2, CH_3	0.92, s		9, 10, 11, 15
24	21.4, CH_3	0.87, s		6, 10, 11, 12
25	28.1, CH_3	1.02, s		14, 18, 19, 20
1'	152.8, C			

Table S4. NMR data of Darumycin D (**4**) in CD_3OD.

No	δ_C [ppm]	δ_H [ppm], mult (J)	HHCOSY	HMBC (H→C)
1	116.3, CH	5.92, s		1', 2, 3, 7
2	133.0, C			
3	59.8, C			
4	80.0, CH	3.60, dd (10.7, 4.1)	5	2, 3, 5, 6, 21
5	29.1, CH_2	a: 1.58, m b: 1.72, m	4, 6	3, 4, 6, 7
6	41.8, CH	1.59, m	5	2, 4, 8, 22, 24
7	38.4, C			
8	36.1, CH_2	a: 1.22, m b: 1.55, m	9	2, 6, 9, 10, 22
9	28.3, CH_2	a: 1.90, m b: 1.70, m	8	7, 11, 15, 23
10	42.9, C			
11	38.6, C			
12	22.6, CH_2	a: 1.88, m b: 1.92, m	13	11, 13, 14, 24
13	31.2, CH_2	a: 1.56, m b: 1.52, m	12	11, 12, 14, 15, 19
14	137.2, C			
15	133.5, C			
16	27.3, CH_2	a: 2.07, m b: 1.86, m	17	14, 15, 17, 18
17	21.3, CH_2	a: 1.67, m b: 1.56, m	16, 18	15, 16, 19
18	41.1, CH_2	a: 1.50, m b: 1.35, m	17	14, 16, 17, 19, 20, 25
19	35.6, C			
20	29.9, CH_3	0.95, s		14, 18 ,19 ,25
21	23.5, CH_3	1.40, s		2, 3, 4
22	25.4, CH_3	1.21, s		2, 6, 7, 8
23	24.2, CH_3	0.92, s		9, 10, 11, 15
24	21.4, CH_3	0.87, s		6, 10, 11, 12
25	28.1, CH_3	1.02, s		14, 18, 19, 20
1'	152.8, C			

Table S5. NMR data of Darumycin E (**5**) in CD_3OD.

No	δ_C [ppm]	δ_H [ppm], mult (J)	HHCOSY	HMBC (H→C)
1	116.9, CH	5.95, s		2, 6, 7, 8
2	132.7, C			
3	59.7, C			
4	79.9, CH	3.56, dd (10.8, 3.8)	5	3, 4, 6
5	31.0, CH_2	a: 2.01, m b: 1.85, m	4, 6	3, 4, 6, 7, 11
6	41.8, CH	1.84, m	5	4, 5, 10, 22, 24
7	38.5, C			
8	36.9, CH_2	a: 1.24, m b: 1.62, m	9	2, 6, 7, 9, 10
9	28.3, CH_2	a: 2.52, td (14.7, 2.3) b: 1.66, m	8	7, 8, 10, 11, 15, 23
10	42.7, C			
11	50.5, C			
12	22.5, CH_2	2.03, m	13	6, 13, 14, 24
13	26.9, CH_2	a: 2.24, m b: 1.82, m	12	11, 12, 14
14	135.7, C			
15	134.9, C			
16	27.1, CH_2	a: 1.87, m b: 2.09, m	17	14, 15, 18
17	21.3, CH_2	a: 1.68, m b: 1.55, m	16, 18	15, 19
18	41.1, CH_2	a: 1.49, m b: 1.34, m	17	14, 16, 17, 19, 20, 25
19	35.5, C			
20	29.9, CH_3	0.96, s		14, 18, 19, 25
21	23.4, CH_3	1.37, s		2, 3, 4
22	23.5, CH_3	1.21, s		2, 6, 7, 8
23	25.6, CH_3	1.21, s		9, 10, 11, 15
24	180.0, C			
25	28.1, CH_3	1.02, s		14, 18, 19, 20
1'	152.9, C			

Table S6. NMR data of Darumycin F (**6**) in CD_3OD.

No	δ_C [ppm]	δ_H [ppm], mult (J)	HHCOSY	HMBC (H→C)
1	117.3, CH	5.97, s		2, 3, 7
2	132.2, C			
3	59.6, C			
4	79.6, CH	3.55, dd (11.8, 4.2)	5	3, 5, 6, 21
5	30.9, CH_2	a: 1.99, m b: 1.70, m	4, 6	3, 4, 6, 7, 11
6	42.1, CH	1.90, m	5	2, 4, 5, 7, 8, 10, 12, 24
7	38.3, C			
8	36.6, CH_2	a: 1.64, m b: 1.25, m	9	6, 7, 10, 22
9	28.2, CH_2	a: 2.39, td (14.6, 3.1) b: 1.72, m	8	7, 8, 10, 11, 15, 23
10	42.8, C			
11	50.8, C			
12	26.4, CH_2	a: 2.23, ddd (14.0, 5.3, 1.2) b: 1.84, m	13	10, 11, 14, 24
13	27.0, CH_2	a: 2.09, m b: 1.87, m	12	11, 12, 14, 15
14	135.9, C			
15	134.4, C			
16	22.3, CH_2	2.05, m	17	14, 15, 18
17	21.2, CH_2	a: 1.69, m b: 1.55, m	16, 18	15, 19
18	41.0, CH_2	a: 1.51, m b: 1.35, m	17	14, 16, 20, 25
19	35.5, C			
20	29.8, CH_3	0.97, s		14, 18, 19, 25
21	23.2, CH_3	1.36, s		2, 3, 4
22	23.2, CH_3	1.08, s		2, 6, 7, 8
23	25.4, CH_3	1.18, s		15, 9, 10, 11
24	177.3, C			
25	28.1, CH_3	1.02, s		14, 18, 19, 20
24-OMe	51.6, CH_3	3.65, s		24
1’	152.9, C			

Table S7. NMR data of Darumycin G (**7**) in CD_3OD.

No	δ_C [ppm]	δ_H [ppm], mult (J)	HHCOSY	HMBC (H→C/N)
1	117.6, CH	5.96, s		N_1, 2, 3, 7
2	131.9, C			
3	58.9, C			
4	89.1, CH	2.99, dd (11.8, 4.0)	5	N_2, 3, 4-OMe
5	24.9, CH_2	a: 2.19, m b: 1.56, m	4, 6	3, 4, 6, 7
6	42.7, CH	1.74, dd (12.6, 1.8)	5	2, 4, 11, 24
7	39.0, C			
8	35.3, CH_2	a: 1.79, m b: 1.54, m	9	6, 10
9	28.3, CH_2	a: 2.66, m b: 1.88, m	8	7, 8, 11
10	43.4, C			
11	50.6, C			
12	30.9, CH_2	a: 2.71, dd (18.7, 6.7) b: 2.32, bd (19.2)	13	6, 10, 11, 13, 14, 24
13	114.3, CH	5.54, d (6.4)	12	11, 12, 15, 19
14	143.6, C			
15	139.5, C			
16	123.9, CH	5.83, t (4.2)	17	10, 14, 17, 18
17	24.4, CH_2	a: 2.28, m b: 2.18, m	16, 18	15, 16, 18, 19
18	37.3, CH_2	1.42, m	17	14, 16, 17, 19, 20
19	34.9, C			
20	29.2, CH_3	1.05, s		14, 18, 19, 25
21	23.4, CH_3	1.32, s		N_2, 2, 3, 4
22	23.8, CH_3	1.04, s		2, 6, 7, 8
23	27.2, CH_3	1.23, s		9, 10, 11, 15
24	177.4, C			
25	28.4, CH_3	1.05, s		4, 18, 19, 20
4-OMe	57.4, CH_3	3.44, s		4
24-OMe	51.6, CH_3	3.65, s		24
1'	152.9, C			
N_1	94.5, NH			
N_2	98.0, NH			

Table S8. NMR data of Pentaprenylguanidine (**8**) in CD_3OD.

No	δ_C [ppm]	δ_H [ppm], mult (J)	HHCOSY	HMBC (H→C)
1'	158.7, C			
1	40.4, CH_2	3.71, d (6.8)	2	1', 2, 3
2	119.2, CH	5.20, tq (9.8, 1.1)	1	1, 4, 21
3	142.9, C			
4	40.7, CH_2	2.00, m		2, 5
5	27.5, CH_2	2.07, m		3, 4, 6, 7
6	125.1, CH	5.06, m		5
7	136.7, C			
8	41.0, CH_2	1.91, m	9	6, 10, 22
9	28.0, CH_2	2.01, m	8, 10	7, 11
10	125.6, CH	5.03, m	9	8, 12, 23
11	136.1, C			
12	41.0, CH_2	1.91, m	13	10, 14, 23
13	27.7, CH_2	2.01, m	12, 14	11, 15
14	125.6, CH	5.03, m	13	12, 16, 24
15	136.0, C			
16	41.0, CH_2	1.91, m	17	14, 18, 24
17	27.8, CH_2	2.01, m	16, 18	15, 19
18	125.6, CH	5.03, m	17	16, 20, 25
19	132.2, C			
20	17.9, CH_3	1.52, bs		18, 19, 25
21	16.6, CH_3	1.65, bs		2, 3, 4
22	16.3, CH_3	1.54, bs		6, 7, 8
23, 24	16.3, CH_3	1.52, bs		10, 11, 12, 14, 15, 16
25	26.1, CH_3	1.59, bs		18, 19, 20

Table S9. ^{1}H NMR ($CDCl_3$) data of Darumycin F **(6)** (*S*)-MTPA ester and Darumycin F (*R*)-MTPA ester) and their $\Delta\delta_{S-R}$ values.

	Darumycin F (*S*)-MTPA ester δ_H (*J* in Hz)	Darumycin F (*R*)-MTPA ester δ_H (*J* in Hz)	$\Delta\delta_{S-R}$ (δS -δR)
1	5.80 s	5.88 s	- 0.08
4	4.81 dd (11.5, 3.5)	4.76 dd (11.5, 3.5)	+0.05
5	2.02 m	2.18 m	- 0.16
	1.42 m	1.68 m	- 0.26
6	1.84 d (13)	1.89 d (13)	- 0.05
8	1.43 m	1.49 m	- 0.06
	1.11 m	1.14 m	- 0.03
9	2.20 m	2.21 m	- 0.01
	1.62	1.64 m	- 0.02
12	1.95 m	1.97 m	- 0.02
	1.71 m	1.72 m	- 0.01
13	1.96 m	1.97 m	- 0.01
	1.74 m	1.74 m	0.00
16	1.98 m (2H)	1.98 m (2H)	0.00
17	1.61 m	1.61 m	0.00
	1.44 m	1.44 m	0.00
18	1.43 m	1.43 m	0.00
	1.35 m	1.35 m	0.00
20	0.97 s (3H)	0.97 s (3H)	0.00
21	1.29 s (3H)	1.33 s (3H)	- 0.04
22	0.91 s (3H)	0.98 s (3H)	- 0.07
23	1.09 s (3H)	1.10 s (3H)	- 0.01
25	3.50 s (3H)	3.58 s (3H)	- 0.08
26	0.94 s (3H)	0.94 s (3H)	0.00

Table S10. Bacterial strains used in this work.

Strains	Description	Reference or Source
Micromonospora rubida JCM 32386	Type strain	Japan Collection of Microorganisms, RIKEN BRC
S. albus Del14	Cluster-free heterologous host strain	[254]
S. lividans DelYA9	Cluster-free heterologous host strain	[255]
S. albus Del14 cos15AAmInt-5E12	S. *albus* strain Del14 containing the cos15AAmInt-5E12 vector	This work
S. lividans ΔYA9 cos15AAmInt-5E12	*S. lividans* ΔYA9 containing the cos15AAmInt-5E12 vector	This work
S. albus Del14 cos15AAmInt-5E12del-darG	S. *albus* strain Del14 containing the cos15AAmInt-5E12del-darG vector, with the deletion of the methyltransferase *darG* gene	This work
S. albus Del14 cos15AAmInt-5E12del-darM	S. *albus* strain Del14 containing the cos15AAmInt-5E12del-darM vector, with the deletion of the methyltransferase *darM* gene	This work
S. albus Del14 cos15AAmInt-5E12del-darA	S. *albus* strain Del14 containing the cos15AAmInt-5E12del-darA vector, with the deletion of the cyclase *darA* gene	This work
S. albus Del14 cos15AAmInt-5E12del-darC	S. *albus* strain Del14 containing the cos15AAmInt-5E12del-darC vector, with the deletion of the cytochrome P450 oxygenase *darC* gene	This work
S. albus Del14 cos15AAmInt-5E12del-darG/darM	S. *albus* strain Del14 containing the cos15AAmInt-5E12del-darG/darM vector, with the double deletion of the *darG* and *darM* genes	This work
S. albus Del14 cos15AAmInt-5E12del-darK	S. *albus* strain Del14 containing the cos15AAmInt-5E12del-darK vector, with the deletion of the hypothetical protein *darK* gene	This work
S. albus Del14 cos15AAmInt-5E12del-darL	S. *albus* strain Del14 containing the cos15AAmInt-5E12del-darL vector, with the deletion of the hypothetical protein *darL* gene	This work
S. albus Del14 cos15AAmInt-5E12del-darC/darG	S. *albus* strain Del14 containing the cos15AAmInt-5E12del-darC/darG vector, with the double deletion of the *darC* and *darG* genes	This work

S. lividans ΔYA9 cos15AAmInt-5E12del-darA	*S. lividans* ΔYA9 containing the cos15AAmInt-5E12del-darA vector, with the deletion of the cyclase *darA* gene	This work
E. coli ET12567 pUB307	Donor strain for intergeneric conjugation	[274]
E. coli GB05-red	Strain used for Red/ET	[275]
E.coli EPI300-T1R	Strain used for Construction of inducible-copy-number genomic libraries using the CopyControl™ Cloning System, with clones that are resistant to contaminating phage T1 and T5	Lucigen

Table S11. Plasmids used in this work.

Plasmids	**Description**	**Reference or Source**
pCos15A_AmInt	pCos15A_gus_AmInt, with *aac(3)IV*, *oriT*, and integrase, where *gus* gene was deleted	[300]
pUC19	Plasmid containing *bla* gene, which encodes a β-lactamase enzyme (ampicillin resistance gene)	[351]
pCos15AAmInt-5E12	Cosmid 5E12 containing darumycin gene cluster	This work
cos15AAmInt-5E12-darG-del	Cosmid 5E12 containing darumycin gene cluster with *darG* (methyltransferase) gene deletion	This work
cos15AAmInt-5E12-darM-del	Cosmid 5E12 containing darumycin gene cluster with *darM* (methyltransferase) gene deletion	This work
cos15AAmInt-5E12-darG/darM-del	Cosmid 5E12 containing darumycin gene cluster with *darG/darM* (both methyltransferases) genes deletion	This work
cos15AAmInt-5E12-darA-del	Cosmid 5E12 containing darumycin gene cluster with *darA* (cyclase) gene deletion	This work
cos15AAmInt-5E12-darC-del	Cosmid 5E12 containing darumycin gene cluster with *darC* (cytochrome P450 oxygenase) gene deletion	This work
cos15AAmInt-5E12-darC/darG-del	Cosmid 5E12 containing darumycin gene cluster with *darC/darG* (cytochrome P450 oxygenase and methyltransferase) genes deletion	This work
cos15AAmInt-5E12-darK-del	Cosmid 5E12 containing darumycin gene cluster with *darK* (hypothetical protein) gene deletion	This work
cos15AAmInt-5E12-darL-del	Cosmid 5E12 containing darumycin gene cluster with *darL* (lysylphosphatidylglycerol synthase) gene deletion	This work

Table S12. Primers used in this work.

Primer name	Sequence (5'-3')	Description	Source
cos_5E12_L_F cos_5E12_L_R	GCTGCTGTCATTGGTGTGC GCAGGACCTCATCGACGA	To sequence the insert containing the darumycin cluster from the left side of the cluster	This work
cos_5E12_R_F cos_5E12_R_R	TTCAGACCGAAGTTGCCCAA GCCTCATCTGGAAGTGGGAC	To sequence the insert containing the darumycin cluster from the right side of the cluster	This work
rubida_groF_F rubida_groF_R	GCAGTTGGACGGCGATGA TCGAATTCAACGACCCGGAC	To test for *groF* homolog gene presence	This work
rubida_groH_F rubida_groH_R	GCGGTAGATGATTCCCACGT TCTTCCGGGAGTACGTGACC	To test for *groH* homolog gene presence	This work
del-MT1-F del-MT1-R	CGAGGACATGCTCGGCGACAGT CATCACTTCGGGTACTTCCCGGA CGGCGGTTTAAACAGCTGTTCCG GGGATCCGTC ATGAGCCCCCGCACCTCCTGCGC GTAGTCGCCCAGCGCCGAGATC CGCTCGTTTAAACTGTAGGCTGG AGCTGCTTCG	For construction of cos15AAmInt-5E12-darG-del	This work
del-MT2-F-Bst del-MT2-R-Bst	TCAAACCGGTCGGCAGCAGGCT CGTCGGCCACGCGGCGGTAGCG CCTGGTGTATACCGTCAGGTGGC ACTTTTCG AGCAGACCGGGTTCGTGAGCCG GATACAACCGTCGGCGTCCCGCC GGGTGGTATACTTACCAATGCTT AATCAGTG	For construction of cos15AAmInt-5E12-darM-del	This work
del-cycl-F del-cycl-R	TAGAGATAGTTGACCAGGGGCG TCAGCGGATAGTCCTGGTGCGTC ACGCTGTTTAAACCGTCAGGTGG CACTTTTCG	For construction of cos15AAmInt-5E12-darA-del	This work

	CTACCGCGGCTTCAAGGAACAC ACCTACGGGATGCCGATCGCGG CGCTGGGTTTAAACTTACCAATG CTTAATCAGTG		
del-P_450-F del-P_450-R	GTGGCCTCGACGTAGCTGAACTG GTCGCCGATGCACTTGCGGGCGC CGCCGTTTAAACCGTCAGGTGGC ACTTTTCG CCTCACGCTCGGGCCGGTGCGG ATCGTGGTCGTCTGCGACCCGGA ACTCAGTTTAAACTTACCAATGC TTAATCAGTG	For construction of cos15AAmInt-5E12-darC-del	This work
del-ubiq-F del-ubiq-R	TGCCCGGCGACGACCCCTCCGTC GTCCCGTGGTACGTCCGGCTCCT GGAGGTTTAAACCGTCAGGTGG CACTTTTCG TGGCGTAGAAGCGGAGCAGGTC AGGGGTGTGGATGCCCAACTTC GCCCGAGTTTAAACTTACCAATG CTTAATCAGTG	For construction of cos15AAmInt-5E12-darK-del	This work
del-LysP-F del-LysP-R	CTCAACCTTGTCGCCCAGGTCGT CCGGGCCGGCAGTTGGGTGGTG ATGCTGTTTAAACCGTCAGGTGG CACTTTTCG GGAACAGCAGCGCAAAACCGAG GGCGGCGTCCGGCGCGACGTGC AGCAGAGTTTAAACTTACCAATG CTTAATCAGTG	For construction of cos15AAmInt-5E12-darL-del	This work
chk-MT1-del-F chk-MT1-del-R	GAGGTGGTGGTGAAGGAGTT ACCAGGTAGACCCCGAACT	To confirm *darG* gene deletion	This work
chk-MT2-del-F chk-MT2-del-R	AACCTGGGCACGTTCGAG CAATCGTCCGGCTGCCAC	To confirm *darM* gene deletion	This work
chk-cyclase-del-F chk-cyclase-del-R	CGGACCAGATCGCATAGGC GAGCACTACACACAGGACGT	To confirm *darA* gene deletion	This work
chk-P450-del-F chk-P450-del-R	GCCTCGAACTTGCCCTTGTA TGAGCTGGGAAAACGGTGAG	To confirm *darC* gene deletion	This work
chk-LP-del-F chk-LP-del-R	GCTTCGCGGCTCACCAGA GTGCCAGGTCAATGCCGG	To confirm *darL* gene deletion	This work

chk-ubi-del-F chk-ubi-del-R	GACGTGTTGGTCGCCAGCTA GGACGCCCTCATGCTTGA	To confirm *darK* gene deletion	This work

Table S13. Toxicity profile of darumycin derivatives. In vitro cytotoxicity was evaluated performing a MTT assay (half maximal inhibitory concentration IC50 ± standard deviation). In vivo toxicity was assessed by determination of the maximum tolerated concentration (MTC) in zebrafish (*Danio rerio*) embryos. CHO, chinese hamster ovary; DOX, doxorubicin.

	In vitro IC_{50} [µg/mL]		*In vivo* MTC [µg/mL]
	HepG2	**CHO-K1**	***Danio rerio***
DarA	8.95 ± 3.6	> 37	5
DarB	> 37	> 37	10
DarC	5.5 ± 0.3	4.6 ± 0.05	1
DarD	14.7 ± 3.7	23.4 ± 0.03	1
DarE	> 37	> 37	> 25
DarF	17.5 ± 2.9	21.3 ± 1.8	5
DarG	14.3 ± 3.9	32.7 ± 1.5	1
Pentaprenylguanidine	4.65 ± 0.7	0.8 ± 0.05	1
DOX	0.1 ± 0.02	0.01	-

List of Figures

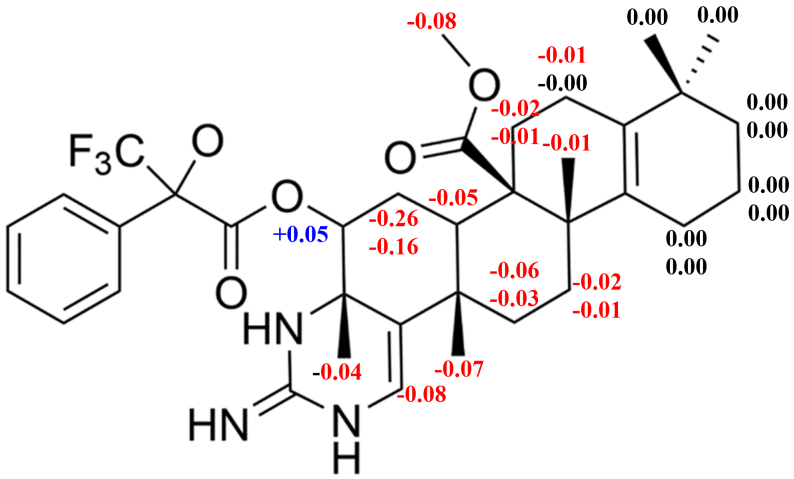

Figure S1. Structure of the Darumycin F **(6)** Mosher conjugate.

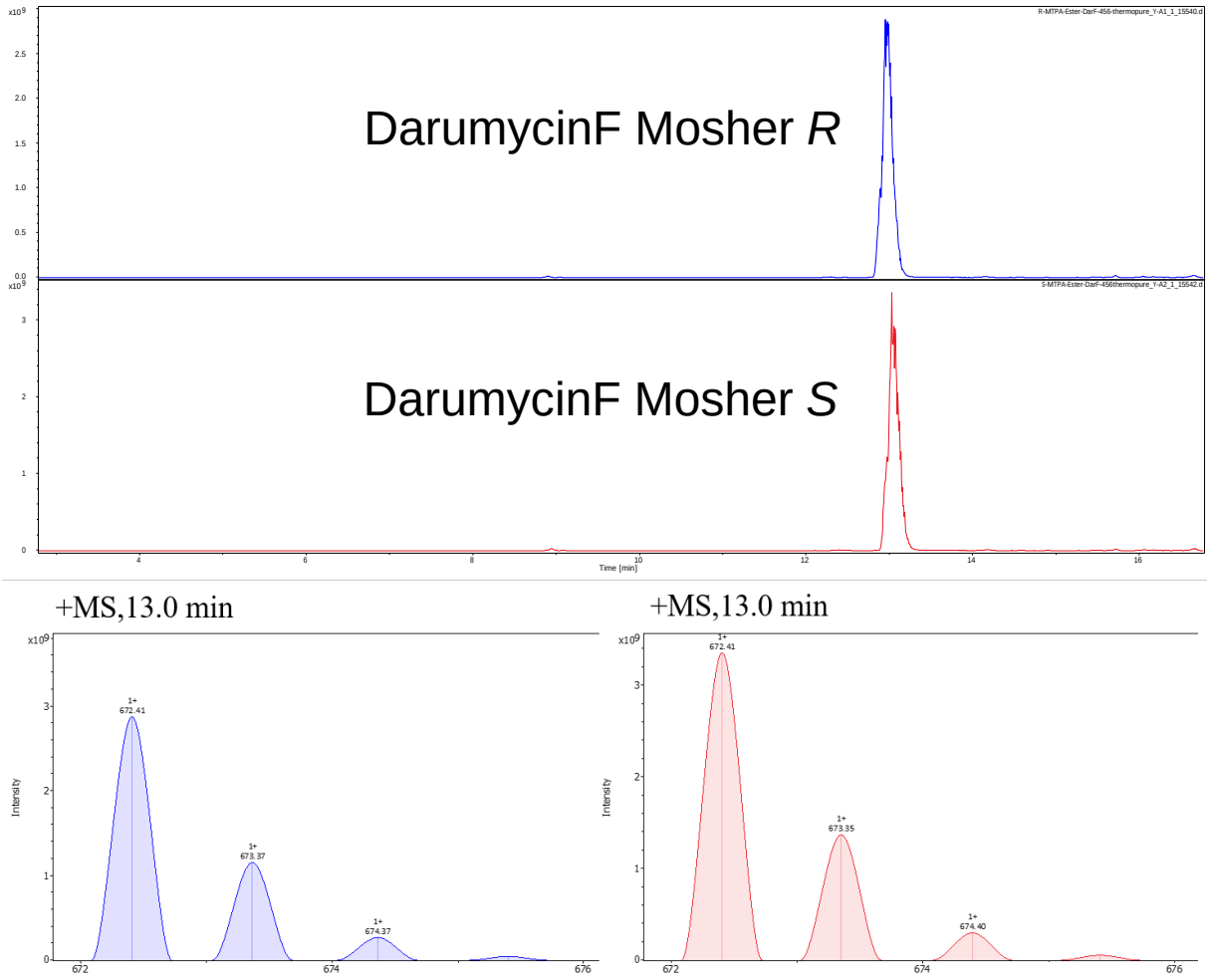

Figure S2. HPLC chromatogram, and mass spectra (*m/z*) of the Darumycin F **(6)** Mosher conjugate.

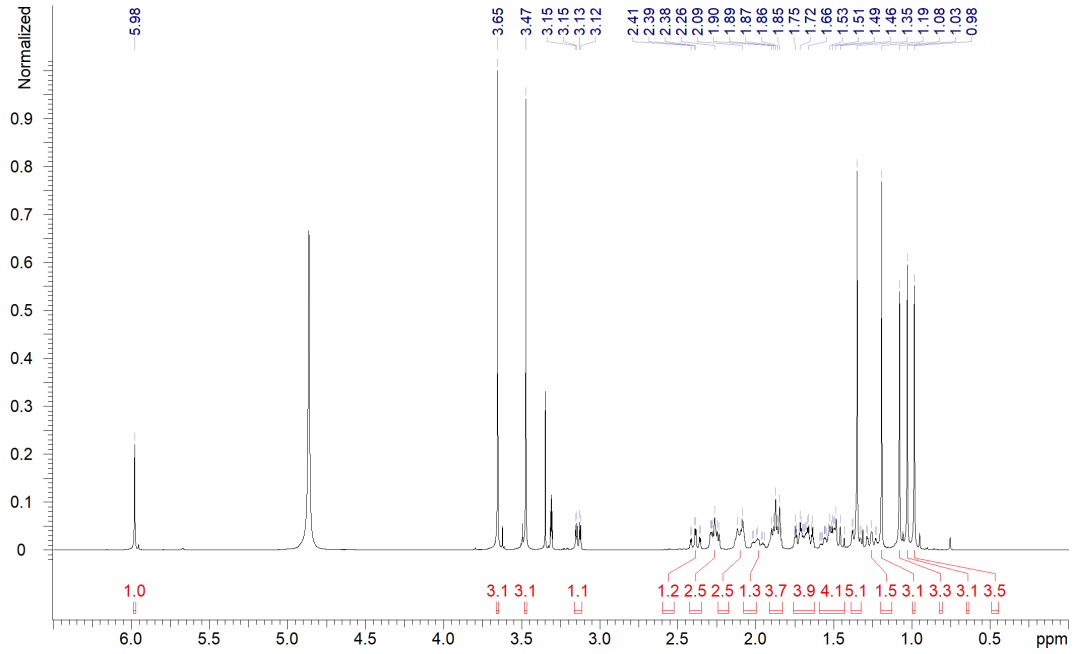

Figure S3. ^{1}H NMR spectrum (500MHz) of Darumycin A **(1)** in CD_3OH.

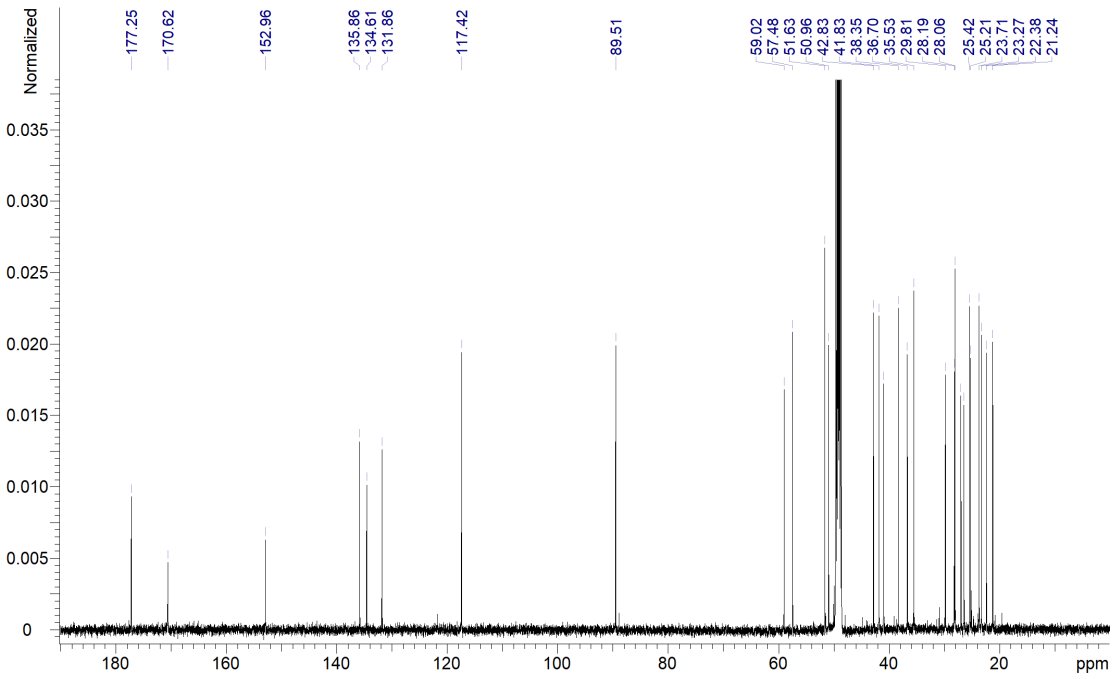

Figure S4. 13C NMR spectrum (125 MHz) of Darumycin A **(1)** in CD3OH.

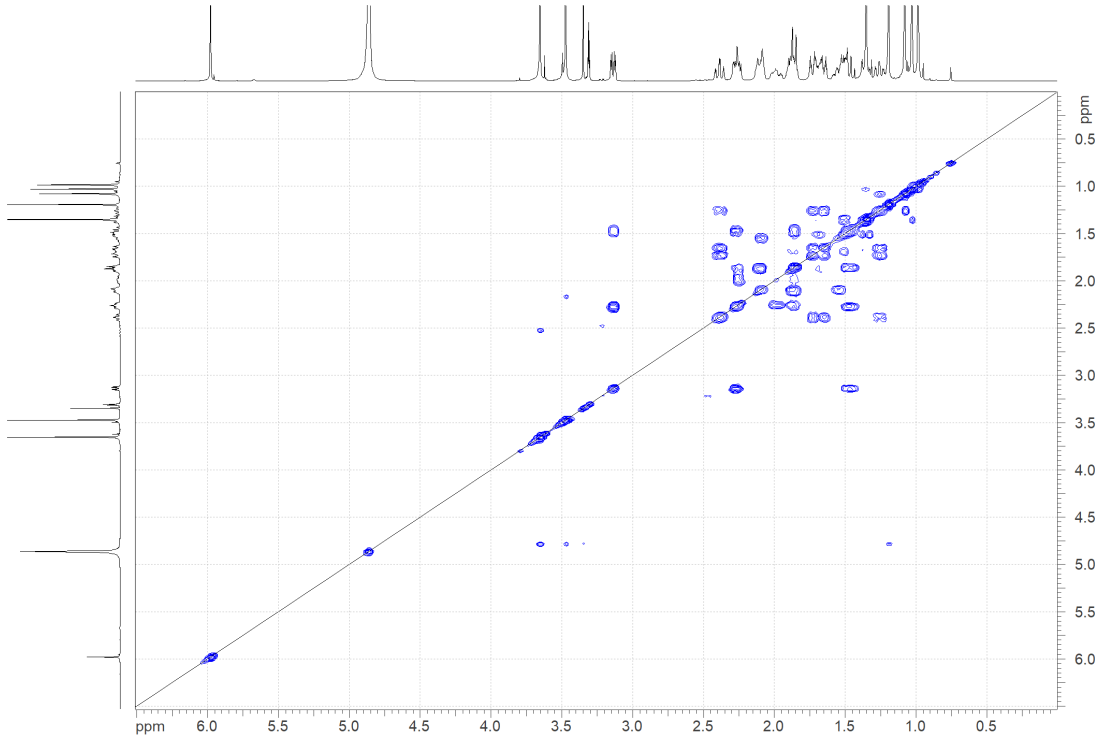

Figure S5. H-H COSY spectrum (500 MHz) of Darumycin A **(1)** in CD_3OH.

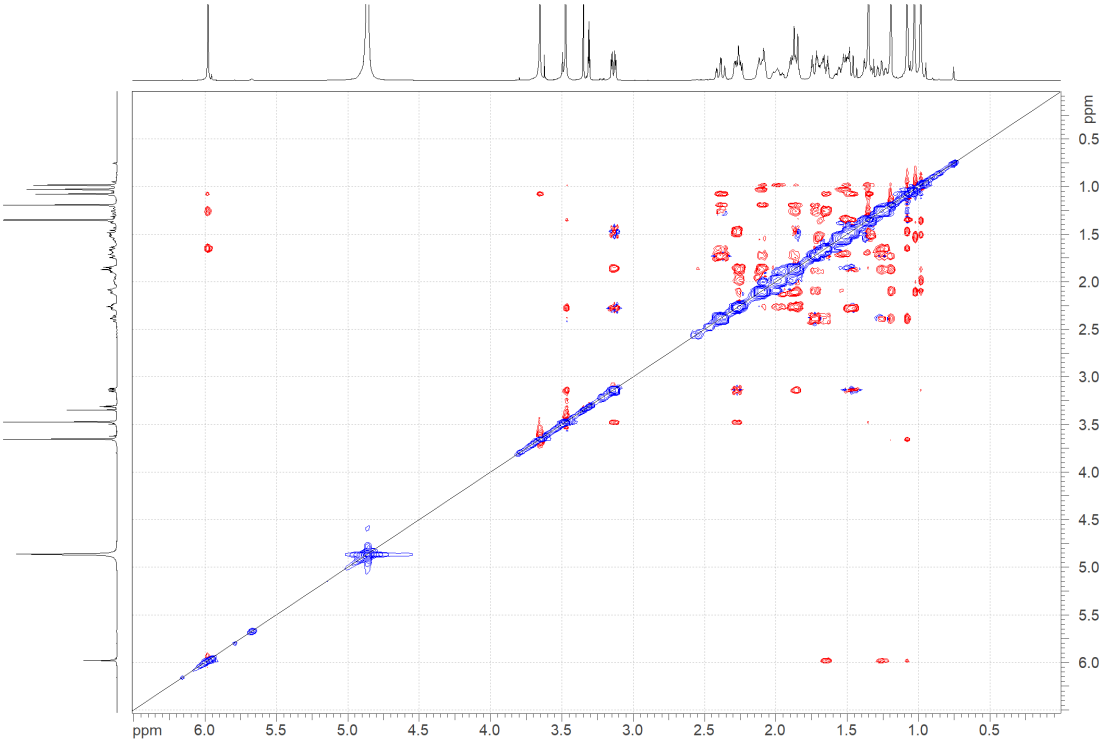

Figure S6. NOESY spectrum (500 MHz) of Darumycin A **(1)** in CD_3OH.

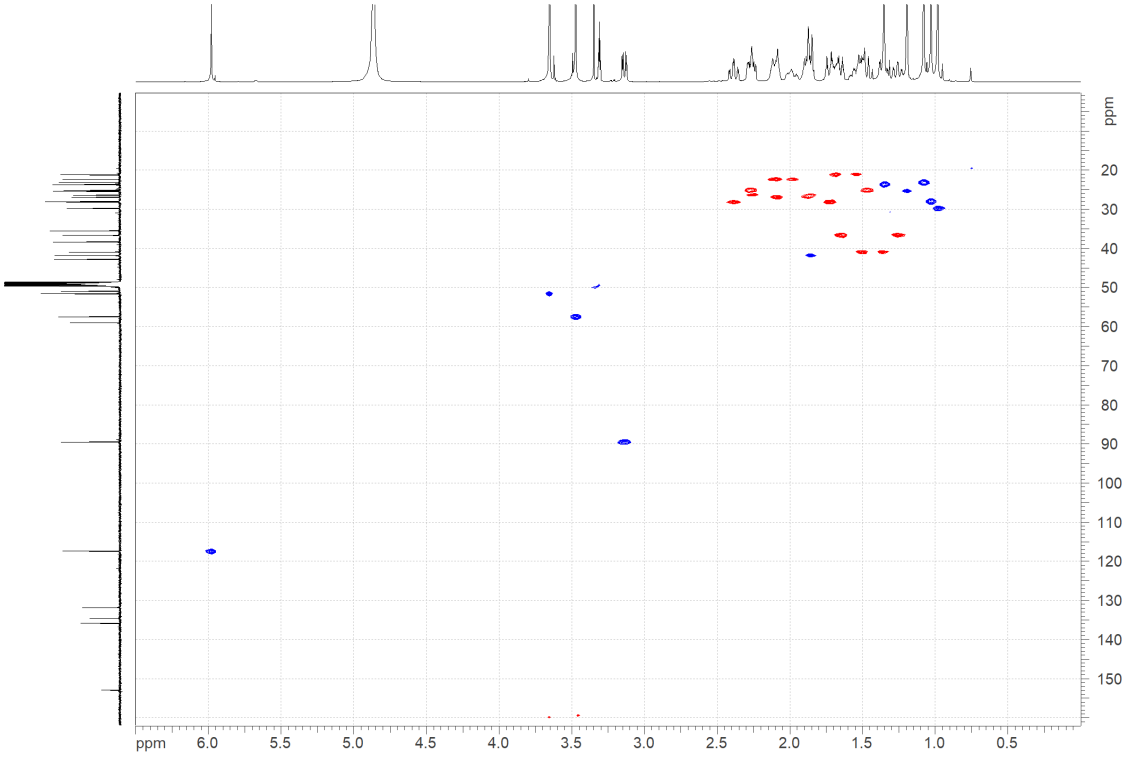

Figure S7. Edited HSQC spectrum (500 MHz) of Darumycin A **(1)** in CD_3OH.

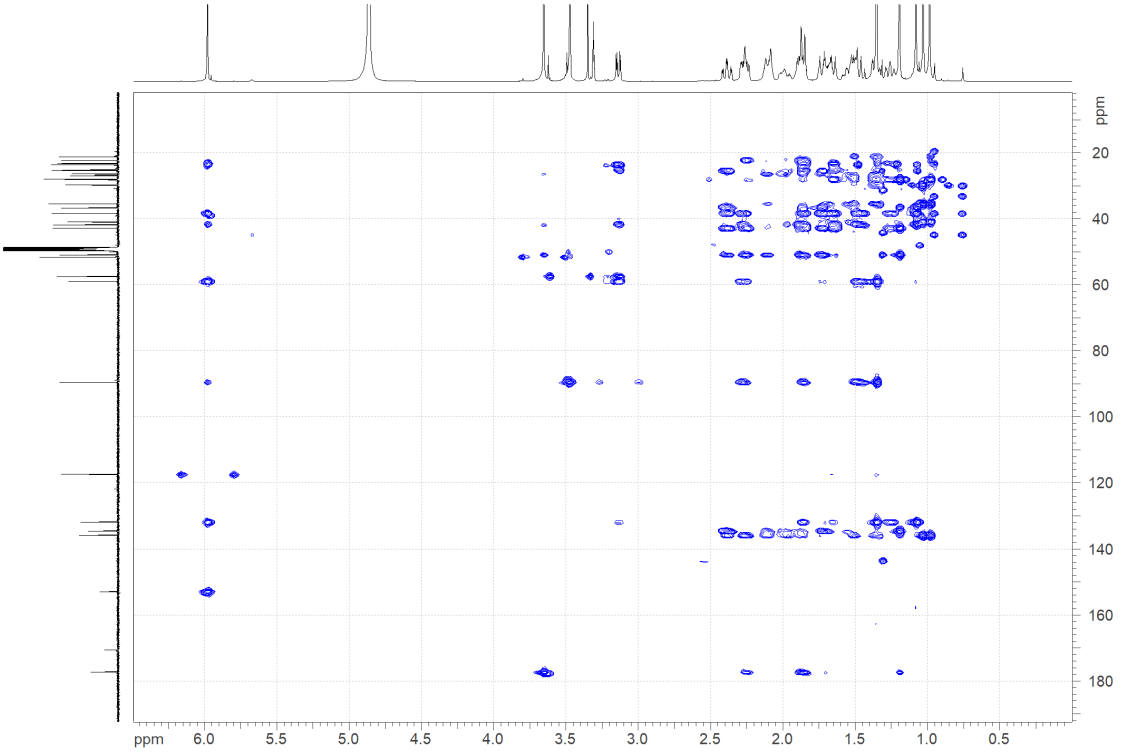

Figure S8. ^{13}C HMBC spectrum (500 MHz) of Darumycin A **(1)** in CD_3OH.

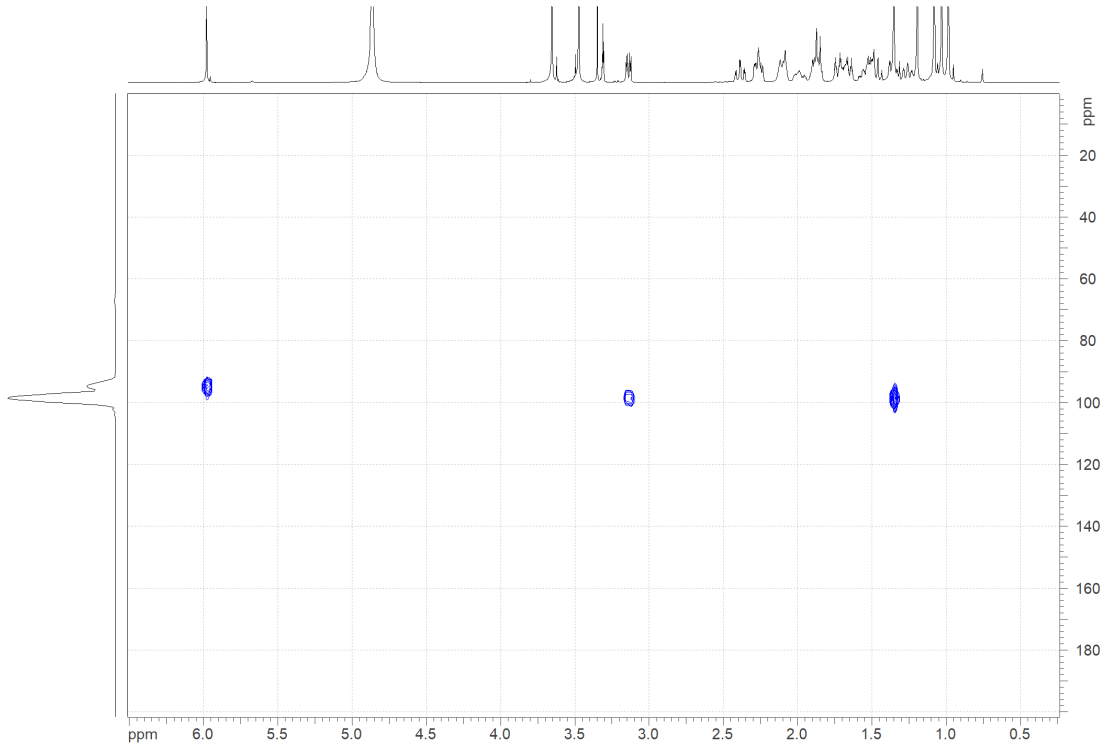

Figure S9. ^{15}N-HMBC spectrum (500 MHz) of Darumycin A **(1)** in CD_3OH.

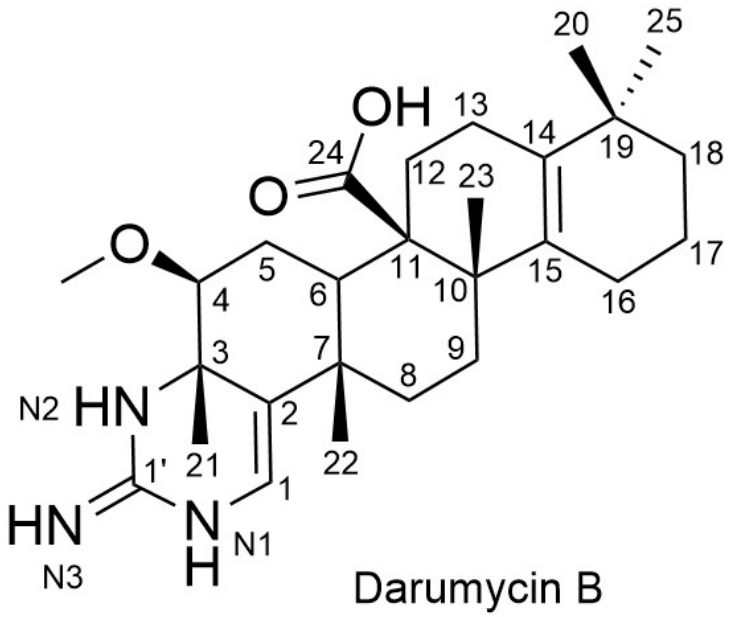

Figure S10. Structure of Darumycin B **(2)**.

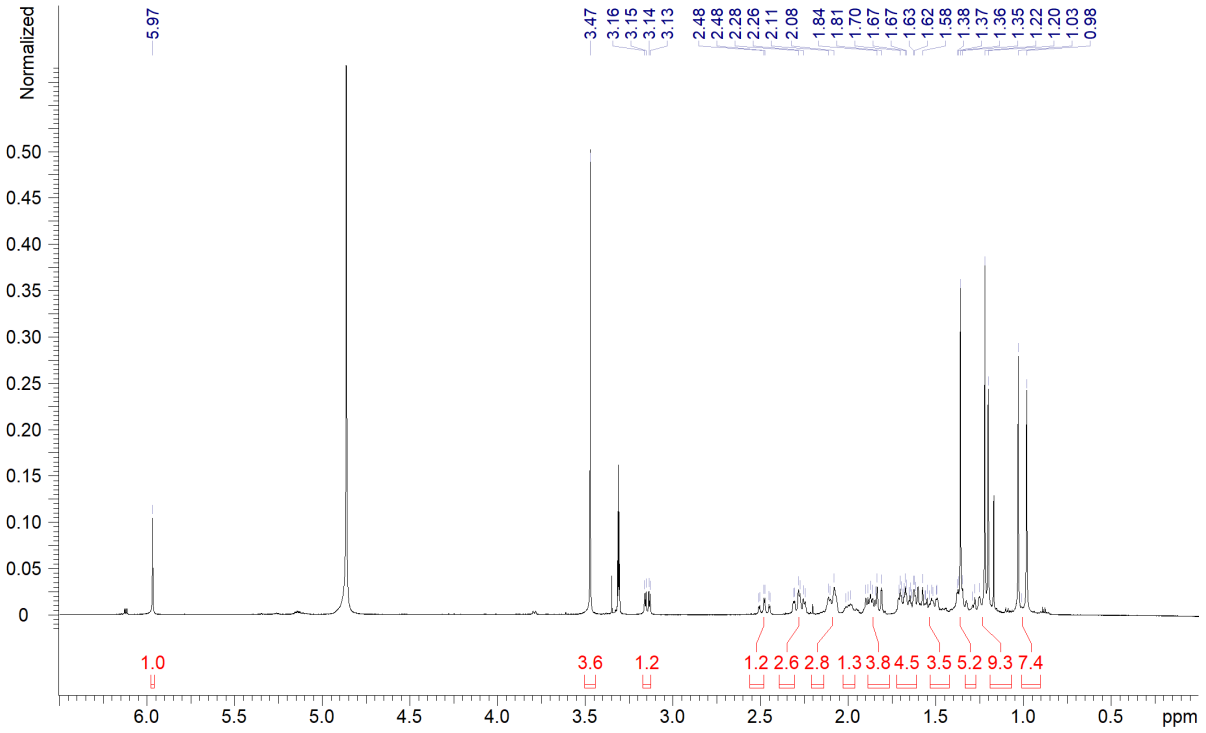

Figure S11. ^{1}H-NMR spectrum (500 MHz) of Darumycin B **(2)** in CD_3OD.

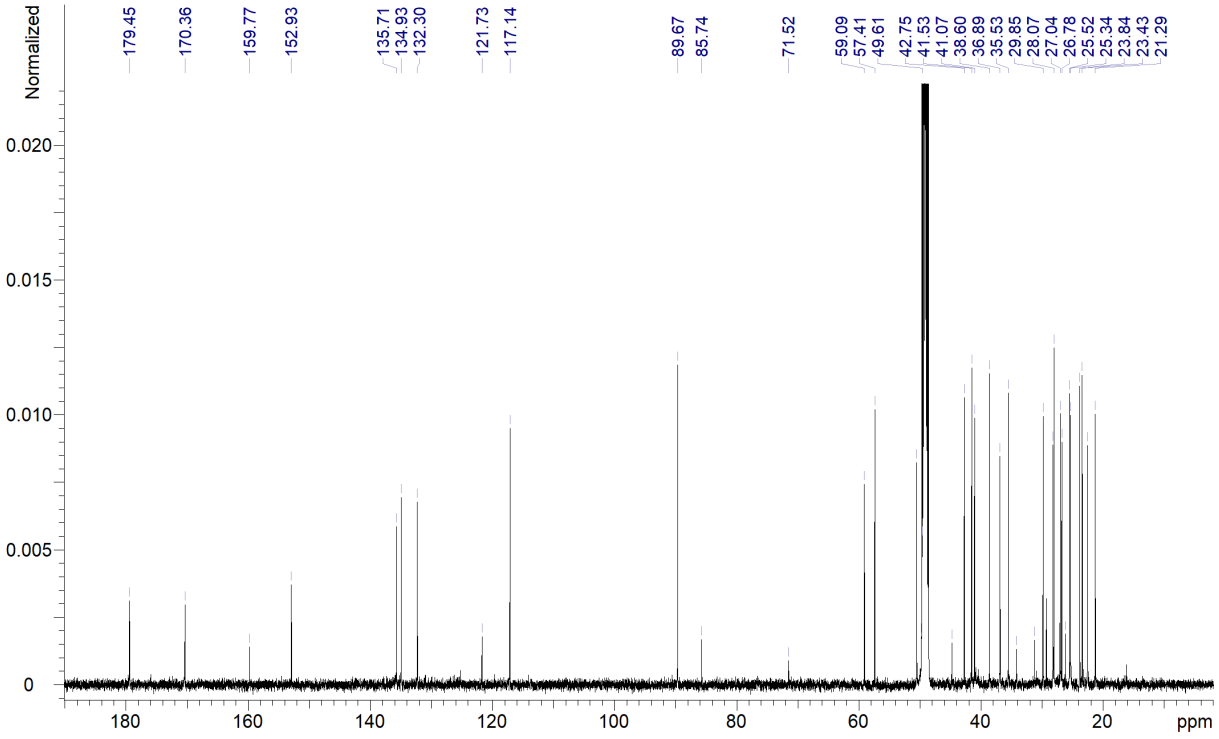

Figure S12. ^{13}C-NMR spectrum (125 MHz) of Darumycin B **(2)** in CD_3OD.

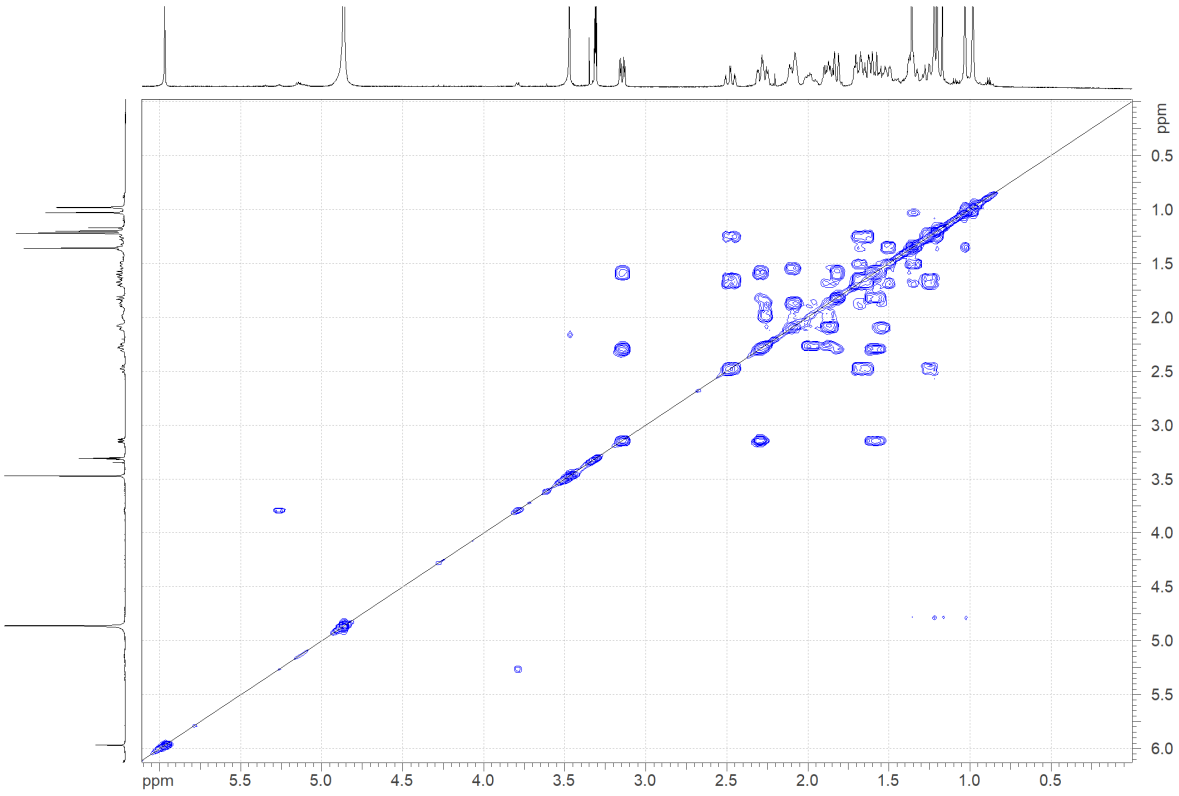

Figure S13. H-H COSY spectrum (500 MHz) of Darumycin B **(2)** in CD_3OD.

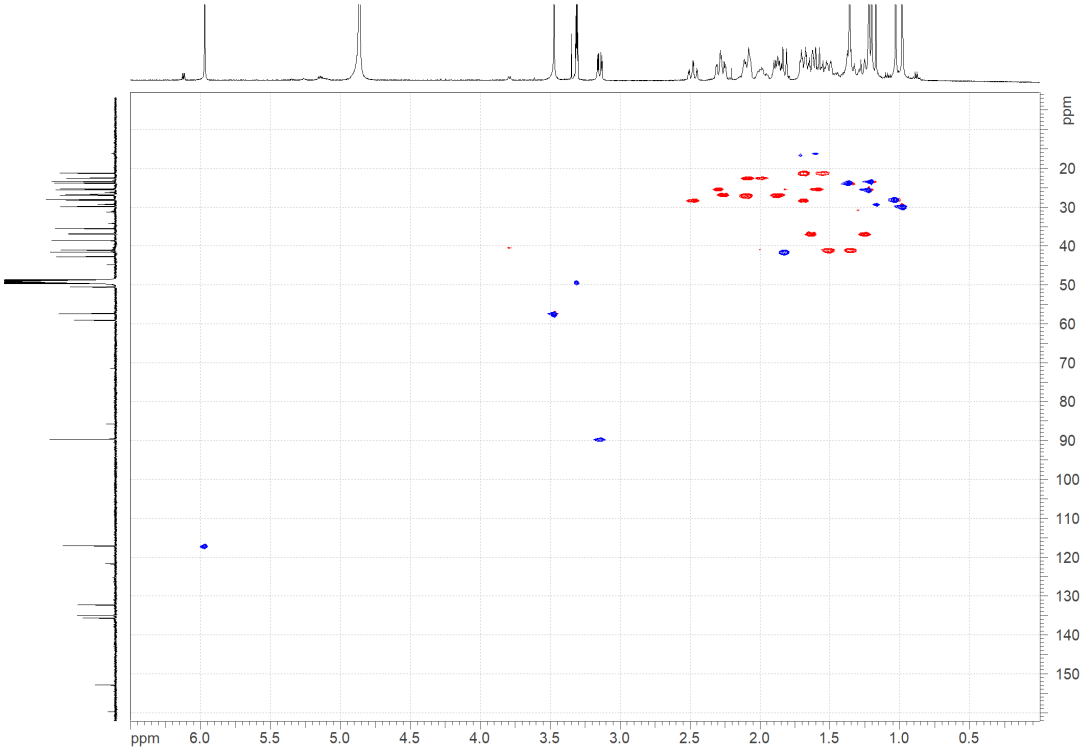

Figure S14. Edited HSQC spectrum (500 MHz) of Darumycin B **(2)** in CD_3OD.

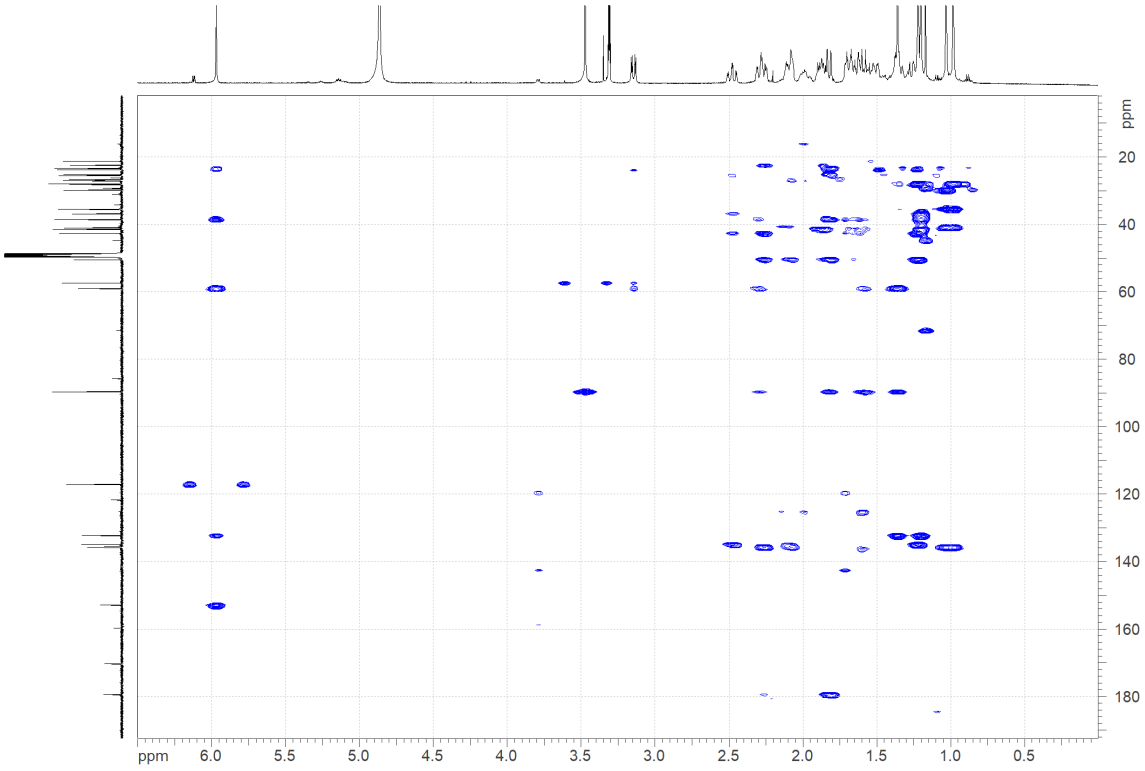

Figure S15. HMBC spectrum (500 MHz) of Darumycin B **(2)** in CD_3OD.

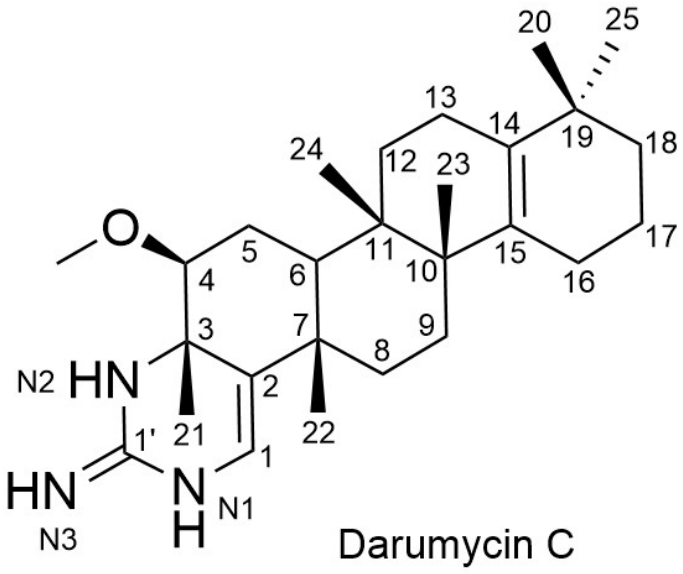

Figure S16. Structure of Darumycin C **(3)**.

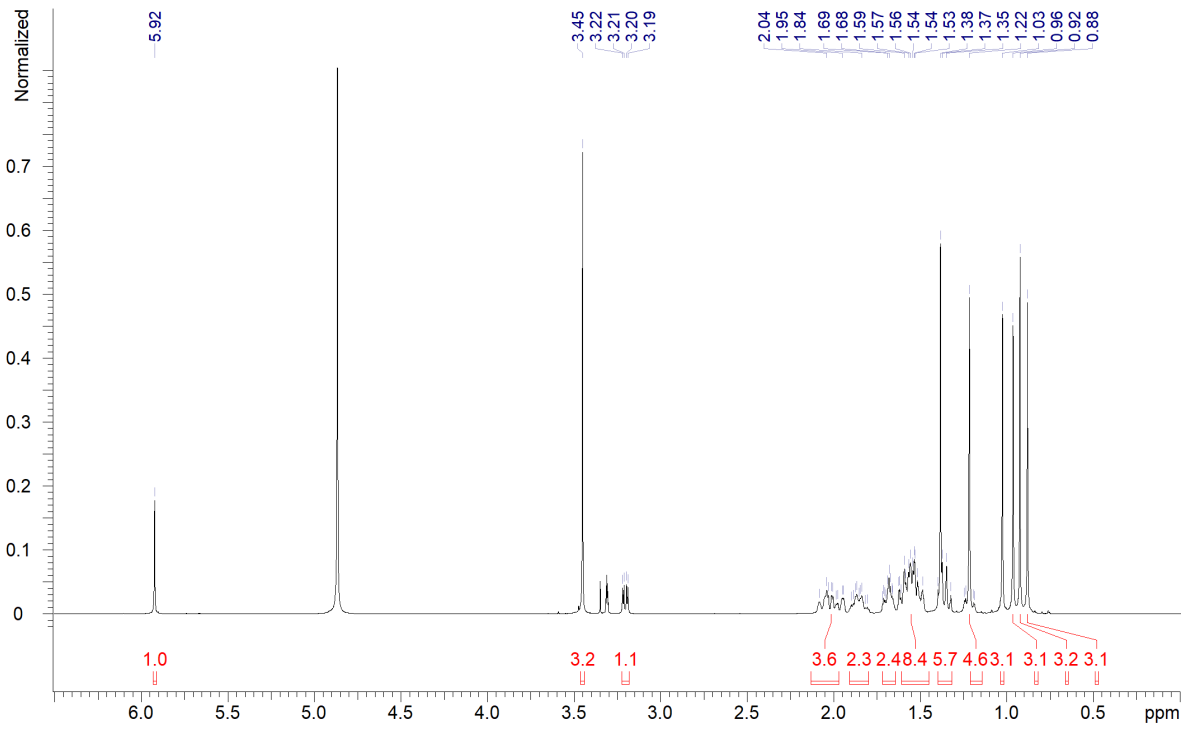

Figure S17. ^{1}H-NMR spectrum (500 MHz) of Darumycin C **(3)** in CD_3OD.

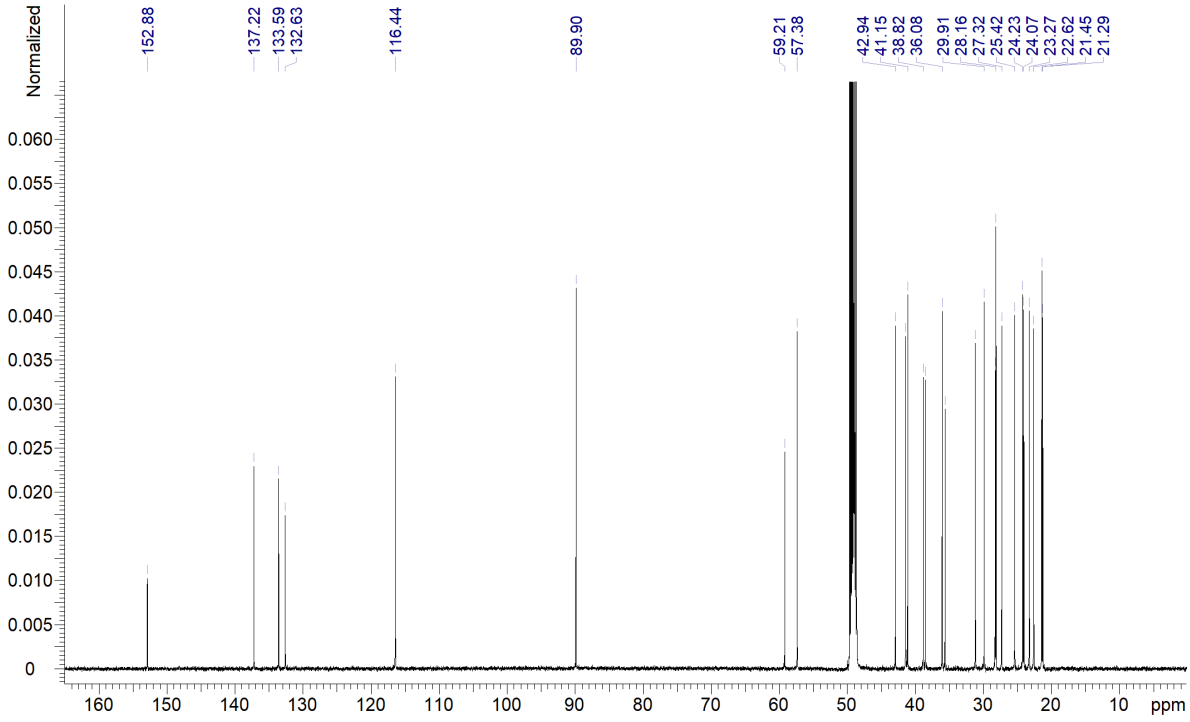

Figure S18. ^{13}C-NMR spectrum (125 MHz) of Darumycin C **(3)** in CD_3OD.

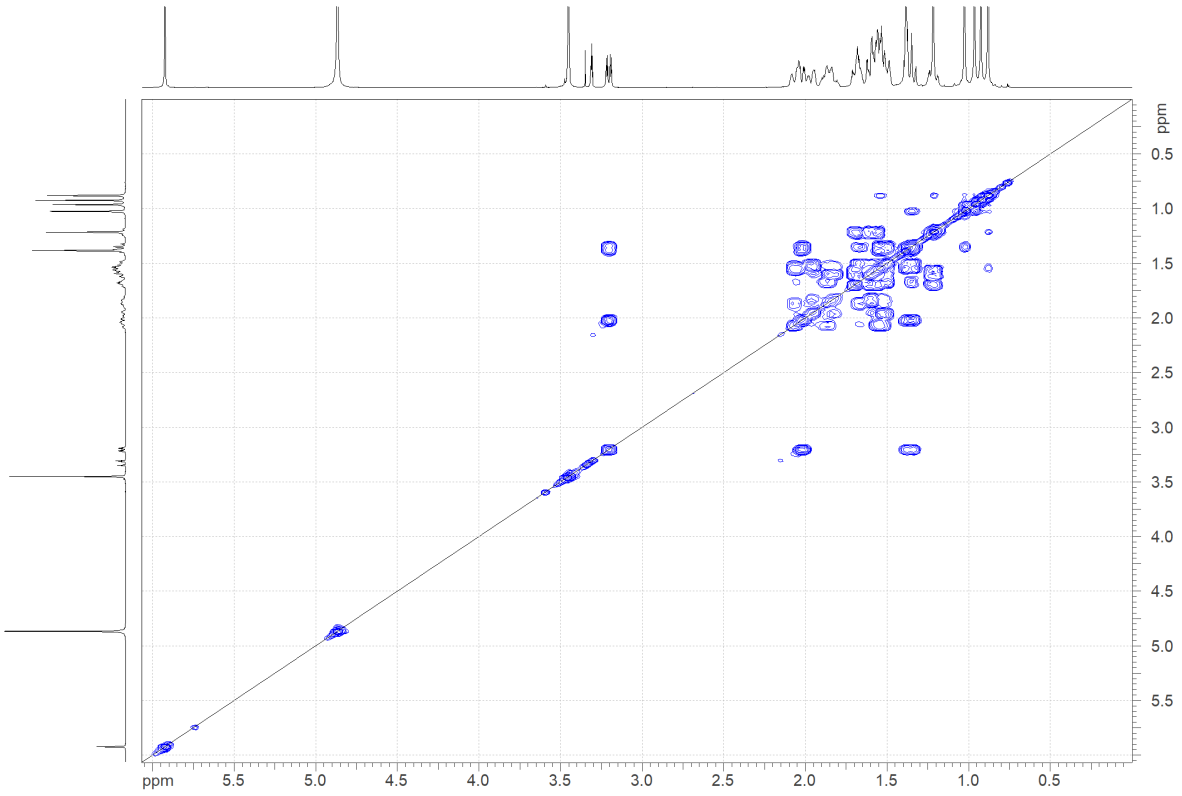

Figure S19. H-H COSY spectrum (500 MHz) of Darumycin C **(3)** in CD_3OD.

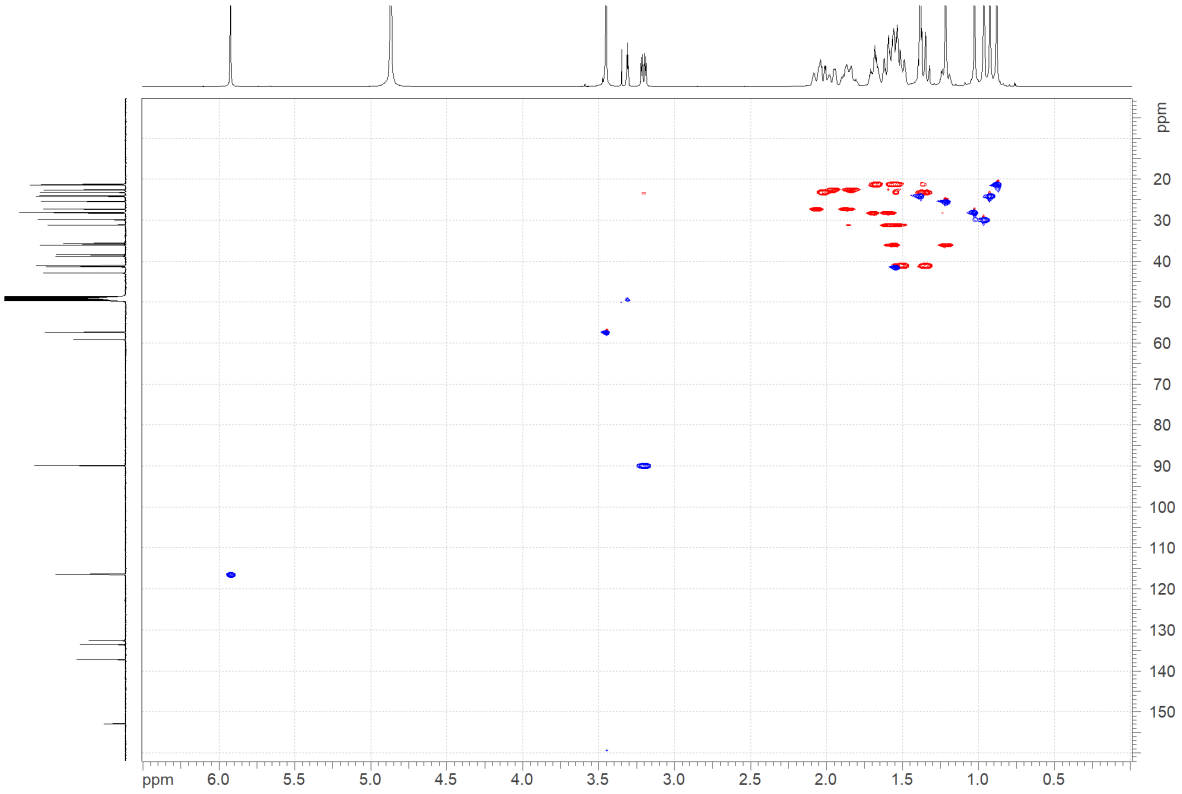

Figure S20. Edited HSQC spectrum (500 MHz) of Darumycin C **(3)** in CD_3OD.

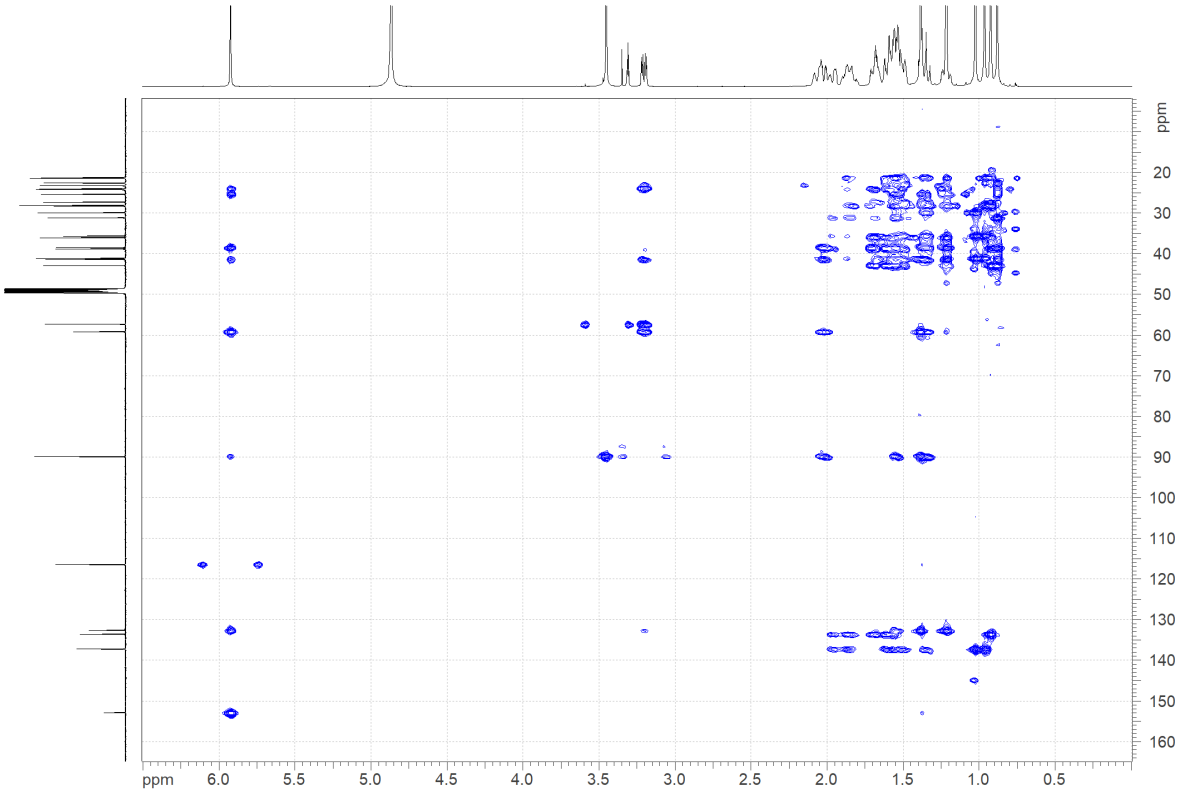

Figure S21. HMBC spectrum (500 MHz) of Darumycin C **(3)** in CD_3OD.

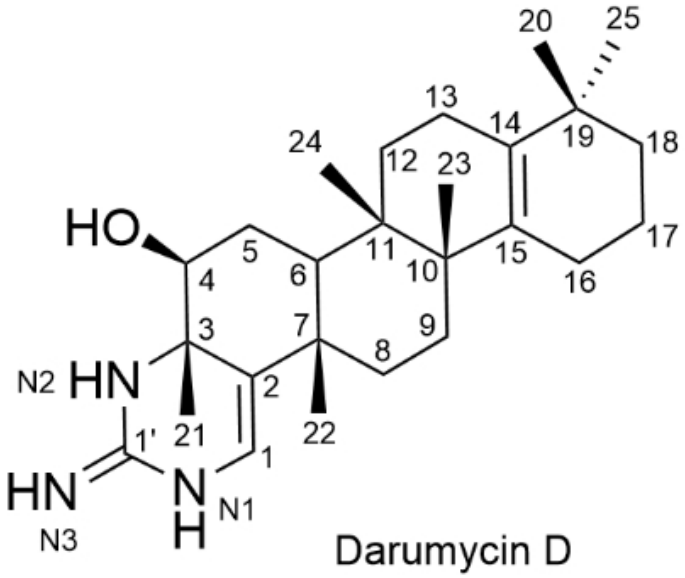

Figure S22. Structure of Darumycin D **(4)**.

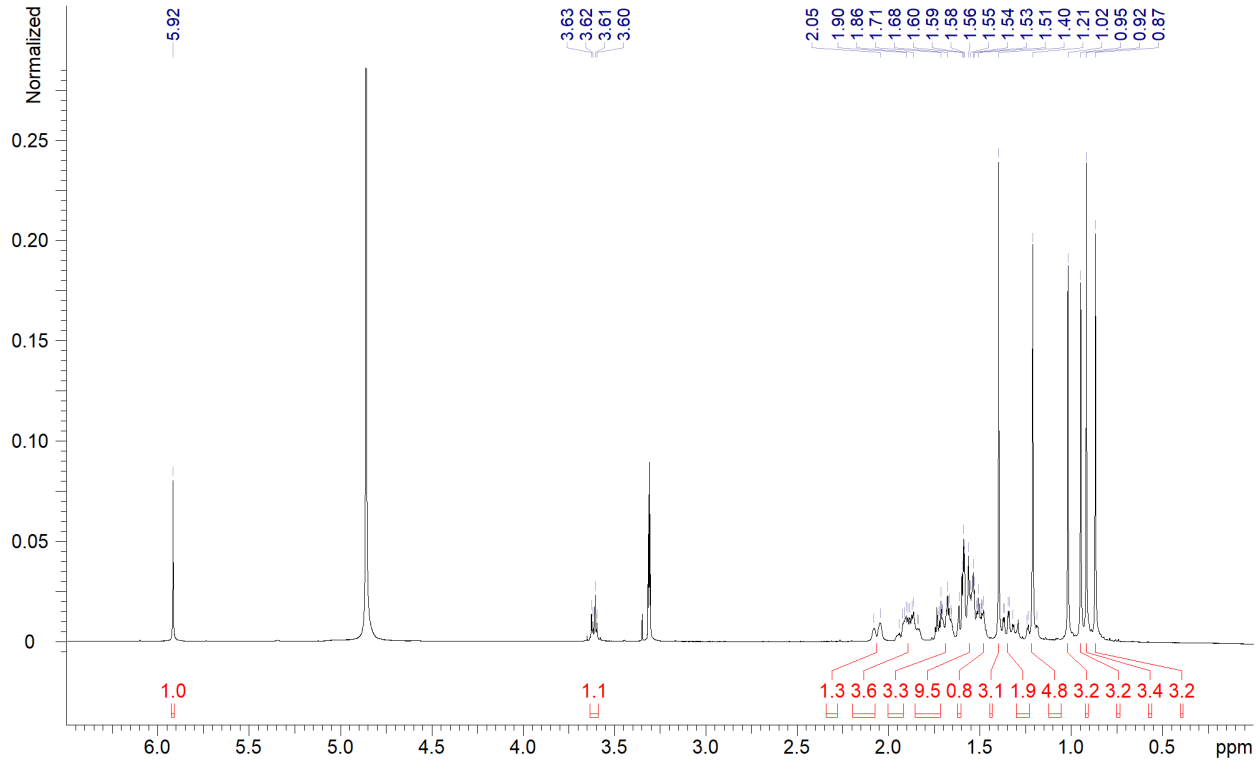

Figure S23. ^{1}H-NMR spectrum (500 MHz) of Darumycin D **(4)** in CD_3OD.

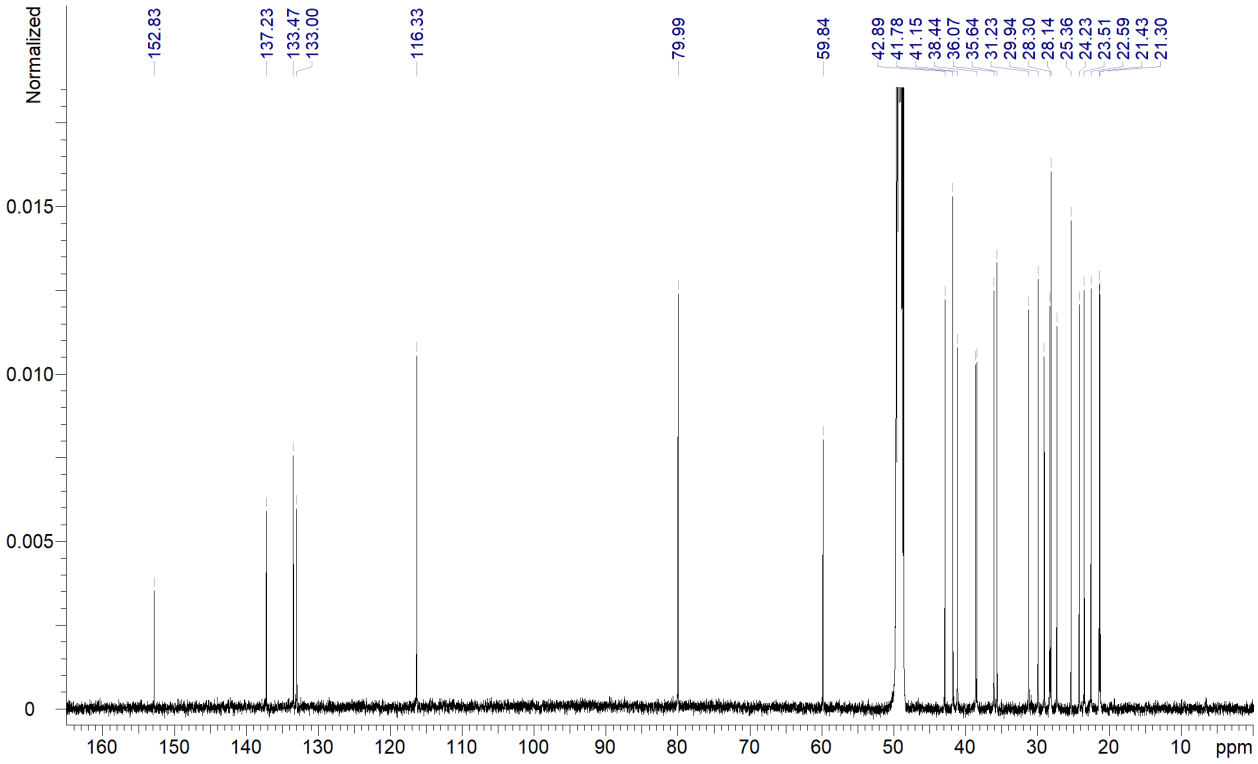

Figure S24. ^{13}C-NMR spectrum (125 MHz) of Darumycin D **(4)** in CD_3OD.

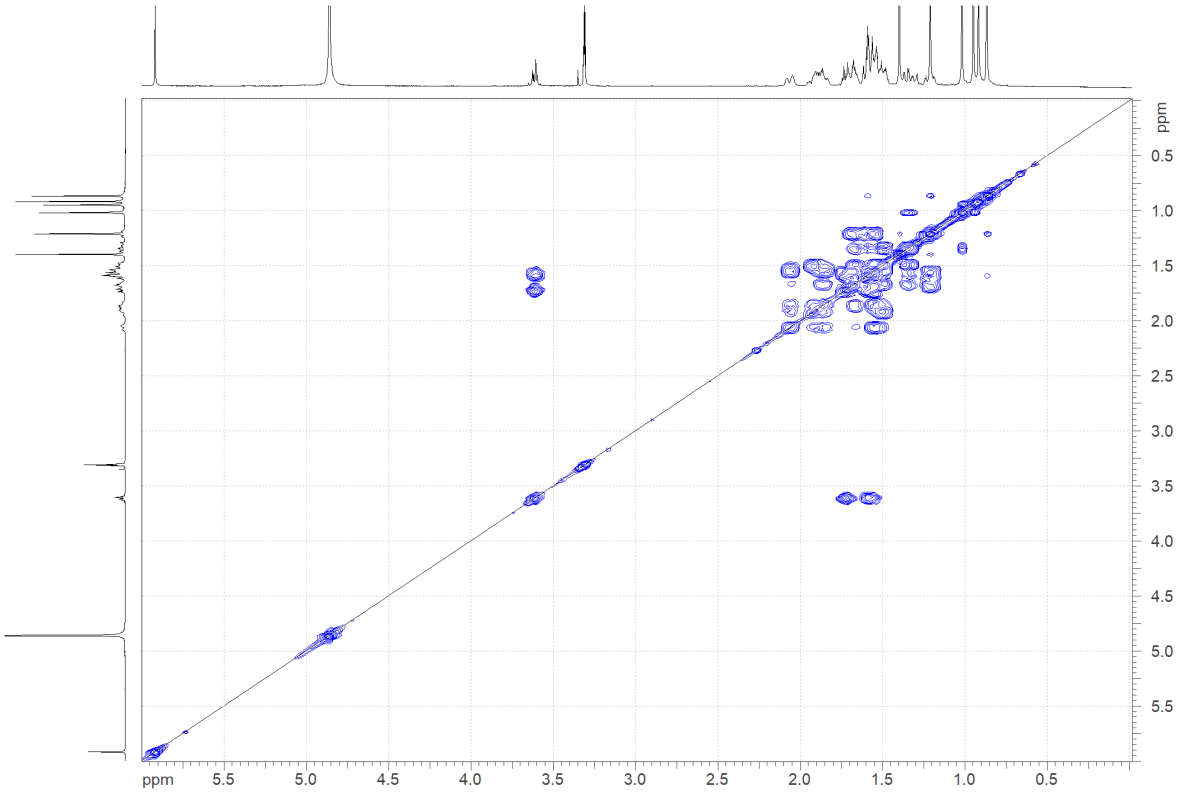

Figure S25. H-H COSY spectrum (500 MHz) of Darumycin D **(4)** in CD_3OD.

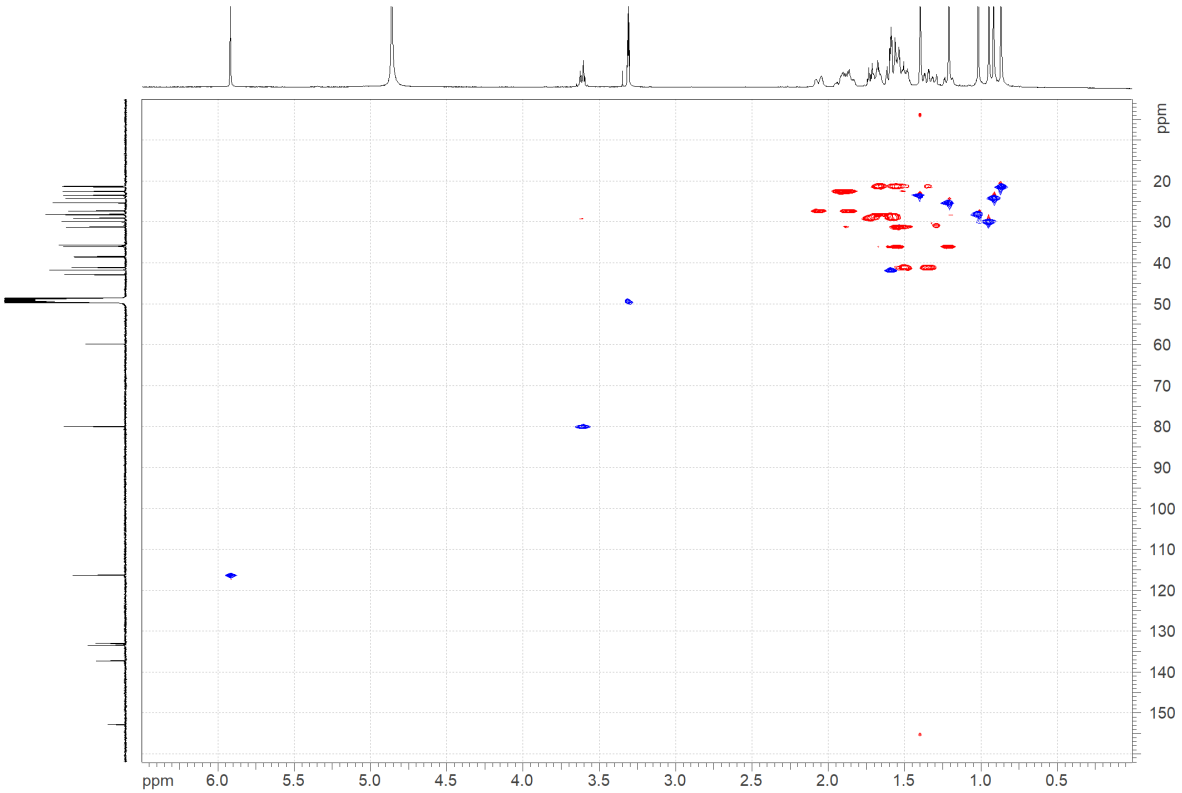

Figure S26. Edited HSQC spectrum (500 MHz) of Darumycin D **(4)** in CD_3OD.

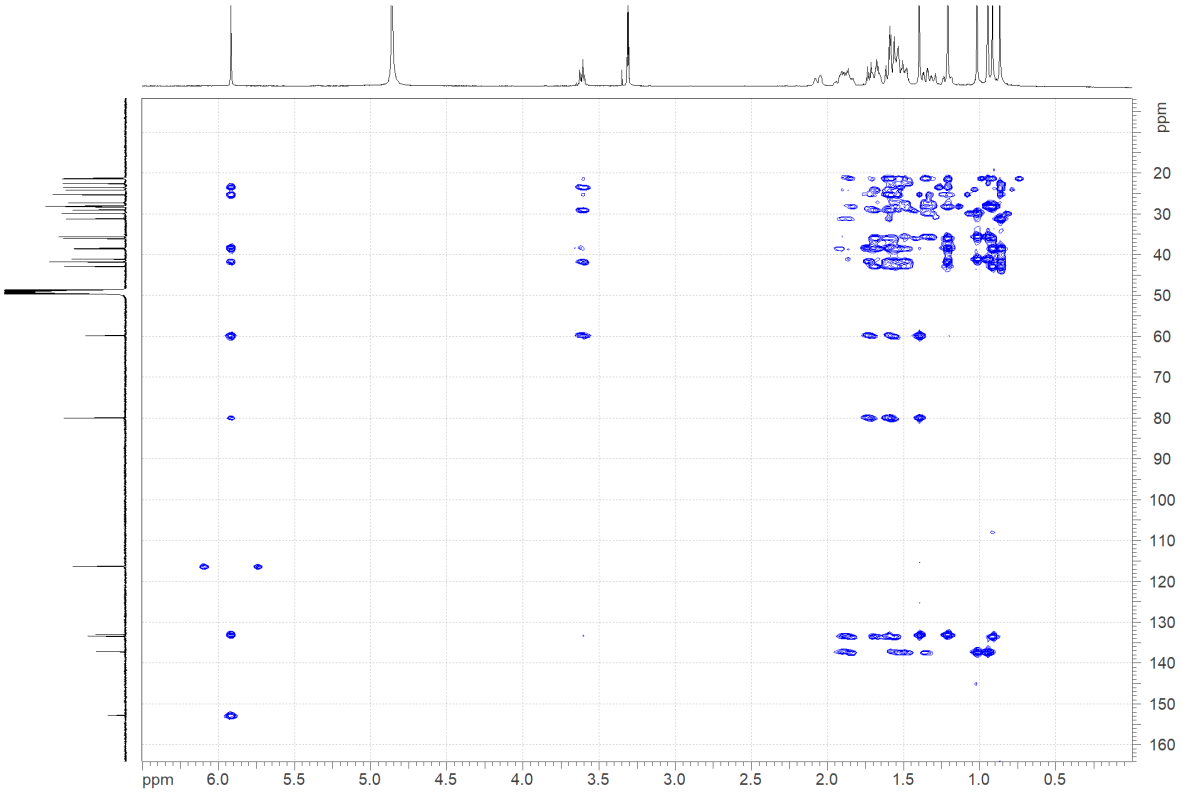

Figure S27. HMBC spectrum (500 MHz) of Darumycin D **(4)** in CD_3OD.

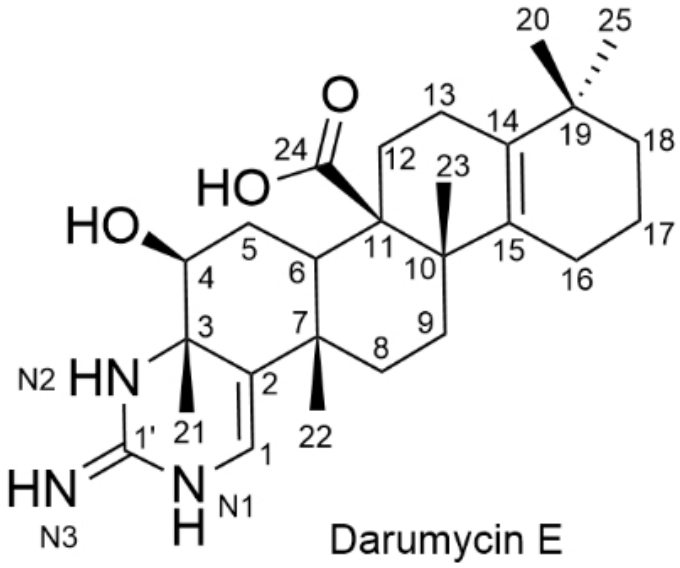

Figure S28. Structure of Darumycin E **(5)**.

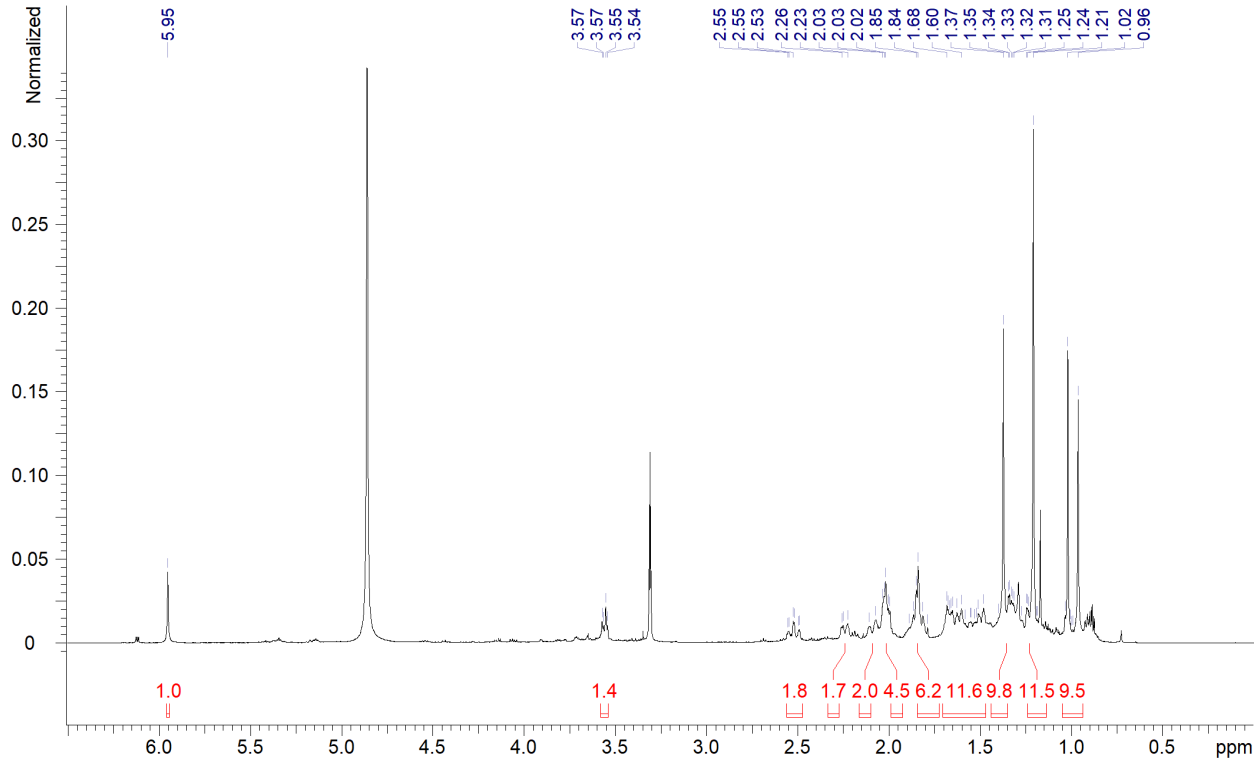

Figure S29. ^{1}H-NMR spectrum (500 MHz) of Darumycin E **(5)** in CD_3OD.

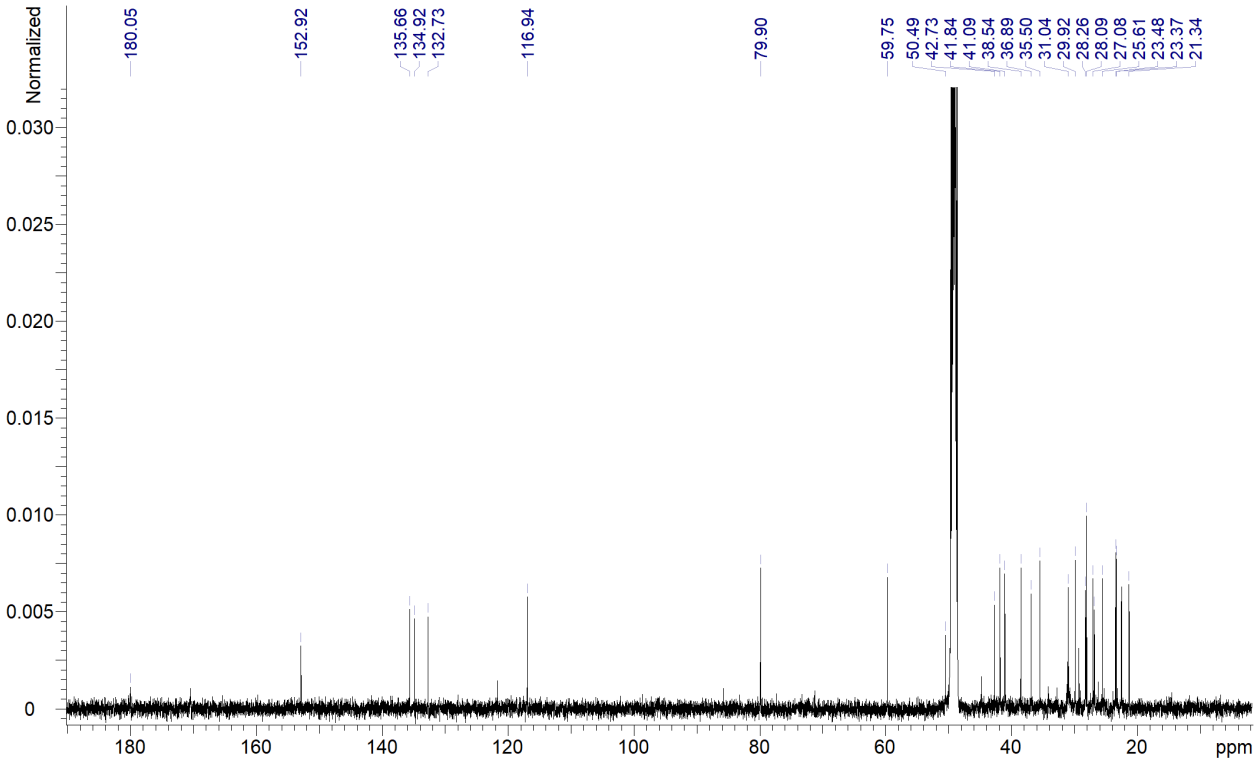

Figure S30. ^{13}C-NMR spectrum (125 MHz) of Darumycin E **(5)** in CD_3OD.

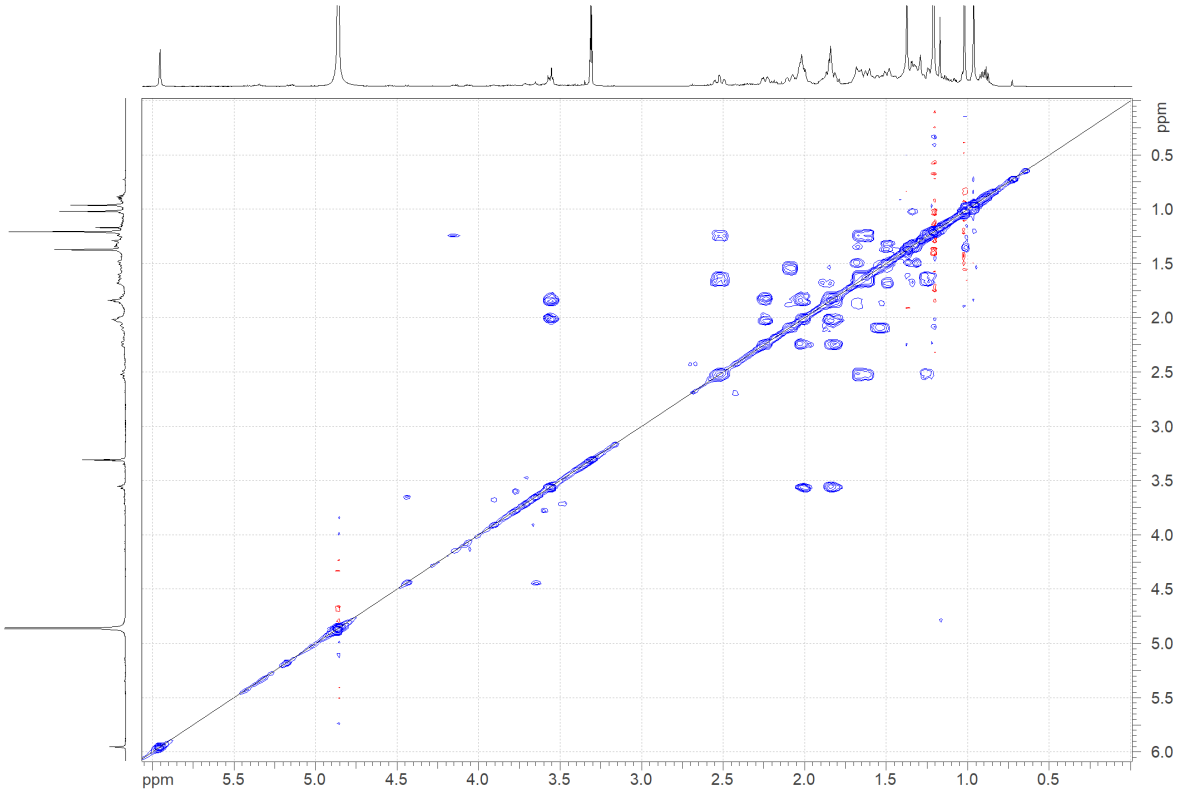

Figure S31. H-H COSY spectrum (500 MHz) of Darumycin E **(5)** in CD_3OD.

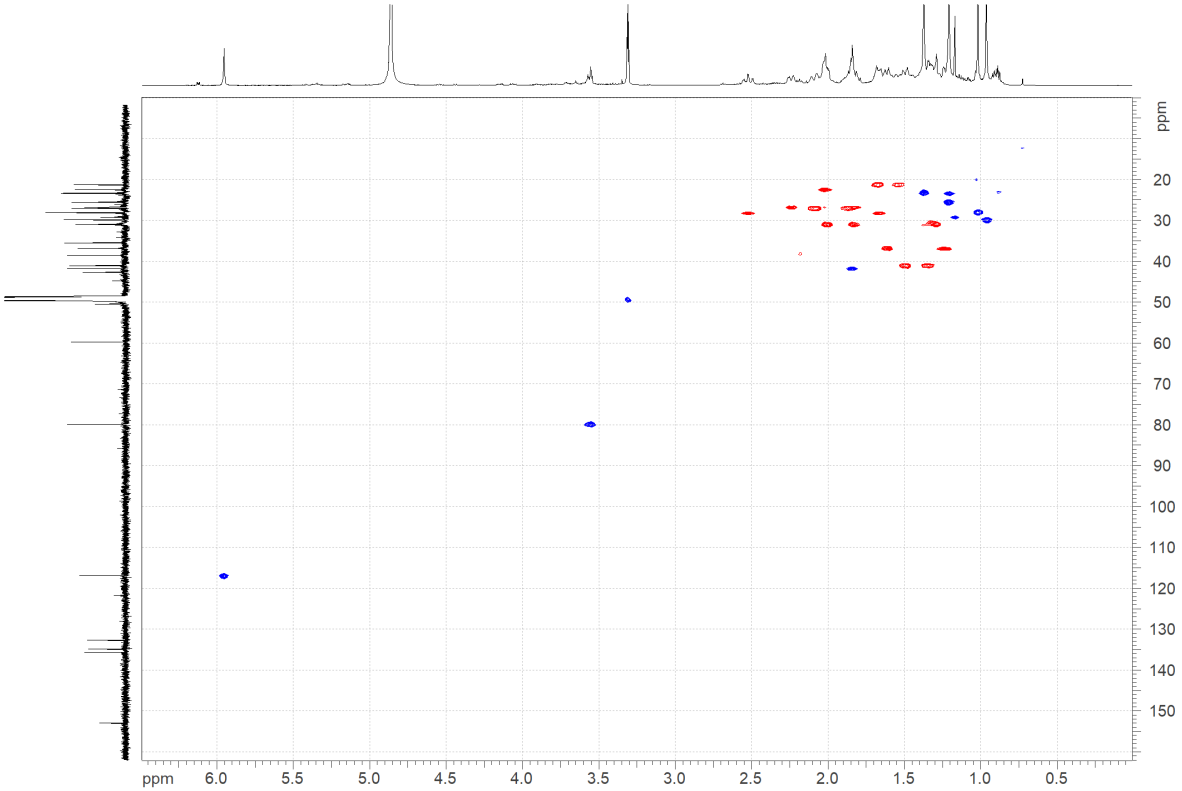

Figure S32. Edited HSQC spectrum (500 MHz) of Darumycin E **(5)** in CD_3OD.

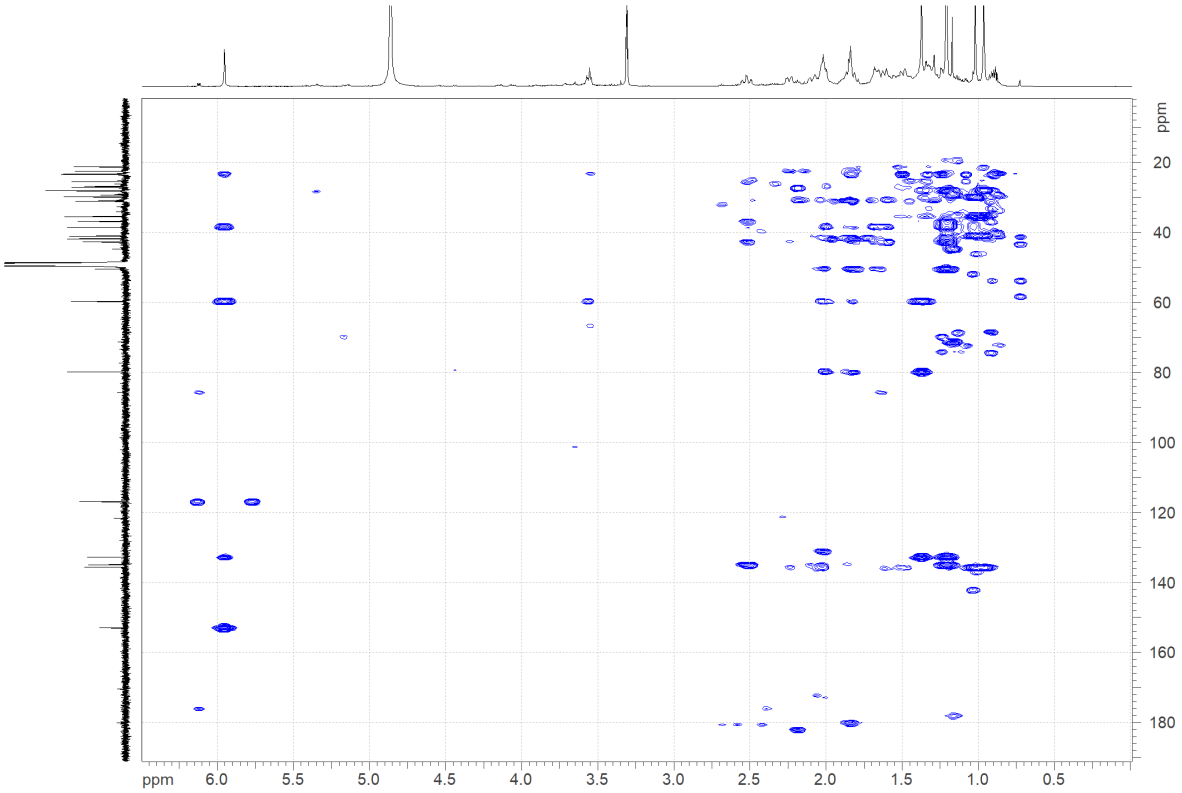

Figure S33. HMBC spectrum (500 MHz) of Darumycin E **(5)** in CD_3OD.

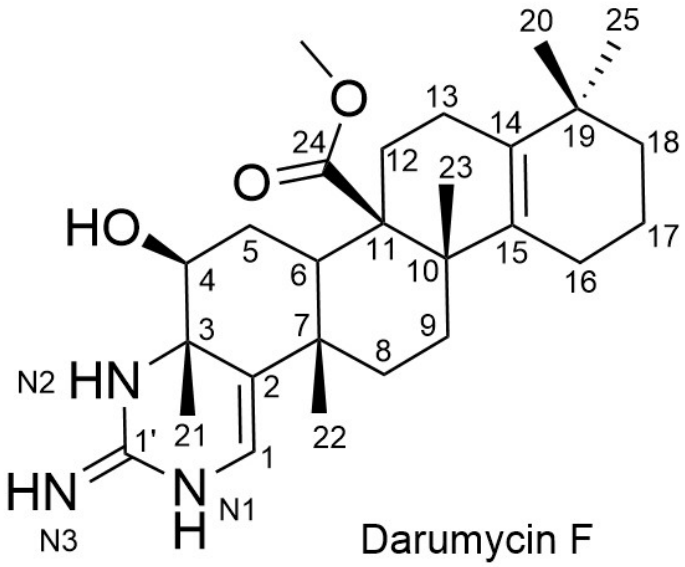

Figure S34. Structure of Darumycin F **(6)**.

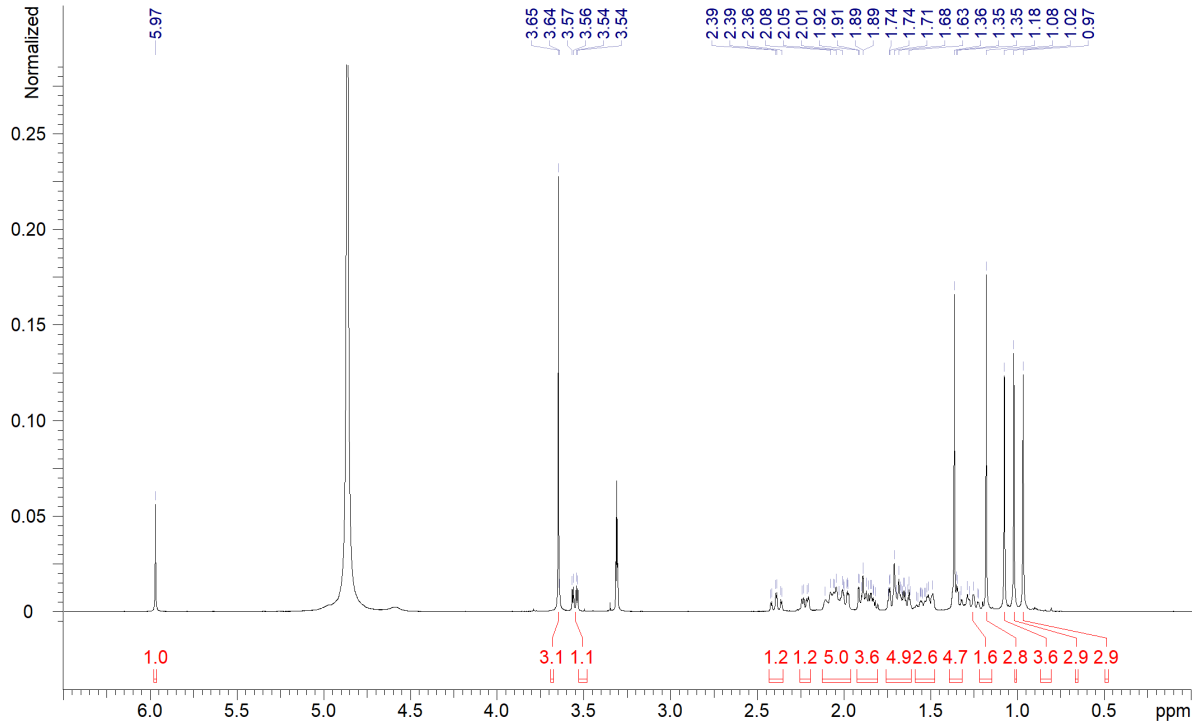

Figure S35. ^{1}H-NMR spectrum (500 MHz) of Darumycin F **(6)** in CD_3OD.

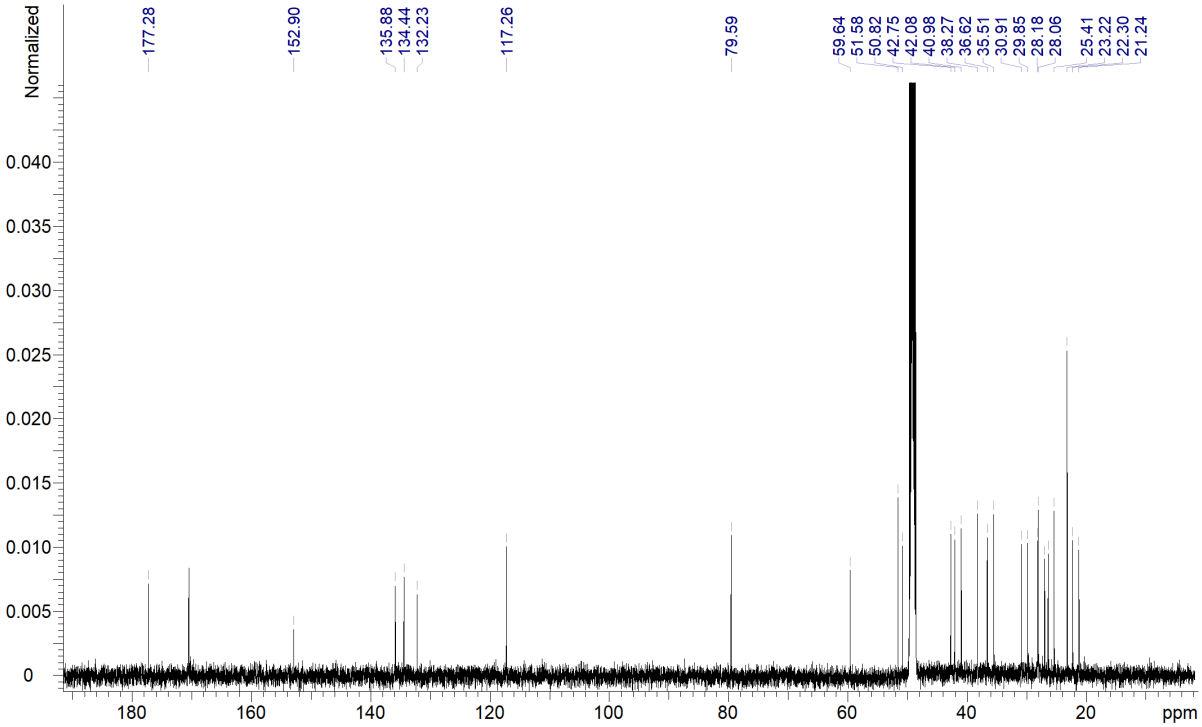

Figure S36. ^{13}C-NMR spectrum (125 MHz) of Darumycin F **(6)** in CD_3OD.

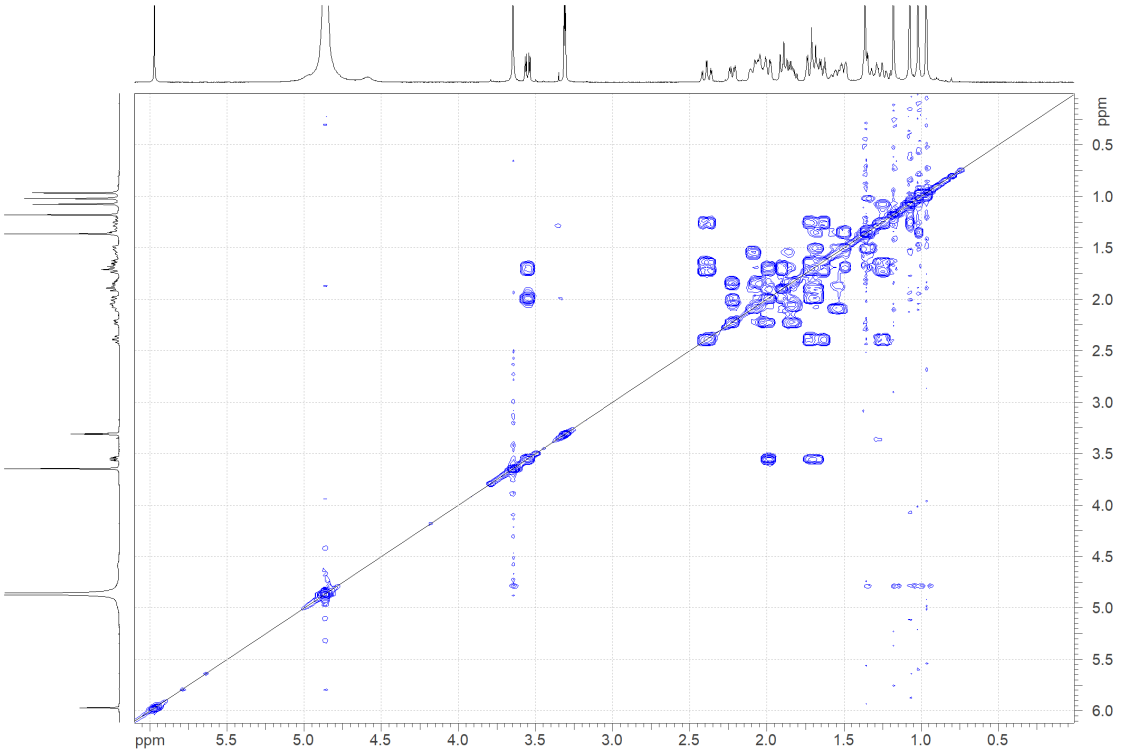

Figure S37. H-H COSY spectrum (500 MHz) of Darumycin F **(6)** in CD_3OD.

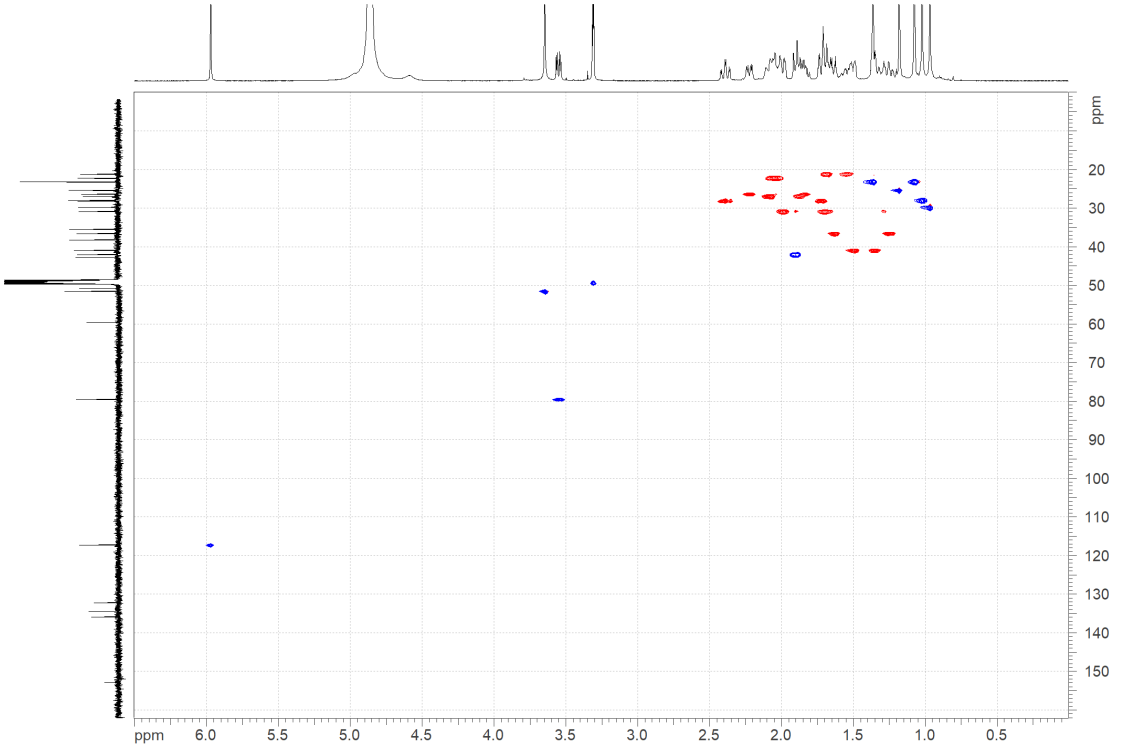

Figure S38. Edited HSQC spectrum (500 MHz) of Darumycin F **(6)** in CD_3OD.

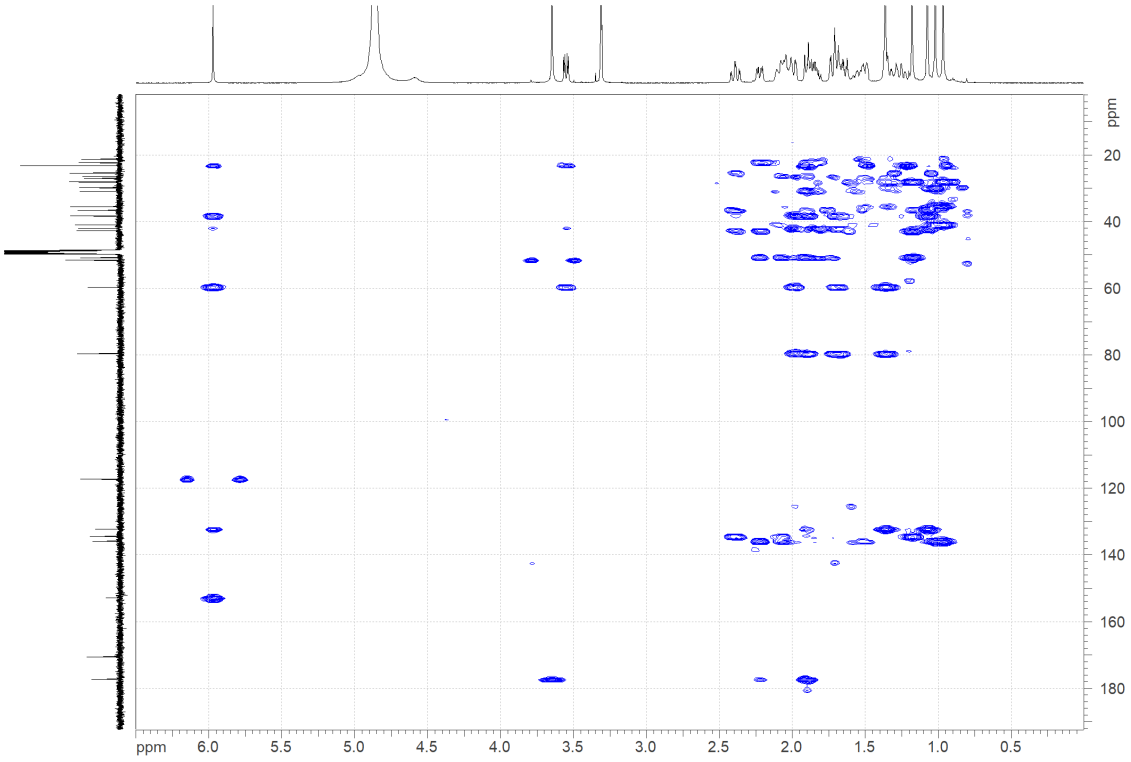

Figure S39. HMBC spectrum (500 MHz) of Darumycin F **(6)** in CD_3OD.

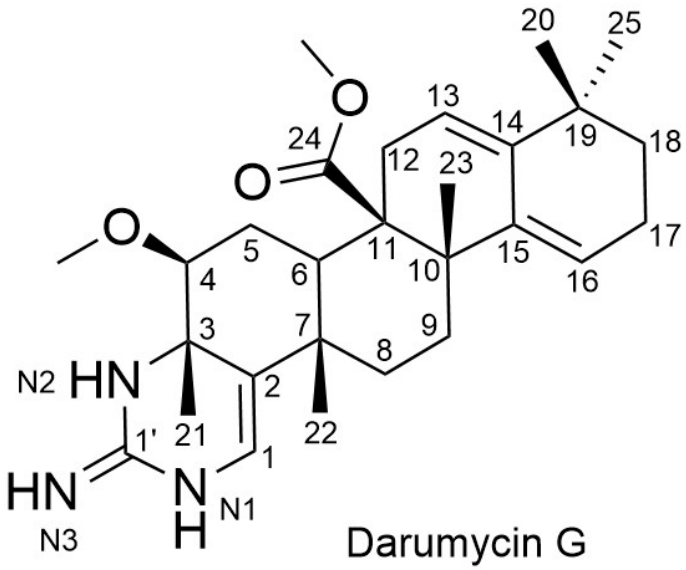

Figure S40. Structure of Darumycin G **(7).**

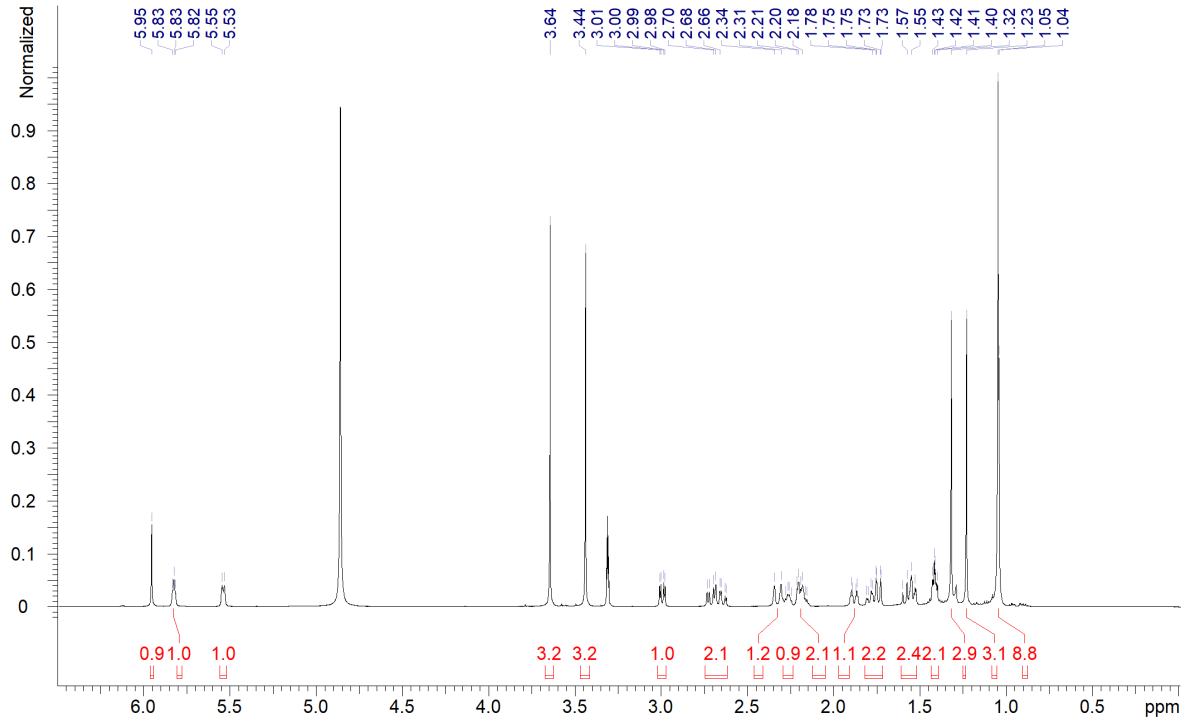

Figure S41. ^{1}H-NMR spectrum (500 MHz) of Darumycin G **(7)** in CD_3OD.

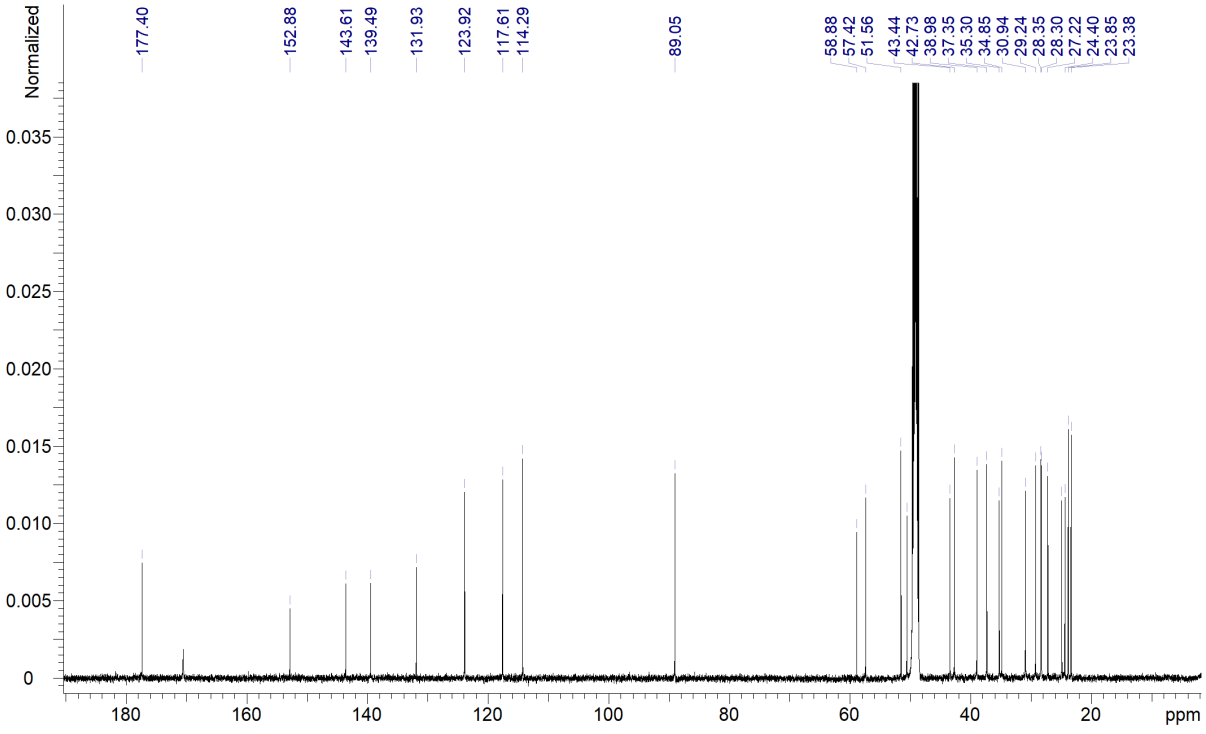

Figure S42. ^{13}C-NMR spectrum (125 MHz) of Darumycin G **(7)** in CD_3OD.

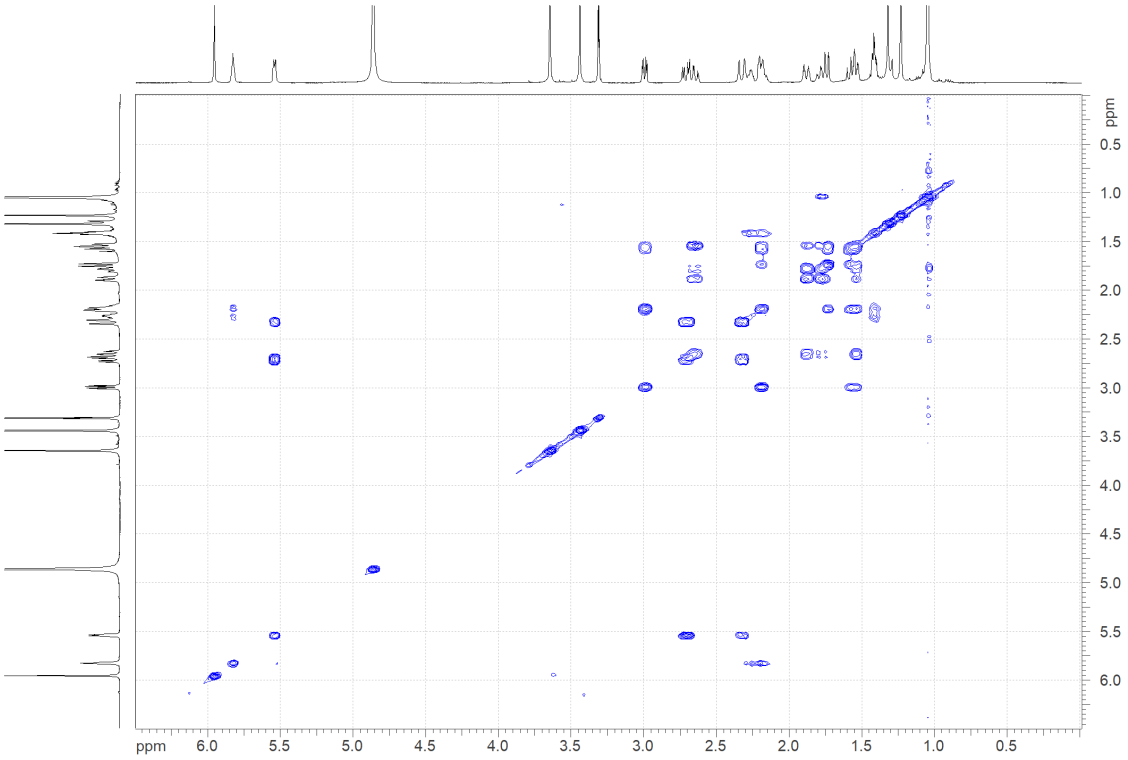

Figure S43. COSY spectrum (500 MHz) of Darumycin G **(7)** in CD_3OD.

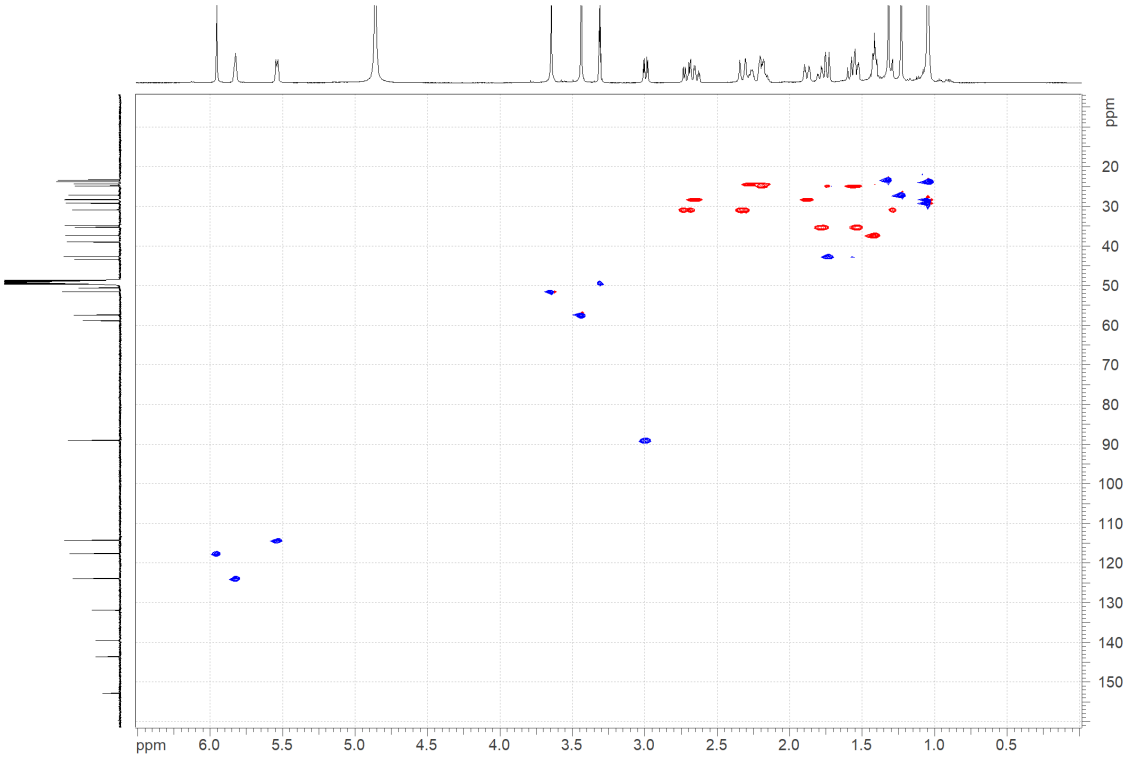

Figure S44. Edited HSQC spectrum (500 MHz) of Darumycin G **(7)** in CD_3OD.

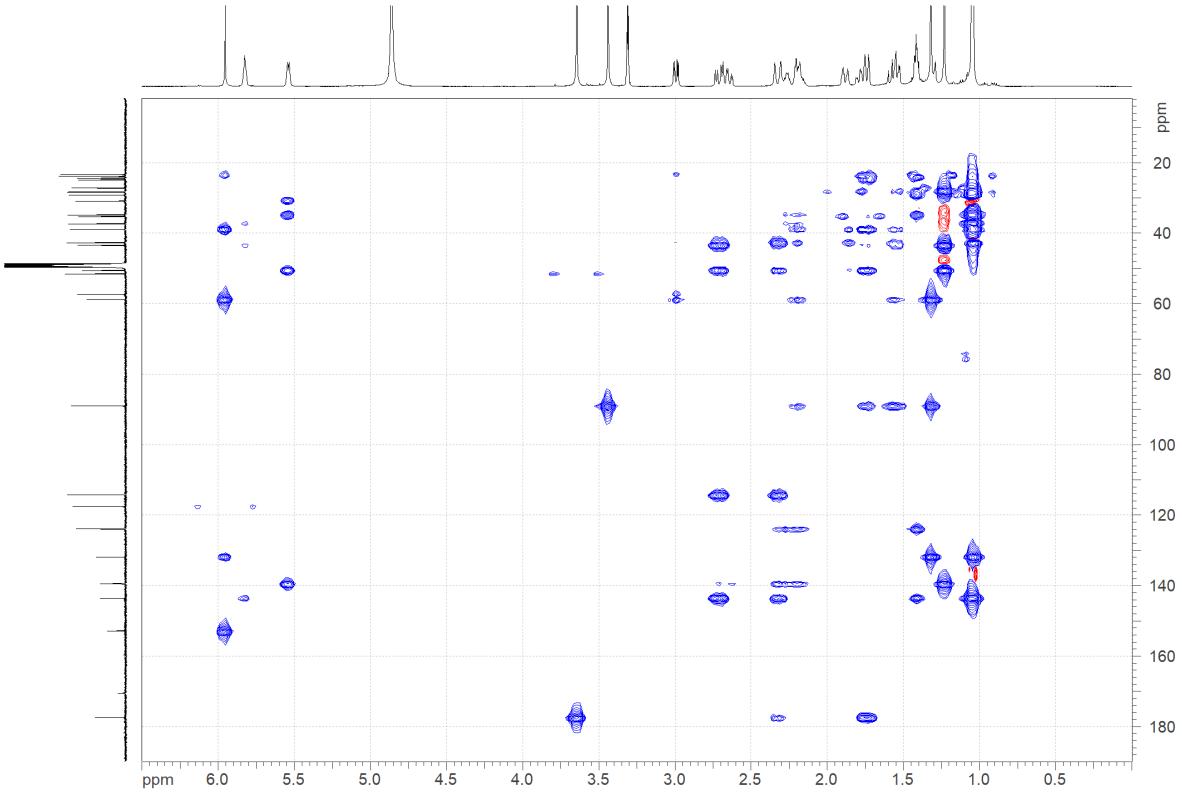

Figure S45. ^{13}C-HMBC spectrum (500 MHz) of Darumycin G **(7)** in CD_3OD.

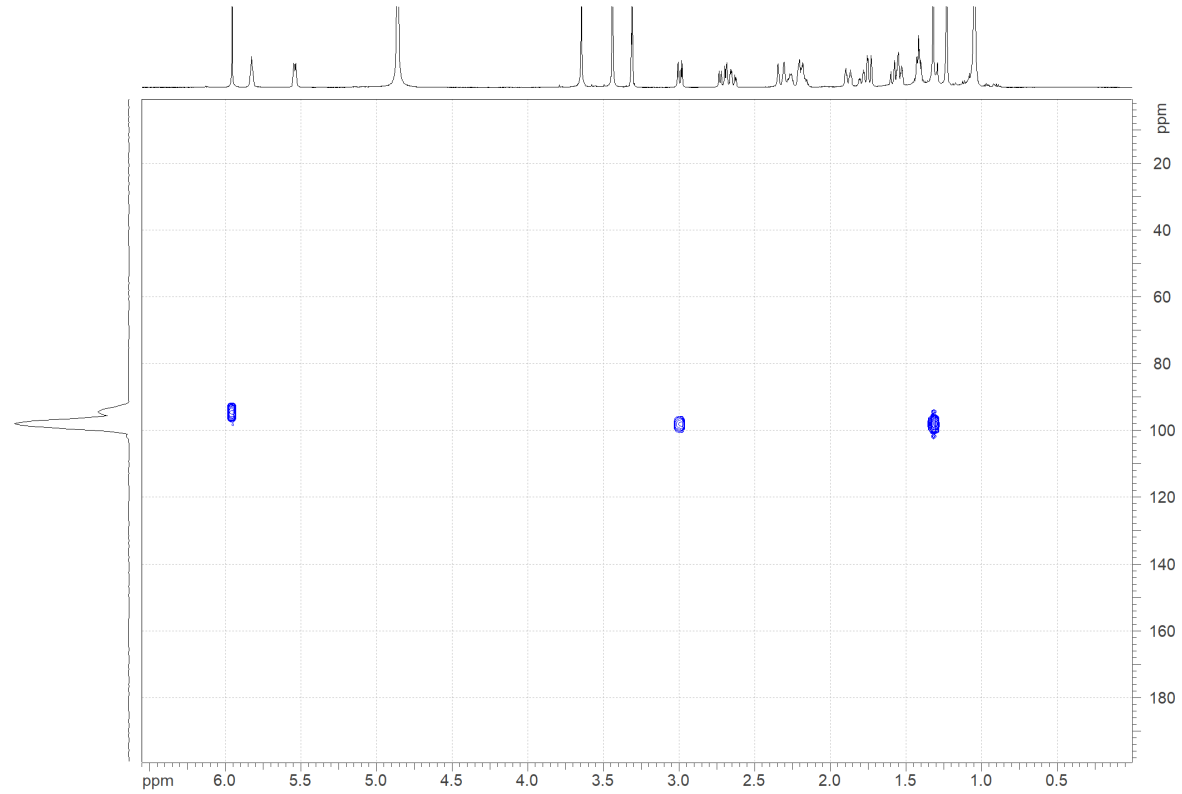

Figure S46. ^{15}N HMBC spectrum (500 MHz) of Darumycin G **(7)** in CD_3OD.

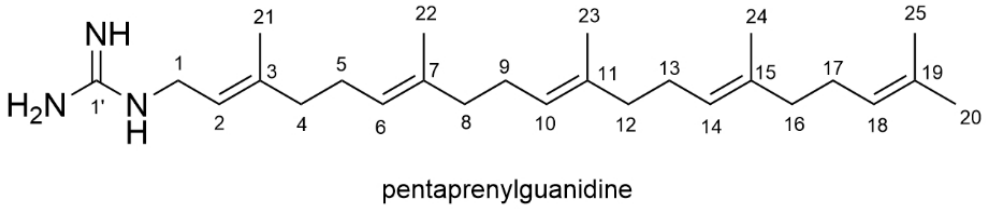

Figure S47. Structure of pentaprenylguanidine **(8)**.

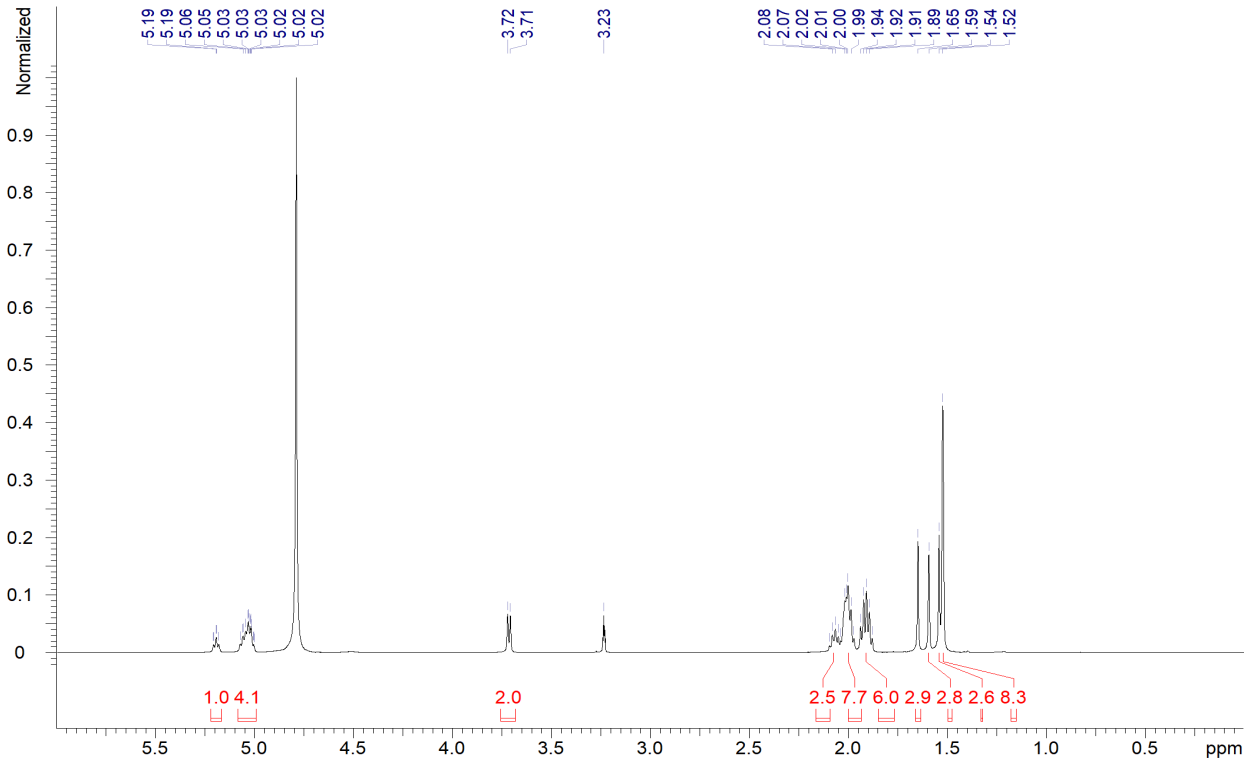

Figure S48. ^{1}H-NMR spectrum (500 MHz) of pentaprenylguanidine **(8)** in CD_3OD.

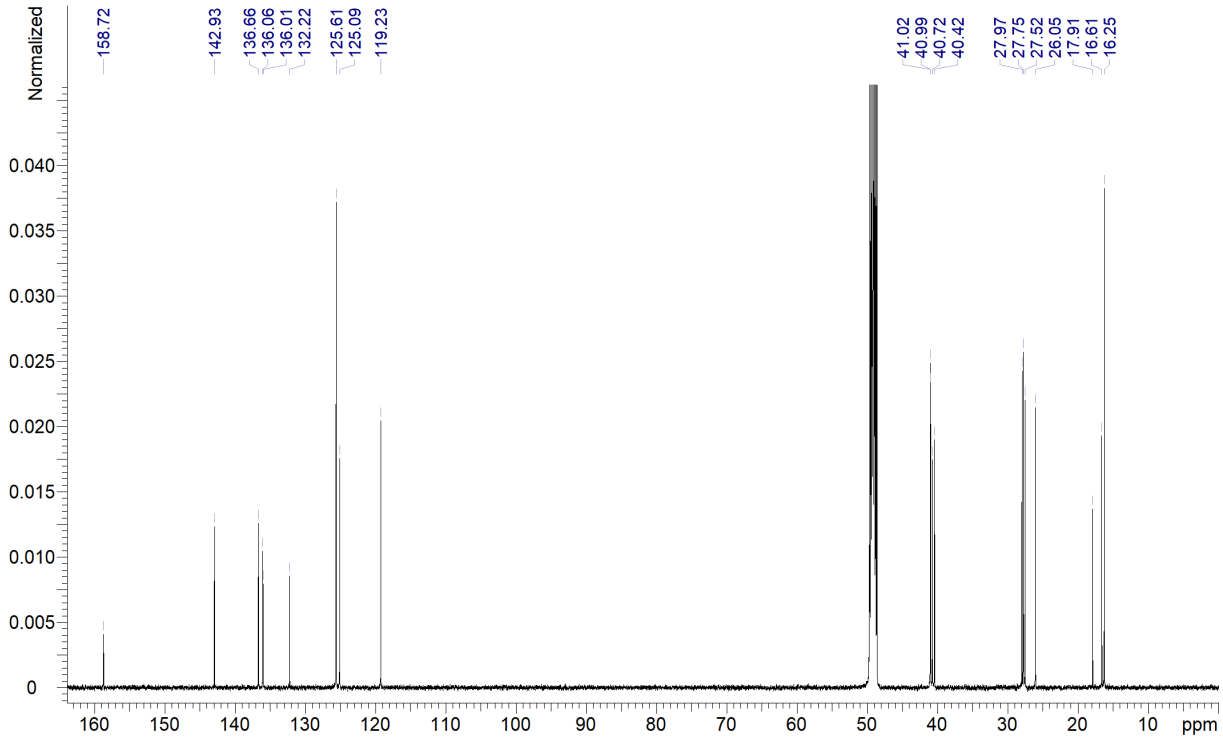

Figure S49. ^{13}C-NMR spectrum (125 MHz) of pentaprenylguanidine **(8)** in CD_3OD.

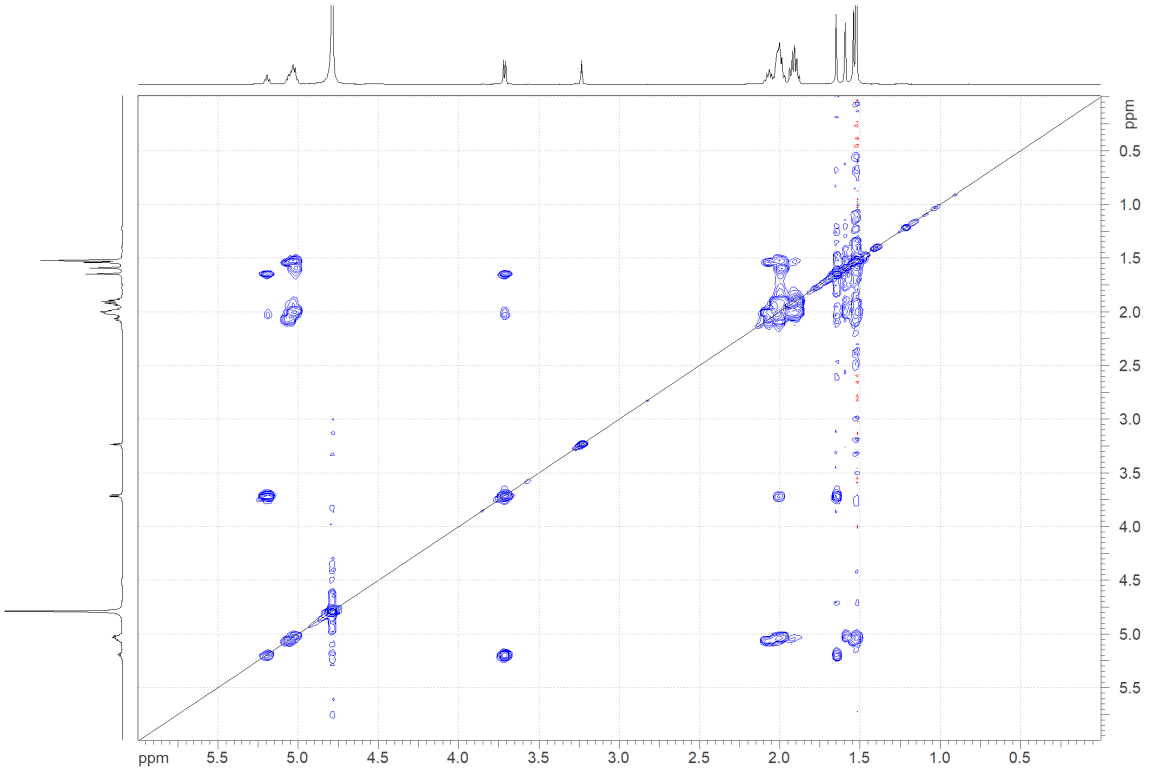

Figure S50. H-H COSY spectrum (500 MHz) of pentaprenylguanidine **(8)** in CD_3OD.

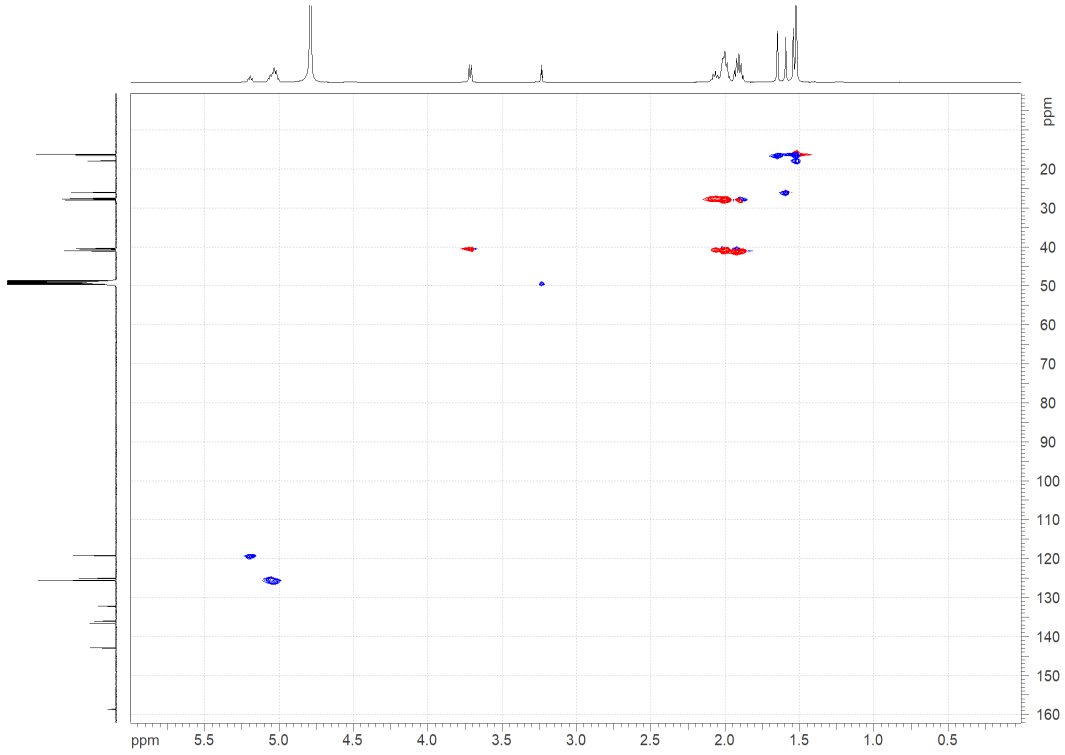

Figure S51. Edited HSQC spectrum (500 MHz) of pentaprenylguanidine **(8)** in CD_3OD.

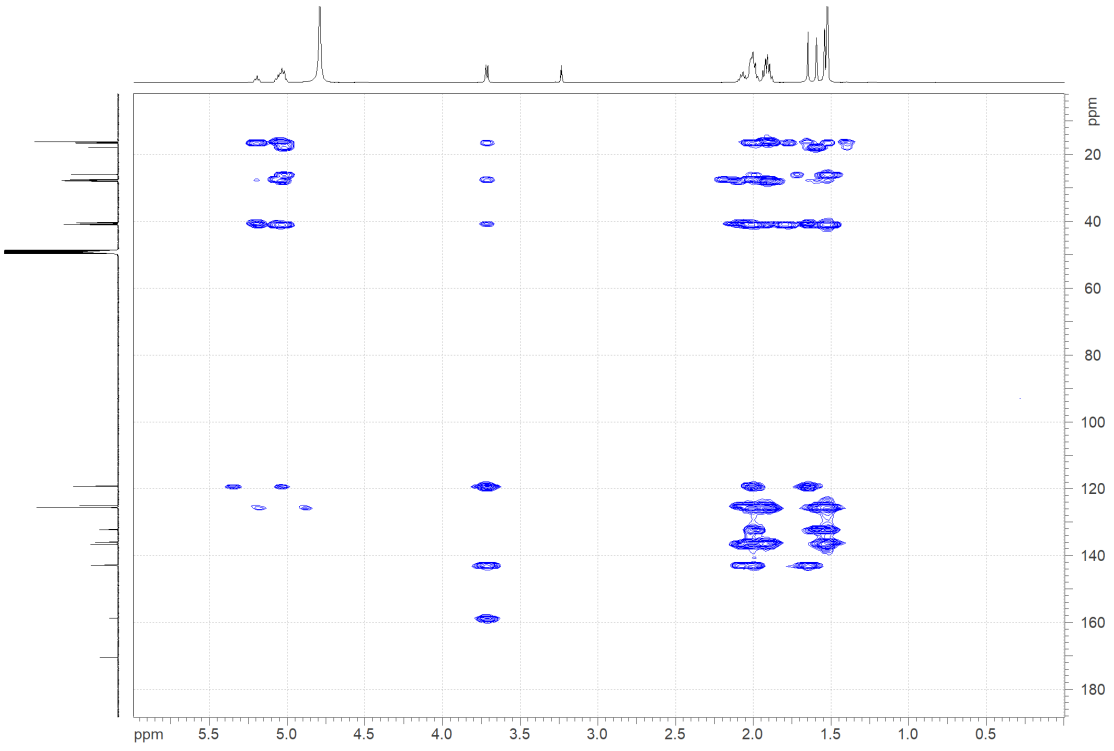

Figure S52. HMBC spectrum (500 MHz) of pentaprenylguanidine **(8)** in CD_3OD.

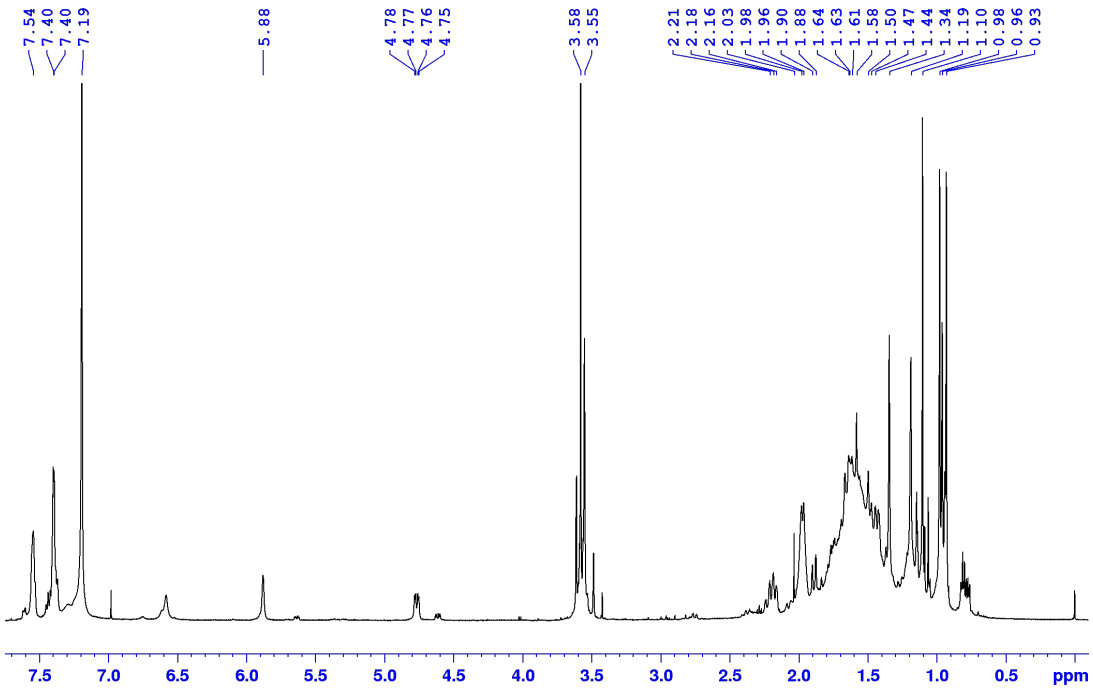

Figure S53. ^{1}H NMR spectrum (500MHz) of Darumycin F **(6)** (*R*)-MTPA ester in $CDCl_3$.

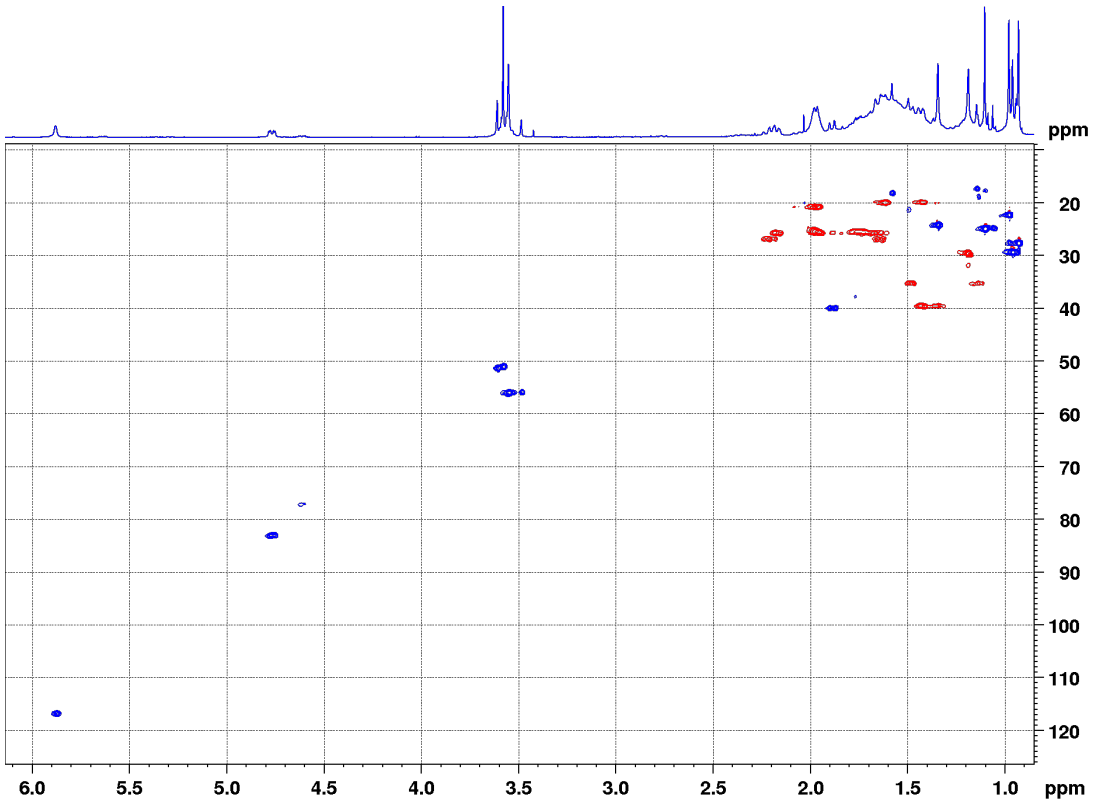

Figure S54. Edited HSQC spectrum (500 MHz) of Darumycin F **(6)** (*R*)-MTPA ester in $CDCl_3$.

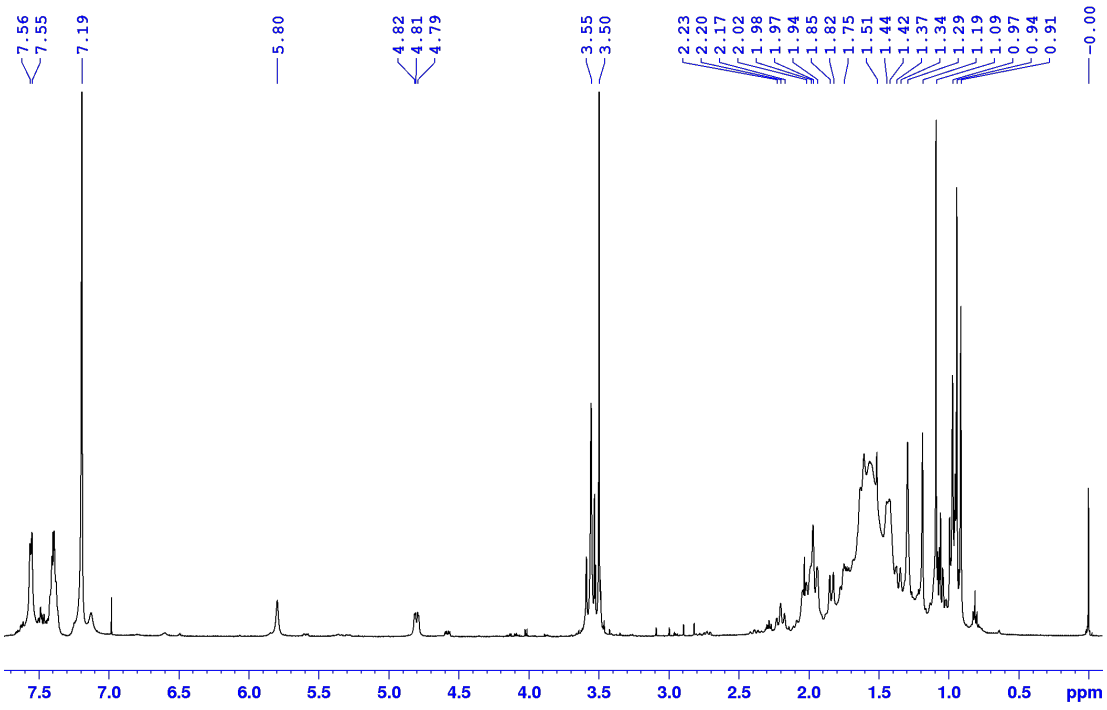

Figure S55. ^{1}H NMR spectrum (500MHz) of Darumycin F **(6)** (*S*)-MTPA ester in $CDCl_3$.

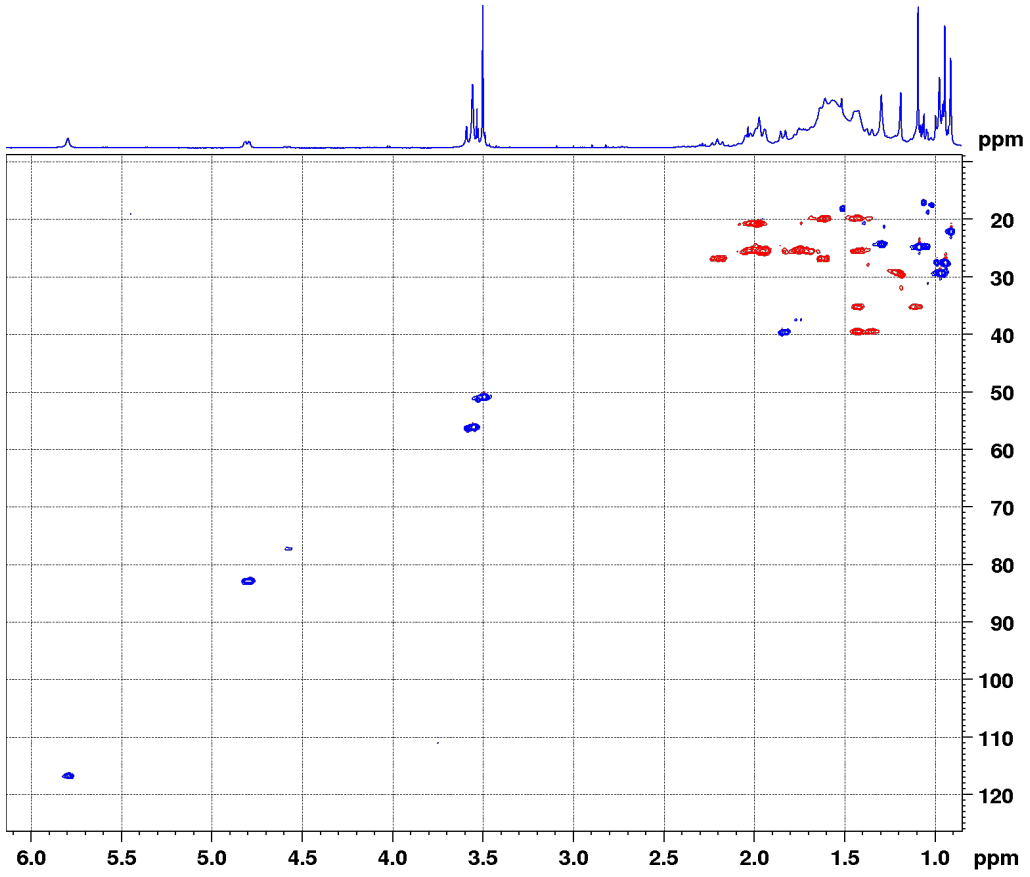

Figure S56. Edited HSQC spectrum (500 MHz) of Darumycin F **(6)** (*S*)-MTPA ester in $CDCl_3$.

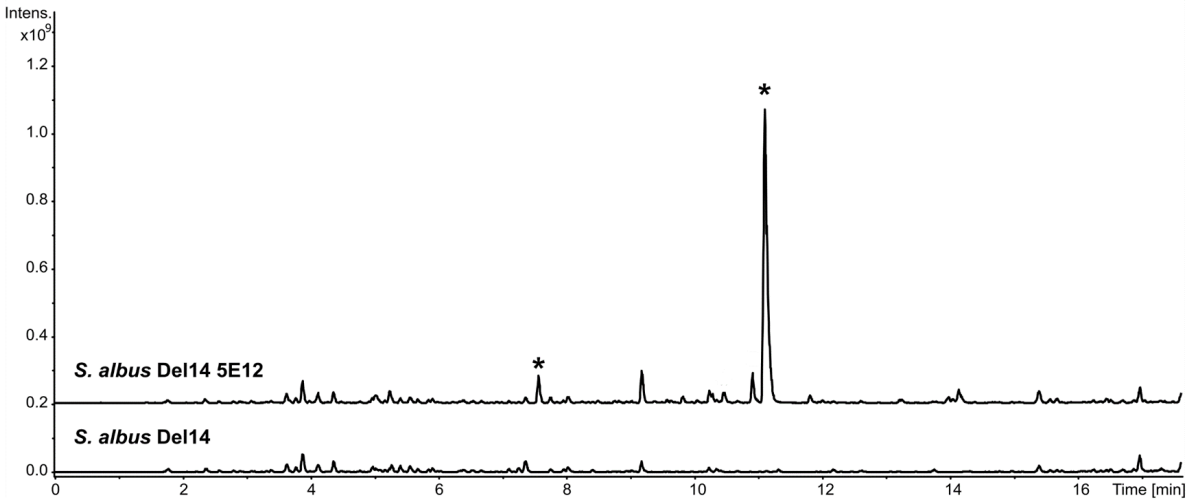

Figure S57. HPLC-MS chromatograms depicting the heterologous expression of the cosmid P05_E12 with darumycin cluster into *S. albus* Del14.The novel peaks are marked by marked by (*) asteriscs, representing darumycins G (left) and A (right).

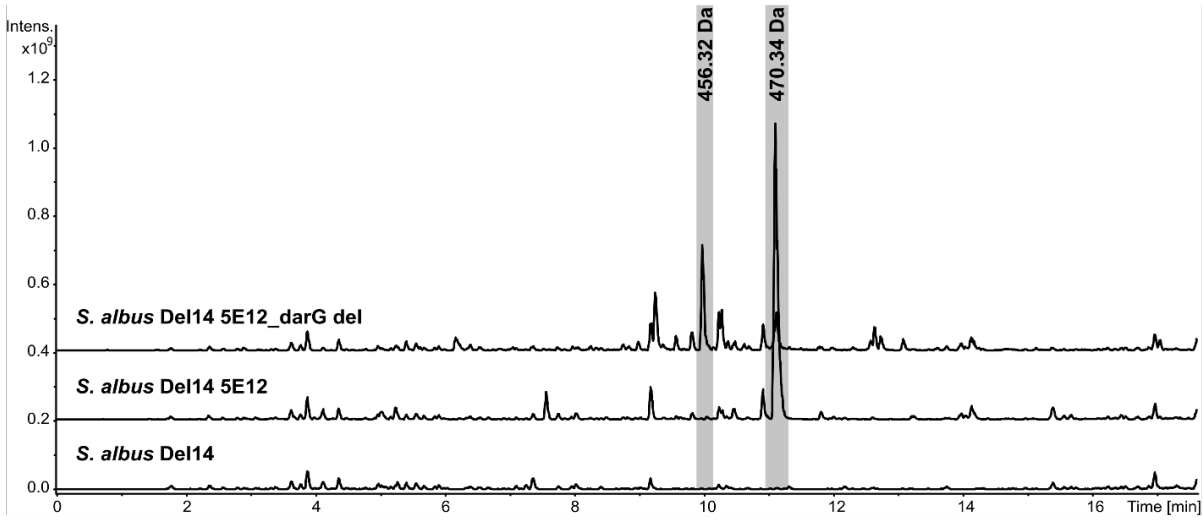

Figure S58. HPLC-MS chromatograms of the strains *S. albus* Del14, *S. albus* Del14 cos15AAmInt-5E12, *S. albus* Del14 cos15AAmInt-5E12_darG del. The peaks representing darumycin A and darumycin F derivative are marked by grey rectangles.

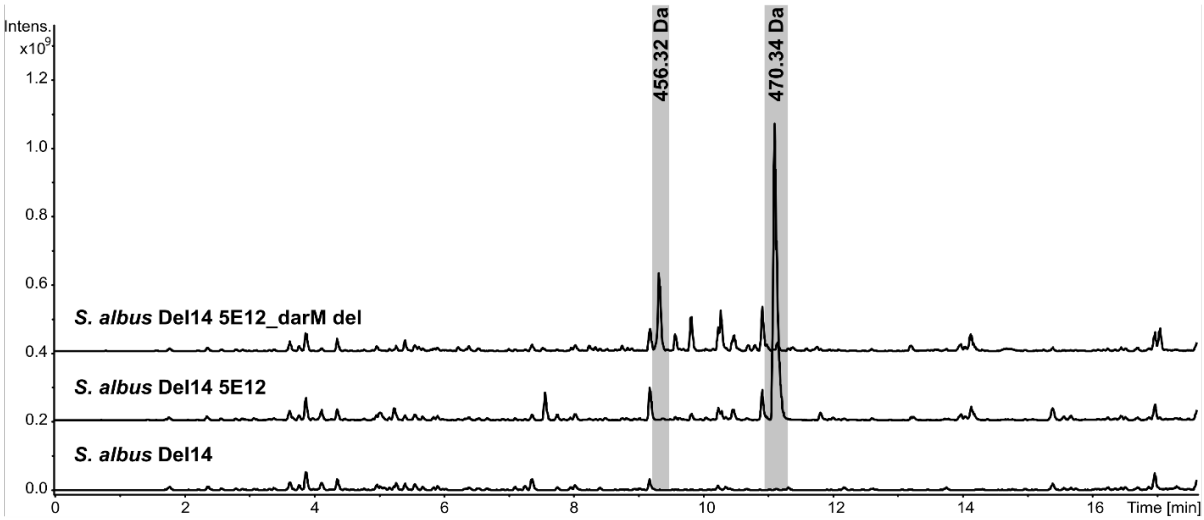

Figure S59. HPLC-MS chromatograms of the strains *S. albus* Del14, *S. albus* Del14 cos15AAmInt-5E12, *S. albus* Del14 cos15AAmInt-5E12_darM del. The peaks representing darumycin A and darumycin B derivative are marked by grey rectangles.

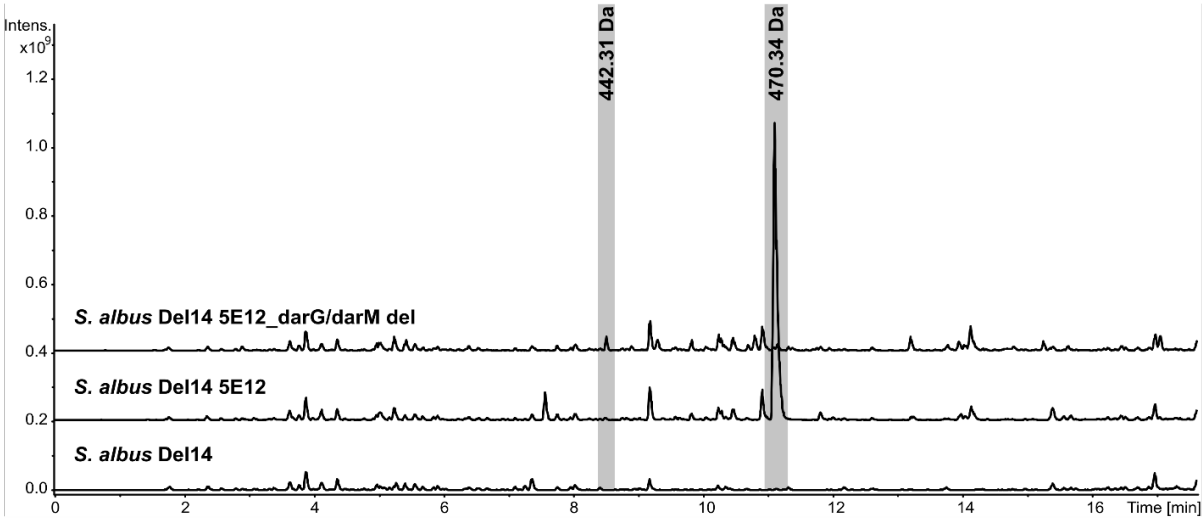

Figure S60. HPLC-MS chromatograms of the strains *S. albus* Del14, *S. albus* Del14 cos15AAmInt-5E12, *S. albus* Del14 cos15AAmInt-5E12_darG/darM del. The peaks representing darumycin A and darumycin E derivative are marked by grey rectangles.

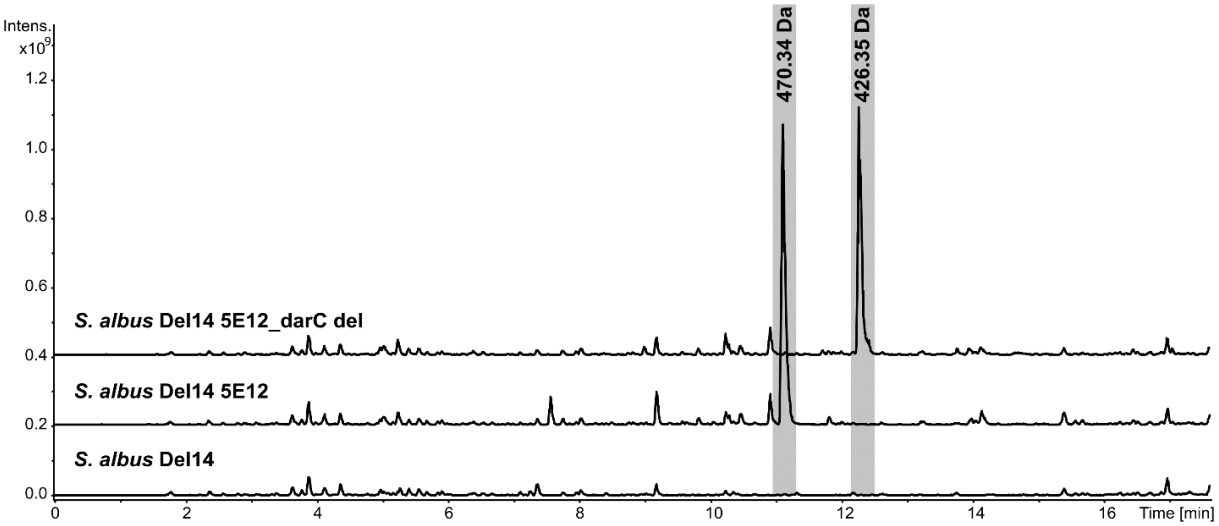

Figure S61. HPLC-MS chromatograms of the strains *S. albus* Del14, *S. albus* Del14 cos15AAmInt-5E12, *S. albus* Del14 cos15AAmInt-5E12_darC del. The peaks representing darumycin A and darumycin C derivative are marked by grey rectangles.

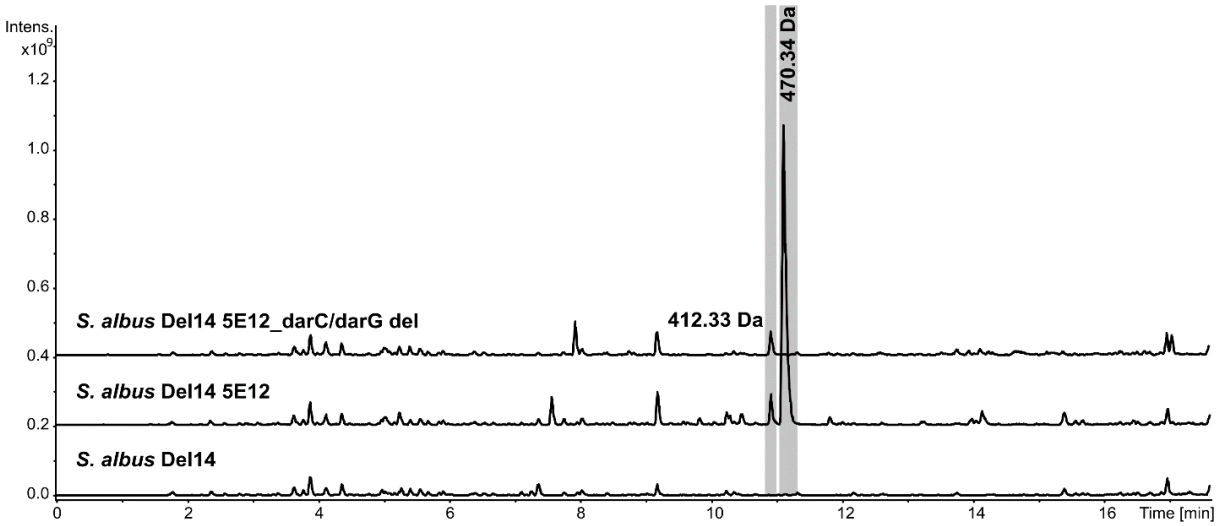

Figure S62. HPLC-MS chromatograms of the strains *S. albus* Del14, *S. albus* Del14 cos15AAmInt-5E12, *S. albus* Del14 cos15AAmInt-5E12_darC/darG del. The peaks representing darumycin A and darumycin D derivative are marked by grey rectangles.

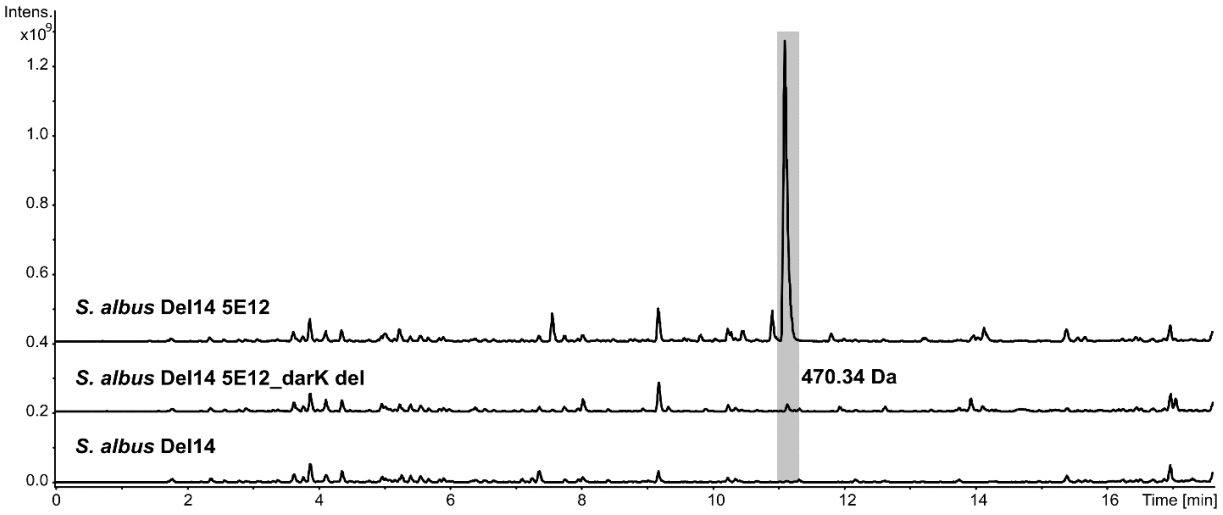

Figure S63. HPLC-MS chromatograms of the strains *S. albus* Del14, *S. albus* Del14 cos15AAmInt-5E12, *S. albus* Del14 cos15AAmInt-5E12_darK del. The peaks representing darumycin A are marked by a grey rectangle.

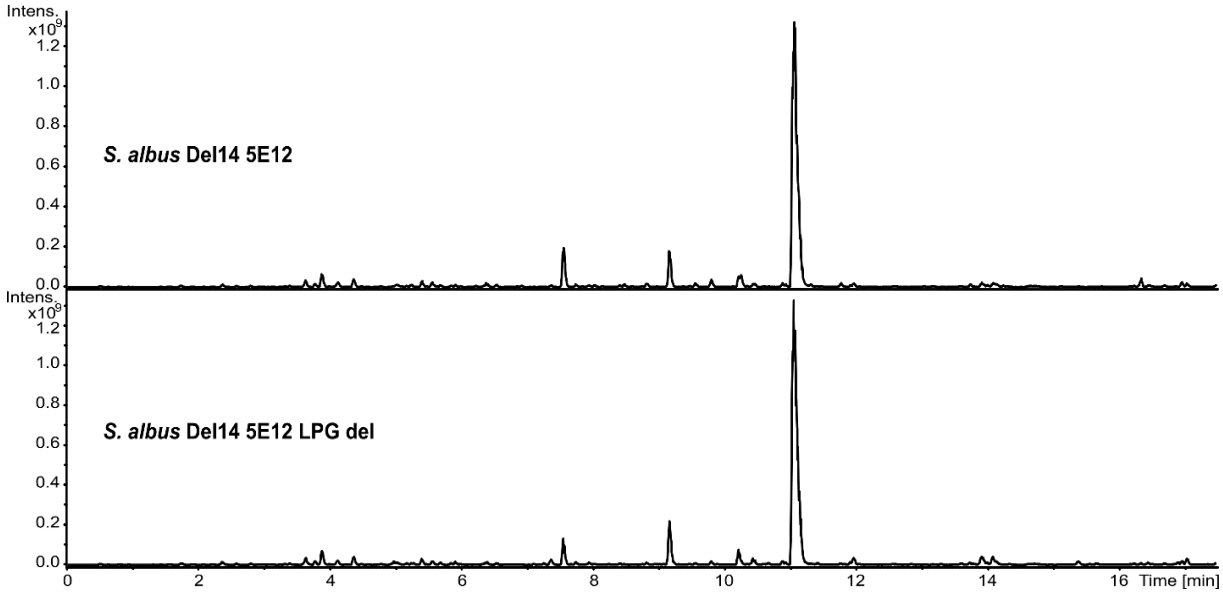

Figure S64. HPLC-MS chromatograms of the strains *S. albus* Del14, *S. albus* Del14 cos15AAmInt-5E12, S. albus Del14 cos15AAmInt-5E12_darL del.

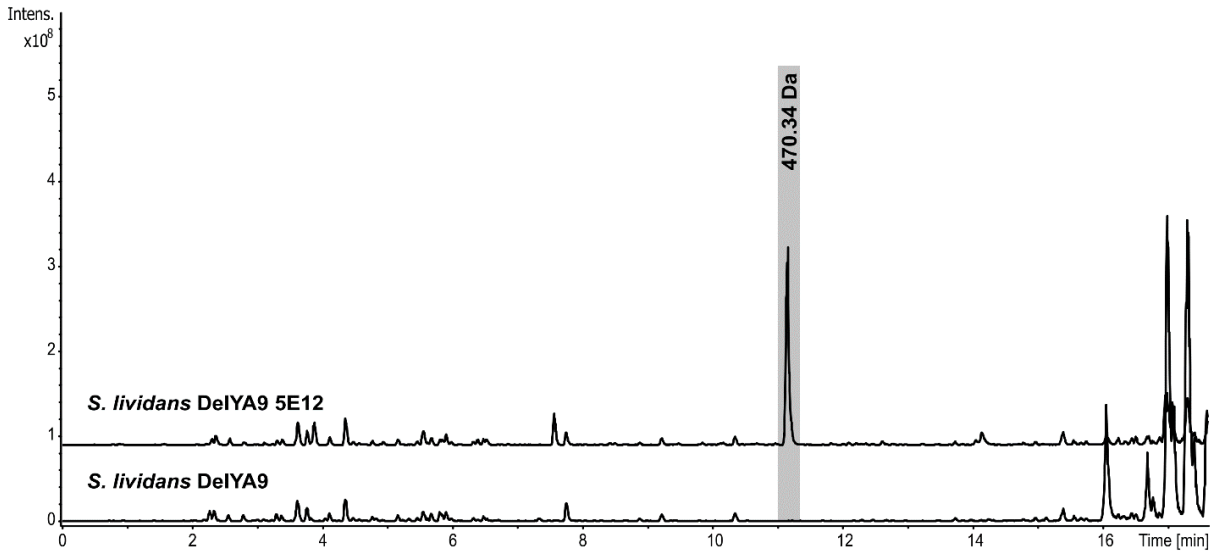

Figure S65. HPLC-MS chromatograms of the strains *S. lividans* DelYA9, *S. lividans* DelYA9 cos15AAmInt-5E12. The peak representing darumycin A is marked by a grey rectangle.

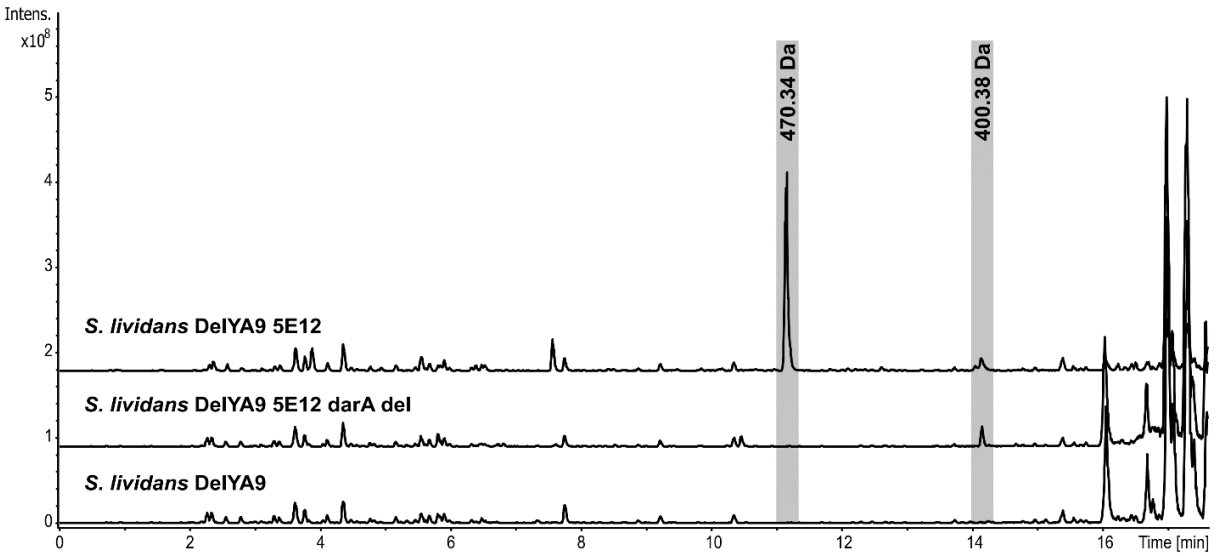

Figure S66. HPLC-MS chromatograms of the strains *S. lividans* DelYA9, *S. lividans* DelYA9 cos15AAmInt-5E12, *S. lividans* DelYA9 cos15AAmInt-5E12_darA del. The peaks representing darumycin A and pentaprenylguanidine derivative are marked by grey rectangles.

3. General Discussion

In this section, the findings presented across the three preceding chapters are integrated into a coherent narrative, that traces the discovery and characterization of novel guanidine-bearing terpenoids. Beginning with the identification and characterization of the guanidine-bearing triterpenenoids gromomycins (**Chapter 2.1**), it then explores the genome mining-guided discovery of gromomycin derivatives and characterization of mechanisms of action of this group of antibiotics (**Chapter 2.2**, partly **Chapter 2.1**). The discussion concludes with the discovery of new guanidine-bearing sesterterpenoids darumycins, and the investigation of their biosynthetic pathway and biological activities (**Chapter 2.3**).

Gromomycins: identification, isolation, proposed biosynthetic pathway and bioactivity profiling. Through chemical screening of antibiotically inactive crude extract, we have discovered a novel class of antibiotics named gromomycins (**Figure 1, A**). Gromomycins show remarkable activity against a range of pathogens, including methicillin-resistant, vancomycin-intermediate, and daptomycin-resistant *S. aureus*, as well as vancomycin-resistant enterococci, indicating an absence of cross-resistance with primary MRSA agents. Moreover, gromomycins exhibit substantial efficacy against *M. tuberculosis* and *A. baumannii*, highlighting an antibacterial spectrum that extends beyond typical Gram-positive pathogens. These unique compounds are pentacyclic triterpenes featuring a cyclic guanidino group that forms a distinctive fifth six-membered ring. To elucidate the biosynthesis of gromomycins and further broaden the spectrum of these compounds through genome mining and biosynthetic engineering, it was critical to identify the biosynthetic gene cluster responsible for their synthesis. Traditional bioinformatics tools, such as antiSMASH, alone proved insufficient pointing on the complex and unusual biosynthetic pathways of gromomycins.

The innovative adaptation of classical genetic tools, specifically transposon mutagenesis coupled with HPLC MS analysis and combined with heterologous expression techniques successfully pinpointed the elusive BGC. Particularly for compounds like gromomycins, which follow unconventional biosynthetic routes, the application of classical tools with a novel twist facilitates the discovery of targeted BGCs. For instance, the discovery of albucidin BGC was achieved by combining random NTG (N-methyl-N'-nitro-N-nitrosoguanidine) mutagenesis with liquid LC-MS and genome analysis.[352] Similarly, the identification and analysis of mansouramycin's BGC was achieved using the older, now rarely used co-synthesis method.[353] These examples underscore the importance of adapting and evolving traditional methodologies to meet the challenges presented by modern natural product

research. By revisiting and modifying classical techniques, researchers can uncover the genetic blueprints of compounds with complex and rare biosynthetic origins.

The biosynthesis of gromomycins is particularly noteworthy. Triterpenoid biosynthesis always begins with the head-to-head dimerization of farnesyl diphosphate by squalene synthase, resulting in the formation of squalene. This compound then undergoes cyclization catalyzed by triterpene synthases, for instance squalene-hopene cyclase is producing pentacyclic hopene, the precursor of hopanoids. Following oxidation to (*S*)-2,3-epoxysqualene, lanosterol synthase facilitates the biosynthesis of lanosterol, a precursor to steroids and saponins. In contrast, the GroD enzyme shows strong similarity to the class I terpene synthases having two conserved DDxD and DTE motifs for binding of Mg^{2+} ions that in turn binds the substrate's diphosphate. This let us suggest that GroD combines in an iterative head-to-tail mode six prenyl monomers, to form hexyprenyl diphosphate, a crucial intermediate in gromomycin biosynthesis.

Notably, during the biosynthesis of gromomycins, the diphosphate residue in hexaprenyl diphosphate precursor is substituted by an arginine-derived guanidine group before cyclization. This step is likely catalyzed by the *groH*-encoded prenyltransferase, which shows resemblance to several terpene synthases and a notable similarity to prenyltransferases. Evidentely, the *in vitro* enzymatic reaction with GroH protein should be assesed to fully characterize this unique biosynthesic step. The linear precursor then undergoes conversion to gromomycins, a process hypothesized to involve the gene products of *groA*, *groB*, *groC*, and *groF*, as their deletion leads to the accumulation of the linear precursor hexaprenylguanidine. In particular, the GroF protein is shown to contain a terpene cyclase domain, similar to the TvTS cyclase from *Talaromyces verruculosus*,[256-257] and the FlvF cyclase-like protein from *Aspergillus flavus*,[258] suggesting its role as gromomycin cyclase. Furthermore, the three Rieske oxygenases, GroA, GroB, or GroC are proposed to be involved in the cyclization process of gromomycins through the introduction of C4-OH group, as these enzymes are known to catalyze hydroxylation reactions.[260]

Finally, cytochrome P450 oxygenase GroI is proposed to incorporate a keto group at C-17 position, followed by the GroE enzyme reducing the keto group to a hydroxyl group. The hydroxylated gromomycin is unstable and subsequently degrades to gromomycin A during the purification process.

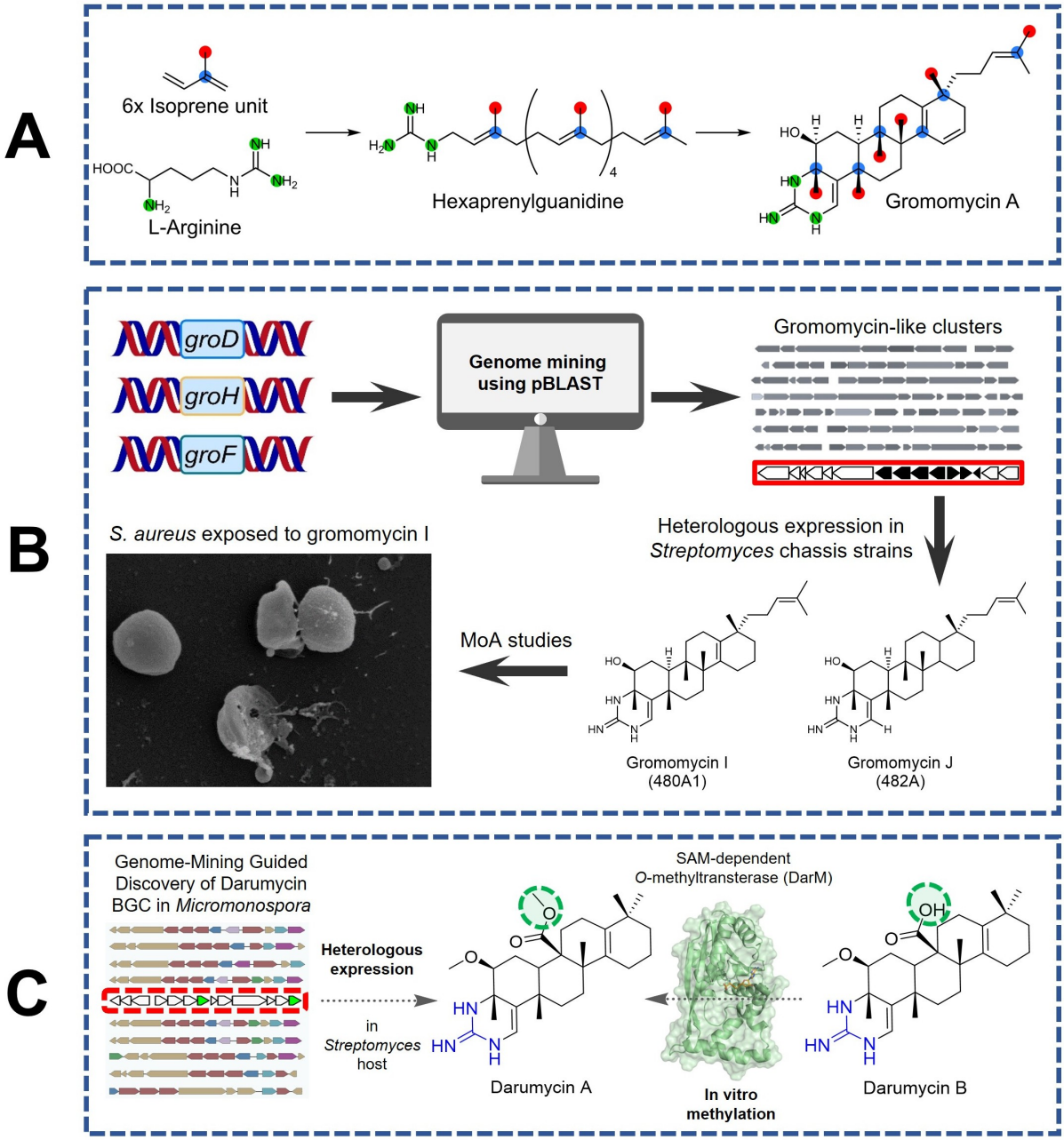

Figure 1. Graphical abstract of this dissertation. **A**. Chapter 2.1. Gromomycins: An Unprecedented Class of Triterpene Antibiotics Produced by a Novel Biosynthetic Pathway; **B**. Chapter 2.2. Genome Mining–Driven Isolation of New Gromomycins and Insights into Their Mode of Action; **C**. Chapter 2.3. Expanding the Chemical Space of Sesterterpene Antibiotics: Discovery and Characterization of Darumycins.

Genome Mining-Driven Isolation of New Gromomycins and Insights into Their Mode of Action. Elucidation of the gromomycin biosynthetic pathway laid the foundation for a genome mining approach, which was further used to explore the distribution of gromomycin-like BGCs (*gro*BGCs) and to identify new derivatives (**Figure 1, B**). The genome mining with the *gro* genes as "hooks" have revealed that this biosynthetic pathway is widely distributed within various *Streptomyces* and non-*Streptomyces* actinobacteria.

While many *gro*BGCs were found to be identical to the prototype cluster from *Streptomyces* sp. Je 1–332, many others include an additional gene encoding a protein with a methyltransferase domain. Cloning and expressing such *gro*BGC from *Streptomyces flavoviridis* resulted in expanding gromomycins chemical space with new methylated derivatives (gromomycins E-H).[300] Intriguingly, the antimicrobial activity seems to be strongly dependent on the structure of the side chain (unmethylated vs methylated derivatives), which prompted the search for new gromomycin variants.

In contrast, several other *gro*BGCs are lacking some genes identified in the prototype cluster. In particular, the *gro*BGC from *A. xinjiangensis* strain lacks *groI* and *groE*, which encode CYP450 monooxygenase and reductase, involved in the tailoring steps of gromomycin biosynthesis. The cloning and heterologous expression of this BGC led to the isolation of 3 additional gromomycin members, highlighting the significant potential of underexplored actinobacteria in the field of antibiotic discovery. Other noteworthy *gro*BGCs were found to contain not only additional methyltransferases, but also genes encoding putative FAD-dependent oxidoreductase and uroporphyrinogen decarboxylase, as in *Streptomyces sp.* NPDC021212 strain. Interestingly, this high distribution of *gro*BGCs across various bacterial taxa is not restricted only to *Actinomycetota* phylum. In particular, so far the smallest *gro*BGC, which includes only the three core genes, was found in the genome of *Pendulispora albinea*, the representative of *Myxococcota* phylum. Such extraordinary examples are particularly worth investigating, indicating the high potential of this newly discovered class of NPs.

The bioactivity profile of gromomycins covers a broad range of Gram-positive bacteria, including multidrug-resistant strains. This makes the further studies of this group of antibiotics clinically relevant. There is a very noticeable structure-activity relationship within gromomycin family. For instance, gromomycins C and I with the double bond in positions C14-C15 and C15-C16 have relatively strong bioactivity, while gromomycin J with a saturated bond in these positions demonstrated significantly reduced antibacterial activity. Also, we observed a significant variation in the toxicity of different gromomycin derivatives both in cell-based and zebra fish embryo models. This variation is most likely due to binding to fetal bovine serum proteins present in cell culture medium, which partly masks gromomycin toxicity

Gromomycins ability to inhibit growth of clinically relevant pathogens, including vancomycin-resistant *Enterococcus faecium* (VRE) and daptomycin resistant *S. aureus*, prompted the deeper studies of the mode of action of these compounds. Gromomycins proved to effectively overcome the existing resistance mechanisms to conventional antibiotics. Furthermore, the killing kinetics analysis revealed a rapid, concentration-dependent bactericidal

rather than bacteriostatic effect. Moreover, the recovery of bacterial growth observed after treatment with gromomycins does not appear to result from the development of resistance. This was later confirmed by many repeated but unsuccessful attempts to generate resistant mutants, even after prolonged serial passaging under subinhibitory concentrations. The inability to select for gromomycin-resistant mutants strongly suggests a non-specific mode of action and/or the absence of a conventional protein target.[303]

The non-selective nature of bactericidal activity of gromomycins and their amphiphilic nature point towards an interaction with the bacterial cell envelope. Indeed, gromomycin treatment caused rapid membrane depolarization and loss of ion homeostasis in *S. aureus*, confirming membrane disturbance as the key lethal event. SEM and TEM microscopy analysis have revealed significant cell damage, including membrane deformation, pore formation and leakage of cellular contents, which is consistent with the loss of membrane integrity. The formation of mesosome-like and vesicular structures further support a mechanism involving lipid bilayer perturbation.[304-305] This observed phenomenon is similar to that of other membrane-active compounds, like the antimicrobial peptide gramicidin S, which is known to disrupt the lipid bilayer through interaction with membrane lipids and promote the emergence of inclusion bodies.[306]

Moreover, the modulation of gromomycin activity by unsaturated fatty acids and lipids indicates that gromomycins interact directly with membrane lipids. The antibiotic activity was neutralized by mixing with unsaturated fatty acids and negatively charged phosphatidylglycerols. In such case, the amphiphilic scaffold of compound most likely facilitates its insertion into the membrain bilayer, herewith the hydrophobic triterpenoid core interacts with lipid acyl chains, and the positively charged guanidino group binds to anionic headgroups of lipids or cell wall components.[307] While it remains unclear whether gromomycins form an actual ion channel, it can be speculated that, upon reaching a critical concentration, additional molecules insert into the membrane or oligomerize to form transient pores. This in turn leads to disruption of membrane integrity and ultimately results in cell lysis.

Overall, the discovery of gromomycins marks a new chapter in bacterial natural products research. These compounds comprise a new family of secondary metabolites with an unusual chemical scaffold not previously observed in bacteria. Combined with their membrane-disruptive mechanisms of biological activity, large chemical space, and novel biosynthetic logic, the discovery of gromomycins paves the way for the further identification of new terpene antibiotics.

Darumycins: BGC identification, heterologous expression, isolation, proposed biosynthetic pathway, in vitro studies, and bioactivity profiling. (**Figure 1, C**) Investigation of the *gro*BGCs phylogenetic distribution revealed their vast presence, escpecially across *Streptomyces* strains. (Bratiichuk D., Fries F. et. al. (2025) *Genome Mining–Driven Isolation of New Gromomycins and Insights into Their Mode of Action* [Manuscript submitted for publication]). However, as demonstrated in the previous chapter, the non-*Streptomyces* actinobacteria could serve as a source of gromomycin related compounds, when judged on structure and organization of their gromomycin-like BGCs (*gro*BGCs). The genome mining with the focus on non-*Streptomycetes* actinobarteria yielded more than a dozen *gro*BGCs, with the most interesting ones found in the genomes of *Micromonospora sp.* NBC_01405 and *Micromonospora rubida*. These BGCs harbor additional genes encoding methyltransferase domain-containing protein. While methyltransferases are not new to the *gro*BGCs family, as shown with *S. flavoviridis* cluster,[300] the presence of two additional genes coding for methyltransferases in *M. rubida gro*BGC, hinted at the possible biosynthesis of new derivatives. Indeed, expression of *M. rubida gro*BGC in heterologous host led to the accumulation of new metabolited distinct from gromomycins. Surprisingly, the observed masses of these compounds suggested that they are not triterpenes, like gromomycins, but are new sesterterpenes. The isolation and structure characterization have confirmed this prediction. New compounds, named darumycins, differ from gromomycins by the lack of prenyl moiety on ring D, presence of methylated carboxyl group at C-24 and a methyl group at C-4.

The general organization of the darumycin BGC has high similarity to the gromomycin cluster,[300] indicating that both share common biosynthetic logic, but differ in the number of isoprene polymerization steps and tailoring modifications. Based on bioinformatic and functional analyses, the three genes, *darD, darB* and *darA* are supposed to play similar roles compared to their gromomycin homologs *groD, groH* and *groF*. The DarD enzyme is proposed to catalyze the condensation of five isoprenoid precursors to form pentaprenyl diphosphate, mirroring the role of GroD in gromomycin biosynthesis. Likewise, DarB is hypothesized to function as a prenyltransferase, catalyzing the formation of pentaprenylguanidine, which serves as the linear intermediate in darumycin biosynthesis. Subsequently, a putative cyclase DarA, together with a set of Rieske oxygenases DarE, DarF, and DarI, catalyze darumycin cyclization.

The methylation pattern of darumycin distinguishes these compounds from gromomycins. Two methyltransferases, DarG and DarM, are proposed to act sequentially, introducing methyl groups at hydroxy and carboxy moieties, respectively. Both proteins were expressed in *E. coli* and their functions were tested *in vitro*. DarG and DarM were shown to act

as SAM-dependent methyltransferases, each recognizing a specific substrate. The DarG is accepting as substrate compounds lacking the hydroxyl methyl group, while DarM preferentially methylates intermediates with a free carboxyl group. The inability of DarM to act on the intermediate lacking a terminal carboxyl group implies that structural maturation of the scaffold is required for DarM catalytic engagement. Such differential substrate preferences do suggest that DarM and DarG are site-specific, but do not necessarily act in a defined order.

The oxidation step, introducing the carboxyl group at position C-24 is suggested to be catalyzed by P450 oxygenase DarC. A similar activity has been previously described for a bacterial cytochrome P450 oxidase, catalyzing a multistep, regioselective oxidation of an inert methyl group to produce a carboxyl product through formation of the hydroxyl and aldehyde intermediates in pyrroindomycin biosynthesis.[354] Furthermore, a *Streptomyces*-derived cytochrome P450 enzyme has been documented to catalyze the conversion of a methyl group to a carboxyl group, through diol and aldehyde intermediates in indolosesquiterpene alkaloids, xiamycins.[336] In addition, a *Micromonospora*-derived cytochrome P450 monooxygenase RosC, catalyzes the three-step oxidation reactions, which leads to the formation of a hydroxy, formyl, and carboxy groups during rosamicin biosynthesis.[337]

In addition to core biosynthetic enzymes, the darumycin cluster contains several auxiliary and/or regulatory genes. For instance, the *darK* product appears to influence darumycin production, possibly functioning as a transcriptional regulator similar to to the RNA polymerase sigma factor RpoN.[329] The *darH* is annotated as a protein – tyrosine phosphatase. These regulatory enzymes can modulate secondary metabolism indirectly through dephosphorylation of transcription factors or biosynthetic enzymes, as shown with AfsR transcriptional regulator.[333, 335]

Based on bioinformatic and functional analyses, as well as targeted gene deletions we have suggested the darumycin biosynthetic pathway, which starts with a stepwise assembly of the pentaprenylguanidine intermediate, its cyclization, the subsequent methylation of the hydroxyl group, oxidation of the C-24 methyl group generating the carboxyl moiety, culminating in the methylation of the latter. It is noteworthy that even though both DarG and DarM methyltransferases are specific to a certain substrate, the available biochemical data do not allow an unambiguous determination of the chronological order of the methylation events *in vivo*. This ambiguity leaves another possibility, where both methyltransferases act after the introduction of the carboxyl group by DarC oxygenase.

Darumycins show a similar to gromomycins pattern of bioactivity. They have strong activity against Gram-positive bacteria and mycobacteria, but limited efficiency on Gram-negative bacteria due to low permeability. Furthermore, the differences in methylation and carboxylation were shown to affect antibacterial potency: the single demethylated darumycins B and F, and particularly the double demethylated darumycin E show reduced activity, suggesting that the polar functional groups influence the hydrophobic interactions essential for membrane binding. Furthermore, the highly hydrophobic darumycins C and D have stronger antibacterial activity in comparizon even to darumycins A and G. This observation suggests that darumycins, like gromomycins, exert their antibacterial effect throught interaction with the bacterial membrane.

4. Conclusions and Outlook

In this dissertation, the three chapters represent a single coherent narrative. It starts with the discovery of gromomycins, their isolation, the biosynthetic pathway studies, and characterization of biological activity. Gromomycins, derived from *Streptomyces* bacteria, are pentacyclic triterpenes with a cyclic guanidino group, and demonstrate a high activity against some of the most challenging pathogens, including methicillin-resistant *S. aureus* (MRSA) and *M. tuberculosis*. What makes them particularly exciting is their unique biosynthesis, which follows a previously unknown pathway for triterpene skeleton assembly. Additionally, the gromomycin BGC was identified through transposon mutagenesis, as bioinformatics tools failed to detect it. The discovery of gromomycin BGC enriched our knowledge about natural products biosynthesis and will serve as a new pattern for bioinformatic instruments dedicated to BGC prediction.

Leveraging our understanding of gromomycin biosynthesis, we have identified new bioactive derivatives via the genome-mining approach, highlighting the significant untapped potential of rare actinobacteria in the field of antibiotic discovery. Mode of action studies have demonstrated that gromomycins act through a previously uncharacterized membrane-targeting mechanism, causing rapid depolarization and potassium ion leakage in *S. aureus*. Their significant activity against vancomycin-resistant *E. faecium* isolates highlights the potential of this new antibiotic family.

Finally, utilizing the genome-mining approach, we have discovered novel guanidine-bearing sesterterpenes, named darumycins. Performing targeted gene deletions within the darumycin BGC generated a number of new bioactive derivatives, enriching the chemical space of the rare sesterterpene class. This, combined with in vitro biosynthetic studies, and characterization of darumycin tailoring methyltransferases, provided critical insights into the biosynthetic pathway of darumycin.

Altogether, these findings expand the chemical diversity of known antimicrobial terpenes, demonstrating the effectiveness of genome mining as a strategy for identifying structurally novel and biologically active natural products. Furthermore, they provide insights into previously uncharacterized membrane-disruptive mechanisms of antibacterial action that hold growing therapeutic relevance in the context of multidrug resistance. As drug resistance continues to rise worldwide, the discovery of gromomycins and darumycins holds promise for addressing some of the most critical public health threats.

The discoveries presented in this dissertation open several promising avenues for future research. A deeper mechanistic understanding of the membrane-targeting activity of gromomycins and darumycins, especially regarding the molecular basis of their interaction with lipid components, may uncover principles relevant for designing safer analogues or selective membrane disruptors. Advancing structural biology efforts, such as resolving the architecture of Gro- and Dar-family enzymes, could reveal novel catalytic strategies in terpene biosynthesis and enable rational pathway engineering. Additionally, the broad distribution of related BGCs identified through genome mining suggests that many more guanidine-bearing terpenoids remain undiscovered. Systematic exploration of rare actinobacteria, coupled with state-of-the-art activation strategies for silent gene clusters, is likely to yield broader chemical diversity and potentially lead to discovery of new therapeutically relevant scaffolds. Finally, integrating synthetic biology with medicinal chemistry may allow the generation of optimized derivatives with reduced toxicity, improved pharmacological profiles and novel antibacterial mechanisms. This would provide a foundation for future antibiotic development in an era of escalating antimicrobial resistance.

References

1. Bharate, S. B.; Lindsley, C. W., Natural Products Driven Medicinal Chemistry. ACS J. Med. Chem.: 2024; Vol. 67, pp 20723-20730.

2. Coy-Barrera, E.; Ogungbe, I. V.; Schmidt, T. J., Natural Products for Drug Discovery in the 21st Century: Innovations for Novel Therapeutics. **2023,** *28* (9), 3690.

3. Atanasov, A. G.; Zotchev, S. B.; Dirsch, V. M.; Supuran, C. T., Natural Products in Drug Discovery: Advances and Opportunities. *Nat. Rev. Drug Discov.* **2021,** *20* (3), 200-216.

4. Newman, D. J.; Cragg, G. M.; Snader, K. M., The Influence of Natural Products Upon Drug Discovery. *Nat. Prod. Rep.* **2000,** *17* (3), 215-234.

5. Elshafie, H. S.; Camele, I.; Mohamed, A. A., A Comprehensive Review on the Biological, Agricultural and Pharmaceutical Properties of Secondary Metabolites Based-Plant Origin. *Int. J. Mol. Sci.* **2023,** *24* (4), 3266.

6. Nakanishi, K., Natural Products Cmistry - Past and Future. In *Natural Products of Woody Plants: Chemicals Extraneous to the Lignocellulosic Cell Wall*, Springer: 1989; pp 13-25.

7. Sanchez, S.; Demain, A. L., Metabolic Regulation and Overproduction of Primary Metabolites. *Microb. Biotechnol.* **2008,** *1* (4), 283-319.

8. Hounsome, N.; Hounsome, B.; Lobo, M. G., Biochemistry of Vegetables. In *Handbook of Vegetables and Vegetable Processing*, 2018; pp 25-46.

9. Marks, B. B.; Nogueira, M. A.; Hungria, M., Microbial Secondary Metabolites and Their Use in Achieving Sustainable Agriculture: Present Achievements and Future Challenges. *Agronomy* **2025,** *15* (6), 1350.

10. O'Brien, J.; Wright, G. D., An Ecological Perspective of Microbial Secondary Metabolism. *Curr. Opin. Biotechnol.* **2011,** *22* (4), 552-558.

11. Pyne, M. E.; Narcross, L.; Martin, V. J. J., Engineering Plant Secondary Metabolism in Microbial Systems. *Plant. Physiol.* **2019,** *179* (3), 844-861.

12. Al-Khayri, J. M.; Rashmi, R.; Toppo, V.; Chole, P. B.; Banadka, A.; Sudheer, W. N.; Nagella, P.; Shehata, W. F.; Al-Mssallem, M. Q.; Alessa, F. M.; Almaghasla, M. I.; Rezk, A. A., Plant Secondary Metabolites: The Weapons for Biotic Stress Management. *Metabolites* **2023,** *13* (6).

13. Van Beirs, C.; El Houari, I.; Vanholme, B., Nature's laboratory: plant metabolic engineering methods using phenylpropanoids as a case study. *Biotechnol. Biofuels Bioprod.* **2025,** *18* (1), 81.

14. Staniek, A.; Bouwmeester, H.; Fraser, P. D.; Kayser, O.; Martens, S.; Tissier, A.; van der Krol, S.; Wessjohann, L.; Warzecha, H., Natural Products – Modifying Metabolite Pathways in Plants. *Biotechnol. J.* **2013,** *8* (10), 1159-1171.

15. Rami, E.; Singh, A.; Favzulazim, S., An Overview of Plant Secondary Metabolites, Their Biochemistry and Generic Applications. *J. Phytopharm.* **2021,** *10*, 421-428.

16. Dictionary of Natural Products, C. P., Taylor & Francis; Group, B. R., FL, USA, [Online Database], https://dnp.chemnetbase.com.

17. Xavier, V.; Spréa, R.; Finimundy, T. C.; Heleno, S. A.; Amaral, J. S.; Barros, L.; Ferreira, I. C. F. R., Terpenes. In *Natural Secondary Metabolites: From Nature, Through Science, to Industry*, Carocho, M.; Heleno, S. A.; Barros, L., Eds. Springer International Publishing: Cham, 2023; pp 107-156.

18. Jha, A., Plant terpenes. In *Phytoconstituents and Antifungals*, Kumar, A., Ed. Academic Press: 2022; pp 77-87.

19. Mabou, F. D.; Yossa, I. B. N., TERPENES: Structural Classification and Biological Activities. *IOSR J Pharm Biol Sci* **2021,** *16*, 25-40.

20. Rudolf, J. D.; Alsup, T. A.; Xu, B.; Li, Z., Bacterial Terpenome. *Nat. Prod. Rep.* **2021,** *38* (5), 905-980.

21. Gross, H.; König, G. M., Terpenoids from Marine Organisms: Unique Structures and their Pharmacological Potential. *Phytochem. Rev.* **2006,** *5*, 115-141.

22. Zhang, F.-L.; Feng, T., Diterpenes Specially Produced by Fungi: Structures, Biological Activities, and Biosynthesis (2010–2020). *J. Fungi* **2022,** *8* (3), 244.

23. Masyita, A.; Mustika Sari, R.; Dwi Astuti, A.; Yasir, B.; Rahma Rumata, N.; Emran, T. B.; Nainu, F.; Simal-Gandara, J., Terpenes and Terpenoids as Main Bioactive Compounds of Essential Oils, their Roles in Human Health and Potential Application as Natural Food Preservatives. *Food Chem. X* **2022,** *13*, 100217.

24. Hanssens, J.; Meneses, D.; Saya, J. M.; Orru, R. V. A., Terpenes and Terpenoids: How Can We Use Them? *Eur. J. Org. Chem.* **2025,** *28* (24), e202401151.

25. Siddiqui, T.; Khan, M. U.; Sharma, V.; Gupta, K., Terpenoids in Essential Oils: Chemistry, Classification, and Potential Impact on Human Health and Industry. *Phytomedicine Plus* **2024,** *4* (2), 100549.

26. Hong, J., Role of natural product diversity in chemical biology. *Curr. Opin. Chem. Biol.* **2011,** *15* (3), 350-4.

27. Holstein, S. A.; Hohl, R. J., Isoprenoids: Remarkable Diversity of Form and Function. *Lipids* **2004,** *39* (4), 293-309.

28. Dembitsky, V. M., Naturally Occurring Norsteroids and Their Design and Pharmaceutical Application. *Biomedicines* **2024,** *12* (5), 1021.

29. Sharmila, A.; Bhadra, P.; Kishore, C.; Selvaraj, C. I.; Kavalakatt, J.; Bishayee, A., Nanoformulated Terpenoids in Cancer: A Review of Therapeutic Applications, Mechanisms, and Challenges. *Cancers* **2025,** *17* (18).

30. Wei, X.; Ning, W.; McCadden, C. A.; Alsup, T. A.; Li, Z.; Łomowska-Keehner, D. P.; Nafie, J.; Qu, T.; Opoku, M. O.; Gillia, G. R.; Xu, B.; Icenhour, D. G.; Rudolf, J. D., Exploring and Expanding the Natural Chemical Space of Bacterial Diterpenes. *Nat. Commun.* **2025,** *16* (1), 3721.

31. Weise, T.; Thürmer, A.; Brady, S.; Kai, M.; Daniel, R.; Gottschalk, G.; Piechulla, B., VOC Emission of Various *Serratia* Species and Isolates and Genome Analysis of *Serratia plymuthica* 4Rx13. *FEMS Microbiol. Lett.* **2014,** *352* (1), 45-53.

32. Garbeva, P.; Avalos, M.; Ulanova, D.; van Wezel, G. P.; Dickschat, J. S., Volatile Sensation: The Chemical Ecology of the Earthy Odorant Geosmin. *Environ. Microbiol.* **2023,** *25* (9), 1565-1574.

33. Cho, J. Y.; Kwon, H. C.; Williams, P. G.; Jensen, P. R.; Fenical, W., Azamerone, a Terpenoid Phthalazinone from a Marine-Derived Bacterium Related to the Genus *Streptomyces* (Actinomycetales). *Org. Lett.* **2006,** *8* (12), 2471-4.

34. Martens, E.; Demain, A. L., Platensimycin and Platencin: Promising Antibiotics for Future Application in Human Medicine. *J. Antibiot. (Tokyo)* **2011,** *64* (11), 705-10.

35. Wissner, J. L.; Almeida, J. R.; Grilo, I. R.; Oliveira, J. F.; Brízida, C.; Escobedo-Hinojosa, W.; Pissaridou, P.; Vasquez, M. I.; Cunha, I.; Sobral, R. G.; Vasconcelos, V.; Gaudêncio, S. P., Novel Metabolite Madeirone and Neomarinone Extracted from *Streptomyces aculeoletus* as Marine Antibiofilm and Antifouling Agents. *Front. Chem.* **2024,** *12*, 1425953.

36. Macherla, V. R.; Liu, J.; Bellows, C.; Teisan, S.; Nicholson, B.; Lam, K. S.; Potts, B. C. M., Glaciapyrroles A, B, and C, Pyrrolosesquiterpenes from a *Streptomyces* sp. Isolated from an Alaskan Marine Sediment. *J. Nat. Prod.* **2005,** *68* (5), 780-783.

37. Ning, W.; Rudolf, J. D., Discovery of Bacterial Terpenoids by Genome Mining. *Methods Enzymol.* **2025,** *717*, 349-385.

38. Liu, X.; Xin, J.; Sun, Y.; Zhao, F.; Niu, C.; Liu, S., Terpenoids from Marine Sources: A Promising Avenue for New Antimicrobial Drugs. *Marine Drugs* **2024,** *22* (8), 347.

39. Amiri Moghaddam, J.; Jautzus, T.; Alanjary, M.; Beemelmanns, C., Recent Highlights of Biosynthetic Studies on Marine Natural Products. *Org. Biomol. Chem.* **2021,** *19* (1), 123-140.

40. Pimentel, L.; Carsanba, E.; Teixeira, F.; Vidigal, S.; Pintado, M.; Oliveira, C.; Rodríguez-Alcalá, L. M., Microbial Production of Terpenes. In *Microbial Production of Food Bioactive Compounds*, Jafari, S. M.; Darvishi Harzevili, F.; Karaca, A. C., Eds. Springer Nature Switzerland: Cham, 2025; pp 997-1033.

41. Sharkey, T. D.; Yeh, S., Isoprene Emission from Plants. *Annu. Rev. Plant Biol.* **2001,** *52* (1), 407-436.

42. Del Prado-Audelo, M. L.; Cortés, H.; Caballero-Florán, I. H.; González-Torres, M.; Escutia-Guadarrama, L.; Bernal-Chávez, S. A.; Giraldo-Gomez, D. M.; Magaña, J. J.; Leyva-Gómez, G., Therapeutic Applications of Terpenes on Inflammatory Diseases. *Front. Pharmacol.* **2021,** *12*, 704197.

43. Hillier, S. G.; Lathe, R., Terpenes, Hormones and Life: Isoprene Rule Revisited. *J. Endocrinol.* **2019,** *242* (2), R9-R22.

44. Ruzicka, L.; Eschenmoser, A.; Heusser, H., Biogenesis of Steroids and Terpenic Compounds. *Experientia* **1953,** *9*, 357-367.

45. Sell, C. S., *A Fragrant Introduction to Terpenoid Chemistry* . Royal Society of Chemistry: 2003.

46. Schwarzbauer, J.; Jovančićević, B., Isoprenoids. In *From Biomolecules to Chemofossils*, Schwarzbauer, J.; Jovančićević, B., Eds. Springer International Publishing: Cham, 2016; pp 27-76.

47. Christianson, D. W., Structural and Chemical Biology of Terpenoid Cyclases. *Chem. Rev.* **2017,** *117* (17), 11570-11648.

48. Ninkuu, V.; Zhang, L.; Yan, J.; Fu, Z.; Yang, T.; Zeng, H., Biochemistry of Terpenes and Recent Advances in Plant Protection. *Int. J. Mol. Sci.* **2021,** *22* (11), 5710.

49. Kang, A.; Lee, T. S., Chapter 2 - Secondary Metabolism for Isoprenoid-Based Biofuels. In *Biotechnology for Biofuel Production and Optimization*, Eckert, C. A.; Trinh, C. T., Eds. Elsevier: Amsterdam, 2016; pp 35-71.

50. Kim, H.-Y.; Kim, J.-H., Sesquiterpenoids Isolated from the Rhizomes of Genus Atractylodes. *Chem. Biodiversity* **2022,** *19* (12), e202200703.

51. Chappell, J.; Coates, R. M., 1.16 - Sesquiterpenes. In *Comprehensive Natural Products II*, Liu, H.-W.; Mander, L., Eds. Elsevier: Oxford, 2010; pp 609-641.

52. Abu-Izneid, T.; Rauf, A.; Shariati, M. A.; Khalil, A. A.; Imran, M.; Rebezov, M.; Uddin, M. S.; Mahomoodally, M. F.; Rengasamy, K. R. R., Sesquiterpenes and their Derivatives-Natural Anticancer Compounds: An Update. *Pharmacol Res.* **2020,** *161*, 105165.

53. Hu, Z.; Liu, X.; Tian, M.; Ma, Y.; Jin, B.; Gao, W.; Cui, G.; Guo, J.; Huang, L., Recent Progress and New Perspectives for Diterpenoid Biosynthesis in Medicinal Plants. *Medicinal Research Reviews* **2021,** *41* (6), 2971-2997.

54. Weaver, B. A., How Taxol/Paclitaxel Kills Cancer Cells. *Molecular biology of the cell* **2014,** *25* (18), 2677-81.

55. Chen, Q.; Li, J.; Ma, Y.; Yuan, W.; Zhang, P.; Wang, G., Occurrence and Biosynthesis of Plant Sesterterpenes (C25), a New Addition to Terpene Diversity. *Plant Commun.* **2021,** *2* (5), 100184.

56. Iobbi, V.; Parisi, V.; Giacomini, M.; De Riccardis, F.; Brun, P.; Núñez-Pons, L.; Drava, G.; Giordani, P.; Monti, M. C.; Poggi, R., Sesterterpenoids: Sources, Structural Diversity, Biological Activity, and Data Management. *Nat. Prod. Rep.* **2025,** *42* (3), 443-481.

57. Ludwiczuk, A.; Skalicka-Woźniak, K.; Georgiev, M. I., Chapter 11 - Terpenoids. In *Pharmacognosy*, Badal, S.; Delgoda, R., Eds. Academic Press: Boston, 2017; pp 233-266.

58. Olatunde, O. Z.; Yong, J.; Tian, D.; Lu, C., Comprehensive Review of Plant-Derived Triterpenoid Types, Structures and Cytotoxicity: an Update from 2015 to 2024. *Org. Biomol. Chem.* **2025,** *23* (25), 5929-6051.

59. Ninkuu, V.; Zhang, L.; Yan, J.; Fu, Z.; Yang, T.; Zeng, H., Biochemistry of Terpenes and Recent Advances in Plant Protection. *Int. J. Mol. Sci.* **2021,** *22* (11).

60. Danila, A., Chapter 12 - Natural Dyes and Pigments in Protective and Healthcare Textiles. In *Renewable Dyes and Pigments*, Ul Islam, S., Ed. Elsevier: 2024; pp 253-269.

61. Trepa, M.; Sułkowska-Ziaja, K.; Kała, K.; Muszyńska, B., Therapeutic Potential of Fungal Terpenes and Terpenoids: Application in Skin Diseases. *Molecules* **2024,** *29* (5).

62. Bouhss, A.; Trunkfield, A. E.; Bugg, T. D. H.; Mengin-Lecreulx, D., The Biosynthesis of Peptidoglycan Lipid-Linked Intermediates. *FEMS Microbiology Reviews* **2008,** *32* (2), 208-233.

63. Sommer, S.; Lang, L. M.; Drummond, L.; Buchhaupt, M.; Fraatz, M. A.; Zorn, H., Odor Characteristics of Novel Non-Canonical Terpenes. *Molecules* **2022,** *27* (12), 3827.

64. Ma, M.; Li, M.; Wu, Z.; Liang, X.; Zheng, Q.; Li, D.; Wang, G.; An, T., The Microbial Biosynthesis of Noncanonical Terpenoids. *Appl. Microbiol. Biotechnol.* **2024,** *108* (1), 226.

65. Nazir, M.; Saleem, M.; Tousif, M. I.; Anwar, M. A.; Surup, F.; Ali, I.; Wang, D.; Mamadalieva, N. Z.; Alshammari, E.; Ashour, M. L.; Ashour, A. M.; Ahmed, I.; Elizbit; Green, I. R.; Hussain, H., Meroterpenoids: A Comprehensive Update Insight on Structural Diversity and Biology. *Biomolecules* **2021,** *11* (7).

66. Fuloria, N. K.; Raheja, R. K.; Shah, K. H.; Oza, M. J.; Kulkarni, Y. A.; Subramaniyan, V.; Sekar, M.; Fuloria, S., Biological Activities of Meroterpenoids Isolated from Different Sources. *Front. pharmacol.* **2022,** *Volume 13 - 2022*.

67. de Lima, M. C. F.; da Silva, L. S.; Wiedemann, L. S. M.; da Veiga, V. F., A Brief History of Terpenoids. In *Terpenoids Against Human Diseases*, CRC Press: 2019; pp 1-15.

68. Breitmaier, E., Terpenes: Importance, General Structure, and Biosynthesis. *Terpenes: Flavors, Fragrances, Pharmaca, Pheromones* **2006,** *1*, 1-3.

69. Croteau, R., The Discovery of Terpenes. In *Discoveries In Plant Biology: (Volume I)*, World Scientific: 1998; pp 329-343.

70. Hoshino, Y., Terpenoids and Membrane Dynamics Evolution. *Frontiers in Ecology and Evolution* **2024,** *Volume 12 - 2024*.

71. Komppa, G., Die vollständige Synthese der Camphersäure und Dehydrocamphersäure. *Ber. Dtsch. Chem. Ges.* **1903,** *36* (4), 4332-4335.

72. Schwab, W.; Davidovich-Rikanati, R.; Lewinsohn, E., Biosynthesis of Plant-Derived Flavor Compounds. *Plant J.* **2008,** *54* (4), 712-732.

73. Câmara, J. S.; Perestrelo, R.; Ferreira, R.; Berenguer, C. V.; Pereira, J. A. M.; Castilho, P. C., Plant-Derived Terpenoids: A Plethora of Bioactive Compounds with Several Health Functions and Industrial Applications-A Comprehensive Overview. *Molecules* **2024,** *29* (16).

74. de Vega, C.; Herrera, C. M.; Dötterl, S., Floral Volatiles Play a Key Role in Specialized Ant Pollination. *Perspect. Plant Ecol.* **2014,** *16* (1), 32-42.

75. Abbas, F.; O'Neill Rothenberg, D.; Zhou, Y.; Ke, Y.; Wang, H.-C., Volatile Organic Compounds as Mediators of Plant Communication and Adaptation to Climate Change. *Physiol. Plant.* **2022,** *174* (6), e13840.

76. Wang, G.; Tang, W.; Bidigare, R. R., Terpenoids As Therapeutic Drugs and Pharmaceutical Agents. In *Natural Products: Drug Discovery and Therapeutic Medicine*, Zhang, L.; Demain, A. L., Eds. Humana Press: Totowa, NJ, 2005; pp 197-227.

77. Helfrich, E. J. N.; Lin, G.-M.; Voigt, C. A.; Clardy, J., Bacterial Terpene Biosynthesis: Challenges and Opportunities for Pathway Engineering. *Beilstein J. Org. Chem.* **2019,** *15*, 2889-2906.

78. Yamada, Y.; Kuzuyama, T.; Komatsu, M.; Shin-Ya, K.; Omura, S.; Cane, D. E.; Ikeda, H., Terpene Synthases are Widely Distributed in Bacteria. *Proc. Natl. Acad. Sci. U S A* **2015,** *112* (3), 857-62.

79. Spellberg, B., The Future of Antibiotics. *Critical Care* **2014,** *18* (3), 228.

80. Miethke, M.; Pieroni, M.; Weber, T.; Brönstrup, M.; Hammann, P.; Halby, L.; Arimondo, P. B.; Glaser, P.; Aigle, B.; Bode, H. B., Towards the Sustainable Discovery and Development of New Antibiotics. *Nat. Rev. Chem.* **2021,** *5* (10), 726-749.

81. Gavagnin, M.; Carbone, M.; Ciavatta, M.-L.; Mollo, E., Natural Products from Marine Heterobranchs: An Overview of Recent Results. *Chem. J. Mold.* **2019,** *14* (2), 9-31.

82. Dai, T.; Wang, Y.; Zhang, W. W.; An, J.; Zhang, S.; Zhang, Z.; Luo, X.; Ding, Y.; Wu, Z.; Liu, Y., Biologically Active Guanidine Alkaloids. *Acta Mater. Med.* **2025,** *4* (4), 570-606.

83. Duca, G.; Aricu, A.; Kuchkova, K.; Secara, E.; Barba, A.; Dragalin, I.; Ungur, N.; Spengler, G., Synthesis, Structural Elucidation and Biological Evaluations of New Guanidine-Containing Terpenoids as Anticancer Agents. *Nat. Prod. Res.* **2019,** *33* (21), 3052-3056.

84. Andreev, K.; Bianchi, C.; Laursen, J. S.; Citterio, L.; Hein-Kristensen, L.; Gram, L.; Kuzmenko, I.; Olsen, C. A.; Gidalevitz, D., Guanidino Groups Greatly Enhance the Action of Antimicrobial Peptidomimetics Against Bacterial Cytoplasmic Membranes. *Biochim. Biophys. Acta.* **2014,** *1838* (10), 2492-2502.

85. Muttathukattil, A. N.; Srinivasan, S.; Halder, A.; Reddy, G., Role of Guanidinium-Carboxylate Ion Interaction in Enzyme Inhibition with Implications for Drug Design. *J. Phys. Chem. B.* **2019,** *123* (44), 9302-9311.

86. Mo, S.; Krunic, A.; Pegan, S. D.; Franzblau, S. G.; Orjala, J., An Antimicrobial Guanidine-Bearing Sesterterpene from the Cultured Cyanobacterium *Scytonema* sp. *J. Nat. Prod.* **2009,** *72* (11), 2043-5.

87. Espinoza-Moraga, M.; Njuguna, N. M.; Mugumbate, G.; Caballero, J.; Chibale, K., In silico Comparison of Antimycobacterial Natural Products with Known Antituberculosis Drugs. *J. Chem. Inf. Model* **2013,** *53* (3), 649-60.

88. Swain, S. S.; Paidesetty, S. K.; Padhy, R. N., Antibacterial, Antifungal and Antimycobacterial Compounds from Cyanobacteria. *Biomed. Pharmacother.* **2017,** *90*, 760-776.

89. Cabanillas, A. H.; Tena Pérez, V.; Maderuelo Corral, S.; Rosero Valencia, D. F.; Martel Quintana, A.; Ortega Doménech, M.; Rumbero Sánchez, Á., Cybastacines A and B: Antibiotic Sesterterpenes from a *Nostoc* sp. Cyanobacterium. *J. Nat. Prod.* **2018,** *81* (2), 410-413.

90. do Amaral, S. C.; Xavier, L. P.; Vasconcelos, V.; Santos, A. V., Cyanobacteria: A Promising Source of Antifungal Metabolites. *Marine Drugs* **2023,** *21* (6), 359.

91. Li, K.; Gustafson, K. R., Sesterterpenoids: Chemistry, Biology, and Biosynthesis. *Nat. Prod. Rep.* **2021,** *38* (7), 1251-1281.

92. Zill, N. A.; Du, Y.; Marinkovich, S.; Gu, D.; Seidel, J.; Zhang, W., Bioactive Natural Product Discovery via Deuterium Adduct Bioactivity Screening. *ACS Chem. Biol.* **2023,** *18* (5), 1192-1199.

93. Carbone, M.; Ciavatta, M. L.; Mathieu, V.; Ingels, A.; Kiss, R.; Pascale, P.; Mollo, E.; Ungur, N.; Guo, Y. W.; Gavagnin, M., Marine Terpenoid Diacylguanidines: Structure, Synthesis, and Biological Evaluation of Naturally Occurring Actinofide and Synthetic Analogues. *J. Nat. Prod.* **2017,** *80* (5), 1339-1346.

94. Putz, A.; Kehraus, S.; Díaz-Agras, G.; Wägele, H.; König, G. M., Dotofide, a Guanidine-Interrupted Terpenoid from the Marine Slug *Doto pinnatifida* (Gastropoda, Nudibranchia). *Eur. J. Org. Chem.* **2011,** *2011* (20-21), 3733-3737.

95. Babot, E. D.; Aranda, C.; Del Rı, O. J.; Ullrich, R.; Kiebist, J.; Scheibner, K.; Hofrichter, M.; Martı Nez, A. T.; Gutiérrez, A., Selective Oxygenation of Ionones and Damascones by Fungal Peroxygenases. *J. Agric. Food Chem.* **2020,** *68* (19), 5375-5383.

96. Serra, S.; Cominetti, A. A.; Lissoni, V., Use of (S)-trans-γ-Monocyclofarnesol as a Useful Chiral Building Block for the Stereoselective Synthesis of Diterpenic Natural Products. *Nat. Prod. Commun.* **2014,** *9* (3), 1934578X1400900312.

97. Stout, E. P.; Yu, L. C.; Molinski, T. F., Antifungal Diterpene Alkaloids from the Caribbean Sponge Agelas citrina: Unified Configurational Assignments of Agelasidines and Agelasines. *European J. Org. Chem.* **2012,** *2012* (27), 5131-5135.

98. Lin, Y.-C.; Chao, C.-H.; Fu, C.-W.; Chiou, S.-F.; Huang, T.-Y.; Yang, Y.-J.; Wu, S.-H.; Chen, S.-L.; Wang, H.-C.; Yu, M.-C.; Huang, H.-C.; Sheu, J.-H., Computationally assisted structure elucidation of new 2-guanidinoethanesulfonyl sesquiterpenoid alkaloids: Agelasidines G–I from the marine sponge Agelas nakamurai. *Tetrahedron* **2022,** *126*, 133077.

99. Coqueiro, A.; Regasini, L. O.; Stapleton, P.; da Silva Bolzani, V.; Gibbons, S., In Vitro Antibacterial Activity of Prenylated Guanidine Alkaloids from Pterogyne nitens and Synthetic Analogues. *J. Nat. Prod.* **2014,** *77* (8), 1972-1975.

100. Tajima, Y.; Murase, H.; Satake, K.; Mitani, Y.; Regasini, L. O.; da Silva Bolzani, V.; Efferth, T.; Nakagawa, H., Nitensidine A, a Guanidine Alkaloid from *Pterogyne nitens*, Induces Osteoclastic Cell Death. *Cytotechnology* **2015,** *67* (4), 585-592.

101. Zárraga, M.; Zárraga, A. M.; Rodríguez, B.; Pérez, C.; Paz, C.; Paz, P.; Sanhueza, C., Synthesis of a New Nitrogenated Drimane Derivative with Antifungal Activity. *Tetrahedron Lett.* **2008,** *49* (32), 4775-4776.

102. Grinco, M.; Morarescu, O.; Lembo, F.; Ungur, N.; Turco, L.; Coretti, L.; Carbone, M.; Celentano, C.; Ciavatta, M. L.; Mollo, E.; Kulcitki, V.; Buommino, E., Synthesis and Antimicrobial Properties of Guanidine-Functionalized Labdane Type Diterpenoids. *Eur. J. Med. Chem.* **2024,** *264*, 115981.

103. Wang, Q.; Quan, S.; Xiao, H., Towards Efficient Terpenoid Biosynthesis: Manipulating IPP and DMAPP Supply. *BIOB.* **2019,** *6* (1), 6.

104. Jahangeer, M.; Fatima, R.; Ashiq, M.; Basharat, A.; Qamar, S. A.; Bilal, M.; Iqbal, H., Therapeutic and Biomedical Potentialities of Terpenoids-A Review. *JPAM* **2021,** *15* (2).

105. Pérez-Gil, J.; Rodríguez-Concepción, M., Metabolic Plasticity for Isoprenoid Biosynthesis in Bacteria. *Biochem J.* **2013,** *452* (1), 19-25.

106. Kuzuyama, T.; Seto, H., Diversity of the Biosynthesis of the Isoprene Units. *Nat. Prod. Rep.* **2003,** *20* (2), 171-83.

107. Rodríguez-Concepción, M.; Boronat, A., Breaking New Ground in the Regulation of the Early Steps of Plant Isoprenoid Biosynthesis. *Curr. Opin. Plant Biol.* **2015,** *25*, 17-22.

108. Oldfield, E.; Lin, F. Y., Terpene Biosynthesis: Modularity Rules. *Angew. Chem. Int. Ed. Engl.* **2012,** *51* (5), 1124-37.

109. Li, C.; Zha, W.; Li, W.; Wang, J.; You, A., Advances in the Biosynthesis of Terpenoids and Their Ecological Functions in Plant Resistance. *Int. J. Mol. Sci.* **2023,** *24* (14), 11561.

110. Brock, N. L.; Dickschat, J. S., Biosynthesis of Terpenoids. In *Natural Products: Phytochemistry, Botany and Metabolism of Alkaloids, Phenolics and Terpenes*, Ramawat, K. G.; Mérillon, J.-M., Eds. Springer Berlin Heidelberg: Berlin, Heidelberg, 2013; pp 2693-2732.

111. Chang, Z.; Li, Y.; Lu, Y.; Xiao, H., Towards Crucial Post-Modification in Biosynthesis of Terpenoids and Steroids: C3 Oxidase and Acetyltransferase. *Enzyme Microb. Technol.* **2023,** *162*, 110148.

112. Kennewick, K. T.; Bensinger, S. J., Decoding the Crosstalk Between Mevalonate Metabolism and T cell Function. *Immunol. Rev.* **2023,** *317* (1), 71-94.

113. Lynen, F., Der Weg von der „aktivierten Essigsäure" zu den Terpenen und Fettsäuren. Nobel-Vortrag am 11. Dezember 1964. *Angew. Chem.* **1965,** *77* (21), 929-944.

114. Wright, L. D.; Cresson, E. L.; Skeggs, H. R.; MacRae, G. D. E.; Hoffman, C. H.; Wolf, D. E.; Folkers, K., Isolation of a New Acetate-Replacing Factor. *J. Am. Chem. Soc.* **1956,** *78* (20), 5273-5275.

115. Rohmer, M.; Knani, M.; Simonin, P.; Sutter, B.; Sahm, H., Isoprenoid Biosynthesis in Bacteria: a Novel Pathway for the Early Steps Leading to Isopentenyl Diphosphate. *Biochem. J.* **1993,** *295 (Pt 2)* (Pt 2), 517-24.

116. Frank, A.; Groll, M., The Methylerythritol Phosphate Pathway to Isoprenoids. *Chem. Rev.* **2017,** *117* (8), 5675-5703.

117. Hemmerlin, A.; Harwood, J. L.; Bach, T. J., A Raison d'être for Two Distinct Pathways in the Early Steps of Plant Isoprenoid Biosynthesis? *Prog. Lipid Res.* **2012,** *51* (2), 95-148.

118. Pérez-Gil, J.; Rodríguez-Concepción, M., Metabolic Plasticity for Isoprenoid Biosynthesis in Bacteria. *Biochem. J.* **2013,** *452* (1), 19-25.

119. Chang, H.-Y.; Cheng, T.-H.; Wang, A. H. J., Structure, Catalysis, and Inhibition Mechanism of Prenyltransferase. *IUBMB Life* **2021,** *73* (1), 40-63.

120. Chen, R.; Gao, B.; Liu, X.; Ruan, F.; Zhang, Y.; Lou, J.; Feng, K.; Wunsch, C.; Li, S. M.; Dai, J.; Sun, F., Molecular Insights Into the Enzyme Promiscuity of an Aromatic Prenyltransferase. *Nat. Chem. Biol.* **2017,** *13* (2), 226-234.

121. Tarshis, L. C.; Yan, M.; Poulter, C. D.; Sacchettini, J. C., Crystal Structure of Recombinant Farnesyl Diphosphate Synthase at 2.6-A Resolution. *Biochemistry* **1994,** *33* (36), 10871-7.

122. Kellogg, B. A.; Poulter, C. D., Chain Elongation in the Isoprenoid Biosynthetic Pathway. *Curr. Opin. Chem. Biol.* **1997,** *1* (4), 570-8.

123. Sacchettini, J. C.; Poulter, C. D., Creating isoprenoid diversity. *Science (New York, N.Y.)* **1997,** *277* (5333), 1788-9.

124. Chen, C.-C.; Zhang, L.; Yu, X.; Ma, L.; Ko, T.-P.; Guo, R.-T., Versatile cis-isoprenyl Diphosphate Synthase Superfamily Members in Catalyzing Carbon–Carbon Bond Formation. *ACS Catalysis* **2020,** *10* (8), 4717-4725.

125. Liu, M.; Ma, Y.; Du, Q.; Hou, X.; Wang, M.; Lu, S., Functional Analysis of Polyprenyl Diphosphate Synthase Genes Involved in Plastoquinone and Ubiquinone Biosynthesis in *Salvia miltiorrhiza*. *Front. Plant Sci.* **2019,** *10*, 893.

126. Arendt, P.; Pollier, J.; Callewaert, N.; Goossens, A., Synthetic biology for production of natural and new-to-nature terpenoids in photosynthetic organisms. *Plant J.* **2016,** *87* (1), 16-37.

127. Zhou, X.; Rao, S.; Wrightstone, E.; Sun, T.; Lui, A. C. W.; Welsch, R.; Li, L., Phytoene Synthase: The Key Rate-Limiting Enzyme of Carotenoid Biosynthesis in Plants. *Front. Plant Sci.* **2022,** *13*, 884720.

128. Hoshino, Y.; Villanueva, L., Four Billion Years of Microbial Terpenome Evolution. *FEMS Microbiol. Rev.* **2023,** *47* (2).

129. Lloyd, C. T.; Iwig, D. F.; Wang, B.; Cossu, M.; Metcalf, W. W.; Boal, A. K.; Booker, S. J., Discovery, Structure and Mechanism of a Tetraether Lipid Synthase. *Nature* **2022,** *609* (7925), 197-203.

130. Heide, L., Prenyl Transfer to Aromatic Substrates: Genetics and Enzymology. *Curr. Opin. Chem. Biol.* **2009,** *13* (2), 171-9.

131. Chunkrua, P.; Leschonski, K. P.; Gran-Scheuch, A. A.; Vreeke, G. J. C.; Vincken, J. P.; Fraaije, M. W.; van Berkel, W. J. H.; de Bruijn, W. J. C.; Kabel, M. A., Prenylation of Aromatic Amino Acids and Plant Phenolics by An Aromatic Prenyltransferase from *Rasamsonia emersonii*. *Appl. Microbiol. Biotechnol.* **2024,** *108* (1), 421.

132. Fan, A.; Li, S.-M., Prenylation of Tyrosine and Derivatives by a Tryptophan C7-Prenyltransferase. *Tetrahedr.Lett.* **2014,** *55* (37), 5199-5202.

133. Melnyk, S.; Rebets, Y.; Bratiichuk, D.; Luzhetskyy, A.; Ostash, B., Gene amir_2071 of *Actinosynnema mirum* DSM 43827 Encodes a Dimethylallyltryptophan Synthase Superfamily Protein Responsible for the Production of Prenylated Tyrosine. *Folia Microbiol.* **2025**.

134. Ronnebaum, T. A.; Eaton, S. A.; Brackhahn, E. A. E.; Christianson, D. W., Engineering the Prenyltransferase Domain of a Bifunctional Assembly-Line Terpene Synthase. *Biochemistry* **2021,** *60* (42), 3162-3172.

135. Wenger, E. S.; Schultz, K.; Marmorstein, R.; Christianson, D. W., Engineering Substrate Channeling in Assembly-Line Terpene Biosynthesis. *bioRxiv* **2024**.

136. Mitsuhashi, T.; Abe, I., Chimeric Terpene Synthases Possessing both Terpene Cyclization and Prenyltransfer Activities. *Chembiochem : a European journal of chemical biology* **2018,** *19* (11), 1106-1114.

137. Wang, Z.; Yang, Q.; He, J.; Li, H.; Pan, X.; Li, Z.; Xu, H. M.; Rudolf, J. D.; Tantillo, D. J.; Dong, L. B., Cytochrome P450 Mediated Cyclization in Eunicellane Derived Diterpenoid Biosynthesis. *Angew. Chem. Int. Ed. Engl.* **2023,** *62* (45), e202312490.

138. Zhang, Q.; Catti, L.; Syntrivanis, L. D.; Tiefenbacher, K., En route to Terpene Natural Products Utilizing Supramolecular Cyclase Mimetics. *Nat. Prod. Rep.* **2019,** *36* (12), 1619-1627.

139. Faylo, J. L.; van Eeuwen, T.; Kim, H. J.; Gorbea Colón, J. J.; Garcia, B. A.; Murakami, K.; Christianson, D. W., Structural Insight on Assembly-Line Catalysis in Terpene Biosynthesis. *Nat. Commun.* **2021,** *12* (1), 3487.

140. Pan, X.; Rudolf, J. D.; Dong, L.-B., Class II terpene cyclases: structures, mechanisms, and engineering. *Nat. Prod. Rep.* **2024,** *41* (3), 402-433.

141. Rudolf, J. D.; Chang, C.-Y., Terpene Synthases in Disguise: Enzymology, Structure, and Opportunities of Non-Canonical Terpene Synthases. *Nat. Prod. Rep.* **2020,** *37* (3), 425-463.

142. Hong, Y. J.; Tantillo, D. J., A Potential Energy Surface Bifurcation in Terpene Biosynthesis. *Nat. Chem.* **2009,** *1* (5), 384-9.

143. Chen, Q.; Li, J.; Ma, Y.; Yuan, W.; Zhang, P.; Wang, G., Occurrence and Biosynthesis of Plant Sesterterpenes (C25), a New Addition to Terpene Diversity. *Plant Commun.* **2021,** *2* (5).

144. Chen, Q.; Li, J.; Liu, Z.; Mitsuhashi, T.; Zhang, Y.; Liu, H.; Ma, Y.; He, J.; Shinada, T.; Sato, T.; Wang, Y.; Liu, H.; Abe, I.; Zhang, P.; Wang, G., Molecular Basis for Sesterterpene Diversity Produced by Plant Terpene Synthases. *Plant Commun.* **2020,** *1* (5), 100051.

145. Siedenburg, G.; Jendrossek, D., Squalene-Hopene Cyclases. *Appl. Environ. Microbiol.* **2011,** *77* (12), 3905-15.

146. Nair, I. M.; Kochupurackal, J., Squalene Hopene Cyclases and Oxido Squalene Cyclases: Potential Targets for Regulating Cyclisation reactions. *Biotechnol. Lett.* **2023,** *45* (5-6), 573-588.

147. Abe, I., The Oxidosqualene Cyclases: One Substrate, Diverse Products. In *Nat. Prod.*, 2014; pp 293-316.

148. Oliaro-Bosso, S.; Caron, G.; Taramino, S.; Ermondi, G.; Viola, F.; Balliano, G., Characterization of the Channel Constriction Allowing the Access of the Substrate to the Active Site of Yeast Oxidosqualene Cyclase. *PloS one* **2011,** *6* (7), e22134.

149. Pan, X.; Du, W.; Zhang, X.; Lin, X.; Li, F.-R.; Yang, Q.; Wang, H.; Rudolf, J. D.; Zhang, B.; Dong, L.-B., Discovery, Structure, and Mechanism of a Class II Sesquiterpene Cyclase. *J. Am. Chem. Soc.* **2022,** *144* (48), 22067-22074.

150. Takahashi, I.; Ogura, K.; Seto, S., Heptaprenyl Pyrophosphate Synthetase from *Bacillus subtilis*. *J. Biol. Chem.* **1980,** *255* (10), 4539-43.

151. Sato, T.; Hoshino, H.; Yoshida, S.; Nakajima, M.; Hoshino, T., Bifunctional Triterpene/Sesquarterpene Cyclase: Tetraprenyl-β-curcumene Cyclase is Also Squalene Cyclase in *Bacillus megaterium*. *J. Am. Chem. Soc.* **2011,** *133* (44), 17540-3.

152. Takigawa, H.; Sugiyama, M.; Shibuya, Y., C(35)-Terpenes from *Bacillus subtilis* KSM 6-10. *J. Nat. Prod.* **2010,** *73* (2), 204-7.

153. Prisic, S.; Peters, R. J., Synergistic Substrate Inhibition of ent-Copalyl Diphosphate Synthase: A Potential Feed-Forward Inhibition Mechanism Limiting Gibberellin Metabolism. *Plant Physiol.* **2007,** *144* (1), 445-454.

154. Durairaj, J.; Girolamo, A. D.; Bouwmeester, H. J.; de Ridder, D.; Beekwilder, J.; van Dijk, A. D. J., An Analysis of Characterized Plant Sesquiterpene Synthases. *bioRxiv* **2018**, 466839.

155. Murai, K.; Lauterbach, L.; Teramoto, K.; Quan, Z.; Barra, L.; Yamamoto, T.; Nonaka, K.; Shiomi, K.; Nishiyama, M.; Kuzuyama, T.; Dickschat, J. S., An Unusual Skeletal Rearrangement in the Biosynthesis of the Sesquiterpene Trichobrasilenol from Trichoderma. *Angew. Chem. Int. Ed. Engl.* **2019,** *58* (42), 15046-15050.

156. Ma, J.; Li, D.; Xu, M.; Xia, Y.; Fang, G.; Wei, Q.; Ma, X.; Zhang, Y.; Zhang, Q.; Hu, Y.; Zhou, J.; Yin, X.; Hu, T., Multifunctional Sesquiterpene Synthase from *Curcuma wenyujin* Reveals the Biosynthetic Mechanism of Sesquiterpenes with Diverse Skeletons. *Int. J. Biol. Macromol.* **2025,** *318*, 145152.

157. Budde, J. L.; Çay, M.-Y.; Dräger, G.; Droste, J.; Hassanin, A.; Davari, M. D.; Kirschning, A., Reprogramming the Cyclization of the Sesquiterpene Synthase BcBOT2 Using 2,3-Z-Configured FPP Derivatives and by Means of "Methyl Mapping". *ACS Catalysis* **2025,** *15* (10), 8125-8139.

158. Huang, J. Q.; Fang, X., Amorpha-4,11-Diene Synthase: a Key Enzyme in Artemisinin Biosynthesis and Engineering. *aBIOTECH* **2021,** *2* (3), 276-288.

159. Faraldos, J. A.; Grundy, D. J.; Cascon, O.; Leoni, S.; van der Kamp, M. W.; Allemann, R. K., Enzymatic Synthesis of Natural (+)-Aristolochene from a Non-Natural Substrate. *Chem. Commun.* **2016,** *52* (97), 14027-14030.

160. Zuzarte, M.; Sousa, C.; Alves-Silva, J.; Salgueiro, L. Plant Monoterpenes and Essential Oils as Potential Anti-Ageing Agents: Insights from Preclinical Data *Biomedicines* [Online], 2024.

161. Janocha, S.; Schmitz, D.; Bernhardt, R., Terpene Hydroxylation with Microbial Cytochrome P450 Monooxygenases. In *Biotechnology of Isoprenoids*, Schrader, J.; Bohlmann, J., Eds. Springer International Publishing: Cham, 2015; pp 215-250.

162. Kakumu, Y.; Chaudhri, A. A.; Helfrich, E. J. N., The Role and Mechanisms of Canonical and Non-Canonical Tailoring Enzymes in Bacterial Terpenoid Biosynthesis. *Nat. Prod. Rep.* **2025,** *42* (3), 501-539.

163. Xiao, H.; Zhang, Y.; Wang, M., Discovery and Engineering of Cytochrome P450s for Terpenoid Biosynthesis. *Trends Biotechnol.* **2019,** *37* (6), 618-631.

164. King, A. J.; Brown, G. D.; Gilday, A. D.; Forestier, E.; Larson, T. R.; Graham, I. A., A Cytochrome P450-Mediated Intramolecular Carbon-Carbon Ring Closure in the Biosynthesis of Multidrug-Resistance-Reversing Lathyrane Diterpenoids. *Chembiochem : a European journal of chemical biology* **2016,** *17* (17), 1593-7.

165. Dong, L. B.; Rudolf, J. D.; Deng, M. R.; Yan, X.; Shen, B., Discovery of the Tiancilactone Antibiotics by Genome Mining of Atypical Bacterial Type II Diterpene Synthases. *Chembiochem : a European journal of chemical biology* **2018**.

166. Wang, L.; Chen, K.; Wang, Z.; Yi, Y.; Zhang, M.; Hasan, A.; Kuang, Y.; Shaker, S.; Yu, R.; Wang, H.; Liu, H.; Ye, M.; Qiao, X., AmAT19, an acetyltransferase from Astragalus membranaceus,

catalyses specific 6α-OH acetylation for tetracyclic triterpenes and steroids. *Org. Biomol. Chem* **2021,** *19* (33), 7186-7189.

167. Choi, H. S.; Han, J. Y.; Cheong, E. J.; Choi, Y. E., Characterization of a Pentacyclic Triterpene Acetyltransferase Involved in the Biosynthesis of Taraxasterol and ψ-Taraxasterol Acetates in Lettuce. *Front. Plant Sci.* **2021,** *12*, 788356.

168. Sarker, L. S.; Mahmoud, S. S., Cloning and Functional Characterization of Two Monoterpene Acetyltransferases from Glandular Trichomes of L. x intermedia. *Planta* **2015,** *242* (3), 709-19.

169. Chang, T. S.; Wu, J. Y.; Ding, H. Y.; Wang, T. Y., Enzymatic Glycosylation of Ganoderma Terpenoid via Bacterial Glycosyltransferases and Glycoside Hydrolases. *Biomolecules* **2025,** *15* (5).

170. Chang, T. S.; Wang, T. Y.; Chiang, C. M.; Lin, Y. J.; Chen, H. L.; Wu, Y. W.; Ting, H. J.; Wu, J. Y., Biotransformation of Celastrol to a Novel, Well-Soluble, Low-Toxic and Anti-Oxidative Celastrol-29-O-β-Glucoside by *Bacillus* Glycosyltransferases. *J. Biosci. Bioeng.* **2021,** *131* (2), 176-182.

171. González-Hernández, R. A.; Valdez-Cruz, N. A.; Macías-Rubalcava, M. L.; Trujillo-Roldán, M. A., Overview Fungal Terpene Synthases and Their Regulation. *World J. Microbiol. Biotechnol.* **2023,** *39* (7), 194.

172. Schmidt-Dannert, C., Biosynthesis of Terpenoid Natural Products in Fungi. *Adv. Biochem. Eng. Biotechnol.* **2015,** *148*, 19-61.

173. Singh, B.; Sharma, R. A., Plant Terpenes: Defense Responses, Phylogenetic Analysis, Regulation and Clinical Applications. *3 Biotech* **2015,** *5* (2), 129-151.

174. Komori, A.; Suzuki, M.; Seki, H.; Nishizawa, T.; Meyer, J. J. M.; Shimizu, H.; Yokoyama, S.; Muranaka, T., Comparative Functional Analysis of CYP71AV1 Natural Variants Reveals an Important Residue for the Successive Oxidation of Amorpha-4,11-Diene. *FEBS Letters* **2013,** *587* (3), 278-284.

175. Zabel, S.; Brandt, W.; Porzel, A.; Athmer, B.; Bennewitz, S.; Schäfer, P.; Kortbeek, R.; Bleeker, P.; Tissier, A., A Single Cytochrome P450 oxidase from *Solanum habrochaites* Sequentially Oxidizes 7-Epi-Zingiberene to Derivatives Toxic to Whiteflies and Various Microorganisms. *Plant J.* **2021,** *105* (5), 1309-1325.

176. Wang, J.; Pichersky, E., Characterization of S-Adenosyl-L-Methionine:(Iso)Eugenol O-Methyltransferase Involved in Floral Scent Production in *Clarkia breweri*. *Arch. Biochem. Biophys.* **1998,** *349* (1), 153-60.

177. Hannich, J. T.; Umebayashi, K.; Riezman, H., Distribution and Functions of Sterols and Sphingolipids. *Cold Spring Harb. Perspect. Biol.* **2011,** *3* (5).

178. McCarty, K. D.; Sullivan, M. E.; Tateishi, Y.; Hargrove, T. Y.; Lepesheva, G. I.; Guengerich, F. P., Processive Kinetics in the Three-Step Lanosterol 14α-Demethylation Reaction Catalyzed by Human Cytochrome P450 51A1. *J. Biol. Chem.* **2023,** *299* (7), 104841.

179. Hernàndez-Sebastiá, C.; Varin, L.; Marsolais, F., Sulfotransferases from Plants, Algae and Phototrophic Bacteria. In *Sulfur Metabolism in Phototrophic Organisms*, Hell, R.; Dahl, C.; Knaff, D.; Leustek, T., Eds. Springer Netherlands: Dordrecht, 2008; pp 111-130.

180. Helfrich, E. J. N.; Lin, G. M.; Voigt, C. A.; Clardy, J., Bacterial Terpene Biosynthesis: Challenges and Opportunities for Pathway Engineering. *Beilstein J. Org. Chem.* **2019,** *15*, 2889-2906.

181. Zhgun, A. A., Fungal BGCs for Production of Secondary Metabolites: Main Types, Central Roles in Strain Improvement, and Regulation According to the Piano Principle. *Int. J. Mol. Sci.* **2023,** *24* (13).

182. Lin, H. C.; Tsunematsu, Y.; Dhingra, S.; Xu, W.; Fukutomi, M.; Chooi, Y. H.; Cane, D. E.; Calvo, A. M.; Watanabe, K.; Tang, Y., Generation of Complexity in Fungal Terpene Biosynthesis: Discovery of a Multifunctional Cytochrome P450 in the Fumagillin Pathway. *J. Am. Chem. Soc.* **2014,** *136* (11), 4426-36.

183. Martín-Sánchez, L.; Singh, K. S.; Avalos, M.; van Wezel, G. P.; Dickschat, J. S.; Garbeva, P., Phylogenomic Analyses and Distribution of Terpene Synthases Among *Streptomyces*. *Beilstein J. Org. Chem.* **2019,** *15*, 1181-1193.

184. Dewett, D.; Lam-Kamath, K.; Poupault, C.; Khurana, H.; Rister, J., Mechanisms of Vitamin A Metabolism and Deficiency in the Mammalian and Fly Visual System. *Dev. Biol.* **2021,** *476*, 68-78.

185. Carazo, A.; Macáková, K.; Matoušová, K.; Krčmová, L. K.; Protti, M.; Mladěnka, P. Vitamin A Update: Forms, Sources, Kinetics, Detection, Function, Deficiency, Therapeutic Use and Toxicity *Nutrients* [Online], 2021.

186. Botelho, J.; Machado, V.; Proença, L.; Delgado, A. S.; Mendes, J. J., Vitamin D Deficiency and Oral Health: A Comprehensive Review. *Nutrients* **2020,** *12* (5).

187. Rizvi, S.; Raza, S. T.; Ahmed, F.; Ahmad, A.; Abbas, S.; Mahdi, F., The Role of Vitamin E in Human Health and Some Diseases. *Sultan Qaboos Univ. Med. J.* **2014,** *14* (2), e157-65.

188. Gomez-Sanchez, C. E.; Gomez-Sanchez, E. P., Cholesterol Availability and Adrenal Steroidogenesis. *Endocrinology* **2024,** *165* (4), bqae032.

189. Jin, H.; McCaffery, J. M.; Grote, E., Ergosterol Promotes Pheromone Signaling and Plasma Membrane Fusion in Mating Yeast. *J. Cell. Biol.* **2008,** *180* (4), 813-26.

190. Eliaš, D.; Tóth Hervay, N.; Gbelská, Y. Ergosterol Biosynthesis and Regulation Impact the Antifungal Resistance and Virulence of *Candida* spp. *Stresses* [Online], 2024, p. 641-662.

191. Sun, T.; Rao, S.; Zhou, X.; Li, L., Plant Carotenoids: Recent Advances and Future Perspectives. *Mol. Horticulture* **2022,** *2* (1), 3.

192. Maoka, T., Carotenoids as Natural Functional Pigments. *J. Nat. Med.* **2020,** *74* (1), 1-16.

193. Caferri, R.; Guardini, Z.; Bassi, R.; Dall'Osto, L., Chapter Two - Assessing Photoprotective Functions of Carotenoids in Photosynthetic Systems of Plants and Green Algae. In *Methods in enzymology*, Wurtzel, E. T., Ed. Academic Press: 2022; Vol. 674, pp 53-84.

194. Liman, G. L. S.; Garcia, A. A.; Fluke, K. A.; Anderson, H. R.; Davidson, S. C.; Welander, P. V.; Santangelo, T. J., Tetraether Archaeal Lipids Promote Long-Term Survival in Extreme Conditions. *Mol. Microbiol.* **2024,** *121* (5), 882-894.

195. Saracco, M.; Schaeffer, P.; Tourte, M.; Albers, S. V.; Louis, Y.; Peters, J.; Demé, B.; Fontanay, S.; Oger, P., Bilayer-Forming Lipids Enhance Archaeal Monolayer Membrane Stability. *bioRxiv* **2025**, 2025.02.20.639260.

196. TouzÉ, T.; Mengin-Lecreulx, D., Undecaprenyl Phosphate Synthesis. *EcoSal Plus* **2008,** *3* (1), 10.1128/ecosalplus.4.7.1.7.

197. Schmerk Crystal, L.; Bernards Mark, A.; Valvano Miguel, A., Hopanoid Production Is Required for Low-pH Tolerance, Antimicrobial Resistance, and Motility in *Burkholderia cenocepacia*. *J. Bacteriol.* **2011,** *193* (23), 6712-6723.

198. Silipo, A.; Vitiello, G.; Gully, D.; Sturiale, L.; Chaintreuil, C.; Fardoux, J.; Gargani, D.; Lee, H.-I.; Kulkarni, G.; Busset, N.; Marchetti, R.; Palmigiano, A.; Moll, H.; Engel, R.; Lanzetta, R.; Paduano, L.; Parrilli, M.; Chang, W.-S.; Holst, O.; Newman, D. K.; Garozzo, D.; D'Errico, G.; Giraud, E.; Molinaro, A., Covalently Linked Hopanoid-Lipid A Improves Outer-Membrane Resistance of a *Bradyrhizobium* Symbiont of Legumes. *Nat. Commun.* **2014,** *5* (1), 5106.

199. Jin, W.; Yang, Z.; Xu, K.; Liu, Q.; Luo, Q.; Li, L.; Xiang, X., A Comprehensive Review of Plant Volatile Terpenoids, Elucidating Interactions with Surroundings, Systematic Synthesis, Regulation, and Targeted Engineering Production. *Biology* **2025,** *14* (5).

200. Wang, S.; Wang, Y., Harnessing Hormone Gibberellin Knowledge for Plant Height Regulation. *Plant Cell Rep.* **2022,** *41* (10), 1945-1953.

201. Baum, M. J.; Cherry, J. A., Processing by the Main Olfactory System of Chemosignals that Facilitate Mammalian Reproduction. *Horm. Behav.* **2015,** *68*, 53-64.

202. Coombes, H. A.; Stockley, P.; Hurst, J. L., Female Chemical Signalling Underlying Reproduction in Mammals. *J. Chem. Ecol.* **2018,** *44* (9), 851-873.

203. Mony, T. J.; Elahi, F.; Choi, J. W.; Park, S. J. Neuropharmacological Effects of Terpenoids on Preclinical Animal Models of Psychiatric Disorders: A Review *Antioxidants* [Online], 2022.

204. Diallo, S.; Kašparová, K.; Šulc, J.; Johny, J.; Křivánek, J.; Nebesářová, J.; Sillam-Dussès, D.; Kyjaková, P.; Vondrášek, J.; Machara, A.; Lukšan, O.; Grosse-Wilde, E.; Hanus, R., Identification of the Trail-Following Pheromone Receptor in Termites. *eLife* **2025,** *13*, RP101814.

205. Kotaki, T.; Shinada, T.; Kaihara, K.; Ohfune, Y.; Numata, H., Structure Determination of a New Juvenile Hormone from a Heteropteran Insect. *Org. Lett.* **2009,** *11* (22), 5234-7.

206. Brülhart, J.; Süß, A.; Oettler, J.; Heinze, J.; Schultner, E., Sex- and Caste-Specific Developmental Responses to Juvenile Hormone in an Ant with Maternal Caste Determination. *J. Exp. Biol.* **2024,** *227* (12).

207. Sorensen, P. W.; Hoye, T. R., 4.05 - Pheromones in Vertebrates. In *Comprehensive Natural Products II*, Liu, H.-W.; Mander, L., Eds. Elsevier: Oxford, 2010; pp 225-262.

208. Galindo-Solís, J. M.; Fernández, F. J., Endophytic Fungal Terpenoids: Natural Role and Bioactivities. *Microorganisms* **2022,** *10* (2).

209. Kramer, R.; Abraham, W.-R., Volatile Sesquiterpenes from Fungi: What are They Good for? *Phytochem. Rev.* **2012,** *11* (1), 15-37.

210. Schulz-Bohm, K.; Martín-Sánchez, L.; Garbeva, P., Microbial Volatiles: Small Molecules with an Important Role in Intra- and Inter-Kingdom Interactions. *Front. Microbiol.* **2017,** *8*, 2484.

211. Hacquard, S., Commentary: Microbial Small Talk: Volatiles in Fungal-Bacterial Interactions. *Front. Microbiol.* **2017,** *8*, 1.

212. Divekar, P. A.; Narayana, S.; Divekar, B. A.; Kumar, R.; Gadratagi, B. G.; Ray, A.; Singh, A. K.; Rani, V.; Singh, V.; Singh, A. K.; Kumar, A.; Singh, R. P.; Meena, R. S.; Behera, T. K., Plant Secondary Metabolites as Defense Tools against Herbivores for Sustainable Crop Protection. *Int. J. Mol. Sci.* **2022,** *23* (5).

213. Abdelgaleil, S. A. M.; Al-Nagar, N. M. A.; Abou-Taleb, H. K.; Shawir, M. S., Effect of Monoterpenes, Phenylpropenes and Sesquiterpenes on Development, Fecundity and Fertility of *Spodoptera littoralis* (Boisduval). *Int. J. Trop. Insect Sci.* **2022,** *42* (1), 245-253.

214. Sayed, S.; Soliman, M. M.; Al-Otaibi, S.; Hassan, M. M.; Elarrnaouty, S.-A.; Abozeid, S. M.; El-Shehawi, A. M. Toxicity, Deterrent and Repellent Activities of Four Essential Oils on Aphis punicae (Hemiptera: Aphididae) *Plants* [Online], 2022.

215. Yuan, Y.; Lei, Y.; Xu, M.; Zhao, B.; Xu, S., Bioactive Terpenes from Marine Sponges and Their Associated Organisms. *Marine Drugs* **2025,** *23*.

216. Derengowski, L. S.; De-Souza-Silva, C.; Braz, S. V.; Mello-De-Sousa, T. M.; Báo, S. N.; Kyaw, C. M.; Silva-Pereira, I., Antimicrobial Effect of Farnesol, a Candida albicans Quorum Sensing Molecule, on Paracoccidioides brasiliensis Growth and Morphogenesis. *Ann. Clin. Microbiol. Antimicrob.* **2009,** *8*, 13.

217. Perochon, A.; Doohan, F. M., Trichothecenes and Fumonisins: Key Players in Fusarium-Cereal Ecosystem Interactions. *Toxins* **2024,** *16* (2).

218. Zhao, B.; Lin, X.; Lei, L.; Lamb, D. C.; Kelly, S. L.; Waterman, M. R.; Cane, D. E., Biosynthesis of the sesquiterpene antibiotic albaflavenone in *Streptomyces coelicolor* A3(2). *J. Biol. Chem.* **2008,** *283* (13), 8183-9.

219. Kim, S.-H.; Ha, T.-K.-Q.; Oh, W. K.; Shin, J.; Oh, D.-C., Antiviral Indolosesquiterpenoid Xiamycins C–E from a Halophilic Actinomycete. *J. Nat. Prod.* **2016,** *79* (1), 51-58.

220. Wang, J.; Soisson, S. M.; Young, K.; Shoop, W.; Kodali, S.; Galgoci, A.; Painter, R.; Parthasarathy, G.; Tang, Y. S.; Cummings, R.; Ha, S.; Dorso, K.; Motyl, M.; Jayasuriya, H.; Ondeyka, J.; Herath, K.; Zhang, C.; Hernandez, L.; Allocco, J.; Basilio, A.; Tormo, J. R.; Genilloud, O.; Vicente, F.; Pelaez, F.; Colwell, L.; Lee, S. H.; Michael, B.; Felcetto, T.; Gill, C.; Silver, L. L.; Hermes, J. D.; Bartizal, K.; Barrett, J.; Schmatz, D.; Becker, J. W.; Cully, D.; Singh, S. B., Platensimycin is a Selective FabF Inhibitor with Potent Antibiotic Properties. *Nature* **2006,** *441* (7091), 358-61.

221. Hu, Y. L.; Zhang, Q.; Liu, S. H.; Sun, J. L.; Yin, F. Z.; Wang, Z. R.; Shi, J.; Jiao, R. H.; Ge, H. M., Building *Streptomyces albus* as a Chassis for Synthesis of Bacterial Terpenoids. *Chem. Sci.* **2023,** *14* (13), 3661-3667.

222. Kim, S.-H.; Lu, W.; Ahmadi, M. K.; Montiel, D.; Ternei, M. A.; Brady, S. F., Atolypenes, Tricyclic Bacterial Sesterterpenes Discovered Using a Multiplexed In Vitro Cas9-TAR Gene Cluster Refactoring Approach. *ACS Synth. Biol.* **2019,** *8* (1), 109-118.

223. Hou, A.; Dickschat, J. S., The Biosynthetic Gene Cluster for Sestermobaraenes-Discovery of a Geranylfarnesyl Diphosphate Synthase and a Multiproduct Sesterterpene Synthase from *Streptomyces mobaraensis*. *Angew. Chem. Int. Ed. Engl.* **2020,** *59* (45), 19961-19965.

224. De Rosa, M.; Gambacorta, A.; Minale, L.; Bu'Lock, J. D., Bacterial Triterpenes. *J. Chem. Soc. Chem. Commun.* **1971,** (12), 619-620.

225. Bird, C., The Identification of hop-22 (29)-ene in Prokaryotic Organisms. *Tetrahedron Lett.* **1971,** *34*, 3187-3190.

226. Wei, J. H.; Yin, X.; Welander, P. V., Sterol Synthesis in Diverse Bacteria. *Front. Microbiol.* **2016,** *7*, 990.

227. Menaa, F.; Wijesinghe, P. A. U. I.; Thiripuranathar, G.; Uzair, B.; Iqbal, H.; Khan, B. A.; Menaa, B. Ecological and Industrial Implications of Dynamic Seaweed-Associated Microbiota Interactions *Marine Drugs* [Online], 2020.

228. Demain, A. L.; Adrio, J. L., Contributions of Microorganisms to Industrial Biology. *Mol. Biotechnol.* **2008,** *38*, 41-55.

229. Dias, D. A.; Urban, S.; Roessner, U., A Historical Overview of Natural Products in Drug Discovery. *Metabolites* **2012,** *2* (2), 303-336.

230. Newman, D. J.; Cragg, G. M., Natural Products as Sources of New Drugs Over the Nearly Four Decades from 01/1981 to 09/2019. *J. Nat. Prod.* **2020,** *83* (3), 770-803.

231. Cook, M. A.; Wright, G. D., The Past, Present, and Future of Antibiotics. *Science Translational Medicine* **2022,** *14* (657), eabo7793.

232. Ligon, B. L. In *Penicillin: Its Discovery and Early Development*, Seminars in Pediatric Infectious Diseases, Elsevier: 2004; pp 52-57.

233. Nelson, M. L.; Levy, S. B., The History of the Tetracyclines. *Annals of the New York Academy of Sciences* **2011,** *1241* (1), 17-32.

234. Thaker, M.; Spanogiannopoulos, P.; Wright, G. D., The Tetracycline Resistome. *Cellular and Molecular Life Sciences* **2010,** *67*, 419-431.

235. Baral, B.; Mozafari, M., Strategic Moves of "Superbugs" Against Available Chemical Scaffolds: Signaling, Regulation, and Challenges. *ACS Pharmacol. Transl. Sci.* **2020,** *3* (3), 373-400.

236. Genilloud, O., Actinomycetes: Still a Source of Novel Antibiotics. *Nat. Prod. Rep.* **2017,** *34* (10), 1203-1232.

237. De Simeis, D.; Serra, S., *Actinomycetes*: A Never-Ending Source of Bioactive Compounds—An Overview on Antibiotics Production. *Antibiot.* **2021,** *10* (5), 483.

238. Meenakshi, S.; Hiremath, J.; Meenakshi, M.; Shivaveerakumar, S., Actinomycetes: Isolation, Cultivation and its Active Biomolecules. *J. Pure Appl. Microbiol.* **2024,** *18* (1).

239. Takahashi, Y.; Nakashima, T., Actinomycetes, An Inexhaustible Source of Naturally Occurring Antibiotics. *Antibiot.* **2018,** *7* (2), 45.

240. Oli, A. K.; Shivshetty, N.; Kelmani, C. R.; Biradar, P. A., Actinomycetes in Medical and Pharmaceutical Industries. In *Actinobacteria: Ecology, Diversity, Classification and Extensive Applications*, Springer: 2022; pp 291-320.

241. Domínguez, Á.; Muñoz, E.; López, M. C.; Cordero, M.; Martínez, J. P.; Viñas, M., Transcriptomics as a Tool to Discover New Antibacterial Targets. *Biotechnol. Lett.* **2017,** *39*, 819-828.

242. van Bergeijk, D. A.; Terlouw, B. R.; Medema, M. H.; van Wezel, G. P., Ecology and Genomics of Actinobacteria: New Concepts for Natural Product Discovery. *Nat. Rev. Microbiol.* **2020,** *18* (10), 546-558.

243. Palermo, A., Metabolomics-and Systems-Biology-Guided Discovery of Metabolite Lead Compounds and Druggable Targets. *Drug Discov. Today* **2023,** *28* (2), 103460.

244. Qi, Y. K.; Tang, X.; Wei, N. N.; Pang, C. J.; Du, S. S.; Wang, K., Discovery, Synthesis, and Optimization of Teixobactin, a Novel Antibiotic Without Detectable Bacterial Resistance. *J. Pept. Sci.* **2022,** *28* (11), e3428.

245. Ruetten, A.; Kirchner, T.; Musiol-Kroll, E. M., Overview on Strategies and Assays for Antibiotic Discovery. *Pharmaceuticals* **2022,** *15* (10), 1302.

246. Gaudêncio, S. P.; Bayram, E.; Lukić Bilela, L.; Cueto, M.; Díaz-Marrero, A. R.; Haznedaroglu, B. Z.; Jimenez, C.; Mandalakis, M.; Pereira, F.; Reyes, F., Advanced Methods for Natural Products Discovery: Bioactivity Screening, Dereplication, Metabolomics Profiling, Genomic Sequencing, Databases and Informatic Tools, and Structure Elucidation. *Marine Drugs* **2023,** *21* (5), 308.

247. Zhang, J. J.; Tang, X.; Moore, B. S., Genetic Platforms for Heterologous Expression of Microbial Natural Products. *Nat. Prod. Rep.* **2019,** *36* (9), 1313-1332.

248. Kang, H.-S.; Kim, E.-S., Recent Advances in Heterologous Expression of Natural Product Biosynthetic Gene Clusters in *Streptomyces* hosts. *Curr. Opin. Biotechnol.* **2021,** *69*, 118-127.

249. Blin, K.; Kim, H. U.; Medema, M. H.; Weber, T., Recent Development of antiSMASH and Other Computational Approaches to Mine Secondary Metabolite Biosynthetic Gene Clusters. *Brief. bioinform.* **2019,** *20* (4), 1103-1113.

250. Blin, K.; Shaw, S.; Kloosterman, A. M.; Charlop-Powers, Z.; Van Wezel, G. P.; Medema, M. H.; Weber, T., antiSMASH 6.0: Improving Cluster Detection and Comparison Capabilities. *Nucleic Acids Res.* **2021,** *49* (W1), W29-W35.

251. Noushahi, H. A.; Khan, A. H.; Noushahi, U. F.; Hussain, M.; Javed, T.; Zafar, M.; Batool, M.; Ahmed, U.; Liu, K.; Harrison, M. T., Biosynthetic Pathways of Triterpenoids and Strategies to Improve their Biosynthetic Efficiency. *J. Plant Growth Regul.* **2022,** *97* (3), 439-454.

252. Tistechok, S.; Roman, I.; Fedorenko, V.; Luzhetskyy, A.; Gromyko, O., Diversity and Bioactive Potential of Actinomycetia from the Rhizosphere Soil of *Juniperus excelsa*. *Folia Microbiol.* **2023,** *68* (4), 645-653.

253. Running, W., Computer Software Reviews. Chapman and Hall Dictionary of Natural Products on CD-ROM. *J. Chem. Inf. Comput. Sci.* **1993,** *33* (6), 934-935.

254. Myronovskyi, M.; Rosenkränzer, B.; Nadmid, S.; Pujic, P.; Normand, P.; Luzhetskyy, A., Generation of a Cluster-Free *Streptomyces albus* Chassis Strains for Improved Heterologous Expression of Secondary Metabolite Clusters. *Metab. Eng.* **2018,** *49*, 316-324.

255. Ahmed, Y.; Rebets, Y.; Estévez, M. R.; Zapp, J.; Myronovskyi, M.; Luzhetskyy, A., Engineering of *Streptomyces lividans* for Heterologous Expression of Secondary Metabolite Gene Clusters. *Microb. Cell Fact.* **2020,** *19* (5), 1-16.

256. Tao, H.; Lauterbach, L.; Bian, G.; Chen, R.; Hou, A.; Mori, T.; Cheng, S.; Hu, B.; Lu, L.; Mu, X., Discovery of Non-Squalene Triterpenes. *Nature* **2022,** *606* (7913), 414-419.

257. Luo, P.; Huang, J.-H.; Lv, J.-M.; Wang, G.-Q.; Hu, D.; Gao, H., Biosynthesis of Fungal Terpenoids. *Natural Product Reports* **2024**.

258. Tararina, M. A.; Yee, D. A.; Tang, Y.; Christianson, D. W., Structure of the Repurposed Fungal Terpene Cyclase FlvF Implicated in the C–N Bond-Forming Reaction of Flavunoidine Biosynthesis. *Biochemistry* **2022,** *61* (18), 2014-2024.

259. Hoshino, T.; Sato, T., Squalene–Hopene Cyclase: Catalytic Mechanism and Substrate Recognition. *Chem. Commun.* **2002,** (4), 291-301.

260. Capyk, J. K.; D'Angelo, I.; Strynadka, N. C.; Eltis, L. D., Characterization of 3-Ketosteroid 9α-Hydroxylase, a Rieske Oxygenase in the Cholesterol Degradation Pathway of *Mycobacterium tuberculosis*. *J. Biol. Chem.* **2009,** *284* (15), 9937-9946.

261. Organization, W. H., *WHO Bacterial Priority Pathogens List*. World Health Organization, Geneva: 2024.

262. Hassoun, A.; Linden, P. K.; Friedman, B., Incidence, Prevalence, and Management of MRSA Bacteremia Across Patient Populations—a Review of Recent Developments in MRSA Management and Treatment. *Critical Care* **2017,** *21* (1), 1-10.

263. Imai, Y.; Hauk, G.; Quigley, J.; Liang, L.; Son, S.; Ghiglieri, M.; Gates, M. F.; Morrissette, M.; Shahsavari, N.; Niles, S., Evybactin is a DNA Gyrase Inhibitor that Selectively Kills *Mycobacterium tuberculosis*. *Nat. Chem. Biol.* **2022,** *18* (11), 1236-1244.

264. Kieser, T.; Bibb, M. J.; Buttner, M. J.; Chater, K. F.; Hopwood, D. A., *Practical Streptomyces Genetics*. John Innes Foundation Norwich: 2000; Vol. 291.

265. Bankevich, A.; Nurk, S.; Antipov, D.; Gurevich, A. A.; Dvorkin, M.; Kulikov, A. S.; Lesin, V. M.; Nikolenko, S. I.; Pham, S.; Prjibelski, A. D., SPAdes: A New Genome Assembly Algorithm and Its Applications to Single-Cell Sequencing. *J. Comput. Biol.* **2012,** *19* (5), 455-477.

266. Meyer, F.; Goesmann, A.; McHardy, A. C.; Bartels, D.; Bekel, T.; Clausen, J.; Kalinowski, J.; Linke, B.; Rupp, O.; Giegerich, R., GenDB—An Open Source Genome Annotation System for Prokaryote Genomes. *Nucl. Acids Res.* **2003,** *31* (8), 2187-2195.

267. Seemann, T., Prokka: Rapid Prokaryotic Genome Annotation. *Bioinformatics* **2014,** *30* (14), 2068-2069.

268. Petzke, L.; Luzhetskyy, A., In vivo Tn 5-based Transposon Mutagenesis of *Streptomycetes*. *Appl. Microbiol. Biotechnol.* **2009,** *83*, 979-986.

269. Steinegger, M.; Söding, J., MMseqs2 Enables Sensitive Protein Sequence Searching for the Analysis of Massive Data Sets. *Nat. Biotechnol.* **2017,** *35* (11), 1026-1028.

270. Müller, A.; Grein, F.; Otto, A.; Gries, K.; Orlov, D.; Zarubaev, V.; Girard, M.; Sher, X.; Shamova, O.; Roemer, T.; François, P.; Becher, D.; Schneider, T.; Sahl, H.-G., Differential Daptomycin Resistance Development in *Staphylococcus aureus* Strains with Active and Mutated gra Regulatory Systems. *Int. J. Med. Microbiol.* **2018,** *308* (3), 335-348.

271. Müller, R.; Fu, C.; Liu, Y.; Walt, C.; Rasheed, S.; Bader, C.; Lukat, P.; Neuber, M.; Haeckl, J.; Blankenfeldt, W., Mycoplanecins, Potent Anti-Tuberculosis Antibiotics: Elucidation of Unusual Biosynthesis and DnaN-Targeting Mode of Action. **2023**.

272. Strähle, U.; Scholz, S.; Geisler, R.; Greiner, P.; Hollert, H.; Rastegar, S.; Schumacher, A.; Selderslaghs, I.; Weiss, C.; Witters, H., Zebrafish Embryos as an Alternative to Animal Experiments—A Commentary on the Definition of the Onset of Protected Life Stages in Animal Welfare Regulations. *Reprod. Toxicol.* **2012,** *33* (2), 128-132.

273. Hoye, T. R.; Jeffrey, C. S.; Shao, F., Mosher ester analysis for the determination of absolute configuration of stereogenic (chiral) carbinol carbons. *Nature Protocols* **2007,** *2* (10), 2451-2458.

274. Flett, F.; Mersinias, V.; Smith, C. P., High Efficiency Intergeneric Conjugal Transfer of Plasmid DNA from *Escherichia coli* to Methyl DNA-Restricting *Streptomycetes*. *FEMS Microbiol. Lett.* **1997,** *155* (2), 223-229.

275. Fu, J.; Teucher, M.; Anastassiadis, K.; Skarnes, W.; Stewart, A. F., A Recombineering Pipeline to Make Conditional Targeting Constructs. In *Methods in enzymology*, Elsevier: 2010; Vol. 477, pp 125-144.

276. Myronovskyi, M.; Rosenkränzer, B.; Luzhetskyy, A., Iterative Marker Excision System. *Appl. Microbiol. Biotechnol.* **2014,** *98*, 4557-4570.

277. Cuozzo, S.; de LeBlanc, A. d. M.; LeBlanc, J.; Hoffmann, N.; Tortella, G., *Streptomyces* Genus as a Source of Probiotics and its Potential for its Use in Health. *Microbiol. Res.* **2023,** *266*, 127248.

278. Donald, L.; Pipite, A.; Subramani, R.; Owen, J.; Keyzers, R. A.; Taufa, T., *Streptomyces*: Still the Biggest Producer of New Natural Secondary Metabolites, a Current Perspective. *Microbiol. Res.* **2022,** *13* (3), 418-465.

279. Parab, S.; Corà, D.; Bussolino, F., Mining Genomes of Actinobacteria. *Met. Actinobacteriol.* **2022**, 221-228.

280. Ding, T.; Yang, L.-J.; Zhang, W.-D.; Shen, Y.-H., The Secondary Metabolites of Rare Actinomycetes: Chemistry and Bioactivity. *RSC adv.* **2019,** *9* (38), 21964-21988.

281. Hifnawy, M. S.; Fouda, M. M.; Sayed, A. M.; Mohammed, R.; Hassan, H. M.; AbouZid, S. F.; Rateb, M. E.; Keller, A.; Adamek, M.; Ziemert, N.; Abdelmohsen, U. R., The Genus *Micromonospora* as a Model Microorganism for Bioactive Natural Product Discovery. *RSC Adv.* **2020,** *10* (35), 20939-20959.

282. Nonthakaew, N.; Sharkey, L. K.; Pidot, S. J., The Genus *Nocardia* as a Source of New Antimicrobials. *NPJ Antimicrob. Resist.* **2025,** *3* (1), 5.

283. Singh, T. A.; Passari, A. K.; Jajoo, A.; Bhasin, S.; Gupta, V. K.; Hashem, A.; Alqarawi, A. A.; Abd_Allah, E. F., Tapping Into Actinobacterial Genomes for Natural Product Discovery. *Front. Microbiol.* **2021,** *12*, 655620.

284. Song, Z.; Xu, T.; Wang, J.; Hou, Y.; Liu, C.; Liu, S.; Wu, S., Secondary Metabolites of the Genus *Amycolatopsis*: Structures, Bioactivities and Biosynthesis. *Molecules* **2021,** *26* (7), 1884.

285. Zhao, P.; Xue, Y.; Gao, W.; Li, J.; Zu, X.; Fu, D.; Feng, S.; Bai, X.; Zuo, Y.; Li, P., Actinobacteria–derived peptide antibiotics since 2000. *Peptides* **2018,** *103*, 48-59.

286. Bentley, S. D.; Chater, K. F.; Cerdeño-Tárraga, A.-M.; Challis, G. L.; Thomson, N.; James, K. D.; Harris, D. E.; Quail, M. A.; Kieser, H.; Harper, D., Complete Genome Sequence of the Model Actinomycete *Streptomyces coelicolor* A3 (2). *Nature* **2002,** *417* (6885), 141-147.

287. Ikeda, H.; Ishikawa, J.; Hanamoto, A.; Shinose, M.; Kikuchi, H.; Shiba, T.; Sakaki, Y.; Hattori, M.; Ōmura, S., Complete Genome Sequence and Comparative Analysis of the Industrial Microorganism *Streptomyces avermitilis*. *Nat. Biotechnol.* **2003,** *21* (5), 526-531.

288. Ohnishi, Y.; Ishikawa, J.; Hara, H.; Suzuki, H.; Ikenoya, M.; Ikeda, H.; Yamashita, A.; Hattori, M.; Horinouchi, S., Genome Sequence of the Streptomycin-Producing Microorganism *Streptomyces griseus* IFO 13350. *J. Bacteriol.* **2008,** *190* (11), 4050-4060.

289. Tokovenko, B.; Rebets, Y.; Luzhetskyy, A., Automating Assessment of the Undiscovered Biosynthetic Potential of Actinobacteria. *BioRxiv* **2016**, 036087.

290. Schorn, M. A.; Alanjary, M. M.; Aguinaldo, K.; Korobeynikov, A.; Podell, S.; Patin, N.; Lincecum, T.; Jensen, P. R.; Ziemert, N.; Moore, B. S., Sequencing Rare Marine Actinomycete Genomes Reveals High Density of Unique Natural Product Biosynthetic Gene Clusters. *Microbiology* **2016,** *162* (12), 2075-2086.

291. Anand, S.; Prasad, M. V. R.; Yadav, G.; Kumar, N.; Shehara, J.; Ansari, M. Z.; Mohanty, D., SBSPKS: Structure Based Sequence Analysis of Polyketide Synthases. *Nucleic Acids Res.* **2010,** *38*, W487-W496.

292. Anker, A. S.; Friis-Jensen, U.; Johansen, F. L.; Billinge, S. J.; Jensen, K., ClusterFinder: a Fast Tool to Find Cluster Structures from Pair Distribution Function Data. *Acta Cryst.* **2024,** *A80* (2), 213-220.

293. Kim, J.; Yi, G.-S., PKMiner: a Database for Exploring Type II Polyketide Synthases. *BMC Microbiol.* **2012,** *12* (1), 169.

294. Skinnider, M. A.; Merwin, N. J.; Johnston, C. W.; Magarvey, N. A., PRISM 3: Expanded Prediction of Natural Product Chemical Structures from Microbial Genomes. *Nucleic Acids Res.* **2017,** *45* (W1), W49-W54.

295. Baltz, R. H., Natural Product Drug Discovery in the Genomic Era: Realities, Conjectures, Misconceptions, and Opportunities. *J. Ind. Microbiol. Biotechnol.* **2019,** *46* (3-4), 281-299.

296. Biermann, F.; Wenski, S. L.; Helfrich, E. J. N., Navigating and Expanding the Roadmap of Natural Product Genome Mining Tools. *Beilstein J. Org. Chem.* **2022,** *18*, 1656-1671.

297. Ziemert, N.; Weber, T.; Medema, M., Genome Mining Approaches to Bacterial Natural Product Discovery. In *Comprehensive Natural Products III. Oxford: Elsevier*, Liu HW (Ben), B. T., Ed. Elsevier: United Kingdom, 2020; Vol. 6, pp 19-33.

298. Kalkreuter, E.; Pan, G.; Cepeda, A. J.; Shen, B., Targeting Bacterial Genomes for Natural Product Discovery. *Trends Pharmacol. Sci.* **2020,** *41* (1), 13-26.

299. Chen, R.; Wong, H. L.; Burns, B. P., New Approaches to Detect Biosynthetic Gene Clusters in the Environment. *Medicines (Basel, Switzerland)* **2019,** *6* (1).

300. Tistechok, S.; Bratiichuk, D.; Sucipto, H.; Gummerlich, N.; Stierhof, M.; Gromyko, O.; Fries, F.; Fedorenko, V.; Müller, R.; Zapp, J., Gromomycins: An Unprecedented Class of Triterpene Antibiotics Produced by a Novel Biosynthetic Pathway. *Angew. Chem. Int. Ed.* **2025,** *64* (22), e202422270.

301. Morlacchi, P.; Wilson, W. K.; Xiong, Q.; Bhaduri, A.; Sttivend, D.; Kolesnikova, M. D.; Matsuda, S. P., Product Profile of PEN3: the Last Unexamined Oxidosqualene Cyclase in *Arabidopsis thaliana*. *Org. lett.* **2009,** *11* (12), 2627-2630.

302. Qiao, W.; Feng, W.; Yang, L.; Li, C.; Qu, X.; Zhang, Y., De Novo Biosynthesis of the Anticancer Compound Euphol in *Saccharomyces cerevisiae*. *ACS Synthetic Biology* **2021,** *10* (9), 2351-2358.

303. Zasloff, M., Antimicrobial Peptides of Multicellular Organisms. *Nature* **2002,** *415* (6870), 389-395.

304. Tempelaars, M. H.; Rodrigues, S.; Abee, T., Comparative Analysis of Antimicrobial Activities of Valinomycin and Cereulide, the *Bacillus cereus* Emetic Toxin. *Appl. Environ. Microbiol.* **2011,** *77* (8), 2755-62.

305. Li, X.; Feng, H. Q.; Pang, X. Y.; Li, H. Y., Mesosome Formation is Accompanied by Hydrogen Peroxide Accumulation in Bacteria During the Rifampicin Effect. *Mol. Cell Biochem.* **2008,** *311* (1-2), 241-247.

306. Hartmann, M.; Berditsch, M.; Hawecker, J.; Ardakani, M. F.; Gerthsen, D.; Ulrich, A. S., Damage of the Bacterial Cell Envelope by Antimicrobial Peptides Gramicidin S and PGLa as Revealed by Transmission and Scanning Electron Microscopy. *Antimicrob. Agents Chemother.* **2010,** *54* (8), 3132-3142.

307. Brogden, K. A., Antimicrobial Peptides: Pore Formers or Metabolic Inhibitors in Bacteria? *Nat. Rev. Microbiol.* **2005,** *3* (3), 238-250.

308. Epand, R. M.; Epand, R. F., Lipid Domains in Bacterial Membranes and the Action of Antimicrobial Agents. *Biochim. Biophys. Acta* **2009,** *1788* (1), 289-94.

309. Arisetti, N.; Fuchs, H. L. S.; Coetzee, J.; Orozco, M.; Ruppelt, D.; Bauer, A.; Heimann, D.; Kuhnert, E.; Bhamidimarri, S. P.; Bafna, J. A.; Hinkelmann, B.; Eckel, K.; Sieber, S. A.; Müller, P. P.; Herrmann, J.; Müller, R.; Winterhalter, M.; Steinem, C.; Brönstrup, M., Total Synthesis and Mechanism of Action of the Antibiotic Armeniaspirol A. *Chem. Sci.* **2021,** *12* (48), 16023-16034.

310. Castro-Falcón, G.; Straetener, J.; Bornikoel, J.; Reimer, D.; Purdy, T. N.; Berscheid, A.; Schempp, F. M.; Liu, D. Y.; Linington, R. G.; Brötz-Oesterhelt, H., Antibacterial Marinopyrroles and Pseudilins Act as Protonophores. *ACS Chem. Biol.* **2024,** *19* (3), 743-752.

311. Dijksteel, G. S.; Ulrich, M. M. W.; Middelkoop, E.; Boekema, B., Review: Lessons Learned From Clinical Trials Using Antimicrobial Peptides (AMPs). *Front. Microbiol.* **2021,** *12*, 616979.

312. Semrau, S.; Monster, M. W. L.; van der Knaap, M.; Florea, B. I.; Schmidt, T.; Overhand, M., Membrane Lysis by Gramicidin S Visualized in Red Blood Cells and Giant Vesicles. *Biochim. Biophys. Acta.* **2010,** *1798* (11), 2033-2039.

313. Lim, L. M.; Ly, N.; Anderson, D.; Yang, J. C.; Macander, L.; Jarkowski III, A.; Forrest, A.; Bulitta, J. B.; Tsuji, B. T., Resurgence of Colistin: A Review of Resistance, Toxicity, Pharmacodynamics, and Dosing. *Pharmacotherapy* **2010,** *30* (12), 1279-1291.

314. Deschner, F.; Mostert, D.; Daniel, J.-M.; Voltz, A.; Schneider, D. C.; Khangholi, N.; Bartel, J.; Pessanha de Carvalho, L.; Brauer, M.; Gorelik, T. E.; Kleeberg, C.; Risch, T.; Haeckl, F. P. J.; Herraiz Benítez, L.; Andreas, A.; Kany, A. M.; Jézéquel, G.; Hofer, W.; Müsken, M.; Held, J.; Bischoff, M.; Seemann, R.; Brötz-Oesterhelt, H.; Schneider, T.; Sieber, S.; Müller, R.; Herrmann, J., Natural Products Chlorotonils Exert a Complex Antibacterial Mechanism and Address Multiple Targets. *Cell Chem. Biol.* **2025,** *32* (4), 586-602.e15.

315. Orlov, D. S.; Nguyen, T.; Lehrer, R. I., Potassium Release, a Useful Tool for Studying Antimicrobial Peptides. *J. Microbiol. Methods.* **2002,** *49* (3), 325-328.

316. Katz, L.; Baltz, R. H., Natural Product Discovery: Past, Present, and Future. *J. Ind. Microbiol. Biotechnol.* **2016,** *43* (2-3), 155-176.

317. Rossiter, S. E.; Fletcher, M. H.; Wuest, W. M., Natural Products as Platforms To Overcome Antibiotic Resistance. *Chem. Rev.* **2017,** *117* (19), 12415-12474.

318. Hutchings, M. I.; Truman, A. W.; Wilkinson, B., Antibiotics: Past, Present and Future. *Curr. Opin. Microbiol.* **2019,** *51*, 72-80.

319. Bérdy, J., Bioactive Microbial Metabolites. *J. Antibiot.* **2005,** *58* (1), 1-26.

320. Behie, S. W.; Bonet, B.; Zacharia, V. M.; McClung, D. J.; Traxler, M. F., Molecules to Ecosystems: Actinomycete Natural Products *in situ*. *Front. Microbiol.* **2017,** *7*, 2149.

321. McClung Dylan, J.; Du, Y.; Antonich Dominic, J.; Bonet, B.; Zhang, W.; Traxler Matthew, F., Harnessing Rare Actinomycete Interactions and Intrinsic Antimicrobial Resistance Enables Discovery of an Unusual Metabolic Inhibitor. *mBio* **2022,** *13* (3), e00393-22.

322. Watve, M. G.; Tickoo, R.; Jog, M. M.; Bhole, B. D., How Many Antibiotics are Produced by the Genus *Streptomyces*? *Arch. Microbiol.* **2001,** *176* (5), 386-390.

323. Bérdy, J., Thoughts and Facts About Antibiotics: Where We are Now and Where We are Heading. *J. Antibiot.* **2012,** *65* (8), 385-395.

324. Jeong, H.; Choe, Y.; Nam, J.; Ban, Y. H., A Guide to Genome Mining and Genetic Manipulation of Biosynthetic Gene Clusters in *Streptomyces*. *J. Microbiol.* **2025,** *63* (4), e2409026.

325. Zhu, S.; Xu, H.; Liu, Y.; Hong, Y.; Yang, H.; Zhou, C.; Tao, L., Computational Advances in Biosynthetic Gene Cluster Discovery and Prediction. *Biotechnol. Adv.* **2025,** *79*, 108532.

326. Heimann, D.; Kohnhäuser, D.; Kohnhäuser, A. J.; Brönstrup, M., Antibacterials with Novel Chemical Scaffolds in Clinical Development. *Drugs* **2025,** *85* (3), 293-323.

327. Murray, C. J.; Ikuta, K. S.; Sharara, F.; Swetschinski, L.; Aguilar, G. R.; Gray, A.; Han, C.; Bisignano, C.; Rao, P.; Wool, E., Global Burden of Bacterial Antimicrobial Resistance in 2019: a Systematic Analysis. *The Lancet* **2022,** *399* (10325), 629-655.

328. Sun, X.; Qiu, S.; Luo, X.; Jin, P.; Zhao, J.; Wu, X.; Yang, J.; Wang, X.; Song, J.; Xiang, W., *Micromonospora rubida* sp. nov., a Novel Actinobacterium Isolated from Soil of Harbin. *Antonie van Leeuwenhoek* **2021,** *114* (6), 697-708.

329. Liu, Y.; Shi, H.; Wang, Z.; Huang, X.; Zhang, X., Pleiotropic Control of Antibiotic Biosynthesis, Flagellar Operon Expression, Biofilm Formation, and Carbon Source Utilization by RpoN in *Pseudomonas protegens* H78. *Appl. Microbiol. Biotechnol.* **2018,** *102* (22), 9719-9730.

330. Kuban-Jankowska, A.; Kostrzewa, T.; Gorska-Ponikowska, M., Bacterial Protein Tyrosine Phosphatases as Possible Targets for Antimicrobial Therapies in Response to Antibiotic Resistance. *Antioxidants* **2022,** *11* (12).

331. Martín, J. F.; Liras, P.; Sánchez, S., Modulation of Gene Expression in Actinobacteria by Translational Modification of Transcriptional Factors and Secondary Metabolite Biosynthetic Enzymes. *Front. Microbiol.* **2021,** *12*, 630694.

332. Passot, F. M.; Cantlay, S.; Flärdh, K., Protein Phosphatase SppA Regulates Apical Growth and Dephosphorylates Cell Polarity Determinant DivIVA in *Streptomyces coelicolor*. *Mol. Microbiol.* **2022,** *117* (2), 411-428.

333. Floriano, B.; Bibb, M., afsR is a Pleiotropic but Conditionally Required Regulatory Gene for Antibiotic Production in *Streptomyces coelicolor* A3(2). *Mol. Microbiol.* **1996,** *21* (2), 385-96.

334. Atsushi, M.; Soon-Kwang, H.; Hiroshi, I.; Sueharu, H.; Teruhiko, B., Phosphorylation of the AfsR Protein Involved in Secondary Metabolism in *Streptomyces* Species by a Eukary Otic-Type Protein Kinase. *Gene* **1994,** *146* (1), 47-56.

335. Lee, P. C.; Umeyama, T.; Horinouchi, S., AfsS is a Target of AfsR, a Transcriptional Factor with ATPase Activity that Globally Controls Secondary Metabolism in *Streptomyces coelicolor* A3(2). *Mol. Microbiol.* **2002,** *43* (6), 1413-30.

336. Zhang, Q.; Li, H.; Li, S.; Zhu, Y.; Zhang, G.; Zhang, H.; Zhang, W.; Shi, R.; Zhang, C., Carboxyl Formation from Methyl via Triple Hydroxylations by XiaM in Xiamycin A Biosynthesis. *Organic Letters* **2012,** *14* (24), 6142-6145.

337. Iizaka, Y.; Kanai, H.; Suzuki, T.; Maruyama, Y.; Kurita, M.; Sano, M.; Watanabe, A.; Fukumoto, A.; Saito, R.; Anzai, Y., Artificial Control of the Multistep Oxidation Reactions Catalyzed by the Cytochrome P450 Enzyme RosC. *Appl. Microbiol. Biotechnol.* **2020,** *104* (8), 3403-3415.

338. Nozoe, S.; Morisaki, M.; Tsuda, K.; Iitaka, Y.; Takahashi, N.; Tamura, S.; Ishibashi, K.; Shirasaka, M., The Structure of Ophiobolin, a C25 Terpenoid Having a Novel Skeleton. *J. Am. Chem. Soc.* **1965,** *87* (21), 4968-4970.

339. Choi, B. K.; Trinh, P. T. H.; Lee, H. S.; Choi, B. W.; Kang, J. S.; Ngoc, N. T. D.; Van, T. T. T.; Shin, H. J., New Ophiobolin Derivatives from the Marine Fungus *Aspergillus flocculosus* and Their Cytotoxicities against Cancer Cells. *Mar. Drugs* **2019,** *17* (6).

340. Guo, K.; Liu, Y.; Li, S.-H., The Untapped Potential of Plant Sesterterpenoids: Chemistry, Biological Activities and Biosynthesis. *Nat. Prod. Rep.* **2021,** *38* (12), 2293-2314.

341. Yan, D.; Arakelyan, J.; Wan, T.; Raina, R.; Chan, T. K.; Ahn, D.; Kushnarev, V.; Cheung, T. K.; Chan, H. C.; Choi, I.; Ho, P. Y.; Hu, F.; Kim, Y.; Lau, H. L.; Law, Y. L.; Leung, C. S.; Tong, C. Y.; Wong, K. K.; Yim, W. L.; Karnaukhov, N. S.; Kong, R. Y. C.; Babak, M. V.; Matsuda, Y., Genomics-Driven Derivatization of the Bioactive Fungal Sesterterpenoid Variecolin: Creation of an Unnatural Analogue with Improved Anticancer Properties. *Acta Pharm. Sin. B.* **2024,** *14* (1), 421-432.

342. Zhang, P.; Qi, J.; Duan, Y.; Gao, J. M.; Liu, C., Research Progress on Fungal Sesterterpenoids Biosynthesis. *J. Fungi* **2022,** *8* (10).

343. Lee, Y. J.; Kim, S. H.; Choi, H.; Lee, H. S.; Lee, J. S.; Shin, H. J.; Lee, J., Cytotoxic Furan- and Pyrrole-Containing Scalarane Sesterterpenoids Isolated from the Sponge *Scalarispongia* sp. *Molecules* **2019,** *24* (5).

344. Chen, L.-J.; Wu, G.-L.; Liu, J.; Lv, F.-Y.; Ng, P. Y.; Luo, Q.; Yang, F.; Mao, Z.-F.; Lin, H.-W., Bioactive Scalarane-Type Sesterterpenoids from the Yongle Islands Marine Sponge *Phyllospongia foliascens*. *Tetrahedron* **2025,** *188*, 134958.

345. Chang, Y.-C.; Tseng, S.-W.; Liu, L.-L.; Chou, Y.; Ho, Y.-S.; Lu, M.-C.; Su, J.-H. Cytotoxic Sesterterpenoids from a Sponge *Hippospongia* sp. *Mar. Drugs* [Online], 2012, p. 987-997.

346. Kim, S.-H.; Lu, W.; Ahmadi, M. K.; Montiel, D.; Ternei, M. A.; Brady, S. F., Atolypenes, Tricyclic Bacterial Sesterterpenes Discovered Using a Multiplexed in vitro Cas9-TAR Gene Cluster Refactoring Approach. *ACS Synth. Biol.* **2018,** *8* (1), 109-118.

347. Kim, M. C.; Winter, J. M.; Asolkar, R. N.; Boonlarppradab, C.; Cullum, R.; Fenical, W., Marinoterpins A–C: Rare Linear Merosesterterpenoids from Marine-Derived Actinomycete Bacteria of the Family *Streptomycetaceae*. *J. Org. Chem.* **2021,** *86* (16), 11140-11148.

348. Gu, B.; Goldfuss, B.; Schnakenburg, G.; Dickschat, J. S., Subrutilane—A Hexacyclic Sesterterpene from *Streptomyces subrutilus*. *Angew. Chem. Int. Ed.* **2023,** *62* (48), e202313789.

349. Hoye, T. R.; Jeffrey, C. S.; Shao, F., Mosher Ester Analysis for the Determination of Absolute Configuration of Stereogenic (Chiral) Carbinol Carbons. *Nat. Protoc.* **2007,** *2* (10), 2451-8.

350. Seco, J. M.; Quiñoá, E.; Riguera, R., The Assignment of Absolute Configuration by NMR. *Chem. Rev.* **2004,** *104* (1), 17-118.

351. Yanisch-Perron, C.; Vieira, J.; Messing, J., Improved M13 Phage Cloning Vectors and Host Strains: Nucleotide Sequences of the M13mp18 and pUC19 Vectors. *Gene* **1985,** *33* (1), 103-19.

352. Myronovskyi, M.; Rosenkränzer, B.; Stierhof, M.; Petzke, L.; Seiser, T.; Luzhetskyy, A., Identification and heterologous expression of the albucidin gene cluster from the marine strain Streptomyces albus subsp. chlorinus NRRL B-24108. *Microorganisms* **2020,** *8* (2), 237.

353. Shuai, H.; Myronovskyi, M.; Rosenkränzer, B.; Paulus, C.; Nadmid, S.; Stierhof, M.; Kolling, D.; Luzhetskyy, A., Novel biosynthetic route to the isoquinoline scaffold. *ACS Chemical Biology* **2022,** *17* (3), 598-608.

354. Wang, J.; Xu, Y.; Chen, D.; Tao, J.; Wang, H.; Liu, W., A Bacterial Cytochrome P450 Enzyme Catalyzes Multistep Oxidation Reactions in Pyrroindomycin Biosynthesis. *Chin. J. Chem.* **2023,** *41* (19), 2439-2445.